DIPARTIMENTO DI SCIENZE DELLA TERRA
UNIVERSITÀ DI PISA

Corso di Dottorato Regionale in Scienze della Terra
PhD Course in Earth Sciences

XXXII Ciclo – 32th Cycle
2016 – 2019

Saverio Bartolini Lucenti

Evolutionary history of Canidae (Carnivora, Mammalia) and Lyncodontini (Mustelidae, Carnivora) in the Plio-Pleistocene of the Old World

Tutore - Supervisor: **Prof. Lorenzo Rook**

Coordinatore del Corso di Dottorato
Prof. Carlo Baroni

Optime loquor, sed adhuc inter mala volutor plurima. Non est quod me ad formulam meam exigas: cum maxime facio me et formo et ad exemplar ingens attollo; si processero quantumcumque proposui, exige ut dictis facta respondeant.

Contents

Abstract

Carnivora is the most diverse order of Mammalia and includes some of the most iconic of all mammals. Among them, members of the families Canidae and Mustelidae possess a great array of adaptations to different sorts of habitats and environmental conditions. The evolutionary history of Canidae has been deeply studied, allowing paleontologists to reconstruct their major evolutionary and biogeographic events: from their origin in the middle Eocene in North America to their dispersion into Old World by the end of the Miocene. The evolutionary history and systematics of Mustelidae is more debated, and especially that of the tribe Lyncodontini. Nowadays, this group is represented by two genera (*Galictis* and *Lyncodon*) of South America, but in Plio-Pleistocene times it was widespread in North America and throughout the Old World.

The present study aims to answer some of taxonomic and evolutionary history issues of selected Plio-Pleistocene taxa of Canidae (*i.e.*, *Canis*, *Eucyon*, *Nyctereutes*, *Vulpes*) and of Lyncodontini from various Old-World localities. Different methodologies and approaches were used to achieve these objectives, from traditional morphometrics, phylogenetic analyses, multivariate statistics to the use of 3D imaging techniques, such as laser scans and computed tomography scans that helped, for instance, the study the internal cranial anatomy of fossil taxa.

Among European Lyncodontini, "*Mustela*" *ardea* from Issoire and Perrier-Les Etouaires represents a problematic taxon. The generic attribution is disputed, as different authors ascribed the taxon to *Pannonictis*, whereas other preferred the ascription to *Enhydrictis*. Even the attributed authorship of the specific name to Bravard (1828) appears dubious as the author did not report the name "ardea" in any of its works. A bibliographic search and the revision of the type and referred material from French and Italian localities allowed to identify the correct authorship (Gervais, 1848-1852) and recognize the peculiarity of the taxon. Many features support the attribution of the species to a new genus, *Martellictis*. This result appears to the supported also by the first phylogenetic analysis on fossil Lyncodontini.

The description of the lyncodontine sample from the Early-Middle Pleistocene site complex of Monte Tuttavista (Sardinia), revealed the presence of two endemic taxa distinct from the coeval continental relatives: *Pannonictis baroniensis* and *Enhydrictis praegalictoides*. The stouter *P. baroniensis* is represent by fewer specimens coming from Early Pleistocene fissures. *E. praegalictoides* is by far more abundant than the other lyncodontine. It shows a mixed pattern of derived features, that testify to the close affinity with the

middle Pleistocene *E. galictoides* from other localities of Sardinia, but also other primitive ones that do not occur in the latter mustelid. The record of these new species expands our knowledge of the biogeography of Lyncodontini in Eurasia and enriches the diversity of the tribe during the Early and middle Pleistocene.

Of living Canidae, *N. procyonoides* is the only living representative of the genus *Nyctereutes*. Although confined to eastern Asia (despite introduced populations are presensently thriving in central-eastern Europe), the fossil record of this genus testifies to its presence in Africa and to a greater diversity. Different analyses were applied to the study of a large sample, representing almost all of the known species of the genus, in order to characterize the ecomorphology and refine the taxonomy of the genus across the Old World. *N. procyonoides* possesses several adaptations to hypocarnivory, also shared by some of the derived fossil taxa, as confirmed by diet estimation analyses and the first cladistic analysis performed on fossil and extant species of *Nyctereutes*. Among the results, the earliest appearance of a derived taxon in western Europe predates the known occurrence of about one Myr and implies the coexistence between primitive and derive species. Moreover, the morphometric and morphological analyses on the sample from Çalta (Turkey, ca 4 Ma), suggest the ascription of this sample to a new taxon, presenting primitive-like and derived characteristics. *Nyctereutes* sp. nov. from Çalta might be the link between eastern Eurasian record of derived species and that of western Eurasia. The result is also supported by the first phylogenetic analysis, here carried out.

The fossil record of *Vulpes* is scanty across Eurasia, but particularly in Europe. The taxonomical tangle of the European Plio-Pleistocene species has its roots in the fragmented and few type material on which these species were described. From the revision of several samples from Hungary, the type and paratype specimens of *V. alopecoides*, *V. praecorsac* and *V. praeglacialis* and the study of the variability of extant *Vulpes* species (*e.g.*, *V. lagopus* and *V. vulpes*), it seems plausible and more parsimonious to consider the Plio-Pleistocene *Vulpes* from Europe as belonging to a single species. Of the three known species, *V. alopecoides* (Del Campana, 1913) (not Forsyth Major, 1875 or 1877 as generally cited) has priority.

The genus *Eucyon* arose in North America during the Late Miocene. It was among the first Canini to disperse into Old World, where it thrived becoming an important element of Eurasian and African Pliocene faunas. The study of the paratype specimens of *C. ferox* reveals the presence of several of the diagnostic features of *Eucyon*, suggesting the possible reattribution to the latter genus, as *E. ferox*. The characteristics shared with *Canis* might be the result of ecological adaptation to hypercarnivorous diet (as suggested by

other dentognathic features). To assess the dietary preferences of this and other taxa, an ecological interpretation of several *Eucyon* spp. and *Eucyon*-like taxa was performed using various methods from literature. The results suggest that the majority of these species were mesocarnivores comparable to modern *C. latrans* or *C. aureus*. Nevertheless, *E. ferox* possess a pattern of morphologies and morphometric ratios consistent with a diet tending to hypercarnivory. *E. ferox* is the first member of *Eucyon* to show such adaptations.

In the framework of the biogeographical dispersion of *Canis* across Eurasia and Africa, the study of material recovered from the site of Wadi Sarrat (Tunisia, ca 800 ka) revealed its peculiarity compared to the taxa presently known in the fossil record of Africa and even in comparison to modern jackals (both of *Lupulella* and *Canis*). Compared to Eurasian taxa, the similarity in morphometric proportions is evident, but morphologically it cannot be ascribed to any known species. The description of *Canis othmanii* in the site of Wadi Sarrat is an important record of the radiation and dispersal of *Canis s. l.* species during the Epivillafranchian.

Two populations of Late Pleistocene wolves from Apulia (southern Italy) were studied. These samples come from Avetrana bed 8 (Taranto province) and Ingarano (Foggia province). The results confirm the distinction during the first half of the Late Pleistocene between the slender and peculiar Apulian wolves and the northern Italian population of *C. lupus* (similar to other European sample of similar age). The preliminary analysis of the sample from Ingarano (MIS 3) confirms the affinity with the Apulian wolves (*e.g.*, Grotta Romanelli, Melpignano). On the contrary, the sample of Avetrana (MIS 3-2) shows unusual morphometric proportions in comparison to other Apulian samples, more similar to those of northern Italian and French ones. This result suggests the dispersion into southern Italy of populations of *C. lupus* from northern Italy or other regions of Europe, replacing the earlier and slender Apulian forms.

Storia evolutiva di Canidae (Carnivora, Mammalia) e Lyncodontini (Mustelidae, Carnivora) nel Plio-Pleistocene del Vecchio Mondo

Riassunto

L'ordine Carnivora è il più ricco in specie della classe Mammalia e include alcuni tra i mammiferi più conosciuti. Tra questi, i membri delle famiglie Canidae e Mustelidae possiedono una grande varietà di adattamenti ad un gran numero di condizioni ambientali e habitat differenti. La storia evolutiva dei canidi è ben nota e studiata, di modo che è possibile ricostruire i principali eventi biogeografici e evolutivi che li hanno riguardati, dalla loro origine nell'Eocene medio in Nord America fino alla loro dispersione nel Vecchio Mondo alla fine del Miocene. Al contrario la sistematica e l'evoluzione della famiglia Mustelidae è dibattuta, e ancor complessa è la situazione della tribù Lyncodontini. Nonostante oggigiorno quest'ultimo gruppo sia composto solo da due generi (*Galictis* and *Lyncodon*), presenti esclusivamente in Sudamerica, nel Pliocene e nel Pleistocene specie di questa tribù erano distribuite sia in Nord America che nel Vecchio Mondo.

Lo studio qui presentato cerca di rispondere ad alcuni degli interrogativi ancora aperti su alcuni taxa di Canidae (*i.e.*, *Canis*, *Eucyon*, *Nyctereutes*, *Vulpes*) e di Lyncodontini del Plio-Pleistocene provenienti da varie località del Vecchio Mondo. A tale scopo sono state utilizzate diverse metodologie che vanno dalla morfometria tradizionale alla statistica multivariata; dalle analisi filogenetiche all'uso di tecnologie di ricostruzione 3D come scansioni in luce strutturata o ancora di metodologie non invasive per lo studio di anatomie interne di campioni fossili tramite l'impiego dalla Tomografia Assiale Computerizzata (TAC).

Caso piuttosto emblematico della *querelle* tassonomica che interessa i Lyncodontini fossili euroasiatici è quello di "*Mustela*" *ardea* rinvenuta e descritta dai siti ad Issoire e Perrier-Les Etouaires. In letteratura, l'attribuzione generica di questo taxon è dibattuta da più di un secolo, in quanto alcuni autori suggeriscono di attribuirla a *Pannonictis* mentre altri suggeriscono una maggiore affinità con *Enhydrictis*. Neppure l'attribuzione della denominazione "ardea" a Bravard (1828) sembra corretta, poiché non risulta che Bravard abbia mai riportato tale nome in nessuno dei suoi scritti. Un'approfondita ricerca bibliografica, unita alla revisone dei campioni tipo e quelli attribuiti a tale specie, provenienti da siti italiani e francesi del Pleistocene inferiore, ha permesso di identificare

in Gervais (1848-1852) e di riconoscere la peculiarità del taxon. Nel complesso, numerose delle caratteristiche anatomiche che caratterizzano il materiale esaminato supportano l'attribuzione di questa specie al nuovo genere *Martellictis*. Tale risultato si accorda con quello della prima analisi filogenetica condotta su Lyncodontini fossili.

La descrizione del materiale di Lyncodontini recuperati dal complesso di siti carsici del Monte Tuttavista (Sardegna), risalenti al Pleistocene inferiore e medio, ha rivelato la presenza di due taxa endemici diversi rispetto ai loro coevi corrispettivi continentali: *Pannonictis baroniensis* e *Enhydrictis praegalictoides*. Il primo rappresenta una forma di lincodontino piuttosto robusta e al momento è conosciuto per un numero di resti piuttosto esiguo, se confrontato al record di *E. praegalictoides*, tutti provenienti da fessure risalenti al Pleistocene inferiore. Quest'ultimo invece presenta allo stesso tempo un insieme di caratteristiche derivate, che lo accomunano a *E. galictoides* proveniente da altre località sarde del Pleistocene medio, e di caratteristiche più primitive che non si ritrovano nella ben nota specie endemica della Sardegna. Il record di due nuove specie dal Pleistocene inferiore-medio della Sardegna arricchisce la diversità della tribù e amplia la nostra conoscenza delle dinamiche biogeografiche del gruppo nell'area mediterranea.

Tra i canidi attuali, il cane procione, *N. procyonoides*, costituisce l'unico rappresentante del genere *Nyctereutes*. Sebbene ad oggi la sua distribuzione naturale sia limitata alla parte orientale dell'Asia (le popolazioni europee sono il risultato di introduzioni più o meno involontarie nello scorso secolo), nel record fossile si conoscono diverse specie che vivevano anche nel continente africano. Studiando un campione che comprende tutte le specie conosciute e proveniente dai siti più importanti del Vecchio Mondo, sono state utilizzate diverse analisi per poter comprendere l'ecomorfologia e migliorare la tassonomia del genere nell'intero Vecchio Mondo. *N. procyonoides* possiede numerosi adattamenti ad una dieta ipocarnivora e tali adattamenti si riscontrano anche in alcune specie fossili, definite appunto derivate. Ciò è confermato da analisi volte a stimare quantitativamente le preferenze ecologiche della dieta ma anche dai risultati della prima analisi filogenetica basata sulle specie fossili e attuale del genere *Nyctereutes*. Tra i risultati più significativi di queste analisi abbiamo il più antico record di un taxon che mostra adattamenti verso l'ipocarnivoria in Europa occidentale, retrodatando la comparsa di tali morfotipi di circa un milione di anni e implicando la coesistenza nello stesso sito di specie più primitive (meno adattate all'ipocarnivoria) e specie più derivate. In più la le analisi morfologiche e morfometriche dei campioni di *Nyctereutes* rinvenuti Çalta (Turchia, ca 4 Ma) suggeriscono l'attribuzione di questo taxon a una nuova specie per la presenza di morfologie primitive

assieme ad altre più derivate. Tale specie, *Nyctereutes* sp. nov. di Çalta potrebbe costituire il collegamento tra i ritrovamenti di specie derivate dell'Eurasia orientale e quelli invece occidentali. Tale risultato e interpretazione sembra essere di fatto supportata dai risultati dell'analisi filogenetica.

Il record fossile di *Vulpes* in Eurasia è scarso e specialmente in Europa. Il complesso dibattito e il confuso status tassonomico del materiale europeo attribuibile a *Vulpes* risalente al Plio-Pleistocene deve la sua origine alla natura frammentaria e al ridotto numero dei materiali tipo sui quali queste specie sono state descritte. Dalla revisione dei campioni provenienti da diversi siti ungheresi, dei tipi e paratipi di *V. alopecoides*, *V. praecorsac* and *V. praeglacialis* e grazie allo studio della variabilità dentale mostrata da varie specie attuali (tra cui la volpe rossa e quella artica), appare più plausibile e parsimonioso considerare la modesta variabilità morfologica come variabilità intraspecifica piuttosto che interspecifica, riducendo il numero di specie ad una soltanto. Delle tre specie sopracitate, *V. alopecoides* (Del Campana, 1913) è quella che ha la priorità secondo i codici della nomenclatura zoologica.

Il genere *Eucyon* comparve in America settentrionale durante il Miocene superiore e fu tra i primi membri della tribù Canini a raggiungere il Vecchio Mondo, andando incontro a radiazione e diventando un importante elemento delle faune del Pliocene eurasiatico e africano. Dallo studio dei paratipi della specie *C. ferox* emerge chiaramente la presenza di caratteristiche diagnostiche tipiche del genere *Eucyon*, implicando una più corretta attribuzione del taxon questo genere, come *E. ferox*. Le poche caratteristiche che lo avvicinerebbero a *Canis* potrebbero essere il risultato di adattamenti ecologici a una dieta ipercarnivora (come anche suggerito da alcune morfologie dentognathiche). Al fine di accertare questa interpretazione ma anche in modo da comprendere le preferenze nella dieta e di predazione di altre specie di *Eucyon* e taxa affini ad *Eucyon* sono state condotte diverse analisi che utilizzano rapporti morfometrici informativi sugli adattamenti craniodentali funzionali alla dieta. I risultati suggeriscono che la maggior parte di tali specie era mesocarnivora, con dieta simile a quella de gli odierni coyote, *C. latrans*, e sciacalli dorati, *C. aureus*. Per quanto riguarda *E. ferox* invece sia i parametri morfometrici che le caratteristiche morfologiche indicano una dieta decisamente tendente all'ipercarnivoria. *E. ferox* di fatto costituisce, ad oggi, il primo rappresentante del genere *Eucyon* che mostra tali adattamenti e preferenze ecologiche.

Nel quadro delle dispersioni biogeografiche che riguardarono il genere *Canis* in Eurasia e Africa nel Pleistocene, si rivela particolarmente interessante il record del canide nel

sito di Wadi Sarrat (Tunisia, ca 800 ka). Esso non presenta somiglianza morfologiche ne morfometriche con gli sciacalli attuali (né del genere *Lupulella* né *Canis*), ma neppure con altri canidi fossili africani, quanto piuttosto possiede somiglianze con i pattern morfometrici dentali di taxa eurasiatici. Ciononostante le caratteristiche morfologiche del tipo escludono la possibile attribuzione a specie attualmente note. Il record di *Canis othmanii* dal sito di Wadi Sarrat assume una notevole importanza a scala regionale e continentale perché testimonia la continua espansione e la radiazione di *Canis s. l.* nell'Epivillafranchiano dell'Eurasia e Africa.

Infine, sono state studiate due popolazioni di lupi fossili risalenti al Pleistocene superiore della Puglia. Tali popolazioni provengono dal livello 8 del sito di Avetrana (TA) e da Ingarano (FG). I risultati confermano la presenza nella penisola italiana di due distinte associazioni di *C. lupus* durante la prima metà del Pleistocene superiore. Da una parte i cosiddetti "Apulian wolves" caratterizzati da alcune caratteristiche peculiari e dalla struttura più minuta rispetto all'altro gruppo di lupi caratteristici dell'Italia settentrionale, con robustezza e caratteristiche affini ad altre popolazioni europee coeve.

L'analisi preliminare del campione di Ingarano (MIS 3) confermano l'affinità di quest'ultimo con gli "Apulian wolves" provenienti da siti quali Grotta Romanelli e Melpignano. Al contrario, il campione di Avetrana livello 8 (leggermente più tardo come cronologia, risalente al MIS 3-2) mostra chiare affinità morfometriche con il gruppo di lupi del Italia settentrionale, rispetto alle forse più esili e precedenti dell'Italia meridionale. Questo suggerisce l'arrivo in Italia meridionale di popolazioni di *C. lupus* dal nord o da altre regioni d'Europa che sostituirono le forme "pugliesi" durante le ultime fasi glaciali.

1. Introduction

1.1. The order Carnivora Bowdich, 1821

The order Carnivora is the fifth largest mammalian order of the 29 presently accepted by researchers (Hunter, 2011). It includes 16 extant families (Eizirik et al., 2010) with more than 260 species (Goswami, 2010) and a remarkable fossil record with at least 7 extinct families and more than 350 fossil genera described (McKenna & Bell, 1997). This considerable diversity is reflected in their wide range of locomotion and lifestyles, enabling them to live in all six continents (Nowak, 2005). Adaptation to such different habitats requires a degree of ecological plasticity and specialization, particularly in diet. While the name "Carnivora" apparently implies a strict diet (from the Latin *carnĭvŏrus* – "flesh-eating", made of "*cărnis*" – meat – and "*vŏro, vŏras, voravi, voratum, vŏrāre*" – devour), "carnivorans", *i.e.*, name used to indicate the member of the order, display a wide array of adaptations to other food items such as insects, fruits and even leaves. Carnivorans have been separated ecologically into three groups based on their food habits (see *inter alios* by Crusafont-Pairó & Truyols-Santonja, 1956; Van Valkenburgh, 1988; Wesley-Hunt, 2005): i) hypocarnivores, *i.e.*, slightly carnivorous, where 70% of the food do not include vertebrates; ii) mesocarnivores, which are moderately carnivorous, having around 50-70% of diet composed of meat; iii) hypercarnivores, highly carnivorous having >70% of the diet composed of vertebrate food. Hypocarnivory is a very peculiar adaptation of some carnivorans to a more omnivorous diet, like the majority of ursids, raccoons, coatis, etc. The most notable of these carnivorans are the giant panda, *Ailuropoda melanoleuca* (David, 1869), and the red panda, *Ailurus fulgens* Cuvier, 1825, which are specialized in eating only fibrous plant material. On the opposite side of the dietary spectrum, large felids, African wild dogs, and spotted hyenas belong to the first category. These diverse feeding behaviors are obviously reflected, in the distinct dental morphologies possessed by the different

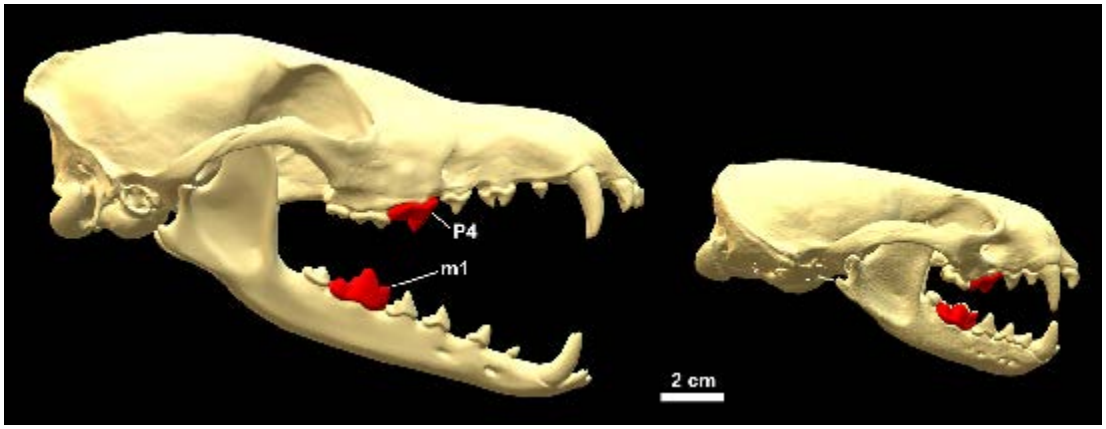

Figure 1.1 – Carnivorans' carnassials teeth shown in a Canidae (*Canis simensis* Rüppell, 1840), on the left, and in a Mustelidae [*Lutra lutra* (Linnaeus, 1758)], on the right.

carnivorans, but all the members of Carnivora share common features in their teeth: carnassial teeth. Despite the variable number of teeth among the order, every carnivoran has two pairs of blade-like teeth that enhance the slicing ability. The teeth serving this purpose are the last upper premolar (P4) and the first lower molar (m1) (Fig. 1.1). These teeth distinguish extant and fossil carnivorans from other mammals, especially those with meat-eating adaptations, which are not true carnivorans (*e.g.*, Creodonta, a group of extinct mammals specialized in a carnivorous diet, but which are not carnivorans).

In the last decades, molecular phylogenies have changed the way zoologists and other scientists used to described relationship between mammals. Murphy et al. (2001), defined four superordinal groups that include all placental mammals: Laurasiatheria, Euarchontoglires, Xenarthra and Afrotheria. Carnivora fi in the former along with Pholidota (their closest allies), Cetartiodactyla (made of the even-toed ungulates and cetaceans), Perissodactyla (odd-toed ungulates), Chiroptera (bats), and Eulipotyphla (shrews, moles and hedgehogs). Wesley-Hunt & Flynn (2005) studied the phylogenetic relationship between Carnivoramorpha (group including modern Carnivora and early stem carnivorans, Wyss & Flynn, 1993) (Fig. 1.2). Two major groupings characterize the phylogenetic tree of Carnivora: Caniformia and Feliformia (Fig. 1.2). Mustelidae and Canidae are both members

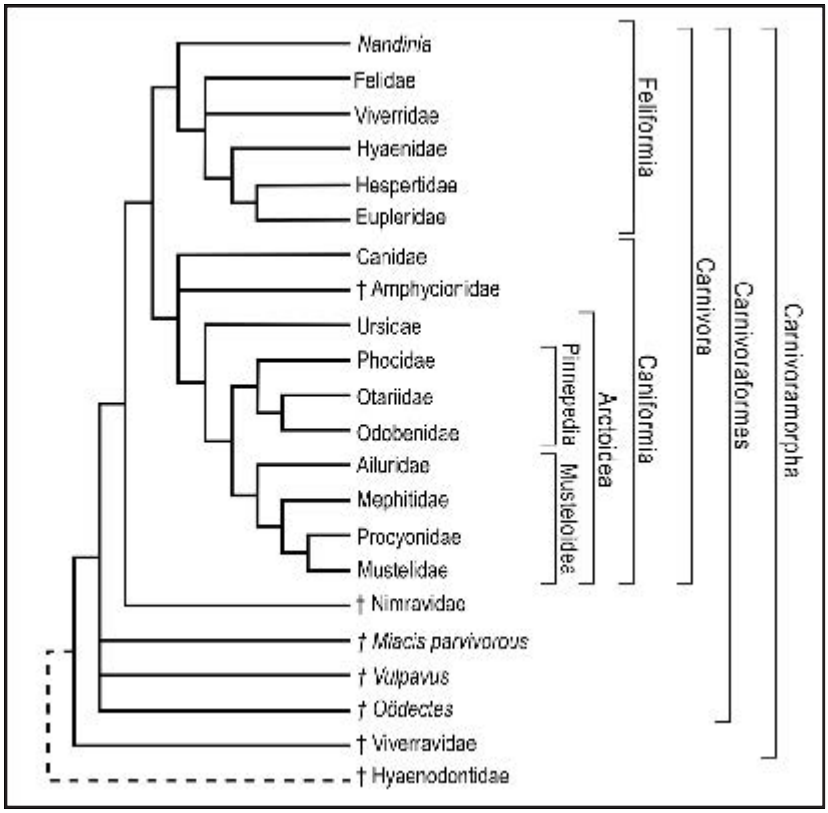

Figure 1.2 – Phylogenetic tree of the Carnivoramorpha (Flynn et al., 2005a; Wesley-Hunt & Flynn, 2005; Spaulding, 2007; Finarelli, 2008), modified from Flynn et al. (2010).

of Caniformia, along with bears, red pandas, raccoons, etc. Canidae Fischer, 1817 is one of the first Carnivora to appear in the fossil record, and the earliest of the living families of the order. The time and location of Mustelidae origin are still discussed (see section 1.2). The early radiation of Canidae is still reflected in the elongated snout as well as the almost complete dental formula I 3/3; C 1/1; P 4/4; M 2-3/2-4. They display not only the typical carnivoran shearing carnassials but also more generalist dental features like the postcarnassial crushing molars. On the contrary, mustelids developed various dietary adaptations, with significant changes to their teeth morphology. For instance, a shared feature among mustelids is the reduction in the number of molars (*i.e.*, loss of the upper second molar and of the lower third molar; Marmi et al., 2004).

Canidae was even one of the first families to be identified and described, thanks to pioneering zoological research. A key problem, in the early days of research

on Carnivora, was that the different species of carnivorans (and of canids as well) had been described on postcranial elements, teeth morphology, or soft tissue elements, which made their classification very demanding. Turner (1848) realized that whereas dental traits are obviously related to diet some skeletal features are unrelated to food procurement. For instance, the basicranial area is among the most significant features taxonomically. Flower (1869) followed Turner and divided carnivorans into three groups (nowadays superfamilies) based on the differential development of the intrabullar septum and on the degree of partitioning of the auditory bulla. These groups include: Aeluroidea (which comprises Felidae, Viverridae, Herpestidae, Hyaenidae) with a fully developed septum; Cynoidea (includes only Canidae) with a partial septum (as shown in Fig. 1.3); and Arctoidea (made up of Procyonidae, Mustelidae, Phocidae, Odobenidae, Otariidae, Ursidae and Amphicyonidae) (Turner, 1840; Flower, 1969; Mivart, 1890).

In the last century, a great number of scientists confirmed the taxonomic significance of these characters, but formulated various hypotheses about their origin and implications in the evolution of the different families (Van Kampen, 1905; Pocock, 1929; Van der Klaauw, 1931; Keen et al., 1940; Segall, 1943; Hough, 1948; Hunt, 1974; Novacek, 1977; Wang & Tedford, 1994, Ivanoff, 2000; 2001; 2007; Prevosti, 2010). Ivanoff (2000; 2001) showed that these anatomical differences are the outcome of the distinct ontogenetic developments: the intrabullar septa present in the tympanic bulla, represent non-reabsorbed bony walls that separated different areas of the bulla during its "growing" (*i.e.*, ontogeny). Ivanoff (2001) points out that the characteristics of these septa directly depends on the development of the inflated in the bulla. As in the three groups defined by Flowers (1869) (Aeluroidea, Arctoidea and Cynoidea) the sinuses arise in different areas of the bulla, these septa cannot be considered homologous between the groups (Ivanoff, 2001). Canids have a quite low and generally in the shape of a horseshoe/crescent-shaped intrabullar septum [or "circular" as in some extinct canids and in the maned wolf, *Chrysocyon*

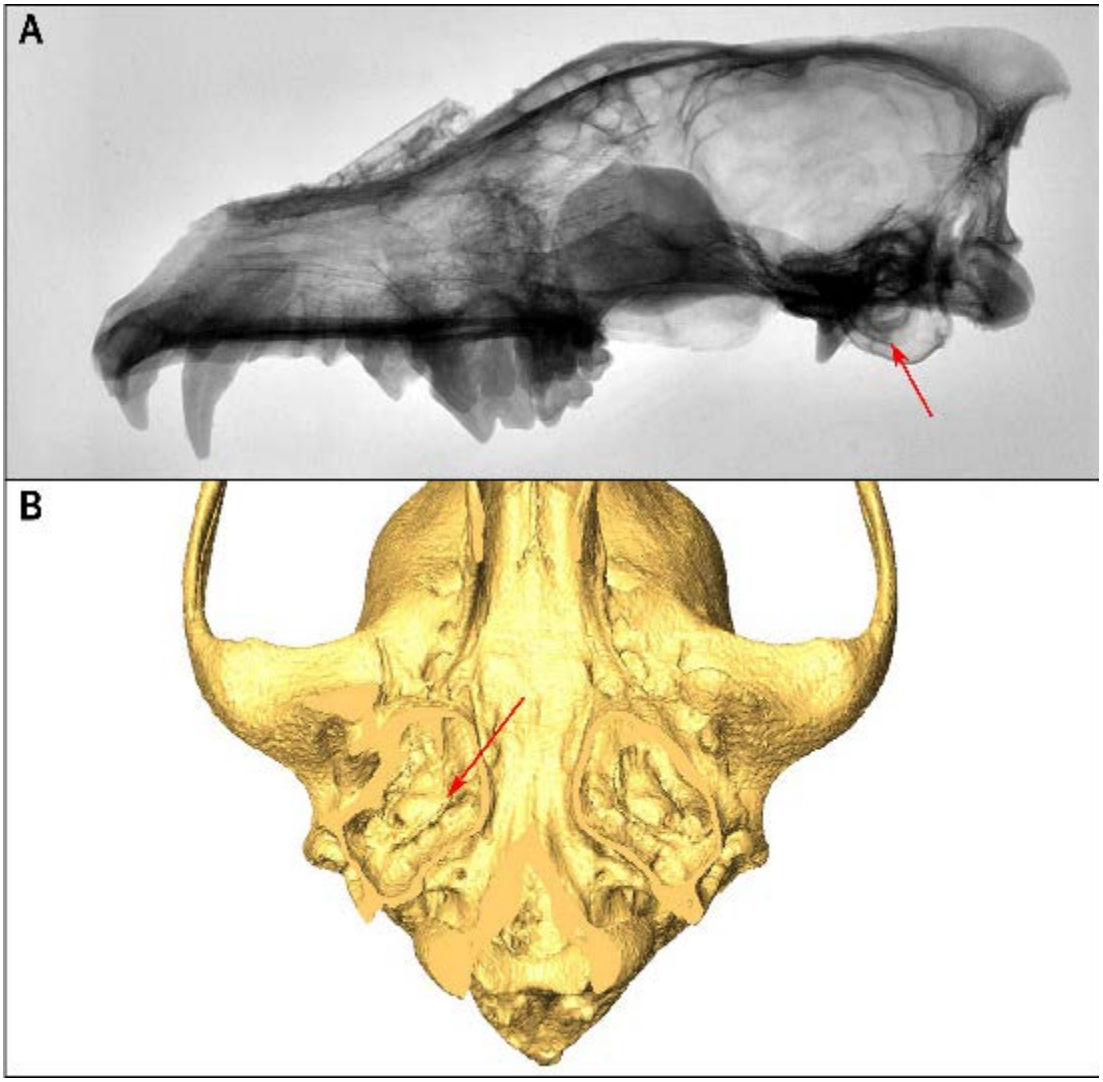

Figure 1.3 – Morphology of the intrabullar septum in Canidae shown in a radiograph of a fossil *Canis lupus* Linnaeus, 1758 (**A**) and in a 3D reconstruction of the CT scan of an extant African golden wolf *Canis anthus* Cretzschmar, 1826 from Somalia (**B**).

brachyurus (Illiger, 1815), see Ivanoff, 2007]. This bone structure partially divides the tympanic chamber into two chambers, called hypotympanic and epitympanic. It is commonly considered the product of an inward-bending of the edge of the caudal entotympanic bone (*e.g.*, Hough, 1953; Tedford, 1976; Wang & Tedford, 1994). Ivanoff, in his studies on cranial morphogenesis (Ivanoff 2000; 2001; 2007), describes two different osteological origins for two different portions of the septum: whereas the dorsal portion derives from the caudal entotympanic, the ventral portion comes from the ectotympanic (Ivanoff, 2007). Ivanoff (2019),

showed the complexity of the ectotympanic bone in Canidae, further clarifying the composition of the intrabullar septum in this family and the evolution of the ectotympanics in Carnivora. From his results, it appears clear that Aeluroidea retains the most primitive anatomical pattern of the groups, whereas Arctoidea and Cynoidea confirms as a related clade with corresponding pattern, of which cynoid's one is the most advanced (Ivanoff, 2019).

1.2. Family Mustelidae Fischer, 1817

1.2.1. Overview of the debate on phylogeny and evolutionary history of Mustelidae

Mustelidae are member of Caniformia (Fig. 1.2) that have adapted to a strikingly diverse range of habitats and ecological niches, with peculiar locomotion (from fossorial to semi-acquatic life-style) and dietary habits (piscivore in otters to specialized on rodents in martens and weasels) (Nowak, 2005). This huge variability, considering also a rather extensive record of more than 84 fossil genera (Wolsan, 1993; McKenna & Bell, 1997), has clouded the phylogenetic affinities of Mustelidae and other carnivorans, and those within the family as well. The first attempts to study these patterns used morphological data, as revelator of ecomorphological similarities, to divide Mustelidae into various subfamilies. One of the most followed schemes was that of Simpson (1945) that divided mustelids into five subfamilies: Lutrinae, Melinae, Mellivorinae, Mephitinae and Mustelinae. In the last two decades molecular phylogenies provided much evidence that skunks (*Conepatus* Gray, 1837; *Mephitis* Geoffroy-Saint Hilaire & Cuvier, 1795; *Spilogale* Merriam, 1890) and the *Mydaus* Cuvier, 1821, the stink badger, form an independent lineage (family Mephitidae) separated from Mustelidae (see Dragoo & Honeycutt, 1997; Flynn & Nedbal, 1998). Apparently, the common ancestor of all Mephitidae split from the other close allied families (*i.e.*, Ailuridae, Mustelidae and Procyonidae) before the differentiation of these latter groups. The number of subfamilies of Mustelidae is of the numerous issues inflaming the debates on these

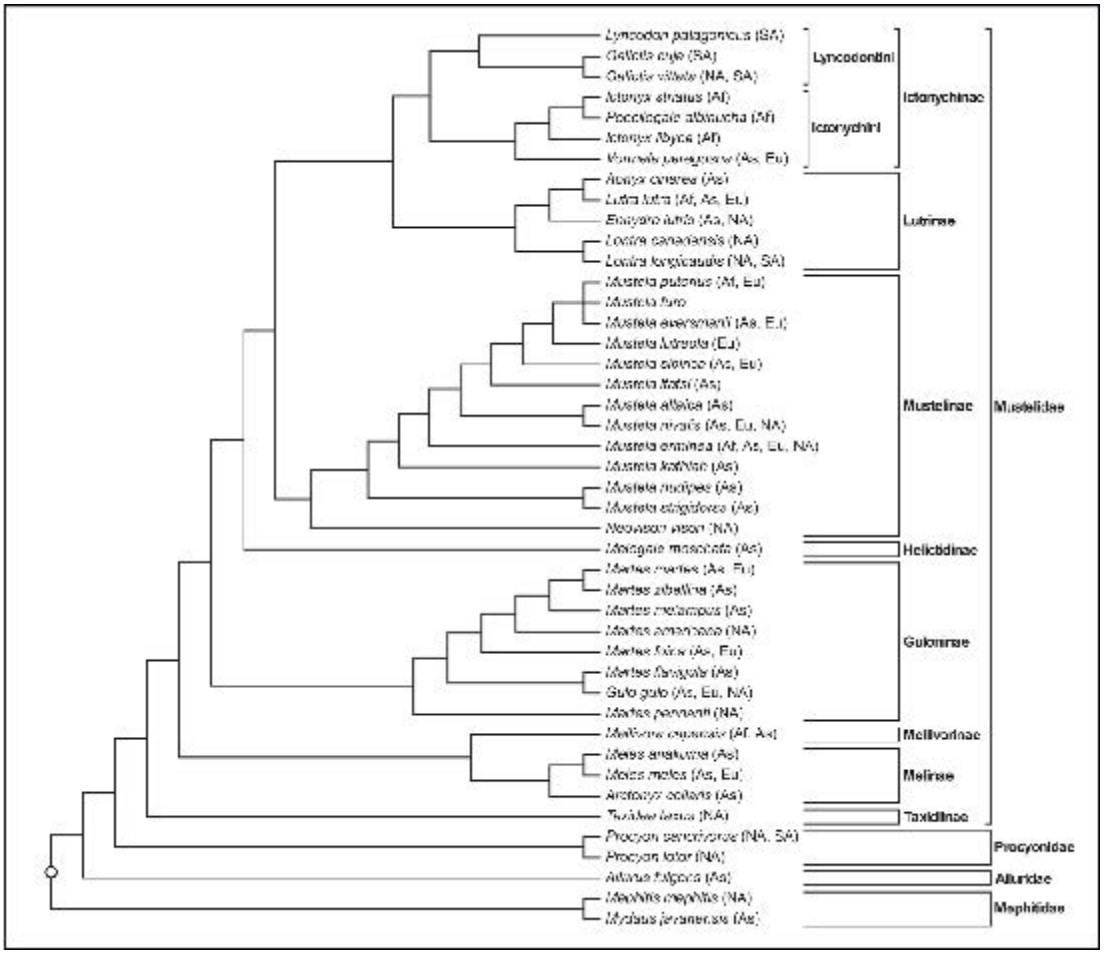

Figure 1.4 – Strict consensus tree resulting from a maximum parsimony analysis performed by Sato et al. (2012) on Musteloidea (see text). In brackets are reported the geographical distribution of the species. Modified from Sato et al. (2012).

mustelids (see Nascimento, 2014 and reference therein). Sato et al. (2012) listed 8 subfamilies (Fig. 1.4): Guloninae (*e.g.*, wolverines, martens), Helictidinae (ferret-badger), Ichtonychinae (*e.g.*, striped polecats, grisons; see section 1.3.), Lutrinae (otters), Melinae (badgers), Mellivorinae (honey-badger), Mustelinae (*e.g.*, minks, polecats), Taxidinae (North American badgers). This scheme is followed here.

Many studies, attempting to reconstruct the evolutionary history and phylogenetic relationships of weasel-like carnivorans, use the term "Musteloidea" (*inter alios* Flynn & Nedbal, 1998; Delisel & Strobeck, 2005; Sato et al., 2006; 2009; 2012; Yonezawa et al., 2007) to indicate the monophyletic group that includes the families Ailuridae (red pandas), Mephitidae (skunk and stink badgers), Mustelidae and

Procyonidae (raccoons). This grouping is used to study the actual phylogenetic relationships of these carnivorans, often unclear and confused (see Sato et al., 2012 and references therein). Several of the phylogenies on Musteloidea implemented the information of the fossil record as time-constraining data to calibrate molecular reconstructions (*inter alios* Yonezawa et al., 2007; Koepfli et al., 2008, Sato et al., 2009; 2012). The earliest basal musteloid appears to be the North American *Mustelavus priscus* Clark, 1936 (Late Eocene-Early Oligocene, Prothero & Emry, 2004). This lead Yonezawa et al. (2007) to suggest a North American origin for Musteloidea, idea challenged by Sato et al. (2009; 2012), who acknowledged the resemblance of *M. priscus* to musteloids but consider it as a stem-taxon, basal to the divergence between Pinnipedia and musteloids (minimum age of divergence 33.7 Ma, Sato et al., 2012). Shared view among researchers is to consider *Mustelictis olivieri* de Bonis (1997) from Mas de Got (France, 32.8-30.9 Ma, Luterbracher et al., 2004) a true musteloids. After this time, musteloids radiated in Eurasia and the first appearance datum in North America dates to the early Miocene (ca 23 Ma, Baskin, 1998; Tedford et al., 2004). Regarding Mustelidae, several alternative hypotheses regarding time and location of their origin have been made. Most recent ones, based on various molecular methodologies, range between the Early Miocene (ca 20.2 Ma of Yonezawa et al., 2007; 26.2-20.9 Ma of Koepfli et al., 2008) and the Early-Middle Miocene transition (16.3 Ma of Sato et al., 2009; 15.6-13.0 Ma of Eizirik et al., 2010; ca 16.1 Ma of Sato et al., 2012). The fossil record apparently disproves younger timings as one of the earliest records of Mustelidae is the genus *Plesictis* Pomel, 1846 from Europe (MN1, ca 23-22.5 Ma). Other relevantly old findings are those of *Dehmictis* Ginsburg & Morales, 1992 (subfamily Melinae, Ginsburg & Morales, 2000; Gulinae according to Valenciano et al., 2018) from the Early Miocene (MN 3, ca 20-18 Ma, Valenciano et al., 2018). Despite doubts put forward by some (Sato et al., 2012 and reference therein) on the actual position of *Dehmictis* or *Plesictis* within Musteloidea, other early fossil mustelids are known

from the fossil record: *e.g.*, *Iberictis azanzae* Ginsburg & Morales, 1992 and *Iberictis buloti* Ginsburg & Morales, 1992 from MN4 (ca 17 Ma) of France and Spain (Valenciano et al., 2018 and reference therein) and *Taxodon sansanensis* Lartet, 1851 from France (MN6, 15.0-13.6 Ma; Peigné, 212). Furthermore, there is general consensus among paleontologists to consider the Early Miocene Oligobuninae as a valid subfamily of Mustelidae (see Baskin, 1998), instead of considering them as part of a separate family of primitive mustelids, as postulated by Wolsan (2005) and Sato et al. (2009). Valenciano et al., 2016 tested if the terrestrially-adapted members of Oligobuninae could be considered part of the crown Mustelidae, showing high support to the monophyly of the clade (thus confirming the results of Wang et al., 2005 and Finarelli, 2008). Altogether, these records favor an earlier differentiation of Mustelidae from other Musteloidea. Koepfli et al. (2008) proposed a link between global climatic and paleoenvironmental changes occurred in the Neogene and timings of diversification of Mustelidae (following evidence from other mammalian taxa, *e.g.*, *inter alios* Matthee et al., 2004; Johnson et al., 2006; Gilbert et al., 2006). The hypothesis of Koepfli et al. (2008) has also been followed also by others (*e.g.*, Sato et al., 2009). Two radiation moments were identified for mustelids (Fig. 1.5): the first one gave origin mainly to badges and martens (subfamilies Guloninae, Helictidinae Melinae, Mellivorinae Taxidinae) and took place after the Mid-Miocene Climatic Optimum when climate other environmental factors (*e.g.*, sea level) experienced profound changes. Vegetation passed from widespread closed tropical and subtropical habitats to more open environments (*e.g.*, Transverse, 1988), affecting animal communities. This first burst appears to be consistent with the major faunal turnover recorded in Europe, known as the middle Vallesian crisis (Janis, 1993; Fortelius et al., 1996). Koepfli et al. (2008) suggested that this faunal "crisis" greatly affected these earliest mustelids, probably forest-dweller taxa, and caused the extinction of their lineages. The disappearance of these taxa, might have freed ecological niches soon exploited by

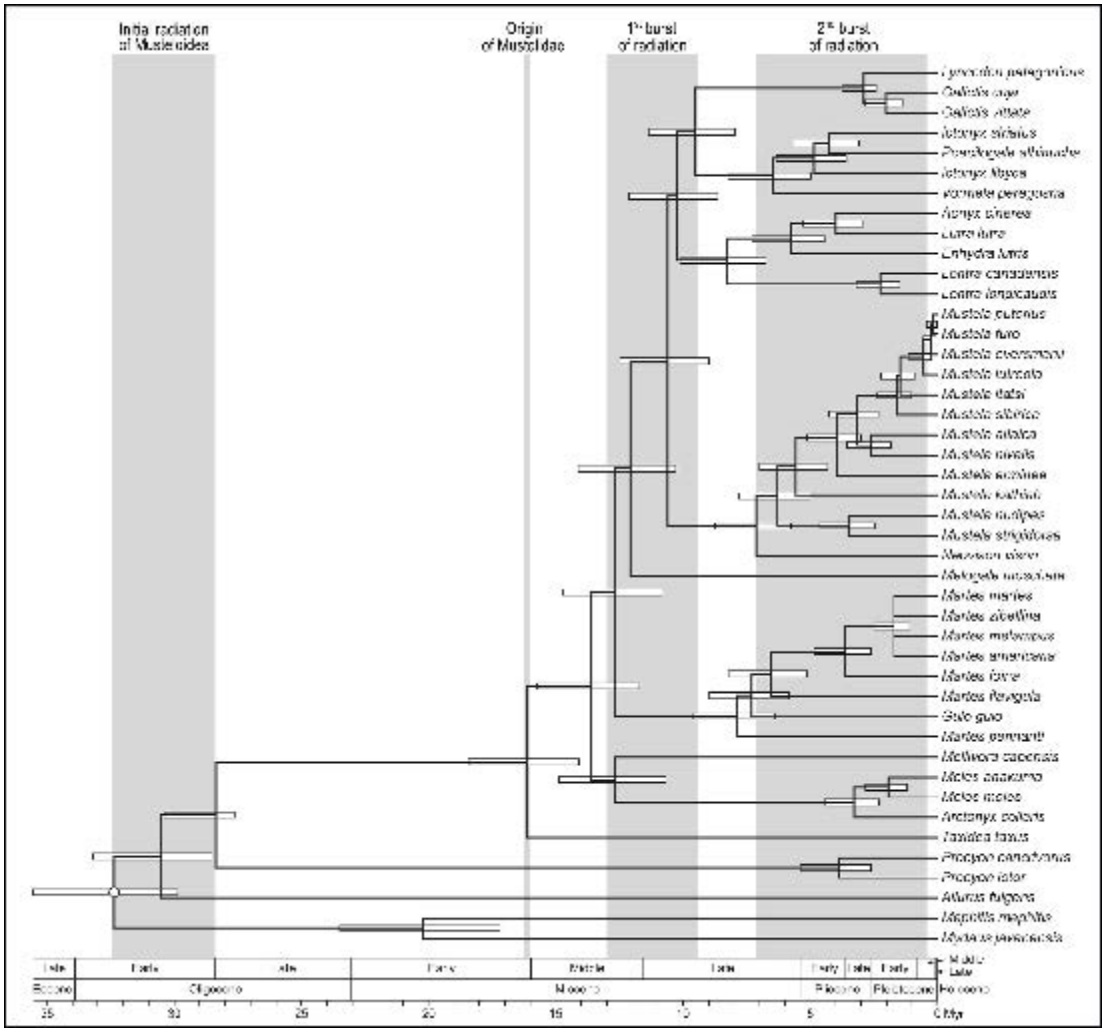

Figure 1.5 – Chronogram of Musteloidea obtained from a Bayesian analysis by Sato et al. (2012) Horizontal bars at the nodes represent the uncertainty in ages of their origins. Interval of radiation (in gray) following Koepfli et al. (2008), and Sato et al. (2009; 2012).

the first burst of radiation of Mustelidae. The second burst in diversity took place during the from the late Miocene to the end of the Gelasian (5.3-1.8 Ma), and involved the crown taxa like weasels, polecats and otters (Ictonychinae, Lutrinae, Mustelinae).

1.3. Tribe Lyncodontini (Ictonychinae, Mustelidae, Carnivora)

1.3.1. Taxonomic issues around Lyncodontini

Nowadays the tribe Lyncodontini Pocock, 1921 (Ictonychinae, Mustelidae, Carnivora) includes two extant genera and three different species: the greater

grison, *Galictis vittata* (Schreber, 1776); the lesser grison, *Galictis cuja* (Molina, 1782), and the Patagonian weasel, *Lyncodon patagonicus* (de Blainville, 1842). The scientific literature on these mustelids is confusing and marked by harsh debates on several issues, partially settled recently. For instance, the taxonomic status of the tribe, its true systematic rank (as a tribe or a subfamily) and its composition (in terms of genera and species) or the relationship with other mustelids are unsolved matters on which researchers have not reached a unanimous agreement.

The first to study these mustelids was Pocock (1921), who established the subfamilies Grisoninae Pocock, 1921 and Lyncodontinae Pocock, 1921. According to this author, the former subfamily included the neotropical greater and lesser grisons, at the time respectively included in the genera *Grison* Oken, 1816 and *Grisonella* Thomas, 1912, whereas *Lyncodon* Gervais, 1844 is the only genus of the second one. Pilgrim (1932) included in the subfamily Grisoninae the genera *Eira* Smith, 1842, *Trochictis* Meyer, 1842, *Enhydrictis* Forsyth Major, 1901, "Mustelidae gen. indet. sp. n." of Zdansky, 1927 and *Pannonictis* Kormos, 1931. Nevertheless, Schreuder (1935) excluded them from the subfamily *Eira* and *Trochictis* for the retention of various dental features. Recently, the genus *Eira* has been related to different subfamilies of Mustelidae: Mustelinae, see among others Presley, 2000; or Guloninae, see Sato et al., 2012 and references therein). Other emendations to taxonomy of Grisoninae were made as Hershkovitz (1949) pointed out that the generic name "*Grison*" used by Oken (1816) was invalid, and suggested using the more pertinent name *Galictis* Bell, 1826. Following Hershkovitz (1949), few years later Reig (1956) created the subfamily name Galictinae Reig, 1956 as an alternative to Grisoninae of Pocock (1921).

In the last twenty years, much research has tried to clarify this intricate subject, improving the knowledge of this group of mustelids both from a paleontological point of view and from the neontological one. Recent molecular phylogenies (*e.g.*, Koepfli et al., 2008; Sato, 2016) have shown that the Galictinae is a solid clade

with extant South American species (*i.e.*, *Galictis* and *Lyncodon*) and Old World ones (*i.e.*, the genera *Ictonyx* Kaup, 1835, the striped polecat, *Poecilogale* Thomas, 1883, the African striped weasel, and *Vormela* Blasius, 1884, the marbled polecat) (see Fig. 1.4). Furthermore, Koepfli et al. (2008) and Sato et al. (2012) showed that the genus *Ictonyx* is paraphyletic as *Ictonyx lybicus* (Hemprich & Ehrenberg, 1833) is the sister taxon of *Ictonyx striatus* (Perri, 1810) and *Poecilogale albinucha* Thomas, 1883. Koepfli et al. (2008) suggested grouping all the taxa under *Ictonyx*, whereas Sato et al. (2012) favored ascribing *I. libycus* to *Poecilictis* Thomas & Hinton, 1920, as *Poecilictis libyca*. The latter hypothesis follows several previous studies by numerous authors, *e.g.*, among others Bryant et al. (1993); Spassov (2001), and is used in Cuzin (2013).

The correct name of the subfamily to which attribute these mustelids is debated. Although Wilson & Reeder (2005) grouped *Galictis* and *Ictonyx* under the subfamily of Mustelinae, a number of recent studies (Wolsan & Sato, 2010; Bornholdt et al., 2013; Nascimento, 2014; Sato et al., 2012; Sato, 2016; Puzachenko et al., 2017) suggest using Ictonychinae Pocock, 1921, as Galictinae Reig, 1956 represent a junior synonym of the former (International Commission on Zoological Nomenclature, 1999, Article 23). According to Sato et al. (2012), the subfamily Ictonychinae include two consistent clades (namely, tribes): Ictonychini Pocock, 1921, consisting of the genera *Ictonyx–Poecilogale–Vormela–Poecilictis*, and Lyncodontini Pocock, 1921, made up of *Galictis–Lyncodon*.

On the paleontological side, research has shown that the past variability and geographic distribution of this group of mustelids during Plio-Pleistocene times has been underestimated, particularly in the Asian part of Eurasia. Two new genera belonging to this subfamily have been described from the Early and Middle Pleistocene of Asia. The different species of the large *Eirictis* Qiu et al., 2004 were recognized in several Chinese localities: Nihewan basin (Teihlard de Chardin & Piveteau, 1930), Longdan (Qiu et al., 2004), Renzidong (Jin & Liu, 2009). More

recently, *Oriensictis* Ogino & Otsuka, 2008 was described from cave deposits of Matsugae Cave in Kyushu Island (Japan). Geraads (2016) described the first fossils of a taxon of the tribe Lyncodontini from northern Africa. Recovered in the Algerian site of Tighennif (or Ternifine), the sample is ascribed to new species *Enhydrictis hoffstetteri* Geraads, 2016. This discovery expands the areal of Plio-Pleistocene Lyncodontini, up to now unknown in the African continent.

Albeit molecular studies have revealed the strong affinity between *Ictonyx* and related taxa and *Galictis-Lyncodon*, and the priority of Ictonychinae Pocock, 1921 on Galictinae Reig, 1956, the paleontological literature has not "absorbed the lesson". After Reig (1956), a biologist and a paleontologist himself, Galictinae was used to refer to this group of mustelids (*e.g.*, Colombero et al., 2012; Fejfar et al., 2012; Peters & de Vos, 2012). Baskin (1998; 2011) referred the tribe of Galictinae with the name Galictini Reig, 1956 to identify the that includes the Old World fossil taxa (*i.e.*, *Enhydrictis*, *Pannonictis*, *Oriensictis*, *Eirictis*) and the New World ones (namely *Lutravus* Furlong 1932, *Cernictis* Hall, 1935, *Trigonictis* Hibbard, 1941, *Stipanicicia* Reig, 1956 and *Sminthosinis* Bjork, 1970), in addition to the extant *Galictis* and *Lyncodon*.

The taxonomy for the analyses and discussion presented in this work, follows Sato et al., 2012 as far as names of the subfamily and tribe are concerned (*i.e.*, subfamily Ictonychinae, tribe Lyncodontini), and Baskin (2011) regarding its fossil composition.

1.3.2. An overview of the diversity of the Plio-Pleistocene Eurasian Lyncodontini

As mentioned above, Qiu et al. (2004) erected the genus *Eirictis*, on the basis of the material from the Early Pleistocene of Longdan (Dongxiang, Gansu, China). García and Howell (2008) recognized the validity of the diagnostic features used by the authors to discriminate this new genus from *Pannonictis* (especially the absence of a hypocone on P4). In the genus of Longdan, Qiu et al. (2004) included

the sample of that same site, which was attributed to new species *Eirictis robusta* Qiu et al., 2004, and also the specimens of "*P.*" *pachygnatha* Teilhard de Chardin & Piveteau, 1930 of Nihewan Basin. Recently, Jin & Liu (2009) described the taxon from the Early Pleistocene site Renzidong Cave (eastern China) as a different species of the same genus, *Eirictis variabilis* Jin & Liu, 2009.

The Middle Pleistocene genus *Oriensictis* is composed of, according to Ogino &Otsuka, *Oriensictis nipponica* (Naora, 1968) from Japan and of *Oriensictis melina* (Pei, 1934) recovered in Zhoukoudian 1 (previously described as *Lutra melina* by Pei, 1394).

Of the Eurasian taxa, *Pannonictis* is the best known and characterized (see, among others, García & Howell, 2008; Colombero et al., 2012). This taxon is most probably the oldest member of the Lyncodontini of Eurasia. Its earliest specimens might be those from the late Miocene *Hipparion*-beds from China reported by Zdansky (1927), who described a mustelid remains as Mustelidae gen. indet. sp. indet.. As many authors pointed out (Kormos, 1931; Pilgrim, 1932; Schreuder, 1935; Rook, 1995; García & Howell, 2008), this taxon could be referred to as *Pannonictis* sp. Zdanski (1927). Although García & Howell, 2008 suggested to ascribe it *P. pachygnatha*, the unspecified attribution is favored here. The latter species, *P. pachygnatha*, was described in localities of the Early Pleistocene Nihewan Basin in China (Teilhard de Chardin & Piveteau, 1930) and also recorded in the other Chinese sites of the Yushe Basin (Teilhard de Chardin & Leroy, 1945) and the Mongolian one of Shamar (Sotnikova, 1980). This species was rather robust and large-sized. The earliest European representatives of the genus *Pannonictis* is that of the Early Pliocene (MN 15) of Wölfersheim (Germany), reported by Morlo & Kundrát (2001). Apart from this early discovery, the genus is reported from Upper Valdarno in Tuscany (Martelli, 1906) in the Early Pleistocene with the species *Pannonictis nestii* (Martelli, 1906), from the younger site of Pietrafitta in Umbria (Rook, 1995) and Pirro Nord (Colombero et al. 2012). Additionally, several

specimens from Sima del Elefante (Sierra de Atapuerca, Spain) were referred to *Pannonictis* cf. *nestii* by García & Howell (2008). The type species of the genus were described by Kormos (1931) in the complex of cavities of Villany-Kalkberg (Hungary). This species is the large *Pannonictis pliocaenica* Kormos, 1931. Two of the richest localities of this site complex are Villany 3 and 5 that span between 2 and 1.5 Ma (Jánossy, 1986; Spassov, 2000). Kormos (1933) reassessed the material from these localities and described the small *Pannonictis pilgrimi* Kormos, 1933. The identity and validity of these three European species (*i.e.*, *P. nestii*, *P. pliocaenica*, and *P. pilgrimi*) is debated in literature. Several hypotheses were put forward: some authors (*e.g.*, García et al., 2008 and reference therein) suggested grouping *P. nestii* with the critical "*Mustela*" *ardea* Gervais 1848-1852, whereas other scholars adverse this proposal (*e.g.*, Viret, 1954; Ficcarelli and Torre, 1967; Rook, 1995; Sotnikova et al., 2002). Viret (1954) synonymized *P. pilgrimi* to "*M.*" *ardea*, whereas Ficcarelli and Torre (1967) suggested uniting the former with *P. nestii*. García & Howell (2008) favored the inclusion of *P. pilgrimi* in *P. pliocaenica*, considering the marked size difference as a strong sexual dimorphism: in their opinion *P. pliocaenica* would represent the larger male individuals, whereas *P. pilgrimi* the smaller females. The genus *Pannonictis* has also been recovered from Mediterranean islands. In the endemic fauna of the Monte Pellegrino (Sicily), De Gregorio (1886) described *Mustela arzilla* De Gregorio, 1886, later referred to the new genus *Mustelercta* Gregorio, 1925. This taxon is very similar to *Pannonictis* and probably close to *P. nestii* (see Rook, 1995; Burgio & Fiore, 1997). An unidentified species of *Pannonictis* was reported by Abbazzi et al. (2004) from the some of the fissure of the Monte Tuttavista site complex (Nuoro, Sardinia). These findings were related to the latest part of the Early Pleistocene (roughly to the Calabrian, see Palombo & Rozzi, 2014).

The most peculiar taxon within the European record of Lyncodontini is by far *Enhydrictis*. The genus was erected for the endemic mustelid recovered from the Late

Pleistocene deposits of the locality of Monte S. Giovanni (Sardinia) and described as *Enhydrictis galictoides* Forsyth Major, 1901. According to Forsyth Major (1901), the form had a strong affinity with the extant South American Ictonychinae *G. cuja*, *G. vittata*, and *Eira barbara* (Linnaeus, 1758). In the fossil record, the genus *Enhydrictis* is more elusive than *Pannonictis* and, apart from *E. galictoides*, is only known from few other Sardinian and Corsican localities *e.g.*, the older *Enhydrictis* sp., from the fissure fillings of Monte Tuttavista (Abbazzi et al., 2004). Many authors regarded the peculiar features that typify this genus (*e.g.*, strong postorbital constriction, shorter muzzle) as adaptations to an aquatic lifestyle (Forsyth Major, 1901 in primis, but also Pilgrim, 1932; Ficcarelli & Torre, 1967). In the last two centuries, a number of different Pliocene and Early Pleistocene remains referable to a small- to medium-sized mustelid were described under different names, such as *Mustela ardea* Gervais, 1848-1852 or *Proputorius olivolanus* Martelli, 1906. Viret (1950; 1954) included all of them in the taxon *Enhydrictis ardea* (Gervais, 1848-1852). Since then, many authors (Rabeder 1976; Spassov 1999; 2000; García & Howell, 2008; García et al. 2008; Fejfar et al. 2012; Peter & de Vos, 2012) questioned the generic attribution of the species, and preferred the ascription to *Pannonictis*. Since the genus *Enhydrictis*, as initially defined, is an endemic, highly peculiar and highly specialized taxon of the Late Pleistocene of Sardinia, its use for continental and older species appears doubtful. The following session specifically discuss the issues concerning the taxon "*Mustela*" *ardea*.

In North America, the one most probably related to *Pannonictis* is the Early Pleistocene *Trigonictis* (Rook, 1995). Numerous authors have proposed synonymizing these two genera (*e.g.*, Kurtén & Anderson, 1980; Repenning, 1967), but the presence of primitive features and some characters (*e.g.*, the morphology of the M1 and the development of its cusps), which cannot be found in either *Pannonictis* or in *Enhydrictis*, would suggest maintaining *Trigonictis* as a separate genus.

Two different, yet related, issues were here taken into consideration and discussed in the present work. The first regards the problematic taxon "*Mustela ardea*" and its systematic position whereas the second concerns the description of the largest sample of fossil Lyncodontini of Eurasia recovered in the Sardinian site of Monte Tuttavista.

*1.3.3. "*Mustela*" ardea: the taxonomic* vexata quaestio *of a Pleistocene lyncodontine*

Since the first descriptions in the first half of the XIX Century of the species "*M.*" *ardea*, its generic attribution has been harshly debated. Moreover, the correct authorship is still disputed. Indeed, several authors refer the species to Mr. Auguste Bravard (1828). In the first half of the XIX century, museums of natural history across Europe started frequent cooperation with amateur naturalists, travelers, owners of private collections in order to expand their exhibition (Secord 1994; Cohen, 1999). The French architect, along with other local naturalists and amateur paleontologists, collaborated with the Museum d'Histoire Naturelle de Paris, especially with George Cuvier (Podgorny, 2001), collecting material in the region of Auvergne. As a report of its discoveries in the locality of Côte de Ardé, near Issoire (Auvergne-Rhône-Alpes, central-southeastern France), he wrote (1828) its "*Monographie de la montagne de Perrier, près d'Issoire (Puy-de-Dome), et de deux espèces fossiles du genre* Felis*, découvertes dans l'une de ses couches d'alluvion*". In this volume, Bravard reports the presence of a small mustelid but simply with the common name "marte" (Bravard, 1828: 8, 11, 111). As correctly noted by Peters & de Vos (2012), Bravard (1828) does not contain any reference to the genus *Mustela* Linnaeus, 1758 or even to the specific name "*ardea*". Furthermore, Jorbert & Croizer (1828), a previous work already cited in Bravard (1828: 138-139), reports a "martre" (Jorbert and Croizer, 1828: 25). Even in other works by Bravard (*i.e.*, Bravard, 1843, 1846), written before his trip to South America around 1850 (see Podgorny, 2001), do not report any description of this mustelid

of the names "*Mustela ardea*". The first description and illustration of the single specimen of the taxon collected by Bravard in Auvergne is contained in a later work. Gervais (1848-1852) reports: "*Portion de maxillaire inférieur portant la molaire carnassière précédée de six alvéoles, indiquant trois avant-molaires, chacune à deux racines, et suivie d'un alvéole qui est celle de la dent tuberculeuse. Longueur de la carnassière 0,011 [m]. Son talon est un peu excavé. Cette pièce a été recueillie à Ardé, près Issoire, par M. Bravard, qui lui a donné le nom spécifique sous lequel nous la représentons.*" [Portion of the lower maxillary bone possessing the carnassial molar preceded by six alveoli, indicating three premolars, each of which with two roots, and followed by one alveolus of the second molar. The length of the carnassial is 0.011 (m). Its talon is slightly furrowed. This specimen has been collected at Ardé near Issoire by Mr. Bravard, who has given it the specific name under which we cite it.]. Few years later, Gervais (1859) included the species in the nowadays invalid genus *Putorius* Cuvier, 1817, comparing the specimen to the extant polecat (Gervais, 1859: 252: "*Plus robuste et plus grand que le Putois*"). Podgorny (2001) points out that in 1847, Bravard sold part his collection to the Museum National d'Histoire Naturelle of Paris, which constitutes the "Bravard collection" still present in the museum. As in his works, Gervais referred to the authorship of the species to Bravard with the expression "*Coll.*" (Gervais 1848-1852) and "*Coll. du Mus.*" (Gervais 1859), it is likely that Bravard had labelled the specimen with the name "*Mustela ardea*" with no description or illustration in an article or book. Therefore, *Mustela ardea* Bravard constitutes a *nomen nudum* (failing to satisfy the requirements of Art. 12, International Commission on Zoological Nomenclature, 1999) and should be therefore cited as *M. ardea* Gervais, 1848-1852. The authorship was not only issue regarding this Pleistocene taxon. Indeed, even its true generic attribution and its taxonomic status remain matter of dispute among scholars. These *querelle* started around the half of the last century. Schaub (1949) synonymized the "*M.*" *ardea* material together with the small mandible of *P. olivolanus* of Olivola (Tuscany,

Italy) described by Martelli (1906). Furthermore, he suggested relating the taxon "*M.*" *ardea* to the genus *Pannonictis* for its generalized affinity to *P. pliocaenica* of Hungary. Viret (1950) studied the species *Mustela ardea* Gervais, 1848-1852: although he agreed with Schaub (1949) in considering the French and Italian specimens as a single species, he pointed out a stronger affinity with the genus *Enhydrictis*. A few years later, the same author (Viret, 1954) described the mustelid remains recovered from the Early Pleistocene site of St. Vallier. He related these fossils to the mandibles of "*E.*" *ardea* in Viret (1950) (*i.e.*, the type specimen described by Gervais, 1848-1852 and the one from Olivola), as the features of the latter were close the skull recovered in St. Vallier (*e.g.*, the narrow width of the ascending ramus of the mandible and the narrow cranial region between mandibular fossa and M1). Given the apparent similarity to *E. galictoides*, Viret (1954) proposed a co-generic attribution of these two species. In the same paper, the author synonymised *P. pilgrimi* with "*E.*" *ardea*, for the slender and short corpus of the mandible. Other scholars favored the hypothesis of a synonymy between *P. pilgrimi* and "*E.*" *ardea* (*i.e.*, Kurtén, 1968; Rabeder, 1976; Willemsen, 1988; Fejfar et al., 2012). On the contrary, other authors noted that *P. pilgrimi* possesses a more convex dorsal profile of the cranium, in lateral view; a proportionately longer muzzle; and a stouter ascendant ramus of the mandible compared to that of "*E.*" *ardea* (Ficcarelli & Torre, 1967; Rook, 1995). Several authors (*e.g.*, Ficcarelli & Torre, 1967; Willemsen, 1988; Rook, 1995) follow the hypothesis of Viret (1954), assigning the taxon "*M.*" *ardea* to *Enhydrictis*. Morlo & Kundrát (2001), in their description of the material from Wölfersheim (MN 15, early Pliocene) reported the earliest sample of "*E.*" *ardea*. Nevertheless, it should be mentioned that these particular specimens need a deep revision, which would assess the numerous peculiar features retained the taxon described by Morlo &Kundrát (2001) as they contrast both with the diagnostic characteristics of *Enhydrictis* and of "*Mustela*" *ardea*. Since Viret (1954), many other scholars (*e.g.*, Rabeder, 1976; Spassov, 1999,

2000) preferred following Schaub (1949)'s attribution of "*M.*" *ardea* to *Pannonictis*, instead of *Enhydrictis*. Notably, Fejfar et al. (2012) supported this attribution for the morphology of the auditory region and the tympanic bullae, deemed closer to *P. pliocaenica*, rather than to *E. galictoides*.

1.3.4. Monte Tuttavista (Sardinia): an outstanding record of Early-Middle Pleistocene Lyncodontini

Sardinia is a stimulating location for the study of the evolution of fossil vertebrates in an insular context, more than any other Mediterranean island. Its important fossil record is as old as the Eocene-Oligocene times (Kotsakis et al., 1997; Mennecart et al., 2017; Zoboli & Pillola, 2017a) and ends with Holocene deposits. Among this large timespan, the record of Sardinian Quaternary vertebrates is so abundant that complete biochronological and paleobiogeographic studies on the dispersion and evolution of these taxa can be made (see among others Palombo & Rozzi, 2014). In literature, to reconstruct the most probable patterns and dynamics of turnover in this island faunal associations, scholars applied the basic principles of biochronology (faunal composition of the association, first and last occurrences of a selected species and evolutionary trends identified in a lineage). The use of such a methodology was possible because anagenetic trends, dimensional and/or morphological ones, were recognised in several of the Quaternary vertebrates, *e.g.*, *Cynotherium* Studiati, 1857 (Abbazzi et al., 2005), *Praemegaceros* Portis, 1920 (Van der Made & Palombo, 2006) and *Prolagus* Pomel, 1853 (Angelone et al., 2008). The results favored the grouping of the sites into two faunal complexes (FC, Palombo, 2009): the older *Nesogoral* faunal complex, spanning approximately from the Late Pliocene to most of the Calabrian, and the younger *Microtus* (*Tyrrhenicola*) faunal complex, extending from the late Early Pleistocene (late Calabrian) to the Holocene. Each of these faunal complexes is further subdivided into two faunal subcomplexes (FsC) to help in the correlation of the local faunas. Palombo &

Rozzi (2014) reviewed the biochronology of the various Sardinian sites and offered a reliable key for understanding the evolution of the Quaternary associations of the isle. According to these authors, the first arrival of taxa might have occurred between 2.9-2 Ma (Late Piacenzian-end of Gelasian). Subsequent important faunal changes in the composition Sardinian assemblages took place for the combined effect of the arrival of new taxa and the extinction of some elements of the Late Pliocene-Early Pleistocene faunal complex. Thus, marking the transition to the *Microtus* (*Tyrrhenicola*) faunal complex. In this dynamic context of turnovers, the site of Monte Tuttavista represents an incredible source of information for the paleontology of Sardinia. Discovered in 1995 by an amateur naturalist and located on the slopes of Mt. Tuttavista (from which the locality takes its name; Abbazzi et al., 2004), the site actually consists of a complex of numerous karst fissures opened in the Mesozoic limestones, which were exploited quarries in the area south of the town of Orosei (Nuoro, eastern Sardinia). The abundant numbers of fossils recovered in the infill of the fissures include many different taxa (about 70 taxa; Abbazzi et al., 2004), referable to both the *Nesogoral* and the *Microtus* (*Tyrrhenicola*) faunal complexes (Palombo & Rozzi, 2014). The oldest fissures can be correlated to the FsC Capo Figari/Orosei 1, *e.g.*, VII, VII-mustelide, X-ghiro and IV-macaca for the presence of taxa like *Asoletragus gentryi* Palombo et al. 2006, "*Asoriculus*" spp., *Chasmaporthetes melei* Rook et al., 2004, *Mustela* sp., *Macaca* aff. *M. majori*, *Nesogoral* aff. *N. melonii*, *Nesogoral* sp. 2, *Pannonictis* sp., *Prolagus figaro* López Martínez, 1974, "*Rhagapodemus*" *minor* (Brandy, 1978), *Sus sondaari* Van der Made, 1999, *Talpa* aff. *T. tyrrhenica*, *Tyrrhenoglis figariensis* Zammit et al. 1982, and *Tyrrhenoglis majori* Engesser, 1976 (Abbazzi et al., 2004; Rook et al., 2004; Angelone et al., 2008; Moncunill-Sole et al., 2016). The appearance of the primitive *M.* (*T.*) *sondaari* is recorded in the fissures X-4 and X-3-uccelli, therefore marking the beginning of the FsC Orosei 2. The remaining fissures (*i.e.*, XI-canide, XI-3; XI-dicembre 2001; XI rondone; XI-marzo 2001; IV-5; IV-20,

VII-2 and VI-banco 6) were referred to the recent FsC Dragonara (see Palombo & Rozzi, 2014). Angelone et al. (2008), on the basis of the morphological and morphometric data, put forward the possibility that the infill of the fissure IX-prolagus may be the result of a prolonged deposition or, alternatively, of taphonomic mixing as a consequence of secondary re-infilling. In addition to helping clarify biochronological issues, the record of Monte Tuttavista provides a great deal of information on the evolutionary history and on the pattern of arrival and dispersion in Sardinia between the Latest Pliocene until the Late Pleistocene. Whereas island faunal assemblages are typically impoverished and ecologically unbalanced due to the absence of predators (MacArthur & Wilson, 1963), the fossil record of Monte Tuttavista yielded an unusual abundance of carnivores. Abbazzi et al. (2004) reported the presence of five carnivorans in the fissures, at different stratigraphic levels: the endemic canid *Cynotherium* (from the fissures IV-20, V, VI-B6, VII-2, XI-cervo, XI-prolagus, X-3uccelli, XI-canide and XI-dicembre 2001), an erratic specimen of *Chasmapothetes melei* from the oldest fissures (*e.g.*, VI-3 and VII) and *Mustela* sp. from the fissure IV-3. In addition to these taxa, *Pannonictis* sp. has been recovered from the older infills, VII-mustelide and VI-3, whereas *Enhydrictis* sp. comes from more recent fissures (*e.g.*, IX-prolagus). As Abbazzi et al. (2004) pointed out, the diverse carnivore guild in the faunal assemblages of Monte Tuttavista suggests reconsideration of the paleobiogeographic dynamics established in Sardinia during the Plio-Pleistocene times.

1.4. Family Canidae Fischer, 1817

1.4.1. Overview of the evolutionary history of Canidae

Among the order Carnivora, Canidae is one of the earliest families to appear in the fossil record, along with the extinct Viverravidae and Miacidae (from which they probably evolved) (Fig. 1.2), and the oldest family of extant carnivorans. Fossil canids were recorded in the middle Eocene deposits of North American as

far back as 40 Ma (Bryant, 1992; Wang, 1994; Munthie, 1998), whereas Ursidae appeared during the Late Eocene (~37 Ma) in North America (Kemp, 2005) and Felidae only during Late Oligocene (~30 Ma) in Europe (Morlo, 1996; Turner, 1996; Agustí & Antón, 2002). Since their origin, the majority of their evolutionary history took place in North America, and the first canid record in Eurasia dates to the late Miocene (*inter alios* Sotnikova & Rook, 2010 and references therein).

At present, 13 genera and about 36 species of extant canids are known (MacDonald & Sillero-Zubiri, 2004; Castelló, 2018). Their fossil record is one of the best and most diverse of Carnivora, with more than 33 fossil genera described (Wang, 1994; Wang e al, 1999; Tedford et al., 2009). Their taxonomical diversity is increasing thanks to the lively scientific debate on the status of some of the extant species (*e.g.*, *Canis lycaon* Schreber, 1776; see Grewal et al., 2004 and section 1.8.1. for additional examples). In the last twenty years, various researchers have done genetic studies on dogs and wild canids (*e.g.*, Wayne et al., 1997; Zrzavý & Řičánková, 2004; Lindblad-Toh et al., 2005; Wayne & Ostrander, 2007; Koepfli et al., 2015; Zrzavý et al., 2018). Fig. 1.6 shows one of most widely accepted molecular phylogeny of extant Canidae (Lindblad-Toh et al., 2005).

All extant canids belong to a single subfamily of Canidae, subfamily Caninae. Unlike Mustelidae (see section 1.2) taxonomical status of subfamilies of Canidae is more straightforward and has been deeply studied and described in the last decades. In their evolutionary history Canidae compose it: Hesperocyoninae, Borophaginae and Caninae. All members of the former clades became extinct respectively during the middle Miocene and before the end of the Early Pleistocene (Fig. 1.7). The earliest true genus of canids is *Hesperocyon* Scott, 1890 from the Cypress Hills formation (Saskatchewan, United States) correlated to Late Eocene (37-40 Ma, Duchesnean following the North American Land Ages, NALMA; see Vandenberghe et al., 2012). These were fox-like animals, characterized by a small size (close to modern civets, ca 1-2 kg in weight), possessed two apomorphies

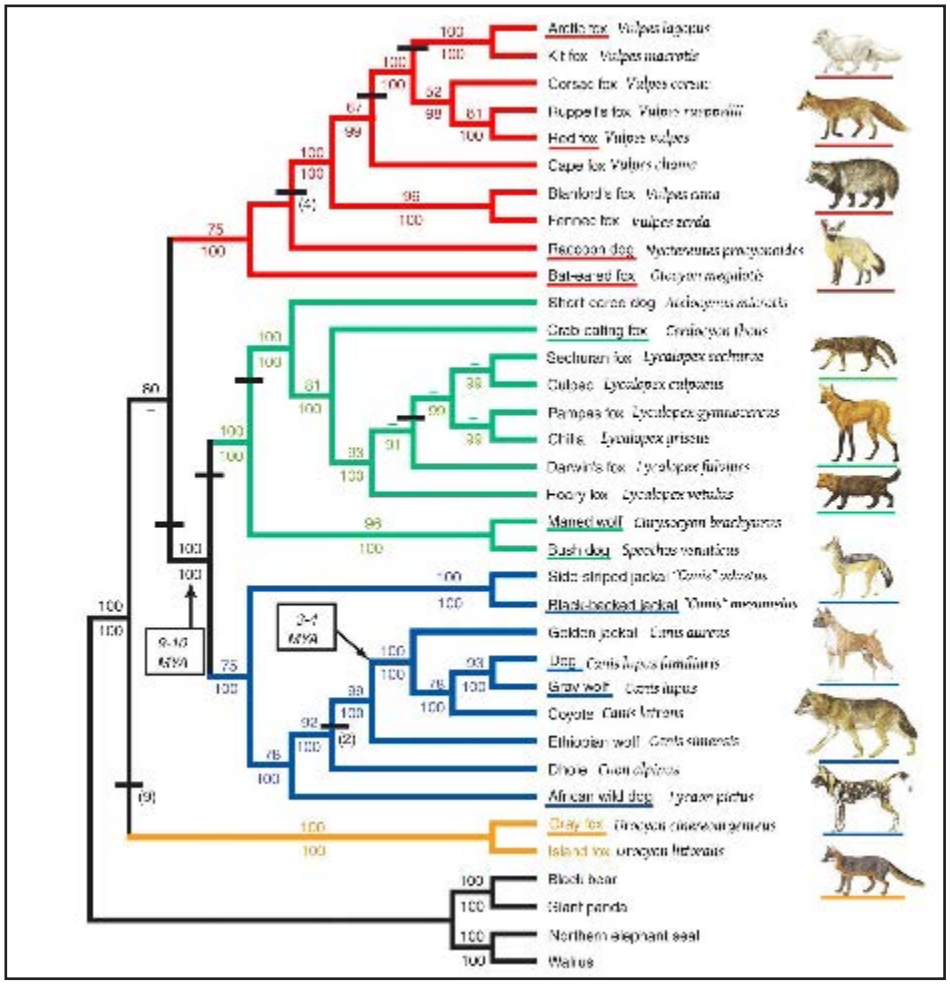

Figure 1.6 – Phylogenetic tree based on molecular analysis on selected extant Canidae. Colors identify different clades: yellow, gray fox clade; red, tribe Vulpini; green, South American canids; blue, *Canis sensu lato* clade. Note the paraphyly of the genus *Canis*.

comparted to coeval carnivorans-carnivoramorphans: an ossified tympanic bulla and a talonid (crushing portion) on lower carnassial (Wang, 1994). The Eocene age (especially Early Eocene) was a period of climatic optimum (Zachos et al., 2001) and North American habitats were probably dominated by wooded-areas (among others: Dilcher, 1973; Markwick, 1998; Fricke et al., 2004), with only small open areas. During their early evolution, hesperocyonines seemed to have taken advantage by the expansion of these environments, occurred at the end of the Eocene and the beginning of the Oligocene, when a global cooling shift is registered by $\delta^{18}O$ (Zachos et al., 2001). Despite small initial forms, Hesperocyoninae radiated in the Oligocene, to reach their maximum diversity during the Late Oligocene

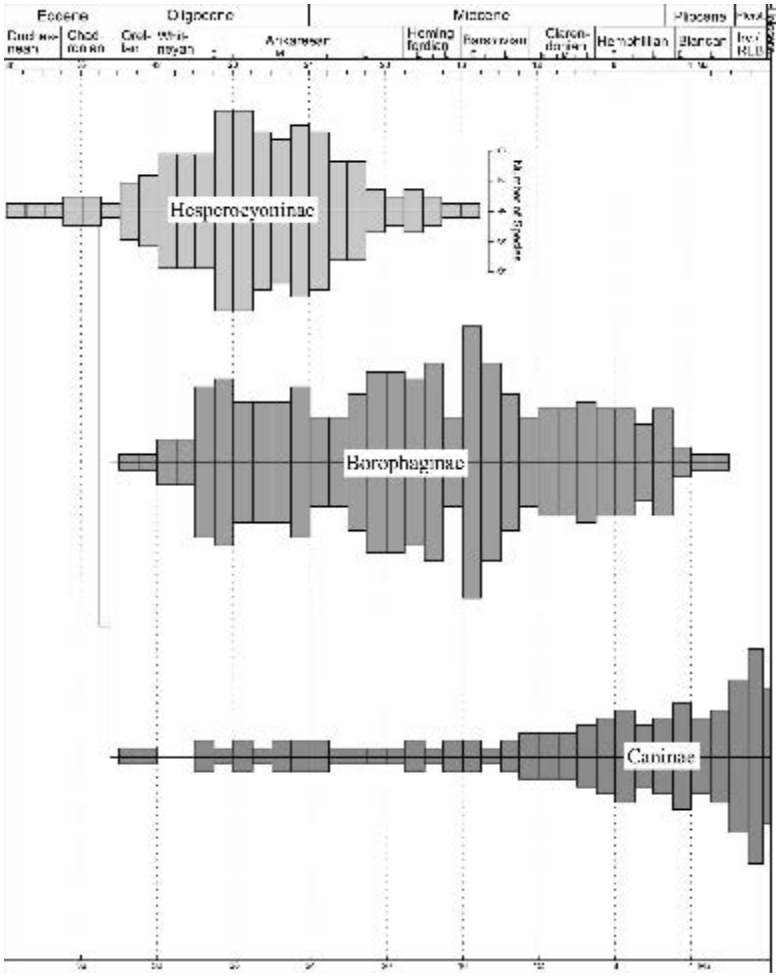

Figure 1.7 – Diversity of Canidae during their evolutionary history. Selected intervals correspond to 1 Myr (Tedford et al., 2009).

(ca 30 Ma; early Arikaneean, Vandenberghe et al., 2012), when some lineages evolved primitive hypercarnivorous traits, independently one from another: *i.e.*, single cuspulid on the m1 talonid as well as reduced upper molars. Other taxa (*Enhydrocyon* Cope, 1879, *Osbornodon* Wang, 1994 and *Ectopocynus* Wang, 1994) display particular bone-cracking dental features, *e.g.*, increased premolar size (Wang, 1994; Wang et al., 2004). At present, there is no fossil evidence of hypocarnivorous hesperocyonines. The last hesperocyonines became extinct in the Middle Miocene. The second radiation of Canidae is that of the subfamily Borophaginae, during the Early Oligocene (Fig. 1.7). Teeth morphology discriminate a borophagines from a hesperocyonines: the former possessed bicuspidate and basined m1 talonid (Wang et al., 1999), compared to the single-cusped one of hesperocyonines. Caninae

shares with borophagines the double-cusped m1 talonid. These dental features guaranteed a totally different plasticity to this group (as to canines), and let them develop both hypo- and hypercarnivorous adaptations. In their early evolution (Oligocene-early Miocene, Arkineean times), borophagines shows dental features suggestive of hypocarnivorous or omnivorous diets, compared to the contemporary predatory hesperocyonines. Some genera (*Cynarctoides* McGrew, 1938; *Cinarctus* Matthew, 1902) developed extreme hypercarnivorous teeth resembling those of Procyonidae and even artiodactyls (Wang et al., 1999; 2003; 2004). After the demise of Hesperocyoninae and probably benefiting from various ecological niches left empty by their relatives, borophagines diversified rapidly and greatly. During this burst, the most renowned forms of hypercarnivorous borophagines appear, from the large wild dog-like *Aelorudon* Leidy, 1858 until the extreme development of bone-cracking features in *Borophagus* Cope 1892 and *Epicyon* Leidy, 1858 (see Wang et al., 1999 for exhaustive discussion on these forms). Among those forms there is the largest canid of the fossil record, *Epicyon haydeni* Leidy, 1858, reaching the size of a small bear (reconstructed shoulder height: 90 cm, Wang & Tedford, 2008). By the late Miocene and during the Pliocene, borophagines declines significantly, possibly as a competition with canines. Last members of the subfamily probably disappeared by the end of the Gelasian (the late Blancan, Hilgen et al., 2012). The subfamily Caninae appeared in the Early Oligocene of North America, more or less contemporarily to borophagines (Fig. 1.7). The early *Leptocyon* Matthew, 1918 is characterized by the slender rostrum, squared-shaped M1, elongated and shallow mandible, elongated premolars and bicuspidate m1 talonid (Tedford et al., 2009). Their record is scanty from the Early-Middle Oligocene (Orellan-Whitneyan, Vandenberghe et al., 2012) but it becomes richer in the Late Oligocene (Early-Middle Arikareean). Nevertheless, the real burst in diversity of Caninae is reached only by the end of the Miocene. The rapid radiation is testified by the arise of hypocarnivorous taxa *Metalopex* Tedford

and Wang, 2008 that thrived in this period (late Clarendonian-Hemphillian times, Hilgen et al., 2012). Tedford et al. (2009) related this genus to modern gray foxes (genus *Urocyon* Baird, 1858) for the common enlargement of the crushing surfaces of carnassials and molars (parallel to Miocene *Cynarctoides*-like borophagines). The success of these hypocanivorous species might have resulted from the gradual decline of the small-sized borophagines (Wang et al., 1999). First *Vulpes* Frisch, 1775 species and the earliest member of the tribe Canini, genus *Eucyon* Tedford & Qiu, 1996 were recovered from various Late Miocene (Hemphillian) deposits of North America. For Caninae, Late Miocene was also a moment of dispersal out of North American continent into the Old World, as testified to by several records in the Eurasia (Crusafont-Pairó, 1950; Rook, 1992; Vislobokova et al., 2003; Montoya et al., 2009; Sotnikova &Rook, 2010) and Africa (Morales et al., 2005; de Bonis et al., 2007; Howell García, 2007) (see sections 1.5.-1.8.). Ancestor of modern South American canids (Fig. 1.2) apparently appeared in North America in Late Miocene (Tedford et al., 2009) and spread south only during the Late Pliocene, after the emergence of the Panamanian land bridge (Marshall et al., 1982). The absence of borophagines in the Eurasian record has been long noticed and discussed (see Wang et al., 1999, and reference therein). The two hypothesis have been put forward to describe this absence: the first one correlates the absence of borophagines in Eurasia with the almost complete absence of hyenids in North America. Considering the strong and convergent specializations that characterizes borophagines and bone-cracking hyenids, ecological competition might have prevented the replacement of one these groups in case of dispersion in the "foreign" continent. Only one hyenid taxon, *Chasmoporthetes ossifragus* Hay 1921 (see Berta, 1981; Kurtén et al., 1988) reached North America in the Early Pleistocene (late Blancan-early Irvingtonian; Pillans & Gibbard, 2012). Explanations for the success of the spreading of these taxa might lie in the fact that borophagines were declining or nearly extinct (Wang et al., 1999) and that *C. ossifragus* was not a bone-cracker

feeder but rather a cursorial predator, thus probably not in direct competition with bone-cracking borophagines (Wang & Tedford, 2008). Another explanation might involve ecological preference of habits. The environments of the Beringian region might have served as biogeographic filter, actively facilitating or impeding the crossing of the land bridge to species. Some evidence shows Beringia of the Late Miocene-Early Pliocene dominated by forested areas (Wallace & Wang, 2004), preventing borophagines, adapted to open environments, to reach Eurasia.

During Pleistocene times, several of the genera that dispersed out of North America in the Neogene (*e.g.*, *Canis* Linnaeus, 1758, *Vulpes*), re-entered in the North American continent in successive dispersive waves (Wang & Tedford, 2008).

1.5. *Nyctereutes* Temminck, 1838

1.5.1. Overview of the extant Nyctereutes procyonoides *(Gray, 1834)*

Nowadays, raccoon dogs are classified under the monospecific genus *Nyctereutes* Temminck, 1838. *Nyctereutes procyonoides* (Gray, 1834), is a small canid characterized by short legs and tail compared to its body length, and by its fur pattern, especially of the facial mask, which bears resemblance to that of the true raccoon (genus *Procyon* Storr, 1780). *N. procyonoides* inhabits two separated areas of Eurasia (Ward & Wurster-Hill, 1990). The natural range extends from the eastern part of Russia to southern China, in the Korean peninsula and Japanese archipelago, whereas the artificial one spans from eastern to central Europe. This range is the result of the accidental or intentional introduction, during the 1920s and 1930s, and the consequent spreading across Europe. Nowadays, European raccoon dogs are diffused from Finland to Hungary and from France to the Caucasus. Ecologically, the extant raccoon dog is an opportunistic feeder that possesses several cranial and dentognathic specialization to a diet composed of a great variety of food items (Ward & Wurster-Hill, 1990). Its main adaptations lie in numerous cranial and dentognathic features that improve the efficiency in the chewing process while

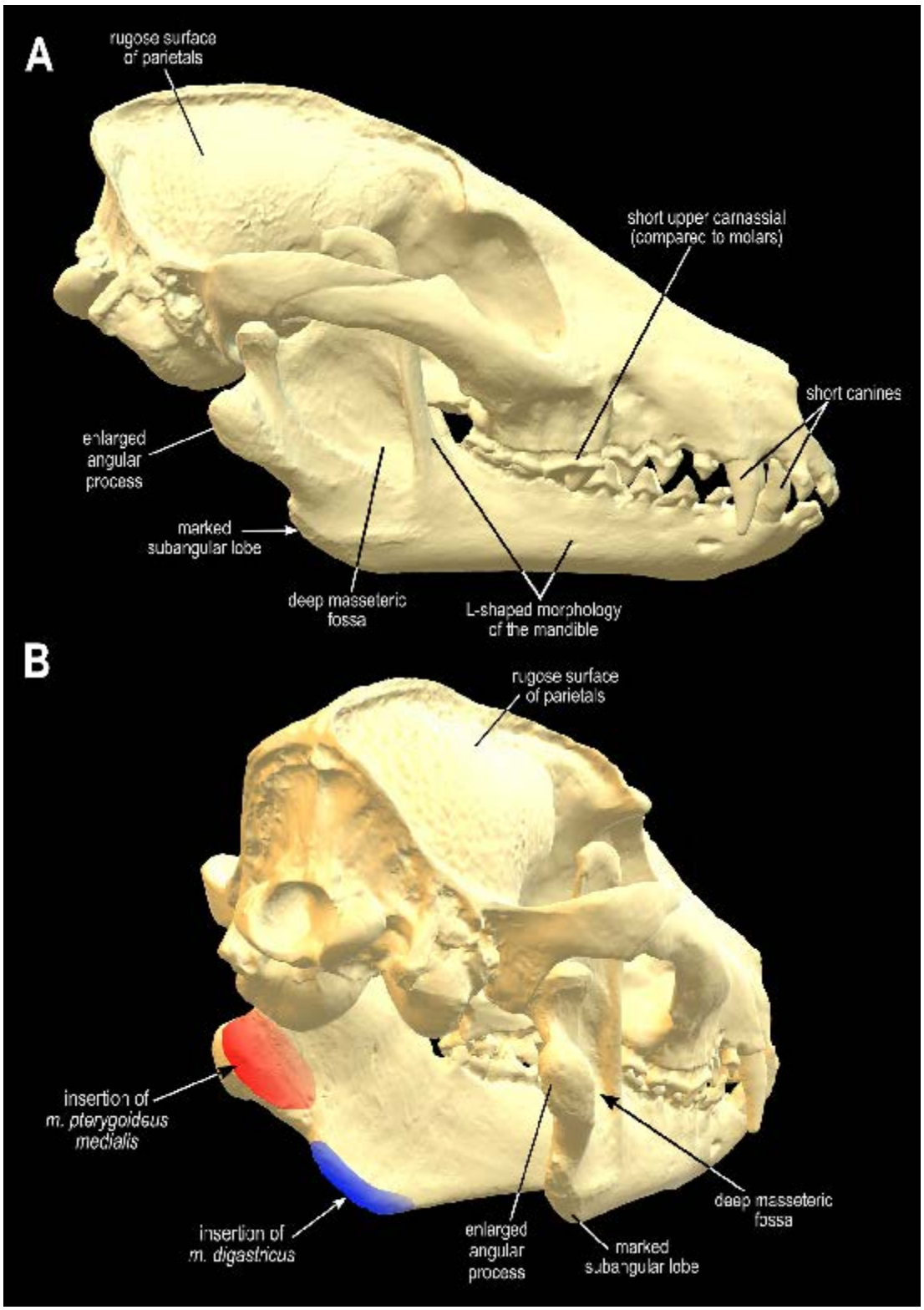

Figure 1.8 – Some of the diagnostic features of the skull of *Nyctereutes procyonoides* (Gray, 1834), in lateral (**A**) and caudolateral view (**B**).

feeding (Fig. 1.8). This species is further classified into six subspecies, according to the geographical distribution and some displayed morphological features (Allen, 1938; Ellerman and Morrison-Scott, 1951). The subspecies dwelling on the Asian mainland are *Nyctereutes procyonoides koreensis* Mori, 1922 from the Korean Peninsula; *Nyctereutes procyonoides orestes* Thomas, 1923 from southern China (Yunnan and Sichuan Province); *Nyctereutes procyonoides procyonoides* Gray, 1834 from eastern China; and *Nyctereutes procyonoides ussuriensis* Matschie, 1908 from eastern Siberia and northern China (Wozencraft, 2008; Sillero-Zubiri, 2010). *Nyctereutes procyonoides albus* Hornaday, 1904 and *Nyctereutes procyonoides viverrinus* Temminck, 1838 are the Japanese subspecies, occurring, respectively, on the island of Hokkaido and on the islands of Honshu, Kyushu, and Shikoku (Saeki, 2009; Sillero-Zubiri, 2010). This subdivision is well established in the literature; however, the complex taxonomic status of the subspecies remains unclear (Kauhala et al., 1998; Pitra et al., 2010; Kim et al., 2013). Much evidence (chromosomal, molecular and morphological) reveals the peculiarity of the Japanese populations of raccoon dogs when compared to the continental populations (Ward et al., 1987; Wada & Imai, 1991; Wada et al., 1991; Kim et al., 2013). Consequently, some authors (Kim et al., 2015) have even proposed the inclusion of the population from Japan in a separate species, *i.e.*, *Nyctereutes viverrinus* Temminck, 1838 (comprising the subspecies *N. v. viverrinus* and *N. v. albus*).

Moving up from the subspecific level, the confusion and debate on the taxonomy and the relationship of the genus *Nyctereutes* with other canids remains. Apart from Frechkop (1959), who ascribed *Nyctereutes* to Procyonidae, others have widely acknowledged its peculiar pattern of morphologies as a canid genus (Huxley, 1880; Gaspard, 1964; Kleiman, 1967; Radinsky, 1973; Clutton-Brock et al., 1976). Nevertheless, this odd set of features made the position within the Canidae difficult to resolve. Berta (1988), who performed one of the first cladistic analyses on living and fossil species of Canidae, found that *Nyctereutes* groups

with the South American canids, *Cerdocyon* Hamilton Smith, 1839, *Atelocynus* Cabrera, 1940 and *Speothos* Lund, 1839. Similar results were reported by Tedford et al. (1995), in which *Speothos* and *Atelocyon* cluster together as a sister group of the clade that includes *Cerdocyon* and *Nyctereutes*. Berta (1988) and Tedford et al. (1995) considered that the strong affinity of the latter two genera lay in the presence of features like the presence of a developed subangular lobe (shared with *Speothos*, *Urocyon* and *Otocyon* Müller, 1836), the expansion of the angular process (as in other South American taxa), the development of the scars of the *m. pterygoideus medialis* on the lingual side of the angular process (as in *Atelocynus* and *Speothos*) and low-crowned canines (comparable to those of *Urocyon* and *Otocyon*). Tedford et al. (2009) erected the subtribe Cerdocyonina, within the tribe Canini, including all the South American canids and the Eurasian raccoon dog. Molecular phylogenetic studies (Wayne et al., 1997; Bardeleben et al., 2005; Lindblad-Toh et al., 2005; Wayne & Ostrander, 2007; Chen & Zhang, 2012; Zhao et al., 2016; Zrzavý et al., 2018) have revealed a different pattern of affinities: *Nyctereutes* separates from the monophyletic clade of South American canids and roots at the base or within the group of foxes, close to the bat-eared fox, *Otocyon* (Fig. 1.6). The position of *Nyctereutes* near the base of the tribe Vulpini implies that these morphologies retained by both the former and *Cerdocyon* (as well as other taxa) simply constitutes convergent adaptations. Homoplasies may represent a source of confusion that can blur the actual affinities between species (*inter alios* Henning, 1966; Wiley et al., 1991; Poe & Wiens, 2000; Simões et al., 2016), as revealed by previously cited molecular data.

1.5.2. Paleontological record of raccoon dogs in the Old world

Despite the reduced specific diversity, up to ten different species were described in literature (Bates, 1937; Soria & Aguirre, 1976; Ficcarelli et al., 1984; Tedford & Qiu, 1991; Werdelin & Dehghani, 2011; Figs. 1.9-1.10). Among the attributed

record of Nyctereutes, the oldest occurrence appears to be in Morocco, in the site of Lissasfa (Casablanca). Geraads (2011) described a small maxillary fragment with partially preserved P4 and M1, with an estimated age of 6-5.5 Ma. The authors discussed the resemblance with younger *Nyctereutes*, noting nonetheless some peculiarities, *e.g.*, small-sized P4 protocone, enlarged P3 alveolus (Geraads, 2011). Besides this uncertain record, the earliest widely-accepted record is that of the early Early Pliocene *Nyctereutes tingi* Tedford & Qiu, 1991 from localities of the Yushe Basin (Shanxi, China) and from the Zanda Basin (Tibet, China) (Fig. 1.9). Li et al. (2003) reported the existence of another early *Nyctereutes* from the deposits Gaotege local fauna (Nei Mongol, Mongolia), roughly coeval to the record of *N. tingi* of China (early Gaozhuangian, Qiu et al., 2013; see Fig. 1.9). This taxon may represent a new undescribed species (Li et al., 2003). Younger deposits of the Yushe Basin yielded another species of fossil raccoon dog, *Nyctereutes sinensis* (Schlosser, 1903) (Fig. 1.9). Compared to the older *N. tingi*, this taxon possesses peculiar features (*e.g.*, prominent subangular lobe, larger angular process), more similar to the extant *N. procyonoides*. On the other side of Eurasia, the oldest

Figure 1.9 – Resuming chronological scheme of the known occurrences of *Nyctereutes* spp. in the fossil record of the Old World. Degree of inclination of locality names approximate the degree of uncertainty on their dating. Data from: Boule (1889); Depéret (1890); Teilhard De Chardin & Piveteau (1930); Bates (1937); Villalta (1952); Viret (1954); Kurtén (1965); Vekua (1972); Soria & Aguirre (1976); Kurtén & Crusafont-Pairó (1977); Horowitz (1979); Ficcarelli et al. (1984); Tedford & Qiu (1991); Koufos (1997); Ginsburg (1998); Spassov (2000); Sotnikova et al. (2002); Li et al. (2003); Monguillon et al. (2004); Sotnikova (2004); Jin & Liu (2009); Dennell (2010); Geraads et al. (2010); Werdelin & Sanders (2010); Geraads (2011); Werdelin & Dehghani (2011); Dong et al. (2013); Tedford et al. (2013); Wang et al. (2013a; 2013b); Koufos (2014). **Abbreviations** – **AaO**, Ahl al Oughlam (Morocco); **CDP**, Collepardo (Italy); **Chikoian FC**, Chikoian Faunal Complex (Mongolia, Russia); **ELFN**, Elandfontein (South Africa); **LPVv**, La Puebla de Valverde (Spain); **Laetoli UB**, Laetoli Upper Beds (Tanzania); **MEL**, Megalo Emvolon (Greece); **PLEt**, Perrier-Les Etouaires (France); **Tabun C**, Tabun Cave (State of Palestine); **VLR**, Villarroya (Spain); **ZKD**, Zhoukoudian (China).

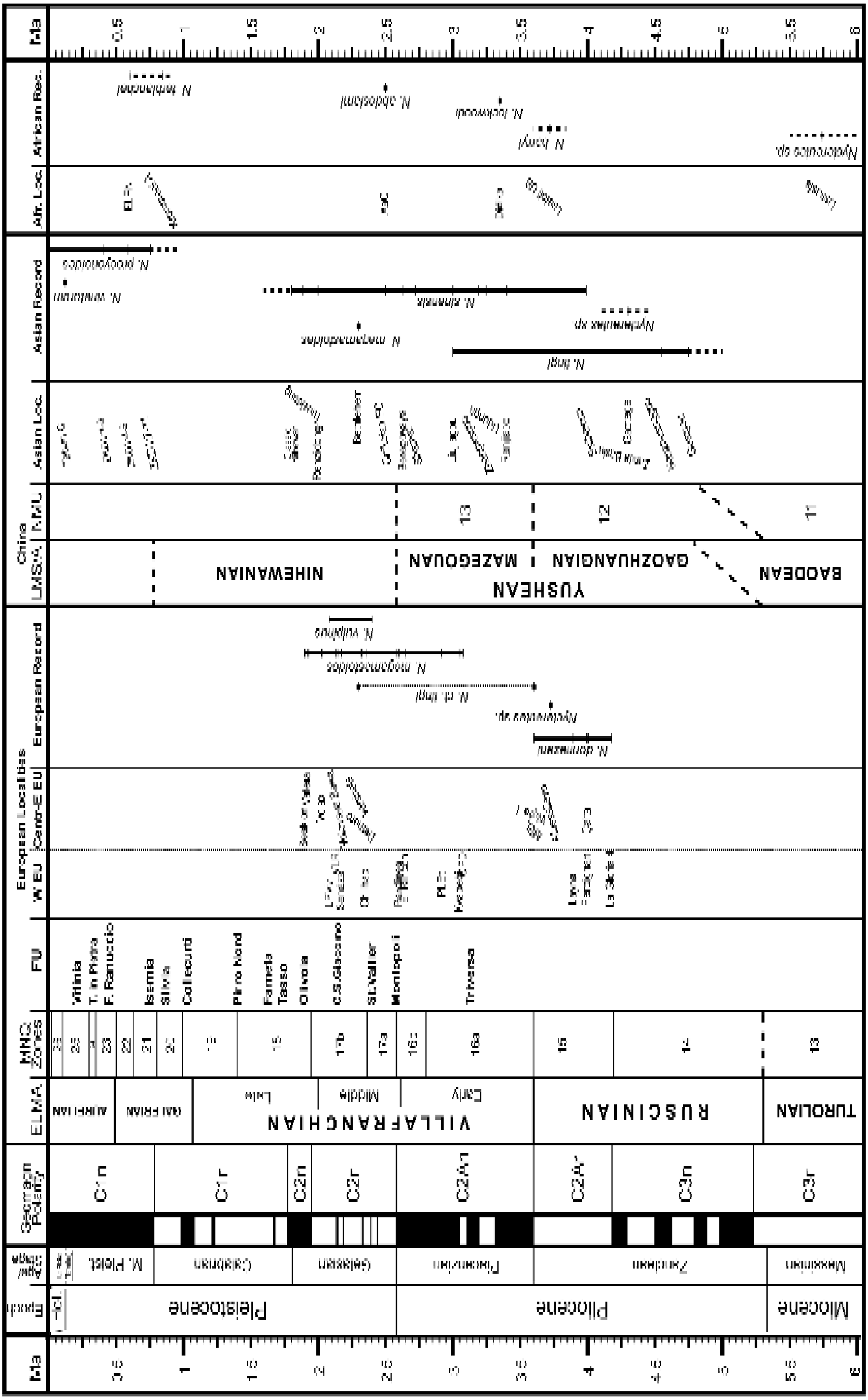
Ma
African Rec.
Afr. Loc.
Asian Record
Asian Loc.
European Record
FU
MNQ Zones
ELMA
Geomagn. Polarity
Epoch
Pleistocene
Pliocene
Miocene
VILLAFRANCHIAN
RUSCINIAN
TUROLIAN
NIHEWANIAN
YUSHEAN
MAZEGOUAN
GAOZHUANGIAN
BAODEAN

form described in western Europe is *Nyctereutes donnezani* (Depéret, 1890), firstly discovered in Perpignan (France) and then reported from older localities such as La Gloria 4 (Spain; Alcalá-Martínez, 1994). These sites are referred to the Early Pliocene, MN14-15 (around 4 Ma) (Domingo et al., 2013; Clauzon et al., 2015), more or less coeval to the occurrence of *N. sinensis* (Figs. 1.9-1.10). Other records of the species are Layna (Spain, Soria & Aguirre, 1976), Çalta (Turkey, Ginsburg, 1998), both 4 Myr-old localities, and Węże 1 (Poland, MN15, Ivanoff et al., 2014). *N. donnezani* has been regarded as the western European correspondent of earlier *N. tingi*, for their consistent morphological affinity in comparison to *N. sinensis* or the extant *N. procyonoides* (Tedford & Qiu, 1991). Spassov (2000), reports an unidentified and unstudied *Nyctereutes* sp. from MN15 locality of Musselievo (Bulgaria).

Fig. 1.10 shows that the fossil distribution range of *Nyctereutes* was not limited to Eurasia as *Nyctereutes* spp. were recovered also from several regions of Africa (see *inter alios* Geraads et al., 2010; Werdelin & Dehghani, 2011). The earliest of these findings is the dubious ?*Nyctereutes barryi* Werdelin & Dehghani, 2011 from the Upper Laetoli Bed (Tanzania, 3.75 Ma, Harrison, 2011). This taxon possesses several features resembling *N. tingi*, as noted by Werdelin & Dehghani (2011) who deemed the taxon to be intermediate between *N. tingi* and *N. donnezani*.

It is worth mentioning that in scientific literature a particular terminology has been historically used when describing fossil species. Several dentognathic features possessed by *N. procyonoides* (Fig. 1.8) are diagnostic for the genus and, at least part of them, were acquired by the extant raccoon dogs' ancestors as the result of progressive adaptations towards a hypocarnivorous diet. Among these characteristics, there are the reduction of slicing portions of the carnassials and enlargement of the crushing surface of the molars, the developed subangular lobe in the mandible corpus, the expansion of the angular process with the consequent the development of the insertion areas of the muscle *pterigoideus*

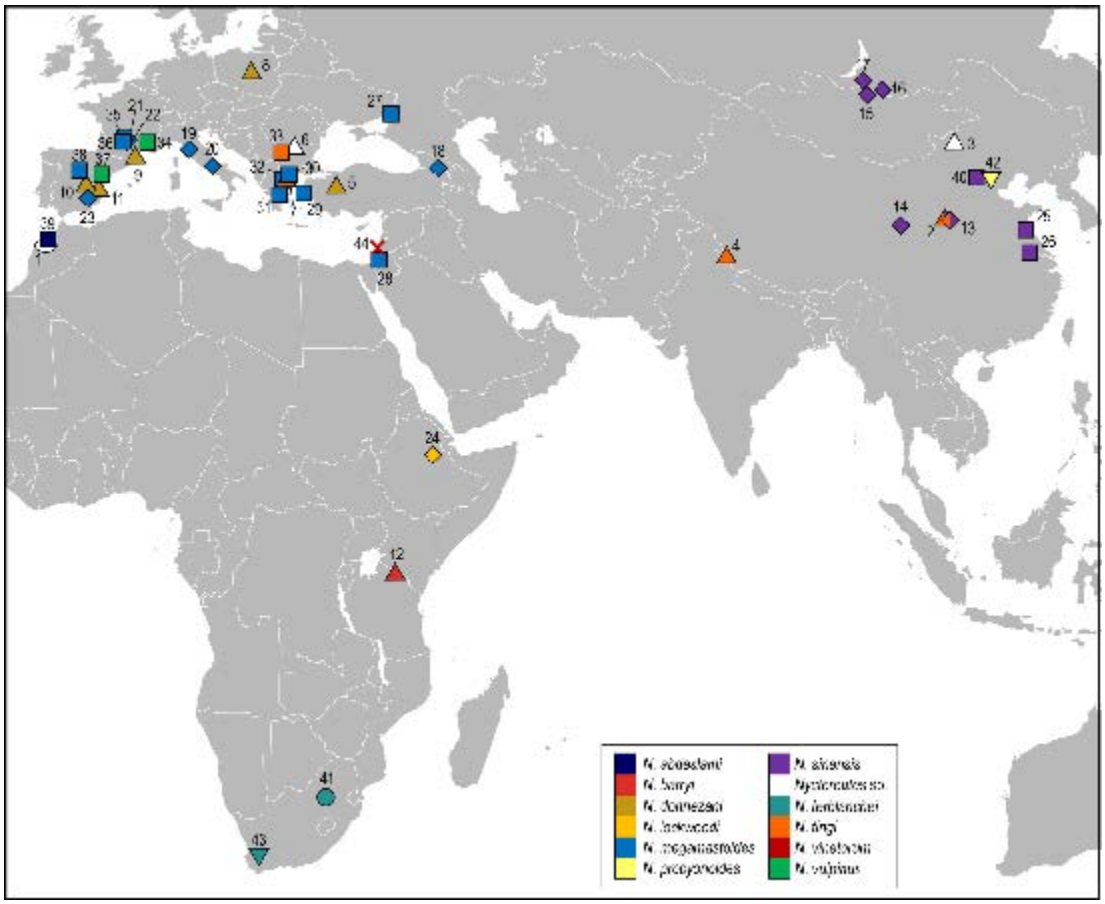

Figure 1.10 – Map showing the global occurrences of fossil *Nyctereutes* (described in section 1.5.). **Localities** – ***Tortonian*** (+): **1**, Lissasfa (Morocco); ***Zanclean*** (triangle): **2**, Guaigou, Nanzhuanggou, Baihaicun, Yushe Basin (China); **3**, Gaotege, Nei Mogol (China); **4**, Zanda Basin, Tibet (China); **5**, Çalta (Turkey); **6**, Musselievo (Bulgaria); **7**, Megalo Emvolon (Greece); **8**, Węże 1 (Poland); **9**, Perpignan (France); **10**, La Gloria 4 (Spain); **11**, Layna (Spain); **12**, Laetoli, Upper beds (Tanzania); ***Piacenzian*** (diamond): **13**, Liujiagou and Zhanwagou, Yushe basin (China); **14**, Renjiapo (China); **15**, Shamar (Mongolia); **16**, Beregovaya, Transbaikalia (Russia); **17**, Udunga, Transbaikalia (Russia); **18**, Kvabebi (Georgia); **19**, Montopoli (Italy); **20**, Collepardo (Italy); **21**, Perrier-Les Etouaires (France); **22**, Pardines (France); **23**, EL Rincon (Spain); **24**, Dikika (Ethiopia); ***Gelasian*** (square): **25**, Tuozidong (China); **26**, Renzidong (China); **27**, Volovaya Balka (Russia); **28**, Bethlehem (State of Palestine); **29**, Vatera (Greece); **30**, Volax (Greece); **31**, Sesklon (Greece); **32**, Dafnero-1 (Greece); **33**, Varshets (Bulgaria); **34**, St Vallier (France); **35**, Senéze (France) **36**, Chihlac (France) **37**, La Puebla de Valverde (Spain); **38**, Villarroya (Spain); **39**, Ahl al Oughlam (Morocco); **40**, Nihewan Basin (China); ***Calabrian*** (circle): **41**, Kromdraai A (South Africa); ***middle Pleistocene*** (inverted triangles): **42**, Zhoukoudian Locality 1 (China); **43**, Elandsfontein (South Africa); ***Late Pleistocene*** (x): **44**, Tabun Cave, Level C (State of Palestine).

medialis, on the medial side of this process. Soria & Aguirre (1976) were among the first to study critically fossil raccoon dogs considering their complete record, taking into account the interspecific and intraspecific variability and the principal features of the fossil and of the extant species of the genus. They acknowledged the peculiarity of *N. procyonoides* and identified in certain mandibular and dental characters (*i.e.*, depth of mandible corpus; morphology of the angular region; inclination of the ascending ramus; the premolars and molars morphology) the key features for the evolutionary differentiation of raccoon dogs. Specifically, Soria & Aguirre (1976) outlined the first pattern of morphological affinity and relation between the species of *Nyctereutes*. This was achieved thanks to the recognition of "primitive" taxa (with *e.g.*, poorly developed subangular lobe and elongated and buccolingually narrow premolars) and of "derived" taxa (in which *e.g.*, there is a marked development of the subangular lobe and stouter premolars) that resemble the extant *N. procyonoides* (Soria & Aguirre, 1976). Since this pivotal work, in the scientific literature on *Nyctereutes*, this terminology was used by several scholars to discuss the morphological set of features a fossil raccoon dog possessed (Ficcarelli et al., 1984; Tedford & Qiu, 1991; Argant, 2004; Monguillon et al., 2004), with no explicit reference to the phylogenetic relationship of a taxon. Therefore, the terminology used while introducing the several taxa follows the same intent: to express the degree of development of the set of morphological features, without implying any evolutionary inference. In this terms, *N. tingi*, *N. donnezani* and *N. barryi* can be considered primitive taxa, for the absence and/or incipient development of these characters (as also noted by Soria & Aguirre, 1976; Tedford & Qiu, 1991; Werdelin & Dehghani, 2011), whereas *N. sinensis* is rather derived, resembling the morphologies of the living raccoon dog.

The first pulse of diversity of raccoon dog around ca 4 Ma (Fig. 1.10) was characterized by the coexistence of primitive and derived species in eastern Asia (*N. tingi* and *N. sinensis*), the westward dispersion of primitive taxa as apparently

testified to by the record of *N. tingi* in the Zanda basin (Wang et al., 2013a) and Megalo Emvolon (Koufos, 1997), of *N. donnezani* from Europe and Turkey (Depéret, 1890; Soria & Aguirre, 1976; Ginsburg, 1998), and of *N. barryi* from Tanzania. If confirmed, the unusual MN17 occurrence of *N.* cf. *tingi* in Varshets (Bulgaria, Spassov, 2000) might testify to the long persistence of primitive Asian forms in the European fossil record.

In Late Pliocene (Mazegouan age) *N. sinensis* thrived in eastern Asia (Fig. tempocal), persisting in the Yushe Basin with the last occurrence of *N. tingi* (Liujiagou locality) and spreading to reach Mongolia and Transbaikalia. Last records of *N. sinensis* are those of the Early Pleistocene (middle Nihewanian) of Renzidong, Tuozidong and Nihewan Basin. A second burst of paleodiversity is that between 3.5-2 Ma (Figs. 1.9-1.10), when several forms appeared in the record of Africa and Europe. Several sites of western Eurasia recorded the presence of the derived species *Nyctereutes megamastoides* (Pomel, 1842), one the most renowned fossil species of this genus. Indeed, this Late Pliocene-Early Pleistocene species had large range of distribution, spanning from Spain to Georgia (Fig. 1.10). These localities include: Chilhac, Perrier-Les Etouaires, Pardines, Senéze, (France; Argant, 2004; Monguillon et al., 2004); Kvabebi (Georgia; Vekue, 1972); Dafnero-1, Sesklon, Volaks, Vatera-F (Greece; Koufos, 2014); Montopoli, Collepardo (Italy; Del Campana, 1917; Gliozzi et al., 1997); Bethlehem (Palestine; Horowitz, 1979); Volovaya Balka (Russia; Sotnikova et al., 2002); El Rincon, Villarroya (Spain; Villalta, 1952; Alberdi et al., 1997). Many authors supported the idea that this taxon originated from *N. donnezani* (Soria & Aguirre, 1976; Argant, 2004; Monguillon et al., 2004). Beside this possibility, during the late Pliocene in Europe, primitive and derived forms of raccoon dogs never coexisted, rather *N. donnezani* was replaced by *N. megamastoides.* Therefore, the European record apparently contrasts with the Asian one (see Tedford et al., 2013). Moreover, the retention of strongly derived dental and cranio-mandibular features in *N. megamastoides*, led some scholars to suggest

the idea of close relationship between *N. megamastoides* and *N. sinensis* (among the first Soria & Aguirre, 1976), although some morphological differences remain. The sample from St. Vallier (France), historically attributed to *N. megamastoides* (Viret, 1954; Martin, 1971) was classified as a separate taxon from *N. megamastoides.* The first to acknowledged the difference between the from *N. megamastoides*-forme tipique were Soria & Aguirre (1976) who identified the presence in the sample from St. Vallier of some features resembling the genus *Vulpes* (*e.g.*, elongation of the premolars and of both the carnassials; and the mesiodistal shortening of the M2). The authors put forward the attribution to the subspecies *Nyctereutes megamastoides vulpinus* Soria & Aguirre, 1976. Monguillon et al. (2004) upranked the taxon as a separated species. Here this interpretation is followed. Apart from St. Vallier, this taxon occurs in La Puebla de Valverde (Spain, Kurtén & Crusafont-Pairó, 1978).
Apart from the controversial taxon ?*N. barryi* , the African record of *Nyctereutes* is relatively scanty but diverse. Younger although still early Pliocene in age (3.35 Ma, Geraads et al., 2010), the primitive *Nyctereutes lockwoodi* Geraads et al., 2010 from Dikika (Ethiopia) shows several peculiar and unusual morphologies, which justify the separation in a different species. Other findings in Africa are the Early Pleistocene species *Nyctereutes abdeslami* Geraads, 1997 from Morocco and the South African *Nyctereutes terblanchei* (Broom in Broom & Schepers, 1946). The former, described from the site of Ahl al Oughlam in Morocco (2.5 Ma), possesses several derived dentognathic features that resemble those of *N. sinensis*, *N. vulpinus* and particularly of *N. megamastoides*. Argant (2004) acknowledged these similarities and suggested a possible affinity between Eurasian species and the North African taxon. *N. terblanchei* from Kroomdrai A and Elandfontein was reviewed by Ficcarelli et al. (1984) who recognized mandibular and dental features in this species, similar to those of *N. megamastoides* and *N. sinensis*. Geraads et al. (2010) suggested the possibility of a close relation (possibly as ancestor-descendant) between *N. lockwoodi* and *N. terblanchei*. Reynolds (2012) questioned the generic

attribution of this species, though the peculiar features of the type specimen (KA 1290, see Werdelin & Peigné, 2010) cannot be mistaken with those of modern jackals (*e.g.*, the subangular lobe, the deep angular process, the vertical ramus of the mandible, etc.).

After 2 Ma, and during the last part of the Early Pleistocene, the findings of *Nyctereutes* across the whole Old World become more and more scarce and the diversity of the genus declined. The first record of the extant *N. procyonoides* appears to be that of middle Pleistocene deposits of China (Zhoukoudian locality 1, Pei, 1934; Tedford & Qiu, 1991). The only other fossil species proposed until today is the Palestinian *Nyctereutes vinetorum* (Bates, 1937). Nevertheless, this taxon could be a larger form of the extant species (Kurtén, 1965).

1.6. *Vulpes* Frisch, 1775

1.6.1. Fossil record of Vulpes *Frisch, 1775 from Mio-Pleistocene times*

Molecular phylogenies on extant Canidae have shown that the genus *Vulpes* is monophyletic (Zrzavý & Řičánková, 2004; Lindblad-Toh et al., 2005; Wayne & Ostrander, 2007; Zrzavý et al., 2018; see Fig. 1.6), including counting up to 12 species (Castellò, 2018), naturally widespread throughout the world (with the exception of Australia and South America). Nevertheless, caution should be advised when using the term "fox". Indeed, generally refers to small-sized canids without explicit implication of a phylogenetic affinity with animals of the genus *Vulpes*. For instance, the species of *Urocyon* are commonly referred to as the gray fox [*Urocyon cinereoargenteus* (Schreber, 1776)], the island fox [*Urocyon littoralis* (Baird, 1858)] and the Cuzomel island fox (*Urocyon* sp., see Cuarón et al., 2004; Gompper et al., 2006). The same can be said for several small-sized South American canids *e.g.*, the Culpeo fox [*Lycalopex culpeo* (Molina, 1782)], the Sechuran fox [*Lycalopex sechurae* (Thomas, 1900)] or the crab-eating fox (*Cerdocyon thous* Hamilton Smith, 1839). Further reference to "fox(es)" in the present work, refer to members of the

genus *Vulpes* and their closely allied taxa (unless stated otherwise).

Of Caninae, the fossil record of *Vulpes* is one of the most fragmentary of the subfamily. Its fossils are known from North America and the Old World, but they are utterly scarce and scattered, especially in Eurasia and Africa. The two oldest records of the genus are the North American *Vulpes stenognatus* Savage, 1941 and *Vulpes kernensis* Tedford et al., 2009, both Hemphillian in age (Figs. 1.11-1.12). The latter is known only for two specimens coming from a locality in the Kern River Formation (locality CIT 49) generically referable to the early Hemphillian (Savage et al., 1954; Lindsay et al., 1987; Tedford et al., 1987). It should be note that a correlative fauna to that of Kern River Fm. was found in the Mehrten Formation (San Joaquin Valley), which was calibrated to 8.2 Ma thanks to a tuff

Figure 1.11 – Resuming chronological scheme of the known occurrences of fossil *Vulpes* spp. in both the Old and New World. Degree of inclination of locality names approximate the degree of uncertainty on their dating. Data from: Del Campana (1913); Teilhard De Chardin & Piveteau (1930); Pei (1934); Broom (1939); Villalta (1952); Thenius (1954); Viret (1954); Odintzov (1965); Bonifay (1971); Rabeder (1976); Kurtén & Crusafont-Pairó (1977); Janossy (1986); Sher (1986); Qiu & Tedford (1990); Moullé (1992); Terzea (1996); Ginsburg (1998); García & Arsuaga (1999); Spassov (2000); Qiu et al. (2004); Tedford et al., (2004; 2009); Moigne et al. (2006); de Bonis et al. (2007); Garrido (2008); Werdelin & Sanders (2010); Geraads (2011); Pacheco et al. (2011); Pazonyi (2011); Tedford et al. (2013); Wang et al. (2013a; 2013b); Wang et al. (2014); Koufos (2014); Madurell-Malapeira et al. (2014); Geraads et al. (2015); Rovinsky et al. (2015); Gasparik & Pazonyi (2018); Krijsman et al. (2019). **Abbreviations** – **AaO**, Ahl al Oughlam (Morocco); **APL1**, Apollonia-1 (Greece); **Atap. TD6**, Atapuerca Trinchera Dolina 6 (Spain); **Atap. TE**, Atapuerca Trinchera Elefante (Spain); **B. Leon 5**: Barranco Leon 5 (Spain); **CGR**, Cal Guardiola (Spain); **DA 2C**, Deutsch Altenburg 2C (Austria); **DrMk**, Drimolen Makondo (South Africa); **ELFN**, Elandfontein (South Africa); **EVT**, Vallparadís Estació; **F. Nueva 3**, Fuente Nueva 3; **LPVv**, La Puebla de Valverde (Spain); **LVal**, Le Vallonnet (France); **Mkps3**, Makapansgat 3 (South Africa); **NHH4**, Nagyharsanyhegy 4; **OCat**, Odessa Catacombs (Ukraine); **OH1-GR1**, Oulad Hamida1-Grotte des Rhinoceros (Morocco); **SH2**, Somssich-Hill 2; **Th1-GH**, Thomas 1 Quarry-Grotte des Hominides (Morocco); **ThCr**, Thousand Creek (U.S.A.); **VLR**, Villarroya (Spain); **ZKD**, Zhoukoudian (China).

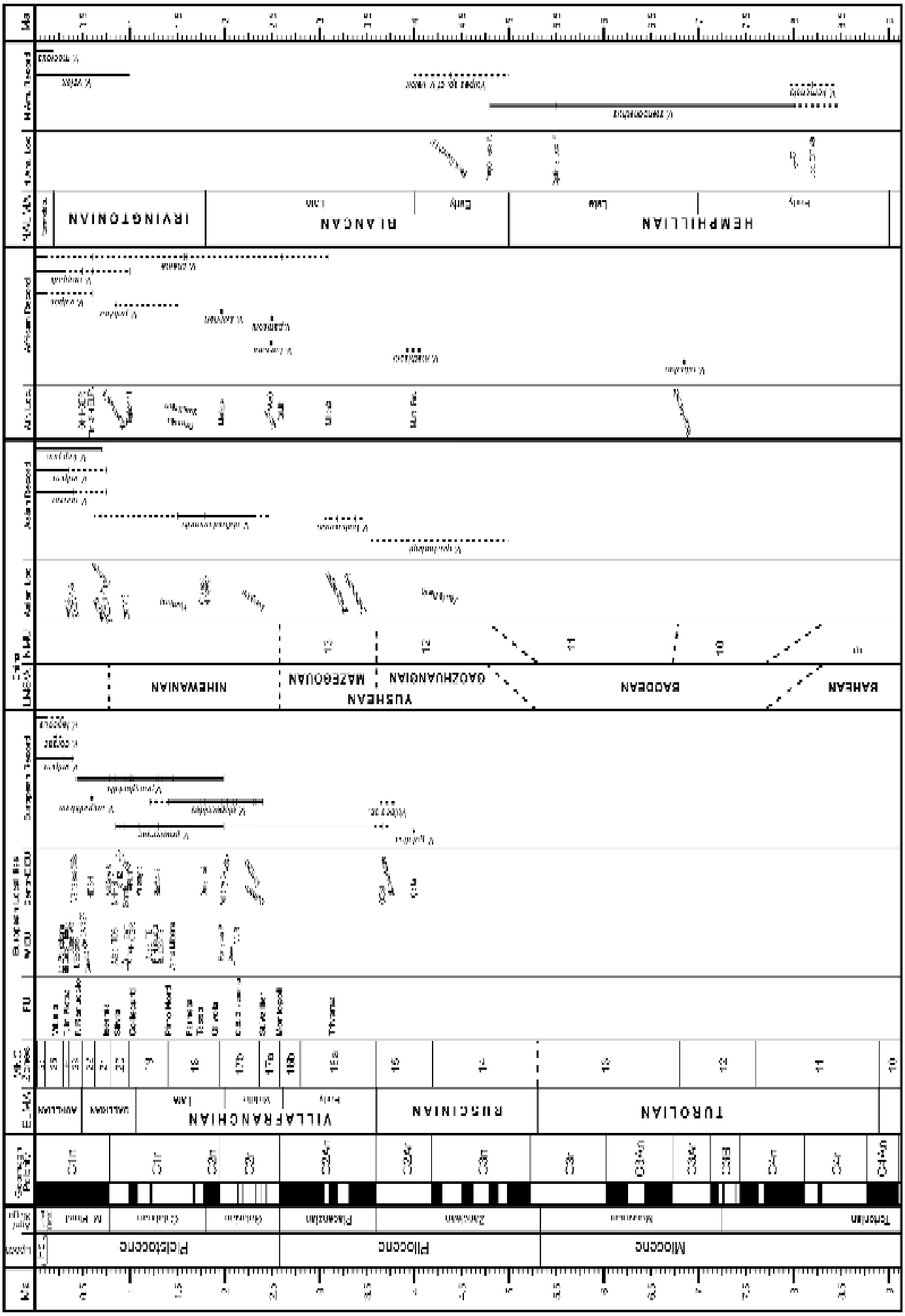
IRVINGTONIAN
BLANCAN
HEMPHILLIAN
NIHEWANIAN
MAZEGOUAN
GAOZHUANGIAN
YUSHEAN
BAODEAN
BAHEAN
VILLAFRANCHIAN
RUSCINIAN
TUROLIAN
Pleistocene
Pliocene
Miocene

Figure 1.12 – Map showing the global occurrences of fossil foxes (described in section 1.6.). **Localities** – ***early Hemphillian*** (asterisk): **1**, Rattlesnake 3, Oregon (U. S. A.); **2**, Burmeister Locality, Oregon (U. S. A.); **3**, University of Oregon Locality 2451, Oregon (U. S. A.); **4**, University of Oregon Locality 2489, Oregon (U. S. A.); **5**, Aphelops Draw, Nebraska (U. S. A.); **6**, UNSM Locality Ft 40, Nebraska (U. S. A.); **7**, Thousand Creek Fm., Nevada (U. S. A.); **8**, Alturas I, California (U. S. A.); **9**, Lava Mountains Fauna, California (U. S. A.); **10**, Ward's North Valley Pit, Texas (U. S. A.); **11**, CIT locality 49, California (U. S. A.); ***late Hemphillian*** (oval): **12**, Black Wolf Creek, Colorado (U. S. A.); **13**, Optima Local Fauna, Oklahoma (U. S. A.); **14**, Miami Quarry, Texas (U. S. A.); **15**, Goodnight area, Texas (U. S. A.); **16**, Chamita Formation, New Mexico (U. S. A.); **17**, Golgotha Watermill Pothole site, Nebraska (U. S. A.); **18**, Wikieup Big Sandy Formation, Arizona (U. S. A.); **19**, Old Cabin Quarry, Arizona (U. S. A.); **20**, Redington Quarry, Arizona (U. S. A.); **21**, Nichol's Mine, Florida (U. S. A.); **22**, Yepomera, Chihuahua (Mexico); ***early Blancan*** (right-pointing triangle):**23**, Beck Ranch Local Fauna, California (U. S. A.); ***Tortonian*** (plus): **24**, Toros Menalla (Chad); ***Zanclean*** (triangle): **25**, Odessa Catacombs (Ukraine); **26**, Musselievo (Bulgaria); **27**, Çalta (Turkey); **28**, Zanda Basin, Tibet (China); **29**, Mursi Formation (Ethiopia); ***Piacenzian*** (diamond): **30**, Zhangwagou, Yushe Basin (China); **31**, Makapansgat 3 (South Africa); ***Gelasian*** (square): **32**, Ahl al Oughlam (Morocco); **33**, Fonelas P1 (Spain); **34**, La Puebla de Valverde (Spain); **35**, Villarroya (Spain); **36**, St Vallier (France); **37**, Villany 3 (Hungary); **38**, Varshets (Bulgaria); **39**, Dafnero-1 (Greece); **40**, Volax (Greece); **41**, Dmanisi (Georgia); **42**, Longdan, Linxia Basin (China); **43**, Nihewan Basin (China); **44**, Taung (South Africa); **45**, Malapa (South Africa); ***Calabrian*** (circle): **46**, Venta Micena (Spain); **47**, Barranco Leon 5 (Spain); **48**, Fuente Nueva 3 (Spain); **49**, El Chaparral (Spain); **50**, Trinchera Elefante, Atapuerca (Spain); **51**, Trichera Dolina 6, Atapuerca (Spain); **52**, Vallparadís Estació (Spain); **53**, Cal Guardiola (Spain); **54**, Le Vallonnet (France); **55**, Tasso, Upper Valdarno (Italy); **56**, Pirro Nord (Italy); **57**, Deutsch Alternburg 2C (Austria); **58**, Gombasek (Slovakia); **59**, Betfia 2 (Romania); **60**, Villany 5 (Hungary); **61**, Somssich-Hill 2 (Hungary); **62**, Villany 8 (Hungary); **63**, Nagyharsanyhegy 4 (Hungary); **64**, Apollonia-1 (Greece); **65**, Yuanmou (China); **66**, Kromdraai A (South Africa); **67**, Tighennif/Terfine (Algeria); ***middle Pleistocene*** (inverted triangles): **68**, Caune de l'Arago (France); **69**, Lunel-Viel (France); **70**, L'Escale (France); **71**, Hundsheim (Austria); **72**, Zhoukoudian Locality 1 (China); **73**, Zhoukoudian Locality 6 (China); **74**, Zhoukoudian Locality 3 (China); **75**, Olyorian Fauna (Siberia).

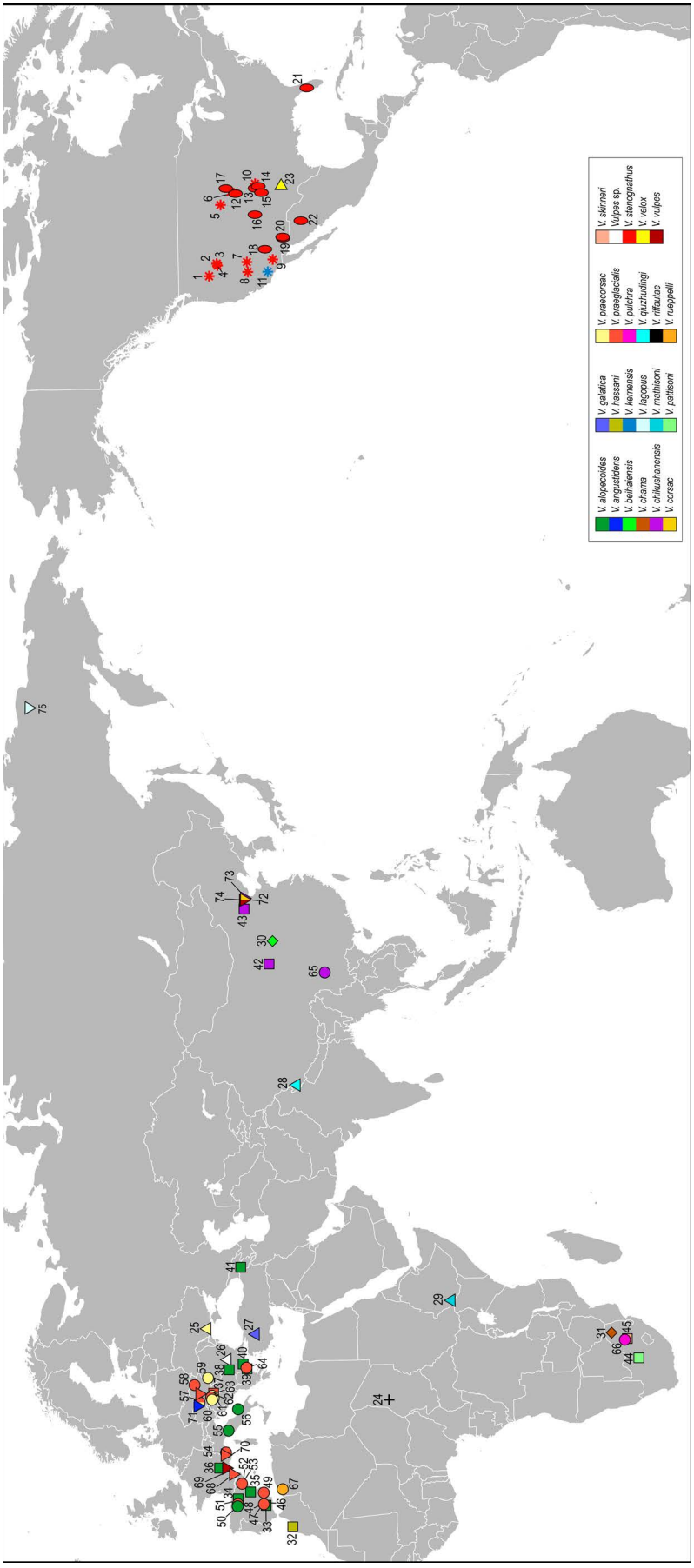
V. skinneri
Vulpes sp.
V. stenognathus
V. velox
V. vulpes
V. praecorsac
V. praeglacialis
V. pulchra
V. qiuzhudingi
V. riffaltae
V. rueppelli
V. galatica
V. hassani
V. kermensis
V. lagopus
V. mathisoni
V. pattisoni
V. alopecoides
V. angustidens
V. beihaiensis
V. chama
V. chikushanensis
V. corsac

layer (Bartow et al., 1983; Baron et al., 2008). The record of *V. stenognathus* is far more extensive compared to that of *V. kernensis*, as both cranial and postcranial elements were retrieved from numerous different sites across North America. Among Caninae, *Vulpes* is one of the first genus to enter into the Old World, as a 7 Myr old species was described from Chad (Fig. 1.11): *Vulpes riffautae* de Bonis et al. 2007 was small-sized, between a modern fennec, *Vulpes zerda* (Zimmermann, 1780), and the Rüppell fox, *Vulpes rueppelli* (Schinz, 1825). Unfortunately, this taxon is difficult to fully characterize as it is known only for two hemimandibles (de Bonis et al., 2007). Another early African species is *Vulpes mathisoni* Geraads et al., 2015 from the ca 4 Myr-old Mursi Formation of Ethiopia. This small species shows hypocarnivorous features in its dentition and it appears to related to the Africa *Vulpes pallida* (Cretzschmar, 1826) and *Vulpes chama* (Smith, 1833) and the Indian *Vulpes bengalensis* (Shaw, 1800) (Geraads et al., 2015). In Eurasia, the earliest occurrences are the MN14-15 records of *Vulpes qiuzhudingi* Wang et al., 2014 from the Zanda Basin (Tibetan Plateau), *Vulpes galaticus* Ginsburg, 1998 from Çalta (Turkey), *Vulpes praecorsac* Kormos, 1932 from the Pliocene deposits of Odessa catacombs (Odinzov, 1965), and *Vulpes* sp. from Musselievo (Bulgaria; Spassov, 2000) (Fig. 1.11). Although age calibration of Zanda Basin is rather uncertain (a large timespan of 1.4 Myr, 5.0-3.6 Ma) and the limited record (two hemimandible fragments), *V. qiuzhudingi* represents one of the largest and surely the oldest species of *Vulpes* to show hypercarnivorous adaptations (Wang et al., 2014). The only other species that shows comparable adaptations is *Vulpes lagopus* (Linnaeus, 1758), and therefore, if confirmed, *V. qiuzhudingi* would represent the earliest ancestor of the extant arctic fox. In east Asia, around 3.3-3.2 Ma, *Vulpes beihaiensis* Qiu & Tedford, 1990 thrived in the Yushe Basin (China). The small-sized Chinese species is well represented by cranial and mandibular specimens, morphologically resembling the extant *Vulpes corsac* (Linnaeus, 1768) (see Qiu & Tedford, 1990). Compared to other canids recovered from the Yushe basin (see section 1.5., 1.7.-

1.8.), the genus *Vulpes* is surely the least represented. Together with the record of *V. praecorsac* of Odessa (explained in detail below), the record of a *Vulpes* sp. in the Bulgarian site of Musselievo (correlated to the second half of the MN15, Popov, 2001) represent one of the earliest records of Europe (Spassov, 2000). The name Ginsburg (1998) gave to the fox species from Çalta, *V. galaticus*, violates the Art. 31.2 of the International Code on Zoological Nomenclature (1999) and should be therefore cited as *Vulpes galatica* Ginsburg, 1998.

During the Quaternary, the fossil record of *Vulpes* testifies to a significant increase in diversity especially in Africa. Geraads (1997) described a small form of fox from Ahl al Oughlam (Morocco) as *Vulpes* aff. *rueppelli*, later ascribed to *Vulpes hassani* Geraads, 2011. *V. hassani* is smaller compared to *V. rueppelli* but larger than *V. pallida*. It further possesses some different dental features (*e.g.*, absence of P4 parastyle, P4 L intermediated between that of *V. pallida* and *V. rueppelli*, when compared to the M1-M2 L; Geraads, 2011). The record South Africa consists of three species: the 1.977 Myr-old *Vulpes skinneri* Hartstone-Rose et al., 2013 from Malapa Cave; the *Vulpes pulcher* Brooms, 1939 from Kroomdrai A (and probably Swartkrans); and *Vulpes pattisoni* Broom in Broom & Schepers, 1946 from Taung. All these species were described almost exclusively on mandibular specimens (although a rib attributed to *V. skinneri* was described by Hartstone-Rose et al., 2013). The name introduced by Broom (1939) to describe the small fox from Kroomdrai A has to be amended according to the International Commission on Zoological Nomenclature (1999: Art. 31.2), and the species cited as *Vulpes pulchra* Broom, 1939. In the original and following descriptions (*e.g.*, Ewer, 1956), *V. pulchra* is considered much larger than *V. chama*, but Hartstone-Rose et al. (2013) showed this is true only for certain proportions (*e.g.*, p4, m1 and m2 L), whereas for others the two species are very similar one another. Hartstone-Rose et al. (2013) put forward the hypothesis that the type specimen of *V. pattisoni* is that of a subadult/young adult, explaining the apparent size gap between the

hemimandible corpus and the size of the m2. *V. skinneri* is close in size to *V. chama* but with proportionally larger m2 and stronger angular process (Hartstone-Rose et al., 2013). After *V. beihaiensis* of Yushe basin, foxes disappear from the east Asian record for the rest of the Yushean. In early Nihewanian localities, like Longdan (Qiu et al., 2004), Classic Nihewan fauna (Teihlard de Chardin, 1940) and Yuanmou (Wang et al., 2013b) appears *Vulpes chikushanensis* Young, 1930. Despite these earlier findings, the species was described by Young (1930) from Chi ku shan (according to modern romanization Jigushan, known as Zhoukoudian Loc. 6), therefore its record extends in the middle Pleistocene. This medium-sized fox has been considered close to *V. corsac* (Qiu & Tedford, 1990) and to *V. praecorsac* from Odessa Catacombs (Qiu et al., 2004).

The Early Pleistocene European record of *Vulpes* is rather confused and debated. Four species were described: *Vulpes alopecoides* (Del Campana, 1913) (see below section 1.6.1.) from Tasso (Upper Valdarno, Italy), *Vulpes praeglacialis* (Kormos, 1932) and *V. praecorsac* from Villany (Hungary) and *Vulpes angustidens* Thenius, 1954 from Hundsheim (Germany). The scarce record used to erect these species, has created a strong debate among scholars to understand the possible relationship with extant foxes, especially *Vulpes vulpes* (Linnaeus, 1758) and *V. lagopus*, or with one another. *V. praecorsac* is characterized reduction of metaconids of m1 and m2 and proportionally large premolars, feature shared with *V. vulpes* and *V. corsac* (Tedford et al., 2009). As evident even from the name, Kormos (1932) proposed a close relationship between the small-sized fox *V. praecorsac* from Villany and the slender extant *V. corsac.* The presence of some dental differences between the two taxa was explained as the retention of archaic features in the Early Pleistocene compared to the extant Corsac fox. In the extensive Canidae record recovered from the Catacomb of Odessa, Odtinzov (1965) described the smaller remains as belonging to *V. praecorsac*, mainly for their size (smaller than other fossil foxes known at the time but still larger from the types of Villany). If the attributions

to *V. praecorsac* should be confirmed, this species would have a great hiatus (ca 1.6 Ma) between its first appearance in eastern Europe and later record. Other central-southern European sites with *V. praecorsac* are Villany 3-5 (Hungary; Jánossy, 1986), Betfia-2 (Romania; Terzea, 1996), Deutsch Altenburg 2C (Austria; Rabeder, 1976), and Somssich-Hill 2 (Gasparik & Pazonyi, 2018).

In literature, *V. alopecoides* has been reported from Early Pleistocene sites as St. Vallier (France; Viret, 1954); Dafnero-1 (Greece; Koufos, 2014), Villarroya (Spain; Villalta, 1952), La Puebla de Valverde (Spain; Kurtén & Crusafont-Pairò, 1977), Volax, Sesklon, Kastritsi, Makinia (Greece; Koufos, 2014), Fonelas-P1(Spain; Garrido, 2008), Dmanisi (Georgia; Krijgsman et al., 2019), Upper Valdarno (Italy; Del Campana, 1913), Pirro Nord (Italia; Petrucci et al., 2013) and *Vulpes* cf. *alopecoides* was reported from Trinchera Elefante TE9 (Spain; Carbonell et al., 2008) (Figs. 1.11-1.12). This species was originally considered affine to the lineage of *V. corsac* (Stehlin, 1933) but then generally reinterpreted as the ancestor of modern red fox (Viret, 1954; Kurtén, 1968; Rabeder, 1976). *V. praeglacialis* comes from late Early Pleistocene localities like: Villany 3-5 (Hungary; Jánossy, 1986), Venta Micena, Barranco Leon-5, Fuente Nueva 3 (Spain; Madurell-Malapeira et al., 2014), Betfia-2 (Romania; Terzea, 1996), Cal Guardiola, Vallparadís Estació (Spain; Madurell-Malapeira et al., 2014), Apollonia-1 (Greece; Koufos, 2018), El Chaparral (Spain; Madurell-Malapeira et al., 2014), Le Vallonnet (France; Moullé, 1992), Gombaszög/Gombasek (Slovakia; García & Arsuaga, 1999), Deutsch Altenburg 2C (Austria; Rabeder, 1976), Villany 8-6 (Hungary; Jánossy, 1986), Atapuerca Trichera Dolina 6 TD6 (Spain; García & Arsuaga, 1999), Cuane de l'Arago (France; Moigne et al., 2006), L'Escale (France; Bonifay, 1971) (Fig. 1.11). Kormos (1932) deemed *V. praeglacialis* to be close to extant arctic fox, thus ascribing the fossil taxon to *Alopex* Kaup, 1829 (former generic name of *V. lagopus*). Rabeder (1976) put forward different hypotheses regarding the affinities of Early-middle Pleistocene foxes. Studying the material from Deutsch-Altenburg 2C, the author

included *V. alopecoides*, *V. praeglacialis* and *V. angustidens* from Hundsheim in a phyletic line leading to the modern *V. vulpes*. This lineage seems to characterized by the increase in size and a modest reduction of the molars (Rabeder, 1976). The authors favored the inclusion of *V. praecorsac* in the lineage of *V. corsac*, but excluded an ancestor-descendant relationship between the two species. According to Rabeder (1976), the arctic fox diverged from the fossil stock of *Vulpes* during the Pliocene, well before the European record (somewhat predating the interpretation of Wang et al., 2014 on *V. qiuzhudingi*).

The modern red fox appeared in the middle Pleistocene of Eurasia (Kurtén, 1968). Pei (1934) ascribed to "*V.* cf *vulgaris*" (Pei, 1934: 37; = *V. vulpes*) few dental specimens of Locality 1 of Zhoukoudian (ZKD) and several cranial fragments of Locality 3 of ZKD. Age calibration of the ZKD localities has been problematic. According to Li et al. (2014), *V. vulpes* remains comes from layers 8-11 of Locality 1, the oldest of the assemblage, dated around 780-700 ka (Shen et al., 2009). Locality 3 appears to be younger than Locality 1 (Jiangzuo et al., 2018), therefore >400 ka (Shen et al., 2009). Although the attribution of Pei (1934) should be revised, the record of Locality 1 might be the earliest of *V. vulpes* of Old World. More certain attributions come from the French sites of Lunel-Viel (Bonifay, 1971), the oldest record of the species in Europe. A doubtful middle Pleistocene single occurrence of *V. vulpes* comes from Thomas Quarry 1, level "Grotte des Hominides" (correlated to ca 600 ka Geraads, 2011) in North Africa. Indeed Geraads (2011), discussing the weathered mandible with worn premolars and carnassial and commented "*In any case, this poor specimen, being of very doubtful age and perhaps even sub-fossil, is of little significance.*" Geraads, 2011: 432). Late Pleistocene deposits (*e.g.*, Doukkala and "Grotte de Gazelles") offers more valid evidence of the arrival of the red fox into North Africa (Geraads, 2011).

The extant *V. lagopus* is firstly recorded in the Siberian Olyorian Fauna around 700 ka (Sher, 1986; Lister, 2004) but never reached western Eurasia until the late middle

Pleistocene-Late Pleistocene (Kahlke, 2014). During the recent glacial stages (MIS5d-2) it is part of the widespread *Mammuthus-Coelodonta* faunal complex that ranged from eastern Siberia to Spain (Kahlke, 2014).

The earliest record of thee extant *V. corsac* seems to be that of Zhoukoudian Locality 1 (layers 1-3,5, 8 and 9) of the early middle Pleistocene (Pei, 1934). In the late Pleistocene seems to have been recorded in Swiss and bohemian localities (Stehlin, 1933; Kurtén, 1968) but it far more abundant in Asian record from the Urals to China (Kosintsev, 2007).

Modern Rüppell fox earliest appearance datum might be that of *V.* cf. *rueppelli* from Tighennif (Ternifine, Algeria; Geraads, 2011), probably referable to Jaramillo subchron (ca 1 Ma, Geraads, 2016). Geraads (2011; 2016) suggested this form to the derived from *V. hassani* of Ahl al Oughlam, although no phylogeny has ever tested the affinity of fossil foxes.

Werdelin & Peigné (2010) listed several record of *V. chama* from numerous Late Pliocene-Pleistocene sites of the Cradle of Humankind: Makapansgat Mbs 3, Sterkfontein, Drimolen, Swartkrans, Elandsfontein Main Site and 4, Saldanha Sea Harvest, Elands Bay Cave, Swartklip. Recently, Herries et al. (2015) described a new record of the species from the 2.61 Myr-old site of Drimolen Makondo (Herries et al., 2018). The fossil history of the other species of *Vulpes* is still greatly unknown.

The North American record of foxes is even more discontinuous than the European one (Kurtén & Anderson, 1980): from Early Pliocene (early Blancan) fossils the record disappears until middle Pleistocene times (late Irvingtonian; Tedford et al., 2009). *Vulpes velox* (Say, 1823) might have arisen from the form *Vulpes* sp. cf *V. velox* (see Tedford et al., 2009) or from Eurasian taxa dispersed into North America. Despite the issue of their origin, both the kit (*Vulpes macrotis* Merriam, 1888) and swift fox thrived in North America by the latest middle Pleistocene- Late Pleistocene (Rancholabrean, Schultz, 1938; Jefferson, 1991).

1.6.2. Nomenclature note on "Canis alopecoides"

In scientific literature the authorship of the Eurasian species *V. alopecoides* has been attributed to Forsyth Major (1875a) or (1877) (*e.g.*, Viret, 1954; Koufos 1992; 1993; 2014; Koufos & Kostopoulos, 1997a; Radulescu et al., 2003; Petrucci et al., 2013). In his review of the Plio-Pleistocene faunas of the Upper Valdarno Basin, published by the Tuscan Society of Natural Sciences in three accounts (1875a; 1875b;1877), Forsyth Major never mentioned the name "*Canis alopecoides*". In the first part, Forsyth Major (1875) cites "*Canis vulpes*" as part of the faunal association of Upper Valdarno, as already described by de Blainville (1841). No other reference to fossil foxes can be found in the other volumes (Forsyth Major, 1875b; 1877). Explanation of the reason why the specific name is always related to Forsyth Major, is reported in Del Campana (1913: 246): "*Questa specie non è mai stata oggetto di una descrizione da parte del Forsyth Major. Sta sotto tale denominazione un frammento di mascellare superiore destro che porta ben conservati i due molari. Fu trovato l'anno 1880 dal sig. Enrico Bercigli nella località del Valdarno superiore denominata "il Tasso", e dal medesimo donata al Museo fiorentino di Geologia e Paleontologia. Il MAJOR nelle sue frequenti fermate presso il Museo di Geologia e Paleontologia di Firenze, vide il fossile in questione e riconosciutolo da un sommario esame come specie affatto distinta, lo pose sotto il nome nuovo di* Canis alopecoides" [This species has never been described by Mr. Forsyth Major. It is reported under such a denomination a right upper maxillary fragment bearing the two well-preserved upper molars. It was found in 1880 by Mr. Enrico Bercigli in the Upper Valdarno site named "Il Tasso", who personally donated it to the Florentine Museum of Geology and Paleontology. During his numerous visits to the Museum of Geology and Paleontology of Florence, Major saw this fossil and, after a short examination by which he acknowledged the specimen as a different (unknown) species, he attributed the name of *Canis alopecoides*]. If Del Campana (1913) is to be believed and the specimen was found

by Mr. E. Bercigli in 1880, Forsyth Major could never have mentioned the species in his works between 1875-1877. Most probably the identification by Forsyth Major, therefore, was only reported on a label of the Museum of Florence. This attribution remained in literature, but *C. alopecoides* clearly represents a *nomen nudum* (failing to satisfy the requirements of Art. 12, International Commission on Zoological Nomenclature, 1999). Del Campana (1913) described and reported the photographs of the specimen in buccal and occlusal view (Del Campana, 1913: Tab. XII, Figs. 6a-6b). The species should be, therefore, cited as "*Canis alopecoides* Del Campana, 1913". In the same manuscript, Del Campana relates to *C. alopecoides* a maxillary fragment which was later referred *Nyctereutes* (Del Campana, 1917; see also section 3.3.). Therefore, the not all the material originally described and figured by Del Campana (1913) are part should constitute the type of *C. alopecoides*. The only specimen from Upper Valdarno referable to the species housed at IGF is IGF 12110.

1.7. *Eucyon* Tedford & Qiu, 1996

1.7.1. Record of Eucyon *from the Old and New World*

After the demise of Hesperocyoninae (Wang, 1994), while Borophaginae were thriving (Wang et al., 1999), the late Miocene (latest Clarendonian-early Hemphillian) was a moment of great diversification for Caninae (see section 1.4.; Fig. 1.7). In this time span, the basal taxa of both tribes Vulpini (*i.e.*, genera *Vulpes* and *Metalopex*) and Canini (Tedford et al., 2009) arose from the last forms of genus *Leptocyon*. In this radiation, the latter tribe is represented by the early genus *Eucyon*, whose first record is that of *Eucyon davisi* (Merriam, 1911) from the early Hemphillian deposits of Oregon, North America (around 8 Ma; Tedford et al., 2009; Fig. 1.13). From that moment on, this group of small- to medium-sized canids remained an important element in the Northern American carnivorans guild for the whole Hemphillian to the early Blancan (Fig. 1.13). With the description

of the new genus, Tedford & Qiu (1996) attempted to provide a solution to the taxonomical issues recognized by researchers who worked on certain taxa clearly different from members of the tribe Vulpini, yet basal to modern Canini (*inter alios* Berta, 1988; Tedford et al., 1991; Rook, 1992). *Eucyon* shares with Canini three synapomorphies: the presence of a frontal sinus invading the postorbital process (unlike Vulpini that generally possess the vulpine crease on the dorsal side of these processes); enlarged paraoccipital processes; loss of the laterally everted zygomatic arches, feature characteristic of Vulpini (Tedford & Qiu, 1996).Furthermore, *Eucyon* possesses a distal accessory cuspulid on the p4 (according to Tedford & Qiu, 1996 feature only displayed by modern wolf and their closed allies), whereas it lacks the transverse cristid connecting he m1 hypoconid and entoconid. In Canini, this cristid is among the diagnostic feature of *Canis sensu lato* lineage (see section 1.8.1.). Despite the limits of the original description, in last two decades several authors have included in *Eucyon* numerous new taxa (Morales et al., 2005; Spassov & Rook, 2006; Howell & García, 2007; García, 2008; Haile-Selassie &

Figure 1.13 – Resuming chronological scheme of the known occurrences of *Eucyon* spp. in both the Old and New World. Degree of inclination of locality names approximate the degree of uncertainty on their dating. Data from: Teilhard De Chardin & Piveteau (1930); Crusafont-Pairó (1950); Odintzov (1967); Martin, 1973; Pons-Moyá & Crusafont-Pairó (1978); Sotnikova (1989); Rook (1992; 1993; 2009); Tedford & Qiu (1996); Kostopoulos & Sen (1999); Li et al. (2003); Radulescu et al. (2003); Tedford et al., (2004; 2009); Morales et al. (2005); Sotnikova (2006); Spassov & Rook (2006); Howell & García (2007); García (2008); Haile-Selassie & Howell, 2009; Montoya et al. (2009); Sotnikova & Rook (2010); Werdelin & Sanders (2010); Geraads (2011); Tedford et al. (2013); Wang et al. (2013b); Werdelin & Lewis (2013); Wang et al. (2014); Koufos (2014); Werdelin et al. (2015). **Abbreviations** – **AEVL 1**, Amba east Vertebrate Locality 1 (Ethiopia); **ALA**, Alatini (Greece); **BRS-CM**, Brisighella-Cava Monticino (Italy); **CAS**, Casino Basin (Italy); **Chkh-1**, Chonokhariakh-1 (Mongolia); **ELFN**, Elandfontein; **KN-LsC**, Khirgis Nur Lower subcomplex (Mongolia); **KN-UsC**, Khirgis Nur Upper subcomplex (Mongolia); **OCat**, Odessa Catacombs (Ukraine); **Po-Le**, Podpusk-Lebyazh'e (Mongolia); **SdN**, Sangin Dalay Nur (Mongolia); **ThCr**, Thousand Creek (U.S.A.); **VER**, Verduno (Italy); **VMo**, Venta del Moro (Spain).

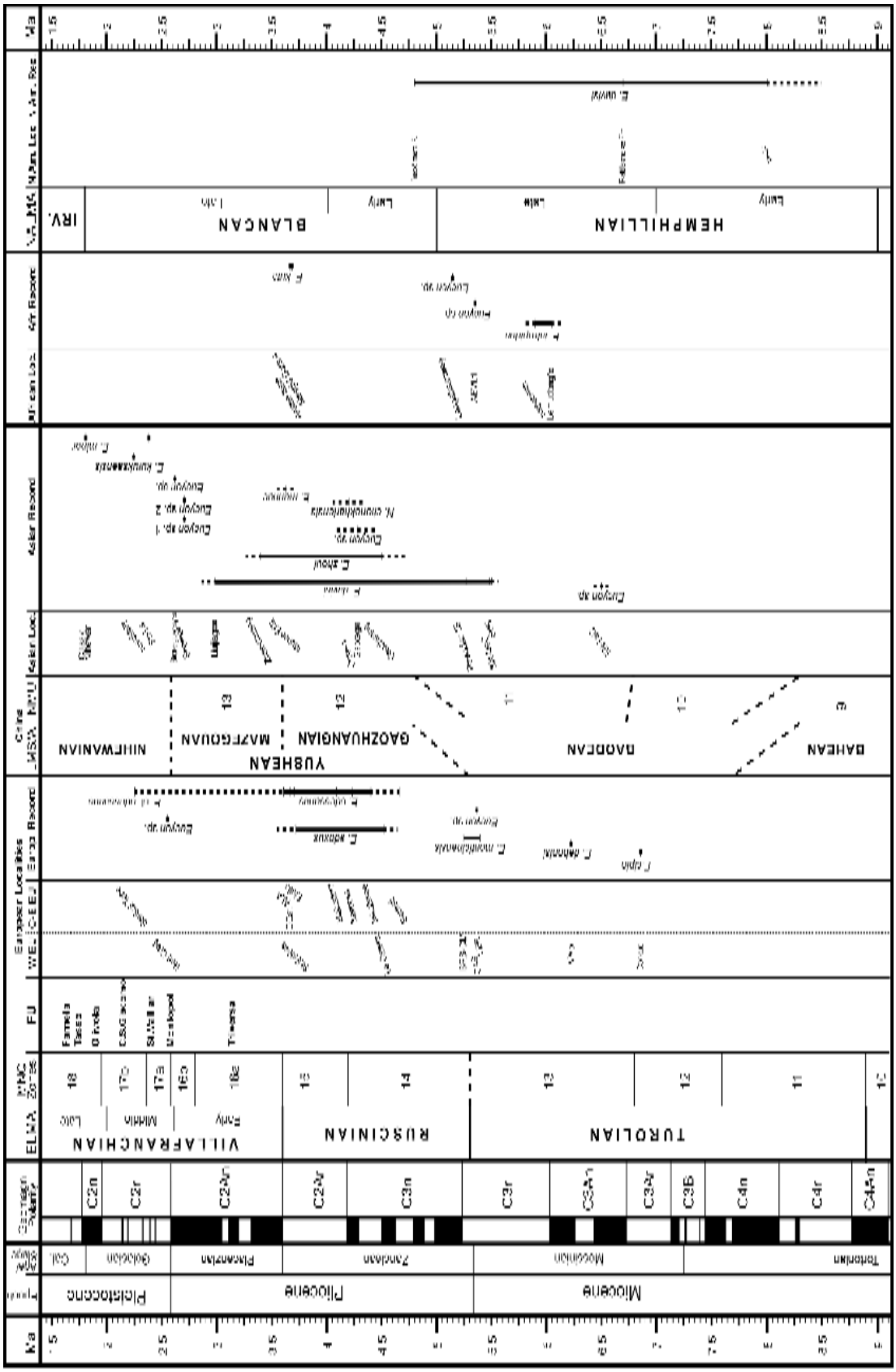

Howell, 2009; Montoya et al., 2009; Werdelin et al., 2015). Other researchers refined the diagnosis of *Eucyon*. Rook (2009) discussed the characters originally put forward by Tedford & Qiu (1996) and added other ones: *e.g.*, a simple angular process, modestly expanded insertion for the inferior ramus of the m. pterigoideus medialis on the medial side of the angular process, and proportionally elongated limbs (radio/tibia ratio >80%). Tedford et al. (2009) revised the diagnosis including the development of the mastoid process (which enlarges in a ridge- or knob-like structure) and included a deep discussion of the cranial and dentognathic features of *Eucyon* compared to *Canis s. l.* species, *i.e.*, the rostrocaudally shorter expansion of the frontal sinus, which does not completely inflate the postorbital process; fan-shaped caudal morphology of the occipital triangle; nuchal crest enlarged at level of the external occipital protuberance; the latter does not overhangs the occipital condyles; I2 and I3 close in size; I3 basal cingulum not prominent; similar sized M1 paracone and metacone; absent of feebly developed M2 metaconule, connected to the protocone by the postprotocrista; entepicondylar foramen on the humerus may be present. These improvements better characterize the genus, allowing more precise attributions of fossil specimens.

After the appearance in the North American record of *E. davisi*, representative of this primitive canid genus dispersed into the Old World in the latest Miocene (Fig. 1.13). Early Asian findings include *E. davisi* and *Eucyon* sp. in Kazakhstan and several Mongolian localities (Khirgis Nur-2 lower and upper subcomplex, Sangin Dalay Nur, Pavlodar 1B, Sotnikova & Rook, 2010) and *E. davisi* and *Eucyon zhoui* Tedford & Qiu, 1996 from the Yushe Basin (China; Tedford &Qiu, 1996). Apparently, the western European record pre-dates the Asian one (Fig. 1.13). The enigmatic species "*Canis*" *cipio* Crusafont-Pairó, 1950 is the earliest member of Canini to be recorded in western Eurasia. This canid comes from the Spanish sites of Concud Cerro della Gariata and Los Mansuetos, both referable to MN12 and dated to 6.9–6.8 Ma (van der Made et al., 2006). The scantiness of

the referred material makes the "*C.*" *cipio* issue thorny: the type specimen (IPS 1988) is a maxillary fragment with P3-M2 and the only other specimen known is an isolated m1. The initial attribution to the genus *Canis* was repeatedly rejected by many scholars (see among others Rook, 1993; 2009; Wang & Tedford, 2008), who acknowledged the basal position of this taxon compared to true *Canis* member, favoring the affinity to *Eucyon*-like canids. Other early record of *Eucyon* in western Europe are the MN 13 record of *Eucyon debonisi* Montoya et al., 2009 from Venta del Moro, Spain (6.23 Ma, Gibert et al., 2013), and the Italian *Eucyon monticinensis* (Rook, 1992) from Brisighella-Cava Monticino and Verduno, and *Eucyon* sp. from the Casino Basin, near Siena (Rook, 2009). Other MN13 Old World record is the African *Eucyon intrepidus* Morales et al., 2005 from the Kenyan locality of Kapsomin and Lemudong'o (Howell & García, 2007). Two other African records are the small-sized *Eucyon* sp. from the Ethiopian Amba east Vertebrate Locality 1, (Kuseralee Member, Sagantole Formation, Middle Awash, 5.5-5.2 Ma; Haile-Selassie & Howell, 2009) and the South African Langebaanweg record (Earliest Pliocene) of Eucyon sp. composed of a cranium, a mandible and postcranial material never described (Rook, 1993).

Considering all these late Miocene-Early Pliocene occurrences, Sotnikova & Rook (2010) defined the "*Eucyon* event" to remark the synchronous character of the spreading of the genus across the Old World. This geologically instant spreading, coupled with the considerable increase in diversity of Caninae (not only *Eucyon*), deeply influenced the latest Miocene and the Early Pliocene Oloarctic communities. *Eucyon*, *Vulpes* and *Canis*, along with *Nyctereutes* in Eurasia, became common elements in Pliocene sites and radiated into various species (Qiu et al., 2004; Rook, 2009; Tedford et al., 2009; Figs. 1.9-1.14) or even short-lived taxa, *e.g.*, *Nurocyon chonokhariensis* Sotnikova, 2006.

Renowned Pliocene Eurasian species are *Eucyon odessanus* (Odintzov, 1967) from Odessa Catacombs and *Eucyon adoxus* (Martin, 1973) from La Calera (Spain) and

Saint-Estéve (France). Originally described as *Vulpes odessana* by Odintzon (1967) from the extensive record of catacombs of Odessa, it has been recognized from other MN14-15 localities of eastern Europe like Etulia, Nikolskoe and Novaja Karbolia (Moldova, Rook, 1993), Beresti and Malusteni (Romania, Radulescu et al., 2003). Other localities with canids attributed to *E. odessanus* are two hemimandibles from Megalo Emvolon/Alatini (Greece, Koufos, 1997; Rook, 2009) and a rather late attribution by Kostopoulos & Sen (1999) from Sarikol Tepe (MN 17; Turkey). Another Early Pleistocene occurrence of *Eucyon* in Europe is that from Red Crag Formation, assigned to *E. adoxus* by Pons-Moyá-Crusafont-Pairó (1978) but later cited as *Eucyon* sp. (Rook, 1992; 1993). While in North America the species was already extinct, E. davisi thrived in Asia at least until the Mazegouan, as testified by its Yushe Basin record (Liujiagou, Tedford & Qiu, 1996). Spassov & Rook (2006) attributed two rather large mandible specimens from the late MN15 Muhor-Erig site (Mongolia) to *Eucyon marinae* Spassov & Rook, 2006. This taxon seems to possess some features consistent with hypercarnivorous diet (*e.g.*, reduced m1 metaconid and entoconid; Spassov & Rook, 2006). Other findings of *Eucyon* from the Tranbaikalian and Mongolian regions might be related to this taxon (Sotnikova & Rook, 2010): *Eucyon* sp. from Beregovaya (Transbaikalia) and *Eucyon* sp. 1 from Shamar (Mongolia; Sotnikova, 2004). *Eucyon* sp. 2 from Shamar described by Sotnikova (2004) shows a mixed pattern of primitive and derived features, possibly belonging to a new species. Interesting although taxonomically complex is the record of Kuruksay (Tajikistan, Sotnikova, 1989), dated to the Early Pleistocene, MN 17. *Canis kuruksaensis* Sotnikova, 1989 is represented by a cranium and two hemimandible fragments. These specimens possess typical *Eucyon* features (*e.g.*, caudal fan-like shape of the nuchal crest; lack of a crista transversa between m1 entoconid and hypoconid) and other more advanced ones (*e.g.*, P4 elongated compared to the M1; larger M1 paracone compared to the metacone).Nevertheless, there is the general consensus in considering this

species as an *Eucyon* one (Tedford personal comm. in Spassov & Rook, 2006). Contemporary findings in Podpusk–Lebyazh'e (Kazakhstan) appear to be related to the small Early Pleistocene *Eucyon minor* (Teilhard de Cardin & Piveteau, 1930) (Fig. 1.13). This small-size species was described from Sangkanho, Nihewan Basin (China) on a fragmentary mandible with typical *Eucyon* features in the lower teeth (distal accessory cuspulid on p4 and no cristid between m1 hypoconid and entoconid). Nowadays, this Chinese record represent the latest occurrence of the genus *Eucyon*. In Africa, during the most of the Pliocene no record of *Eucyon* can be found (Fig. 1.13). Recently, Wederlin et al. (2015) described two rather large hemimandibles from the Afar Region, particularly from Aralee Issie (3.82-3.57 Ma) and Mesgid Dora locality 4, ascribing that to the new species *Eucyon kuta* Werdelin et al., 2015.

1.7.2. Scientific debate around Eucyon *and* Eucyon*-like taxa*

Tedford & Qiu (1996) explicitly acknowledged the paraphyletic nature of the *Eucyon*, which in truth it embraces several taxa, primitive compared to *Canis s. l.* group but probably originated from different ancestors. Recently a total evidence phylogenetic analysis by Zrzavý et al. (2018) supported this hypothesis, as some *Eucyon* species stem at the base of *Canis s. l.* group (*i.e.*, *E. zhoui* and *E. marinae*). Some authors have cast doubts on the actual possibility of recognition of the genus (Geraads, 2011; Werdelin et al., 2015), whereas some others have put forward the idea of alternative denomination for some of the species referred to *Eucyon* (Ivanoff, 1996; Sotnikova & Rook, 2010). As a consequence of this debate, the systematic status of some *Eucyon* species and *Eucyon*-like taxa is disputed. The discussion surrounding "*C.*" *cipio* has already been outlined in the previous section. The late Pliocene *E. adoxus* was interpreted as *Canis* (Martin, 1973) and *Vulpes* (Pons-Moyá & Crusafont-Pairó, 1978), but now is generally referred to *Eucyon* (*inter alios* Rook, 2009). Ivanoff, 1996 put forward the hypothesis of ascribing the

"*Eucyon*" *odessanus* material to a different genus, intermediate between *Eucyon* and *Canis*, based on its peculiar cranial features. Similarly, the position of the taxon from Kuruksay is debated in literature and its peculiarity lies in the set of features that was interpreted by Sotnikova & Rook (2010) as the most affine to *Canis* among *Eucyon*-like taxa. For this reason, it will be here addressed it as "*E.*" *kuruksaensis*. The position of *N. chonokhariensis* from Chonokhariakh (Mongolia) in the phylogenetic analysis of Zrzavý et al. (2018), *i.e.*, clustered within *Nyctereutes*-group. The odd result may be due to the scantiness of the type material of *Nurocyon* Sotnikova, 2006 (*i.e.*, one cranium and a maxillary fragment). Sotnikova (2006) pointed out some hypocarnivorous features in the upper teeth of this taxon, *i.e.*, the similar size of M1 and M2 paracone compared to the metacone, the relative size of the M1 metaconule. The result markedly contrasts with the diagnostic cranial and dentognathic morphologies possessed by *Nurocyon* compared to those of raccoon dogs, and even other member of Vulpini. Most probably the superficial similarity between *Nyctereutes* and *Nurocyon* is the result of independent development of hypocarnivorous features in *Nurocyon*, resulting from convergent evolution (as already noted by Sotnikova, 2006). The rather distinctive set of cranial characteristics possessed by *N. chonokhariensis* suggests a close affinity to *Eucyon*-like species, although showing more derived features shared with *Canis* spp. Sotnikova & Rook (2010) deemed *E. adoxus* and *C. ferox* to be the only two taxa of the Oloarctic Canini with a remote resemblance to *Nurocyon* (Sotnikova, 2006 put forward the redescription of *E. adoxus* under *Nurocyon*). The scantiness of the African material makes the African species particularly dubious. Of these, García (2008) described a taxon from Aramis (Ethiopia) as *Eucyon wokari* García, 2008. Nevertheless, this record has been questioned by several authors (Rook, 2009; Sotnikova & Rook, 2010; Werdelin et al., 2015) for the presence of several features uncommon in *Eucyon* but often present in some taxa of Vulpini (*i.e.*, the M3 alveolus; a feeble yet evident transverse cristid). Following this possible

attribution to Vulpini, its record was not reported in Fig. 1.13.

1.8. *Canis* Linnaeus, 1758

1.8.1. Neontological controversy on Canis sensu lato*-group*

Several of the most iconic and renowned species of Canidae belong to the genus *Canis*. In recent years, the clade of species related to *Canis* (see Fig. 1.6) has been object of numerous scientific papers showing the existence of underestimated pattern of affinities (Rueness et al., 2011; Gaubert et al., 2012; Koepfli et al., 2015; Bertè, 2017; Viranta et al., 2017). Particularly, molecular research showed that the genus *Canis* as commonly used in conservation biology and by science popularization is paraphyletic (*inter alios* Wayne et al., 1997; Zrzavý & Řičánková, 2004; Lindblad-Toh et al., 2005; Wayne & Ostrander, 2007; Koepfli et al., 2015; Zrzavý et al., 2018) as "*Canis*" *mesomelas* Schreber, 1776 and "*Canis*" *adustus* Sundevall, 1847 cluster outside of the clade including *Lycaon pictus* (Temminck, 1820), *Cuon alpinus* (Pallas, 1811) and the true *Canis* species (Fig. 1.6). This considered, many scholars (*inter alios* Zrzavý & Řičánková, 2004, Viranta et al., 2017) has proposed two possible solutions to address this issue: one is to include all the species of the clade *Canis sensu lato* (*i.e.*, "*C.*" *adustus*, "*C.*" *mesomelas*, *C. alpinus*, *L. pictus*, and the other *Canis* spp.) within the genus of *Canis*. Alternatively, the side-striped jackal, "*C.*" *adustus*, and the black-backed jackal, "*C.*" *mesomelas* could be included under different generic names. Zrzavý & Řičánková (2004) found that the side-striped and the black-backed jackals do not cluster together into a clade, but stem separately at the base of the *Canis-Cuon-Lycaon* clade. Therefore, the authors proposed to refer the side striped jackal to the genus *Schaeffia* Hilzheimer, 1906 and the black backed one to *Lupulella* Hilzheimer, 1906. In other molecular phylogenies (*e.g.*, Lindblad-Toh et al., 2005; Zrzavý et al., 2018) these canids form a monophyletic clade and are synonymized under *Lupulella* (that has priority on *Schaeffia* following the Article 23, International Commission on Zoological

Nomenclature, 1999). The different generic attribution for the two African jackals based exclusively on molecular ground opens the issue for field zoologists and paleontologists of finding the morphological evidence supporting this distinction. No work has endeavored to address this problem yet.

1.8.2. Short review of the fossil record of **Canis** *across the Old World*

Figure 1.14 – Resuming chronological scheme of the known occurrences of species of *Canis s.l.* group in both the Old and New World. Generic names of the fossil species were reported as described by original authors (see text). Degree of inclination of locality names approximate the degree of uncertainty on their dating. Data from: Del Campana, 1913; Teilhard De Chardin & Piveteau (1930); Broom (1948); Thenius (1954); Ewer, 1956; Rabeder (1976); Kotlia (1987); Sotnikova (1989); Rook (1993; 1994); Vekua (1995); Koufos & Kostopoulos (1997a; 1997b);García & Arsuaga (1999); Werdelin & Lewis (2000; 2013); Sotnikova (2001); Qiu et al. (2004); Tedford et al., (2004; 2009); Lacombat et al. (2006); Garrido (2008); Garrido & Arribas (2008); Martínez-Navarro et al. (2009); Boudadi-Maligne (2010); Patniak & Nanda (2010); Sotnikova & Rook (2010); Werdelin & Sanders (2010); Brugal & Boudadi-Maligne (2011); Geraads (2011); Pacheco et al. (2011); Werdelin & Dehghani (2011); Tong et al. (2012); Madurell-Malapeira et al. (2013; 2014); Petrucci et al. (2013); Tedford et al. (2013); Wang et al. (2013b); Cherin et al. (2014); Ghezzo & Rook (2014); Koufos (2014); Wang et al. (2014; 2015); Bartolini Lucenti & Rook (2016); Bartolini Lucenti et al. (2017); Gasparik & Pazonyi (2018); Jiangzuo et al. (2018). **Abbreviations** – AaO**,** Ahl al Oughlam (Morocco); **ABou**, Aïn Boucherit (Algeria); **AHan**, Aïn Hanec (Algeria); **APL1**, Apollonia-1 (Greece); Ata**p. TD6**, Atapuerca Trinchera Dolina 6 (Spain); **Atap. TE**, Atapuerca Trinchera Elefante (Spain); **B. Leon 5**: Barranco Leon 5 (Spain); **CGR**, Cal Guardiola (Spain); **Chikoian FC**, Chikoian Faunal Complex (Mongolia, Russia); **DA 2C**, Deutsch Altenburg 2C (Austria); **DrMk**, Drimolen Makondo (South Africa); **ELFN**, Elandfontein (South Africa); **EVT**, Vallparadís Estació; **F. Nueva 3**, Fuente Nueva 3; **TSn**, Fan Tsun (China); **HDSH**, Hundsheim (Germany); **K Fora KBS**, Koobi Fora KBS (Kenya); **Laetoli UB**, Laetoli Upper Beds (Tanzania); **LVal**, Le Vallonnet (France); **Mkps3**, Makapansgat 3 (South Africa); MOSB, Mosbach (Germany); **OH1-GR1**, Oulad Hamida1-Grotte des Rhinoceros (Morocco); SSMZ, Shanshenmiaozui (China); **Stkfn**: Sterkfontein (South Africa); **Th1-GH**, Thomas 1 Quarry-Grotte des Hominides (Morocco); **ThCr**, Thousand Creek (U.S.A.); **UISIW**, Upper Indian Siwalik (India); **UPSIW**, Upper Pakistan Siwalik (Pakistan); **ZKD**, Zhoukoudian (China).

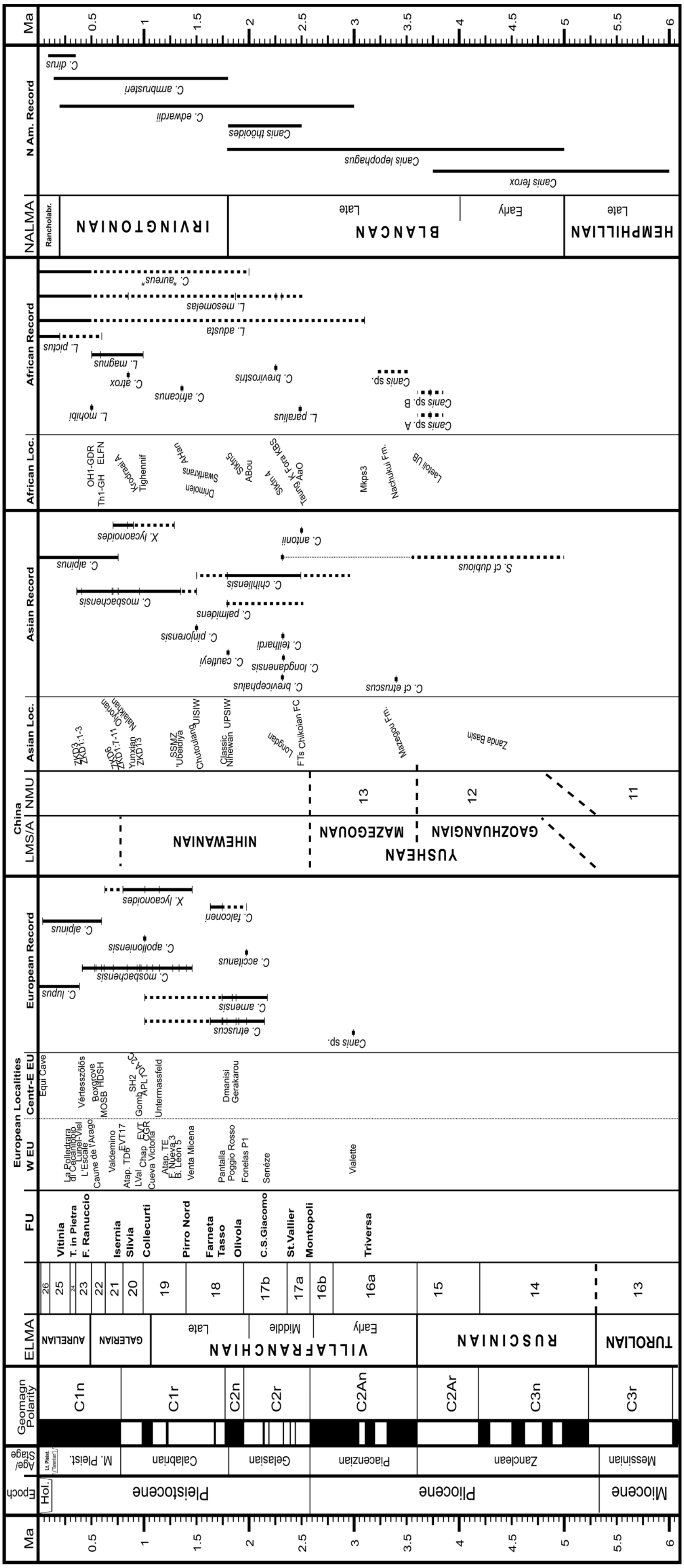

Ma
N Am. Record
C. dirus
C. armbrusteri
C. edwardii
Canis thooides
Canis lepophagus
Canis ferox
NALMA
Rancholabr.
IRVINGTONIAN
BLANCAN
Late
Early
HEMPHILLIAN
African Record
C. "aureus"
L. mesomelas
L. adusta
L. pictus
L. magnus
C. atrox
C. africanus
C. brevirostris
Canis sp.
L. mohibi
L. paralius
Canis sp. B
Canis sp. A
African Loc.
Asian Record
X. lycaonoides
C. antonii
C. alpinus
S. cf dubious
C. chihliensis
C. mosbachensis
C. palmidens
C. pinjorensis
C. teilhardi
C. cautleyi
C. longdanensis
C. brevicephalus
C. cf etruscus
Asian Loc.
Zanda Basin
China
NMU
LMS/A
NIHEWANIAN
MAZEGOUAN
GAOZHUANGIAN
YUSHEAN
European Record
C. falconeri
C. apolloniensis
C. accitanus
C. lupus
C. arnensis
C. etruscus
Canis sp.
European Localities
W EU
Centr-E EU
FU
Vitinia
T. in Pietra
F. Ranuccio
Isernia
Slivia
Collecurti
Pirro Nord
Farneta
Tasso
Olivola
C.S.Giacomo
St.Vallier
Montopoli
Triversa
ELMA
AURELIAN
GALERIAN
VILLAFRANCHIAN
Late
Middle
Early
RUSCINIAN
TUROLIAN
Geomagn Polarity
C1n
C1r
C2n
C2r
C2An
C2Ar
C3n
C3r
Age/ Stage
M. Pleist.
Calabrian
Gelasian
Piacenzian
Zanclean
Messinian
Epoch
Hol.
Pleistocene
Pliocene
Miocene

Within the scenario of evolutionary radiation of Caninae during latest Miocene, the first species attributed to genus *Canis* is *Canis ferox* Miller & Carranza-Castañeda, 1998 recovered in the Lower Rancho Viejo Beds (New Mexico, United States), and referred to late Hemphillian (Miller & Carranza-Castañeda, 1998; Flynn et al., 2005b). Tedford et al. (2009) recognized the basal position of *C. ferox* in their phylogeny of Caninae, as this taxon stems at the base of the clade of *Canis s. l.* (the clade including *Canis*, *Xenocyon* Kretzoi, 1938, *Cuon* Hodgson, 1838 and *Lycaon* Brookes, 1827). Other research also confirms this (*e.g.*, Zrzavý et al., 2018). In Eurasia, the record of *Canis* (with the exception of "*C.*" *cipio*, now generally referred to *Eucyon*, see section 1.7.) begins in eastern Asia in the Late Pliocene (early Piacenzian, early Villafranchian) and in central Asia and Europe in the Early Pleistocene (Gelasian, MN17, Coste S. Giacomo Faunal Unit) (see Fig. 1.14). The earliest record of *Canis* is the 3.4 Myr-old *Canis* sp. from Mazegou Formation in the Yushe Basin (Shanxi Province, China; Flynn et al., 1991), later identified as *Canis* cf. *etruscus* (Qiu & Flynn 2013; Qiu & Tedford 2013). Three species have been customarily distinguished from the Late Pliocene-Early Pleistocene of Asia: the large-sized *Canis antonii* Zdanski, 1924 and *Canis chihliensis* Zdanski, 1924; and the smaller and coyote-sized *Canis palmidens* Teilhard de Chardin & Piveteau, 1930 somewhat equivalent to the North American *Canis edwardii* Gazin, 1942. The former two species possess several hypercarnivorous features (Tong et al., 2012), resembling some later European species (see Rook, 1994), possibly related to the clade of hypercarnivorous canids such as *Xenocyon*, *Lycaon* and *Cuon* (see Tedford et al., 2009). Another interesting record related to the fossil hypercarnivorous taxa is the Early Pliocene of Zanda Basin *Sinicuon* cf. *dubius* (Wang et al., 2015). Indo-Pakistan area are renowned for their Plio-Pleistocene record, although much geological and paleontological research is needed to refine the understanding of its biochronology, deposition processes etc. (Patniak & Nanda, 2010). The canid record of the region includes: *Canis curvipalatus* Bose, 1880 (although it might

represent an early representant of the lineage of *Otocyon*, see Wang & Tedford, 2008; thus not included in Fig. 1.14); the Early Pleistocene *Canis cautleyi* Bose, 1880 and *Canis pinjorensis* Gaur, 1987; and the middle Pleistocene taxon *Canis vitastensis* Kotlia, 1987 (though some of the morphological features of the holotype adverse the ascribtion to *Canis*, *e.g.*, the presence of the m2 paraconid; the taxon was excluded from Fig. 1.14).The affinities of *C. cautleyi* and *C. pinjorensis* are still unclear. The former is probably part of the late Villafranchian canids *ex gr. Canis etruscus* Forsyth Major 1877 (see Torre, 1979; Rook, 1993).

Based on current evidence, the genus *Canis* is not recorded in Europe until the Early Villafranchian (Late Pliocene) — a summary of the chronological distribution of Late Pliocene and Pleistocene medium- and large-sized canids of Europe is provided in Fig. 1.14. Historically, from a biochronological viewpoint, the first appearance datum of *Canis* spp. in western Europe marked the onset of the so-called "Wolf event", dated to ca. 2.0–1.8 Ma (Azzaroli, 1983; Azzaroli et al., 1988). However, subsequent discoveries have indicated an earlier dispersal of canids into Europe, based on scarce specimens attributed to *Canis* cf. *etruscus* from Coste S. Giacomo FU (late Middle Villafranchian, Italy; Rook & Martinez-Navarro, 2010) and specimens of *Canis* sp. from the Vialette (Early Villafranchian, ca. 3 Ma; Lacombat et al., 2008; Fig. 1.14). These finds not only predate the Wolf event as classically defined, but show its diachronous nature (Sotnikova & Rook, 2010), thus questioning its significance as a biochronological event (Sardella & Palombo, 2007). Because of this fact, some authors (Martínez-Navarro, 2010; Rook & Martinez-Navarro, 2010) have suggested to redefine the faunal turnover that took place ca. 2 Ma as the "*Pachycrocuta brevirostris* event", based on the dispersal of this large superscavenger hyenid into Eurasia.

Subsequently from the oldest dispersal of true *Canis* into Europe, during the Pleistocene, several different species of canids are recorded in this continent. Ever since the pioneering study by Del Campana (1913), for many years the complex

taxonomic status of extinct species of *Canis* in Europe has been investigated (summarized in Brugal & Boudadi-Maligne, 2011; Cherin et al., 2014; Bartolini Lucenti & Rook, 2016). At least three species are currently considered valid, being mostly distinguished on the basis of general size and proportions, as well as particular craniodental and/or postcranial features: *C. etruscus* (ca. 2.0 Ma, Olivola, Italy); *Canis arnensis* Del Campana, 1913 (ca 1.8 Ma, Upper Valdarno); and *Canis mosbachensis* Soergel, 1925 (ca 1.4 Ma, southern and central Europe). The taxonomic distinction of these species is relatively well founded based on the diagnostic features reviewed by several authors (respectively, Sotnikova, 2001; Cherin et al., 2014; Bartolini Lucenti & Rook, 2016), even if the taxonomic status of *C. mosbachensis* as a distinct species (instead of subspecies) from *C. lupus* is still debated (see Flower & Schreve, 2014). The phylogenetic relationships among these species and relative to extant species of the genus, in any case, are still highly debated (*e.g.*, Kurtén, 1974; Tedford et al., 2009; Brugal & Boudadi Maligne, 2011), and some additional species of more dubious taxonomic validity or generic ascription are distinguished by other authors (see below).

Among the earliest and well-documented evidence of *Canis* from the Early Pleistocene of Europe comes from the Italian sites of Olivola (Val di Magra, Tuscany, ca. 2 Ma; Rook & Martínez-Navarro, 2010) and Poggio Rosso (Upper Valdarno, Tuscany; ca. 1.9–1.8 Ma; Napoleone et al., 2001, 2003), where three different species of canids are recorded (Del Campana, 1913; Torre, 1968; Azzaroli, 1983; Rook, 1992): *C. arnensis*, *C. etruscus* and *Canis falconeri* Forsyth Major, 1877 (Fig. 1.14). Martínez-Navarro & Rook (2003) transferred the latter species from genus *Canis* to *Lycaon*, but not all scholars agree with this conclusion (Hartstone-Rose et al. 2010; Tong et al., 2012). The medium-sized *C. etruscus* and *C. arnensis* are characteristic elements of the early Late Villafranchian faunas of southern Europe (Torre, 1967; Koufos, 1987; Cherin et al., 2014; Bartolini Lucenti & Rook, 2016). Outside Italy, they have also been found in several Greek sites (Koufos,

2014), and *C. etruscus* has been further recovered from Fonelas-P1 in Spain (ca. 1.9–1.7 Ma; Garrido & Arribas, 2008), which is roughly coeval to Olivola and Upper Valdarno. Similarly, *C. arnensis* has also been recorded in France, since *Canis senezensis* from Senèze (ca. 2 Ma; Martin, 1973) is currently considered its junior synonym (Boudadi-Maligne, 2010; Bartolini Lucenti & Rook, 2016). The Early Pleistocene site of Fonelas P-1 mentioned above represents the earliest record of canids in the Iberian Peninsula, with as many as four species identified (Garrido, 2008; Garrido & Arribas, 2008): *Vulpes alopecoides* Del Campana, 1913, *C. falconeri*, *C. etruscus*, and the small *Canis accitanus* Garrido & Arribas, 2008, described from this site.

Around 1.5 Ma, an important faunal turnover (see Palombo & Sardella, 2008) lead to a decrease in the diversity of canids, coinciding with the appearance and dispersal of two new species of medium- to large-sized canids (Sotnikova & Rook, 2010): *C. mosbachensis* and *Xenocyon lycaonoides* Kretzoi, 1938. Both species are recorded in three sites (Venta Micena, Barranco León, and Fuente Nueva 3) from the Early Pleistocene of the Guadix-Baza Basin in southern Spain, spanning approximately 1.4–1.2 Ma (Duval et al., 2011, 2012; Toro-Moyano et al., 2013). Subsequently, during the late Early Pleistocene and Epivillafranchian (latest Early Pleistocene, ca. 1.2–0.8 Ma; Kalkhe, 2006; 2007; Madurell-Malapeira et al., 2010; 2014; Bellucci et al., 2015), medium- to large-sized canids are generally represented in Europe by two species: *C. mosbachensis* and *X. lycaonoides* (Fig. 1.14). *C. mosbachensis* (or *C. ex gr. mosbachesis* like *Canis apolloniensis* Koufos & Kostopoulos, 1997b) became very common during the late Early Pleistocene and the Middle Pleistocene of Eurasia (*e.g.*, see Sotnikova, 2001; Martínez-Navarro et al., 2009; Petrucci et al., 2013). Even if the phylogeny of fossil Canidae is still matter of strong debate, there is general consensus among scholars to consider *C. mosbachensis* as the ancestor of *C. lupus* (*e.g.*, Torre 1967; Sotnikova, 2001; Sotnikova & Rook, 2010).

The record of Canidae in Africa is the rather poor and scattered across the

continent. Generally present in the recovered fossil faunas, the number of Canidae specimen recovered from these sites is considerably inferior to other major families of Carnivora (like, Felidae or Hyaenidae). Despite this bias, the African record of Canidae is nonetheless interesting (see the sections 1.5.-1.7.) as it includes some of the earliest record of Vulpini and one of the oldest *Canis* of the entire Old World. Unfortunately, the material from Nachukui Formation south of the Turkwel River in Turkana (northern Kenya), dated between 3.52-3.2 Ma (Ward et al., 1999), is too few and damaged to be confidently attributed (Werdelin & Lewis, 2000). The recent description of two fragments possibly referable to *Canis* in Laetoli (Werdelin & Dehghani, 2011), might reveal as the oldest of the genus in the continent (ca 3.7-3.6 Ma; Fig. 1.14.). The record of *Canis* remain fragmented and scarce throughout the Pliocene and Pleistocene. Several taxa were described from renowned localities (such as Sterkfontein, Transvaal caves, Kroomdrai, Olduvai gorge) but their taxonomic status has been questioned: *e.g.*, *Thos terblanchei* is widely considered a *Nyctereutes* (Ficcarelli et al., 1984; though it should be noted that Reynolds, 2012 adverse this long and documented interpretation; see section 1.5.1.); *Thos antiquus* Broom, 1937 (probably junior synonym of *L. mesomelas*, see Ewer, 1956); *Canis atrox* Broom, 1948 could be related to the *Xenocyon-Lycaon* lineage. *Canis brevirostris* Ewer, 1956 does not possess typical dental morphologies of *Canis*, in addition to other cranial ones (*e.g.*, the presence of a depression on the dorsal side of the frontals). One of the most abundant area in canids remains of the continent is North Africa. Two hypercarnivorous taxa were recovered: the large African wild dog-like "*Canis*" *africanus* Pohle, 1928 (see Arambourg, 1979) from Aïn Hanech (Algeria) and *Lycaon magnus* Ewer & Singer, 1956 from few middle Pleistocene sites (Tighennif, Thomas-1 Quarry, Grotte de Rhinoceros; Geraads, 2011). These species are similar to the South African type specimen. More peculiar are the records of *Canis* aff. *aureus* of Ahl al Oughlam and the small canid from Grotte de Rhinoceros. Some author proposed to ascribe the former to the genus *Eucyon*

(see *inter alios* Werdelin & Peigné, 2010), but Geraads (2011) erected the species *Lupulella paralius* Geraads, 2011 for this sample. The medium-sized canid from Morocco probably was strictly related to *Lupulella mohibi* Geraads, 2011 of Grotte de Rhinoceros, a rather odd and unusual small canid with cranial features similar to *Canis* spp. *s.l.* but with teeth morphology resembling *Nyctereutes* ones. In general, the record of Canidae from North Africa shows a wide continental distribution of the known species (all closely related to African taxa).

1.8.3. Focus on Late Pleistocene Canis lupus *of the Italian peninsula*

The wolf *Canis lupus* Linnaeus, 1758, when compared to other *Canis* species, is a medium- to large-sized social canid with a slender body, elongated limbs and a massive skull with a proportionately short muzzle (Boitani et al., 2003). Its body size is characterised by marked sexual dimorphism: males (20–80 kg) are larger than females (15–55 kg) (Mech, 1970; Boitani et al., 2003).

In general, Canidae retains more primitive dental features when compared to other Carnivora (Ungar, 2010), and this provides them with a great degree of adaptability and a wide ecological tolerance (Macdonald & Sillero-Zubiri, 2004). Wolves are widespread in the Old and the New World, inhabiting ecosystems spanning from the arctic tundra to the Arabian desert (Mech, 1970; Boitani, 1995). Adaptation to such a wide range required the emergence of local morphological differentiations and/or genetic divergences, and these differences have been acknowledged in the approximately forty subspecies described in the scientific literature (Wilson & Reeder, 2005). One of these subspecies is *Canis lupus italicus* Altobello 1921 (see, among others, Randi, 2011).

According to the ecogeographic Bergmann's Rule, carnivores with a large distribution frequently show marked geographical variations in body size (see, among others, Meiri et al., 2004). Research on the extant *C. lupus* (*e.g.*, see Carbyn, 1987; Boudadi-Maligne, 2010) suggests that this carnivore follows this rule, as the

body size is larger in populations from higher latitudes than in those from lower latitudes; the exception here is the arctic wolf (*Canis lupus arctos* Pocock, 1935), which shows a medium size.

The taxonomy of the Middle-Late Pleistocene wolves and the evolutionary history of European canids, in general, remain matters of debate among scholars. This is due to the particular pattern of features shared by all canids (*e.g.*, the retention of primitive dentition) that complicate the clear identification of true diagnostic characters that define interspecific (or intersubspecific) variability. This is particularly true if these diagnostic features are considered, rather than differences related to intraspecific/subspecific variance that are not relevant for taxonomical and evolutive purposes (Mecozzi et al., 2017). Although the taxonomic status of *C. mosbachensis* is strongly debated among the specialists (see Mecozzi et al., 2017, for discussion), the prevailing consensus is that the Mosbach wolf is the ancestor of *C. lupus* (Sotnikova & Rook, 2010; Sardella et al., 2014; Bartolini Lucenti et al., 2017).

The earliest true *C. lupus* in Europe appears in the late Middle Pleistocene site of the Lunel-Viel cave (France, dated around 400-350 ka; Brugal & Boudadi-Maligne, 2011) and has been ascribed to the subspecies *Canis lupus lunellensis* Bonifay, 1971. In Italy, the first occurrence of the modern wolf comes from the late Middle Pleistocene La Polledrara di Cecanibbio site (MIS 9; Gliozzi et al., 1997; Anzidei et al., 2012). A global climatic cooling trend, starting in the late Middle-Late Pleistocene and culminating during the Last Glacial Maximum (Ramstein et al., 1997; Kahlke, 2014), produced drastic environmental changes that profoundly affected the structure of faunal assemblages (Gliozzi et al., 1997). The places where "thermophile" species persisted during glacial stages have been described as glacial refugia (*e.g.*, the Italian and the Iberian Peninsulas and the Balkan region; Stewart et al., 2010). During the last 400 kyr, the range of species was strongly affected by the glacial/interglacial cycles. The current consensus is that each species possesses

a certain degree of plasticity for adaptation to variable climatic conditions. At the same time, however, each species responds to climatic changes in its own way (Taberlet et al., 1998; Stewart, 2008; Stewart et al., 2010).

Several studies have recently focused on the dispersal and the variations in body size of the modern wolf lineage in western Europe in correlation with the climate changes registered during the Middle and Late Pleistocene. Most of this work supports the idea that *C. lupus* underwent an increase in body size, from the small *C. l. lunellensis* to the larger last glacial stage wolves (see, among others, Van der Made et al., 2014). Boudadi-Maligne (2012) suggested that the large-sized wolves from southwestern France, chronologically referable to the last part of MIS 3 and MIS 2, should be referred to as the subspecies *Canis lupus maximus* Boudadi-Maligne, 2012. This subspecies was reported from sites that are characterised by faunal associations suggestive of a cold climatic condition, as testified, for instance, by the presence of medium and large-sized ungulates [*e.g.*, *Rangifer tarandus* (Linnaeus, 1758)] (Boudadi-Maligne, 2012).

2. Materials and Methods

2.1. Studied fossil specimens and comparative samples

2.1.1 Studied material for sections 3.1.-3.2.

The examined and described fossils of "*Mustela*" *ardea* are housed in the IGF (see abbreviation below, section 2.3.), in the collections of the MdC and those of the UCBL-1, and in the Paleontology and the Paleontology collection of the MNHN. The material of Monte Tuttavista are kept in the collections of the Soprintendenza Archeologia, Belle Arti e Paesaggio per le province di Sassari e Nuoro, and the "Museo Archeologico Nazionale (Polo Museale della Sardegna)" in Nuoro (Sardinia, Italy). Numbers and abbreviation used for the specimens are laboratory/field names, composed of a first part in roman numbers that indicates the quarry (*e.g.*, "VII") and of a second part, which identifies the fissure (*e.g.*, "mustelide") (see below, section 2.3.1.). The last part is the progressive number of inventory for each fissure. These numbers will be eventually replaced by a national catalogue code, yet unavailable at the time of the preparation of this study. The fossil comparative sample include: *Enhydrictis galictoides* from Monte S. Giovanni (housed in the IGF); *Pannonictis nestii* from Upper Valdarno (in the collections of the IGF) and Pirro Nord (from the collections of the DST-UNITO); *Pannonictis pliocaenica* from Villany-Kalkberg and *Pannonictis pilgrimi* from Villany and Beremend (both housed in the collection of HNHM, Budapest, Hungary); *Trigonictis* spp. from various North American localities (Paleontological collections of the AMNH). All the relevant literature on the Plio-Pleistocene Lyncodontini was inspected (Viret, 1954; Ficcarelli & Torre, 1967; Rook, 1995; Morlo & Kundrat, 2001; Qiu et al., 2004; García & Howell, 2008; García et al., 2008; Ogino & Otsuka, 2008; Jin & Liu, 2009; Colombero et al., 2012; Fejfar et al., 2012; Peters & De Vos, 2012; Geraads, 2016). Extant specimens from the MZUF were also used for morphological and morphometric comparisons.

The extant comparative sample includes specimens of *Galictis cuja*, *G. vittata*, *Lutra lutra*, *Lontra longicaudis* (Olfers, 1818), *Lontra provocax* (Thomas, 1908), *Mustela putorius* Linnaeus, 1758, *Mustela nivalis* Linnaeus, 1758, and *Eira barbara*. All craniodental measurements were taken to the nearest 0.1 mm with a digital caliper, following Driesch (1976). Cranial and postcranial nomenclature follows Barone (1966), Ercoli (2015). Dental nomenclature used in the work follows Biknevicius & Van Valkenburg (1996); Popowics (2003) and Ungar (2010) with some variations (see Fig. 2.1).

2.1.2. Studied material for sections 3.3.-3.7.

The studied sample of *Nyctereutes* is consistently large (more than five hundred cranial and postcranial specimens from more than thirty localities of the Old World) housed in several institutions and museums: AMNH; AUT; ICP; IGF; HNHM; MdC; MNCN; MNHN; UCBL-1. We also reviewed the relevant literature

Figure 2.1 – Occlusal morphology and dental nomenclature used in the present study for Lyncodontini (**A-B**, **E-F**) and Caninae (**C-D**, **G-H**). Upper teeth of the lyncondontine *Galictis vittata* showing nomenclature of the cusps (**A**) and of cingula, basins and other features (**B**). Upper teeth of the Vulpini *Nyctereutes procyonoides* showing nomenclatures of the cusps (**C**) and of cingula, basins and other features (**D**). Lower teeth of *Galictis vittata* showing nomenclature of the cuspids (**E**) and of cingulids, basins and other features (**F**). Lower teeth of *Vulpes vulpes* showing nomenclatures of the cuspids (**G**) and of cingulids, basins and other features (**H**). Lines indicate dental features, whereas arrows point out areas and basins. Dotted lines are features not present in the photographed taxon that may be present in other taxa studied. **Nomenclature abbreviations**: **bc**, buccal cingulum; **bmn**, buccal molar notch; c, cingulum; **cd**, cingulid; **cn**, carnassial notch; **crdt**, transverse cristid; **dac**, distal accessory cuspule; **dacd**, distal accessory cuspulid; **dcd**, distal cingulid; **dmn**, distal molar notch; **End**, entoconid; **Enld**, entoconulid; **Hy**, hypocone; **Hyd**, hypoconid; **hyfd**, hypoflexid; **mc**, mesial cingulum; **Me**, metacone; **mec**, metaconule; **Med**, metaconid; **mesd**, mesoconid; **Ms**, metastyle; **Pa**, paracone; **pacrd**, paracristid; **Pad**, paraconid; **pas**, parastyle; **poprc**, postprotocrista; **ppac**, preparacrista; **Pr**, protocone; **prc**, protoconule; **Prd**, protoconid; **prmc**, medial protocone crista; **tb**, talon basin; **tdb**, talonid basin; **tdn**, talonid notch; **trb**, trigon basin; **trdb**, trigonid basin.

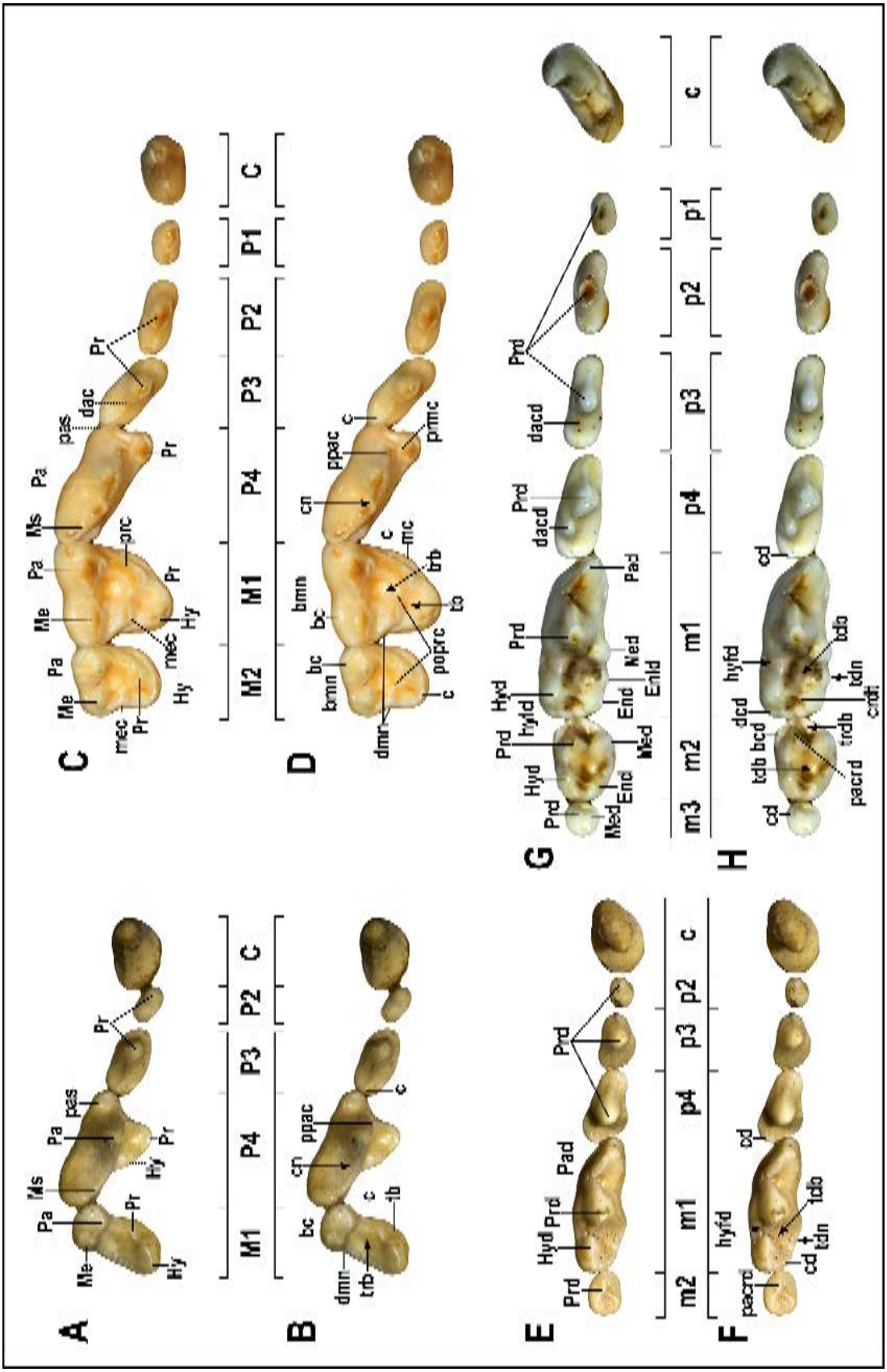
A
B
C
D
E
F
G
H
M1
P4
P3
P2
C
M2
M1
P4
P3
P2
P1
C
m2
m1
p4
p3
p2
c
m3
m2
m1
p4
p3
p2
p1
c
Me
Pa
Ms
Pa
pas
dac
Pr
Hy
mec
Pr
Hy
pmc
Pr
bc
bmn
cn
ppac
c
dmn
mic
brb
tb
popra
pmic
Hyd
Prd
hyld
End
Med
Enld
Pad
dacd
tdb
bcd
hyfd
cd
tdn
tdo
pacrd
cndt

on Plio-Pleistocene raccoon dogs (Martin, 1971; Soria & Aguirre, 1976; Torre 1979; Tedford & Qiu, 1991; Monguillon et al., 2004). All the material was directly examined, with the exception of *N. lockwoodi*, whose data were collected from Geraads et al. (2010). *N. barryi* and *N. terblanchei* were studied using bibliographic references as well as casts of the type material held, respectively, at MNHN and IGF (see abbreviations below). The fossil species were considered to come from the following regions: *N. abdeslami* from Ahl al Oughlam (Morocco); *N. barryi* from Laetoli (Tanzania); *N. donnezani* from Perpignan (France), La Gloria 4 and Layna (Spain); *N. megamastoides* from the Perrier-Les Etouaires (France), Kvabebi (Georgia), Dafnero (Greece), Lower Valdarno Basin (Italy), and Villarroya (Spain); *N. sinensis* from the Yushe Basin and Nihewan Basin (China); *Nyctereutes* sp. from Çalta (Turkey); *N. terblanchei* from Kroomdrai A (South Africa); *N. tingi* from the Yushe Basin (China) and Megalo Emvolon (Greece); and *N. vulpinus* from St. Vallier (France) and La Puebla de Valverde (Spain). *N. vinetorum* was excluded from the analysis because of the scantiness of its record. Other relevant literature on Plio-Pleistocene raccoon dogs was also reviewed (Martin, 1971; Soria & Aguirre, 1976; Torre, 1979; Tedford & Qiu, 1991; Monguillon et al., 2004; Geraads et al., 2010; Ivanoff et al., 2014). The extant comparative sample includes specimens of *N. procyonoides*, *Vulpes vulpes*, *Vulpes lagopus* and *Cerdocyon thous* housed in the MZUF and AMNH. Measurements were taken to the nearest of 0.1 mm following Driesch (1976) and Tedford et al. (2009). Cranial and postcranial nomenclature follows Berta (1988), Rook (1993), Barone (1966), Evans & Lahunta (2013). Dental nomenclature used in the work follows Biknevicius & Van Valkenburg (1996); Wang & Tedford (2008); Tedford et al. (2009) and Ungar (2010) with some variations (see Fig. 2.1).

2.1.3. Studied material for section 3.8.

The studied and revised fossil specimen of *Vulpes* come from several locality of

western Europe, as St. Vallier (France), Dafnero-1, Apollonia-1 (Greece), Kvabebi (Georgia), Villany (Hungary), Pirro Nord, Upper Valdarno (Italy), Cal Guardiola, Puebla de Valverde, Vallparadís Estació, Venta Micena, Villarroya, (Spain). The fossil materials are housed in several European institutions: AUT, DST-UNIFI, ICP, IGF, MdC, UCBL-1. To evaluate reliable morphological features that allow the distinction between the European species, the type specimens of three of the four known species of Europe, *i.e.*, *V. alopecoides*, *V. praeglacialis*, and *V. praecorsac* housed at IGF, HNHM and MAFI were reviewed. Comparative material of late Miocene to Early Pleistocene foxes from Eurasia and Africa here considered are those held in the American Museum of Natural History (New York, U.S.A.) and Musée National d'Histoire Naturelle (Paris, France). Relevant literature on these canids was also taken into consideration (Pei, 1934; Broom, 1948; Ewer, 1956; Rabeder, 1976; Qiu & Tedford, 1990; Qiu et al., 2004; Garrido, 2008; Geraads, 2011; Hartstone-Rose et al., 2013; Koufos, 2014; Geraads et al., 2015). Extant comparison sample includes *Vulpes corsac*, *Vulpes lagopus* and *Vulpes vulpes* housed in the collections of the AMNH, GNM, HNHM, and MZUF. Measurements were taken to the nearest of 0.1 mm following Driesch (1976) and Tedford et al. (2009). Cranial and postcranial nomenclature follows Berta (1988), Rook (1993), Barone (2006), Evans & Lahunta (2013). Dental nomenclature used in the work follows Biknevicius & Van Valkenburg (1996); Wang & Tedford (2008); Tedford et al., (2009) and Ungar (2010) with some variations (see Fig. 2.1).

2.1.4. Studied material for section 3.9.

The examined fossil material includes the types and paratypes of *Canis ferox* from latest Miocene to Early Pliocene localities of North America, *Eucyon* species, "*Eucyon*-like" taxa (*sensu* Sotnikova & Rook, 2010), and medium-sized species of *Canis* from both North America and Eurasia. Extant specimens from the AMNH, MZUF and ICP collections were also used for morphological and morphometric

comparisons. The extant comparative sample includes specimens of *Canis anthus*, *Canis aureus* Linnaeus, 1758, *Canis latrans* Say, 1823, *Canis lupus*, *Canis simensis*, *Cuon alpinus*, *Lupulella adusta*, *Lupulella mesomelas*, *Lycaon pictus*, *Nyctereutes procyonoides*, and *Vulpes lagopus* housed in the AMNH and MZUF. Measurements were taken to the nearest of 0.1 mm following Driesch (1976) and Tedford et al. (2009). Cranial and postcranial nomenclature follows Berta (1988), Rook (1993), Evans & Lahunta (2013). Dental nomenclature used in the work follows Biknevicius & Van Valkenburg (1996); Wang & Tedford (2008); Tedford et al., (2009) and Ungar (2010) with some variations (see Fig. 2.1).

2.1.5. Studied material for section 3.10.

The specimen OS10-02, included in this study, comes from the site of Wadi Sarrat and is housed at the ONM. Comparative material of Early Pleistocene canids here considered are those held in the ICP and in the IGF. Material of the following extant species housed in the IPHES and in the MZUF were used for comparative purpose: *Canis aureus*, *Canis anthus*, *Lupulella mesomelas*, *Lupulella adusta*, *Lycaon pictus*, and *Canis lupus*. Measurements were taken to the nearest of 0.1 mm following Driesch (1976) and Tedford et al. (2009). Cranial and postcranial nomenclature follows Berta (1988), Rook (1993), Barone (2006), Evans & Lahunta (2013). Dental nomenclature used in the work follows Biknevicius & Van Valkenburg (1996); Wang & Tedford (2008); Tedford et al., (2009) and Ungar (2010) with some variations (see Fig. 2.1).

2.1.6. Studied material for sections 3.11.-3.12.

For the morphological and morphometric study of the canid sample from Avetrana bed 8 and Ingarano, the materials temporarily housed in the DST-SAP and in the DST-UNIFI, were examined. During the various excavation campaigns, the collected materials were marked with several acronyms (Avetrana: A8-; Ave8;

Ave-07-; A8C-; Ingarano: IN-; ING-); specimens without field labels/numbers are indicated with "AND-" if they come from Avetrana, and "INGND-" is they come from Ingarano, The comparison dataset was built considering the available studies on *C. lupus* from the Aurelian (late Middle –Late Pleistocene) of southern Europe (Bonifay, 1971; Boudadi-Maligne, 2010; 2012; Bertè, 2014; Sardella et al., 2014; Gatta et al., 2016; Salari et al., 2017). The material of the extinct *Canis mosbachensis* Soergel, 1925 from Pirro Nord (Italy), housed in the DST-UNIFI, and of the sample from Vértesszȍlȍs II (Hungary), housed in the Palaeovertebrate Collection of the HNHM, were considered as fossil comparative samples. For extant material considered includes the specimens of the Italian subspecies *C. l. italicus*, *C. simensis*, *C. aureus*, and *C. anthus* housed in the MZUF, as well as from literature (among others, Caloi et al., 1982, 1984). Measurements were taken to the nearest of 0.1 mm following Driesch (1976) and Tedford et al. (2009). Cranial and postcranial nomenclature follows Berta (1988), Rook (1993), Evans & Lahunta (2013). Dental nomenclature used in the work follows Biknevicius & Van Valkenburg (1996); Wang & Tedford (2008); Tedford et al., (2009) and Ungar (2010) with some variations (see Fig. 2.1.). Nomenclature of the brain anatomy are taken from Lyras & Van der Geer (2003) and Evans & Lahunta (2013). The digital endocast were obtained from CT scans of the fossil and extant specimens scanned at the Ospedale S. Giovanni di Dio (Scandicci, Florence). The DICOM data obtained from scans were processed in Slicer3D (ver.4.10.2) and in R using the packages Arothron (Profico et al., 2018a) and Morpho (Schlager, 2017) following the protocol of Profico et al. (2018b).

2.1.6. Studied material for sections 3.13.

The present study is based on the comparative morphological analysis of the medium-sized wolf-like canids (tribe Canini) of the Early Pleistocene-middle Pleistocene of southeastern Europe. The described fossils are housed at the Georgian

National Museum (Tbilisi). As comparative fossil material, late Villafranchian canids from Eurasia housed at AMNH, AUT, ICP, and IGF (see abbreviation below) were studied. This fossil comparative sample includes specimens of *Canis arnensis* Del Campana, 1913 and *C. etruscus* from the Italian sites of Olivola, Upper Valdarno Basin, Coste San Giacomo and Pantalla (Cherin et al., 2014); *Canis apolloniensis* Koufos and Kostopoulos (1997) from Apollonia-1 (Koufos, 2018) *C. chihliensis* and *C. palmidens* from Yushe Basin (Rook, 1993; 1994); remains of *Canis mosbachensis* Soergel, 1925 from Cueva Victoria, Vallparadís (Bartolini Lucenti et al., 2017), Pirro Nord (Petrucci et al., 2013), 'Ubeidiya (Martínez-Navarro et al., 2009), Untermassfeld (Sotnikova, 2001), and Zhoukoudian (Jiangzuo et al., 2018). The relevant literature on late Villafranchian canids was inspected (Del Campana, 1913; Crusafont Pairó, 1950; Thenius, 1954; Torre, 1967; 1974; 1979; Bonifay, 1971; Kurtén, 1974; Pons-Moyà and Moyà-Sola 1978; Pons-Moyà, 1981; Koufos and Kostopoulos, 1997; Wang et al., 1999; Sotnikova, 2001; Garrido and Arribas, 2008; Lacombat et al., 2008; Tedford et al., 2009; Petrucci et al., 2013; Cherin et al., 2014; Koufos, 2014; 2018; Amri et al., 2017; Mecozzi et al., 2017; Jiangzuo et al., 2018). Extant specimens housed at the AMNH, MZUF, ICP and GNM (see abbreviation below) were also used for morphological and morphometrical comparisons. We examined specimens of *Canis aureus* Linnaeus, 1758, *Canis latrans* Say, 1823, *Canis lupaster* Hemprich and Ehrenberg, 1832, *Canis lupus* Linnaeus, 1758, *Lupulella adusta* (Sundevall, 1847), *Lupulella mesomelas* (Schreber, 1775), and *Lycaon pictus* (Temminck, 1820).

2.1.6. Studied material for sections 3.14.

The studied material was formerly stored at the Institut de Paleontologia Miquel Crusafont (Sabadell, Barcelona, Spain) until 1998, later at the Museo Municipal de Prehistoria y Paleontología (Orce, Granada, Spain) until 2016 and, since then, at the Museo Arqueológico de Granada (Spain). As comparative fossil material,

we studied: *Canis apolloniensis* from Apollonia 1 (housed at AUT) *Canis arnensis* from Upper Valdarno and Poggio Rosso (housed at IGF); *Canis chihliensis* from Yushe Basin (housed at AMNH); *Canis etruscus* from Olivola and Upper Valdarno (housed at IGF and MPM); *Canis etruscus* from Dmanisi (housed at GNM); *Canis mosbachensis* from Cueva Victoria, Pirro Nord, Vallparadís Estació, Vértesszőlős II (housed at ICP, DST-UniFI, HNHM); *Canis palmidens* from Yushe Basin (housed at AMNH) and Nihewan Basin (housed at MNHN) (see abbreviations below). Additional comparative material of extant and Late Villafranchian canids was taken from the literature (Del Campana, 1913; Crusafont, 1950; Thenius, 1954; Torre, 1967; 1974; Kurtén, 1974; Pons-Moyà and Crusafont, 1978; Pons Moya, 1981; Rook, 1993; Koufos & Kostopoulos, 1997a; 1997b; Sotnikova, 2001; Garrido and Arribas, 2008; Lacombat et al., 2008; Martínez-Navarro et al., 2009; Tedford et al., 2009; Tong et al., 2012; Petrucci et al., 2013; Cherin et al., 2014; Koufos, 2014; Bartolini Lucenti & Rook, 2016; Bartolini Lucenti et al., 2017). Extant comparison specimens used for morphological and statistical considerations were taken from the collection of the "La Specola" Zoological Section of the Museum of Natural History of the University of Florence. This sample includes specimens of the following species: *Canis lupus* Linnaeus, 1758, *Canis latrans* Say, 1823, *Canis lupaster* Hemprich and Ehrenberg, 1832, *Canis aureus* Linnaeus, 1758, *Lupulella mesomelas* (Schreber, 1775), *Lupulella adusta* (Sundevall, 1847) and *Lycaon pictus* (Temminck, 1820).

2.2. Morphometric and cladistic analyses

2.2.1. Morphometric analyses

To investigate the morphometric difference between the considered and known taxa, different types of analyses and graphs were used. Scatter plots and boxplots were used in sections 3.2., 3.4., 3.5., 3.6., and 3.11. Log-ratio diagrams (Simpson 1941; Simpson et al. 1960) were used to compare different taxa against a chosen

standard. With the log-transformed mean value of each variable for every species, these graphs estimate the difference between these values and those of the selected species, which constitutes the chosen comparative baseline. These plots can be used on cranial, mandibular, dental and/or postcranial variables. In section 3.2., the *P. pliocaenica* was used has a comparative reference for the cranial and dental variability of fossil Eurasian Lyncodontini. The cranial variables used are Tl, NCL, FL, Eu, PoCW, SH, AB, BL, ECW, GPW (see Abbreviation below – Table 2.1), whereas dental ones include p3-m1 L, m1W, Mm1H, Mm1B, P2-M1 L, P4-M1 W (see Abbreviation below – Table 2.1). When the analyses were focused on raccoon dogs, the extant *N. procyonoides* was generally selected as a reference baseline, with the exception of section 3.3., in which the reference species is *N. megamastoides* from different site. The dental variables selected in section 3.6. are the P3 length, the length and width of P4-M2 for the upper teeth, while for the lower dentition the p3 length and the length and width of p4-m2. In section 3.10. the dental variables selected were the upper teeth ones, particularly P1-M2 length and P4-M2 width. To study the variability of "*Canis*" *ferox* (section 3.9.) compared to other *Eucyon* species from Eurasia and North America, log ratio diagrams were used. *E. davisi* was selected to serve for this comparative purpose. The morphometric values considered include cranial (*i.e.*, TL, NCL, SCL, GNL, Eu, Ect, PoCW, SH, AB, GWOC, BL, PL, CBL, ECW, GPW; see Abbreviation below – Table 2.1) and dental values (*i.e.*, length of p4; length and width of m1; length of the trigonid of m1; length and width of m2; length of the m3; length and width of P4; length and width of M1; length and width of M2). In section 3.12., the cranial and dentognathic variables used are TL, NCL, SCL, PL, C-M2 L, LMR, GWOC, Eu, GPW, HPW, SH, AB, LLPR, Mm1H (see Table 2.1). In addition, log-transformed data of the dietary groups and the fossil species "*C.*" *ferox*, *E. adoxus*, *E. davisi*, *E. zhoui* were used to perform principal component and discriminant analyses using RStudio. In sections 3.11.-3.12., the dental variables and the postcranial ones

considered are respectively length and width of P4-M2, of p4-m2 and the length of the m1 trigonid and GL, Bp, DC, SD, and Bd (for the femur, see abbreviations below – Table 2.2). The extant *C. l. italicus* was chosen as reference baseline and, the following fossil species were plotted, in addition to *C. lupus* from Avetrana: *C. l. lunellensis* from French sites (*i.e.*, Lunel-Viel 1, Igue des Rameaux, Aven 1 de la Fage, Coudoulous 1); *Canis lupus santenaisiensis* Argant, 1989 from Aven de l'Arquet; *C. l. maximus* from Grotte de Jaurence, Grotte de Maldidier, Igue du Gral; "Apulian wolves" (Sardella et al., 2014) from various southern Italian localities (*e.g.,* Grotta Romanelli, Ingarano, Melpignano); "northern Italian wolves" from localities like Broion, Buco del Frate, Pocala; and the sample of wolf from Cardamone (Apulia). In section 3.13., the following variables were selected (see abbreviations above): TL, NCL, FL, SCL, GNL, Eu, Ect, POCW, SH, GWOC, PL, ECW, GPW; length and width of P4-M2 and of p4-m2. *C. lupus* was chosen as a reference baseline, and plotted the following European fossil species: *C. apolloniensis* from Apollonia-1, *C. arnensis* from Upper Valdarno; *C. mosbachensis* from the Cueva Victoria and Vallparadís section; Untermassfeld, Pirro Nord and 'Ubeidiya; *C. etruscus* from Olivola, Upper Valdarno and Pantalla; and *Canis* from Dmanisi.

We performed a Principal Components Analysis (PCA) on a dataset of selected $\log_{10}$-transformed cranial measurements, in order to establish the morphological similarities between various canid species, both extinct (*Canis* from Dmanisi, *C. arnensis*, *C. etruscus*, and *C. mosbachensis*) and extant (*C. aureus*, *C. lupus*, *C. lupaster*, *L. adusta*, *L. mesomelas*). In section 3.14., the difference in proportions among several fossil Eurasian species (*i.e.*, *C. etruscus* from Olivola, Upper Valdarno and Pantalla; *C. arnensis* from Upper Valdarno; *C. mosbachensis* from Cueva Victoria, Vallparadís Section, Pirro Nord) and extant ones (i.e., *Lupulella mesomelas*, *L. adusta*, *C. aureus*, *C. lupaster* and *C. lupus*) was studied. The ratio between the length of the P4 and the length of M1-M2 (index A of Bonifay, 1971; here CI) was also used to consider differences in the relative proportions of carnassials and molars. Moreover, paleoecological

inferences were also derived from carbon- and nitrogen-isotope ratios measured in the members of the carnivoran guild of Venta Micena (data from Palmqvist et al., 2008) and also from craniodental ratios that allow differentiating among modern species of canids according to their dietary habits.

2.2.2. Statistical analyses

In section 3.9. statistical tests were used to assess statistical significance between morphometric ratios (see section 2.2.4.). The $\log_{10}$-transformed ratios was applied the Shapiro-Wilks test to assess the normal distribution of the samples. All resulted normally distributed but two, M2S ($p<0.01$) and UM2/1 ($p<0.01$). All the $\log_{10}$-transformed ratios were tested for significant difference between the dietary groups and "*C.*" *ferox* by permutational ANOVA, on those normally distributed, and Kruskal-Wallis test, on M2S and UM2/1. Of the fossil species considered in the study, the only one with sufficiently well-preserved materials to estimate several series of ratios is "*C.*" *ferox*.

In section 3.11. the Kruskal-Wallis Test was used to assessed the degree of affinity of the wolf from Avetrana bed 8 with other Italian and European Late Pleistocene localities. three dental measurements (*i.e.* P4 L, M1 L and m1 L) were considered for the referred sample from Avetrana bed 8 and then compared to those of the taxa included in the log-ratio analysis. We first used the Shapiro-Wilk test to assess the normal distribution of the samples. The result was negative (P4 L, p-value <0.01; M1 L, p-value <0.01, m1 L, p-value <0.01); therefore, a non-parametric test was carried out to evaluate differences in the size of teeth between Avetrana and the other wolf populations. We carried out a Kruskal-Wallis test on each subsample for each variable, testing the null hypothesis that the location parameters of the distribution of x were the same in each group. The alternative is that they differ in at least one distribution.

To analyzed the morphometric affinity of the *Canis* material from Dmanisi (section 3.13), this material was compared with that of other European Late Villafranchian species by means of boxplots and statistical tests. To achieve so, selected measurements and cranio-dentognathic ratios were used to test for statistical difference among the sample of Dmanisi, the other fossil taxa and the extant species of the genera *Canis* and *Lupulella*. The $\log_{10}$-transformed measurements and ratios were firstly tested from normality of distribution through the Shapiro-Wilks. The cranial ratios, SCL/TL, GNL/TL, GWOC/AB and SH/TL, do not deviate considerably from normality of distribution, whereas the other violate the null hypothesis of the test. The non-normally distributed $\log_{10}$-transformed ratios were tested for significant difference by Kruskal-Wallis test whereas those normally distributed, we tested with permutational ANOVA. All statistical analyses, biplots and 3D plots were realized using RStudio ver. 1.2.1335 (R ver. 3.6.).

2.2.3. Cladistic analyses

The maximum parsimony criterion was chosen for the purposes of the analyses, as it is considered one of the best ways to evaluate morphological character arrays (*inter alios* Spencer & Wilberg, 2013). The analysis was performed using TNT 1.5 (Goloboff & Catalano, 2015), on selected morphological characters that were treated as unpolarized and non-additive. In section 3.1., thirty cranial and dentognathic characters for 8 Lyncodontini genera were selected. The cladistic analysis of section 3.7. is based on 115 characters (106 of these concerned cranial, dentognathic and cerebral features and 9 postcranial ones; see Appendix 3.7.1. for a detailed list of characters) and 11 fossil and extant taxa of *Nyctereutes*. The freeware program Mesquite 3.6 (Maddison & Maddison, 2018) was used to build the matrix and obtain the Consistency Index (CI), the Retention Index (RI) and the Tree Length (TL).

2.2.4. Ecomorphological investigation

The molar ratio index (Asahara, 2013a) was used to investigate the dietary preferences of *N. sinensis* from Yushe Basin (section 3.5.), of *N. donnezani* from Layna (section 3.6.) and in section 3.7. in comparison to some extant subspecies - *i.e.*, *N. p. albus* and *N. p. viverrinus* - and fossil species of this genus (data also taken from Asahara & Takai, 2016). The method described by Asahara (2013a) consists in calculating the occlusal surface of the m1 and the m2, and then estimate the ratio between the two surfaces (*i.e.*, m2/m1 score). In Canidae, this molar ratio proves to be related to the differences in diet (Asahara, 2013a; 2013b; 2014; Asahara et al., 2016). After measuring the tooth length and width, the occlusal area following Kavanagh et al. (2007) was calculated. We used these new scores to plot all the data in a biplot diagram of m1 occlusal surface versus m2/m1 score of each extant populations or fossil species to compare them with the results by Asahara & Takai (2016).

Selected morphometric ratios (described by Van Valkenburgh, 1989; Van Valkenburgh & Koepfli, 1993; Van Valkenburgh et al., 2003) were used to investigate the dietary habits of "*C.*" *ferox* and some *Eucyon* species (section 3.9.). Van Valkenburgh (1989) used several cranial and dentognathic ratios as indicators of predatory behavior and diet of extant carnivorans, showing the reduced influence of body size. Carnivorans' weight appears be an important element only in relation to prey size and predatory strategy (*i.e.*, if a taxon is pack- or solitary hunter), as shown by Van Valkenburgh & Koepfli (1993) and Carbone et al. (1999). The ratios used here are the relative blade length of the lower carnassial (RBL), the premolar shape (RPS), the relative molar grinding areas, both upper and lower (respectively RUGA and RLGA), the size of the trigonid blade of the m1 (M1BS), the relative size of the second molar (M2S), relative resistance of the dentary to bending in the sagittal plane (IxM2), the mechanical advantage of the *m. temporalis*

(MAT) and of the *m. masseter* (MAM), relative size of the second upper incisor (I2), of the third upper one (I3), and of the upper canine (C1), the relative rostral breath of the cranium (C1C1), the ratio between the squared roots of the area of M2 and M1 (UM2/1). All indices were calculated following the description in Van Valkenburgh (1989) and Van Valkenburgh & Koepfli (1993). The body size of extinct species was estimated following body mass regression against the length of m1 and of condylobasal length of the cranium (Van Valkenburgh, 1990). On the two regressions, the cranial one was preferred as Losey et al. (2015), showed a considerable degree of percent error in the prediction obtained with the dental regression formula. Van Valkenburgh & Koepfli (1993) described two least square regression functions describing typical and maximum prey size in extant Canidae, subsequently modified by Van Valkenburgh et al. (2003). We used these regression equations attempting to estimate the prey size of fossil species. Data on extant species are partially taken from Van Valkenburgh (1989) (RPS, body mass), from Van Valkenburgh & Koepfli (1993), and personal dataset.

2.3. Site and Institutional abbreviations

AMNH, American Museum of Natural History, New York (U. S. A.); **AUT**, Aristotle University Thessaloniki (Greece); **DST-SAP**, Earth Science Department of Sapienza, University of Rome (Italy); **DST-UNIFI**, Earth Science Department of the University of Florence (Italy); **DST-UNITO**, Earth Science Department of the University of Turin (Italy); **GNM**, Georgian National Museum, Tbilisi (Georgia); **HNHM**, Hungarian Natural History Museum, Budapest (Italy); **ICP**, Institut Català de Paleontologia, Bellaterra (Spain); **IGF**, Geological and Paleontological Section of the Natural History Museum of the University of Florence (Italy); **IPHES**, Institut Català de Paleoecologia Humana i Evolució Social, Tarragona (Spain); **MAFI**, Hungarian Institute of Geology and Geophysics, Budapest (Hungary); **MdC**, Musée des Confluences, Lyon (France); **MNCN**,

Museo Nacional de Ciencias Naturales, Madrid (Spain); **MNHN**, Musée National d'Histoire Naturelle, Paris (France); **MZUF**, La Specola, Zoological section of the Natural History Museum of the University of Florence (Italy); **ONM**, Museum of the National Office of Mines, Tunis (Tunisia); **UCBL-1**, Université Claude-Bernard Lyon-1, Lyon (France).

2.3.1. Monte Tuttavista quarry abbreviations

IV-mac, IV-macaca; IX-pro, IX-prolagus; VII-ms, VII-mustelide; X-3u, X-3uccelli;

2.4. Measurement abbreviations

Table 2.1 – List of cranial abbreviations, in alphabetical order.

Abbr.	Description
AB	Skull height without the sagittal crest (from Basion to Inion)
Ac1-m2 L	Length of the lower toothrow from the distal side of the canine alveolus to the distal side of the m2 alveolus
AC1-M2 L	Length of the upper toothrow from the distal margin of the upper canine alveolus to the distal margin of the M2 alveolus
Ac1-m3 L	Length of the lower toothrow from the distal side of the canine alveolus to the distal side of the m3 alveolus
AM1-M2 L	Length of the upper toothrow from the mesial margin of the M1 alveolus to the distal margin of the M2 alveolus
AP1-M2 L	Length of the upper toothrow from the distal margin of the P1 alveolus to the distal margin of the M2 alveolus
Ap1-p4 L	Length of the lower toothrow from the mesial side of the p1 alveolus to the distal side of the p4 alveolus
AP1-P4 L	Length of the upper toothrow from the mesial margin of the P1 alveolus to the distal margin of the P4 alveolus
Ap2-p4 L	Length of the lower toothrow from the mesial side of the p2 alveolus to the distal side of the p4 alveolus
AP2-P4 L	Length of the upper toothrow from the mesial margin of the P2 alveolus to the distal margin of the P4 alveolus
BL	Basal length of the cranium (from Basion to Prosthion)
C1-M2 L	Length of the upper toothrow from the upper canine to the M2
CBL	Condylobasal length of the cranium (from the caudal tip of the condyles to Prosthion)
c-m2 L	Length of the lower toothrow from the canine to the m2
c-m3 L	Length of the lower toothrow from the canine to the m3
CoL	Length of the occipital condyle
CoW	Width of the occipital condyle
Ect	Breadth across the zygomatic process of the frontals

Abbr.	Description
ECW	Width across the external surface of the upper canines
Eu	Greatest breadth of the braincase
FL	Facial length (from the level of the tip of the zygomatic process of the frontal to the Prosthion)
FMH	Height of the foramen magnum
FMW	Width of the foramen magnum
GHOr	Height of the orbit
GNL	Greatest length of the nasals
GPW	Greatest width of the palate (between P4-M1 notch)
GWOC	Greatest width across the occipital condyles
GWOT	Greatest width of the occipital triangle
Hbu	Height of the tympanic bulla
HPrac	Height of the mandible between the dorsal margin of the condyloid process and the ventral one of the angular process
HPW	Width of half of the palate (from the M2 to the medial side of the palatine bone)
HR	Height of the mandibular ramus, from the ventral side of the angular process to the dorsal tip of the coronoid process
IoD	Interorbital distance
LBu	Craniocaudal length of the tympanic bulla
LCM	Length of the cranium from Basion to the distal margin of the canine alveolus
LCN	Length of the nuchal crest (from the inion to the lateral tip of the occipital triangle)
LCT	Length of the crushing part of the lower teeth (from the talonid of the m1 to the m3)
LLMR	Length of the lower molar row
LLPR	Length of the lower premolar row
Lm3-Pa	Length of the distal part of the mandible from the distal side of the m3 alveolus to the angular process
Lm3-Pc	Length of the distal part of the mandible from the distal side of the m3 alveolus to the condyloid process
LMca	Length of the mandible from the mesial side of the canine and the tip of the angualr process
LST	Length of the slicing part of the lower teeth (from the p1 to the trigonid of m1)
m1-m2 L	Length of the lower toothrow from the p2 to the p4
M1-M2 L	Length of the upper toothrow from the M1 to the M2 (Length of the Molar row)
M2B	Length of the cranium from the distal side of the M2 to the mesial side of the bulla (caudal to the foramen lacerum)
Mm1B	Mandibular breadth below the central point of m1
Mm1H	Mandibular height at level of the distal side of the alveolus of m1
MOH	Height of the maxillary area below the orbit (from the interadicular septum of the M1 to the correspondent margin of the orbit)
Mp1H	Mandibular height at level of the distal side of the alveolus of p1
Mp2H	Mandibular height at level of the distal side of the alveolus of p2
Mp3-p4B	Mandibular breadth below the space between p3 and p4
Mp4H	Mandibular height at level of the distal side of the alveolus of p4

Abbr.	Description
NCL	Length of the neurocranium (from Inion to the level of the tip of the zygomatic process of the frontal)
P1-M2 L	Length of the upper toothrow from the P1 to the M2
P1-P4 L	Length of the upper toothrow from the P1 to the P4 (Length of the premolar row)
p2-p4L	Length of the lower toothrow from the p2 to the p4
PL	Palate length (from Staphyion to Prosthion)
PoCW	Shortest width of the postorbital constriction
PWP1	Width of the palate between the P1
PWP2	Width of the palate between the P2
SCL	Splanchnocranial length (from Nasion to Prosthion)
SH	Skull height (from Basion to dorsal level of the sagittal crest)
SMW	Shortest width of the mandible between the distal to the m3 and the angle of the mandible
TL	Total length of the cranium (from Inion to Prosthion)
Zyg	Greatest width of the zygomatic arches

Table 2.2 – List of postcranial abbreviations, in alphabetical order.

Abbr.	Description
B	Greatest breadth of the bone
Bd	Breadth of the distal epiphysis
BFcd	Breath of the caudal articular surface of the vertebrae or of the cuboid
BFcr	Breath of the cranial articular surface of the vertebrae or of the cuboid
BG	Breadth of the glenoid cavity of the scapula
Bp	Breadth of the proximal epiphysis
BPacd	Breadth across the caudal articular process
BPC	Greatest breadth across the coronoid process of the ulna
BPtr	Breadth across the transverse process
BT	Breadth of the trochlea of the humerus
D	Greatest depth of the bone
DC	Depth of the caput femoris
Dd	Depth of the distal epiphysis
Dp	Depth of the proximal epiphysis
DPA	Depth across the *processus anconeus* of the ulna
GB	Greatest breadth of the bone
GL	Greatest length of the bone
GLC	Greatest length of the humerus (from the caput)
GLP	Greatest length of the glenoid process of the scapula
H	Greatest height of the bone
LaD	Length of *arcus dorsalis*
LAPa	Length of the arch of the axis (including the articular processes)
LCDe	Greatest length of the corpus of the axis including the dens
ScH	Height of the scapula (measured on the cranial side)

3. Results and Discussions

In the following sections, the results of the analyses performed on the various considered samples are described in detail. Due to their complexity and depth of the investigations, each sections is treated as separated case study, explaing all the research of the particular topic and discussing the implication of the results in a wider framework.

3.1. The revision of the species "*Mustela*" *ardea* Gervais, 1848–1852 (Mammalia, Mustelidae)

3.1.1. Context

Considering the numerous issues surrounding the taxon "*Mustela*" *ardea* (*i.e.*, the correct authorship, the generic attribution and its taxonomic status as a species; explained in deatil in section 1.3.), a deep revision of its features and the affinities compared to the other Lyncodontini was needed. The analyzed specimens of the species come from the French sites of Perrier (precisely Cote d'Arde, Issoire) and of St. Vallier (both MN17) and the Italian site of Olivola (late Gelasian).

3.1.2. Methods

Thanks to the study of an extended sample of fossil and extant Lyncodontini (section 2.), the diagnostic features of the four Eurasian fossil genera were analyzed morphometrically and morphologically. Furthermore, the first cladistic analysis for the fossil Lyncodontini was here carried out. For this purpose, eight fossil and extant genera of the Ictonychinae (from America and Eurasia) and as an outgroup, *Mustela* Linnaeus, 1758 was chosen. For the analysis, thirty cranial and dentognathic characters were selected. They were treated as unpolarised and non-additive. The character descriptions and the resulting data matrix are provided below (see section 3.1.6.). The analysis used TNT version 1.5 (Golobov & Catalano,

2016) to provide a 50% major cut-off tree using the traditional search setting (TBR algorithm and 2000 random addition sequences), based on 6 tree resulting from the most-parsomony analysis. To build the data matrix of these characters and manage the tree resulting from the analysis and to export it in a graphic format, the freeware software Mesquite version 3.31 (build 765) (Maddison & Maddison, 2017) was used.

3.1.3. Systematic Paleontology

Order **Carnivora** Bowdich, 1821

Family **Mustelidae** Fischer, 1817

Subfamily **Ictonychinae** Pocock, 1921

Tribe **Lyncodontini** Pocock, 1921

Genus ***Martellictis*** Bartolini Lucenti, 2018

Generic diagnosis. The genus includes small-sized mustelids similar to or smaller than other fossil Eurasian Lyncodontini mustelids. The cranium is rather short in comparison to that of *Enhydrictis* and *Pannonictis*. In lateral view, the cranium is not flattened markedly as in *Enhydrictis*. The frontals are rather elevated on the muzzle, giving the cranium an arched dorsal profile, similar to that of *Pannonictis*. The orbital fossa, mesial to the margin of the orbit, is not as deep as in *Enhydrictis*. The region of the postorbital constriction is elongated compared to *Pannonictis*, with a more marked constriction compared to the latter or to *Eirictis*, but not to the extent seen in *Enhydrictis*. In dorsal view, the braincase has a globular shape unlike *Pannonictis*, *Enhydrictis*, *Galictis*, *Lyncodon* and *Stipanicicia*, in which the dorsal outline is pear shaped and elongated caudally. In ventral view, the medial portion of the tympanic bullae is inflated. Unlike *Pannonictis* and *Galictis*, the embayment on the cranial side of the bulla is rather poorly developed. The palate of *Martellictis* is elongated, as testified to by the retention of the first upper premolars, feature

that contrasts with the rostrally large and much shortened palate of *Oriensictis*. In dental morphology, *Martellictis* differs from *Enhydrictis* for the possession of the better-developed P4 protocone, by the oval morphology of P3 and p4 and by the stouter and mesiodistally shorter m1, with a round and buccolingually larger talonid, in occlusal view. It differs from *Pannonictis* for the morphology and degree of development of the P4 hypocone and of the cusps on M1. The cup-like morphology of the protocone area, instead of a cone-shaped one, and the retention of the P4 hypocone, even if reduced, marks the distinction from *Eirictis*. *Oriensictis* is different from *Martellictis* for the lingual expansion of the P4 protocone, the prominent lutrine-like P4 hypocone, the development of the M1 protocone and the strongly buccolingually compressed m1. Some dentognathic features (*e.g.*, the elongated braincase, the extreme reduction of the upper and lower dentition, the teeth morphologies) of *Lyncodon* and *Stipanicicia* contrast evidently with the features of *Martellictis*. The genus *Cernictis* possesses a stouter m1 compared to *Martellictis*, especially considering the talonid. *Sminthosinis* has a cone-shaped P4 protocone, different morphology of the M1 cusps and a longer m1 paraconid, features that contrast to *Martellictis*. The corpus of the mandible in *Martellictis* is considerably shorter and more slender when compared to that of *Pannonictis*, *Oriensictis*, *Enhydrictis* and especially to that *Eirictis*, so is the ascending ramus.

A summarizing synthesis of the main characters of a generic diagnosis of the Eurasian genera *Martellictis*, *Enhydrictis*, *Eirictis*, *Oriensictis* and *Pannonictis* is provided in Table 3.1.2.

Derivatio nominis. The name is a tribute to prof. Alessando Martelli (1876-1934; professor of Mineralogy and Geology in Florence's National Forestry Institute) who was the first to acknowledge the peculiarity of the mustelid from Olivola, establishing the taxon *Proputorius olivolanus*.

Type species. *M. ardea* Gervais, 1848-1852 (monospecific).

Martellictis ardea (Gervais, 1848-1852)

(Fig. 3.1.1)

1828 martre Jorbert & Croizer, p. 25

1828 marte Bravard, p. 8

1859 *Mustela ardea* Gervais, pl. XXVII, fig. 5

1906 *Proputorius olivolanus* Martelli, p. 603, pl. VIII, fig. 2a,b

1949 *Pannonictis ardea* Schaub, p. 500, fig. 5

1950 *Enhydrictis ardea* Viret, p. 166

1954 *Enhydrictis ardea* Viret, p. 83, pl. 4, figs. 1-2

1967 *Enhydrictis ardea* Ficcarelli and Torre, p. 140, figs. 1.f, 2.f, 3.d, 4.b, 5.h-I and m, 6.f-g, 7.e; pl. XXI, fig. 18

1976 *Pannonictis ardea* Rabeder, p. 39, pl. 5-7, figs. 12-15, 19

1988 *Enhydrictis ardea* Willemsen, p. 313, pl. 2- 4

1995 *Enhydrictis ardea* Rook, p. 853

2000 *Pannonictis ardea* Spassov, p. 92

2002 *Enhydrictis ardea* Sotnikova et al., p. 380

2008 «*Enhydrictis*» *ardea* García & Howell, p. 2

2008 «*Enhydrictis*» *ardea* García et al., p. 3, fig. 2

2012 «*Enhydrictis*» *ardea* Colombero et al., p. 668

2012 *Pannonictis ardea* Fejfar et al., p. 99, fig. 3

Holotype. MNHN.F.PET2008, left hemimandible fragment with m1, recovered from Côte de Ardé (Perrier-Etouaires, Puy-de-Dôme, Auvergne-Rhône-Alpes, France).

Localities. Côte de Ardé, Olivola (Martelli, 1906), Saint Vallier (Viret, 1954),

Table 3.1.1 – Resume of the cranial and dentognathic differences of five fossil genera of Lyncodontini from Eurasia: *i.e.*, *Pannonictis* Kormos, 1931; *Enhydrictis* Forsyth Major, 1901; *Eirictis* Qiu et al., 2004; *Oriensictis* Ogino & Otsuka, 2009; and *Martellictis*. (1) Ficcarelli & Torre, 1967; (2) García & Howell, 2008; (3) Qiu et al., 2004; (4) Viret, 1954; *modified here.

	Pannonictis	*Enhydrictis*	*Eirictis*	*Oriensictis*	*Martellictis*	Ref.
Cranium, in lateral view	modestly flattened	consistently flattened	-	-	not flattened	
Dorsal profile of the cranium, in lateral view	arched	straight	arched	-	arched, frontals rather elevated on the muzzle	
Cranium length	long	long	-	-	short	
Muzzle	long and robust	short and robust	long and very robust	-	long and robust	
Temporal region	developed	developed	developed	-	shortened	(1)
Development of zyg. arches	long zygomatic arches	long zygomatic arches	long zygomatic arches	-	short zygomatic arches	
Postorbital constriction	slightly marked	consistently marked	slightly marked	-	marked	(1); *
Frontals caudal to postorb.proc.	very short	long	short	-	short	(1)
Infraorbital foramen	small	large	small	-	large	(2)
Orbital fossa	shallow	deep	shallow	-	shallow	
Anterior margin of the orbit	not marked	prominent, crest-like		-	marked, crest-like	
Braincase	generally elongated	elongated (drop-shape)	-	-	globular	
Tympanic bullae	markedly inflated and protruding	flattened	-	-	inflated only in medial portion	
Tympanic bullae mesial embayment	strong	absent	-	-	weak	
P3 and p4 shape	oval	rounded	oval	oval	oval	(1)
P4 protocone area	cup-like	cup-like	cone-shaped	cup-like	cup-like	(3)
P4 protocone	long (reaches ½ of p4)	short (reaches ⅓ of p4)	long (reaches ½ of p4)	short (reaches ⅓ of p4)	long (reaches ½ of p4)	(2)
P4 hypocone	present	reduced (slightly bulging)	absent	present	reduced (cuspid-like cingulum)	(3)
Position of m1 metaconid	posterior to protoconid.	in line with protoconid	posterior to protoconid	posterior to protoconid	posterior to protoconid.	(1)
Robustness of mandible	robust	robust	very robust	robust	gracile	(4)
Masseteric fossa	very deep	deep	very deep	deep	shallow	
Ascending ramus	robust	robust	robust	-	slender	(1)

Deutsch-Altenburg (Rabeder, 1976), Tegelen (Willemsen, 1988), Ivanovce (Fejfar et al., 2012).

Morphological and morphometric comparisons. The species *Martellictis ardea* was extensively described by several authors (among others, Schaub, 1949; Viret, 1954). A revised punctual comparison with other Plio-Pleistocene Eurasian species of the tribe Lyncodontini is here reported. In size, *Martellictis ardea* is similar to *E. galictoides* from Monte San Giovanni and *Enhydrictis* sp. of Monte Tuttavista, *Pannonictis nestii* from Pietrafitta, *P. pilgrimi* from Villany and Beremend (Ficcarelli & Torre, 1967; Abbazzi et al., 2004; García & Howell, 2008). The postorbital constriction of *M. ardea* is less marked compared to these latter species. On the contrary, it is more prominent when compared to *Eirictis* (Qiu et al., 2004), to *P. pliocaenica* from Villany-Kalkberg and *P.* cf. *nestii* from Atapuerca TE (García & Howell, 2008). The tympanic bullae of *P. pilgrimi* and *P. pliocaenica* from Hungary possess a marked medial inflation and a sharp and pronounced notch on the cranial side of the bulla. These features contrast with the morphology of *M. ardea* (Fig. 3.1.1). *E. robusta* from Longdan and some specimens of *P. pilgrimi* and *P. nestii* (see Rook, 1995) shares with *M. ardea* the button-like P1 placed close to the C. A P1 is absent in *Enhydrictis* spp. (as noted by Ficcarelli & Torre, 1967) and only rarely present in *P. pliocaenica* from Villany-Kalkberg. In contrast to *E. galictoides*, the mesial margin of P4 is lobed, as in some species of *Pannonictis* (*e.g.*, *P. nestii*, *P. pilgrimi* or *P. pliocaenica*). The P4 protocone and the lingual cingulum are reduced in comparison to those of *P. nestii* from Pirro Nord. Moreover, the protocone area is cup-shaped similar to that of *Enhydrictis*, *Oriensictis* and *Pannonictis*, and in strong contrast to that of *Eirictis*, which is characterized by the prominent conical cusp. The P4 hypocone is present but not as developed as it is in *O. nipponica* from Matsugae cave (see Ogino & Otsuka, 2008) or *P. pilgrimi* and *P. pliocaenica* from Hungary. It resembles more closely the condition visible in *E.*

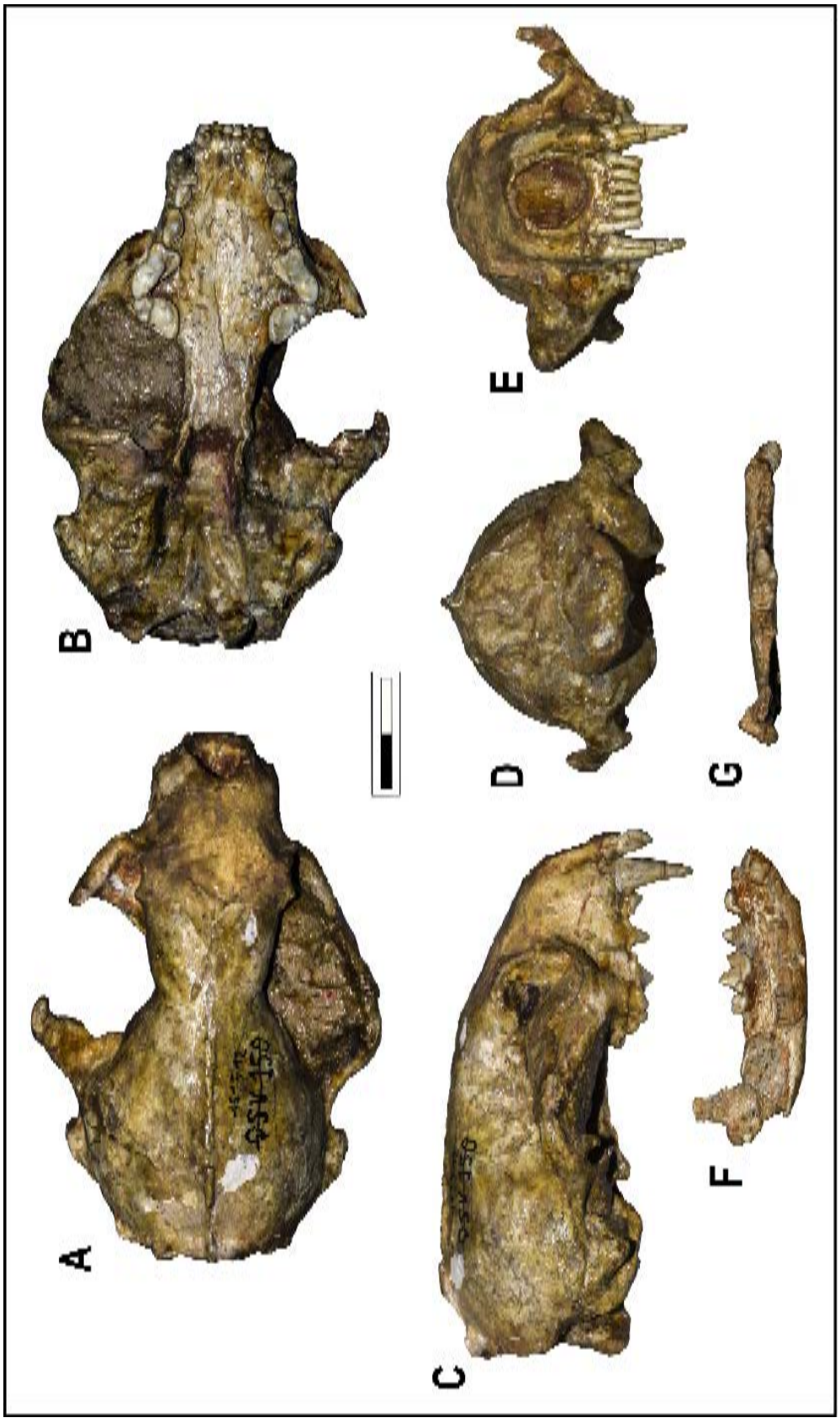

Figure 3.1.1 – *Martellictis ardea* from St. Vallier (France) and Olivola (Italy). **A-E**: **MHNL 20161912** (QSV 150 in Viret, 1954), cranium in dorsal (**A**), ventral (**B**), left lateral (**C**), caudal (**D**), and rostral (**E**) views. **F-G**: **IGF 4297**, right hemimandible in buccal (**F**) and occlusal (**G**) views. Scale bar equals 2 cm.

galictoides from Sardinia (Ficcarelli & Torre, 1967). The M1 shows an enlarged lobed talon, distally directed, unlike *P. pliocaenica* and similar to *E. galictoides, P. nestii*, and *P. pilgrimi*, although in the former this lobe it is more reduced than in the latter species. A narrowing occurs between the trigon cusps and the talon of M1, as can be found in *Pannonictis* species and unlike in *E. galictoides*. Moreover, the buccal side of the M1 of *M. ardea* is shorter mesiodistally compared to the lingual side, in a condition similar to *P. nestii* from Pietrafitta and contrast with the morphologies of *Enhydrictis* spp. or *P. pliocaenica*. The mandible corpus of *M. ardea* from Perrier, Olivola and St. Vallier is shallow, slender and it is rather shortened rostrocaudally if compared to other Lyncodontini, *e.g.*, most of all *Eirictis* spp. from China but also *P. pliocaenica* Villany-Kalkberg, *P. pilgrimi* from Beremend, *P. nestii* Upper Valdarno and *Enhydrictis* spp. from Sardinia. The lower carnassial of *M. ardea* possesses a short and enlarged paraconid and a large metaconid that ends distally compared to the distal wall of the protoconid. On the m1 talonid, the hypoconid is larger compared to that of *O. nipponica* from Matsugae cave, *E. robusta* from Longdan, *E. variabilis* from Renzidong and *E. galictoides* from Monte San Giovanni. A low furrow separates the m1 hypoconid from a distal accessory cuspulid, features absent in *Eirictis*, *Enhydrictis* or *Oriensictis*. Lingually to this distal accessory cuspulid, a high cristid borders the distal and distolingual portion of the m1 talonid. The distal cristid is not so elevated in *P. pliocaenica* from Villany-Kalkberg, whereas unworn specimens of *P. nestii* from Pirro Nord and Upper Valdarno and of *P. pilgrimi* from Beremend also show an accessory cuspulid distal to the hypoconid.

3.1.4. Discussion

3.1.4.1. Taxonomic remarks on Martellictis

The analysis of the cranial and dentognathic features of the highly disputed species "*Mustela*" *ardea* Gervais, 1848-1852 revealed numerous peculiarities that do not

fit with the diagnosis of other genera of Lyncodontini described in literature, namely *Enhydrictis* Forsyth Major, 1901, *Eirictis* Qiu et al., 2004, *Oriensictis* Ogino & Otsuka, 2008, *Pannonictis* Kormos, 1931. Among these differences, the most evident are the degree of embayment of the mesial side of the tympanic bullae and their modest medial inflation; the prominence of the postorbital constriction; the globular shape of the braincase, in occlusal view; the cup-like P4 protocone, the presence and development of the P4 hypoconid; the development and morphology of the cusps on M1; and the occlusal shape of the cuspulids of m1, in occlusal view. From the morphological analysis, it appears evident that some morphologies retained by *M. ardea* resemble those of *Pannonictis* spp., whereas others *Enhydrictis* spp. This fact might have led numerous scholar to assign the species to the latter genus (Viret, 1954; Ficcarelli & Torre, 1967; Rook, 1995) whereas others to the former one (Schaub, 1949; Rabeder, 1976; Fejfar et al., 2012). Nonetheless, to choose between one and the other attribution would mean to set aside part of the peculiar features possessed by *Martellictis ardea*. This is particularly true for the cranial ones, and among others the morphology of the tympanic bullae, whose morphology is one of the most systematically relevant characteristics for Carnivora (as noted by Fejfar et al.2012).

3.1.4.2. An updated review of the diversity of the Plio-Pleistocene Lyncodontini

Fig. 3.1.2. resumes the most important and verified sites that record the palearctic genera of Lyncodontini. Numerous authors (*e.g.*, Kormos, 1931; Pilgrim, 1932; Schreuder, 1935; Rook, 1995; García & Howell, 2008) suggested that the earliest record of the widespread *Pannonictis* is most probably the one reported by Zdansky (1927) from the late Miocene Hipparion-beds of China. Although García & Howell, 2008 suggested ascribing the taxon to *P. pachygnatha*, it would be better more prudent to refer to it as *Pannonictis* sp. indet. Zdanski (1927). In Asia, three Late Pliocene-Early Pleistocene localities provide important record of *Pannonictis*.

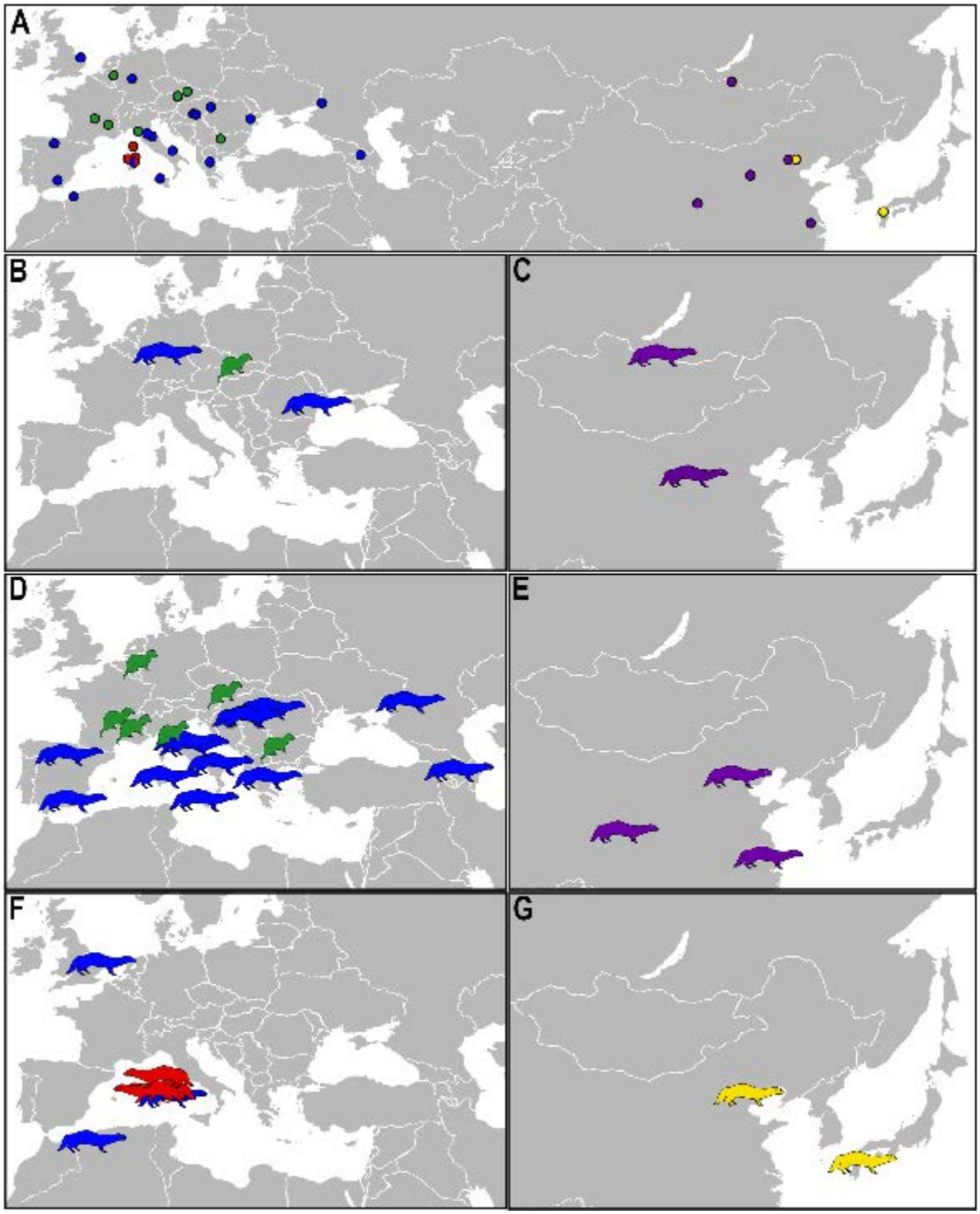

Figure 3.1.2 – Geographic and chronological distribution of Eurasian Lyncodontini from Early Pliocene to Late Pleistocene times. Color legend: **blue**, *Pannonictis* Kormos, 1931; **green**, *Martellictis*; **purple**, *Eirictis* Qiu et al., 2004; **red**, *Enhydrictis* Forsyth Major, 1901; **yellow**, *Oriensictis* Ogino & Otsuka, 2009. **A**, Schematic representation of all the localities reporting specimens of Lyncodontini, references in the text. **B-C**, Pliocene European (B) and Asian (C) occurrences of Lyncodontini - *Eirictis*: Shamar (Mongolia; Sotnikova et al., 2002), Nihewan Basin (China; Qiu et

The lyncondontine material of Chinese Yushe Basin (Teilhard de Chardin & Leroy, 1945) and Nihewan Basin (Teilhard de Chardin & Pivetau, 1930), and of the Mongolian site of Shamar (Sotnikova, 1980) were ascribed to the large-sized species *P. pachygnatha* (although the generic attribution was questioned by Qiu et al., 2004; see later).

Among the earliest European representatives of *Pannonictis* there is the record from the Early Pliocene (MN 15) of Wölfersheim (Germany) (Fig. 3.1.2). From this site, Morlo & Kundrát (2001) described two dental specimen of *Pannonictis* sp. and few others of "*E.*" *ardea*. As the authors pointed out, the material is considerably old for the Eurasian Lyncodontini record, probably the earliest record of *Pannonictis*-

al., 2004); *Martellictis*: Ivanovce (Slovakia, Fejfar et al., 2012); *Pannonictis*: Wölfersheim (Germany; Morlo & Kundrát, 2001); Etulia (Moldova, Sotnikova et al., 2002). **D-E**, European (D) and Asian (E) localities of the Early Pleistocene (*partim*, *i.e.*, until the end of Late Villafranchian) - *Eirictis*: Longdan (China, Qiu et al., 2004); Renzidong (China, Jin & Liu, 2009); Yushe (China, Teilhard de Chardin & Leroy, 1945); *Martellictis*, Perrier-Etouaires (France, Schaub, 1949); Saint Vallier (France, Viret, 1954); Tegelen (The Netherlands, Willemsen, 1988); Olivola (Italy, Martelli, 1906); Deutsch-Altenburg 2C (Austria, Rabeder, 1976); Varshets (Bulgaria, Spassov, 2000); *Pannonictis*: Atapuerca TE (Spain; García & Howell, 2008); Barranco Leon 5, Fuente Nueva 3 (Spain, Madurell-Malapeira et al., 2014); Monte Tuttavista – VII Mustelide (Sardinia, Italy, Abbazzi et al., 2004); Upper Valdarno (Italy, Martelli, 1906); Pietrafitta (Italy, Rook, 1995); Pirro Nord (Italy, Colombero et al., 2012); Monte Pellegrino (Sicily, Italy, Burgio & Fiore, 1997); Villany (Hungary, Jánossy, 1986); Csarnota 1 (Hungary, Jánossy, 1986); Beremend (Hungary, Jánossy, 1986); Betfia 2-4/ Püspökfurdö (Romania, Jánossy, 1986); Livakkos (Greece, Koufos, 2014); Khapry (Russia, Sotnikova et al., 2002); Palan-Tyukan (Azerbaijan). **F-G**, late Early Pleistocene (Epivillafranchian) – Late Pleistocene localities of Europe (F) and Asia (G) - *Enhydrictis*: Monte Tuttavista – numerous younger fissures (Sardinia, Italy, Abbazzi et al., 2004); Monte San Giovanni (Sardinia, Italy, Forsyth Major, 1901), Grotta della Dragonara (Sardinia, Italy, Masseti, 1995); Oletta cave (Corsica, France, Ferrandini & Salotti, 1995); *Oriensictis*: Zhoukoudian (China, Pei, 1934); Matsugae Cave (Japan, Ogino & Otsuka, 2008); *Pannonictis*: West Runton (Great Britain, Stuart, 1982); Tighennif/ Ternifine (Algeria, Geraads, 2016); Monte Tuttavista – X-3-Uccelli (Sardinia, Italy, Abbazzi et al., 2004).

like mustelids in Europe. The fragmented right P4 (SMF 2000/212) and the right m2 (SMF 2000/213) could be reasonably ascribed to the genus *Pannonictis*, but the specimens of "*Enhydrictis*" possesses several features that contrast significantly with the type specimens of the genus. The hypothesis of a primitive state of this taxon, even considering ages, cannot compensate the "lack of some typical features" (Morlo & Kundrát, 2001: 170) or the prominence of other morphologies. These elements cast doubts on the generic and specific attribution of the material, even if the specimens are close in size to *M. ardea* from St. Vallier. Among the most evident discrepancies, there is the high conical cusp on the P4 protocone area, unlike the majority of the Lyncodontini of Eurasia, which generally possess a cup-like protocone area girdled by a swelling cingulum. A close condition can be found in *Eirictis*, whose P4 possesses a conical cusp in the protocone area (Qiu et al., 2004). Another point of similarity between the Wölfersheim specimen and *Eirictis* is the lack of a hypocone on the lingual side of the P4 (a diagnostic feature of the latter, see Qiu et al., 2004 and García & Howell, 2008). The morphology of the right M1 (SFM2000/217) from Wölfersheim differs from that of other Lyncodontini taxa, as it has an enlarged buccal cingulum that expands buccally and appears continuous between the paracone and the metacone. Moreover, the M1 is proportionately shortened buccolingually. In contrast, the species of *Pannonictis*, *Enhydrictis*, *Martellictis*, *Eirictis* and *Oriensictis* have the cingulum divided into two lobes, a larger one for the paracone and the smaller for the metacone (Ficcarelli & Torre, 1967; Abbazzi et al., 2004; Qiu et al., 2004; García & Howell, 2008; Ogino & Otsuka, 2008). Similarly to *Enhydrictis* from Monte San Giovanni and Monte Tuttavista, in occlusal view, the M1 is not so curved distally. Nevertheless, when closely compared to the M1 of *Enhydrictis* spp., the M1 metacone of SMF 2000/217 is more developed than that in the Sardinian taxa. The development of the cusp resembles that of some *Pannonictis* species (*e.g.*, *P. pilgrimi* and *P. pliocaenica* from Hungarian localities) or to *M. ardea* from St. Vallier. The hypocone is missing

or greatly reduced in the German specimen, whereas it is generally enlarged in *Pannonictis* and *Eirictis*. Lingually, the area of the hypocone differs greatly even from *M. ardea* from St. Vallier as the latter shows a prominent distal extension of the M1, giving the tooth a peculiar shape in occlusal view. The upper and lower canines (respectively SMF 2000/214 and SMF 2000/215) are short mesiodistally. The left m1 SMF 2000/218, and particularly its paraconid, is shorter mesiodistally compared to that of *Enhydrictis* from Monte San Giovanni and Monte Tuttavista (Ficcarelli & Torre, 1967) and *E. robusta* from Longdan (Qiu et al., 2004), but similar to the m1 of the holotype of *M. ardea* from Côte de Ardé. In occlusal view, the metaconid is less separated from the protoconid compared to *Pannonictis* and *Martellictis*, but it is also more developed and stouter than in *Enhydrictis* and *Eirictis* spp. Among the Lyncodontini of Eurasia, *Oriensictis* has the largest and the most individualized m1 metaconid (Ogino & Otsuka, 2008). In occlusal view, a round cristid girdles the m1 talonid of SMF 2000/218, departing from the hypoconid and extends to the lingual side of the talonid. A similar morphology can be seen in some *Pannonictis* spp. (*e.g.*, *P. nestii* from the Pirro Nord and Upper Valdarno) or in *Oriensictis* from Matsugae Cave (Ogino & Otsuka, 2008). The m1 talonid of *Enhydrictis*, *Eirictis* and *Martellictis* tends to be more elongated. All these features considered, the attribution to the genus *Enhydrictis* or the species *M. ardea* appears rather unlikely. Some features are suggestive of an affinity with the genus *Eirictis* (*e.g.*, the P4 protocone, the absence of a P4 hypocone) although these specimens are considerably smaller and more slender compared to the average individuals of *Eirictis*. In conclusion, the record from Wölfersheim reports possibly the earliest European specimens of a member of the genus *Pannonictis* and a few other specimens of an undetermined taxon, though surely not related to the genus *Enhydrictis* nor with the species *M. ardea*. Future revision and additional material could help clear out these doubts on *Eirictis*? sp. indet.

The first *Pannonictis* species to be described is the Early Pleistocene *P. nestii*, from

the Upper Valdarno in Tuscany (Martelli, 1906) and the younger site of Pietrafitta in Umbria (Rook, 1995). García & Howell (2008) referred several specimens recovered in the site of Sima del Elefante (Sierra de Atapuerca) to *Pannonictis* cf. *nestii*. García et al. (2008) grouped *P. nestii* with "*E.*" *ardea*, without any discussion of the morphological evidence supporting this synonymy. On this matter, other scholars disagree (see among others Viret, 1954; Ficcarelli & Torre, 1967; Rook, 1995; Sotnikova et al., 2002). Another important record of *Pannonictis* is that of *P. pliocaenica* from the complex of cavities of Villany-Kalkberg (Hungary). Other two of the richest localities for Lyncodontini remains of this complex are Villany 3 and 5, which span between 2 and 1.5 Ma (Jánossy, 1986; Spassov, 2000). From these localities, Kormos (1933) described *P. pilgrimi*, distinguished from *P. pliocaenica* for its smaller size and some peculiarities. In the scientific literature, various hypotheses of synonymy were provided for *P. pilgrimi*. In addition to those reported above regarding the disputed synonymy to "*E.*" *ardea* (see Viret, 1954), Ficcarelli & Torre (1967) suggested uniting this species with *P. nestii*, rather than with *M. ardea*. By contrast, García & Howell (2008) proposed the inclusion of *P. pilgrimi* in *P. pliocaenica*, addressing the issue of the large size difference to a strong degree of sexual dimorphism. In this view, *P. pliocaenica* would represent the larger male individuals, whereas *P. pilgrimi* would represent the smaller females. The genus *Pannonictis* has also been recovered in the few Mediterranean islands: *Pannonictis arzilla* (De Gregorio, 1886) was described from the endemic fauna of the Monte Pellegrino (Sicily). This taxon is probably close to *P. nestii* (see Rook, 1995; Burgio & Fiore, 1997). Furthermore, the Early-Middle Pleistocene quarries of Monte Tuttavista (Nuoro, Sardinia) yielded few but significant specimens of *Pannonictis* sp. (see section 3.2.).

Recently, Peters & De Vos (2012) described some dentognathic remains from the Dutch locality of Langenboom (Noord-Brabant) attributing them to "*Pannonictis*" *ardea*. As described by Peters & De Vos (2012), the sample possesses several

peculiarities worth noting. For instance, the presence of a cuspular P4 protocone girdled by a prominent cingulum, the absence of P4 hypocone (or a greatly reduced one), the large and slightly distally curved M1, the continuous and marked buccal cingulum on the M1, the presence of the M1 protocone and protoconule but no metaconule, and the absence of the M1 hypocone. On the lower teeth, the p3 and p4 are markedly elongated mesiodistally, in occlusal view. The p4 shows a large distal accessory cuspulid, visible in all views. The m1 specimen of Langenboom has a mesiodistally elongated paraconid, an enlarged and strongly individualized metaconid and a round talonid. Many of these features resemble those of the fossils from Wölfersheim (Morlo & Kundrát, 2001; see the discussion above), although in size the specimens from Langenboom are larger compared to those from the German sample. As for the German sample, the attribution to the genus *Pannonictis* and to the species *M. ardea* appears unlikely. As the Langenboom fauna resembles that of St. Vallier and Tegelen (Peters & De Vos, 2012), the similarity between the German and the Dutch findings would suggest the occurrence in the Pliocene-Earliest Pleistocene of central-western Europe of a previously unknown form of mustelid, probably related to *Eirictis*.

As can be noted in Fig. 3.1.2, the genus *Pannonictis* is considerably widespread across Eurasia, with a broad geographic range spanning from Spain (García & Howell, 2008; Madurell-Malapeira et al., 2014) to Great Britain (Stuart 1982), southeastern Russia and Moldova (Sotnikova et al., 2002), China and Mongolia (Sotnikova, 1980).

Qiu et al. (2004) erected the genus *Eirictis* for the species of Longdan (Dongxiang, Gansu, China; Early Pleistocene), and García & Howell (2008) recognized its validity, especially in comparison to *Pannonictis*. Qiu et al. (2004) included in *Eirictis*, *E. robusta* from Longdan and *E. pachygnata* from Nihewan. Among the distinctive features of *Eirictis*, the latter authors remarked the absence of a hypocone on the P4. Jin & Liu (2009) included in this genus the new species *E. variabilis*, erected for

the findings of Renzidong Cave (eastern China).

Another Asian taxon of Lyncodontini comes from the Middle Pleistocene Matsugae cave deposits (northern Kyushu) of West Japan, the genus *Oriensictis* with the species *O. nipponica* (Naora, 1968). The authors propose the inclusion of the species *Lutra melina* Pei, 1934 from Zhoukoudian 1 (Middle Pleistocene, China) in the genus *Oriensictis*.

The most peculiar taxon within the European record of Lyncodontini is *Enhydrictis galictoides* from the Late Pleistocene Sardinian locality of Monte San Giovanni (Forsyth Major, 1901; Ficcarelli & Torre, 1967) (Fig. 3.1.2). The genus *Enhydrictis* is more elusive than *Pannonictis* in the fossil record, and is known only from few other Sardinian and Corsican localities. Many authors (Forsyth Major, 1901; Pilgrim, 1932; Ficcarelli & Torre, 1967) regarded the peculiar features of the genus as adaptations to an aquatic lifestyle (*e.g.*, strong postorbital constriction, shorter muzzle, etc.).

Geraads (2016) recently reported the first fossil taxon of the tribe Lyncodontini of northern Africa. The author described the sample from Tighennif (or Ternifine, Algeria; Fig. 3.1.2) and ascribed the scarce sample to the new species *E. hoffstetteri*. This discovery expands the areal of Plio-Pleistocene Lyncodontini, shanding new light on their dispersion dynamics, at present unknown in the African continent. Unfortunately, no complete cranial or mandibular specimens were found, making it is difficult to ascribe precisely the material to a species, as the major diagnostic characters are missing (*e.g.*, the postorbital constriction, the height of the cranium, the shape of the braincase, the presence and/or the development of hypocone on the P4 and features of the m1 talonid; see Table 3.1.1). Nevertheless, there are several features displayed by the holotype and the referred specimens of *E. hoffstetteri* (Fig.1 in Geraads 2016: page 447) that cast doubts on the attribution of the Algerian material to the genus *Enhydrictis*. Among these, briefly discuss here, the morphology of M1. It tends to be arched distally and stretched and

possesses an enlarged talon compared to the trigon cusps. In occlusal view, the M1 of *Enhydrictis* is not curved distally. The M1 metacone of *E. hoffstetteri* is smaller than the paracone but still prominent and it is evidently girdled by a large and round cingulum especially on the distal side. On the contrary, the specimens of *Enhydrictis* from Monte S. Giovanni or Monte Tuttavista, the metacone is greatly reduced and does not show a marked cingulum around it (Ficcarelli & Torre, 1967; Abbazzi et al., 2004). The position of the enlarged M1 protocone and protoconule of *E. hoffstetteri* differs from the condition of *Enhydrictis* spp. as in the specimens from Tighennif they lie in the centre of the tooth, whereas in latter taxa they are placed towards the lingual side of the M1, close to the hypocone. In contrast to the condition seen in *M. ardea*, the talon tends to narrow towards the hypocone area. The features of the M1 of Tighennif taxon are similar to those retained by some species of *Pannonictis* (*e.g.*, *P. pliocaenica* from Villany-Kalkhberg). The considerable height and breadth of the mandible corpus of TER-2008 contrast with the slender and shallow mandibles of *M. ardea* and resemble those of robust forms like *Pannonictis pliocaenica* or even *Eirictis*. In the lower teeth, the prominent and high wrinkled pattern of the basal cingulid of the canine is similar to that shown by some species of *Pannonictis* (*e.g.*, *P. pliocaenica* from Villany or *P.* cf. *nestii* from Atapuerca, Garcia & Howell, 2008). Furthermore, the stout and shortened m1, especially considering the talonid, and the enlarged metaconid, extended lingually, contrast with the principal features visible in specimens of *Enhydrictis* spp. (*e.g.*, large metaconid but close to the protoconid). By contrast, *M. ardea* possesses a buccolingually wider m1 compared to that of TER-2008, and a stouter and shorted paraconid. Altogether, these morphologies are suggestive of a closer affinity of the taxon from Tighennif (Ternifine) to the genus *Pannonictis*, rather than to *Enhydrictis*. Probably the species "*E.*" *hoffstetteri* should be referred to as *Pannonictis hoffstetteri*. The misinterpretation might have arisen as a consequence of the underestimation of the diversity of Plio-Pleistocene Lyncodontini of Eurasia.

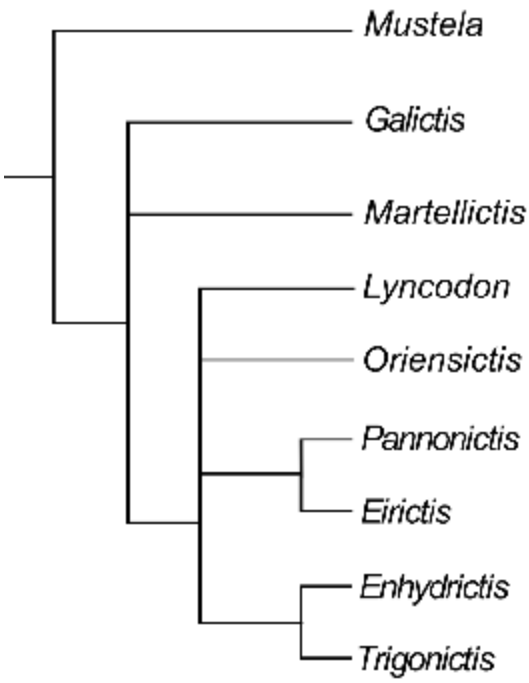

Figure 3.1.3 – The 50% major cut-off cladogram of selected Eurasian and American Lyncodontini mustelids produced with a cladistic analysis in TNT, based on 30 craniodental characters (see section 3.1.2.).

Geraads (2016) suggests to include the cluster of all the genera in *Enhydrictis* sensu lato, without taking into consideration the numerous differences that characterize the Lyncodontini (for further discussion on the variability of Lyncodontini see also Garcia & Howell, 2008 and Colombero et al., 2012).

Recently, Jiangzuo et al. (2019) reported the discovery of new specimens a Lyncodontini from the Jinyuan cave (Puwan, Dalian, Liaoning Province; Early-Middle Pleistocene). In their description, the authors suggest to synonymize the genera *Enhydrictis* and *Oriensictis* under the former (following Article 23 of the International Commission on Zoological Nomenclature, 1999) and, thus, ascribe the sample to the species *Enhydrictis melina* (Pei, 1934). Jiangzuo et al. (2019) propose considering *Oriensictis* only as a subgenus for the Asian forms of *Enhydrictis*. The inclusion of the Asian species *E. melina* and *E. nipponica* within the European and endemic genus *Enhydrictis* leads the authors to put forward the hypothesis of the dispersion and radiation across Eurasia. The presence in the Paratethys region (Caucasus) of *M. ardea*, the basal form to the monophyletic clade of *Enhydrictis*,

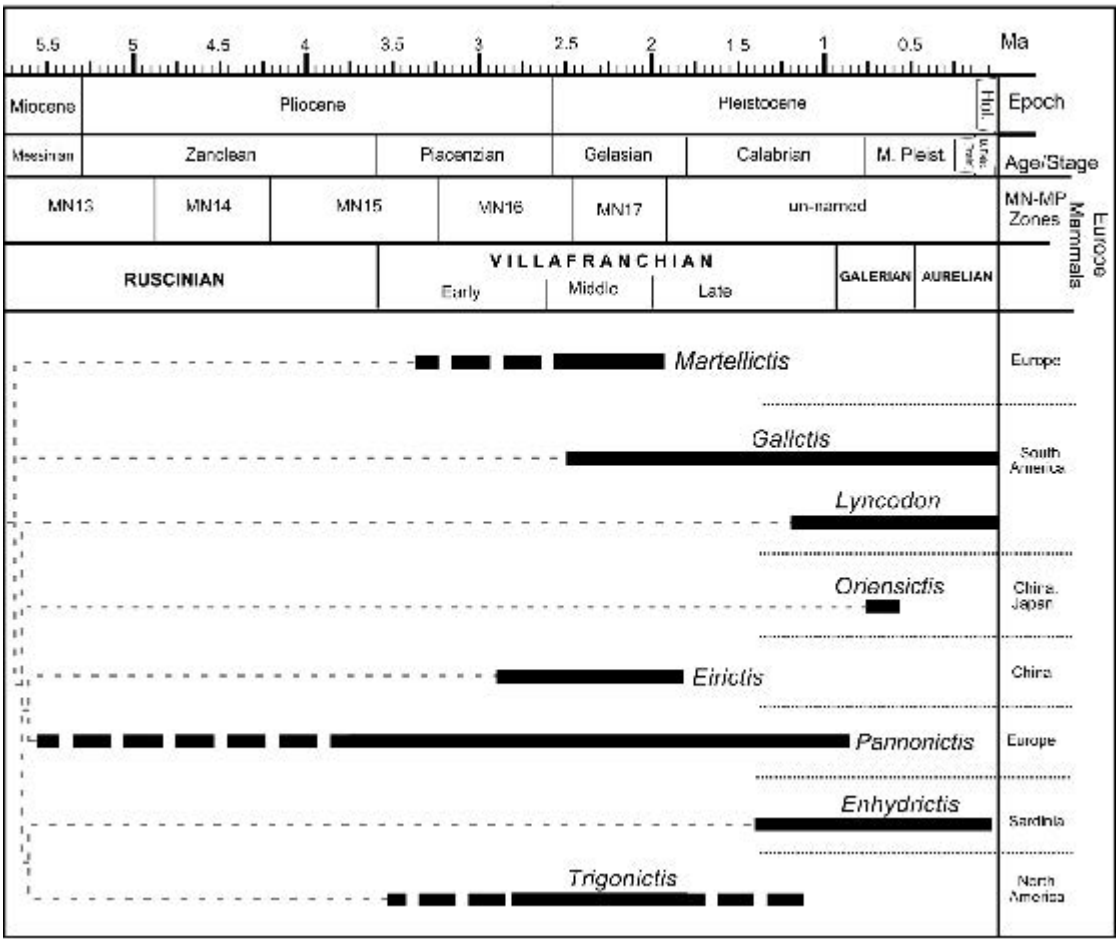

Figure 3.1.4 – Stratigraphic ranges and postulated phyletic relationships for genera of the tribe Lyncodontini discussed in this report. The relationship is largely based on the cladogram in Fig. 3.1.4. Based on the following references: Bjork, 1970; Yensen & Tarifa, 2003; Abbazzi et al., 2004; Qiu et al., 2004; García et al., 2008; Ogino & Otsuka, 2008; Rodrigues et al., 2015.

might have led to the appearance of taxa with similar and comparable adaptations at the two extremes of Eurasia. The hypothesis proposed by Jianzuo et al. (2019), although interesting, is feebly supported on both morphological and analytical ground. The similarities between cranial morphologies of the taxon from Jinyuan cave and the type specimen from Sardinia appear evident, particularly the apparent flatness and the postorbital constriction. Nevertheless, other features and the upper dental morphology are coherent with that of *Oriensictis*, whereas differing greatly from *E. galictoides*. The lateral expansion of the palate, the development of the P4 protocone and the hypocone area, the presence of a P4 protoconule, the enlargement of the M1 protocone, the presence of the M1 metaconule are all

features that markedly contrast with the type specimens of *Enhydrictis*. The latter genus shares several cranial features with the members of the subfamily Lutrinae, the flattened cranium, bulging orbits, etc. (see among others Ficcarelli & Torre, 1967). Noteworthy, these features are the same identified by Jiangzuo et al. (2019), also shared with the taxon from Jinyuan cave. The analogous features recognized in these taxa might have arisen from convergent adaption to similar environments, hypothesis mentioned by Jiangzuo et al. (2019) but not thoroughly analyzed.

Of the numerous Ictonychinae of North America, the one most probably related to *Pannonictis* is the Early Pleistocene *Trigonictis* (as noted by Rook, 1995). Numerous authors have proposed synonymizing these two genera (*e.g.*, Repenning, 1967; Kurtén & Anderson, 1980), but the presence of primitive features and some characters in the former (*e.g.*, the morphology of the M1 and the development of its cusps), which cannot be found in either *Pannonictis* or in *Enhydrictis*, would suggest maintaining *Trigonictis* as a separate genus.

As shown from the analyses and the resuming Tabs 3.1.1-3.1.2, the morphological pattern of the cranial and dentognathic features of *M. ardea* differ prominently from those of other Eurasian taxa of Lyncodontini, thereby supporting the recognition of a new genus. This has important implications in the complex taxonomic dispute of Eurasian Lyncodontini as it forces a reconsideration of their Plio-Pleistocene paleodiversity as well as their morphological affinities and relationships.

3.1.4.3. Cladistic analysis and its implications

A cladistic analysis was carried out on the basis of the character matrix for fossil and extant genera of Eurasian and American Lyncodontini, as described in the section 3.1.2. The fossil genera of the tribe Lyncodontini were selected among the holoarctic fossil taxa based on the completeness of their fossil record and the number of characters recognizable in the type specimens of these taxa. According to recent molecular phylogenies (*e.g.*, Sato et al., 2012; Sato, 2016) the two closest

subfamilies to Ictonychinae are Lutrinae and Mustelinae. As the members of the former subfamily possess several prominent adaptations to an aquatic lifestyle, the outgroup genus chosen in the cladistic analysis is *Mustela* Linnaeus, 1758.

The analysis used TNT ver. 1.5 to provide a 50% major cut-off tree (Fig. 3.1.3.) based on the six shortest trees (see Appendix). This analysis represents the first attempt to investigate the phylogeny of fossil Eurasian Lyncodontini at a generic level. It produced relatively well resolved tree, with a consistency index (CI) of 0.645 and a retention one (RI) of 0.352. As it is visible in Fig. 3.1.3., there are different degrees of possible affinities previously underestimated in the literature. *Lyncodon* and *Oriensictis* equally differ from the two clustered groups, *i.e.*, *Pannonictis-Eirictis* and *Enhydrictis-Trigonictis*. With the distinction of the Eurasian "pannonictine" group (*i.e.*, *Pannonictis-Eirictis*) from *Martellictis*, on the one side, and from *Enhydrictis* and the American *Trigonictis*, on the other, the resulting arrangement testifies to previously unnoticed relationships in the tribe Lyncodontini. The obtained tree supports the peculiarity of the set of morphological features of *Martellictis*, as pointed out by its position in the phylogenetic tree (Fig. 3.1.3). Together with the South American *Galictis*, it is the sister taxon of all the other Eurasian Lyncodontini and of the American *Lyncodon* and *Trigonictis*. In this configuration, the affinity of *Martellictis* to *Pannonictis* or to *Enhydrictis* is not as close as expected from literature (see sections 1.1. and 3.1.3.2.). Indeed set of features possessed by *Martellictis* is suggestive of a primitive state among Lyncodontini. Thus, the distinction of these taxa into different genera seems well supported. Fig. 3.1.3 also points out the difference between the endemic genus *Enhydrictis* and the European taxa of Lyncodontini, suggesting that its evolution set in the insular context of Sardinia and Corsica (Fig. 3.1.2), from mainland ancestors like *Martellictis* or *Pannonictis* (notably, the latter is present in the record of Sardinia, *i.e.*, Monte Tuttavista see Abbazzi et al., 2004). The schematic representation in Fig. 3.1.4, relates the phylogenetic relationship between the Lyncodontini genera of the cladistics

analysis here performed and the past and present distribution of these taxa.

3.1.5. Conclusions

The taxonomic tangle of the Plio-Pleistocene tribe Lyncodontini of Eurasia is intricate and debated since the beginning of the last century. The dispute arose mainly due to the scantiness and the sparse nature of their fossil record. Before the 1950s, few and pivotal studies were done on these taxa but, since then, only few authors have worked on their systematics. In recent years, the tribe of Lyncodontini has regained the interest of scholars (*e.g.*, García et al., 2008). Among the most discussed species, there is "*Mustela*" *ardea*: its generic attribution, either assigned to *Pannonictis* (Schaub, 1949; Rabeder, 1976; Fejfar et al., 2012;) or to *Enhydrictis* (Viret, 1954; Ficcarelli & Torre, 1967; Rook, 1995) and even its correct authorship (Peters & De Vos, 2012), were all matter of harsh debate.

Thanks to a deep morphological revision of Eurasian and American material, the presented analyses point out the need of a different generic name for the peculiar Lyncodontini sample coming from sites of Perrier-Etouaires, St. Vallier and Olivola. This proposal is based on evident morphological features of the specimens from these and other localities (Fig. 3.1.2), which differ markedly from other fossil taxa of the same subfamily (see Table 3.1.1). Moreover, it provides a clearer taxonomic scenario for the tribe. The results are also supported by the first cladistics analysis, based on eight genera of Eurasian and American Lyncodontini and thirty selected characters. The distinction of *Martellictis* appears evident, as well as its differences with *Enhydrictis* and *Pannonictis* (Figs. 3.1.3-3.1.4).

Martellictis ardea becomes a widespread and important element within this highly complex systematic debate, particularly as it testifies to a greater paleodiversity of the Eurasian Plio-Pleistocene Mustelidae than that assumed in the last century. Although a different generic attribution for the species *M. ardea* poses new questions regarding the origin and of the dispersion of this group of mustelids in western

Eurasia from or into the American continent, it also helps resolving part of the debate on these taxa. For instance, the presence of a primitive-like *Martellictis ardea* in Pliocene-Earliest Pleistocene continental sites implies that the genus *Enhydrictis*, which shows several derived dental and skeletal features, represents a distinct and endemic genus exclusive of the insular context of late Early to Late Pleistocene of Sardinia and Corsica. In the light of this new taxonomic arrangement and in order to acknowledge the previously underestimated diversity of fossil Lyncodontini, a revision of the collections of European fossil mustelid is urgent and desirable.

3.1.6. Appendix

3.1.6.1. Character list and description

1. Cranial height, in lateral view: (0) not flattened; (1) consistently flattened.
2. Dorsal profile of the cranium; in lateral view: (0) strongly arched; (1) modestly arched; (2) straight.
3. Cranium rostrocaudal length: (0) long; (1) short.
4. Temporal region and the development of zygomatic arches: (0) developed and long zygomatic arches; (1) shortened and short zygomatic arches.
5. Postorbital constriction: (0) slightly marked; (1) marked; (2) consistently marked.
6. Frontals development posterior to the postorbital processes: (0) very short; (1) short; (2) long.
7. Infraorbital foramen: (1) small; (1) large.
8. Orbital fossa: (0) shallow; (1) deep.
9. Anterior margin of the orbit: (0) not marked; (1) crest-like and marked; (2) very sharp and prominent margin.
10. Braincase morphology; in dorsal view: (0) elongated; (1) globular.
11. Tympanic bullae; general shape: (0) markedly inflated and protruding in lateral view; (1) inflation limited to medial portion; (2) flattened.
12. Tympanic bullae mesial embayment: (0) strong; (1) weak; (2) absent.
13. P4 hypocone: (0) absent; (1) reduced to cuspid-like cingulum; (2) present.
14. Distal extension P4 protocone: (0) absent (cuspid-like protocone); (1) short

(reaches a third of the P4); (2) long (reaches half of the P4).

15. P3 and p4 shape: (0) oval; (1) rounded.
16. Robustness of mandible: (0) gracile; (1) robust; (2) very robust.
17. Masseteric fossa: (0) shallow; (1) deep; (2) very deep.
18. Ascending ramus: (0) slender; (1) robust.
19. Mesial margin of the P4: (0) embayed; (1) continuous cingulum-like.
20. M1 constriction: (0) present; (1) missing.
21. P1: (0) present; (1) absent.
22. m1 metaconid: (0) present; (1) absent.
23. P4 protocone: (0) conical cusp; (1) shelf only.
24. p4 distal accessory cuspulids: (0) absent; (1) present.
25. M1 metacone: (0) reduced compared to paracone; (1) equal in size to the paracone; (2) lost.
26. Diastemata between lower premolars: (0) absent; (1) present.
27. m1 trigonid length: (0) longer or equal to talonid; (1) shorter.
28. M1 metaconule: (0) absent; (1) present.
29. Sagittal crest: (0) end at the occipital; (1) hangs over the occipitals.
30. Reduction of the upper premolars: (0) no reduction (presence of P2); (1) reduction (no P2).

3.1.6.2. Data matrix

Table 3.1.2 – Matrix of the 30 cranial and dentognathic characters for the 9 genera used in the cladistic analysis.

	1	**2**	**3**	**4**	**5**	**6**	**7**	**8**	**9**	**10**	**1**	**2**	**3**	**4**	**5**	**6**	**7**	**8**	**9**	**20**	**1**	**2**	**3**	**4**	**5**	**6**	**7**	**8**	**9**	**30**
Mustela	0	0	0	0	0	2	0	0	0	0	0	2	0	0	0	0	0	0	0	0	1	1	0	0	0	0	0	0	0	0
Pannonictis	0	0	0	0	0	0	0	0	0	0	0	0	0	2	0	1	2	1	0	0	0	0	1	1	0	1	0	1	1	0
Eirictis	0	0	?	0	0	1	0	0	0	0	?	?	2	2	0	2	2	1	1	0	0	0	0	0	0	1	0	0	?	0
Martellictis	0	1	1	1	1	1	1	0	1	1	1	1	1	2	0	0	0	0	0	0	0	0	1	0	0	1	0	0	1	0
Enhydrictis	1	2	0	0	2	2	1	1	2	0	2	2	1	1	1	1	1	1	1	1	1	0	1	0	0	1	0	1	0	0
Galictis	0	0	0	0	0	0	0	0	0	0	1	0	0	2	0	0	0	0	0	0	1	1	1	0	2	0	1	0	0	0
Lyncodon	0	0	0	1	0	?	?	0	?	0	0	1	2	2	0	1	1	0	?	0	1	1	?	0	1	?	0	0	0	1
Oriensictis	?	?	?	?	?	?	?	?	?	?	?	?	?	0	2	0	1	?	?	0	1	1	0	0	?	0	?	0	1	?	0
Trigonictis	?	?	?	?	?	?	?	?	?	?	?	?	?	1	2	1	1	1	1	0	1	?	0	0	0	0	1	0	0	?	0

3.1.6.3. Tree resulting from phylogenetic analysis

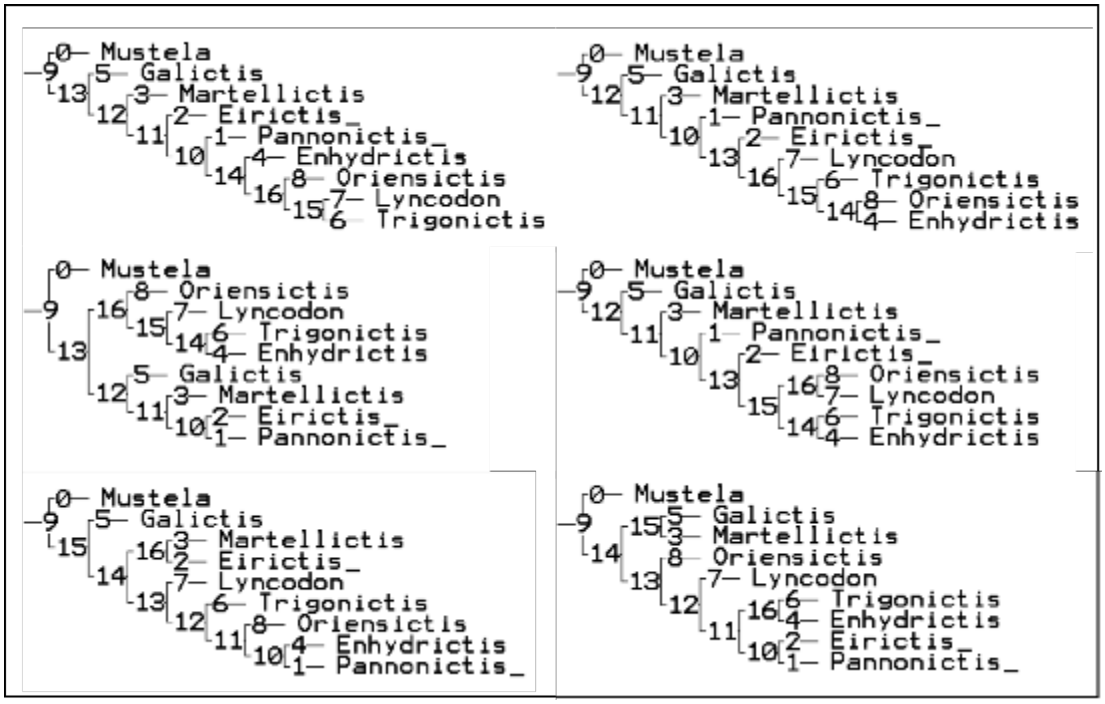

Figure 3.1.5 – Additional tree obtained from the analysis Six equally parsimonious trees that produced the 50% major cut-off tree in Fig. 3.1.3.

3.2. Taxonomy and evolution of the insular Lyncodontini of Monte Tuttavista (Early and middle Pleistocene; Orosei, Sardinia)

3.2.1. Context

In this study, the fossil record of the mustelids of the tribe Lyncodontini recovered in the karst infill of Monte Tuttavista are described. The interpretation of this extensive record might shed new light on the origin and evolution of Sardinian insular carnivore guilds and the complex evolutionary history of Lyncodontini.

3.2.2. Systematic Paleontology

Order **Carnivora** Bowdich, 1821.

Family **Mustelidae** Fischer, 1817.

Subfamily **Ictonychinae** Pocock, 1921.

Tribe **Lyncodontini** Pocock, 1921.

Genus ***Pannonictis*** Kormos, 1931

Pannonictis baroniensis Rook et al., 2018

(Figs. 3.2.1-3.2.2)

1998 Mustelidae gen. sp. nov. nov. - Cordy, p. 40.

2003 *Pannonictis* sp. - Rook et al., p. 20, Fig. 11

2004 *Pannonictis* sp. - Abbazzi et al., p. 627, Fig. 11a-c, f-g.

Holotype. VII-ms-1003: fragmented cranium (Fig. 3.2.1).

Repository. Soprintendenza Archeologia, Belle Arti e Paesaggio per le province di Sassari e Nuoro.

Type locality. Monte Tuttavista quarry area (Orosei, Sardinia). The type specimen comes from the fissure named VII-mustelide.

Figure 3.2.1 – *Pannonictis baroniensis* from Monte Tuttavista. **A**, **C** and **E**: **VII-erratico-1**, skull, in dorsal (**A**), ventral (**C**), and right lateral (**E**) views. **B**, **D** and **F**: **VII-ms-1003**, cranium in dorsal (**B**), ventral (**D**), and left lateral (**F**) views.

Referred Age. The presence in the type locality of primitive taxa characterizing the *Nesogoral* Faunal Complex (Sondaar, 2000), such as *Chasmaporthetes melei*, *Sus sondaari* and *Macaca majori* (Abbazzi et al., 2004), testifies to an Early Pleistocene age, Late Gelasian-Early Calabrian, for the fissure VII-mustelide.

Derivatio nominis. The name "*baroniensis*" is derived from the "Baronie" geographic area in Sardinia, where Monte Tuttavista is located.

Hypodigm. Unregistered fissure filling (possibly in the area of quarry VII): VII-erratico-1, skull with mandible in occlusion.

Filling labelled VII-mustelide: VII-ms-7, distal fragment of a left radius; VII-ms-8, r fragment of a right radius; VII-ms-1, fragment of a right ulna; VII-ms-9, fragment of a left ulna; VII-ms-5, fragment of a right pelvis; VII-ms-6, fragment of a left pelvis fragment; VII-ms-2, fragment of a left femur; VII-ms-10, distal fragment of a left femur; VII-ms-3,fragment of a left tibia; VII-ms-4, fragment of a left fibula.
Filling labelled X-3uccelli: X-3u-9, left P2; X-3u-10, right I3; X-3u-11, right humerus missing distal part.

Diagnosis. In size, the species is intermediate between *P. nestii* and the larger *P. pliocaenica*. The strong muzzle and cranium are elongated. The margin of the orbit slightly marked, and the orbital fossa depression appears shallow or absent. The postorbital processes are small and the frontal sinuses are elongated caudally and well developed. The postorbital constriction is not so marked. Tympanic bullae possess a marked V-shaped embayment on their mesial margin and an inflation located on the medial portion. There are no P1 nor p1, unlike *M. ardea*, *P. pliocaenica*, *P. pilgrimi* and *P. nestii* that have evident P1. The P4 protocone area expands lingually and enlarged, and with a cup-like morphology, unlike *Eirictis* species. The P4 hypocone is reduced. The M1 morphology is peculiar, with a large paracone and markedly reduced metacone; the cingula are prominent around the buccal side of the paracone and on the mesial margin of M1, but there is no visible distinction of a cingulum around the metacone. The mandible corpus is robust and the ramus large.

Description. *Cranium*. VII-erratico-1 is a fragmented cranium with the articulated mandibles but VII-Ms-1003 is a complete cranium. The left side of VII-erratico-1 is strongly damaged (Fig. 3.2.1), as the muzzle and the tempo-occipital area are missing. Both specimens lack the zygomatic arches (Fig. 3.2.1A-B). The muzzle is long and strong. The cranium tends to be elongated. The cranial profile shows a marked curvature of the muzzle and a straight outline in the dorsocaudal

portion of the skull. The frontal sinus appears modestly inflated and elongated caudally. The postorbital constriction is not marked. The braincase is elongated caudally. Although the caudal parietal and occipital regions are missing, it seems to be inflated. In caudal view, the nuchal crest is bell shaped damaged. In VII-erratico-1, a red-brownish crust covers the ventral side, preventing the possibility of description of the features, whereas in VII-ms-1003 the palate ends distally to the M1, almost at the level of the postorbital constriction. The bullae of VII-erratico-1 are well preserved (Fig. 3.2.1), large and bulging. In lateral view, they are fairly prominent. Ventrally, the bullae appear bulging, especially on the medial portion, and possesses a prominent embayment on the rostral border.

Upper teeth. There is no P1. The P2 possesses only a single cusp, with a rather high crown. The P3 possesses a markedly high protocone, with no distal accessory cuspule, but a prominent distal cingulum on the buccal margin. The P4 and M1 are missing in VII-erratico-1 but preserved in VII-ms-1003. The P4 has a large protocone area, made of a large basin with a tiny cuspule on the cingulum that girdles this basin. Where cingulum reaches the lingual side of the paracone there is a small cuspid. The protocone extends only to one third of the P4 (Fig. 3.2.1D). The paracone is high and stout, and the metastyle is long and sharp. The M1 has a considerably larger paracone compared the metacone, which is strongly reduced (Fig. 3.2.1D). No cingulum bounds the metacone, whereas a large and prominent one girdles the mesial portion of the paracone. The protocone is enlarged. A strong cingulum is found on the mesiolingual side of the tooth, separated by a furrow from the protocone; on the distolingual side of the tooth is a cingular hypocone. The distal portion lacks a metaconule of the M1, thus appearing flat. The M1 hypocone is a prominent and rather individualized from the distolingual cingulum.

Mandible. The mandible corpus is stout (Fig. 3.2.1E), with a curved ventral margin. A similar curvature is visible in the line of the teeth, with the p4 in the lowest point of the curvature. The masseteric fossa is deep. The angular process is hook-shaped

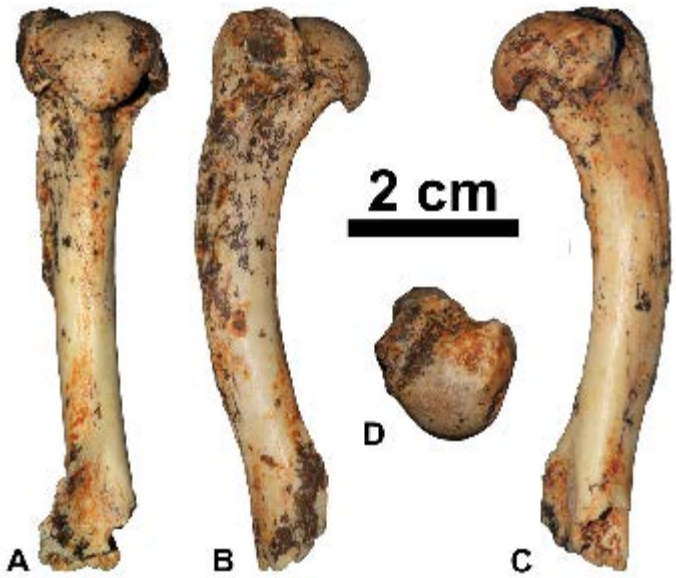

Figure 3.2.2 – *Pannonictis baroniensis* from Monte Tuttavista. **A-D**: **X-3u-11**, right humerus, in cranial (**A**), lateral (**B**), medial (**C**) and proximal (**D**) views.

and well-developed. In medial view, an oval surface girdled by prominent crests for the insertion of the m. pterigoideus medialis. The ramus is enlarged mesiodistally and it seems to be rather high, although broken in the dorsal part.

Lower teeth. The incisors are reduced and simple. The lower canines have a basal rugose and large cingulid at the base; they are larger compared to C. There is no p1. The p2 is single-cusped, with a small elongation of the distal part. The p3 is similar to the p2 but more elongated distally and larger. The p4 is large, with a tiny cuspulid on the distal cingulid. The m1 possesses a short paraconid, high protoconid. On the buccal side, there is a feeble cingulid. Although in VII-erratico-1 the mandibles are attached to the cranium (Fig. 3.2.1E), the metaconid of the left m1 is visible. It is enlarged, with a small cuspulid on its distal side. The talonid of m1 possesses a large hypoconid, a small accessory cuspulid located distally to the former, and a cristid-like structure as a lingual border.

Postcranial elements. The majority of the postcranial specimens recovered and ascribed to *Pannonictis* are very fragmentary. Humerus. X-3u-11 (Fig. 3.2.2) possesses a large head ending ventrally with a sharp pointy margin, in mediolateral

view. A large greater tubercle is present, but not higher than the head of the humerus. In cranial view (Fig. 3.2.2A), the surface of the diaphysis is rugose, and two marked crests border this rough area. These crests merge into a single one that becomes shallow close to the distal epiphysis. In lateral view (Fig. 3.2.2B), the humerus shows a large and round insertion area for the *m. infraspinatus*. A prominent and sharp crest departs below the greater tubercle, and reaches almost the half level of the diaphysis, ending in the humeral crest. The deltoid tuberosity is slightly evident from the rest of the crest. In medial view (Fig. 3.2.2C), the intertubercular furrow is not deep.

Comparisons. Although partially damaged, the specimens from the fissures VII-mustelide, X-3uccelli and of VII-erratico-1 possess several morphologies suggestive of the attribution to the genus *Pannonictis*. For instance, the strong embayment on the mesial side of the tympanic bulla, the scarcely marked postorbital constriction and the stout mandible exclude attribution of the referred sample to the genera *Enhydrictis* and *Martellictis*. Of these features, the tympanic bullae possessed by VII-erratico-1 and VII-ms-1003 closely resemble those of *P. pliocaenica*, contrasting with the shape of *M. ardea* or *Enhydrictis* (Fig. 3.2.3). Other features support the distinction between *Pannonictis* from Monte Tuttavista and *M. ardea* from St. Vallier: whereas in the latter the cranium is shortened and the nuchal crest, in caudal view, has a triangular outline, the former possesses an elongated cranium and the enlargement of the dorsal part of the supraoccipital shield. *M. ardea* shows a reduced development of the temporal region in comparison to that of the material from Monte Tuttavista. The considered specimens' slender proportions also contrast with that of *Eirictis* species like *E. robusta* from Longdan (Qiu et al., 2004). In shape, the cranium is similar to that of *P. pliocaenica* from Villany-Kalkberg and of *P.* cf. *nestii* from Sima del Elefante. Nonetheless, *Pannonictis* from Monte Tuttavista differs in some respects from the other species, *e.g.*, for the wider palate

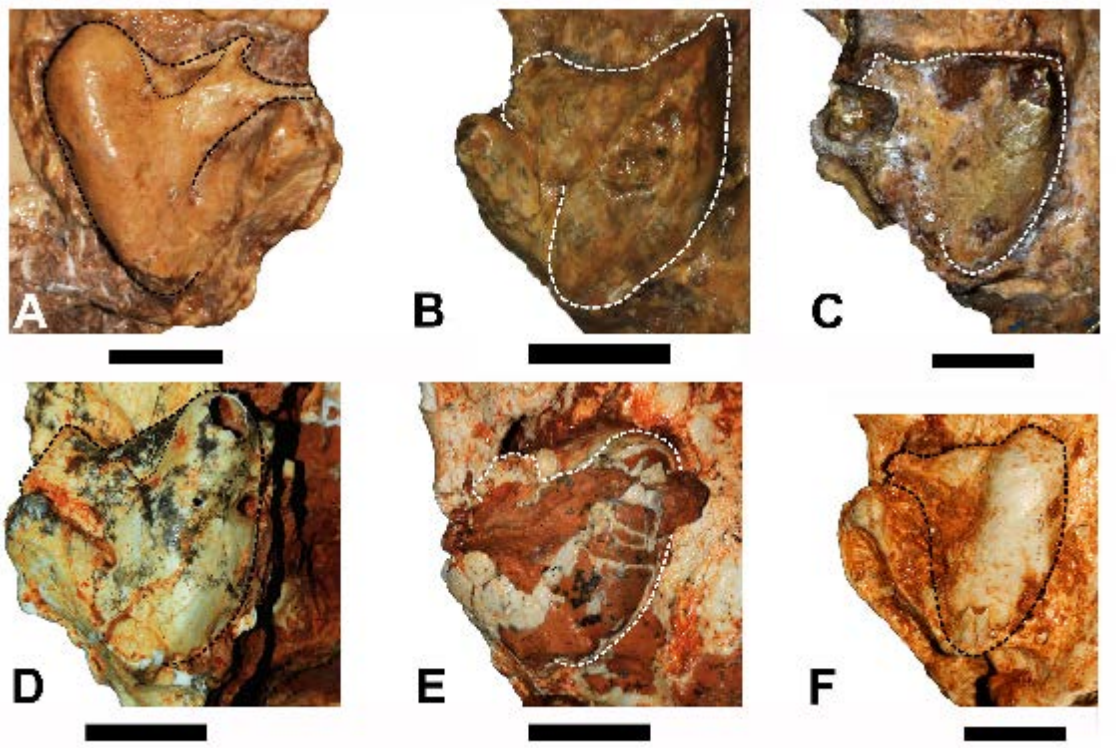

Figure 3.2.3 – Detailed pictures and schematic outlines of the tympanic bullae in some taxa of the tribe Lyncodontini. **A**: *Pannonictis pliocaenica* from Villany (Hungary); **B**: *Martellictis ardea* from St. Vallier (France); **C**: *Enhydrictis galictoides* from Monte S. Giovanni (Sardinia); **D**: *Pannonictis baroniensis* (VII-erratico-1) from Monte Tuttavista (Sardinia); **E**: *Pannonictis baroniensis* (VII-ms-1003) from Monte Tuttavista (Sardinia); **F**: *Enhydrictis praegalictoides* (IX-pro-121) from Monte Tuttavista (Sardinia). Scale bars equals 1 cm.

at level of the P3-P4 and the stouter muzzle compared to *P. pilgrimi* from Villany and *P.* cf. *nestii* of Sima del Elefante or the proportionally narrower braincase compared to *P. pliocaenica*. *Pannonictis* from Monte Tuttavista does not have the P1, which is or may be present in *M. ardea*, *P. nestii*, *P. pilgrimi*, *P. pliocaenica*, and the larger specimens of *P.* cf. *nestii* from Atapuerca (Garcia & Howell, 2008). The P4 of *Pannonictis* from Monte Tuttavista does not show the marked mesial notch displayed by other taxa, like *P. nestii* from Pietrafitta, *P. pilgrimi* and *P. pliocaenica* from Villany and *P.* cf. *nestii* from Atapuerca. Furthermore, the P4 protocone of *P. pliocaenica* is large; it expands prominently lingually and possesses a large hypocone, whereas the P4 protocone of *Pannonictis* from Monte Tuttavista is less expanded lingually and has only a small and slightly evident hypocone. In terms

of the expansion on the lingual side, VII-ms-1003 is similar to *P. nestii* from Pirro Nord. Nevertheless, in the latter taxon, the protocone extends beyond the mesial margin of the P4 and, in VII-ms-1003, the mesial protocone lies at the same level of the margin of the tooth.

The development of the mesiobuccal cingulum resemble that of *P. nestii* and *P. pilgrimi*. The shape of the M1 paracone and metacone of *Pannonictis* from Monte Tuttavista differs with the morphology of *P. pilgrimi* from Villany as in the latter, the buccal cusps are similar in size, whereas in the considered taxon, the metacone is considerably smaller than the paracone. This resembles *P. pliocaenica* and *P.* cf. *nestii* from Atapuerca. The occlusal morphology of the M1 of *P. pliocaenica* is peculiar for its rectangular shape, unlike that of *Pannonictis* of Monte Tuttavista. In the studied sample, theM1 talon is distally elongated, emphasized by the position of the M1 hypocone, and there is a prominent enlargement of the mesiolingual cingulum. This elongation is similar to that of the M1 of *M. ardea*, *P. nestii*, and *P. pilgrimi,* but none of these taxa possess the great expansion of the cingulum on the mesiolingual side of the tooth.

The hemimandible of *Pannonictis* from Monte Tuttavista is rather deep, as in other species of *Pannonictis*, (*e.g.*, *Pannonictis* cf. *nestii* from Atapuerca, *P. nestii* from Pirro Nord and Upper Valdarno, *P. pliocaenica* from Villany-Kalkberg). It differs from *Eirictis* spp. because these taxa have mandibles with a stouter corpus and from *P. pilgrimi* from Villany or *M. ardea* from St. Vallier and Olivola for their very shallow and thin mandible (see also Fig. 3.2.6). The ramus in the considered specimens is enlarged mesiodistally, like that of *Pannonictis* cf. *nestii* from Atapuerca, *P. nestii* from Pirro Nord and Pietrafitta and *P. pliocaenica* but it contrasts to that of *M ardea* or *P. pilgrimi*. Assessment of the features of the lower teeth is difficult, although the m1 is mesiodistally elongated, as in other species of the genus *Pannonictis*. It possesses a well-developed metaconid and a stout hypoconid, but the distal accessory cuspulid posterior to the hypoconid seems to be less prominent and

individualized when compared to *M. ardea*, *P. nestii*, *P. pilgrimi*, *P. pliocaenica*.

The humerus X-3u-11 differs from the other postcranial specimens of mustelids recovered from other fissures of the Monte Tuttavista site complex. X-3u-11 can be confidently assigned to *Pannonictis* for the robustness of the diaphysis when compared to the more slender morphologies of types of *Enhydrictis*. Other features support this attribution visible in the specimens, such as the prominent greater tubercle and the developed deltoid crest. The specimen of Fig. 3.2.2 is stouter and proportionally elongated proximodistally compared to that of *P. nestii* from Pirro Nord. In lateral view, the greater tubercle of *Pannonictis* from Monte Tuttavista is enlarged and more elevated on the head. The insertion area of the *m. infraspinatus* is reduced in *P. nestii* compared to that of the Sardinian taxon. On the lateral margin, a prominent crest arises from the distal part of the greater tubercle, more developed if compared to that of the specimen from Pirro Nord. The supracondylar crest is reduced in the specimen of Monte Tuttavista in comparison to *P. nestii*, in cranial view.

Observing the general proportions in Figs. 3.2.4-3.2.5 and Tabs 3.2.1-3.2.8 (in section 3.2.5. Appendix), the remains of *Pannonictis* from Monte Tuttavista are intermediate in size between the large forms like *E. pachygnatha*, *E. robusta*, the larger individuals of *P. pliocaenica* and the smaller *M. ardea*, *P. nestii* and *P. pilgrimi*. Fig. 3.2.6 summarizes the values of the robustness index (*i.e.*, the ratio of breadth/height of the mandible at level of m1): *E. galictoides*, *E. pachygnatha* and *P. pliocaenica* possess rather stout mandibles, whereas *M. ardea* has a the most shallow and thin mandible corpus of all the Plio-Pleistocene species. The mandible of *Pannonictis* from Monte Tuttavista falls within the variability of *P. nestii*. The log-ratio diagrams (Fig. 3.2.7A-3.2.8A) point out the very peculiar dental and cranial pattern of proportions of the *Pannonictis* material from Monte Tuttavista, when compared to all other species of *Pannonictis*, confirming the evidence derived from morphological comparison and the attribution to a different species compared to

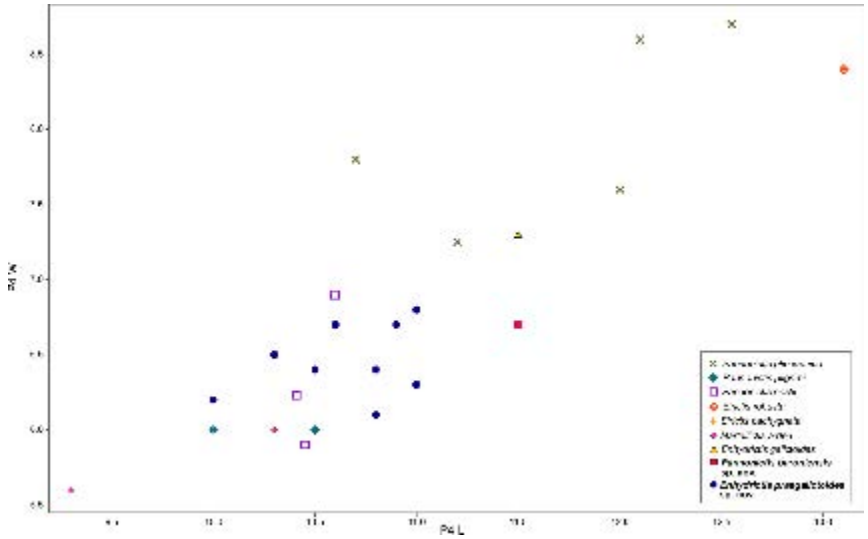

Figure 3.2.4 – Biplot of the P4 length and width in several species of Lyncodontini. Symbols are explained in the legend.

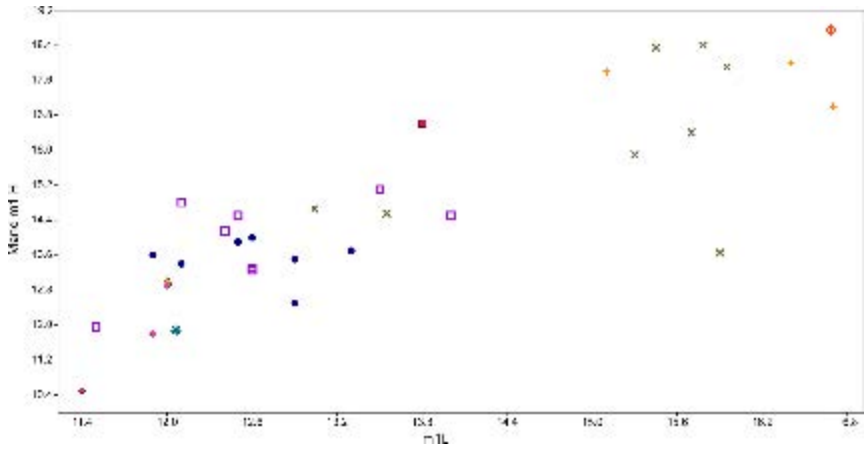

Figure 3.2.5 – Biplot of the m1 length and mandibular height at the level of m1 in several species of Lyncodontini. Symbols are the same as in Fig. 3.2.4.

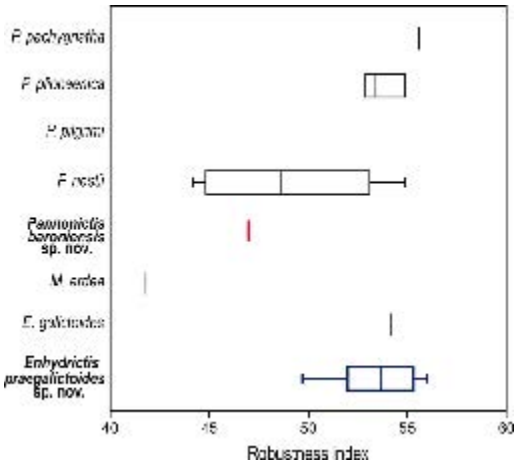

Figure 3.2.6 – Boxplot of the variation in the robustness index in various fossil Lyncodontini.

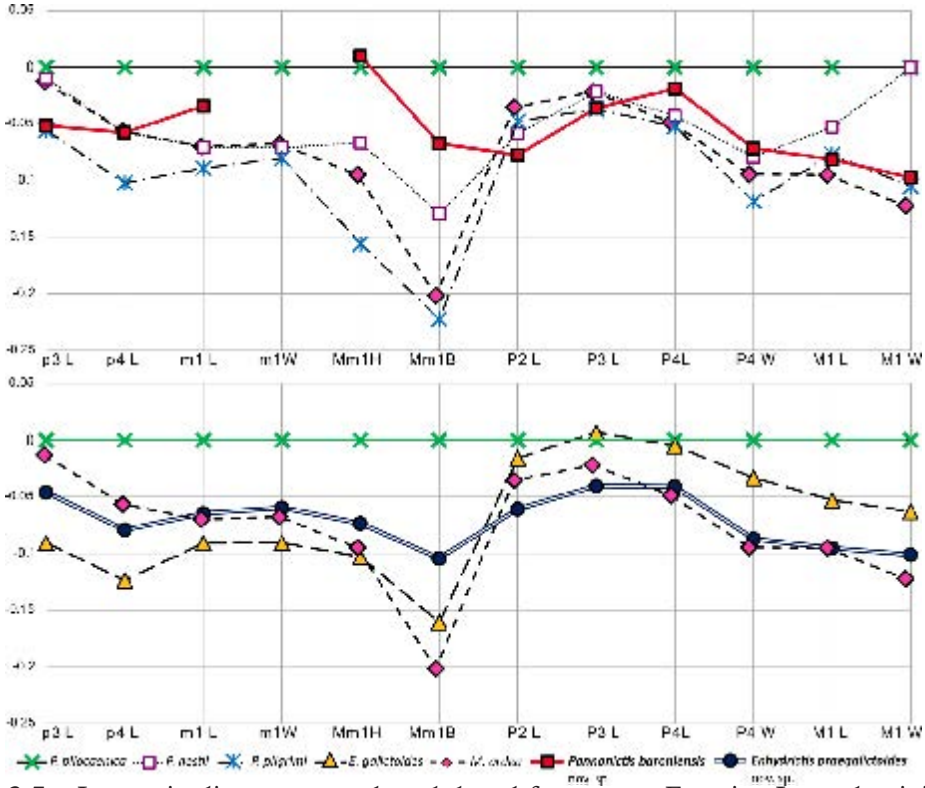

Figure 3.2.7 – Log–ratio diagrams on selected dental features on Eurasian Lyncodontini fossil species: **A**, *Pannonictis* from Monte Tuttavista, *P. pliocaenica, P. nestii*, *P. pilgrimi*, *Martellictis ardea*; **B**, *P. pliocaenica*, *Martellictis ardea*, *Enhydrictis galictoides* and *Enhydrictis* from Monte Tuttavista. *P. pliocaenica* is used as a reference.

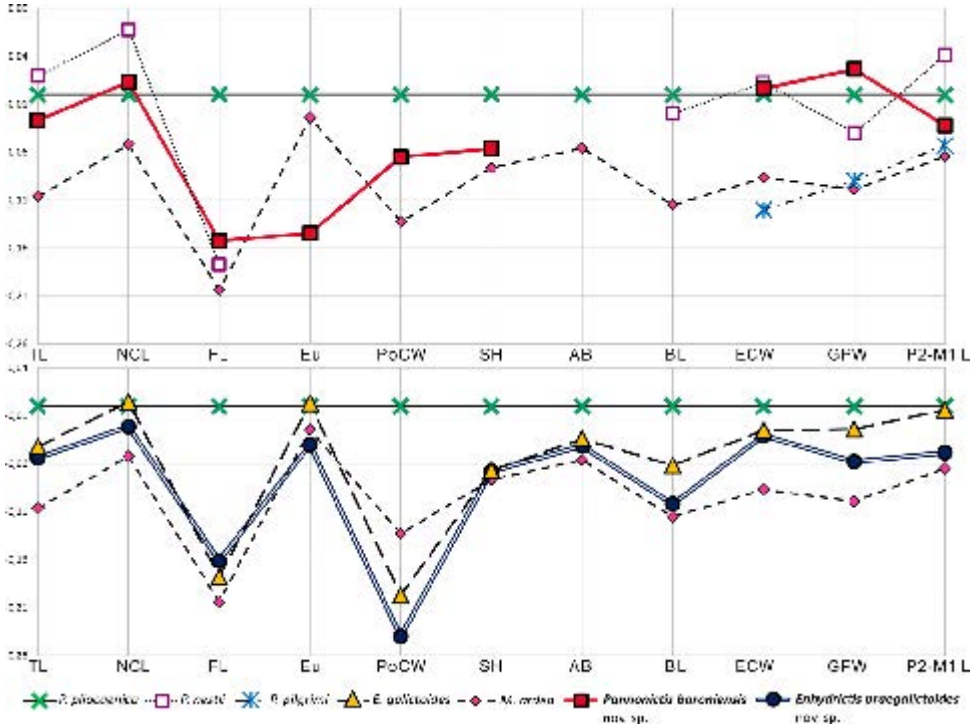

Figure 3.2.8 – Log–ratio diagrams of selected cranial features on Eurasian Lyncodontini fossil species; **A** and **B** same as Fig. 3.2.7.

the continental relatives.

Genus ***Enhydrictis*** Forsyth Major, 1901

Enhydrictis praegalictoides Rook et al., 2018

(Figs. 3.2.9-3.2.11; Tables 3.2.1-3.2.8)

Enhydrictis sp. Rook et al. 2003 – p. 20 – Fig. 12

Enhydrictis sp. Abbazzi et al. 2004 – p. 627

Holotype. IX-pro-121 – skull with associated atlas (Fig. 3.2.9). Among the extremely abundant hypodigm material, some postcranial material probably belongs to the type individual, as a right (IX-pro-98) and a left (IX-pro-99) fragmentary humerus.

Repository. Soprintendenza Archeologia, Belle Arti e Paesaggio per le province di Sassari e Nuoro.

Type locality. Monte Tuttavista quarry area (Orosei, Sardinia). The type specimen and hypodigm specimen come from fissure filling labelled IV-macaca, IX-prolagus, X-4, and X-5.

Referred Age. The occurrence of primitive representatives of taxa characterizing the classical "*Praemegaceros-Tyrrhenicola* complex" (Sondaar et al. 1986), such as *Tyrrhenicola henseli* and *Rhagamys orthodon* (Abbazzi et al. 2004), is suggestive of a Middle Pleistocene age for the IX-pro assemblage.

Derivatio nominis. The name refers to the morphological features possessed by this species; these features are similar to but more primitive than those of *Enhydrictis galictoides*.

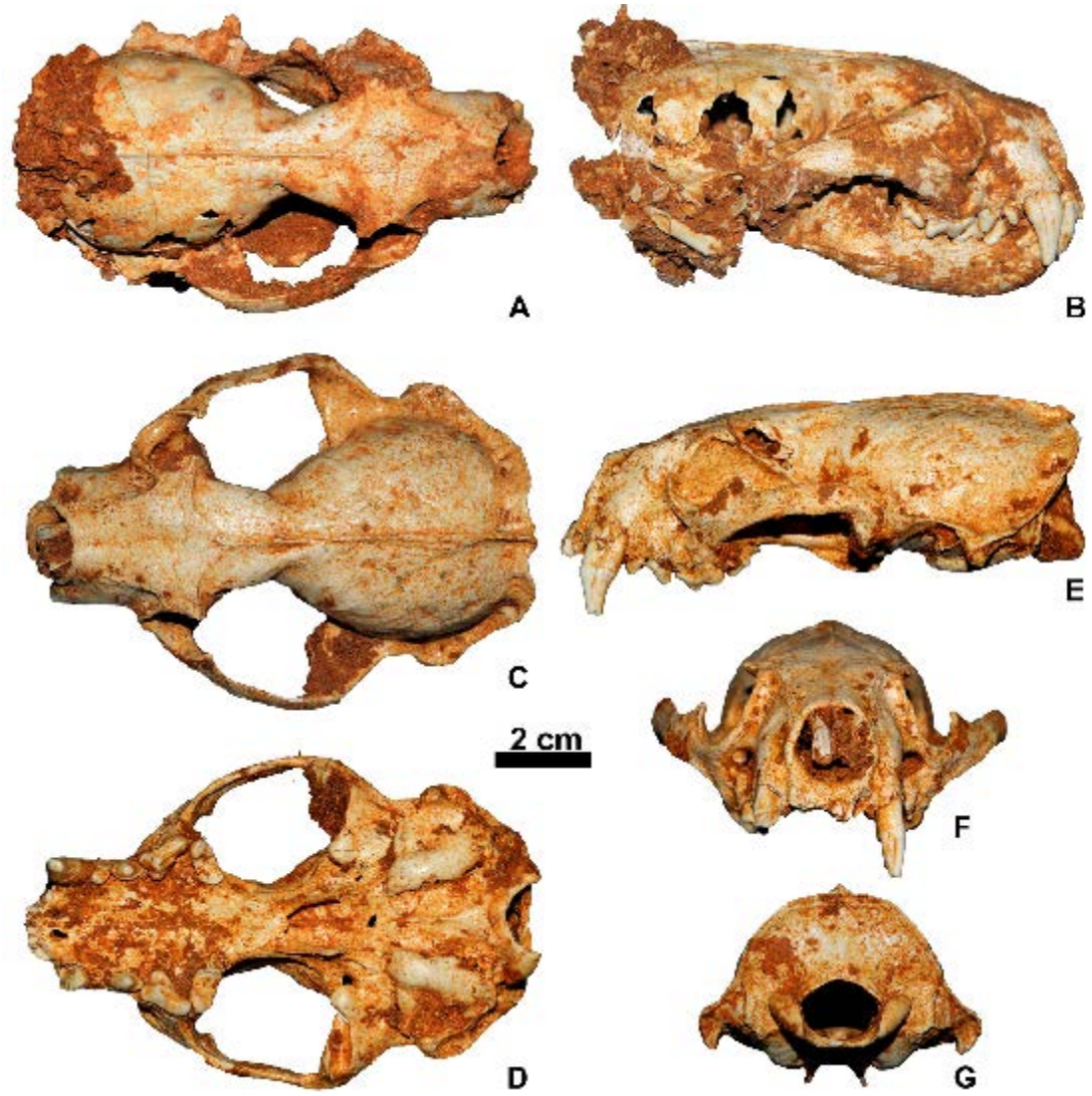

Figure 3.2.9 – *Enhydrictis praegalictoides* from Monte Tuttavista. **A-B**: **IX-pro-120**, skull, in dorsal (**A**), right lateral (**B**) views. **C-G**: **IX-pro-121**, cranium in dorsal (**C**), ventral (**D**), left lateral (**E**), rostral (**F**) and caudal (**G**) views.

Hypodigm. Filling labelled IV-macaca: IV-mac-2, left calcaneum; IV-mac-3, right M1; IV-mac-4, axis fragment; IV-mac-5, caudal vertebra; IV-mac-8, left m2; IV-mac-9, right m2; IV-mac-10, right I2; IV-mac-11, left I3, juvenile; IV-mac-12, caudal vertebra; IV-ma-13, left metacarpal II.

Filling labelled IX-prolagus: IX-prolagus-1, anterior portion of cranium; IX-pro-2, right hemimandible with p2-m1; IX-pro-3, right hemimandible with p3-m1; IX-pro-4, left hemimandible fragment with damaged m1; IX-pro-5, right hemimandible fragment with p2 roots and complete p3-p4; IX-pro-6, right tibia without proximal epiphysis; IX-pro-7, diaphysis and distal articular surface of left femur; IX-pro-8, diaphysis and distal articular

surface of left femur; IX-pro-9, distal portion of right humerus; IX-pro-10, left astragalus; IX-pro-11, right calcaneum; IX-pro-12, fragment of right pelvis (acetabulum); IX-pro-13, fragment of left pelvis (acetabulum); IX-pro-14, fragment of proximal epiphysis of left ulna; IX-pro-15, fragment of diaphysis of humerus; IX-pro-16, left I metacarpal; IX-pro-17, diaphysis and distal epiphysis of left femur; IX-pro-18, diaphysis and damaged distal epiphysis of left femur; IX-pro-19, diaphysis and distal epiphysis of left juvenile femur (missing distal articulation); IX-pro-20, fragment of diaphysis; IX-pro-21, four corpora vertebralis; IX-pro-22, right c1; IX-pro-23, right hemimandible with c1, p2-m1 and root of m2, IX-pro-24, right maxillary fragment with P4-M1 and zygomatic arch base; IX-pro-25, left humerus; IX-pro-26, diaphysis and distal epiphysis of left humerus; IX-pro-27, right tibia; IX-pro-28, left tibia; IX-pro-29, left pelvis (acetabulum + iliac wing); IX-pro-30, part of the diaphysis of right humerus; IX-pro-31, left tibia; IX-pro-32,distal fragment of left tibia; IX-pro-33, distal part of right ulna; IX-pro-34, left radio; IX-pro-35, left radius missing proximal portion; IX-pro-36,right caput femoris; IX-pro-37, right C1; IX-pro-38, left M1; IX-pro-39, proximal fragment of right ulna; IX-pro-40, proximal fragment of left ulna; IX-pro-41, left III metatarsus; IX-pro-42, right III metatarsus; IX-pro-43, right V metatarsus; IX-pro-44, right IV metacarpus; IX-pro-45, right III metacarpus; IX-pro-46, left V metatarsus; IX-pro-47, distal epiphysis of metapodials; IX-pro-48, distal epiphysis of left radius; IX-pro-49, I phalanx; IX-pro-50, I phalanx; IX-pro-51, I phalanx; IX-pro-52, I phalanx; IX-pro-53, I phalanx; IX-pro-54, I phalanx; IX-pro-55, I phalanx; IX-pro-56, I phalanx; IX-pro-57, I phalanx; IX-pro-58, II phalanx; IX-pro-59, II phalanx; IX-pro-60, II phalanx; IX-pro-61, II phalanx; IX-pro-62, right maxillary fragment of with P3-P4; IX-pro-63, left P4; IX-pro-64, left P3; IX-pro-65, right P3; IX-pro-66, right I3; IX-pro-67, right I3; IX-pro-68, left I2; IX-pro-69, left C; IX-pro-70, c; IX-pro-71, right m1; IX-pro-72, right m1; IX-pro-73, left m1; IX-pro-74, partial diaphysis of ulna; IX-pro-75, part of axis; IX-pro-76, right cranial fragment; IX-pro-77, right scapula; IX-pro-78, left scapula; IX-pro-79, cranium; IX-pro-80, cranium (two separated fragments); IX-pro-81, cranium; IX-pro-82, right hemimandible; IX-pro-83, rostral portion of the cranium; IX-pro-84, right pelvis (without pubic ramus); IX-pro-85, left pelvis (ischiatic ramus and fragment of acetabulum); IX-pro-86, left diaphysis of tibia; IX-pro-87, right distal epiphysis tibia; IX-pro-88, right radius; IX-pro-89, damaged proximal epiphysis of right radius; IX-pro-90,

right calcaneum; IX-pro-91, I phalanx; IX-pro-92, cranial fragment; IX-pro-93, proximal epiphysis of left ulna; IX-pro-94, left scapula fragment; IX-pro-95, left scapula fragment; IX-pro-96, left humerus (same individual of IX-Pr-97 and IX-Pr-120); IX-pro-97, right humerus missing the distal epiphysis (same individual of IX-Pr-97 and IX-Pr-120); IX-pro-100, distal epiphysis of left humerus; IX-pro-101, left ulna; IX-pro-102, right ulna with damaged proximal epiphysis; IX-pro-103, right radius; IX-pro-104, distal epiphysis of left radius; IX-pro-105, distal epiphysis of left radius; IX-pro-106, diaphysis of left radius; IX-pro-107, proximal epiphysis of left radius; IX-pro-108, left tibia; IX-pro-109,part of the proximal epiphysis and diaphysis of a right tibia; IX-pro-110, proximal epiphysis of a right tibia; IX-pro-111, left pelvis fragment; IX-pro-112, right pelvis fragment; IX-pro-113, right scapula; IX-pro-114, right scapula fragment; IX-pro-115, fragments of costae; IX-pro-116, vertebrae; IX-pro-117, I phalanx; IX-pro-118, left I3; IX-pro-119, right m2; IX-pro-120, complete cranium with mandibles; IX-pro-122, fragment of zygomatic arches; IX-pro-123, caudal vertebra; IX-pro-124, left scapula; IX-pro-125, left humerus without diaphysis and proximal epiphysis; IX-pro-126, fragment of right pelvis; IX-pro-127, occipital shield; IX-pro-128, diaphysis and distal epiphysis of left femur; IX-pro-129, right tibia; IX-pro-130, right radius; IX-pro-131, right ulna; IX-pro-132, vertebra; IX-pro-133, vertebra; IX-pro-134, vertebra; IX-pro-135, vertebra; IX-pro-136, left maxillary fragment; IX-pro-137, left and right mandibles; IX-pro-138, I phalanx; IX-pro-139, I phalanx; IX-pro-140, I phalanx; IX-pro-141, I phalanx; IX-pro-142, II phalanx; IX-pro-143, II phalanx; IX-pro-144, left V metacarpus; IX-pro-145, left IV metacarpus; IX-pro-146, left III metatarsus; IX-pro-147, right calcaneum; IX-pro-148, right astragalus; IX-pro-149, proximal fragment of left ulna; IX-pro-150, right C; IX-pro-151,proximal fragment of left ulna; IX-pro-152, diaphysis and distal epiphysis of left femur; IX-pro-153, left tibia, missing distal epiphysis; IX-pro-154, right pelvis without pubis ramus; IX-pro-155, left hemimandible ramus with p2 and p3; IX-pro-156, axis; IX-pro-157, cervical vertebra; IX-pro-158, cervical vertebra (VI); IX-pro-159, vertebra; IX-pro-160, thoracic vertebra; IX-pro-161, thoracic vertebra; IX-pro-162, thoracic vertebra; IX-pro-163, vertebral corpus; IX-pro-164, vertebral corpus; IX-pro-165, vertebral corpus; IX-pro-166, vertebral corpus; IX-pro-167, vertebral corpus; IX-pro-168, 15 costae; IX-pro-169, bone breccia block; IX-pro-170, bone breccia block; IX-pro-171, bone breccia block.

Filling labelled X-4: X-4-19, right c1; X-4-26, C1; X-4-27, left i3; X-4-28, right i3; X-4-29, left p2; X-4-30, right P2.
Filling labeled X-5: X-5-1, cranial fragment with I1-M1.

Diagnosis. The material from Monte Tuttavista retains the diagnostic features of the genus *Enhydrictis* Forsyth Major, 1901 but with more primitive morphologies compared to *E. galictoides*. The cranium is short in lateral view, in contrast to that of *Pannonictis* and *Martellictis* spp., but tends to be slightly bulging in the caudal part of the braincase. The tympanic bullae are inflated only in their medial part and have a straight mesial margin, straighter than that of *M. ardea* and without the mesial embayment found in *Pannonictis* spp. The P4 protocone area has a cup-like morphology and the hypocone is reduced but visible. M1 is elongated buccolingually. The paraconid on the m1 is slender buccolingually; the m1 metaconid and hypoconid are well developed.

Description. *Cranium*. The cranium is rostrocaudally elongated (Fig. 3.2.9). The snout is strong and short. On both sides external to the orbits, a depression on the frontals makes the margin of the orbital cavity strongly jutting. The frontal sinus has a great posterior expansion and the postorbital processes are reduced. The postorbital constriction is considerably marked. The braincase is inflated, especially caudally. IX-pro-120 and IX-pro-121 show a reduced sagittal crest (Fig. 3.2.9B, E). In caudal view, the supraoccipital shield appears to be fan-shaped. The occipital condyles project caudally beyond the level of the external occipital protuberance. In ventral view, the tympanic bullae are enlarged mediolaterally and rather flattened. The medial walls of the tympanic bullae tend to converge to the median line of the cranium (Fig. 3.2.9D).
Upper teeth. The C is thin and possesses two parallel furrows on its buccal side. No P1 is present (Fig. 3.2.9D). The P2 is conical and single-cusped. The P3 does not possess any distal accessory cuspule but has a strong distolingual cingulum.

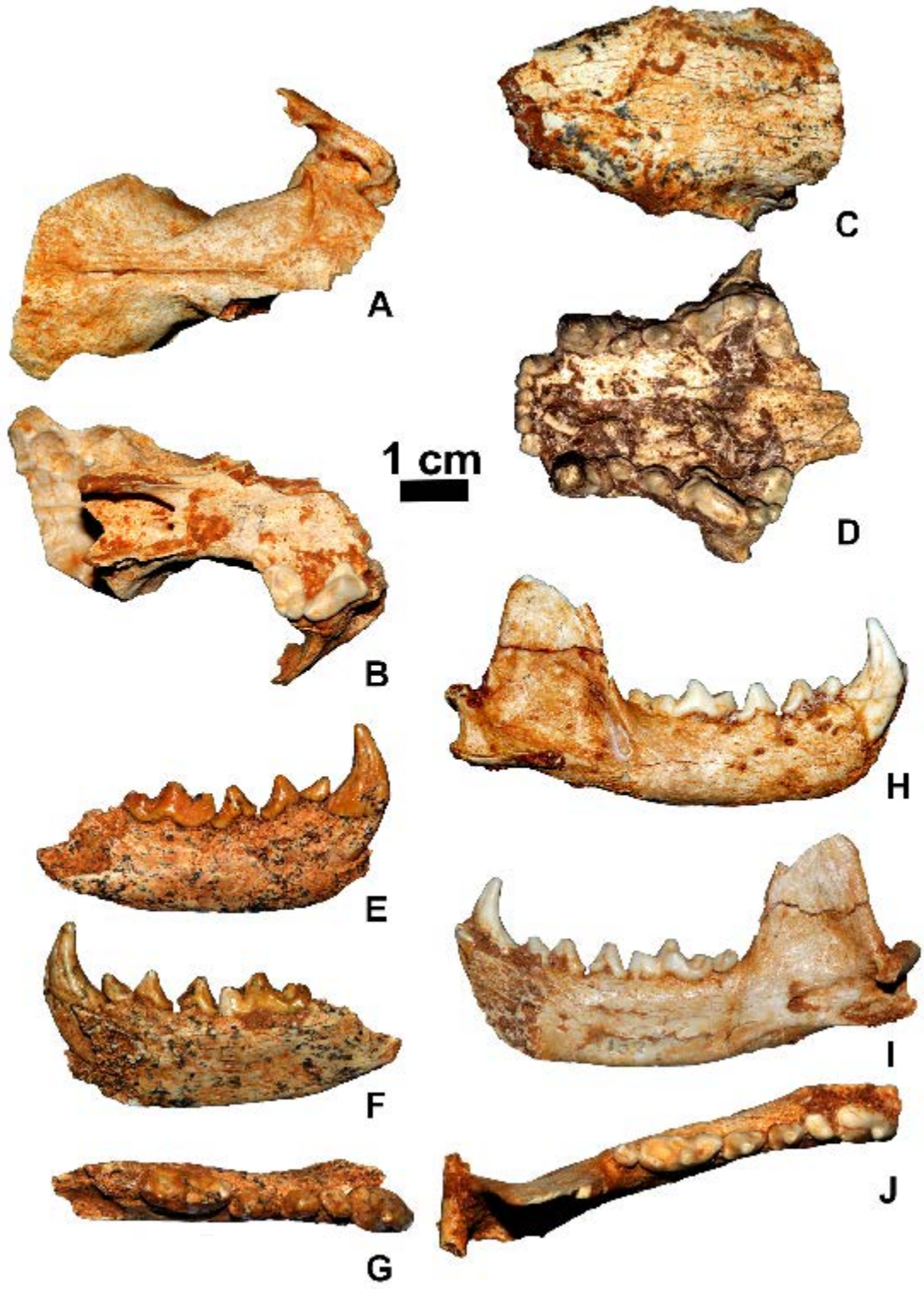

Figure 3.2.10 – *Enhydrictis praegalictoides* from Monte Tuttavista. **A-B**: **IX-pro-79**, cranial fragment, in dorsal (**A**), and ventral (**B**) views. **C**: **IV-mac-34**, cranial fragment in dorsal view. **D**: **X-5-1**, cranial fragment in ventral view. **E-G**: **IX-pro-23**, right hemimandible fragment in buccal (**E**), lingual (**F**) and occlusal (**G**) views. **H-J**: **IX-pro-137**, right hemimandible fragment in buccal (**H**), lingual (**I**) and occlusal (**J**) views.

The P4 protocone has a large basin bounded by a cingular border, with a small cuspule on it (Figs. 3.2.9D and 3.2.10B, D). On its lingual side, this cingulum continues distally, merging with the prominent distolingual cingulum. At this point, there seems to be a swelling of the enamel in the shape of a tiny cuspule, at the midpoint of the tooth (Fig. 3.2.9D). IX-pro-1 does not have any accessory cuspules on the protocone or on the lingual side of the P4. The M1 is bean-shaped and elongated buccolingually, but rather short mesiodistally. The paracone is larger than the metacone, which tends to be reduced. There is a prominent parastyle, on the mesiobuccal side. The protocone is high. M1 possesses a strong cingulum on the distolingual side of the tooth. IX-pro-80 and X-5-1 possess a reduced M1 metaconule (Fig. 3.2.10D).

Mandible. The corpus is short dorsoventrally (Fig. 3.2.10E-J). The dorsal margin of the coronoid process has a D-like shape in lateral view, and it is not very high. The masseteric fossa is deep and large. The ventral margin is straight. The angular process is hook-shaped and, in medial view (Fig. 3.2.10I), it shows two elongated and oval muscular insertion areas, girdled by crests.

Lower teeth. The c is well developed and ached distally. The lower premolars show a mesiodistal elongation and a marked distal cingulid (Fig. 3.2.10G, J). The p2 is conical. The p3 resemble the p2 in shape, but it is larger. The p4 is large, with an accessory cuspulid on the distal cingulid. The m1 possesses a high paraconid, a well-developed protoconid and a large metaconid, although not so individualized from the protoconid. The talonid of m1 possesses a large hypoconid and accessory cuspulids its distal side, and the talonid basin is deep and bounded by a cingulid.

Postcranial elements. Atlas. The atlas is short (Fig. 3.2.11A), with a consistently wider cranial articular surface, compared to the reduced caudal articular fovea. The foramen transversarium is large. The ventral tubercle is reduced. Axis. The axis is not well preserved, if not for small fragments. IV-mac-4 is one of the best preserved specimens (Fig. 3.2.11B-C). Scapula. The coracoid process appears to be

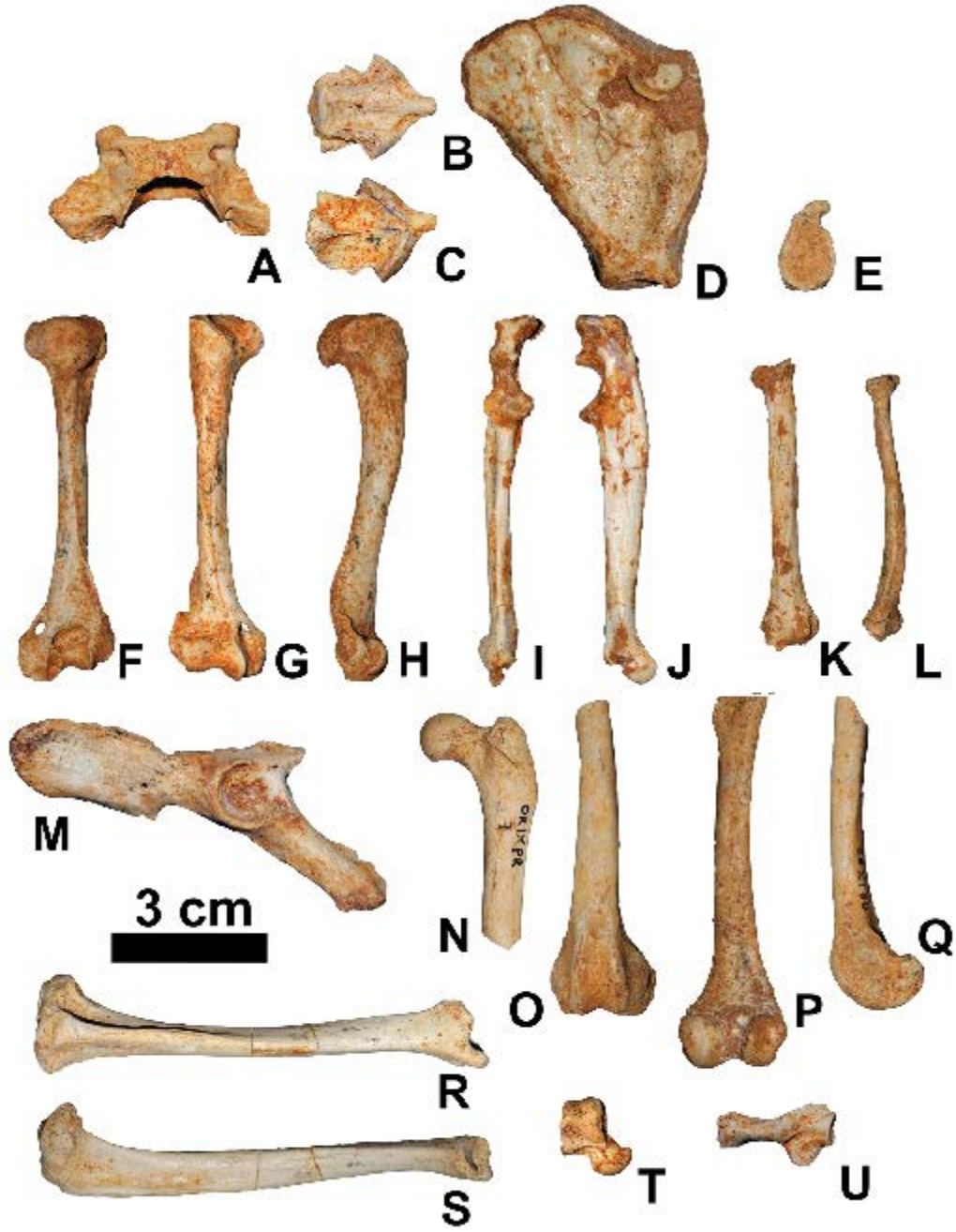

Figure 3.2.11 – *Enhydrictis praegalictoides* from Monte Tuttavista. **A**: **IX-pro-121**, atlas in dorsal view. **B-C**: **IV-mac-4**, fragment of axis in dorsal (**B**), and ventral (**C**) views. **D**: **IX-pro-77**, left scapula in medial view. **E**: **IX-pro-78**, right scapula in distal view. **F-H**: **IX-pro-25**, right humerus in cranial (**F**), palmar (**G**), and lateral (**H**) views. **I-J**: **IX-pro-101**, right ulna in cranial (**I**), and medial (**J**) views. **K**: **IX-pro-103**, right radius in palmar view. **L**: IX-pro-88, right radius in medial view. **M**: **IX-pro-84**, left pelvis in lateral view. **N**: **IX-pro-7**, left femur in cranial view. **O-Q**: **IX-pro-152**, left femur in cranial (**O**), plantar (**P**) and lateral (**Q**) views. **R-S**: **IX-pro-31**, left tibia in cranial (**R**), and lateral (**S**) views. **T**: **IX-pro-148**, right astragalus in dorsal view. **U**: **IV-mac-148**, left calcaneum in dorsal view.

absent or strongly reduced, whereas the supraglenoid tubercle is pointy and long (Fig. 3.2.11D-E). The infraglenoid tubercle is strongly reduced. Humerus. The greater tubercle is enlarged and slightly higher than the well-developed head (Fig. 3.2.11F). On the lateral side (Fig. 3.2.11H), there is a sharp crest and a concave and circular insertion area of the *m. infraspinatus*. The intertubercular furrow is enlarged (Fig. 3.2.11G). The deltoid tuberosity is prominently high and the humeral crest is rather sharp. The lateral supracondylar crest is large and high and as prominent as the lateral epicondyle. The medial epicondyle is large and has on dorsally it presents an epicondylar foramen (Fig. 3.2.11F-G). The distal epiphysis possesses a small and round supratrochlear foramen (Fig. 3.2.11F). Ulna. The ulna is long dorsoventrally, almost as long as the humerus (Fig. 3.2.11I-J). The two coronoid processes greatly differ in size one another: the medial is conspicuously enlarged compared to the lateral one. The diaphysis is rather straight, although the olecranon tends to curve medially. The lateral side of the diaphysis (visible in Fig. 3.2.11I) shows a deep groove. Radius. The proximal articular surface of the radius has an oval shape. The cranial margin of the distal epiphysis (Fig. 3.2.11K) shows a high crest that bounds the grooves for the *m. extensor digitalis communis* and the *m. extensor carpi radialis*. The styloid process is rather elongated (Fig. 3.2.11K-L). Femur. On the proximal epiphysis, the head is well-developed and the neck is long and stout (Fig. 3.2.11N). In plantar view, the teres minor is well developed. The distal epiphysis shows a slight difference between the two distal condyles, in cranial and plantar view (Fig. 3.2.11O-P). the two condyles also have non-parallel median axes. The lateral supracondylar tubercle is less stout and prominent than the medial one. Tibia. The tibia is rather elongated. The proximal articular surface has a large triangular shape in, proximal view. The intercondylar tubercle is short and hook shaped. The tibial tuberosity extends distally *circa* to the midpoint of the tibia (Fig. 3.2.11R). The popliteal notch is rather marked. The medial malleolus is enlarged (Fig. 3.2.11R-S). In plantar view, the astragali sulci are poorly marked.

Astragalus. The astragalus is flattened craniopalmarly and elongated (Fig. 3.2.11T). Calcaneus. The calcaneum is large laterolaterally (Fig. 3.2.11U) with a conspicuous articular surface for the astragalus.

Comparison. The cranial and dentognathic features displayed by the material of the fissures IV-macaca, IX-prolagus, X-4 and X-5 favor the attribution of these specimens to the genus *Enhydrictis*, similar to those recovered from Monte San Giovanni, in north-eastern Sardinia (Forsyth Major, 1901). Among these: the dorsoventrally flattened cranium, the evident postorbital constriction, the shallow tympanic bullae and their three-sided ventral morphology. These features of *Enhydrictis* of Monte Tuttavista differ from those *M. ardea* of various sites in Europe (*e.g.*, St. Vallier and Olivola). The latter possesses a greatly shortened cranium, with a higher distal portion of the braincase in lateral view and the medially inflated tympanic bullae that show a reduced yet visible notch on their mesial side (Fig. 3.2.3). Other differences in the cranium of *M. ardea* are the less pronounced postorbital constriction in, the short portion of the frontals distally to the postorbital processes, the shortened and globular braincase in dorsal view and the more elevated frontals on the muzzle, in lateral view. Even the dental features are suggestive of a considerable difference between *M. ardea* and the Sardinian taxon, as the former possesses the P1, unlike the latter that lacks both the P1 and p1. In occlusal view, the shape of P3 and p4 is round in the *Enhydrictis* from Monte Tuttavista, but oval in *M. ardea* from St. Vallier and Olivola. The upper P4 in the French-Italian taxon shows a marked mesial embayment, while it has a linear mesial margin in the Sardinian one. Whereas in *M. ardea* the M1 is subtriangular, with an expanded lingual talon portion, in the sample from Monte Tuttavista shows a rectangular-like occlusal shape for the M1. The mandible corpus of *M. ardea* is very shallow and rather thin, in contrast to the deep corpus of the *Enhydrictis* of Monte Tuttavista. In the lower teeth, the m1 in *M. ardea* shows an

elongated and slender trigonid shape in occlusal view, similar to *Enhydrictis* and unlike *Pannonictis* spp. Nevertheless, *M. ardea* also possesses a shortened talonid similar to that of *Pannonictis*. All these features testify to the affinity of the material from Monte Tuttavista with the endemic taxon *E. galictoides*. Nevertheless, the specimens of *Enhydrictis* from Monte Tuttavista possess more primitive characters, which allow to distinguish it from *E. galictoides* and its peculiar morphology. The derived features possessed by *E. galictoides* (*e.g.*, the flattened profile of the cranium and the short height braincase in lateral view, the strongly marked postorbital constriction,) are visible in the sample from Monte Tuttavista, but in an incipient form. Other cranial features are *e.g.*, the frontal sinus and the braincase, which are more inflated in the specimens from Monte Tuttavista; the proportionately larger palate at the level of the P3 in *E. galictoides*. Furthermore, the cranium is shorter rostrocaudally compared to that of Monte San Giovanni (Fig. 3.2.9). Probably the most prominent difference lies in the morphology of the bullae: *Enhydrictis* from Monte Tuttavista shares with *E. galictoides* the straight mesial margin of the bulla (unlike *Martellictis* and *Pannonictis*), but the former differs from the second by its merked medial inflation, which is almost absent in the specimens of Monte San Giovanni. Among the differences in the dental morphology are, for example, the presence of an M1 metaconule in the material of Monte Tuttavista or the larger and more individualized m1 metaconid in the considered sample.

The postcranial elements show very few differences between the two samples of *Enhydrictis*, (*e.g.* the more conspicuous medial development of the lesser tubercle and the straighter diaphysis of the tibia in *E. galictoides* compared to *Enhydrictis* from Monte Tuttavista).

Dental biplots (Figs. 3.2.4-3.2.5 and Tabs. 3.2.1-3.2.8 in section 3.2.5. Appendix) show that the specimens of *Enhydrictis* from Monte Tuttavista cluster rather well together and they are close in size to *P. nestii*, whereas those of *E. galictoides* have larger upper P4 (Fig. 3.2.4) but are comparable to *Enhydrictis* from Monte

Tuttavista in terms of the proportions of the mandible (Fig. 3.2.5). The mandible of *Enhydrictis* from Monte Tuttavista possesses a rather high value for the robustness index (Fig. 3.2.6), comparable to that of *E. galictoides* and *Pannonictis* species such as *E. pachygnatha*, *P. nestii*, *P. pilgrim*, and *P. pliocaenica*. The log-ratio diagrams (Fig. 3.2.7B-8B) also point out the dimensional affinity between the remains of *Enhydrictis* from Monte Tuttavista and *E. galictoides*. Indeed, even in proportions, the two taxa are clearly highly comparable (especially cranially, Fig. 3.2.8B). Even *M. ardea* shows similar proportions, both in cranial and dental parameters, compared to these two taxa (Figs. 3.2.7-8). This fact therefore confirms the strong affinity of *M. ardea* to the genus *Enhydrictis,* even considering the primitive pattern of the former (see section 3.1).

3.2.3. Discussion

The morphometric data and morphological features of the Lyncodontini mustelids from Monte Tuttavista confirmed the presence of two different forms, as reported by Abbazzi et al. (2004). The larger and stouter material belongs to the genus *Pannonictis,* whereas the more slender and abundant material shows several features that resemble those of the Sardinian endemic taxon *Enhydrictis*. Our analyses reveal evident differences between the continental taxa known in literature compared to the Sardinian sample. Considering the importance and the number of these differences, *Pannonictis baroniensis* and *Enhydrictis praegalictoides* need to be distinguished from the other continental taxa of Eurasia.

The importance of these species must take into consideration the attempted reconstructions of the biochronology of the Monte Tuttavista site complex. The first attempts were those of Ginesu & Corby (1997), Sondaar (2000), Sondaar & Van Der Geer (2002) and, more extensively, of Abbazzi et al. (2004) (Fig. 3.2.12). The latter authors described to four complexes in the faunal succession: the fissures VI-3, X ghiro, VII, VII-bloccostrada, VII-mustelide and IX-antilope

to the *Nesogoral* Complex (Sondaar, 2000); X-3uccelli and X-mele are considered as part of a new complex, point out this as the phase of colonisation of the ancestors of the subsequent *Microtus* (*Tyrrhenicola*) complex (as well as time of persistence of taxa from the previous phase). The fissures XI-canide, XI-dic.2001, XI-mar2002, XI-3 and XI-rondone represent the first of two faunal subcomplexes of *Microtus* (*Tyrrhenicola*) FC and are referred to the Middle-Late Pleistocene. The most recent fissures are VI banco 6 and VII 2 (Fig. 3.2.12A). Since the work of Abbazzi et al. (2004), no other revisions of the assemblage of Monte Tuttavista were made, but only general reviews of the Sardinian fossil record (*e.g.*, Palombo, 2006; 2009; Palombo & Rozzi, 2014) (Fig. 3.2.12B). Nevertheless, some researchers have studied the taxonomy and the evolution of selected taxa (*e.g.*, Abbazzi et al., 2005; Boldrini et al., 2010; Piras et al., 2012) and have provided useful insights on the succession dynamics of the site or of whole Sardinia. For instance, Angelone et al. (2008) revised the material of *Prolagus* from Monte Tuttavista site complex, suggesting that the chronology of fissure IX-prolagus may be biased by taphonomic mixture, the long-time average of infill of the fissure or even secondary deposition events. In time, this filling will probably span between the end of the Early Pleistocene and the Middle Pleistocene times. A great deal of research has endeavoured to build a biochronology of the complex pattern of colonization and radiation in Sardinia since the Late Miocene. Recently, in their review of Sardinian local assemblages, Palombo & Rozzi (2014) included and chronologically referred other fissures from Monte Tuttavista, such as X-4 and X-5 to the faunal subcomplex Orosei 2 and IX-3 to Dragonara FsC.

Pannonictis baroniensis comes mainly from two fissures: VII-mustelide and X-3uccelli. The cranium VII-erratico-1 was collected from an unregistered fissure in the area of fissure VII. As mentioned above, the faunal assemblage of VII-mustelide supports an early age (possibly one of the oldest) of the complex of Monte Tuttavista. Indeed, the presence of *Nesogoral* spp. and of carnivores (like *C.*

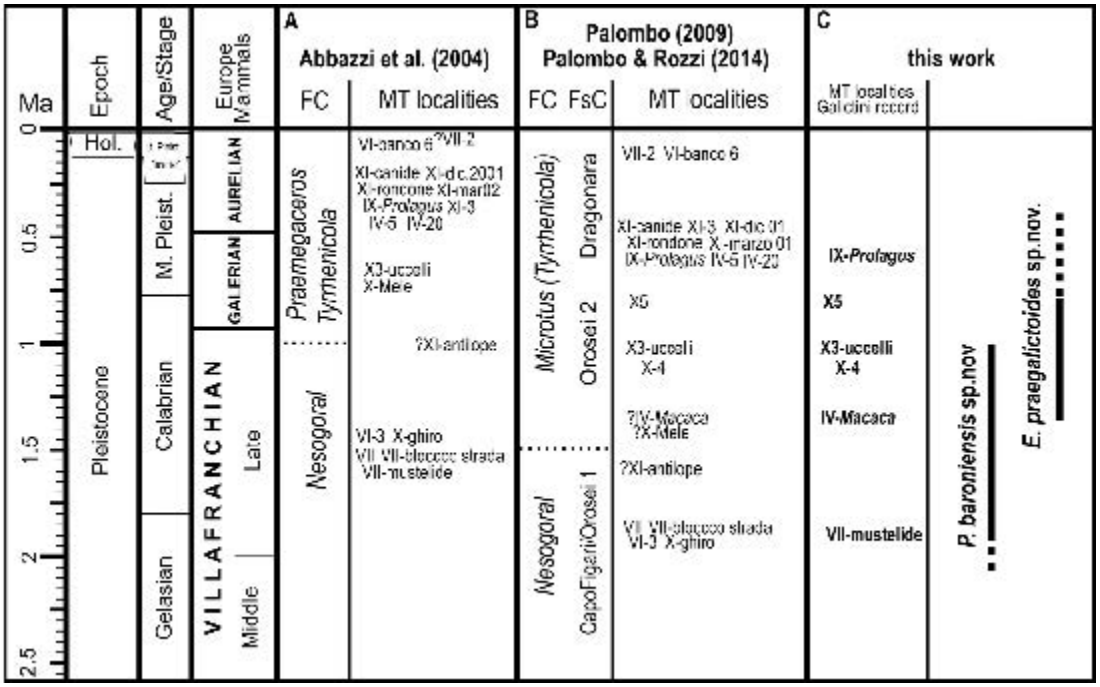

Figure 3.2.12 – Schematic representation of the major research and reviews on the chronology of Sardinian assemblages (focused on the Monte Tuttavista site complex). **A**: Abbazzi et al. (2004) included the first biochronological characterisation of Monte Tuttavista localities. **B**: Palombo (2009) and Palombo & Rozzi (2014) widened the research to include the whole of Sardinia, and they updated and calibrated more precisely the numerous fossiliferous sites (here, only those of Monte Tuttavista). **C**: the quarries of the Monte Tuttavista site complex in which fossil Lyncodontini have been found are here reported and the chronological ranges for these species.

melei) is what relates the fissure to the more ancient of the two Sardinian Faunal Complexes (*i.e.*, *Nesogoral* FC). The record of few specimens unequivocally ascribable to *Pannonictis* in the fissure X-3uccelli, referred the younger Orosei 2 FsC (latest Early Pleistocene), testifies to the persistence of this mustelid when the first *Enhydrictis praegalictoides* had already arrived in the Monte Tuttavista area. As a matter of fact, the oldest record of *E. praegalictoides* is that of IV-macaca, a fissure referred to the second half of the Early Pleistocene and to the end of the *Nesogoral* FC (Palombo & Rozzi, 2014). The abundant material of *E. praegalictoides* occurs in different fissures, but never together with *P. baroniensis*. The features of *E. praegalictoides*, although primitive compared to the Middle-Late Pleistocene *E. galictoides*, are distinctively different from those of *Pannonictis* spp., both in cranial

and in postcranial morphologies (as clear from Figs. 3.2.1-3 and 3.2.9-11) as well as from a morphometric point of view (Figs. 3.2.4-8). In this biochronological frame, the dispersion of the presumably *Pannonictis*-like ancestor(s) of both *P. baroniensis* and *E. praegalictoides* entered to Sardinia during the Late Pliocene-Earliest Pleistocene and then differentiated into *P. baroniensis*, on the one side, and into *E. praegalictoides*, on the other, and developing all the peculiarities that characterize this genus.

3.2.4. Concluding remarks

The dispute of Lyncodontini diversity in recent years has regained the attention of researchers. For instance, the discovery of a member of the tribe in North Africa (Geraads, 2016), probably related to *Pannonictis* (see section 3.1.), has widened the geographical range of the tribe, always considered as exclusive Holoarctic taxa. With the exception of the undetermined mustelid from the late Miocene *Hipparion* beds from China (Zdansky, 1927), the earliest Eurasian records of members of Lyncodontini are those of *Pannonictis* from the Early Pliocene localities of Wölfersheim (Germany) and Etulia (Moldova) (both MN15). Soon after, other taxa appeared in eastern Asia and Europe, such as *Eirictis* from Mongolia and China (Sotnikova et al., 2002; Qiu et al., 2004) or the first specimens attributable to *Martellictis* (Fejfar et al., 2012). These findings testify to the beginning of a radiation that reached its peak during the first half of the Early Pleistocene (García et al., 2008). In the fossil record of Eurasian Lyncodontini evidence of adaptation to insular enviroments and of divergence from continental ancestors were not limited to the genus *Enhydrictis*. Among the middle Pleistocene *Oriensictis nipponica* (Naora, 1968) from Japan or *P.* (*Mustelercta*) *arzilla* from Monte Pellegrino (Sicily), (dated to the Early Pleistocene). Similarly to what happened to this Sicilian taxon, the ancestors of the Sardinian species probably arrived in this Mediterranean island during this phase of expansion all over Eurasia and there thrived. The

presence of an early form of *Enhydrictis*, which already shows several distinctive features compared to other Lyncodontini and other primitive ones in comparison to *E. galictoides*, suggests that the insular environment of Sardinia (and probably also of Corsica) favored the occupation of different ecological niches compared to their continental relatives on the. This eventually led to the divergence of the genus from all other Lyncodontini. As some scholars have noted (Forsyth Major, 1901; Ficcarelli & Torre, 1967; Rook, 1995; García & Howell, 2008), *E. galictoides* shows a few features that are suggestive of an aquatic lifestyle, although this idea is not widely shared (Bate, 1935; Kurtén, 1968). Our analyses indicated that the postcranial material of *E. praegalictoides* is very similar to that of *E. galictoides;* therefore, similar lifestyle seems plausible. Nevertheless, the study of the adaptation of these mustelids to certain habitats is beyond the scope of the present study.

The new taxa from the Early and middle Pleistocene deposits of Monte Tuttavista are two important elements of the tribe Lyncodontini that enrich our knowledge of their evolutionary history and their biogeographic radiation across Eurasia.

3.2.5. Appendix

Cranial and postcranial measurements of Lyncodontini material from Monte Tuttavista are reported in the following pages.

Table 3.2.1 – Cranial measurements of P*annonictis baroniensis* and *Enhydrictis praegalictoides* from Monte Tuttavista. For measurement abbreviations, see the section 2.

Species	Cat. N°	TL	NCL	FL	SCL	GNL	Eu	Ect	PoCW	SH	AB	GWOT	GWOC	BL	PL	CBL	Zyg	ECW	GPW	P2-M1 L	P2-P4 L
P. baroniensis	**VII-erratico-1**	-	-	41.3	-	-	32.8	31.2	20.9	-	-	-	-	-	-	-	-	28.1	-	-	-
P. baroniensis	**VII-ms-1003**	112.3	75.0	45.6	34.3	18.2	32.4	29.8	22.5	33.8			-	-	56.0	-	-		41.2	26.6	22.5
E. praegalictoides	**IV-mac-34**	-	-	-	-	-	-	30.6	-	-	-	-	-	-	-	-	-	-	-	-	-
E. praegalictoides	**IX-pro-1**	-	-	-	-	-	-	32.0	14.0	-	-	-	-	-	-	-	-	25.0	33.7	-	-
E. praegalictoides	**IX-pro-79**	-	-	-	-	-	-	-	13.9	-	-	-	-	-	-	-	-			-	-
E. praegalictoides	**IX-pro-81**	-	-	-	-	-	-	-	14.5	-	-	-	-	-	58.9	-	-	25.8	32.6	26.5	
E. praegalictoides	**IX-pro-120**	109.1	71.2	44.1	-	-	41.4	32.4	14.8	34.8	-	-	-	-	53.8	-	-	26.8	34.5	26.0	22.1
E. praegalictoides	**IX-pro-121**	102.1	67.5	41.1	-	-	41.5	30.3	15.3	31.0	29.3	54.2	26.7	94.8	51.8	101.9	66.3	25.4	35.4	24.8	21.0
E. praegalictoides	**IX-pro-127**	-	-	-	-	-	-	-	-	-	-	-	24.7	-	-	-	-	-	-	-	-
E. praegalictoides	**X-5-1**	-	-	-	-	-	-	-	-	-	-	-	-	-	-	-	-	26.1	33.4	25.3	21.6

Table 3.2.2 – Upper teeth measurements of *Pannonictis baroniensis* and *Enhydrictis praegalictoides* from Monte Tuttavista. For measurement abbreviations, see the section 2.

Species	Cat. N°	Element		C L	C W	P2 L	P2 W	P3 L	P3 W	P4 L	P4 W	M1 L	M1 W
P. baroniensis	**VII-erratico-1**	skull	R	7.1	-	[3.6]	-	6.5	-	-	-	-	-
P. baroniensis	**VII-ms-1003**	cranium	L	-	-	4.3	-	6.4	-	11.2	6.7	6.2	8.1
P. baroniensis	**X-3u-9**	P2	L	-	-	4.3	2.9	-	-	-	-	-	-
E. praegalictoides	**IV-mac-3**	M1	R	-	-	-	-	-	-	-	-	4.6	7.5
E. praegalictoides	**IX-pro-1**	cranial fr	L	-	-	-	-	-	-	10.2	6.6	5.3	8.1
E. praegalictoides	**IX-pro-24**	maxillary fr	R	-	-	-	-	-	-	10.9	6.7	-	-
E. praegalictoides	**IX-pro-38**	M1	L	-	-	-	-	-	-	-	-	5.7	8.9

Species	Cat. N°	Element		C L	C W	P2 L	P2 W	P3 L	P3 W	P4 L	P4 W	M1 L	M1 W
E. praegalictoides	**IX-pro-62**	maxillary fr	R	-	-	-	-	6.4	4.0	10.4	6.3	-	8.3
E. praegalictoides	**IX-pro-63**	P4	L	-	-	-	-			10.8	6.4	-	
E. praegalictoides	**IX-pro-64**	maxillary fr	L	-	-	-	-	6.6	4.0	-	-	-	-
E. praegalictoides	**IX-pro-65**	maxillary fr	R	-	-	-	-	6.7	3.9	-	-	-	-
E. praegalictoides	**IX-pro-69**	C1	L	6.7	5.2	-	-	-	-	-	-	-	-
E. praegalictoides	**IX-pro-76**	cranium	R	-	-	4.3	2.9	6.2	3.9	10.5	6.4	5.3	7.6
E. praegalictoides	**IX-pro-79**	cranial fr	L	-	-	-	-	-	-	10.0	6.2	5.1	7.5
E. praegalictoides	**IX-pro-80**	cranial fr	L	-	-	-	-	-	-	-	-	5.1	8.0
E. praegalictoides	**IX-pro-81**	cranial fr	L	-	-	4.5	2.9	6.5	3.9	10.5	6.1	5.6	7.2
E. praegalictoides	**IX-pro-83**	cranial fr	L	-	-	4.3	2.9	6.3	3.8	-	-	-	-
E. praegalictoides	**IX-pro-120**	skull	L	7.3	-	-	-	6.1	-	11.6	-	-	-
E. praegalictoides	**IX-pro-121**	skull	L	7.1	5.3	4.26	3.2	-	3.9	10.3	6.5	5.0	7.2
E. praegalictoides	**X-5-1**	cranial fr	L	7.6	5.5	4.8	2.9	6.1	4.0	11.0	6.8	5.0	7.3

Table 3.2.3 – Mandibular measurements of *Pannonictis baroniensis* and *Enhydrictis praegalictoides* from Monte Tuttavista. For measurement abbreviations, see the section 2.

Species	Cat. N°	Element		Mp2H	Mp4H	Mm1H	Mm1B	H R	p2-p4 L	m1-m2 L
P. baroniensis	**VII-erratico-1**	skull	L	17.4	16.1	16.6	7.8	-	16.5	16.3
E. praegalictoides	**IX-pro-2**	hemimandible fr	R	-	12.8	13.5	7.3	-	16.8	-
E. praegalictoides	**IX-pro-3**	hemimandible fr	R	-	12.3	12.5	6.7	-	-	-
E. praegalictoides	**IX-pro-4**	hemimandible fr	L	-	-	-	6.9	-	-	-
E. praegalictoides	**IX-pro-23**	hemimandible	R	15.6	12.5	13.7	7.6	-	18.1	-
E. praegalictoides	**IX-pro-82**	hemimandible fr	R	-	-	-	-	32.9	-	-
E. praegalictoides	**IX-pro-120**	skull	L	15.5	12.8	15.2	7.3	30.7	16.7	-
E. praegalictoides	**IX-pro-121**	skull	L	14.7	13.3	13.9	7.7	32.0	-	15.8
E. praegalictoides	**IX-pro-137**	mandibles	L	15.3	12.2	13.4	6.7	32.2	17.0	15.4
E. praegalictoides	**IX-pro-155**	hemimandible	L	16.9	-	-	7.2	33.6	-	-

Table 3.2.4 – – Lower teeth measurements of *Pannonictis baroniensis* and *Enhydrictis praegalictoides* from Monte Tuttavista. For measurement abbreviations, see the section 2.

Species	Cat. N°	Element		c L	c W	p2 L	p2 W	p3 L	p3 W	p4 L	p4 W	m1 L	m1 W	trm1 L	trm1 W	tdm1 L	m2 L	m2 W
P. baroniensis	**VII-erratico-1**	skull	L	8.5-	-	3.1	-	5.9	-	7.0	-	-	-	-	-	-	-	-
E. praegalictoides	**IV-mac-35**	hemimandible fr	L	-	-	-	-	-	-	-	-	-	-	-	-	-	3.6	4.0
E. praegalictoides	**IV-mac-36**	m1	R	-	-	-	-	-	-	-	-	-	-	-	-	5.6	-	-
E. praegalictoides	**IX-pro-2**	hemimandible fr	R	-	-	4.4	3.0	5.6	4.1	6.2	3.9	12.9	5.2	8.4	5.2	-	-	-
E. praegalictoides	**IX-pro-3**	hemimandible fr	R	-	-	-	-	5.5	3.6	6.6	3.9	12.9	5.3	8.1	5.1	-	-	-
E. praegalictoides	**IX-pro-5**	hemimandible fr	R	-	-	-	-	5.9	3.7	6.8	4.1	-	-	-	-	-	-	-
E. praegalictoides	**IX-pro-23**	hemimandible	R	9.5	6.6	5.2	3.5	6.4	4.2	7.0	4.3	13.3	5.7	8.3	5.7	-	-	-
E. praegalictoides	**IX-pro-71**	m1	R	-	-	-	-	-	-	-	-	13.4	5.4	8.7	5.1	-	-	-
E. praegalictoides	**IX-pro-72**	m1	R	-	-	-	-	-	-	-	-	-	5.5	8.5	5.5	-	-	-
E. praegalictoides	**IX-pro-73**	m1	L	-	-	-	-	-	-	-	-	-	-	8.2	5.1	-	-	-
E. praegalictoides	**IX-pro-120**	skull	L	9.4	-	4.4		6.0		6.7	-	-	-	-	-	-	-	-
E. praegalictoides	**IX-pro-119**	m2	L		-	-	-	-	-	-	-	-	-	-	-	-	4.4	4.2
E. praegalictoides	**IX-pro-121**	skull	L	8.9	5.9	-	-	5.9	3.7	6.8	3.9	12.5	5.2	8.6	-	-	3.1	3.5
E. praegalictoides	**IX-pro-137**	mandibles	L	8.9	5.8	4.4	3.4	6.1	4.1	6.6	3.9	12.1	5.3	8.2	5.3	-	3.4	3.4
E. praegalictoides	**IX-pro-155**	hemimandible	L	-	-	4.7	3.6	6.1	4.1	-	-	-	-	-	-	-	-	-
E. praegalictoides	**X-4-19**	c1	R	8.6	5.9	-	-	-	-	-	-	-	-	-	-	-	-	-

Table 3.2.5 – Axial skeleton and scapula measurements of *Pannonictis baroniensis* and *Enhydrictis praegalictoides* from Monte Tuttavista. For measurement abbreviations, see the section 2.

Cat. N°	Element		Atlas			Axis			Scapula	
			BFcr	BRcd	LaD	LCDe	BFcr	BFcd	GLP	BG
IV-mac-4	axis		-	-	-	24.7	20.3	11.3	-	-
IX-pro-121	atlas		26.4	19.0	7.0	-	-	-	-	-
IX-pro-77	scapula	L	-	-	-	-	-	-	15.9	9.1
IX-pro-78	scapula	R	-	-	-	-	-	-	17	10.3
IX-pro-94	scapula	R	-	-	-	-	-	-	16.3	10.3

Cat. N°	Element		Atlas				Axis		Scapula	
			BFcr	BRcd	LaD	LCDe	BFcr	BFcd	GLP	BG
IX-pro-95	scapula	R	-	-	-	-	-	-	16.3	10.8
IX-pro-113	scapula	L	-	-	-	-	-	-	-	9.8
IX-pro-114	scapula	L	-	-	-	-	-	-	-	9.7

Table 3.2.6 – Forelimb measurements of *Pannonictis baroniensis* and *Enhydrictis praegalictoides* from Monte Tuttavista. For measurement abbreviations, see the section 2.

Cat. N°	Element		Humerus					Ulna			Radius				
			GL	GLC	Bp	Dp	Bd	GL	DPA	BPC	GL	Bp	Dp	Bd	Dd
X-3u-11	humerus	R	-	-	17.7	18.1	-	-	-	-	-	-	-	-	-
IX-pro-25	humerus	R	70.6	69.3	16.1	17.1	19.2	-	-	-	-	-	-	-	-
IX-pro-26	humerus	R	-	-	17.6	-	-	-	-	-	-	-	-	-	-
IX-pro-96	humerus	R	79.2	78.3	18.7	19.5	22.8	-	-	-	-	-	-	-	-
IX-pro-97	humerus	L	-	-	19.3	19.8	-	-	-	-	-	-	-	-	-
IX-pro-98	humerus	L	-	-	18.7	19.1	-	-	-	-	-	-	-	-	-
IX-pro-99	humerus	R	-	-	-	-	22.3	-	-	-	-	-	-	-	-
IX-pro-125	humerus	R	-	-	-	-	21.4	-	-	-	-	-	-	-	-
IX-pro-14	ulna	L	-	-	-	-	-	-	-	9.4	-	-	-	-	-
IX-pro-40	ulna	R	-	-	-	-	-	-	12.3	10.2	-	-	-	-	-
IX-pro-93	ulna	R	-	-	-	-	-	-	11.5	7.8	-	-	-	-	-
IX-pro-101	ulna	R	-	-	-	-	-	72.1	12.9	9.7	-	-	-	-	-
IX-pro-102	ulna	L	-	-	-	-	-	-	-	9.8	-	-	-	-	-
IX-pro-131	ulna	L	-	-	-	-	-	-	-	10.3	-	-	-	-	-
IX-pro-34	radius		-	-	-	-	-	-	-	-	55.4	7.4	6.1	-	7.4
IX-pro-35	radius	L	-	-	-	-	-	-	-	-	-	-	-	11.6	7.4
IX-pro-88	radius	R	-	-	-	-	-	-	-	-	51.3	7.9	5.4	10.8	7.0
IX-pro-103	radius	L	-	-	-	-	-	-	-	-	56.1	9.3	6.3	11.5	8.3

Cat. N°	Element		Humerus					Ulna			Radius				
			GL	GLC	Bp	Dp	Bd	GL	DPA	BPC	GL	Bp	Dp	Bd	Dd
IX-pro-104	radius	R	-	-	-	-	-	-	-	-	-	-	-	11.7	8
IX-pro-105	radius	R	-	-	-	-	-	-	-	-	-	-	-	12.0	7.9
IX-pro-130	radius		-	-	-	-	-	-	-	-	-	-	-	8.8	6

Table 3.2.7 – Hindlimb measurements of *Pannonictis baroniensis* and *Enhydrictis praegalictoides* from Monte Tuttavista. For measurement abbreviations, see the section 2.

Cat. N°	Element		Femur				Tibia				Astragalus	Calcaneus	
			Bp	DC	Bd	Dd	GL	Bp	Bd	Dd	GL	GL	GB
IX-pro-7	femur	L	23.7	10.3	-	-	-	-	-	-	-	-	-
IX-pro-8	femur	L	21.0	9.0	-	-	-	-	-	-	-	-	-
IX-pro-17	femur	L	-		20.5	17.2	-	-	-	-	-	-	-
IX-pro-36	femur		-	10.8			-	-	-	-	-	-	-
IX-pro-152	femur	L	-	-	20.7	17.7	-	-	-	-	-	-	-
IX-pro-27	tibia	R	-	-	-	-	84.2	19.4	13.5	8.6	-	-	-
IX-pro-31	tibia	L	-	-	-	-	86.8	19.5	13.7	8.5	-	-	-
IX-pro-32	tibia	R	-	-	-	-	-	-	12.7	8.6	-	-	-
IX-pro-87	tibia	R	-	-	-	-	-	-	13.5	9.0	-	-	-
IX-pro-108	tibia	L	-	-	-	-	82	19.7	13.9	9.0	-	-	-
IX-pro-109	tibia	R	-	-	-	-	-	20.8	-	-	-	-	-
IX-pro-110	tibia	R	-	-	-	-	-	16.3	-	-	-	-	-
IX-pro-129	tibia	R	-	-	-	-	-	16.2	-	-	-	-	-
IX-pro-153	tibia	L	-	-	-	-	-	19.6	15.7	-	-	-	-
IX-pro-10	astragalus	L	-	-	-	-	-	-	-	-	15	-	-
IV-mac-2	calcaneus	L	-	-	-	-	-	-	-	-	-	22.3	12.1
IX-pro-11	calcaneus	R	-	-	-	-	-	-	-	-	-	22.4	13.7
IX-pro-90	calcaneus	R	-	-	-	-	-	-	-	-	-	21.6	12.0

Table 3.2.8 – Metapodial measurements of *Pannonictis baroniensis* and *Enhydrictis praegalictoides* from Monte Tuttavista. For measurement abbreviations, see the section 2.

Cat. N°	Element		Metapodials				
			GL	Bp	Dp	Bd	Dd
IX-pro-16	I mc	L	27.3	4.6	5.9	5.9	4.7
IV-mac-13	II mc	L	25.1	4.8	6.0	5.9	5.3
IX-pro-44	II mc	R	23.5	3.9	5.7	5.6	4.3
IX-pro-45	II mc	R	20.8	4.4	5.1	4.7	3.4
IX-pro-145	II mc ?	L	24.3	3.8	5.2	5.0	4.0
IX-pro-144	V mc	L	18.4	4.8	4.4	5.0	4.1
IX-pro-41	III mt	L	27.8	4.7	5.8	4.8	3.7
IX-pro-42	III mt	R	30.6	4.4	6.6	5.5	4.6
IX-pro-146	III mt	L	32.3	5.1	7.2	5.9	3.8
IX-pro-43	V mt	R	-	5.3	5.4	-	-
IX-pro-46	metapodial		-	-	-	5.5	4.7
IX-pro-47	metapodial		-	-	-	5.5	4.3

3.3. The record of *Nyctereutes* (Carnivora, Canidae) from Lower Valdarno (Tuscany, Italy)

3.3.1. Context

The Lower Valdarno basin has yielded *Nyctereutes* remains from two different localities: San Giusto (Triversa FU, early Villanyian, early Villafranchian, Late Pliocene; Florence), and Montopoli (Montopoli FU, middle Villafranchian, Early Pleistocene, Pisa).

3.3.1.1. San Giusto

San Giusto is a well-known early Villanyian (Late Pliocene) locality that yielded the type specimen of the vole *Mimomys stehlini* Kormos 1931 (Masini & Torre, 1987). Together with other Italian early Villanyian sites (Cascina Arondelli, Asti, Piedmont; Arcille, Grosseto, Tuscany) this fauna is coeval with the large mammal assemblages of the early Villafranchian Triversa FU and are correlated to the Gauss Chron (Sala & Masini, 2007). An unpublished *Nyctereutes* hemimandible fragment from S. Giusto is kept in the collections of the Natural History Museum, Geological and Paleontological section, of the University of Florence with inventory number IGF 10132. The specimen was recovered during a sampling excavation in 1916 and later donated to the Museum by Prof. A. Fucini.

3.3.1.2. Montopoli

Montopoli is an important large mammal fauna site since it is the first middle Villafranchian (Early Pleistocene, see Fig. 1.9) large mammal assemblage. Montopoli is stratigraphically superposed on the fauna of the Triversa unit and shallow-water marine sediments of Early Pleistocene age (Middle Pliocene in papers prior to the IUGS 2009 decision, *e.g.*, cf. Benvenuti et al., 1995). This fauna is celebrated in the literature for its important signs of environmental change given by the dispersals of a

primitive species of the genus *Mammuthus* (Palombo & Ferretti, 2005), the monodactyl horse *Equus* cf. *livenzovensis*, the large deer *Eucladoceros tegulensis*, and *Gazella borbonica*, as well as the disappearance of some taxa with subtropical affinities still characterizing the previous early Villafranchian assemblages (Pradella & Rook, 2007). The Montopoli Faunal Unit (corresponding to unit MN16b in the European MN sub-division) was originally included in the early Villafranchian (Azzaroli, 1977; Azzaroli et al., 1988), but the marked faunal turnover characterizing the transition from the early Villafranchian Triversa FU to the Montopoli FU suggested considering Montopoli as the basal unit of the middle Villafranchian (Caloi & Palombo, 1996; Gliozzi et al., 1997). Montopoli, and the related faunal unit, occurs at the Gauss–Matuyama transition (Lindsay et al., 1980) thus correlating with the recently redefined Plio/Pleistocene boundary (Gelasian Stage, GSSP at Monte san Nicola Section, Sicily; Rio et al., 1994; Gradstein et al., 2004). Del Campana (1913) discussed the attribution of a right maxillary fragment (IGF 10131) from Montopoli to *Canis* (=*Vulpes*) *alopecoides*, but later changed this attribution ascribing it to a raccoon dog (Del Campana, 1917). The specimen, later relabeled in the Florence Museum inventory as *N. megamastoides*, has never been redescribed in detail, although the occurrence of the species has been reported in faunal lists from Montopoli in all the general papers dealing with the biochronology of Italian mammalian faunas (*e.g.* Azzaroli et al., 1982; Caloi & Palombo, 1996; Gliozzi et al., 1997; Palombo et al., 2002).

3.3.2. Systematic Paleontology

Order **Carnivora** Bowdich, 1821

Family **Canidae** Fischer, 1817

Genus ***Nyctereutes*** Temminck, 1838

Nyctereutes megamastoides (Pomel, 1842)

(Fig. 3.3.1; Table 3.3.1)

Referred material. San Giusto (Late Pliocene; Triversa FU): IGF 10132, left, edentulous mandibular fragment.
Montopoli (Early Pleistocene; Montopoli FU): IGF 10131_1, right maxillary fragment with P2-P4; IGF 10131_2, right maxillary fragment with M1 (probably same individual of IGF 10131_1).

Description. *Upper teeth* The second and third upper premolar in the specimen IGF 10131_1 (Fig. 3.3.1) are rather buccolingually flattened, and lack a distal accessory cusp. They are separated by short diastemata. In the P4, the protocone is large and directed mesiolingually. It has a long and low metastylar blade. The M1 (IGF 10131_2) is rather elongated mesiodistally (Fig. 3.3.1). As the occlusal surface is highly worn, the only feature that can be confidently assessed is that the paracone and metacone are of equal size.
Mandible. The hemimandible (Fig. 3.3.1) is broken anteriorly at the level of the alveoli of the p4 and posteriorly slightly above the alveolus of m3. It does not have any teeth. The angular region is only partially preserved but the high-angled subangular lobe is well-preserved. The corpus is quite thick under the m1.

Comparisons. *Montopoli* – The morphology of the upper carnassial differs greatly from the extant *N. procyonoides*, *N. tingi* and *N. donnezani*, especially regarding the enlarged protocone and it mesial position relative to the anterior margin of the P4. In *N. sinensis* from the Yushe basin, the protocone of the P4 lies far mesial of the mesial margin of the paracone, much more so than in IGF 10131_1, whereas the upper carnassial of *N. megamastoides* is very similar to the Montopoli specimen. Focusing on the European species, Fig. 3.3.2 schematically points out the features of the upper carnassials of *N. donnezani* (from Depéret 1980), *N. vulpinus* (from Viret 1954), *N. megamastoides* (from Boule 1889 and DFN-17) and IGF 10131_1.

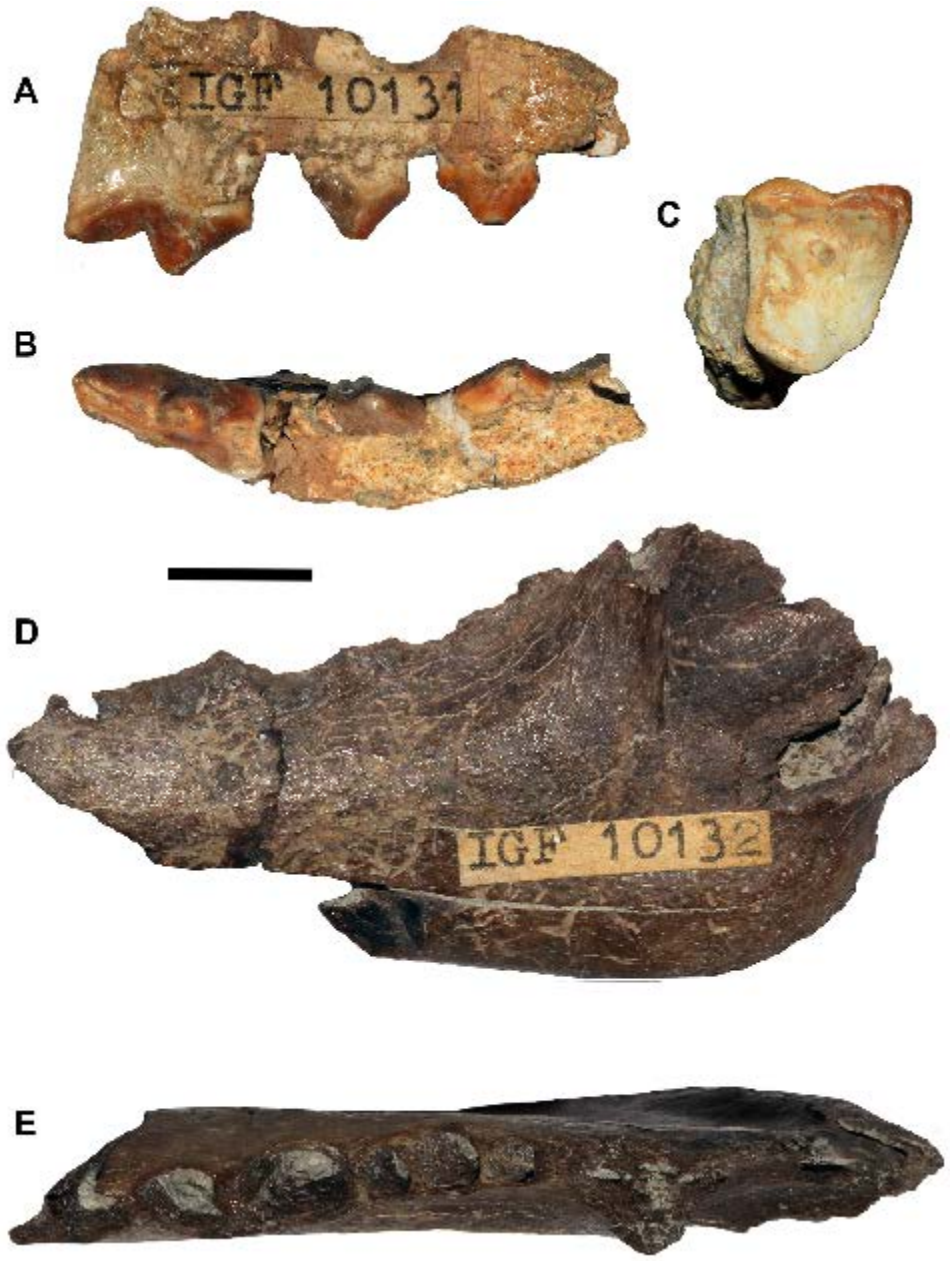

Figure 3.3.1 – *Nyctereutes megamastoides* from the localities of S. Giusto and Montopoli. **A-B**: **IGF 10131_1**, right maxillary fragment in lateral (**A**) and occlusal (**B**) views. **C**: **IGF 10131_2**, right maxillary fragment with M1 in occlusal view. **D-E**: **IGF_10132**, left mandibular fragment in lateral (**D**) and occlusal (**E**) views. The scale bar equals 10 mm.

Cat. N°		P2		P3		P4		M1	
		L	W	L	W	L	W	L	W
IGF 10131_1	R	6.9	3.0	7.5	3.6	12.9	6.4	-	-
IGF 10131_2	R	-	-	-	-	-	-	10.6	12.3

Table 3.3.1 – Upper teeth measurements of *Nyctereutes megamastoides* of the Lower Valdarno.

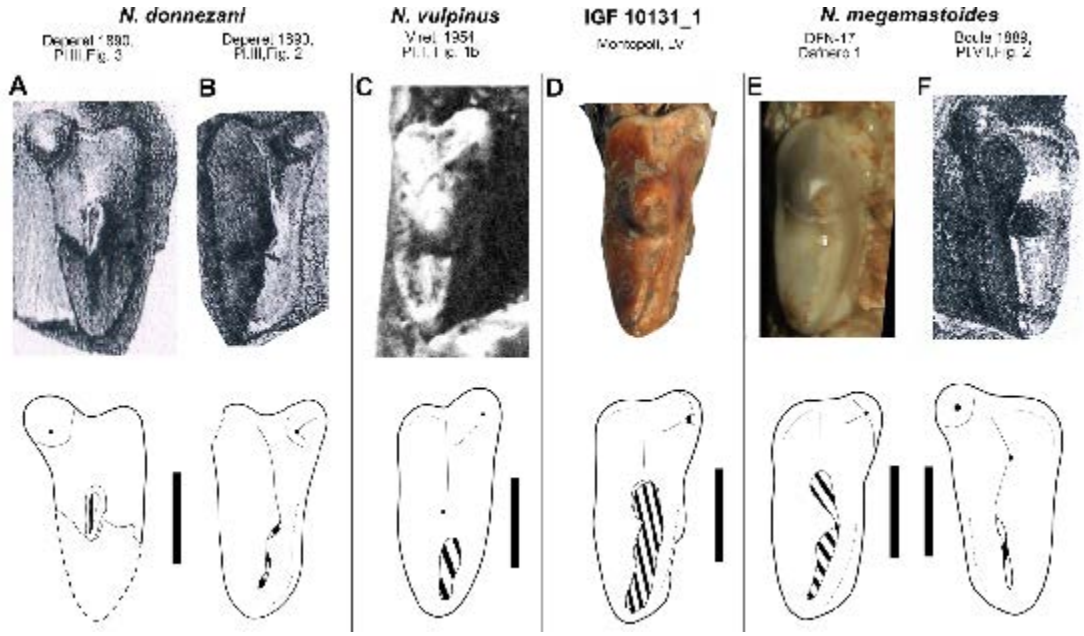

Figure 3.3.2 – Comparison between P4 morphologies of the European species of *Nyctereutes*, in occlusal view: *N. donnezani* from Depéret (1890), Plate III, Fig. 3 (**A**) and Fig. 2 (**B**). *N. vulpinus* from Viret (1954), Plate I, Fig. 1b (**C**). **IGF 10131_1** from Montopoli (**D**). *N. megamastoides* from Dafnero-1 (western Macedonia, Greece), DNF-17 (**E**) and Boule (1889), Plate VII, Fig. 2 (**F**). All scale bars equal 5 mm.

As shown in the figure, the P4 of IGF 10131_1 does not show the embayment on the mesial margin of the tooth that separates the protocone from the rest of the paracone in *N. donnezani*-type specimens reported in Depéret (1890). On the contrary, the mesial margin of P4 of IGF 10131_1 is straight-like in *N. vulpinus* and *N. megamastoides*, especially like DFN-17. Unlike *N. donnezani* and *N. vulpinus*, the P4 of IGF 10131_1 has a mesiodistally short paracone and an elongated metastylar blade. This resembles the condition seen in the holotype of *N. megamastoides* in Boule (1889). Even though the M1 of IGF10131_2 is heavily worn, its buccal margin resembles that of *N. sinensis* and *N. megamastoides.*

The log-ratio diagram of upper teeth measures (Fig. 3.3.3) shows that IGF 10131_1 is close in size to *N. megamastoides*, *N. donnezani*, *N. vulpinus* and *N. sinensis*, whereas *N. procyonoides* and *N. tingi* are on average, respectively, smaller and larger. Although P4 L-P4 W proportions show a trend similar to that of *N. donnezani*, all the other proportions bear resemblance to *N. megamastoides* (*e.g.*, P3L-P4 L of IGF

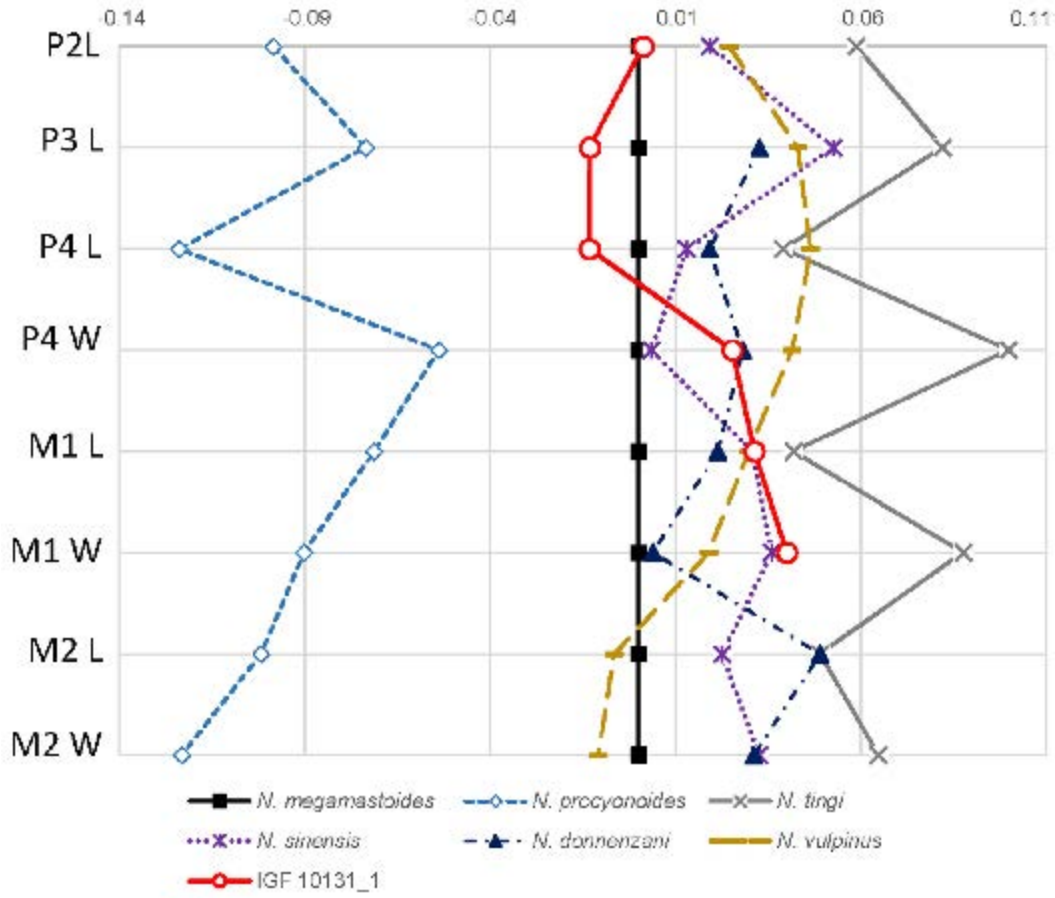

Figure 3.3.3 – Log-ratio diagram based on log-transformed mean of upper teeth measurements of *Nyctereutes* spp. *N. megamastoides* is used as a reference. Tooth measurements taken into consideration are shown on the left side.

10131_1 and the standard *N. megamastoides* are identical in proportions, and the P4 W-M1 L-M1 W points of IGF 10131_1 show only a slight difference between them).

San Giusto - The caudoventral curvature of the subangular lobe is more marked in comparison with primitive forms like *N. donnezani* and *N. tingi*, in which the strong curvature of this part of the mandibular body is missing. In contrast, IGF 10132 resembles *N. megamastoides*, *N. sinensis* and, to some extent, *N. procyonoides*. *N. vulpinus* from St. Vallier does not have such a high angle-curvature, being somewhat intermediate between primitive and derived forms.

3.3.3. Discussions and Conclusions

The morphological features of the *Nyctereutes* remains from the sites of S. Giusto and Montopoli here described (such as the morphology of the P4 of the Montopoli specimen and the high-angled caudoventral curvature of the corpus of the San Giusto mandible) point to a substantial affinity with the Late Pliocene-Early Pleistocene *N. megamastoides* (Pomel, 1842) of Europe. This is also consistent with the stratigraphic history of Pliocene canids. The first record of the family Canidae of western Europe is from the Turolian (Late Miocene) of Concud (Teruel Basin, Spain; Late Miocene, MN12) with the species '*Canis*' *cipio* (see Crusafont Pairó 1950). The scarcity of the material and its peculiar features have led many researchers (*e.g.* Rook, 1992; Wang & Tedford, 2007) to question the taxonomic attribution of the specimens and, recently, Rook (2009) re-assigned the species to the genus *Eucyon*. Other species of the latter genus characterized Late Miocene-Early Pliocene times in Europe: *E. debonisi* in the Late Miocene of Spain (Montoya et al., 2009); *E. monticinensis* from the Messinian Monticino gypsum quarry of Brisighella (Ravenna, Italy; Rook, 1992); *E. odessanus* in the Early Pliocene of southeastern Europe (Odintzov, 1967); and the Early Pliocene *E. adoxus* from the French site of Perpignan (Martin, 1973). The earliest appearence of a *Nyctereutes* species to place during the Early Pliocene, *N. donnezani*, in Spanish sites like La Gloria 4 (MN14) and Layna (MN 15) (Alcalá Martínez & Montoya, 1989-1990). Subsequently, this primitive form is replaced by the more derived forms *N. megamastoides* and *N. vulpinus*. Indeed, from the Latest Pliocene, these two species are the only representatives of the genus in Europe (Monguillon et al., 2004). The presence of a fossil of *Nyctereutes* (IGF 10132) with derived features in the Late Pliocene locality of S. Giusto fits with the European panorama of raccoon dog like canids. Even the maxillary fragment (IGF 10131) recovered from an Early Pleistocene locality of the same basin, shows morphological and mensural affinity to derived forms *Nyctereutes*. All things considered, the fossil material from the Lower Valdarno basin can be reasonably attributed to *N. megamastoides*.

In conclusion, the study of the *Nyctereutes* material of the Lower Valdarno highlights two points: the Montopoli specimen (IGF 10131) confirms the taxonomic attribution of this fossil to *N. megamastoides* (Pomel, 1842), a relatively widespread taxon in the earliest Pleistocene of Europe, whereas the described and figured specimen from San Giusto (IGF 10132) demonstrates the occurrence of an advanced *Nyctereutes* form in the Late Pliocene of Italy for the first time. It also represents one of the earliest records of the species *N. megamastoides* in all of Europe. This early occurrence of a derived *Nyctereutes* species in the Late Pliocene (early Villafranchian) of western Eurasia reveals an evolutionary pattern of the genus different from the one documented in the Early Pliocene of China, where a more advanced species is associated with the primitive *N. tingi*.

3.4. The Late Pliocene record of Caninae from Kvabebi (Georgia)

3.4.1. Context

Vekua (1972) described the fossil assemblage of Kvabebi, a late Pliocene site (MN16a in the European Land Mammal biochronology). Mein (1975a, b) and Agustí et al. (2009) reported the co-occurrence of *N. megamastoides* and *Canis* sp. in eastern Georgia. Agustí et al. (2009) provided a general revision of the Kvabebi fauna and its chronological position. The authors, by providing a magnetostratigraphic calibration of the Kvabebi succession to the late Pliocene (chron 2An.1r), reviewed the faunal list ascribing the canid record to the genera *Nyctereutes* and *Eucyon*.

3.4.2. Geological and chronological context of the Kvabebi site

Kvabebi is located south of Magaro village, in the area of the Sighnaghi region of eastern Georgia that surrounds Kvabebi Mountain, on the southern edge of the Iori Plateau. The Kvabebi section sits in the sedimentary infill of the Kura Basin. The latter, since the late Neogene, has been bordered by the Greater Caucasus to northeast and by the Lesser Caucasus and the Talysh ranges to the southwest (Agustí et al., 2009, fig. 1), and it formed as a northward inland ingression of the Caspian (Popov et al., 2006). The Kvabebi section, which is in the middle part of the Akchagylian stage of the Caspian Paratethys (Vekua, 1972), is ~170m thick and displays a general regressive trend. The lower 110m of the section is built up of a succession of brownish and bluish laminated mudstones. The brownish sediments are of fluvio-lacustrine origin, whereas the bluish color testifies to transgressive (marine) events characterized by a Pliocene (Akchagylian) mollusk fauna (Djikia, 1968). The upper part of the section (from 110m to the top) is formed by a succession of alluvial reddish-brown sediments with no marine fauna. The section is characterised by the occurrence of several sandstone layers, including

the one that yielded the Kvabebi fossil vertebrate assemblage (at meter 40), which is the result of accumulation due to tractive processes in a fluvial-influenced environment (Agustí et al., 2009).

New prospections and excavations conducted at Kvabebi allowed the re-evaluation of the geochronological setting of the section and a revision of the vertebrate fauna assemblage (Agustí et al., 2009). A magnetostratigraphic study allowed placement of the fossiliferous level within the polarity reversals chron 2An.1r, with an age of ca. 3.07 Ma for the Kvabebi site (Agustí et al., 2009). The updated revised list of the Kvabebi vertebrate fauna (Vekua, 1972; Hemmer et al., 2004; Agustí et al., 2009; this study) is as follows:

Reptilia

Testudo cernovi transcaucasica Chkhikvadze, 1979

Aves

Ioriotis gabuniae Burchak-Abramovich & Vekua, 1971;

Struthio transcaucasicus Burchak-Abramovich & Vekua, 1971

Mammalia

Rodentia: *Hystrix* cf. *H. primigenia* Wagner, 1848

Carnivora: *N. megamastoides* (Pomel, 1842); *Eucyon* sp., *Vulpes* cf. *V. alopecoides* (Del Campana, 1913); *Ursus minimus* Devèze & Bouillet, 1827; *Lynx issiodorensis* (Croizet & Jobert, 1828); *Homotherium davitashvili* Vekua, 1972; *Puma pardoides* Owen, 1846; *Dinofelis cristata* (Falconer & Cautley, 1836); *Chasmaportetes lunensis* (Del Campana, 1914); *Perinium kvabebicus* (Bendukize & Vekua, 2012)

Arctiodactyla: *Propotamochoerus provincialis* (Gervais, 1859); *Eucladoceros* sp.; ?*Pseudalces* sp.; *Procapreolus* sp.; *Ioribos aceros* Vekua, 1972; *Protoryx heinrichi* Major, 1891; *Oryx* (*Aegoryx*) sp.; *Parastrepsiceros sokolovi* Vekua, 1968; *Eosyncerus ivericus* Vekua, 1972; *Gazella postmitilinii* Vekua, 1972

Perissodactyla: *Hipparion rocinantis* Hernández Pacheco, 1921; *Stephanorhinus megarhinus* (de Christol, 1834)

Hyracoidea: *Kvabebihyrax kachethicus* Gabunia & Vekua, 1966

Probiscidea: *Anancus arvernensis* (Croizet & Jobert, 1828).

3.4.3. Systematic Paleontology

Order **Carnivora** Bowdich, 1821

Suborder **Caniformia** Kretzoi, 1943

Family **Canidae** Fischer, 1817

Subfamily **Caninae** Fischer, 1817

Tribe **Vulpini** Hemprich & Ehrenberg, 1832

Genus ***Nyctereutes*** Temminck, 1838

Nyctereutes megamastoides (Pomel, 1842)

(Figs. 3.4.1-3.4.2; Tables 3.4.1-3.4.4)

1972 *Nyctereutes megamastoides* Vekua, p. 41, pl. 2, figs. 1, 2, pl. 3, figs.1, 6.

2009 *Nyctereutes megamastoides* Agustí et al., p. 3277.

Holotype. The holotype of *Nyctereutes megamastoides* comes from Perrier-Etouaires (early Pleistocene), France.

Materials. MG 29-2013/455 (K234), juvenile cranium with left dP4 and M1 and right P4–M2; MG 29-2013/456 (K217), cranium; MG 29-2013/457 (K220), cranium with left C1–M2 and right P1–M2; MG 29-2013/567 (K4173), neurocranium; MG 29-2013/568 (K215), cranium; GNM 29-2013/573 (K233), skull; MG 29-2013/581 cranium; MG 29-2013/610 (K227), left C1; MG 29-2013/609 (K237), left M1; MG 29-2013/588 (K221), left hemimandible with i2, c1–p1, m1–m3; MG 29-2013/589 (K224), right hemimandible with p4-m2; MG 29-2013/590 (K235), right hemimandible with dm1 and germinal m1; MG 29-2013/591 (K214), right hemimandible with m1; MG 29-2013/592 (K4177), right hemimandible with p4-m1; MG 29-2013/606, right hemimandible with c1; MG 29-2013/820, left hemimandible with p2–m3; MG 29-2013/612 (K236), c/C; MG 29-2013/613, incisors, c1 and p1; MG 29-2013/605 (K256), left p4; MG 29-2013/611, right m2; MG 29-2013/593, vertebral fragments (K502 and K504); MG 29-2013/458, left humerus (K251), ulna, and radius (K250); MG 29-2013/594, left humerus (K241), ulna (K239), radius (K245), metacarpals II–V, and I phalanx; MG 29-2013/596 (K232), left

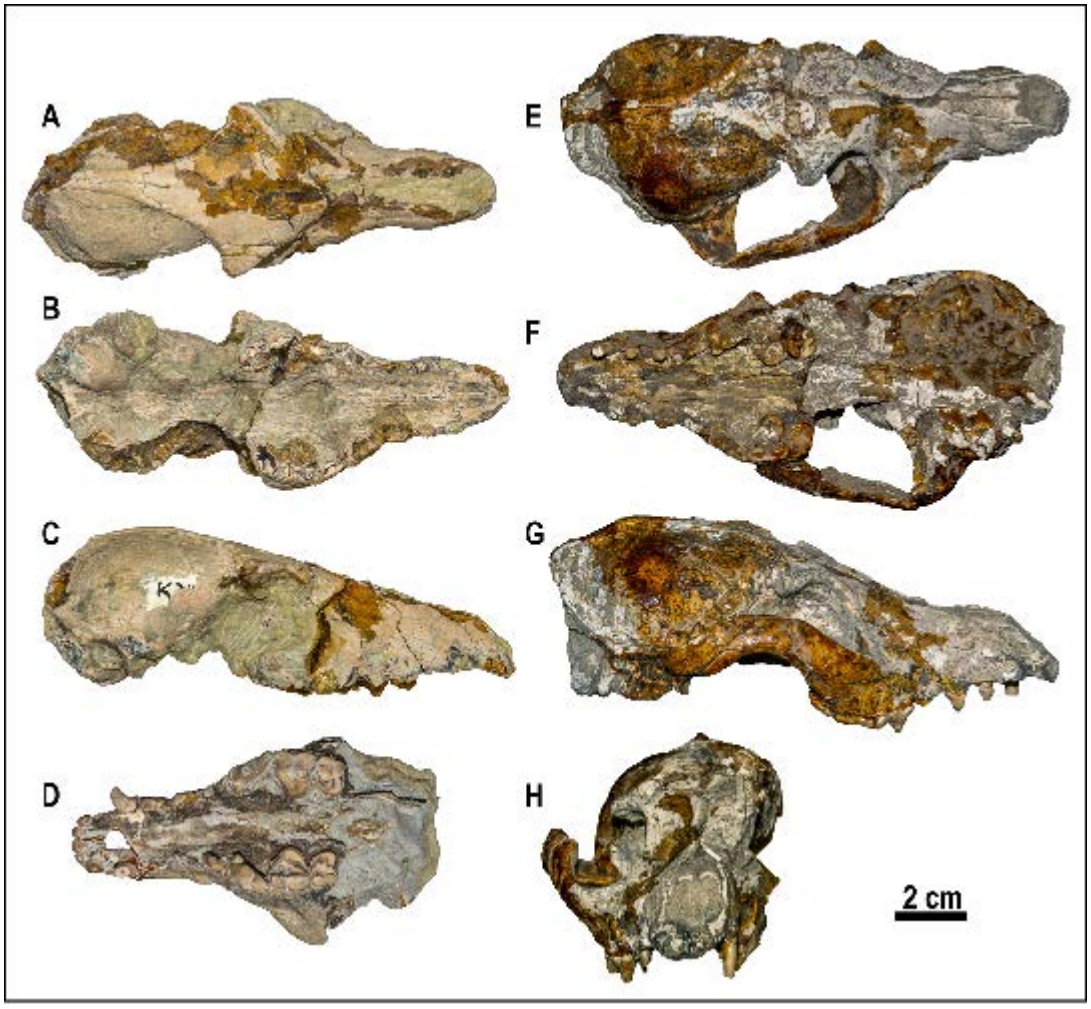

Figure 3.4.1 – *Nyctereutes megamastoides* (Pomel, 1842) from Kvabebi. **A-C**: **MG 29-2013/581** (**K219**), cranium in dorsal (**A**), ventral (**B**) and right lateral (**C**) views. **D**: **MG 29-2013/456** (**K217**), cranial fragment in occlusal view. **E-H**: **MG 29-2013/457** (**K220**), cranium in dorsal (**E**), ventral (**F**), right lateral (**G**) and rostral (**H**) views.

radius; MG 29-2013/602 (K503), right pelvis; MG 29-2013/598 (K501), left femur; MG 29-2013/600 (K226), right femur; MG 29-2013/599 (K820), right tibia; MG 29-2013/601 left calcaneum; MG 29-2013/597 (K253), metapodial fragments and phalanges; MG 29-2013/460 (K254), left phalanges.

Description. *Cranium.* The cranium is elongated rostro-caudally, with a long muzzle and long nasals, which end beyond the maxillofrontal suture. In lateral view, the cranial profile is rather straight on the nasals and frontals aspects and becomes arched only in the caudal portion of the braincase (*e.g.*, Fig. 3.4.1). The frontals show a depression on the midline of the cranium at the level of the

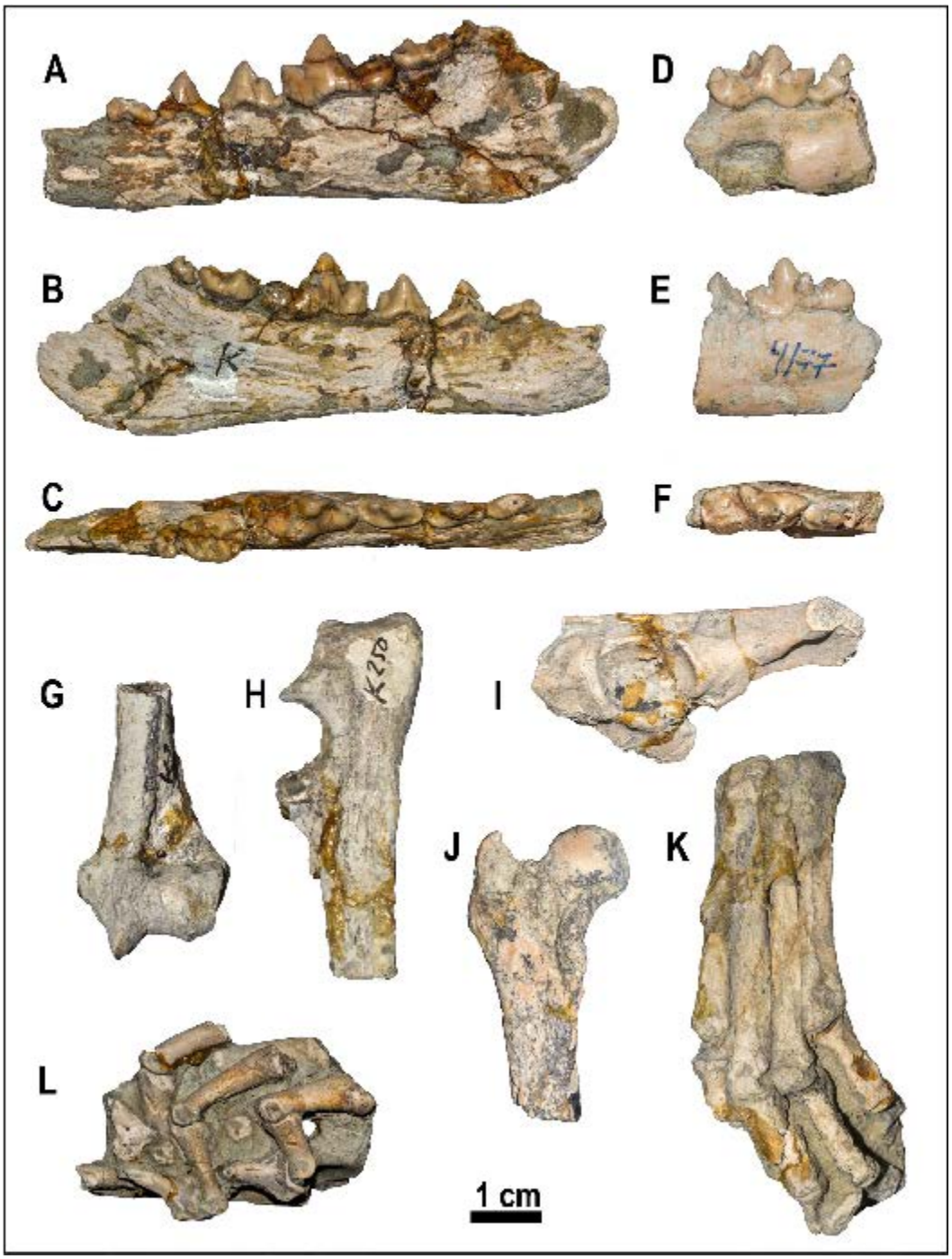

Figure 3.4.2 – *Nyctereutes megamastoides* (Pomel, 1842) from Kvabebi. **A-C**: **MG 29-2013/820**, left hemimandible in buccal (**A**), lingual (**B**), and occlusal (**C**) views. **D-F**: **MG 29-2013/592** (**K4177**), right hemimandible fragment in buccal (**D**), lingual (**E**), and occlusal (**F)** views. **G-H**: **MG 29-2013/458**, left humerus (**K251**) and ulna (**K250**) in caudal (**G**) and right lateral (**H**) views. **I**: **MG 29-2013/602** (**K503**), right pelvis in lateral view. **J**: **MG 29-2013/600** (**K226**), right femur in dorsal view. **K**: **MG 29-2013/597** (**K253**), left metacarpals with phalanges in dorsolateral view. **L**: **MG 29-2013/460** (**K254**), left phalanges in lateral view.

postorbital processes. These are expanded laterally and are well developed. The postorbital constriction is short and marked, so that the frontal sinuses are slightly developed and have a flat external surface. The braincase is rather inflated and globular in shape. The sagittal crest is poorly developed, with some specimens (*e.g.*, K219) showing long parasagittal crests that fuse distally from the frontoparietal suture and others (*e.g.*, K215) having parasagittal crests that fuse at the level of the frontoparietal suture. In caudal view, the supraoccipital shield is "bell"-shaped, with prominent borders and a marked knoblike expansion at level of the mastoid process. In lateral view, the inion does not overhang the condyles. The tympanic bullae are fairly inflated. The paraoccipital processes are not fused with the bulla and are posteriorly directed.

Unfortunately, the only juvenile cranium (MG 29-2013/455 [K234]) is too poorly preserved to assess correctly its morphological features. It appears to be low in dorsoventral height, in lateral view. In dorsal view, the braincase is inflated and the postorbital constriction seems rather marked.

Upper teeth. The incisors possess a main cusp with two small accessory cuspids on both sides of the main cusp. I3 is slightly larger compared to I1-I2, but still maintains an incisor morphology (not canine form) and does not possess the basal cingulum. C1 is very thin and its crown is not very high. Short diastemata are visible between upper premolars. The premolars do not show distal accessory cuspids. The P3 possesses a tiny cuspid on the distal cingulum. The P4 is rather slender and elongated mesiodistally. The protocone is small, pointy, and anteriorly positioned compared to the mesial margin of the tooth. Some specimens (*e.g.*, K217) seem to show a parastyle in the mesiolingual portion of the P4. The paracone is high and the metastylar blade is sharp and short. There is a strong lingual cingulum. The M1 is subquadrate in shape. It possesses an equally developed paracone and metacone, bounded buccally by a strong cingulum. There is a prominent parastyle. The M1 shows a large trigon basin, a prominent protocone, a large protoconule and a low,

but well-developed, metaconule. Lingually, there is a cingular hypocone. On the mesial side, there is a strong cingulum that forms a bulging of enamel in the shape of a small cuspid. The M2 is large mesiodistally and possesses an equal-sized paracone and metacone, a protocone, a protoconule, and a small metaconule. There is a lingual cingulum.

Mandible.The mandible is long and rather shallow, with a straight ventral margin. In the angular region, the subangular lobe is well developed and high-angled, in lateral view. The angular process is large and stout. The masseteric fossa is deep. MG 29-2013/590 (K235) possesses dm1 with a broken paraconid and a pointy and high protoconid; its talonid basin is wide and bounded by an entoconid, hypoconid, and a prominent distal accessory cuspulid.

Lower teeth. Of the lower premolars, only p4 possesses a distal accessory cuspulid, although there is a cuspulid-like distal cingulid on p3 and p4. The p4 also possesses a slightly visible mesial cingulid. The m1 paraconid is short, lower than the p4 protoconid. The protoconid is high, whereas the large metaconid is individualized from the protoconid, slight lingually, and distally positioned compared to the distal margin of the protoconid. In the talonid, the hypoconid is larger based compared to the entoconid, but not sensibly higher. In K4177, there are accessory cuspulids on the talonid (*e.g.*, mesially to the entoconid or distally to the hypoconid). The m2 is enlarged in the mesial portion, especially with a great expansion of the mesiobuccal cingulid. The protoconid and the metaconid are equal in size. Distal to the protoconid is a hypoconid with accessory cuspulids on both mesial and lingual sides. The m3 possesses two large cuspulids and a distal accessory one.

Postcranial elements. The postcranial remains from Kvabebi are generally in a bad state of preservation, so the features of the various bones are difficult to discern.

Humerus. MG 29-2013/458 (K251) and MG 29-2013/594 (K241) are the distal epiphysis of the left humeri (Bd: 21.0 mm and 22.2 mm, respectively), showing a prominent medial epicondyle compared to the lateral one; the trochlea has a sharp

ridge. MG 29-2013/594 (K239) is fragmentary ulna (BPC: 8.6 mm) that possesses a faint lateral coronoid process, whereas the medial one is round and expanded. Ulna. The ulna of MG 29-2013/458 (K251) has DPA = 18.5 mm and BPC = 9.6 mm. Radius. Radius fragments MG 29-2013/458 (K251) and MG 29-2013/596 (K232) have Bp = 11.8 mm and 13.5 mm, and Bd = 9.0 mm. Femur. Two femur fragments are recorded, MG 29-2013/598 (K501) and MG 29-2013/600(K226); the former (Bp = 23.3 mm and DC = 12.3 mm) shows a large head departing from a short neck. The greater trochanter is high and slender, with a deep trochanteric fossa. The lesser trochanter of MG 29-2013/598 (K501) is prominent. In the distal epiphysis, the lateral condyle is considerably larger than the medial, which is also thinner. Tibia. There is no proximal epiphysis of the tibiae preserved, but only a diaphysis with the distal portion MG 29-2013/599 (K820), with Bd = 17.4 mm and Dd = 11.9 mm. Calcaneus. The calcaneus MG 29-2013/601 is rather compressed mediolaterally, so that the *sustentaculum tali* is very reduced (GL = 31.9 mm). MG 29-2013/594 and MG 29-2013/597 are metapodial fragments with associated phalanges. MG 29-2013/594 measures are: Mc II — GL = 39.6 mm; Bp = 4.7 mm; Dp = 7.6 mm; Mc III — GL = 47.4 mm; Bp = 6.3mm; Dp = 72mm; Mc IV — GL = 46.5 mm; Bp = 4.1 mm; Dp = 6.5 mm; Mc V—GL = 38.6 mm; Bp = 7.5 mm; Dp = 6.3 mm.

Comparisons. Most of the Canidae specimens of Kvabebi are ascribable to the genus *Nyctereutes* based on the size and on the morphological features described above. Compared to *N. procyonoides* and to the Eurasian Pliocene species of raccoon dog-like canids, *Nyctereutes* from Kvabebi is similar in size to *N. megamastoides*, *N. sinensis*, and *N. donnezani*, but smaller than *N. tingi*. Some morphological features (*e.g.*, the high angle of the corpus of the mandible in the region of the subangular lobe, subquadrate M1, mesiodistally enlarged M2, etc.) are suggestive of a derived form of *Nyctereutes*, thus differing from primitive morphologies like those characterizing

N. tingi and *N. donnezani* (*e.g.*, poorly developed subangular lobe, reduced width of upper molars). Therefore, *Nyctereutes* from Kvabebi is more similar to species like the extant *N. procyonoides*, *N. sinensis* from the Yushe Basin, and *N. megamastoides* from western Europe. Among these latter species, *N. procyonoides* possesses the greatest number of dental differences compared to *Nyctereutes* from Kvabebi (*e.g.*, the P4 protocone more mesially placed, a stronger parastyle on P4, proportionally buccolingually shorter M1 and M2, the M1 metacone and metaconule reduced in development, the pointy and higher M1 hypocone, the individualized metaconid and reduced buccolingual width of the talonid on the m1). *Nyctereutes* sinensis and *N. megamastoides* are similar in size and in morphological features, so they could represent a single taxon with a wide zoogeographic range (Tedford & Qiu, 1991). Nevertheless, as pointed out by Tedford & Qiu (1991), *N. megamastoides* has a better-developed subangular lobe and more quadrangular upper molars compared to *N. sinensis*. Furthermore, the P4 protocone of *N. sinensis* lies more mesially when compared to the mesial margin of the tooth, more than it does in *N. megamastoides*; this species has an equal-sized M1 paracone and metacone, in contrast to those of *N. sinensis*, which appear well developed in F:AM 96759 (Tedford & Qiu, 1991); the latter species does not possess any or strongly reduced protoconule on M1, which is present in the Villarroya and Dafnero-1 *N. megamastoides*; the mesiolingual cingulum on M1 of *N. sinensis* is not continuous and does not form the cuspid-like enlargement on the mesial side of the M1 of *N. megamastoides*; the M2 of the Chinese species is reduced compared to that of *N. megamastoides*, which has a peculiar "D"-like shape; *N. megamastoides* from Villarroya and Dafnero-1 has a large protoconule and protocone and a low metaconule on the M2, whereas *N. sinensis* seems to possess only a large and prominent protocone; the m1 metaconid of *N. megamastoides* is larger than that of *N. sinensis*; in *N. megamastoides*, the m1 talonid is considerably enlarged compared to the trigonid, whereas in *N. sinensis* the talonid is not oversized compared to the trigonid; the m2 is generally slender

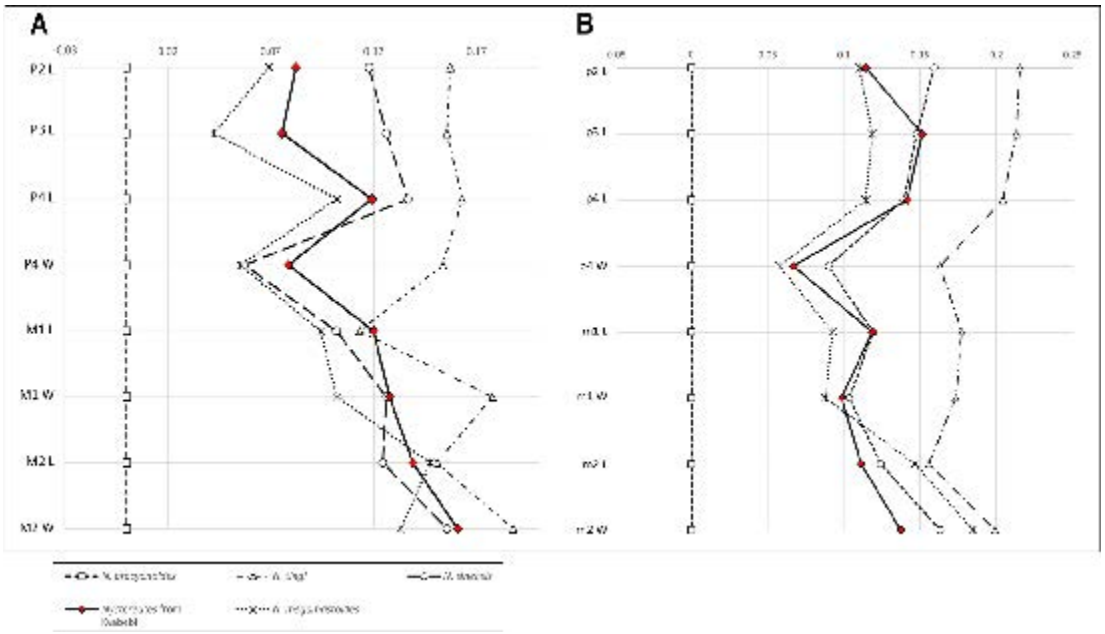

Figure 3.4.3 – Log-ratio diagrams based on selected upper (**A**) and lower teeth (**B**) variables in the described Kvabebi material, as well as in other Pliocene and extant species of *Nyctereutes* (*N. sinensis*, *N. tingi* and *N. megamastoides*; data taken from the literature: Tedford & Qiu (1991) Monguillon et al. (2004) as compared to the extant *N. procyonoides* (used as the reference baseline).

in *N. sinensis* compared to *N. megamastoides* in which it is oval in shape. The m2 protoconid and metaconid are subequal in size in *N. megamastoides*, whereas *N. sinensis* has a larger protoconid; this latter species does not possess any accessory cuspulids on the distolingual side of m1, whereas *N. megamastoides* generally shows the entoconid and may possess accessory cuspulids. Considering these differences, the Kvabebi raccoon dog can be assigned to *Nyctereutes megamastoides*. Cranial, dentognathic, and postcranial measurements of the *Nyctereutes* sample from Kvabebi are shown in Tables 3.4.1–3.4.4.

The log-ratio diagrams (Fig. 3.4.3A-B) were used to compare the mean dental measures of *Nyctereutes* from Kvabebi to those of the extant *N. procyonoides* and other Eurasian Pliocene species, using *N. sinensis* from the Yushe Basin (Tedford & Qiu, 1991) as a standard reference. On the one hand, these diagrams show that *Nyctereutes* from Kvabebi differs considerably both in size and proportions from and from *N. tingi*, the former being much smaller (as expected), and the latter substantially larger, than the Kvabebi raccoon dog. On the other hand, the graphs

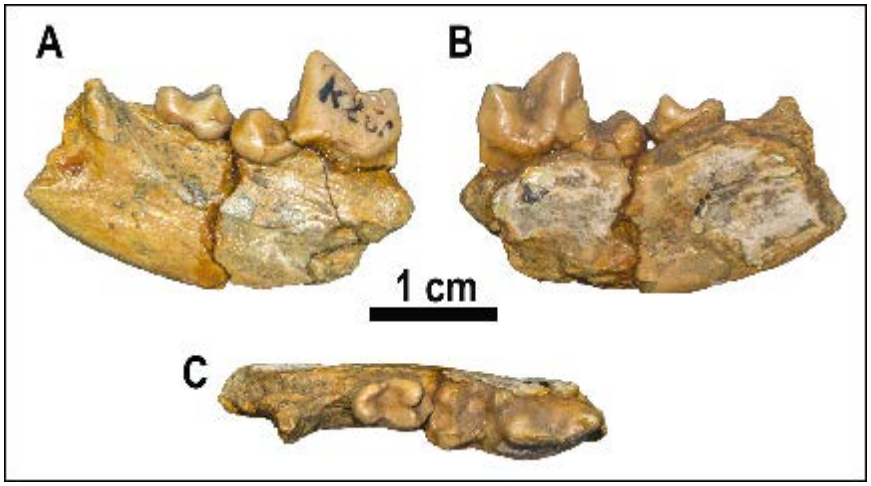

Figure 3.4.4 – *Vulpes* cf. *V. alopecoides* from Kvabebi. **A-C**: **MG-29-2013/461 (K260)**, right hemimandible fragment in buccal (**A**), lingual (**B**), and occlusal (**C**) views.

allow an appreciation of how the Kvabebi sample is similar in size and proportion to both *N. sinensis* and *N. megamastoides*, although with a much greater affinity to the latter. This provides additional support for the taxonomic interpretation of the Kvabebi material as *Nyctereutes megamastoides*.

Genus ***Vulpes*** Frisch, 1775

Vulpes* cf. *V. alopecoides (Del Campana, 1913)

(Fig. 3.4.4)

1972 *Canis* sp. Vekua, p. 50, pl. III, fig. 7

Holotype. The holotype of *Vulpes alopecoides* comes from Tasso (early Pleistocene), Upper Valdarno Basin, Tuscany, Italy.

Materials. MG-29-2013/461 (K260), right hemimandible fragment with m1 and m2.

Description. *Mandible*. The fragment MG-29-2013/461 (K260) is very small in dimensions compared to the other specimens from Kvabebi. The ventral margin of the corpus of the mandible is preserved in a small, curved portion below the m2 (*e.g.*, Fig. 3.4.4).

Lower teeth. The m1 possesses a proportionately high paraconid, a higher and distally curved protoconid and a prominent, slightly individualized metaconid. The latter is in line with the distal margin of the protoconid, so it is not visible in buccal view. The talonid basin is deep, with a large hypoconid and a smaller entoconid. These cuspulids are of the same height and are connected by a cristid. On the buccal side, there is a cingulid. The m2 is bean-shaped, with a larger mesial part compared the distal. The protoconid has a larger base than the metaconid, but both cuspulids have the same height. Mesial to the protoconid is a prominent cristid that ends in a faint accessory cuspulid. On the mesiobuccal side, a cingulid is well developed. Distal to the protoconid, there is a large hypoconid, and the lingual side is bounded by a cristid with a low entoconid.

Remarks. MG 29-2013/461 (K260) measurements are as follows— m1 L: 13.1 mm; m1 W: 5.5 mm; trm1 L: 8.5 mm; m2 L: 6.2 mm; m2 W: 4.4 mm; M m1 B: 4.5 mm; M m1 H: 11.1 mm.

The extant species *V. vulpes* is larger in size compared to the smallest canid from Kvabebi. Moreover, it possesses several features (such as an individualized and large metaconid, a high and pointy accessory cuspulid between entoconid and metaconid and an oval-shaped m2 with numerous distal accessory cuspulids) that cannot be found in MG 29-2013/461 (K260). Unlike the arctic fox *V. lagopus*, the smallest Kvabebi canid possesses the m1entoconid and hypoconid close to one another, a reduced talonid basin and a slender m2. Compared to *V. praecorsac* from the Odessa catacombs and Püspökfürdö/Betfia 2 (Kormos, 1932; Odintzov, 1965), MG 29-2013/461 (K260) shows some differences; for example, a slender m1 protoconid, in lateral view; the lower carnassial is less compressed buccolingually; and the m2 is more elongated mesiodistally and bean-shaped in occlusal view, with a reduced talonid portion compared to the large trigonid. Following the discussion in Madurell-Malapeira et al. (2009), some of the distinctive features of *V.*

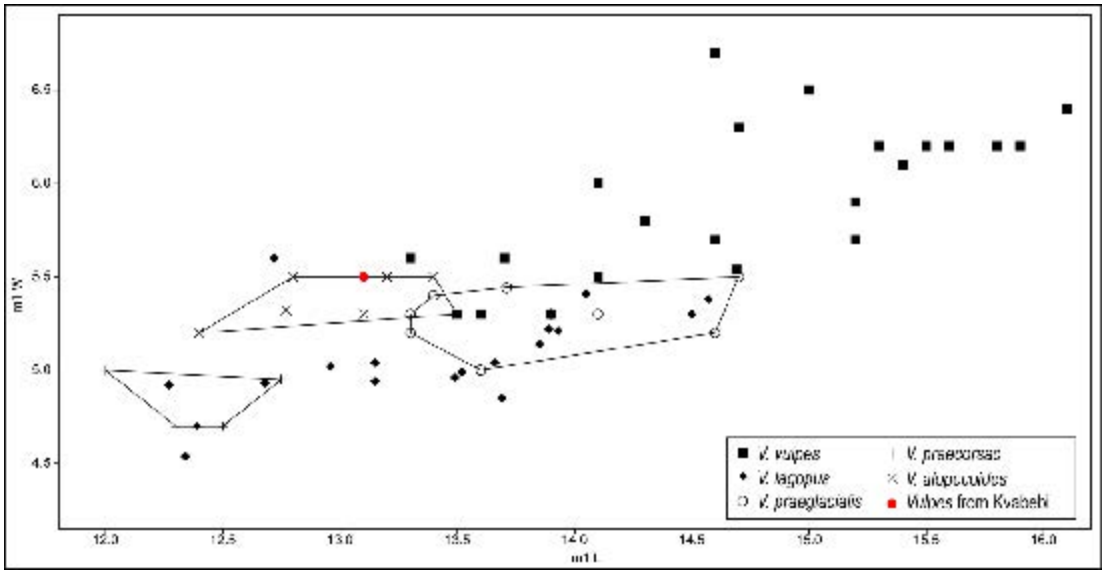

Figure 3.4.5 – Scatter-plot diagram of the m1 length and width in extant and fossil species of the genus *Vulpes*. Symbols are explained in the legend.

praeglacialis are: a large and individualized m1 metaconid; a wide bicuspid talonid with a larger hypoconid; and a large and wide m2, with the protoconid larger than the metaconid. All these features contrast with those of MG 29-2013/461 (K260). In fact, the morphology of the m1 of closely resembles that of *V. alopecoides* from Pirro Nord and Dafnero-1 in general shape, with the distally inclined protoconid, the reduced metaconid, and slightly larger hypoconid compared to the entoconid and the presence of an accessory cuspulid mesial to the entoconid. The talonid of *V. alopecoides* is slightly shorter mesiodistally when compared to the Kvabebi specimen.

The scatter plot of the m1 length and width of *Vulpes* is shown in Fig. 3.4.5 Together with the two extant species, *V. Vulpes* and *V. lagopus*, also including the Eurasian Plio-Pleistocene species *V. praecorsac*, *V. praeglacialis* and *V. alopecoides* for comparison.

All the fossil species fall within the variability of extant *V. lagopus* and are generally smaller than *V. Vulpes*. *V. praecorsac* is characterized by extremely reduced dimensions compared to the other two fossil species, being at the lower dimensional range of the extant *V. lagopus*. *V. praeglacialis* and *V. alopecoides* are comparable in size. An

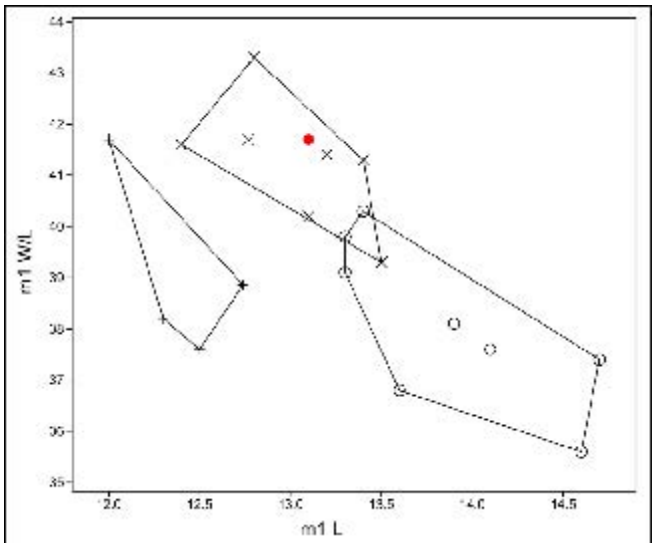

Figure 3.4.6 – Scatter-plot diagram of the m1 width and m1 width/length ratio in fossil species of *Vulpes*. Symbols are the same as in Fig. 3.4.5.

additional scatter plot of m1 L and the ratio of m1 W/L allows an appreciation of the differences in robustness of the lower carnassial of *Vulpes* fossil species, showing that the Kvabebi specimen, like *V. alopecoides*, is characterized by stouter proportions of the m1 (Fig. 3.4.6).

MG 29-2013/461 (K260) falls within the upper dimensional range of the early Pleistocene *V. alopecoides* sample and shares with the same species a comparable degree of robustness. Based on its morphological features, size and proportions, it is possible to identify this specimen as *Vulpes* cf. *V. alopecoides*.

Tribe **Canini** Fischer, 1817

Genus ***Eucyon*** Tedford & Qiu, 1996

***Eucyon* sp.**

(Fig. 3.4.7; Table 3.4.5)

1972 *Nyctereutes megamastoides* Vekua, p. 41

2009 *Nyctereutes megamastoides* Agustí et al., p. 3277

2009 *Eucyon* sp. Agustí et al., p. 3277

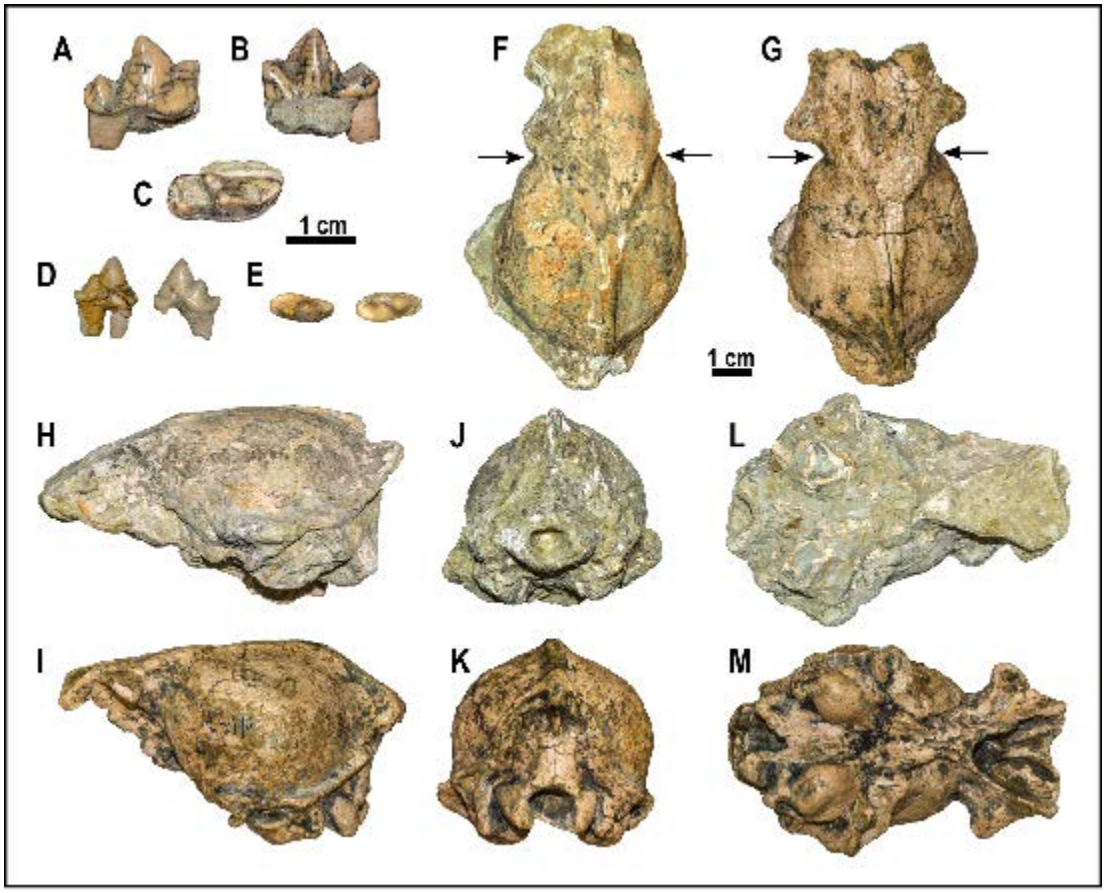

Figure 3.4.7 – *Eucyon* sp. from Kvabebi. **A-C**: **MG 29-2013/603**, right m1 in buccal (**A**), lingual (**B**), and occlusal (**C**) views. **E-D**: **MG 29-2013/607-608**, right and left p4 in buccal (**D**), and occlusal (**E**) views. Comparison between two neurocranial fragments: *Eucyon* sp. **MG 29-1** (**K222**) (**F, H, J, L**) and *N. megamastoides* **MG 29-2013/567** (**K4173**) (**G**, **I**, **K**, **M**) in dorsal (**F-G**), left lateral (**H**), reversed right lateral (**I**), caudal (**J-K**) and ventral (**L-M**) views. Arrows highlight the morphology of the frontals at the level of the postorbital constriction and postorbital processes.

Materials. MG 29-1 (K222), neurocranium; MG 29-2013/607, right p4; MG 29-2013/608, left p4; MG 29-2013/603, right m1.

Description. *Cranium*. MG 29-1 (K222) is a neurocranium preserving partial dorsal portions of the orbits and the frontals. The neurocranium (Fig. 3.4.7) is globular in shape, with inflated frontal sinuses that expand into the postorbital constriction. Their extension into the frontal is also testified by the dorsal outline of the frontals that bulge in lateral view, at level of the postorbital processes. The inflation of the frontal sinuses is also revealed by the smoothness of the parasagittal crest on top

of them. In caudal view, the supraoccipital shield is fan-shaped, with an expansion at level of the mastoid process. The inions fail to overhang the condyles.

Lowet teeth. The two premolars show high protoconids, slightly arched lingually; on their distal sides. There is a distal individualized and large cuspulid, which is not in line with the protoconid, but sets slightly buccally. Distally, there is a cuspulid-like cingulid. In the occlusal view, the m1 is elongated mesiodistally and slender. The paraconid is low, whereas the protoconid is high and slightly inclined backwards. The metaconid is reduced in height and rather individualized from the protoconid; it is positioned slightly distally compared to the distal wall of the protoconid, so that, in buccal view, it is visible behind it. The hypoconid is large and occupies almost all the talonid and has a faint accessory cuspulid on its distal side. The entoconid is reduced. There is a weak cristid connecting the talonid cuspulid. The m1 possesses a buccal cingulid.

Remarks. Cranial and dentognathic measurements of *Eucyon* from Kvabebi are shown in Table 5. The neurocranium MG 29-1 (K222) possesses inflated frontal sinuses, in contrast to all other cranial fragments recovered from Kvabebi. As shown in Fig. 3.4.7, *N. megamastoides* crania [*e.g.*, MG 29-2013/567 (K4173)] generally have marked postorbital constrictions in shape of a strong incision, in dorsal view. On the contrary, the postorbital constriction of MG 29-1 (K222) is slightly distinct. Furthermore, the dorsal portion of the frontals is bulging, compared to the depression visible in *N. megamastoides*. In caudal view, the supraoccipital shield in *Eucyon* is fan shaped (Fig. 3.4.7.K), whereas that of *N. megamastoides* is subrectangular (Fig. 3.4.7.L).

The p4 of *Nyctereutes* possess a short protoconid characterized by large mesial and distal sides (resulting in a low isosceles triangular shape in the buccal shape) and a distal accessory cuspulid that is almost entirely attached to the protoconid. On the contrary, GM 29-2013/607 and GM 29-2013/608 show a high and slender

protoconid with a prominent and individualized distal accessory cuspulid, feature similar to those of Canini species. For its small size (Table 5) and some missing morphological features (*e.g.*, weak cristid between hypoconid and entoconid), MG 29-2013/603 cannot be attributed to *Canis*. The paraconid is large mesiodistally with a subvertical mesial margin similar to *E. odessanus* from Alatini, unlike *E. davisi* and *E. zhoui* from Yushe and *E. adoxus* from Roussillon, which is shorter and distally inclined. *E. zhoui* and *E. adoxus* possess very stout protoconids and larger metaconids compared to the specimen from Kvabebi. Furthermore, *E. adoxus* has a prominent cristid on the buccodistal side of the protoconid that is hardly visible in other *Eucyon* species. *E. marinae* from Muhor-Erig, disregarding its larger size, has a considerably more individualized and larger metaconid compared to MG 29-2013/603, which is also distally pointed. The talonid cuspids of the Kvabebi *Eucyon* bear resemblance to those of *E. davisi* and *E. odessanus*, with a large hypoconid and the entoconid is reduced and placed rather lingually. In fact, *E. zhoui* possesses a thinner talonid (reduced in buccolingual width), whereas *E. marinae* and *E. adoxus* have better developed entoconids. Unlike the majority of *Eucyon* species analysed, MG 29-2013/603 does not possesses accessory cuspulids in the talonid, apart from a small one on the distal side of the hypoconid; a comparable condition occurs in the *E. odessanus* mandibles of Alatini.

Species variability of the lower carnassial of the Pliocene *Eucyon* species from Eurasia is reported in the scatter diagram of Fig. 3.4.8.A. MG 29-2013/603 is smaller than the lower carnassial of all Eurasian eucyons (*E. marinae*, *E. zhoui*, *E. davisi*, *E. minor*, and *E. adoxus*). *E. odessanus* shows a wide dimensional range, and is proportionally slender when compared with the other species. Our specimen falls among the shortest individuals of *E. odessanus* range, although differing for the relatively wider carnassial. Given its relatively small size and robustness (*e.g.*, Fig. 3.4.8.B), it appears better to leave open the specific attribution of the Kvabebi sample, referring to it as *Eucyon* sp.

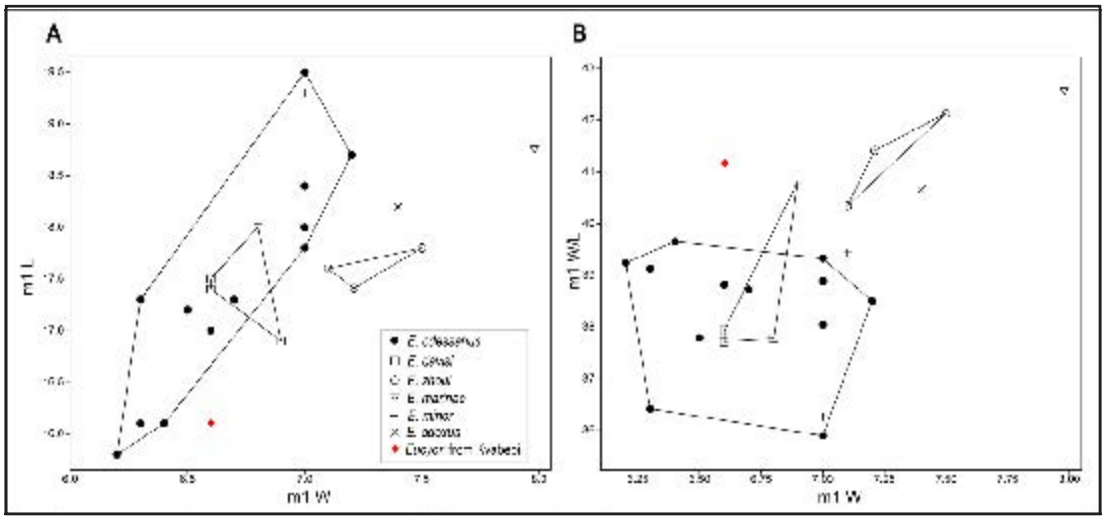

Figure 3.4.8 – Scatter-plot diagrams of the m1 length and width (**A**) and the m1 width and m1 width/length ratio (**B**) in species of the genus *Eucyon*. Symbols are explained in the legend.

3.4.4. Discussion

Vekua (1972), who was the first to report canid material from Kvabebi, described several cranial and postcranial elements of *Nyctereutes megamastoides* and a single hemimandible fragment identified as *Canis* sp. Our revision confirms, in general terms, these original taxonomic attributions (Vekua, 1972; as updated in Agustí et al., 2009), with additional recognition of a third taxon (*Vulpes* cf. *V. alopecoides*).

The occurrence of three sympatric canids is not surprising, since the family shows a great degree of sympatry. At present, Africa, Asia and South America support the greatest canid diversity, with more than 10 living species for each continental area. The red foxes, golden jackals and grey wolves are each sympatric with more than ten other canids (from different geographical regions) within one location; however, canid diversity is usually limited to a maximum of four or five species (Sillero-Zubiri & Macdonald, 2004). The fossil record of canid diversity does not contradict this rule, and the Kvabebi record documents a guild of three sympatric canids.

3.4.4.1. Nyctereutes

The first occurrence of *Nyctereutes* is in early Pliocene, with the species *Nyctereutes tingi* from the Yushe Basin and *N. donnezani* from western European localities. Subsequently, a more derived species (*N. sinensis*) appears in some Chinese sites, together with the more primitive *N. tingi* (Teilhard de Chardin & Pei, 1941). By the late early-middle Pleistocene, *N. sinensis* seems to have been replaced by another derived taxon (*Nyctereutes* sp. in Tedford & Qiu, 1991). In contrast to the coexistence in Asia of primitive and derived forms, in late Pliocene localities in western European (*e.g.*, San Giusto, Villarroya, Perrier-Etouaires) raccoon dog-like canids are represented by the derived species *N. megamastoides*. This species, probably related to *N. donnezani*, may be regarded as the European counterpart of *N. sinensis* for the retention of comparable derived features.

In the early Pleistocene, there is no or little record of *Nyctereutes* in Eurasia. The extant *N. procyonoides* appears in the middle Pleistocene deposits of Zhoukoudian (localities 1 and 13). Even though the phylogenetic relationships of late Pliocene Eurasian species of *Nyctereutes* are still a matter of debate (see Tedford & Qiu, 1991; Monguillon et al., 2004), a closer relation seems plausible between the extant *N. procyonoides* and *N. sinensis*. The occurrence in the Kvabebi sample of *Nyctereutes megamastoides*, as identified by Vekua (1972), testifies to the wide geographic range expansion of this western European taxon.

Recently, Asahara & Takai (2016) attempted to infer dietary preferences in extant and extinct *Nyctereutes* species using the ratio of m2 and m1 surfaces (see also Kavanagh et al., 2007). Their analyses confirmed that primitive species like *N. donnezani* and *N. tingi* had omnivorous diets. In addition, the authors found that *N. sinensis* had a more carnivorous m2/m1 score than for *N. megamastoides*, suggesting a more omnivorous diet for the latter. Using the methodology of Asahara & Takai (2016), *Nyctereutes* from Kvabebi possesses an m2/m1of about 0.53, intermediate between the two derived species. The Kvabebi sample fits with the general framework proposed by Asahara & Takai (2016), in which members of the genus

Nyctereutes underwent dietary transitions or had considerable dietary plasticity in their evolution.

3.4.4.2. Vulpes

The genus *Vulpes* appeared in the late Miocene (ca. 9 Ma, Hemiphillian) of North America (Tedford et al., 2009). As with other members of the subfamily Caninae, it expanded its range early into the Old World, as testified by the African species *V. riffautae* from the late Miocene Toros-Menalla site and by the early Pliocene Chinese *V. beihaiensis* from the Yushe Basin, as well as *V. qiuzhudingi* Wang et al., 2014 from the Tibetan Plateau (the Zanda and Kundun Basins). This latter large-sized species possesses remarkable hypercarnivorous adaptations, suggesting a close relationship to the extant *V. lagopus*.

The earliest European record of *Vulpes* is that of early-late Pliocene *V. praecorsac* in the Odessa catacombs (MN 15, Odintzov, 1965). This small-sized fox has been historically considered the ancestor of the extant *V. corsac* (see Kormos, 1932). Another well-known European species is *V. alopecoides* described by Del Campana (1913) from Tasso (Upper Valdarno) and also recovered from St. Vallier, Senéze (France, Viret, 1954), Villaroya and La Puebla de Valverde (Spain, Kurtén & Crusafont-Pairo, 1977). Kurtén (1968) suggested the synonymy between *V. alopecoides* and *V. praeglacialis*. Nevertheless, the literature reveals no unanimous opinion on the status of these two species (Bonifay, 1971; Rabeder, 1976; García & Arsuaga, 1999). The relationship between the two taxa is beyond the scope of this paper; therefore, both were included in the comparative analyses. MG 29-2013/461 represents the first occurrence of a member the vulpine taxon *V. alopecoides*, the most widespread fox species in the early Pleistocene of western Europe.

3.4.4.3. Eucyon

The genus *Eucyon* appears in the late Miocene (late Clarendonian) record of North America with the species *E davisi*. Its geographic range remained limited to North America until the latest Miocene, when the genus spread into the Old World, occurring in central Asia, Africa, and western Europe (the "*Eucyon* event", Sotnikova & Rook, 2010). *E. davisi* disappears in North America in the earliest Pliocene (latest Hemphillian), and survives into the early Pliocene of eastern Asia (China and Mongolia). The genus *Eucyon* reached a relative high diversity in the Pliocene of Eurasia (Sotnikova & Rook, 2010; Rook, 2009), surviving until the late Pliocene in China (*E. minor*), Mongolia (*E. marinae*), Tadzhikistan (*E. kuruksaensis*), Kazakhstan (*Eucyon* cf. *E. odessanus*), and southeastern Mediterranean regions (*Eucyon* cf. *E. odessanus*, Sarikol Tepe, Turkey).

The occurrence of a *Eucyon* representative within the fauna of Kvabebi completes our knowledge of the late Pliocene history of the advanced eucyons surviving in western Europe and central Asia. The Kvabebi finding predates the explosive radiation of the wolf and coyote-sized Canini that took place in central Asia (reflected in the appearance of *Canis teilhardi*, *C. longdanensis*, *C. brevicephalus*, and *Sinicuon* cf. *S. dubius*) and that continued until the end of the Pliocene (Qiu et al., 2004; Sotnikova & Rook, 2010).

3.4.5. Conclusions

The evolutionary history of the Pliocene Canidae in Eurasia is characterized by taxonomic diversification and range expansion. Diversification of Vulpini and Canini showed a maximum in central Asia at the beginning of the early Pliocene, as evidenced by the appearance of several new taxa (*Nyctereutes tingi*, *V. beihaiensis*, *V. qiuzhudingi, Nurocyon chonokhariensis, E. zhoui*) and by the increase in frequency of other species (like the well-known *Eucyon davisi*). In western Europe, at the beginning of the Pliocene, the canid record is limited to the primitive vulpine *N. donnezani*. The peak of canid diversification in western Europe is recorded later

in the early Pliocene, during the Late Ruscinian (MN 15), with the differentiation of the advanced raccoon dog *N. megamastoides*, the appearance of the small fox *V. praecorsac*, and the emergence of the enigmatic *"Canis" michauxi*, together with the advanced *E. adoxus* and *E. odessanus*. The revision of the Kvabebi assemblage documents the earliest occurrence of the typical (later) early Pleistocene species *V. alopecoides* in the European fossil record. The contemporary early occurrence at Kvabebi of *Vulpes* with *Nyctereutes* and *Eucyon,* clearly supports the established niche partitioning among these three sympatric canids.

3.4.6. Appendix

Tables of measurements of the specimens from Kvabebi here described.

Table 3.4.1 – Cranial measurements of *Nyctereutes megamastoides* (Pomel, 1842) from Kvabebi.

Cat. N°	TL	NCL	FL	Eu	Ect	PocW	SH	AB	GWOC	BL	PL	CBL	ZyG	ECW	GPW	FMW
MG 29-2013/455 (K234)	-	-	-	42.2	-	-	35.2	26.8	-	-	-	-	-	-	-	-
MG 29-2013/457 (K220)	137.6	63.6	76.8	62.9	45.1	31.9	[42.5]	[35.9]	-	123.2	64.9	129.7	82.1	23.2	-	12.9
MG 29-2013/567 (K4173)	-	66.3	-	46.9	43.8	27.1	43.0	34.7	23.3	-	-	-	-	-	-	10.4
MG 29-2013/568 (K215)	-	59.6	-	42.0	42.7	28.2	36.5		23.6						40.3	8.0
MG 29-2013/573 (K233)	-	-	76.9	-	-	-	-	-	-	-	-	-	-	-	-	-
MG 29-2013/581	129.2	[58.0]	73.5	49.1	46.1	30.3	36.6	-	-	-	67.4	-	-	16.8	34.6	-

Table 3.4.2 – Associated upper teeth measurements of *Nyctereutes megamastoides* (Pomel, 1842) from Kvabebi.

Cat. N°		C L	C W	P1 L	P1 W	P2 L	P2 W	P3 L	P3 W	P4 L	P4 W	M1 L	M1 W	M2 L	M2 W	LCR	LPR	LMR
MG 29-2013/455 (K234)	L	-	-	-	-	-	-	-	-	-	-	-	12.1	7.0	8.0	-	-	-
	R	-	-	-	-	-	-	-	-	11.9	6.3	11.0	11.0	-	-			
MG 29-2013/456 (K217)	L	5.7	3.7	4.7	2.5	6.9	2.7			14.0	6.8	11.1	12.9	7.7	9.8	54.4	38.3	18.7
	R	-	-	-	-	-	-	7.5	3.1	14.1	7.2	11.4	12.6	7.5	9.0			
MG 29-2013/457 (K220)	L	5.4	3.7	3.7	2.8	6.1	2.6	7.0	2.8	-	5.6	-	-	-	-	48.7	34.0	17.1
	R	-	-	4.0	2.9	6.0	2.7	-	-	12.6	5.8	11.0	12.6	7.0	8.6			
MG 29-2013/573 (K233)	L	6.1	-	4.5	-	7.2	-	8.1	-	-	-	10.9	-	7.7	-	52.0	-	18.2
	R	-	-	4.7	-	7.0	-	8.3	-	-	-	11.0	-	7.2	-			

Table 3.4.3 – Mandibular measurements of *Nyctereutes megamastoides* (Pomel, 1842) from Kvabebi.

ID		Mand P_4 H	B mand m1	p2-p4 L	LLMR	m1-m2 L
MG 29-2013/588 (K221)	L	14.1	7.0	-	26.0	22.4
MG 29-2013/589 (K224)	R	13.7	5.8	-	-	-
MG 29-2013/591 (K214)	R	13.1	6.7	-	-	-
MG 29-2013/592 (K4177)	R	13.6	-	-	-	-
MG 29-2013/820	L	12.5	7.9	24.4	28.2	24.1

Table 3.4.4 – Associated lower teeth measurements of *Nyctereutes megamastoides* (Pomel, 1842) from Kvabebi.

Cat. N°		c1 L	c1 W	p1 L	p1 W	p2 L	p2 W	p3 L	p3 W	p4 L	p4 W	m1 L	m1 w	m1 trL	m2 L	m2 W	m3 L	m3 W
MG 29-2013/588 (K221)	L	4.5	3.6	3.6	2.1	-	-	-	-	-	-	14.9	5.8	-	7.9	5.8	4.4	3.8
MG 29-2013/591 (K214)	R	-	-	-	-	-	-	-	-	-	-	14.8	6.7	9.5	-	-	-	-
MG 29-2013/592 (K4177)	R	-	-	-	-	-	-	-	-	-	-	14.8	6.6	8.4	-	-	-	-
MG 29-2013/606	R	7.1	4.0	-	-	-	-	-	-	-	-	-	-	-	-	-	-	-
MG 29-2013/820	L	-	-	-	-	7.2	3.0	8.1	3.1	9.1	4.2	15.9	7.7	9.2	8.7	7.5	4.1	4.4

Table 3.4.5 – Summarizing table of *Eucyon* sp. measurements from Kvabebi.

Cat. N°	Element		NCL	Eu	PoCW	SH	GWOC	FMW	L	W	trL
MG 29-1 (K222)	neurocranium		61.7	46.5	29.8	45.4	24.4	[10.0]	-	-	-
MG 29-2013/603	m1	L	-	-	-	-	-	-	16.1	6.6	10.8
MG 29-2013/607	p4	R	-	-	-	-	-	-	8.9	3.7	-
MG 29-2013/608	p4	L	-	-	-	-	-	-	9.3	4.2	-

3.5. Quantitative estimation of the diet in *Nyctereutes sinensis* (Schlosser, 1903)

3.5.1. Context

Recently Asahara & Takai (2016) presented an interesting and easy-to-perform quantitative method to infer the dietary habits of extinct species of the raccoon dog *Nyctereutes*. The method used by the authors consists of calculating the surface of occlusion of the first and second lower molars (m1 and m2), and then estimate the ratio between these two surfaces (m2/m1 score). In Canidae, this molar ratio relates to the differences in diet. This can be done at low resolution, that is to discriminate between hypercarnivorous species and omnivorous (or hypocarnivorous) ones: the former have lower scores, whereas the latter have higher ones. Nevertheless, this method is also capable of acknowledging subtle differences in diet at the subspecific level (Asahara, 2013a, 2014; Asahara et al., 2016). Nowadays, the raccoon dogs are represented only by a single species, *Nyctereutes procyonoides* (Gray, 1834). Its geographic range is divided into two areas, an original Asian range (from northern China to North Vietnam and from eastern Siberia to Korea and Japan) and an introduced central-east European one (Sillero-Zubiri, 2010). As long as diet is concerned, *N. procyonoides* is omnivorous, in general terms, and opportunist, so that its dietary habits are subject to habitat and seasonal changes (see *inter alios* Ward & Wurster-Hill, 1990; Kauhala & Auniola, 2001; Hirasawa et al., 2006; Sutor et al., 2010). The dentognathic features of *N. procyonoides* confirm this omnivory. Its features resemble those of other fossil *Nyctereutes* species, although probably extant *N. procyonoides* is less specialized to a hypocarnivorous diet compared to other fossil taxa, such as the Eurasian *Nyctereutes megamastoides* (Pomel, 1842) or the Chinese *Nyctereutes sinensis* (Schlosser, 1903), the most probable ancestors of *N. procyonoides* (Tedford & Qiu, 1991). For a recent review on the evolutionary history of the fossil *Nyctereutes*. As Asahara & Takai (2016) point out in scientific

literature, there are no quantitative studies exploring the dietary preferences of the fossil species of *Nyctereutes*, in relation to their morphology and anatomofunctional adaptations. Thanks to a large sample of extant *Nyctereutes* and its ecology, the authors were able to make highly plausible inferences on the diet of the fossil taxa of the genus and their affinity in comparison with extant subspecies, especially *N. p. albus* (Hornaday, 1904), from Hokkaido, and *N. p. viverrinus* from Honshu and Kyushu islands (Japan). These two subspecies are significant, as some authors have identified dietary differences between these two Japanese raccoon dogs, with *N. p. albus* characterized by a more carnivorous diet and *N. p. viverrinus* by a more omnivorous one (see *inter alios*, Haba et al., 2008). This seems to be testified to also by the scores in Asahara & Takai (2016): the former has as a mean score value of 0.44; instead, in *N. p. viverrinus* the mean score is 0.49. In their analysis, Asahara & Takai (2016) point out how the various taxa of the genus *Nyctereutes* had considerable dietary plasticity or experienced dietary transitions during their evolution. The two primitive species of Eurasia, *Nyctereutes donnezani* (Depéret, 1890) and *Nyctereutes tingi* Tedford & Qiu, 1991 share the same m2/m1 score of 0.48, indicative of an omnivorous diet as in the case of *N. p. viverrinus*. Regarding *N. sinensis* and *N. megamastoides*, the authors calculate a much lower m2/m1 score for the Chinese form (m2/m1 = 0.42) in comparison with that of the European species (m2/m1 = 0.54). Therefore, according to the authors, *N. sinensis* was more carnivorous than *N. megamastoides*. This result contradicts the observations that can be made on the fossil specimens and with scientific literature. Indeed, besides slight differences, these two forms are highly comparable or even have been considered as morphotypes of a single species with a wide paleogeographic range (Bartolini Lucenti 2017; Rook et al., 2017; Soria & Aguirre, 1976; Tedford & Qiu, 1991). The sample of *N. sinensis* taken into consideration by Asahara & Takai (2016) includes five specimens (out of seven) from Zhoukoudian locality 1 described by Pei (1934) as *Canis* (*Nyctereutes*) *sinensis* which were re-ascribed to a

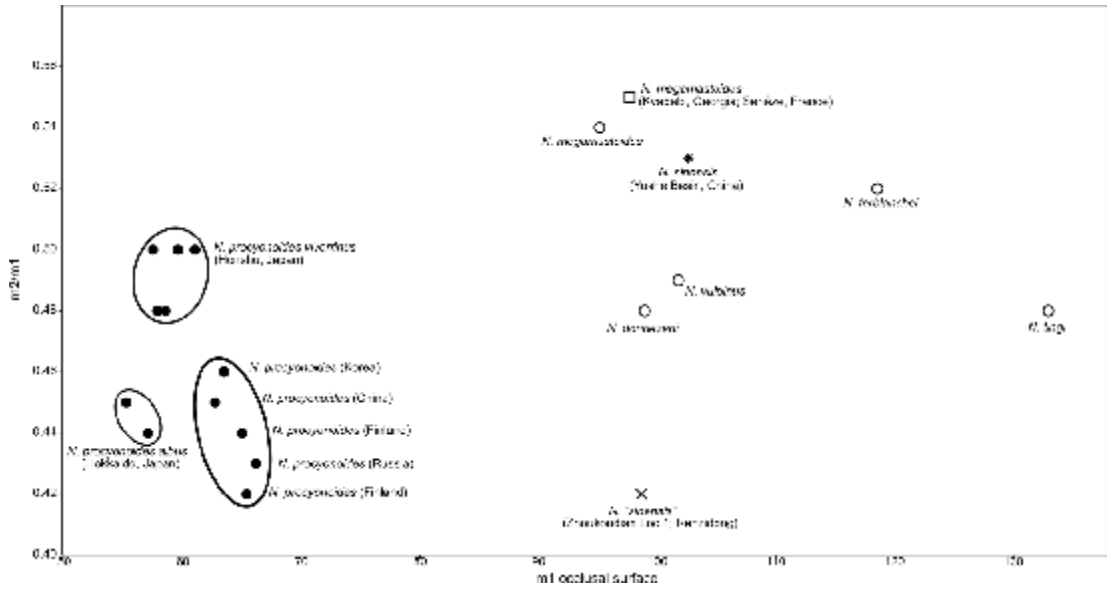

Figure 3.5.1 – Biplot of the m2/m1 scores against the surface of various species and subspecies of *Nyctereutes*. Dots are extant taxa; open circles are extinct ones; asterisk is *N. sinensis* from Yushe Basin; open square is *N. megamastoides* from Kvabebi (Georgia) and Senéze (France); × is *N. procyonoides*-like form from Zhoukoudian loc. 1 (Pei 1934) and Renzidong (Jin & Liu, 2009).

Middle Pleistocene form very close to *N. procyonoides* by Tedford & Qiu (1991). In fact, the m2/m1 score obtained (0.42) fits within the range of the extant raccoon dogs and should be better interpreted as the dietary habit of this early form of *N. procyonoides*. Here are reported new unpublished data of *N. sinensis* that allow refined inferences on the diet of this Chinese relative of the extant raccoon dog.

3.5.2. Discussion and Conclusions

In Fig. 3.5.1, *N. sinensis* score is positioned very closely to that of *N. megamastoides*, contrasting the evidence of Fig. 3.5.1A in Asahara & Takai (2016: 4). The higher value of m2/m1 score implies a proportionally larger crushing surface of the molar, and consequently an advantage for a relatively more omnivorous diet. The new values of m2/m1 from *N. sinensis* profoundly affect the interpretation of this species as described by Asahara & Takai (2016). First of all, as dentognathic features suggest, *N. sinensis* does not tend to a relatively carnivorous diet as *N. p. albus* but shares comparable adaptation to progressively more omnivorous

diet with *N. megamastoides*. In their discussion, Asahara & Takai (2016) suggest that the subangular lobe—derived feature of *N. megamastoides*, *N. sinensis* and *N. procyonoides* probably related to chewing (Malcolm, 1986)—might not be related to an adaptation to omnivory as some *Nyctereutes* subspecies (*e.g. N. p. albus*) and *N.* "*sinensis*" from Zhoukoudian loc. 1 (Pei 1934) and Renzidong (Jin & Liu 2009) possess these relatively more carnivorous scores, although retaining a developed subangular lobe. The evolutionary development of the subangular lobe in the fossil species is well documented in scientific literature: the primitive *N. donnezani* and *N. tingi* have simple mandible, with poorly developed subangular lobe (Soria & Aguirre, 1976; Tedford & Qiu, 1991). Later forms of Eurasia (such as *N. megamastoides* and *N. sinensis*) possess a well-developed subangular lobe and a conspicuous enlargement of the area of the angular process (see section 3.4.). Contemporarily with the appearance of these mandibular features, there is the development of other dental adaptation that suggests a progressively more omnivorous diet such as squared shape of upper molars, conspicuous enlargement, in buccolingual sense, of the talonid of m1 and consequent reduction of the trigonid (see see section 3.4.). Together with the higher, that is relatively more omnivorous, scores of *N. megamastoides–N. sinensis* in comparison with the primitive forms *N. donnezani–N. tingi* (see Table 1), these features are suggestive of evolutionary adaptations towards omnivory both in Europe and in eastern Asia. Therefore, the development of the subangular lobe appears to be linked to diet and to maximization of the chewing efficiency of the primitive and omnivore species of *Nyctereutes*. A comparable condition to the raccoon dog is that of the crab-eating fox *Cerdocyon thous*, which possesses both *Nyctereutes*-like enlarged angular process and a distinctively visible subangular lobe. *Cerdocyon* is omnivorous and an opportunistic hunter, especially at night. Its diet, although seasonally variable, is composed of small vertebrates, eggs, insects and fruits. The development of a subangular lobe in another canid, phylogenetically distant from the raccoon dog (see Wayne & Ostrander, 2007),

but with similar diet habits strongly suggests a relationship between this feature and specialized omnivory. In extant *N. procyonoides*, the subangular lobe is equally developed in all the different subspecies even if they possess different m2/m1 scores (see Table 3.5.1 and Asahara & Takai, 2016:3; Fig. 3.5.1). Nevertheless, this might be due to the dietary plasticity showed by raccoon dogs, to their adaptability to different habitats and to the availability of certain food item, compared to others in other environments. In conclusion, few observations could be made correcting the misinterpretation of the fossil raccoon dog from Zhoukoudian loc. 1 and Renzidong as *N.* "*sinensis*" to an early or strictly related form of *N. procyonoides* (Tedford & Qiu, 1991). Thanks to material housed in the AMNH collections it is possible to see that *N. sinensis* from Yushe basin does not appear to be similar to *N. p. albus* in m2/m1 scores. On the contrary, its actual scores (Table 3.5.1) and its morphology (see section 3.4.) are strongly similar to that of the European *N. megamastoides* and suggestive of a strong adaptation to an omnivorous diet. Besides this, molar ratio appears to be a reliable method to infer diet habits of both extant and fossil *Nyctereutes*.

3.5.3. Appendix

Table 3.5.1 – Measurements of the m1 and m2 (L: length and W: width), estimated surfaces and scores for fossil species and extant subspecies of *Nyctereutes*. The numbers in italic correspond to new data presented here compared to Table 1 of Asahara & Takai (2016:3). [1] Monguillon et al. (2004); [2] Tedford & Qiu (1991); [3] Ficcarelli et al. (1984); [4] Pei (1934), Jin & Liu (2009); [5] Asahara & Takai (2016).

Species	m1 L	m1 W	m2 L	m2 W	m1 occlusal surface	m2 occlusal surface	m2/m1	SD	N
Nyctereutes sinensis (Pliocene-Early Pleistocene, China)	*15.83*	*6.47*	*8.59*	*6.29*	*102.61*	*54.11*	*0.53*	*0.04*	*22*
Nyctereutes megamastoides (Kvabebi, Pliocene, Georgia; Senéze, Early Pleistocene, France)	*15.14*	*6.42*	*8.3*	*6.37*	*97.68*	*53.11*	*0.55*	*0.04*	*3*
Nyctereutes megamastoides (Pliocene-Early Pleistocene, Europe)[1]	15.10	6.30	8.60	6.00	95.13	51.60	0.54	-	9
Nyctereutes vulpinus (Early Pleistocene, St. Vallier)[1]	15.9	6.4	8.4	5.9	101.76	49.56	0.49	-	20
Nyctereutes donnezani (Pliocene, western Europe)[1]	15.7	6.3	8.4	5.7	98.91	47.88	0.48	-	8
Nyctereutes tingi (Latest Miocene to Pliocene, China)[2]	18.09	7.35	9.36	6.79	132.94	63.55	0.48	0.04	8
Nyctereutes terblanchei (Early Pleistocene, South Africa)[3]	17.18	6.9	9.37	6.56	118.54	61.47	0.52	-	6
Nyctereutes procyonoides, fossil (Middle Pleistocene, China)[4]	15.41	6.4	7.87	5.29	98.65	1.61	0.42	0.04	7
Nyctereutes p. albus (Hokkaido, Japan)[5]	-	-	-	-	-	-	0.44	-	203
Nyctereutes p. viverrinus (Honshu and Kyushu, Japan)[5]	-	-	-	-	-	-	0.49	-	809

3.6. Revision of the *Nyctereutes* record from Layna (Spain)

3.6.1 Context

Soria & Aguirre (1976) first described the *Nyctereutes* sample from Layna and attributed it to *N. donnezani*. Here, new raccoon dog material is described (among which a nearly complete cranium) from the same site and report the first diagnoses for both *N. donnezani* and *N. megamastoides*. Furthermore, the record of Layna is discussed in the framework of the evolutionary history of *Nyctereutes* in Eurasia and of the most recent studies of this group of canids.

3.6.2. Geological setting

The karstic site of Layna (Soria Province, Spain) is located in the NW area of the Castillian Range (Iberian Chain), near the homonymous village (Fig. 3.6.1). It was the first Spanish paleontological site declared as a National Paleontological Reserve. The fossils occur in a karstic deposit developed in the lower Lias unit known as the Carniolas Formation that in the studied area, is superposed on the erosional surface of the so-called Parameras de Molina (Aguirre et al., 1974). The richness and diversity of the vertebrate fauna, most particularly of the small mammal species, are one of the most remarkable of the Spanish paleontological record. Although there are many different types of sedimentary infillings, the recorded faunal remains, in the present state of our knowledge, seem to be homogeneous. The age of the site, based on the rodent remains, is Ruscinian (MN15; Early Pliocene) (López-Martínez, 1989; Sesé, 2006). Preliminary magnetostratigraphic studies suggested a normal polarity within the Gauss Chron (Hoyos et al., 1987). More recently, other interpretations of the faunal assemblage have yielded an early age of 3.91 Ma (Domingo et al., 2007; 2013). A further important point about Layna is that it preserves evidence of occupation not only by predatory birds but also by hyenas. This allows taphonomic interpretations of great interest (Aguirre

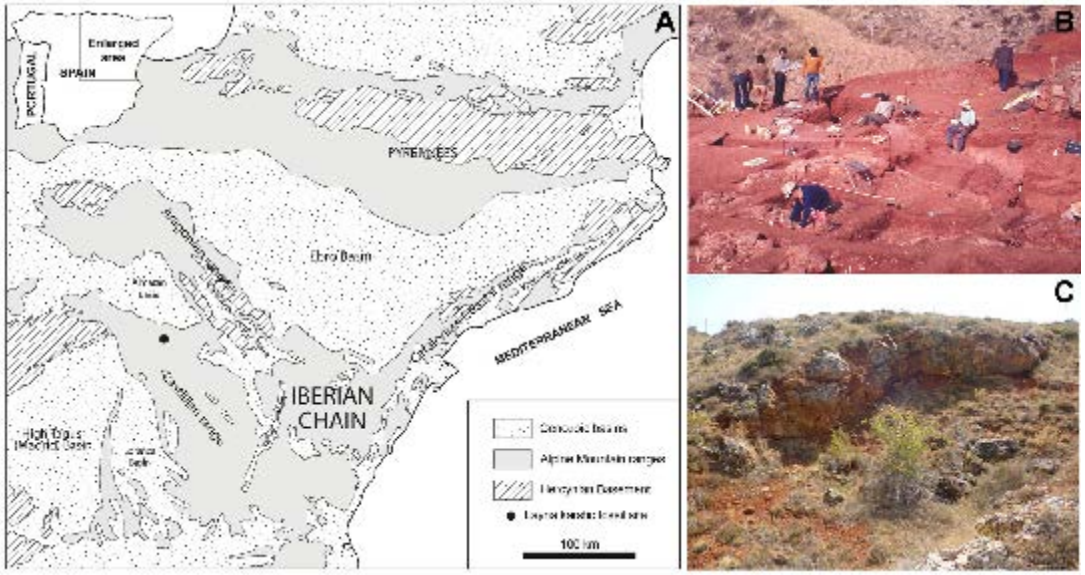

Figure 3.6.1 – Geographic location and photos of the Layna fossil vertebrate site. **A**: Position of the site with the schematic representation of the enlarged area in the Iberian Peninsula on top left. **B-C**: Pictures of the First systematic excavation of Layna locality, directed by Prof. Emiliano Aguirre in 1972 (**B**) and the site nowadays (**C**) (2012). Photo credits: B, Prof. E. Aguirre; C, Prof. J. Morales.

et al., 1981; Pérez & Soria, 1989-90).

3.6.3. Systematic Paleontology

Order **Carnivora** Bowdich, 1821

Suborder **Caniformia** Kretzoi, 1943

Family **Canidae** Fischer, 1817

Subfamily **Caninae** Fischer, 1817

Tribe **Vulpini** Hemprich & Ehrenberg, 1832

Genus ***Nyctereutes*** Temminck, 1838

Nyctereutes donnezani (Depéret, 1890)

(Figs. 3.6.2-3.6.5; Tables 3.6.1-3.6.7)

1890 *Vulpes donnezani* Depéret

Type locality. Perpignan, France

Age. Early Pliocene, MN15

Differential diagnosis. Medium-sized *Nyctereutes*, smaller than *N. tingi* but similar in size to other Eurasian species, such as *N. sinensis*, and considerably larger compared to extant *N. procyonoides*. Upper molars tend to be buccolingually narrow compared to *Vulpes* and also to *N. tingi*, but not mesiodistally elongated as in *N. procyonoides*, *N. sinensis*, *N. vulpinus* and *N. megamastoides*. In the mandible, the subangular lobe is generally more prominent than in *N. tingi*, but not to the extent of species like *N. procyonoides*, *N. sinensis*, *N. vulpinus* and *N. megamastoides*. The angular process is enlarged compared to the hook-shaped morphology observed in *N. tingi*, although *N. megamastoides* and the extant *N. procyonoides* have dorsoventrally larger angular processes. Lower premolars are more buccolingually compressed compared to other species. The m1 is reduced in width resembling that of *N. tingi*, with a talonid not enlarged unlike those of *N. sinensis* or *N. megamastoides*.

Materials. MNCN-39920, left maxillary fragment with M1-M2; MNCN-62478, left maxillary fragment with P4; MNCN-62482, right maxillary fragment with P2; MNCN-62610, cranial fragment in sediment matrix; MNCN-63662, cranium with left I3-P2, P4-M2 and right I3-C1, P2, P4 and M2; MNCN-62599, left I2; MNCN-62600, left I3; MNCN-62494, left C1; MNCN-62496, right C1; MNCN-62483, right P3; MNCN-62479, left P4; MNCN-62480, right P4; MNCN-62491, right M1; MNCN-62493, left M2; MNCN-39916, right hemimandible with p2-p3 and m1-m3; MNCN-39917, right hemimandible with p4-m2; MNCN-39919, right hemimandible with p4-m2; MNCN-62616, right hemimandible with m2; MNCN-62617, right hemimandible with p2; MNCN-62618, right hemimandible, edentulous; MNCN-62619, left hemimandible with m2; MNCN-62620, right hemimandible; MNCN-62621, right hemimandible with p1; MNCN-62625, right hemimandible fragment, edentulous; MNCN-62643, fragment of hemimandible ramus; MNCN-71082, right hemimandible fragment;

MNCN-71083, right hemimandible, edentulous; MNCN-71087, right hemimandible with m1;MNCN-62602, left i1; MNCN-62598, left i2; MNCN-71086, left i2; MNCN-62597, left i3; MNCN-62495, right c1; MNCN-62497, right c1; MNCN-62651, right c1; MNCN-70008, left c1; MNCN-71085, right p3; MNCN-62519, right m1; MNCN-62520, right m1; MNCN-62608, left m1; MNCN-62609, right m1; MNCN-70007, left m3; MNCN-62563, fragment of juvenile diaphysis; MNCN-62575, fragment of left scapula; MNCN-62576, fragment of right scapula; MNCN-62577, fragment of right scapula; MNCN-62632, fragment of left scapula; MNCN-62634, fragment of right scapula; MNCN-62635, fragment of right scapula; MNCN-62502, distal epiphysis of left humerus; MNCN-62503, proximal epiphysis and fragment of diaphysis of left humerus; MNCN-62603, fragment diaphysis of left humerus; MNCN-62604, distal epiphysis of right humerus; MNCN-62631, distal epiphysis of right humerus; MNCN-13651, proximal epiphysis of right radius; MNCN-13652, proximal epiphysis of right radius; MNCN-13654, distal epiphysis of left radius; MNCN-70904_1, distal epiphysis of left radius; MNCN-70904_2 fragment of distal epiphysis of right radius; MNCN-70905, distal epiphysis of left radius; MNCN-70906, proximal epiphysis of left radius; MNCN-70907, fragment of distal epiphysis of right radius; MNCN-62550, fragment of right ulna; MNCN-62551, fragment of left ulna; MNCN-62552, fragment of left ulna; MNCN-62553, fragment of right ulna; MNCN-62554, fragment of left ulna; MNCN-62555, fragment of right ulna; MNCN-62556, fragment of ulna; MNCN-62557, fragment of right ulna; MNCN-62622/549, fragment of right ulna; MNCN-62623, fragment of right ulna; MNCN-70006, fragment of left ulna; MNCN-62614, fragment of pelvis; MNCN-62615, fragment of right pelvis; MNCN-52972, right femur; MNCN-62473/75, proximal epiphysis of right femur; MNCN-62474, proximal epiphysis of right femur; MNCN-62476, proximal epiphysis of right juvenile femur; MNCN-62477, proximal epiphysis of right femur; MNCN-62558, distal epiphysis of left juvenile femur; MNCN-62559, distal epiphysis of left femur; MNCN-62560, distal epiphysis of right femur; MNCN-62561, distal epiphysis of right femur; MNCN-62562, fragment of distal epiphysis of femur; MNCN-62636, proximal epiphysis of left femur; MNCN-62637, distal epiphysis of left femur; MNCN-62638, proximal epiphysis of right femur; MNCN-62484, fragment of distal epiphysis of left tibia; MNCN-62485, distal epiphysis of right tibia; MNCN-62486,

fragment of distal epiphysis of left tibia; MNCN-62487, distal epiphysis of right tibia; MNCN-62488, proximal epiphysis of left tibia; MNCN-62489, fragment of proximal epiphysis of left tibia; MNCN-62490, proximal epiphysis of left tibia; MNCN-62639, proximal epiphysis of left tibia; MNCN-70911, fragment of distal epiphysis of right tibia.

Description. *Cranium.* MNCN-63662 is a rather damaged and broken cranium, especially in the neurocranium portion (Fig. 3.6.2). In dorsal view, the cranium is considerably elongated, especially the splanchnocranium. The nasals are short, as they end before the maxillofrontal suture. In lateral view, the cranial profile is rather straight and the cranium appears short in height, although this morphology might be due at least in part to the dorsoventral diagenetic compression of the neurocranium. The orbit is large and with oval-like shape, in lateral view. The postorbital processes are broken. The specimen is considerably damaged at level of the postorbital constriction and it is difficult to estimate its actual width. This taking into account the state of preservation of the specimen and the morphology of the dorsal portion of the postorbital processes (which show a shallow depression, compatible with the vulpine crease), the frontal sinuses seem to be very poorly developed. The sagittal crest seems to be very low. In dorsal view, the braincase appears inflated, globular, but being broken and deformed, its original morphology is difficult to assess. The occipital region is badly damaged. The tympanic bullae are rather short mesiodistally, rounded in ventral view and considerably inflated. In ventral view, the palate is long and narrow, even at level of M1. It seems to end slightly caudally to the distal margin of M2.

Upper teeth. Incisors possess a large main cusp and two accessory small accessory cusps. The I3 is very similar in morphology to the other incisors. The C is considerably compressed buccolingually, with a high and pointed cusp. The premolars are separated by diastemata. The P1 has a conical, single cusp. The P2 has a large and high protocone and no distal accessory cusps. The P3 is similar to

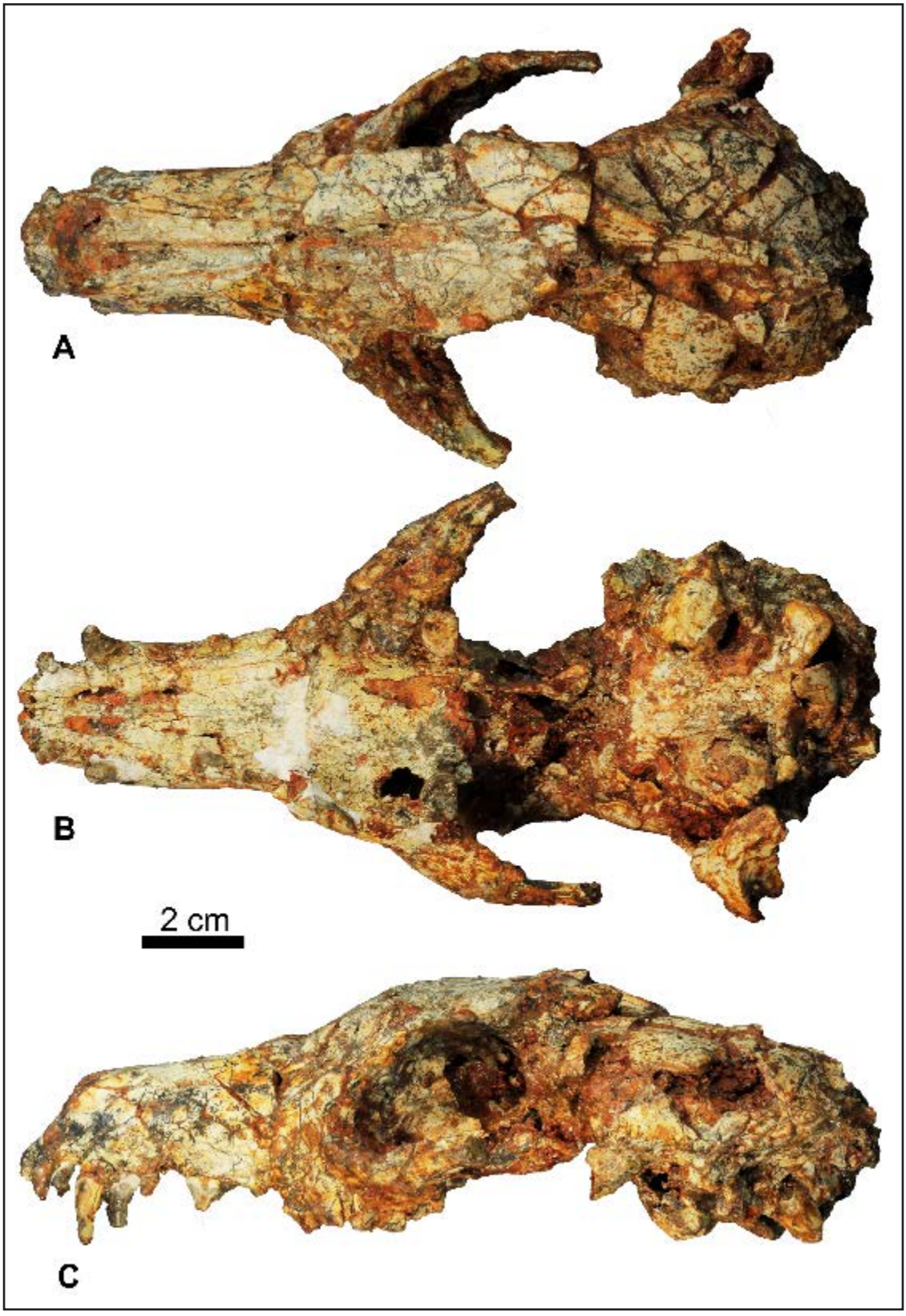

Figure 3.6.2 – *Nyctereutes donnezani* from Layna, MN15 (Spain). **A-C**: **MNCN-63662**, cranium in dorsal (**A**), ventral (**B**) and lateral (**C**) views.

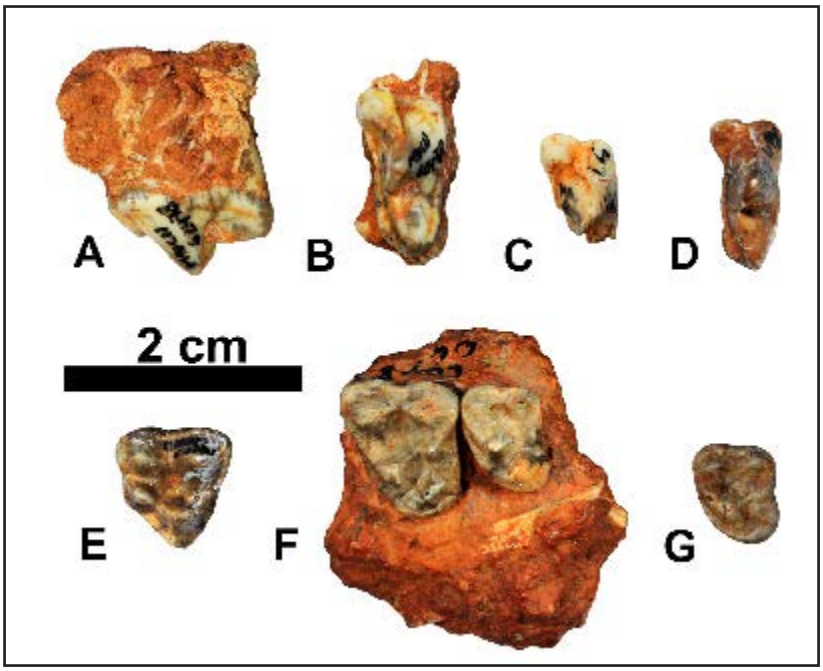

Figure 3.6.3 – *Nyctereutes donnezani* from Layna, MN15 (Spain). **A-B**: **MNCN-62478**, left maxillary fragment with P4, in buccal (**A**) and occlusal (**B**) views. **C**: **MNCN-62479**, left P4, in occlusal view. **D**: **MNCN-62481**, left P4, in occlusal view. **E**: **MNCN-62492**, left M1, in occlusal view. **F**: **MNCN-39920**, left maxillary fragment with M1-M2, in occlusal view. **G**: **MNCN-62493**, left M2, in occlusal view.

P2, but larger, with a distal cusp-like cingulum. The position of the P4 protocone is variable in the analyzed sample, although in the majority of the specimens, it exceeds mesially the mesial margin of the tooth (Fig. 3.6.3B-C; see MNCN-62481 in Fig. 3.6.3D as an example of different protocone mesial development). This cusp is large, high and pointed. On the opposite side of the protocone, there is a prominent and cusp-like mesial cingulum (almost in a parastyle). The P4 is overall compressed buccolingually, with a low but mesiodistally elongated paracone and a short metastylar blade. On the lingual side of the tooth, there is a continuous cingulum. The M1 is extends lingually with an elongated shape in occlusal view (Fig. 3.6.3E-F). The paracone is similar in size compared to the metacone, although higher. The M1 protocone and metaconule are well-developed and there is a prominent protoconule. The hypocone is generally large-based and can be separated from the lingual cingulum by a small furrow. The cingulum is strong on the buccal and on the mesial sides. The M2 possesses a larger paracone compared

to the metacone, a large protocone and smaller but visible protoconule and metaconule (Fig. 3.6.3F-G). The protocone and the metaconule are connected by the postprotocrista. Lingually, there is a cingulum-like hypocone.

Mandible. The corpus is rather low and slender (Fig. 3.6.4). Its ventral margin in lateral view, is slightly arched. In occlusal view, the lower tooth row appears straight. In buccal view, lower premolars do not show diastemata between them. The masseteric fossa is relatively deep and the ramus is rostrocaudally large, stout and rather elevated over the corpus. In the angular region, the subangular lobe is slightly developed, in lateral view, in with the shape of a short bulging of bone. The angular process is large and stout (Fig. 3.6.4I-J and L-M). MNCN-39917 (Fig. 3.6.4A-C) is the specimen in which the distal portion is better preserved but the angular process is broken.

Lower teeth. The incisors are small. The c is low-crowned. The lower premolars are mesiodistally short and possess very high protoconids (Fig. 3.6.4). Both p2 and p3 do not possess distal accessory cuspid. In occlusal view, the p4 is oval-shaped. It has a large accessory cuspid closely attached to the protoconid and a strong distal cingulid. The m1 paraconid is short, whereas the protoconid is high, not arched distally (Fig. 3.6.4). The metaconid is large and individualized from the protoconid, and it slightly projects on the lingual side. On the talonid, there is a large hypoconid and a smaller entoconid (with generally no difference in height between them) not connected by any cristid. Between the metaconid and entoconid, there is generally

Figure 3.6.4 – *Nyctereutes donnezani* from Layna, MN15 (Spain). **A-C**: **MNCN-39917**, right hemimandible fragment with p4-m2 in buccal (**A**), lingual (**B**), and occlusal (**C**) views. **D-F**: **MNCN-39916**, right hemimandible fragment with p2-p3 and m1-m3 in buccal (**D**), lingual (**E**), and occlusal (**F**) views. **G-H**: **MNCN-39919**, right hemimandible fragment with p4-m2 in lingual (**G**), and occlusal (**H**) views. **I-K**: **MNCN-62616**, right hemimandible fragment with m2 in buccal (**I**), lingual (**J**), and occlusal (**K**) views. **L-M**: **MNCN-62618**, right hemimandible fragment in buccal (**L**) and lingual (**M**) views. **N-P**: **MNCN-62504**, left hemimandible fragment with p4-m1 in buccal (**N**), lingual (**O**), and occlusal (**P**) views.

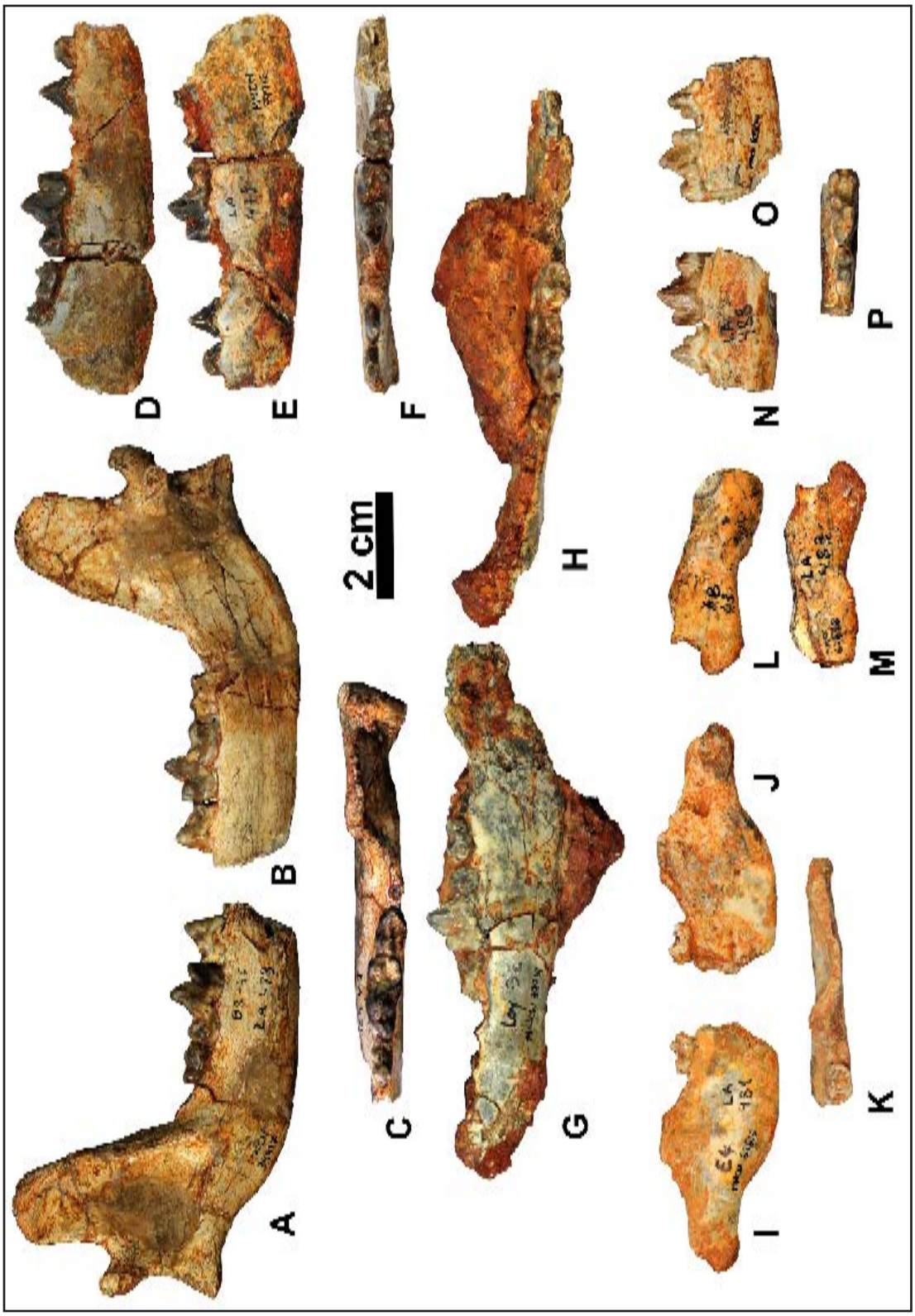
A
B
C
D
E
F
G
H
I
J
K
L
M
N
O
P
2 cm

one large accessory cuspid. In almost all the specimens, a cristid bounds the distal margin of the m1 and connects the distal sides of the entoconid and the hypoconid (Fig. 3.6.4C, F, H, P). The m2 is generally bean-shaped in occlusal view, with a conspicuous mesiobuccal cingulid (Fig. 3.6.4). The protoconid and metaconid are large and equal in size. Mesially to these cuspids, there is generally a round cristid with a cuspulid on it. On the talonid, there is a large hypoconid and, generally, one or more accessory cuspulids behind the metaconid. The m3 is oval and possesses two equal-sized cuspids.

Postcranial elements. Scapula. Among the various scapulae recovered from the site of Layna, only two fragments are in good state of preservation (*i.e.*, MNCN-62577 and MNCN-62633) (Fig. 3.6.5). Nevertheless, these specimens preserve almost only the glenoid cavity and very little portion of the *ala scapulae*. The glenoid cavity outline is sub-rounded in shape. The supragleonoid tubercle is hooked with a stout coracoid process directly and closely attached to the medial margin of the tubercle. Humerus. On the proximal epiphysis, there is a robust head. The greater tubercle is slightly higher compared to the head, and it is considerably enlarged (Fig. 3.6.5). The lesser tubercle is quite prominent and large, in palmar view. On the distal epiphysis, there is a round supratrochlear foramen. In cranial view, the distal articular surfaces appear compressed dorsoventrally in comparison to its width, especially the *capitulum*, although the medial side of the trochlea extends distally (Fig. 3.6.5). Furthermore, the lateral side of the distal articular surface is inclined compared to the medial side and the vertical axis of the diaphysis. The distal epicondyles are both well-developed, although the medial is larger than the lateral. In medial view, MNCN-62502 shows a prominent supratrochlear crest (Fig. 3.6.5). Ulna. The tuberosity of the olecranon is knob-like in shape. On the medial side, there is a deep fossa below this tuberosity. The lateral coronoid process is greatly reduced compared to the medial one, resembling more a small bone prominence. The medial coronoid process is rather thin and compressed mediolaterally instead

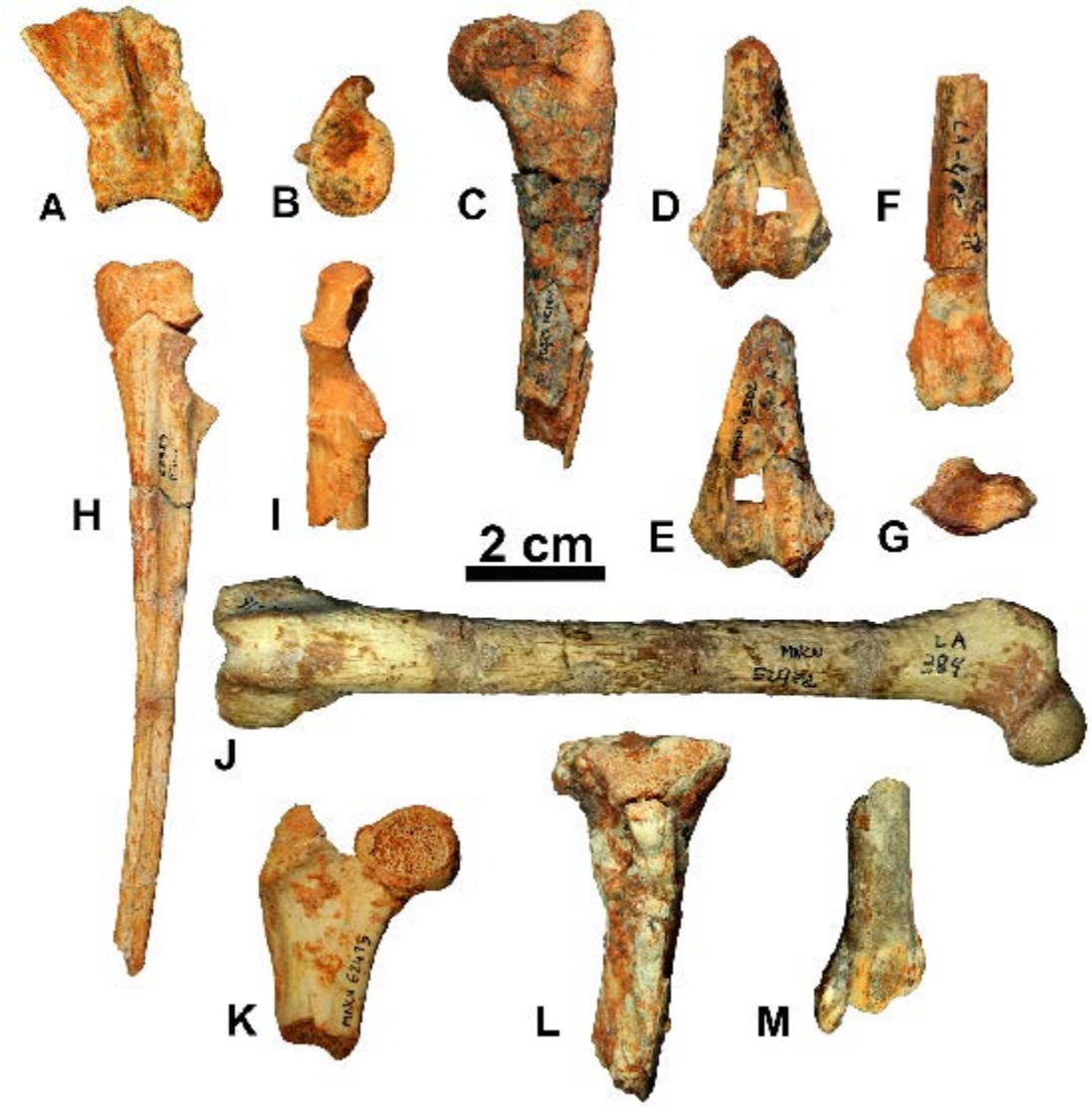

Figure 3.6.5 – *Nyctereutes donnezani* from Layna, MN15 (Spain). **A-B**: **MNCN-62577**, fragment of right scapula, in lateral (**A**) and distal (**B**) views. **C**: **MNCN-62503**, fragment of left humerus in lateral view. **D-E**: **MNCN-62502**, fragment of left humerus in dorsal (**D**) and palmar (**E**) views. **F**: **MNCN-13654**, fragment of left radius in dorsal view. **G**: **MNCN-70905**, fragment of left radius in distal view. **H**: **MNCN-62622/549**, right ulna in lateral view. **I**: **MNCN-62623**, fragment of right ulna in dorsal view. **J**: MNCN-52972, right femur in dorsal view. **K**: **MNCN-62473/75**, proximal epiphysis of right femur in dorsal view. **L**: **MNCN-62488**, proximal epiphysis of left tibia in dorsal view. **M**: **MNCN-62485**, distal epiphysis of right tibia in dorsal view.

of expanding medially, it projects cranially, if observed in proximal view (Fig. 3.6.5I). Radius. In proximal view, the proximal articular area is bean-shaped. The coronoid process is a prominent tip, in cranial view. On the cranial side of the distal portion, there is a swelling of bone, particularly prominent in MNCN-70905 (Fig.

3.6.5G), identified by the wide grooves of the *extensor carpi radialis* and *extensor digitalis communis* muscles. Femur. MNCN-52972 is an almost complete femur, missing only the greater trochanter (Fig. 3.6.5J). It is rather shortened, with thick diaphysis and mediolaterally large epiphyses. In medial view, the lesser trochanter is large and prominent. On the diaphysis, there are no relevant grooves visible. On the cranial side of the distal epiphysis, the ridges of the distal articulation are prominent. In plantar and distal views, the intercondylar space is large. Dorsal to the lateral condyle, in plantar view, there is a prominent supracondylar tuberosity. Tibia. In cranial view, the diaphysis of the tibia seems markedly curved, especially near the proximal epiphysis (Fig. 3.6.5L). Distally, the medial malleolus is rather enlarged and extended distally (Fig. 3.6.5M).

Comparison. Although damaged, MNCN-63662 is one of the most complete crania of *N. donnezani* reported in the literature (Fig. 3.6.2). MNCN-63662 shows numerous similarities with the cranium of *N. tingi* (*e.g.*, F:AM 96575; THP 22714). For instance, both species are large-sized, possess diastemata between upper premolars, and the splanchnocranium is rather elongated compared to the neurocranium. Besides the larger overall size, the crania of *N. sinensis* from Yushe Basin, *N. vulpinus* from St. Vallier or *N. megamastoides* of Europe show a smaller basicranial area compared to that of *N. donnezani* and similar proportions between the neurocranium and the splanchnocranium. Other features cannot be discussed due to the state of preservation of the fossil from Layna.

The set of morphologies of the Layna material is consistently primitive if compared to the features characterizing *N. sinensis*, *N. vulpinus* and *N. megamastoides*. For instance, the latter species show a high angle between the mandibular corpus and ramus, in the area of the subangular lobe; additionally, the development of the angular process or sub-quadrate morphology of M1 and M2 in *N. vulpinus*, *N. sinensis* and particularly *N. megamastoides* cannot be seen in *N. donnezani*.

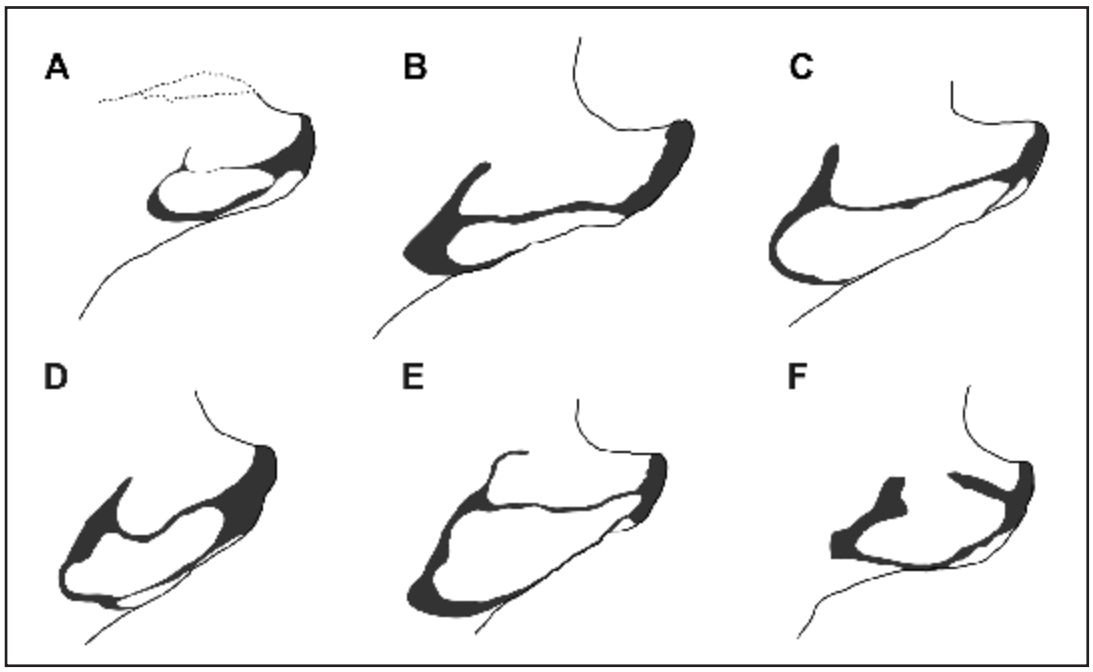

Figure 3.6.6 – Comparative schematic representation of the rami of the *m. pterygoideus medialis* on the medial side of the angular process in different *Nyctereutes* species: (**A**) *N. donnezani* from Layna; (**B**) *N. tingi* from the Yushe Basin; (**C**) *N. vulpinus* from St. Vallier; (**D**) *N. megamastoides* from Senéze; (**E**) *N. sinensis* from the Yushe Basin; (**F**) extant *N. procyonoides*. Muscle insertions are represented by scars or rough surfaces on the angular process. All outlines were rescaled to appear of the same dimensions.

Similarly, *N. procyonoides* exhibits several features that are also highly derived and not comparable to those of *Nyctereutes* from Layna, *e.g.*, the presence of a stronger parastyle on P4, the general morphology of the upper molars, the reduced development of the metacone and metaconule in the M1, the proportionally reduced metaconid on the m1, etc. The dentognathic features of *N. vulpinus* from St. Vallier are rather derived in comparison to those of the considered sample. For example, *N. vulpinus* possesses the M1 paracone slightly larger than the metacone; a quadrate occlusal shape of the M2; a well-developed subangular lobe, stronger than that of *N. donnezani*. Other features that distinguish *N. vulpinus* from the specimens from Layna are the thin and sharp angular process and the relative development of the scars of *m. pterygoideus medialis* on the medial side of this process (Fig. 3.6.6). Although the characters of the taxon from St. Vallier are more

derived than those of *N. donnezani* from Perpignan and *Nyctereutes* from Layna, they are suggestive of a less advanced degree of adaptation to an hypocarnivorous diet similar to that of *N. sinensis* and in contrast to *N. megamastoides*.

The taxa showing primitive morphologies close to those observed in the Layna sample are *N. tingi* from numerous localities of the Yushe Basin (China) and *N. donnezani* from La Gloria 4 (Spain) and Perpignan (France). Among the shared features, the poorly developed subangular lobe, the morphology of the upper molars, and their reduced width can be pointed out.

Regarding the postcranial sample, the humeri from Layna (*e.g.*, MNCN-62503) possess a robust head that extends palmarly, with an oval shape when observed in proximal view. Conversely, in the humerus of *N. megamastoides* from Perrier-Les Etouaires or of the extant *N. procyonoides*, the *caput humeri* is rather round in shape in proximal view. The greater tubercle of the Layna sample resembles that of *N. procyonoides*, whereas it is proportionally larger than that *N. megamastoides.* Compared to these two species, the intertubercular *sulcus* of the specimens from Layna (*e.g.*, MNCN-62503 and MNCN-69984) is reduced and narrow if compared to the condition of *N. megamastoides* and *N. procyonoides*. Moreover, the lesser tubercle appears reduced compared to that of both the extant *N. procyonoides* and *N. megamastoides*. In the distal epiphysis of the humerus, the majority of the specimens from Layna possesses a large, proximodistally high *capitulum*, similar to that of *N. donnezani* of Perpignan and unlike *N. megamastoides* of Perrier-Les Etouaires, *N. vulpinus* from St. Vallier and extant *N. procyonoides*. In distal view, the incision for the articulation of the olecranon of the ulna is proportionally narrower compared to that of *N. megamastoides* and *N. procyonoides*. In the same view, the distal epiphysis appears stout and craniopalmarly enlarged compared to *N. procyonoides*, *N. donnezani* from Perpignan and *N. megamastoides* from Perrier-Les Etouaires. In cranial view, the trochlea of *N. procyonoides* tends to be strongly inclined medially. In the fossil species, this feature is not clearly marked. The

features of the distal portion of the radius resemble those of *N. donnezani* from Perpignan for the elongation in lateral direction of the distal articular surface (in distal view), correspondingly to a compression in craniopalmar direction. This rectangular shape contrasts with the condition seen in *N. megamastoides*. Moreover, another common feature between the specimens from Layna and Perpignan, is the bone swelling on the cranial side of the distal epiphysis, which is conversely smaller in *N. megamastoides*. Both *N. donnezani* from Perpignan and the specimens of Layna possess a well-developed and large groove for the *m. extensor radialis carpi* whereas the ones of the *mm. extensor digitorum communis* and *extensor obliquus carpi* are reduced.

The ulna of *N. megamastoides* shows an enlarged, prominent and shelf-like medial coronoid process, different from that of *N. procyonoides* and especially from that of the sample from Layna and *N. donnezani* from Perpignan. In these two latter taxa, the medial coronoid process although larger than the lateral one, is thinner and receding compared to that of *N. megamastoides*.

The neck of the femur of the specimens of Layna (*e.g.*, MNCN-62473/75 or MNCN-52977), is stout as in *N. donnezani*, while it is more slender in *N. megamastoides* and *N. procyonoides*. The lesser trochanter is prominent in lateral view and well developed compared to *N. megamastoides* from Perrier and especially to the extant *N. procyonoides*. The third trochanter is peculiarly larger in the sample of Layna than in *N. procyonoides*.

A relevant difference between the tibiae of Layna and other Eurasian samples lie in the morphology of the distal articular surface: the plantar margin of the surface is reduced in lateral length compared to the cranial margin, giving a triangular shape to the tibial trochlea in distal view. This feature resembles that of *N. donnezani* from Perpignan but contrast with *N. megamastoides* and *N. procyonoides*.

All measurements of the *Nyctereutes* sample from Layna are shown in Tables 3.6.1-3.6.7 in section 3.6.5.

Log-ratio diagrams (Fig. 3.6.7) were used to test the affinities of the Layna sample in comparison to the variability of the Eurasian fossil taxa. These diagrams were used to compare the mean dental measures of Eurasian Pliocene-Pleistocene species and of the extant *N. procyonoides*, which was used as a standard reference in all the diagrams. The graph of Fig. 3.6.7A highlights the similarity in tooth proportions between the Layna material and *N. donnezani* from Perpignan. Therefore, these morphometric results reinforce those obtained from the morphological comparison and support the attribution of the Layna sample to *N. donnezani*. In general dental proportions, the sample from Layna is significantly larger than the extant *N. procyonoides* but similar in size to the fossil species of *Nyctereutes*, as shown in Fig. 3.6.7A. When considered all together, the proportions and size the Perpignan, La Gloria 4 plus Layna samples (*N. donnezani* from western Europe of Fig. 3.6.7B) fall between those of *N. procyonoides* and *N. tingi*, being the former considerably smaller and the latter substantially larger than the other taxa. Remarkable is the similarity between the pattern of dental proportions of *N. donnezani*, *N. sinensis* and especially *N. vulpinus*, besides the presence of some derived morphological features in the two latter (*e.g.*, equal-sized paracone and metacone on M1; quadrate occlusal shape of M2) (Fig. 3.6.7B). The general dental proportions and size of *N. megamastoides* do not differ significantly from *N. sinensis* and *N. vulpinus*, except for the proportionally longer M2, the enlarged m1 and the wider m2.

Nyctereutes* cf. *megamastoides (Pomel, 1842)

(Fig. 3.6.8)

1842 *Canis megamastoides* Pomel

Type locality. Perrier-Les Etouaires, France.

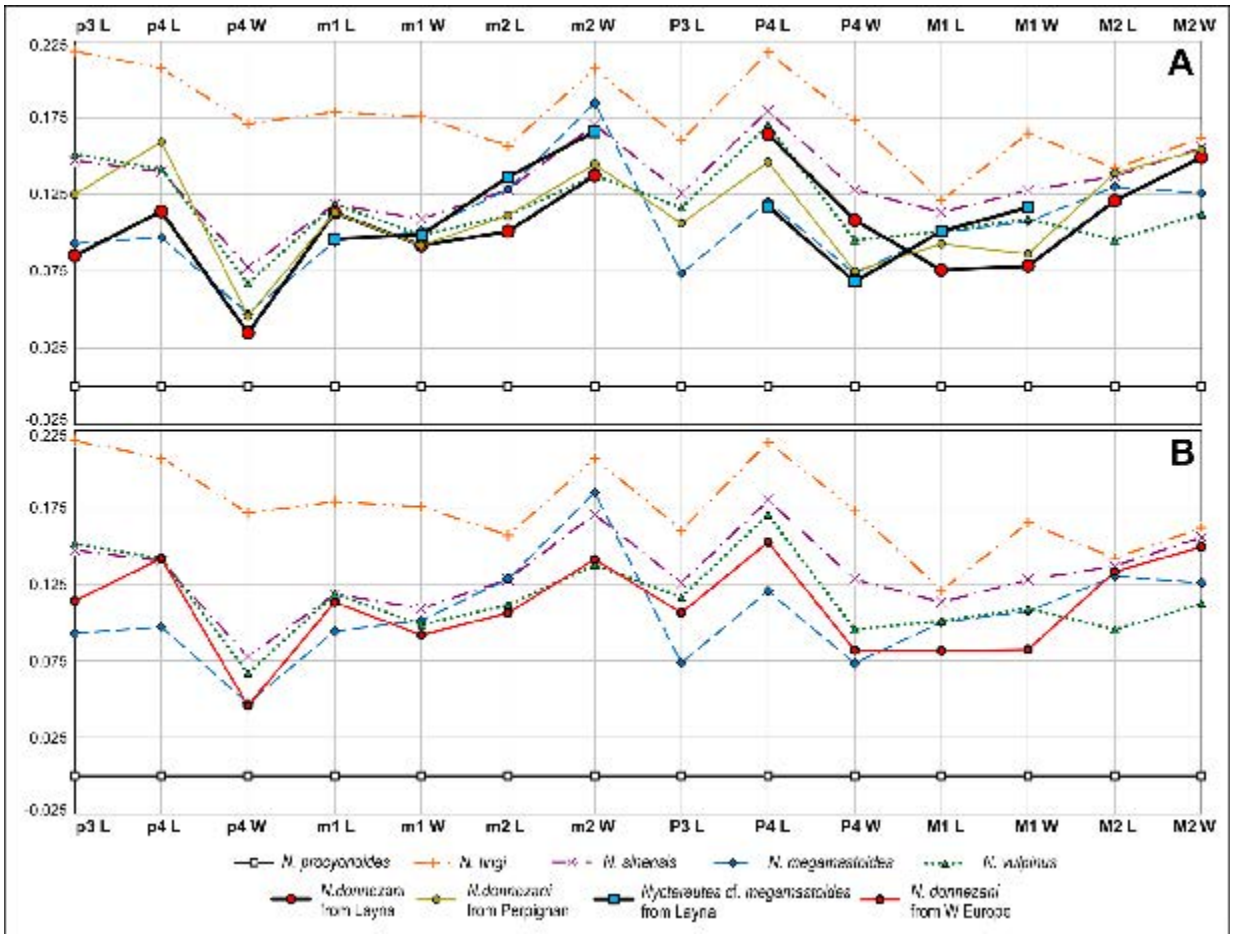

Figure 3.6.7 – Log-ratio diagrams on selected upper and lower tooth variables in Plio-Pleistocene species and selected samples of *Nyctereutes* as compared to the extant *N. procyonoides*. **A**: Log-ratio diagram on the different samples of Layna (*N. donnezani* and *N.* cf. *megamastoides*) in comparison to the Plio-Pleistocene species (*N. sinensis*, *N. tingi*, *N. vulpinus*, *N. megamastoides* and the type sample of *N. donnezani* from Perpignan) and *N. procyonoides*. **B**: Resuming log-ratio diagram showing the pattern of dental proportions in the fossil Eurasian species as compared to the extant *N. procyonoides* (used as the reference baseline). Here the proportions of *N. donnezani* are the resulting from the combination of the sample of La Gloria 4, Perpignan and Layna. The extant *N. procyonoides* is used as the reference baseline in both diagrams.

Age. Late Pliocene, MN16

Differential diagnosis. The cranium tends to be shortened rostrocaudally. The upper molars tend to have squared outline in occlusal view, unlike the buccolingually wider shape of *N. donnezani* and *N. tingi*. In M1 and M2, the paracone and metacone are equal in size like in *N. donnezani* but in contrast to *N. sinensis* and *N. vulpinus*.

Nyctereutes megamastoides possesses a mandible with a greatly developed subangular lobe similar and even more prominent compared to *N. sinensis* and *N. vulpinus*. The angular process in *N. megamastoides* in enlarged in dorsoventral direction, with large insertion areas for branches of the *m. pterigoideus medialis* (particularly the superior one). The m1 trigonid tends to be shortened compared to primitive taxa of the genus and the talonid is buccolingually enlarged. The m1 metaconid is enlarged and extends lingually. The cuspids of the m1 talonid are generally joined by a marked cristid unlike other species of *Nyctereutes*. The m2 is rather enlarged in its mesial portion, with a larger protoconid compared to the metaconid. Accessory cuspids are present in the distal portion of the m2.

Materials. MNCN-39921, left maxillary fragment with P4-M1. MNCN-39918, right hemimandible with m1-m2. MNCN-69984, distal epiphysis of right humerus.

Description. *Upper teeth*. The maxillary fragment MNCN-39921 preserves complete P4 and M1. The P4 (L= 12.1 mm; Lmax= 13.1 mm; W= 6.2 mm) has a large protocone that lies at the same level of the mesial margin of the P4 or slightly advanced (Fig. 3.6.8A-B). Lingually there is a strong cingulum whereas on the mesial side there is a faint one. The paracone is high and pointed and the metastylar blade is short. The M1 (L= 10.6 mm; W= 11.9 mm) is quadrangular in occlusal view (Fig. 3.6.8A-B). The paracone is equal in size as the metacone, but slightly higher. The M1 protocone is large and the metaconule is reduced; the protoconule is evident. On the mesial side, there is an expanded and prominent cusp-like cingulum. The hypocone is large. The buccal cingulum is prominent. *Lower teeth*. The m1 dimensions of MNCN-39918 are: L= 15.1 mm; W= 6.4 mm; trm1 L= 9.8 mm. The m1 protoconid is markedly higher than the low paraconid (Fig. 3.6.8C-E), which is slender in occlusal view. The metaconid is prominently large and separated from the protoconid. Together with the talonid, it extends

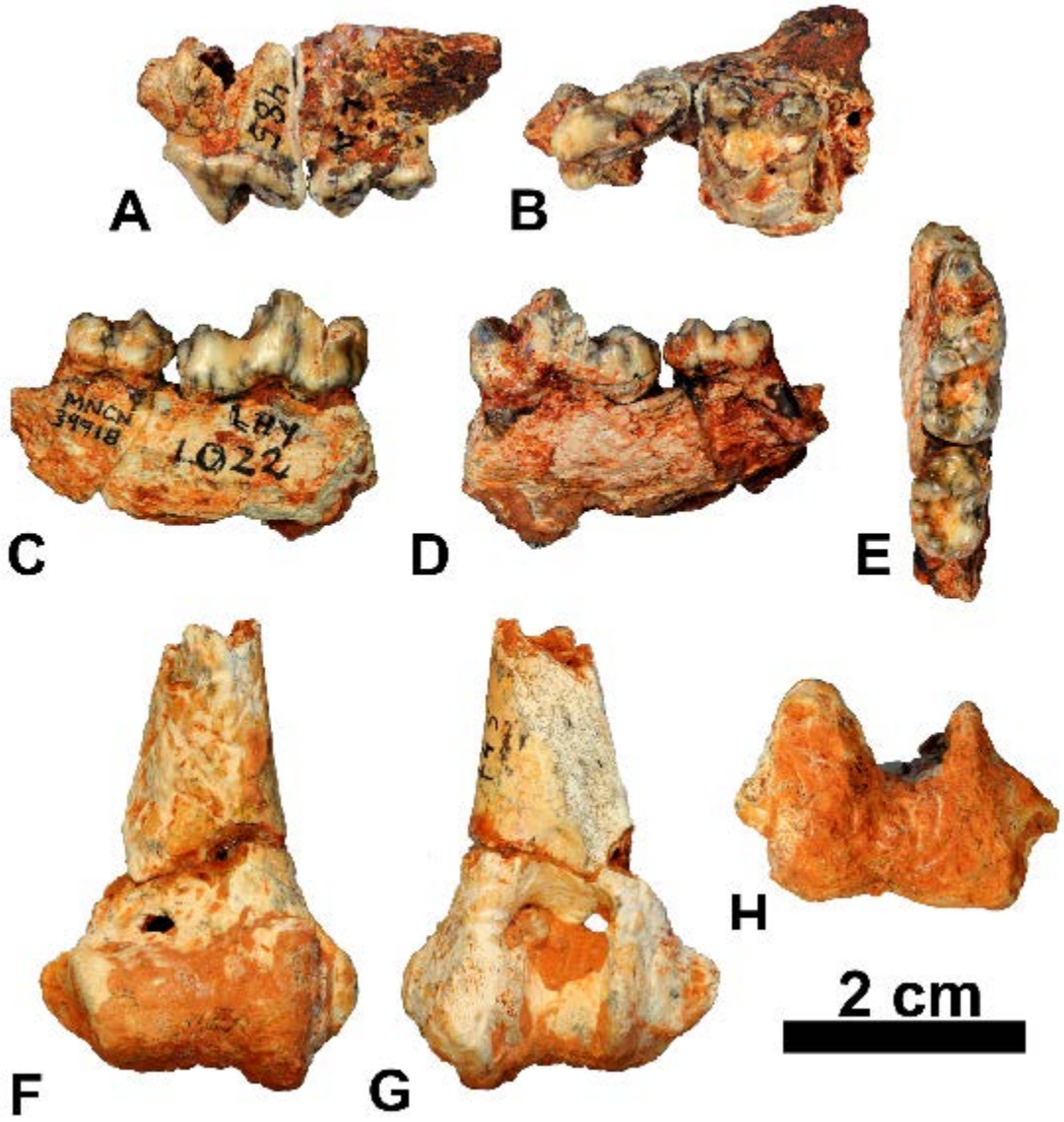

Figure 3.6.8 – *Nyctereutes* cf. *megamastoides* from Layna, MN15 (Spain). **A-B**: **MNCN-39921**, left maxillary fragment with P4-M1 in lateral (**A**), and occlusal (**B**) views. **C-E**: **MNCN-39918**, right hemimandible fragment with m1-m2 in buccal (**C**), lingual (**D**) and occlusal (**E**) views. **F-H**: **MNCN-69984**, fragment distal epiphysis of right humerus, in cranial (**F**), palmar (**G**) and distal (**H**) views.

lingually. The hypoconid is larger and higher compared to the entoconid; a short cristid connects them, prominent, especially on the entoconid. Between the metaconid and the entoconid there are two large accessory cuspids. In occlusal view, the m2 (L= 8.9 mm; W= 6.3 mm) is bean-shaped with a conspicuous buccal development of the cingulid, especially mesially (Fig. 3.6.8E). The protoconid is similar in size to the metaconid. A cristid develops from the mesial side of the

protoconid. On the talonid, there is the hypoconid and three prominent accessory cuspulids behind the metaconid.

Postcranial elements. Humerus. It preserves only the distal portion (Bd= 29.3 mm). In cranial view, the distal articular surface of MNCN-69984 appears elongated laterally especially in the capitulum (Fig. 3.6.8F). The trochlea, although damaged, is very high in proximodistal direction. The lateral side of the distal articular surface is strongly inclined laterally compared to the medial side, which is parallel to the vertical axis of the diaphysis. The epicondyles are well-developed and similar in size, both extended laterally. The olecranon fossa seems deep and large.

Comparisons. The position and the development of the P4 protocone is unusual compared to the rest of the sample from Layna: it is relatively reduced and close the paracone instead of having a strong and advanced mesial margin (Figs. 3.6.3 and 3.6.8). The squared morphology of the upper molar of MNCN-39921 differs greatly from the other molars recovered from Layna. Particularly, the development of the mesial cingulum, with its short but prominent cusps, and the lingual shortening of M1 resemble the features observed in the specimens from Perrier-Les Etouaires, Dafnero-1, or Kvabebi and strongly contrast with those of *N. donnezani* from Layna or Perpignan and those of *N. tingi* from the Yushe Basin. For instance, no specimens of the analyzed sample of these two latter species show a buccolingual reduction of the M1, or possess the cusp-like cingulum. Even the more derived taxa, *N. sinensis* and *N. vulpinus*, do not possess a markedly enlarged and cusp-like cingulum on the mesial side of M1. The morphological analysis of the samples of *N. sinensis* and of *N. vulpinus* reveal that only the 14% and the 22% of the specimens, respectively, possessed large and cusp-like mesial cingulum. On the contrary, *N. megamastoides* and *N. procyonoides* almost always possess this morphology of the mesial cingulum of the M1 (95% and 90% of the considered sample). The morphology of the m1 is peculiar for the conspicuous enlargement of the

metaconid and talonid, especially in occlusal view. The widening of the talonid area of the m1 compared to the trigonid is marked in the derived species *N. megamastoides* whereas in *N. donnezani* or even *N. sinensis* and *N. vulpinus*, this feature is not prominent. The presence of large accessory cuspids on the lingual side of m1 and m2 and the cristid connecting the m1 hypoconid and the entoconid are further features that resemble *N. megamastoides* or *N. vulpinus* as *N. donnezani* does not possess the crista transversa. *N. sinensis* rarely possess accessory cuspid/cuspulids or this cristid between hypoconid and entoconid. Particularly, among the specimens of *N. sinensis* from Yushe Basin and Nihewan Basin only the 5% possessed a crista transversa. On the contrary, in *N. vulpinus* from St. Vallier the percentage of specimens with the cristid is above the 54%, but in the samples attributed to *N. megamastoides* (*e.g.*, Perrier-Les Etouaires, Senéze, Kvabebi), the 90% of the specimens with preserved m1 show a prominent cristid between the m1 hypoconid and entoconid. In the extant *N. procyonoides*, the 72% of the sample displayed a prominent crista transversa. The enlargement of the m1 talonid in buccolingual sense, visible in occlusal view, and the supranumerary cuspulids on the lower molars contrast with the diagnostic features of *N. vulpinus* as described by Soria & Aguirre (1976) (viz. the elongated m1 and a reduced m2).

The humerus MNCN-69984 possesses features contrasting with *N. donnezani* from Perpignan and even other specimens from Layna. It resembles those of the material recovered from Perrier-Les Etouaires and attributed to *N. megamastoides*. For instance, in cranial view, the distal articular surface of MNCN-69984 shows an enlarged trochlea, greatly expanded compared to the short capitulum, similar to *N. megamastoides* from Perrier-Les Etouaires and from Kvabebi and the extant *N. procyonoides*. On the contrary, in *N. donnezani* from Perpignan and Layna, the trochlea and capitulum are similar in height. In lateral view, the distal epiphysis of the humerus of *N. megamastoides* is craniopalmarly more compressed compared to that of *N. donnezani*. The same difference is visible in *N. procyonoides* and *N.*

donnezani.

The log-ratio diagram in Fig. 3.6.7A compares the proportions of the dental sample from Layna tentatively attributed to *N.* cf. *megamastoides* with those of Eurasian samples. Although fragmentary, the pattern of the Layna material in the graph clearly follows that of *N. megamastoides*, thus supporting the taxonomic attribution made on morphological ground.

3.6.4. Discussions and Conclusions

The origin of the genus *Nyctereutes* is still debated and rather dubious. Its earliest occurrence is represented by the species *N. tingi* from the Early Pliocene (correlable to MN14) localities of the Yushe Basin (Tedford & Qiu 1991). Nevertheless, the ancestor of this primitive Asian form is yet unknown. Another issue is the confusion regarding the relationship between *Nyctereutes* and other canids. Tedford et al. (1995; 2009) suggested a close phylogenetic affinity between *Nyctereutes* and *Cerdocyon* because of the retention of shared features like the presence of a developed subangular lobe, the expansion of the angular process, the development of the pterygoideus medialis scars on the lingual side of the angular process and low-crowned canines. For this reason, they ascribed these two genera to the same subtribe Cerdocyonina within the tribe Canini, and therefore deeming a closer affinity to *Canis* Linnaeus, 1758 than to *Vulpes*. On the contrary, several genetic analyses (Wayne et al. 1997; Wayne & Ostrander 2007) grouped *Nyctereutes* within the tribe Vulpini, separated from the South American clade of Canini (which includes *Cerdocyon*). In our opinion, the ancestor of raccoon dog-like canids is a member of Vulpini that spread into Eurasia from North America (center of origin of the tribe Vulpini, see Tedford et al. 2009) at the end of the Miocene and the morphologies shared by *Cerdocyon* and *Nyctereutes* are homoplasies resulting from convergent evolution to ecological adaptations.

After the appearance of *N. tingi*, the first record of a derived form, *N. sinensis*,

is reported from Early Pliocene Chinese sites of the Yushe Basin (correlable to MN15). More or less contemporaneously, in western Europe *N. donnezani* appears in the fossil record, first in Perpignan and subsequently in Layna. The features described above confirm the rather primitive state of this taxon, comparable to that of *N. tingi*. Nevertheless, Tedford & Qiu (1991), in their description of *N. tingi*, pointed out some differences between the Chinese taxon and *N. donnezani*. Among these, there is the larger size, the presence of incipient cristids connecting the hypoconid and the entoconid on m1, and the larger metaconule compared to the protoconule on M1. Other features used by the authors, *e.g.*, the similar size of paracone and metacone in the upper molars and the similar morphology of the angular process, need to be reconsidered since in *N. donnezani* the buccal cusps have different size (Fig. 3.6.3) and the angular process, in medial view, has different morphology (Fig. 3.6.6). In fact, in *N. tingi*, the angular process is rather thin and has the shape of an elongated hook, whereas in *N. donnezani* it is enlarged and, to some extent, is morphologically closer to that of *N. sinensis* and *N. megamastoides*. Another difference between the Chinese and European taxa is that the record of *N. tingi* in the Yushe Basin seems to be uninterrupted from the earliest Pliocene to ca. 3 Ma, whereas *N. donnezani* has been described from few and sparse localities in Spain and France, referable to MN14 and MN15. These localities are La Gloria 4 (4.19 Ma; Domingo et al., 2013), Perpignan (Serrat-d'en-Vacquer, ca. 4 Ma; Clauzon et al., 2015) and Layna (3.91 Ma; Domingo et al., 2013). A coeval record of the genus comes from the Turkish site of Çalta (Ankara Province, North-western Turkey), correlated to some MN15 European localities (see among others Bernor & Sen, 2017). The remains of *Nyctereutes* from Çalta, which include two well-preserved crania (ACA-291 and ACA-292) and some mandibular specimens (*e.g.*, ACA-549 and ACA-294), were attributed to *N. donnezani* by Ginsburg (1998). Several cranial and dentognathic features support this attribution, *e.g.*, the rostrocaudal elongation of the cranium in

dorsal view (although the crania suffered of a certain degree of lateral diagenetic compression, considering the morphology of the nasal area in dorsal view; this compression might result in an overall impression of a prominent rostrocaudal elongation); and the morphology of the subangular region, with no or poorly developed subangular lobe. Other characteristics, on the contrary, differ from the type material of Perpignan and from that of Layna. Unlike *N. tingi*, *N. sinensis* and *N. vulpinus*, the absence or the great reduction of the frontal sinus, the reduced length of the area caudal to the postorbital processes and the marked postorbital constriction are features similar to the condition observed in *N. megamastoides* from Villarroya and from Perrier-Les Etouaires. In tooth morphology, the shape of the upper molars is intermediate between the buccolingually wide teeth of *N. tingi* and the narrower ones of derived species like *N. sinensis* or *N. megamastoides*; the cingulum that bounds the upper molar is better developed compared to that of *N. donnezani* from Perpignan and Layna. The majority of the recovered M1 (83 %) possesses expanded and cusp-like mesial cingulum. Furthermore, the M2 paracone is larger than the metacone like in *N. megamastoides* or *N. vulpinus*. It also possesses a large and prominent M2 metaconule connected by the postprotocrista to the protocone, unlike the specimens of *N. tingi* or *N. donnezani*. The ventral margin of the mandible is short rostrocaudally, and tend to be curved in contrast to the straight ventral margin of the other Eurasian species of *Nyctereutes* (*e.g.*, *N. sinensis*, *N. megamastoides*). The presence of an evident cristid connecting the hypoconid and the entoconid on both the m1 (*e.g.*, ACA-294 and ACA-549; 75% the preserved m1) from Çalta is unusual for *N. donnezani*, *N. tingi* or *N. sinensis* whereas is common in *N. megamastoides* (see previous discussion). Moreover, the m1 metaconid of *Nyctereutes* from Çalta is rather prominent compared to that of *N. donnezani* from Perpignan and Layna, or even *N. tingi* and *N. sinensis* from China; it resembles that of *N. megamastoides* from *e.g.*, from Dafnero-1 or Kvabebi. In dental proportions, the sample from Çalta differs considerably from the Chinese

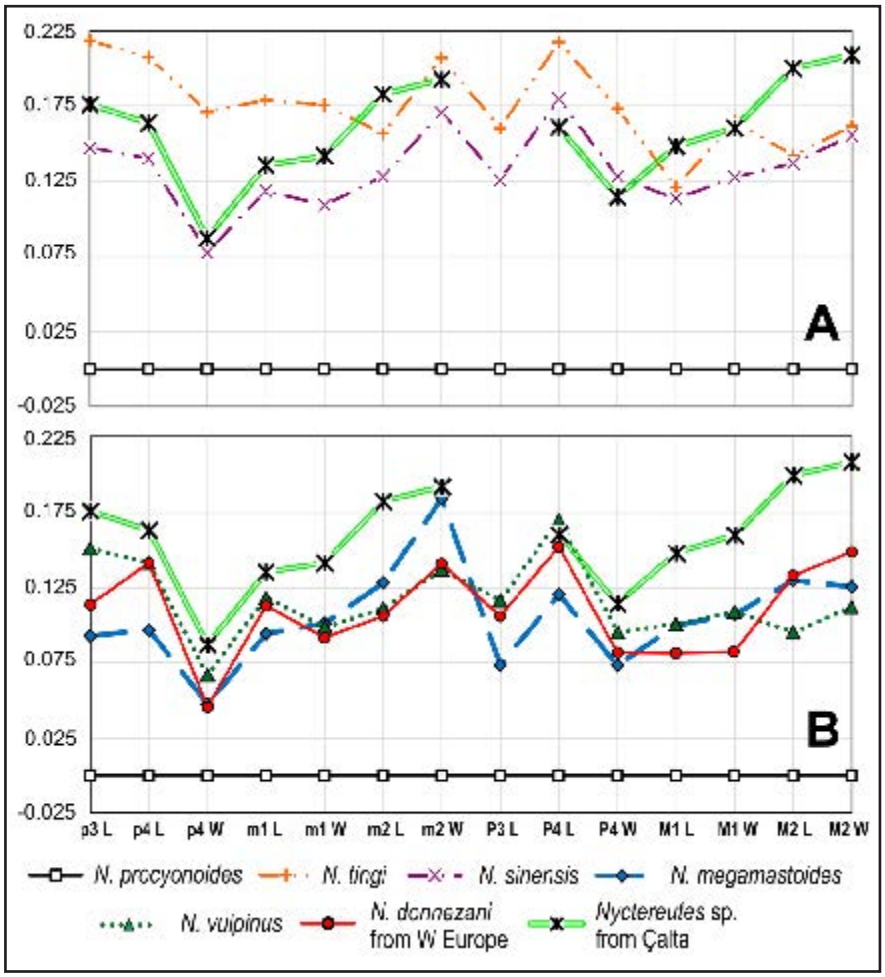

Figure 3.6.9 – Log-ratio diagrams on selected upper and lower teeth tooth variables in *Nyctereutes* from Çalta as compared to the extant *N. procyonoides* (used as the reference baseline) and to *N. tingi* and *N. sinensis* (**A**) and to *N. donnezani*, *N. vulpinus* and *N. megamastoides* (**B**). The extant *N. procyonoides* is used as the reference baseline in both diagrams.

species *N. tingi* and *N. sinensis* (Fig. 3.6.9A). More similarities can be found with the European taxa, especially with *N. megamastoides*, as shown in Fig. 3.6.9B. This mixed pattern of features, with resemblance and difference with various Eurasian taxa, makes the original attribution at least doubtful. For the moment, the sample of Çalta is referred to as *Nyctereutes* sp.

In other localities of southeastern and eastern Europe, some scanty remains of fossil raccoon dogs with primitive features have been described. Spassov (2003) reported *N.* cf. *tingi* from the Bulgarian site of Varshets (referred to the St. Vallier Faunal Unit, MN17), while the remains from Megalo Emvolon (Greece; MN15)

was ascribed to *N. tingi* (Koufos, 1997). If the attributions were confirmed, these remains would extend the distribution of the Chinese species into Europe and, in the case of Varshets material, also in time (from 3 Ma to 2.2 Ma). The maxillary fragment recovered from Weze (Poland, MN15-16) originally described by Stach (1954) as *Nyctereutes* sp., was later referred to as *N.* aff. *donnezani* (Soria & Aguirre, 1976). A reinterpretation of these fossils in the biogeographic framework of the raccoon dog evolutionary history would hopefully provide new evidence to solve some of the above-mentioned issues.

Historically the appearance of derived species of *Nyctereutes* in western Europe, namely *N. megamastoides*, has been referred to the Late Pliocene, around 3 Ma (section 3.3.) and no record of co-occurrence of primitive and derived taxa in European localities is reported in the literature. This contrast with the eastern Asian record of the Yushe Basin, in which *N. tingi* coexists with *N. sinensis* (Tedford & Qiu, 1991). The recognition of *N. megamastoides* within the sample of Layna unveils an unexpected ecological pattern in a European site similar to the correspondent to the Chinese one. This discovery reveals that the earliest arrival of *N. megamastoides*-like raccoon dogs in Europe was much earlier than previously thought, around 3.9 Ma (Domingo et al., 2013). Furthermore, it is remarkable that in dental morphology these specimens resemble the younger *N. megamastoides* recovered from other European sites, *e.g.*, Kvabebi, Lower Valdarno, Dafnero-1. The discovery of the derived taxon *N. megamastoides* in such an early site forces us to reevaluate the paradigms of dispersion and evolution of this taxon and more in general of all the Eurasian raccoon dogs. For instance, the generally accepted hypothesis for the origin of *N. megamastoides*, as the result of anagenetic evolution from *N. donnezani*, seems less likely as the two appeared more or less contemporarily and apparently coexisted in the Spanish site. The alleged homology between *N. sinensis* and *N. megamastoides* based on shared derived features and the view of such species as a single taxon with a large paleobiogeographic range, favored by Tedford

& Qiu (1991), could contrast with the scenario suggested by the discovery of *N. megamastoides* at Layna. With its peculiar derived morphology, the latter species probably evolved in Eurasia more or less contemporarily to and independently from the *N. sinensis* lineage. Moreover, the characterizing cranial and dentognathic features of *N. sinensis* remain stable throughout the Yushe Basin Pliocene succession. Morphometric and morphological evidence might suggest a closer affinity between *N. sinensis* and *N. vulpinus*. This reinterpretation of the dispersal pattern and evolutionary history of Pliocene species, allows us to reconsider the specimens from Çalta. Their size, the mosaic pattern of primitive and derived features, but different from *N. donnezani* and *N. tingi*, combined with the similarity in dental proportions to *N. megamastoides*, are elements that suggest the possible presence of an unknown lineage, parallel to that of *N. tingi-N. donnezani*, and which eventually lead to the appearance of *N. megamastoides* in Eurasia.

Thanks to the method of the molar ratio index, Asahara & Takai (2016) showed that *Nyctereutes* spp. and sspp. possess a certain degree of dietary plasticity. Based on this method applied to the considered sample, a new score for the species *N. donnezani* was calculated (m2/m1= 0.482), different from that known in literature (Fig. 3.6.10). The resulting mean score for *N. donnezani* (0.51) is slightly above the range of variability of the extant *N. p. viverrinus* from Honshu (Japan), whereas it is higher than that of *N. tingi* (0.48) and of other living subspecies of *N. procyonoides*. This suggests that *N. donnezani*, as well as *N. tingi*, had a diet comparable to that of *N. p. viverrinus* (omnivorous, see Asahara & Takai, 2016), although it does not show such a set of derived features in the mandible as extant raccoon dogs. The mean molar ratio score of *N. vulpinus* from St. Vallier (m2/m1=0.48) testify to different dietary preferences in comparison to *N. megamastoides* or *N. sinensis*. Indeed, in the French species, the subangular lobe is moderately developed but the dental morphology is suggestive of a more carnivorous diet compared to taxa like *N. megamastoides* or *N. sinensis*, in which their dental dimensions and morphologies

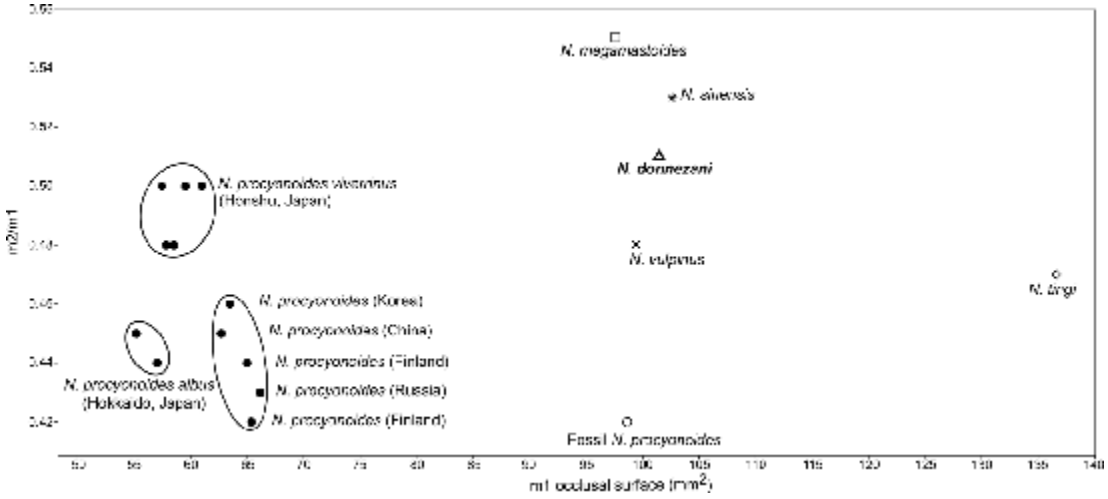

Figure 3.6.10 – Biplot of the m2/m1 scores against the m1 occlusal surface (in mm²) in various species and subspecies of *Nyctereutes* (see section 2.). Fossil species are represented by average values. Black circles represent extant taxa; the open circle represents Chinese fossil *N. procyonoides*-like forms from Zhoukoudian loc. 1 (Pei, 1934) and Renzidong (Jin & Liu, 2009) [n=7]; asterisk represents *N. sinensis* from the Yushe Basin (China) [n=22]; open square represents *N. megamastoides* (from Kvabebi, Georgia and Senéze, France) [n=5]; X represents *N. vulpinus* from St. Vallier (France) [n=8]; open triangle represents *N. donnezani* (from Perpignan, La Gloria 4 and Layna) [n=7]; plus represents *N. tingi* from Yushe Basin (China) [n=4]. Updated from section 3.5.

suggest slightly different diet adaptations. Peculiar among the fossil species *N. vulpinus* may suggest similar niche occupation.

The study of the fossil record shows that the different *Nyctereutes* species have developed dentognathic features to progressively take advantage of a great variety of food items from the earlier species as *N. tingi* and *N. donnezani* to more recent ones as *N. megamastoides* and *N. sinensis*. The former possesses characteristics suggestive of meso- to hypocarnivorous diet. The latter, with shared or similar morphologies to the extant *N. procyonoides*, show a shift in diet a hypocarnivorous diet. The enlargement and development of the crushing parts of teeth (both upper and lower) against slicing parts (see also Soria & Aguirre, 1976; Tedford & Qiu, 1991; and section 3.4.), the higher molar ratios (Fig. 3.6.10), etc. are all evidence of this dietary specialization. It is not clear which of the fossil species is the direct ancestor of *N. procyonoides* (although some scholars deem *N. sinensis* as the most probable), it is clear that it retains derived mandibular and dental features typical

of this clade. Nevertheless, the morphological and morphometric evidence on this species and this subspecies (*e.g.*, the molar ratio index or the elongation and buccolingual compression of lower molars compared to some fossil taxa) suggests an inversion of the trend towards an effective hypocarnivorous diet and that the spectrum of dietary preferences widened toward a greater plasticity in their diet.

In conclusion, the description of the new raccoon dog material recovered at Layna improves our knowledge on the primitive-like species *N. donnezani*, thanks to the discovery of a nearly complete although damaged cranium (MNCN-63662) and several postcranial elements. Furthermore, the study of this sample pointed out the presence of few specimens that do not show the diagnostic features of *N. donnezani*. The morphological and morphometric comparisons of these fossils strongly support an affinity to the derived species *N. megamastoides*, and therefore referred them to as *N.* cf. *megamastoides*. This represents the earliest known record of a derived species in western Europe, backdating its appearance of nearly one Ma. Surely, this record, combined with that of Çalta, opens new questions regarding the origin of derived species of raccoon dogs and has strong implications for our understanding of the pattern of evolution and dispersal of these species around the Old World.

3.6.5. Appendix

3.6.5.1. Table of measurements of the Nyctereutes *sample from Layna.*

Table 3.6.1. – Cranial measurements (mm) of *Nyctereutes donnezani* from Layna.

Cat. N°	FL	SCL	GNL	Ect	ECW	GPW	MOH	PwP1	LB	M2B	FMH	LCM
MNCN63662	82.7	61.8	44.4	35.7	27	44	16.1	18.5	16	35.5	11.8	126.9

Table 3.6.2. – Measurements (mm) of associated upper teeth of *Nyctereutes donnezani* from Layna.

Cat. N°		C L	C W	P1 L	P1 W	P2 L	P2 W	P3 L	P3 W	P4 L	P4 Lmax	P4 W	M1 L	M1 W	M2 L	M2 W
MNCN39920	L	-	-	-	-	-	-	-	-	-	-	-	9.7	11.2	6.4	8.3
MNCN39921	L	-	-	-	-	-	-	-	-	12.1	13.1	6.2	10.6	11.9	-	-
MNCN63662	L	7.2	4.6	3.8	2.5	7.8	2.8	-	-	13.3	15.1	-	10.7	11.2	7.1	9

Cat. N°		C-M2 L	A C-M2 L	P1-M2 L	P1-P4 L	M1-M2 L
MNCN39920	L	-	-	-	-	15.8
MNCN39921	L	-	-	-	-	-
MNCN63662	L	70.3	62.2	58.1	41.3	18

Table 3.6.3. Measurements (mm) of isolated upper teeth of *Nyctereutes donnezani* from Layna.

Cat. N°			L	W	Lmax
MNCN62494	C	L	6.4	4.3	-
MNCN62482	P2	R	6.5	2.9	-
MNCN62478	P4	L	12.8	7.4	14
MNCN62479	P4	L	-	6.1	-
MNCN62481	P4	L	12.8	7	13.1
MNCN62491	M1	R	9.7	-	-
MNCN62492	M1	L	9.95	10.5	-
MNCN62493	M2	L	6.8	8.1	-

Table 3.6.4. – Measurements (mm) of mandibles and associated lower teeth of *Nyctereutes donnezani* from Layna.

Cat. N°		p2 L	p2 W	p3 L	p3 W	p4 L	p4 W	m1 L	m1 W	trm1 L	tdm1 W	m2 L	m2 W	m3 L	m3 W	Mp4H	Mm1H	Mm1B	HR
MNCN39916	R	6.1	2.5	7.5	2.7	-	-	15.6	5.9	10	5.8	7.8	5.4	4.1	3.6	-	-	-	-
MNCN39917	R	-	-	-	-	9.1	3.9	14.8	6.2	9.2	6.1	8	-	-	-	13.9	15.9	7.8	41
MNCN39918	R	-	-	-	-	-	-	15.1	6.4	9.8	6.3	8.9	6.3	-	-	-	-	-	-
MNCN39919	R	-	-	-	-	9.1	-	15.7	-	10	-	8.4	6.7	-	-	-	17	-	-
MNCN62504	L	-	-	-	-	9	3.5	13.6	5.2	8.4	5.1	-	-	-	-	14	-	-	-

Table 3.6.5. – Measurements (mm) of isolated lower teeth of *Nyctereutes donnezani* from Layna.

Cat. N°			L	W	trm1 L	tdm1 W
MNCN62495	c	R	6.8	4.3	-	-
MNCN62497	c	R	6.8	4.3	-	-
MNCN62651	c	R	6.7	4.5	-	-
MNCN70008	c	L	6.6	4,5	-	-
MNCN70009	c	R	6.1	4.4	-	-
MNCN62621	p1	R	3.5	2.1	-	-
MNCN71085	p3?	R	7.1	3	-	-
MNCN62519	m1	R	17	6.3	11	6.3
MNCN62608	m1	L	6.7	-	-	-
MNCN62609	m1	R	6.8	-	-	-
MNCN71087	m1	R	16	6.7	11.7	6.4
MNCN62616	m2	R	7.6	5.2	-	-
MNCN62619	m2	L	8.6	5.7	-	-
MNCN70007	m3	L	4	3.7	-	-

Table 3.6.6 – Measurements (mm) of the forelimb bones of *Nyctereutes donnezani* from Layna.

Cat. N°	Element		Scapula		Humerus		Radius				Ulna	
			GLP	BG	Dp	Bd	Bp	Dp	Bd	Dd	DPA	BPC
MNCN62575	scapula	L	-	10.1	-	-	-	-	-	-	-	-
MNCN62576	scapula	R	19.3	10.7	-	-	-	-	-	-	-	-
MNCN62577	scapula	R	18.5	11.5	-	-	-	-	-	-	-	-
MNCN62632	scapula	L	21.6	13.1	-	-	-	-	-	-	-	-
MNCN62633	scapula	R	-	11	-	-	-	-	-	-	-	-
MNCN62634	scapula	R	18.6	12.2	-	-	-	-	-	-	-	-
MNCN62635	scapula	R	19.1	11.8	-	-	-	-	-	-	-	-
MNCN62503	humerus	L	-	-	25.5	-	-	-	-	-	-	-
MNCN69984	humerus	R	-	-	29.3	25.5	-	-	-	-	-	-
MNCN62502	humerus	L	-	-	-	20.4	-	-	-	-	-	-
MNCN62604	humerus	R	-	-	-	23.3	-	-	-	-	-	-
MNCN62631	humerus	R	-	-	-	22.2	-	-	-	-	-	-
MNCN62622/549	ulna	R	-	-	-	-	-	-	-	-	-	8.8
MNCN62623	ulna	R	-	-	-	-	-	-	-	-	16.7	11
MNCN70006	ulna	L	-	-	-	-	-	-	-	-	18.4	
MNCN62551	ulna	L	-	-	-	-	-	-	-	-	-	9.4
MNCN62552	ulna	L	-	-	-	-	-	-	-	-	17	
MNCN62553	ulna	R	-	-	-	-	-	-	-	-	-	9.8
MNCN62554	ulna	L	-	-	-	-	-	-	-	-	-	8.5
MNCN62555	ulna	R	-	-	-	-	-	-	-	-	-	7
MNCN13652	radius	R	-	-	-	-	12.1	7.7	-	-	-	-
MNCN70906	radius	L	-	-	-	-	13.2	8.5	-	-	-	-
MNCN13651	radius	R	-	-	-	-	12	8.4	-	-	-	-
MNCN13653	radius	R	-	-	-	-	-	-	17	9.6	-	-
MNCN13654	radius	L	-	-	-	-	-	-	15.1	8.6	-	-

Cat. N°	Element		Scapula		Humerus			Radius			Ulna	
			GLP	BG	Dp	Bd	Bp	Dp	Bd	Dd	DPA	BPC
MNCN70904_1	radius	L	-	-	-	-	-	-	15.3	9.8	-	-
MNCN70905	radius	L	-	-	-	-	-	-	16.7	10.3	-	-

Table 3.6.7 – Measurements (mm) of hindlimb bones of *Nyctereutes donnezani* from Layna.

Cat. N°	Element		Femur				Tibia		
			Bp	DC	Bd	Dd	Bp	Bd	Dd
MNCN52972	Femur	R		12	21.4	23.1			
MNCN62473/75	Femur	R	29						
MNCN62477	Femur	R		13.1					
MNCN62636	Femur	L	28.4	12.4					
MNCN62638	Femur	R		12.3					
MNCN62560	Femur	R			23.8	24.7			
MNCN62561	Femur	R			22.3	19			
MNCN62562	Femur	/			22.3	19			
MNCN62637	Femur	L			22.5	18.8			
MNCN62488	Tibia	L					26.2		
MNCN62490	Tibia	L					24.3		
MNCN62639	Tibia	L					25.9		
MNCN62485	Tibia	R						16	11.8
MNCN62487	Tibia	R						15.3	11.4

3.7. Preliminary results of the first phylogeny of the fossil and extant raccoon dogs

3.7.1. Context

In the fossil record, the diversity of the genus was higher than it is today, as during the Plio-Pleistocene up to ten species are known, from both Eurasia as well as Africa (see Bartolini Lucenti, 2018, fig. 1, p. 9). The phylogenetic relationships of all these species have never been tested by any cladistic analysis. In their pivotal work, Soria & Aguirre (1976) presented a dendrogram of the plausible affinities, based on their morphological study of the species known at the time. According to them, *Nyctereutes donnezani* (Depéret, 1890), the earliest raccoon dog of western Europe, was the first member of a phyletic lineage that included *Nyctereutes megamastoides* (Pomel, 1842) and *Nyctereutes vulpinus* Soria & Aguirre, 1976, whereas, in Asia, *Nyctereutes sinensis* (Schlosser, 1903) originated *N. procyonoides*. The description of *Nyctereutes tingi* Tedford & Qiu, 1991, the earliest recognised raccoon dog (Early Pliocene, Yushe Basin, China), led Tedford & Qiu (1991) to interpret this species as the ancestor of the later species of the Old World. This hypothesis is shared by many other scholars (*e.g.,*Monguillon et al., 2004; Geraads et al., 2010; Werdelin & Dehghani, 2011; Rook et al., 2017). Monguillon et al. (2004) proposed an alternative hypothesis for the origin of *N. vulpinus* from St. Vallier, deeming an origin from *N. tingi* more plausible than from the lineage *N. donnezani-N. megamastoides* (*sensu* Soria & Aguirre, 1976).

The relationships of the African taxa are more unclear, probably due to the scantiness and/or the fragmented nature of their record. Ficcarelli et al. (1984) related *Nyctereutes terblanchei* (Broom, 1948) from South Africa to *N. megamastoides* and *N. sinensis* for the similar development of some mandibular features (*e.g.,*the subangular lobe). Similarly, Argant (2004) pointed out some similarities of *Nyctereutes abdeslami* Geraads, 1997 from Morocco and other Eurasian taxa.

The enigmatic *Nyctereutes lockwoodi* Geraads et al., 2010 from Ethiopia seems to represent a separate taxon from most of the other *Nyctereutes* spp. Geraads et al. (2010) considered that *N. lockwoodi* could represent the ancestor of *N. terblanchei* or, in any case, that the former was related to the latter. Moreover, these authors did not exclude the ascription of *N. lockwoodi* to a different genus from *Nyctereutes* (Geraads et al., 2010). *Nyctereutes barryi* Werdelin & Dehghani, 2011 from Laetoli is referred to as an intermediated between the two earliest Eurasian taxa, i.e. *N. tingi* and *N. donnezani* (Werdelin & Dehghani, 2011). Lastly, the dubious taxon *Nyctereutes vinetorum* (Bate, 1937) is known only for a single specimen (see Kurtén, 1965) and it probably represents a large form of the extant *N. procyonoides* (Soria & Aguirre, 1976). Therefore, several issues of the evolutionary history of these canids remain unsolved.

Along with the problems introduced above, the sample of *N. donnezani* from Çalta (Turkey) has been separated from the typical *N. donnezani,* as Bartolini Lucenti et al. (2018) pointed out the dubious nature of its specific attribution. Recently, Zrzavý et al. (2018) carried out a phylogeny of Caninae, and included two species of *Nyctereutes* (i.e. the extant *N. procyonoides* and the fossil *N. lockwoodi*). In their resulting tree, the clade of the raccoon dog includes the problematic *Nurocyon chonokhariensis* Sotnikova, 2006. This configuration is rather surprising, considering all the features of the taxon from Chonokhariakh (Mongolia) which do not resemble any known Vulpini (as derived as it could be). Sotnikova (2006) described the latter taxon as hypocarnivorous, and she did acknowledge some similarities between *Nurocyon* and *Nyctereutes* (*e.g.,*short and robust P4, developed conules on M1). Nevertheless, the author also concluded that the apparently similar features represent a case of convergent evolution to the same dietary habit in two independent groups. The dental features of *Nurocyon* support the hypocarnivorous interpretation but the cranial ones clearly contrast with the diagnostic features of *Nyctereutes*, resembling more derived Canini (like *Eucyon* and especially *Canis*;

Sotnikova 2006; Sotnikova & Rook, 2010). Consequently, the result of Zrzavý et al. (2018), limited to this clade *Nyctereutes-Nurocyon*, should be taken with caution.

3.7.2. Methods

The maximum parsimony criterion was chosen for the purposes of this analysis, as it is considered one of the best ways to evaluate morphological character arrays (inter alios Spencer and Wilberg, 2013). The analysis was performed using TNT 1.5 (Goloboff and Catalano, 2015), based on 115 non-additive and 3 additive characters (111 of these concerned cranial, dentognathic and cerebral features and 9 postcranial ones; see Table 3.7.2 and character list in section 3.7.7.) and 14 taxa. The chosen outgroup is the North American, late Miocene Leptocyon vafer (Leidy, 1858). The latest phylogenies on Canidae are not unanimous with respect to the identity of the closest ally of *N. procyonoides* (see "Introduction" above), although a general consensus has been reached that it belongs to the tribe Vulpini. Several possible options were available for the choice of the outgroup, but a species of *Vulpes* was favoured over the genera *Urocyon* and *Otocyon*. *Urocyon* was excluded based on molecular phylogenetic analyses (*inter alios* Wayne and Ostrander, 2007; Agnarsson et al., 2010; Zhao et al., 2016; Zrzavý et al. 2018) indicating that the grey fox genus stems at the base of the Caninae tree; therefore, it is not closely related to *Nyctereutes*. In the literature, some scholars (*e.g.,*Wayne and Ostrander, 2007; Westbury et al., 2017) have pointed out the closeness between *Otocyon megalotis* (Desmarest, 1822) and *Nyctereutes* within the Vulpini. These analyses show *Otocyon* as the sister taxon of the clade composed of *Nyctereutes* and *Vulpes*. *Otocyon* is characterised by the presence of possible homoplasies shared with *Nyctereutes* (*e.g.,*development of the subangular lobe) and numerous autopomorphies (*e.g.,*the supernumerary number of molars, see Clark, 2005). Some scholars (*e.g.,*Poe and Wiens, 2000; Sereno, 2007) have pointed out that

homoplasies should be avoided when selecting the various types of characters. For the present purposes, this "general rule" suggests caution in the use of *Otocyon* as an outgroup. *Leptocyon vafer* (Leidy, 1858), was preferred over other members of the subfamily Caninae for several reasons, including its basal position to the radiation of Vulpini and Canini (Tedford et al. 2009; Zrzavy et al., 2018); for the presence of several plesiomorphic features, despite being one of the latest taxon of its genus; the relative abundance and satisfactory state of preservation of its fossil record. In addition to this outgroup, two other non-*Nyctereutes* taxa were included. The Late Miocene *Metalopex macconnelli* Tedford et al., 2009 as representative of the genus *Metalopex* Tedford and Wang, 2008, a group of fox-like canids of doubtful affinities. *V. stenognathus* was chosen for its basal position among the species of *Vulpes* as one of the oldest of the genus (Tedford et al., 2009); and its retention of plesiomorphic features among *Vulpes* spp.

The heuristic search was performed using Tree Bisection Reconnection (TBR) algorithm on 99999 random addition replicates to retrieve the highest number of most parsimonious trees. All the characters were treated as unordered for the purposes of this analysis. The default "collapse all zero length tree branches" ("rule 1") option was used to avoid biases due to the high number of "presence/absence" characters (Brazeau, 2011). After generation of the strict consensus tree, the absolute decay (Bremer) index was plotted onto it. The bootstrap was calculated using the tree resulting from the strict consensus technique for the cut-off, setting 99999 replicates and absolute frequencies as options.

The freeware program Mesquite 3.6 was used to obtain the Consistency Index (CI), the Retention Index (RI) and the Tree Length (TL). .

3.7.3. Results

Only two most parsimonious trees (MPTs) were produced by the analysis, from which a strict consensus tree (CI= 0.5595, RI= 0.6021, TL= 252) with collapse

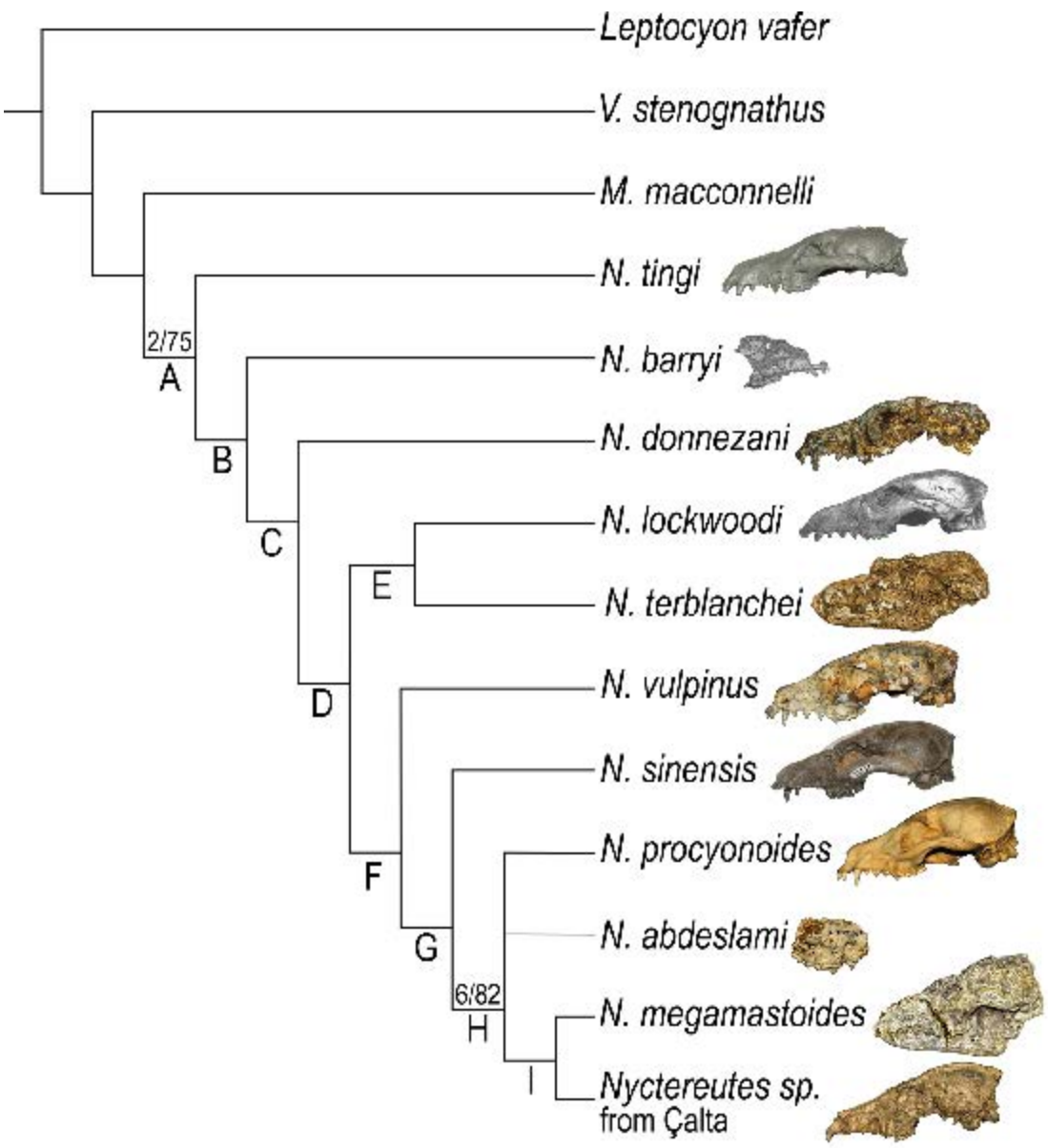

Figure 3.7.1 – Strict consensus tree resulting from the two MPTs. Each node is labeled with a capital letter. Values above the node indicate the absolute decay (Bremer) support and the bootstrap, respectively.

all zero length branches ("rule 1") was generated to have a more supported result. The cladogram (Fig. 3.7.1) shows two major clades of *Nyctereutes,* as well as a polytomy of three taxa.

The root of the strict consensus tree has the following traits (excluding those that are logically incompatible): NCL/FL < 80%; uncertain length of the nasals; V-shaped nasofrontal suture; caudal margin of the infraorbital foramen located

above P3 and inclined rostrodorsally-caudoventrally; U-shaped maxillofrontal suture; zygomatic bone of uncertain shape but with a width between 51 and 56%; zygomaticomaxillary suture with a markedly caudal-oriented notch; low and gently ventral margin of the zygomatic arch; uncertain position of frontal process of the zygomatic bone; frontal sinus absent; depression on the dorsal surface of the zygomatic process of frontal present but not marked; uncertain presence of rugosity on the surface of the parietals; interparietals markedly expanded or rostrally expanded; parasagittal ridges fused rostrally to the frontoparietal suture; mesial margin of the orbit over the distal half of the P4; uncertain position of the external occipital protuberance in lateral view; uncertain morphology of the occipital region in lateral view; reduced nuchal crest with uncertain development; reduced nuchal tubercles; crest-like mastoid process; ovoidal and wide acoustic meatus; reduced difference between height of the acustic meatus and that the bulla; large and caudally expanded paracondylar processes, arched in medial view and fused for all their length with the bulla; medially compressed and elongated palatine fissures; sutura palatina transversa markedly concave caudally and with the rostral margin approximately at level of the P4 paracone or protocone; uncertain presence of accessory foramina palatina; the palate ends at the level of the end of the toothrow; nasal process of the palatine absent; bilobed or rectangular caudal margin of the palatines; ECW/PL under 34%; uncertain shape of the hammulus; uncertain shape of the medial walls of the bullae; uncertain canine morphology; upper premolars compressed buccolingually and elongated distally; the mesial mental foramen under p1 or between p1–p2 and the distal one under p3 or the distal part of p3; caudal border of the mandibular symphysis under p2 or between p2 and p3; uncertain height of the ventral border of the mandibular condyle; uncertain morphology of the condyloid process; coronoid process long at base relative to dorsoventral height; subangular lobe absent; thin and hook-shaped or enlarged dorsoventrally angular process; scar of the m. pterygoideus

medialis with a larger superior fossa compared to inferior one; curved horizontal ramus; mesial margin of the ascending ramus distally inclined; uncertain shape of the scars of the medial m. masseter; uncertain presence of diastema between I2 and I3; no diastema between P2–P3; slightly advanced protocone in P4; marked embayment of the mesial margin in P4; the paracone in P4 is larger mesiodistally compared to the metastyle; upper molars larger lingually than mesiodistally; M1 metacone shorter mesiodistally compared to paracone and parastyle together; metaconule of the M1 reduced at its base compared to the protocone; markedly curved distal notch of M1; reduced mesial cingulum of M1; L/W ratio of the M2 <85%; M2 paracone larger than the metacone; protoconule on M2 absent; crest-like metaconule on M2; M2 postprotocrista present and connected to metaconule; relative upper grinding area between 0.836 and 0.987; the diastema between p1–p2 absent; diastema between p2–p3 present; presence of diastema between p3–p4; uncertain length of the sectorial part of the m1; talonid narrow compared to, or as wide as, the trigonid in m1; m1 entoconid separated from the hypoconid; crown height of the m1 talonid much lower than trigonid cuspid; absence of a transverse cristid connecting talonid cuspids; m1 hypoconid much larger than the entoconid; m1 entoconulid absent; distal basin of the talonid distally open; m1 hypoconulid absent; relative lower grinding area between 0.604 and 0.923; small mesiobuccal cingulum of the m2; paraconid of m2 absent; small m2 paraconid; m2 metaconid smaller than the protoconid; entoconid of m2 absent; m2 mesoconid absent; absence of distal accessory cuspulids on m3; cingulid on m3 absent; uncertain morphology of the prorean gyrus of the cerebrum; pentagonal or heart-shaped outline of the coronal and ansate sulci on dorsal side of the cerebrum; expanded and jutting cranially medial outline of the distocranial border of the distal epiphysis of the humerus; expanded development of the scar of the m. ulnaris medialis on the medial epicondyle of the humerus; the scars of the m. flexor carpi and of the m. flexor digitorum lie craniodistally to that of the m. pronator teres or at the

cranial tip of the distal epiphysis; rounded and well differentiated capitulum of the distal articulation of the humerus; uncertain extension of the lateral epicondyle of the humerus; uncertain development of the interosseous margin of the ulna craniolaterally; lower or slightly lower height of the greater trochanter of the femur related to the height of its head; uncertain cranial morphology of the tibial shaft; uncertain shape of the notch in the distal articulation of the tibia in lateral view; well-developed distal process of the medial malleolus.

Node A (Fig. 3.7.1) represents the speciation event that leads to all the branch of the *Nyctereutes* phylogenetic tree. It is identified by 5 synapomorphies: (1) infraorbital margin of the zygomatic bone with dorsal border thickened and no lateral flare; (2) distinctly rugose surface of the parietals; (3) rostral margin of the *sutura palatina transversa*; (4) low-crowned canines and (5) reduced difference in height between m1 trigonid and talonid.

Node B (Fig. 3.7.1) is a clade comprising *N. barryi*, *N. abdeslami* and the Eurasian group of species of *Nyctereutes*. It is identified by two synapomorphies: (1) caudal border of the mandibular symphysis under the p2 and (2) m1 talonid as wide as the trigonid.

N. donnezani is placed at the base of the Eurasian clade s. l. and the African one, stemming from the node C (Fig. 3.7.1). The node includes tree synapomorphies: (1) presence of the subangular lobe; (2) presence of a diastema between P2 and P3 and (3) presence of a diastema between p2 and p3.

The following node D (Fig. 1) is identified by seven synapomorphies: (1) low and gently curved ventral margin of the zygomatic arch; (2) very high ventral border of the mandibular condyle; (3) straight ventral margin of the horizontal ramus; (4) mesial margin of the ascending ramus straight vertical; (5) presence of diastema between I2 and I3; (6) reduced mesial margin of the P4 and (7) presence of a cingulid on m3.

Node E (Fig. 1) is a clade including *N. lockwoodi* and *N. terblanchei*; it comprises

two synapomorphies: (1) presence of M2 metaconule and (2) absence of the M2 postprotocrista.

N. vulpinus is located at the base of a more derived clade of *Nyctereutes* (Fig. 1). The node F from which this species branches is defined by six synapomorphies: (1) presence of the frontal sinus; (2) acoustic meatus reduced compared to bulla height; (3) paracondylar process directed ventrally and parallel to the distal border of the bulla in lateral view; (4) M2 postprotocrista connected to metacone; (5) trm1L/m1L <64% and (6) relative lower grinding area between 0.924 and 1.243.

The following clade (node G, Fig. 1) includes *N. abdeslami*, *N. procyonoides*, *N. megamastoides*, *N. sinensis* and *Nyctereures* sp. from Çalta. The clade is identified by nine synapomorphies: (1) rostroventral-caudodorsal inclined infraorbital foramen; (2) strong depression on the dorsal surface of the zygomatic process; (3) mesial margin of the orbit over the M1; (4) external occipital protuberance at level of occipital condyles; (5) ovoidal and reduced acoustic meatus; (6) shortened mesiodistally upper premolars; (7) m1 entoconid similar in size to hypoconid; (8) m1 distal basin of the talonid closed by the distal cingulid and (9) presence of accessory cuspulids on m3.

Node H (Fig. 1) comprises *N. abdeslami*, *N. procyonoides* and the common ancestor of *N. megamastoides* and *Nyctereutes* sp. from Çalta. It is identified by sixteen synapomorphies (the largest number of the entire tree): (1) caudal margin of the infraorbital foramen above the mesial root of P4; (2) Zyg/CBL between 57 and 59%; (3) frontal sinus slightly developed caudally to the zygomatic process of the frontals; (4) distally enlarged palatine fissures; (5) diastema between P2-P3 absent; (6) subquadrate upper molars; (7) reduced difference between buccal cuspids of M1; (8) enlarged M1 metaconule; (9) M1 straight distal notch; (10) cuspule-like M1 mesial cingulum; (11) ratio between length and width of the M2 >85%; (12) M2 paracone similar in size to the metacone; (13) presence of the protoconule on M2; (14) tubercular metaconule on M2; (15) 73 relative upper grinding area

between 0.988 and 1.139 and (16) presence of a transverse cristid connecting talonid cuspids on m1.

Finally, the node I (Fig. 1) places *N. megamastoides* and *Nyctereutes* sp. from Çalta in a sister taxa relationship with the following five synapomorphies: (1) interparietals limited to the distal portion of the occipital region; (2) reduced paracondylar process; (3) expanded subangular are; (4) I2-I3 diastema absent and (5) much lower m1 talonid crown height than trigonid.

3.7.4. Systematic Paleontology

Order **Carnivora** Bowdich, 1821

Suborder **Caniformia** Kretzoi, 1943

Family **Canidae** Fischer, 1817

Subfamily **Caninae** Fischer, 1817

Tribe **Vulpini** Hemprich & Ehrenberg, 1832

Genus ***Nyctereutes*** Temminck, 1838

Type species. *Canis viverrinus* Temminck, 1838

Synthetic differential diagnosis of the genus. The genus includes all the Vulpini more closely related to *Nyctereutes procyonoides* than to *Metalopex macconnelli*, *Otocyon megalotis* or *Vulpes vulpes.* Rugose surface of the parietals unlike *Canis, Lupulella*, and *Vulpes*; absence of lateral flare on the infraorbital margin of the zygomatic bone, unlike *Otocyon* and *Vulpes*; low-crowned canines unlike *Canis*, *Lupulella*, and *Vulpes*; absence of supernumerary molars as in *Otocyon*; incipient or developed subangular lobe, unlike *Canis*, *Lupulella*, and *Vulpes*.

***Nyctereutes* sp. nov.**

(Fig. 3.7.2)

Type locality. Çalta (Turkey).

Age. Early Pliocene - MN15 (ca 4.0 Ma).

Diagnosis. Large-sized raccoon dog. Fairly rostrocaudally elongated cranium, with strong postorbital constriction, reduced development of frontal sinus and with nuchal crest jutting caudally. Reduced *diastemata* for the premolars. P4 protocone slightly mesially positioned, with a reduced but evident mesial embayment on the P4. Squared occlusal morphology of M1; paracone larger than metacone; prominent cusp-like and developed M1 mesial cingulum; M1 talon expanded lingually. Buccolingually short M2; metacone smaller than paracone; postprotocrista incomplete. Stout mandible horizontal ramus, with scaphoid ventral margin. Poorly developed subangular region. The m1 talonid slightly larger than trigonid; transverse cristid connecting the hypoconid and entoconid; entoconulid present. Enlarged m2, with a prominent paraconid and large protoconid; evident entoconid and accessory cuspulids on the lingual side.

Holotype. MNHN.F.ACA291, cranium with left P4 and right C, P4–M2.

Referred material. MNHN.F.ACA292, cranium with left I3, P4–M2 and right I3, M1–M2; MNHN.F.ACA298, left maxillary fragment with P4; MNHN.F.ACA296, left M1; MNHN.F.ACA297, right M1; MNHN.F.ACA355, left M1; FSL 212806, hemimandible fragment with p4; MNHN.F.ACA294, right hemimandible with p4–m2; MNHN.F.ACA295, right hemimandible with c–p3; MNHN.F.ACA387, right hemimandible with m1–m2; MNHN.F.ACA548, right hemimandible with m1; MNHN.F.ACA549, right hemimandible with p2–m3. *Lower teeth*. MNHN.F.ACA299, left c; MNHN.F.ACA300, right c*;* MHNH.F.ACA386, III cervical vertebra; MHNH.F.ACA550, fragment of right radius; MHNH.F.ACA551, fragment of right radius; MHNH.F.ACA301, left astragalus.

Description and Comparison. A schematic list of the differences between *Nyctereutes* from Çalta and other species of the genus here considered is given in Table 3.7.1. In section 3.6. a comparison of the dental proportions of the Eurasian species was carried out. The morphometric analysis shows that the sample from Çalta differs from the Chinese species (*i.e.*, *N. tingi* and *N. sinensis*), as its pattern of dental ratios follows that of *N. megamastoides* (Fig. 3.6.9). Ginsburg (1998) ascribed this Turkish taxon to *N. donnezani*. Indeed, some of its morphologies fit in this interpretation, although some others do not. In dorsal view, the rostrocaudal elongation of the cranium resembles that of *N. tingi* of the Yushe Basin and Megalo Emvolon, *N. donnezani* from Perpignan and Layna and *N. lockwoodi* from Dikika. *N. tingi* and *N. donnezani* possess the parasagittal ridges with a reduced medially concave outline in dorsal view, in contrast to those of *Nyctereutes* sp. from Çalta. The development of these marked ridges in the latter taxon is more similar to *N. megamastoides*, *N. procyonoides, N. sinensis*, and *N. vulpinus* for the marked curvature visible in dorsal view. The zygomatic processes of the frontal of *Nyctereutes* from Çalta are prominent, slender and round-pointed, similar to those of *N. megamastoides*, *N. sinensis*, and *N. vulpinus*, unlike the sharp and shorter ones of *N. procyonoides* and *N. tingi*. The postorbital constriction distal to these processes is more marked compared to *N. tingi*, *N. sinensis* and *N. vulpinus*. *N. megamastoides* and *N. procyonoides* share with *Nyctereutes* from Çalta the strong notch between the zygomatic process of the frontal and the rostral part of the braincase. *Nyctereutes* sp. from Çalta has a greatly reduced frontal sinus, comparable to that of *N. megamastoides*. The dorsal surface of the zygomatic process possesses a shallow depression, similar to the condition of *N. sinensis*. The caudal enlargement of the nuchal crest and its lateral extension beyond the level of the condyles characterize the distal part of the cranium of *Nyctereutes* sp. from Çalta. *N. tingi*, *N. sinensis* and *N. vulpinus* possess a similar

Table 3.7.1 – Resuming list of characteristics possessed by *Nyctereutes* nov. sp. from Çalta as opposed to other *Nyctereutes*.

	A	B	*N. eludens*	*N. abdeslami*	*N. barryi*	*N. donnezani*	*N. lockwoodi*	*N. megamastoides*	*N. procyonoides*	*N. sinensis*	*N. terblanchei*	*N. vulpinus*	*N. tingi*
Rostrocaudal elongation of the cranium	present	reduced	A	-	-	A	A	B	B	B	-	B	A
Parasagittal ridges	developed and marked	reduced, medially concave outline in dorsal view	A	-	-	B	B	A	A	A	-	A	B
Zygomatic process of the frontal	prominent and round-pointed	sharp pointed	A	-	-	-	A	A	B	A	-	A	B
Postorbital constriction	promimently marked	less marked	A	-	-	-	-	A	A	B	-	B	B
Nuchal crest, distal projection	beyond the level of occipital condyles	at level or sligthly beyond the condyles	A	-	-	-	A	A	B	A	-	A	B
Ventral outline of the mandible corpus	scaphoid	straight	A	B	A	A	A	B	B	B	B	B	A
Development of the subangular lobe	reduced	developed	A	B	A	b	b	B	B	B	B	B	A
Mesial embayment of P4	absent or reduced	developed	A	A		B		A	A	B	-	B	B
M1 parastyle and mesiobuccal cingulum	pointy	rounded	A	A	B	B	B	A	A	A	-	A	A
Occlusal morphology M1	subsquared	buccally elongated	A	A	B	B	B	A	A	A	-	A	
M1 metaconule	large-based cusp	small-size cusp	A	A		B	A	A		A	-		B
Mesial cingulum of M1	cuspule-like	reduced or simple	A	A	B	B	B	A	A	B	-	B	B
M1 talon	lingually expanded	not expanded	A	A	B	B	B	B	B	B	B	B	B
M2 postprotocrista reaching metaconule	no	yes	A	A	B	A	B	A	A	B	-	B	A
p2 and p3 distal cingulid and accesory cuspulid	absent	present	A	B	B	A	-	B	A	A	A	A	B
m1 talonid	enlarged	as wide as trigonid	A	A	B	B	B	A	A	A	A	A	B
Cristid transversa	present	generally absent	A	A	B	B	B	A	A	B	B	B	B

condition, although less prominently jutting caudally. This morphology is close to that of *N. megamastoides*. *Nyctereutes* sp. from Çalta possesses a scaphoid outline of the ventral margin of the mandible. This shape is shared with *N. donnezani*, *N. tingi* and *N. lockwoodi*. Even *N. barryi* has a dorsoventrally arched ventral margin, although the horizontal ramus is proportionally more slender and shallower when compared to *Nyctereutes* sp. from Çalta. The subangular region of the mandibular specimens from Çalta is partially preserved and does not offer clear evidence of its morphology, but it clearly shows a modest enlargement of this area and a poorly developed curvature. Compared to the coeval species, *N. tingi* and *N. barryi*, *Nyctereutes* from Çalta possesses a comparable scarce development of the subangular lobe. By contrast, *N. donnezani*, from both Perpignan and Layna, shows a subangular region characterised by a more marked bone swelling and a more pronounced ventral concavity in the rostroventral area of the angle. The degree of development of this region of *Nyctereutes* sp. is greatly reduced when compared to the later species (*N. abdeslami*, *N. megamastoides*, *N. sinensis*, *N. vulpinus* and *N. procyonoides*).

The major peculiarities of *Nyctereutes* sp. from Çalta lie in its dental morphology. The P4 protocone is moderately separated from the tooth and its mesial side lies at level of the mesial margin of the tooth or slightly beyond it. This morphology contrasts to that of the other *Nyctereutes*, with the exception of *N. barryi*. *Nyctereutes* sp. from Çalta shows a slightly developed embayment on the mesial side of the P4, unlike those of *N. megamastoides* and *N. abdeslami*, which do not have it. Nevertheless, the development of this notch is not as marked as that visible in *N. tingi*, *N. sinensis*, *N. vulpinus* or even *N. donnezani*. The first upper molar possesses several peculiarities. *N. tingi*, *N. megamastoides*, *N. sinensis* and *N. vulpinus* share with

Figure 3.7.2 – *Nyctereutes* sp. nov. from Çalta. **A-C**: **MNHN.F.ACA292**, cranium in dorsal (**A**), ventral (**B**), and lateral (**C**) views. **D-F**: **MNHN.F.ACA291**, cranium in dorsal (**D**), ventral (**E**), and lateral (**F**) views. **G-I**: **MNHN.F.ACA-549**, right hemimandible in buccal (**G**), lingual (**H**), and occlusal (**I**) views.

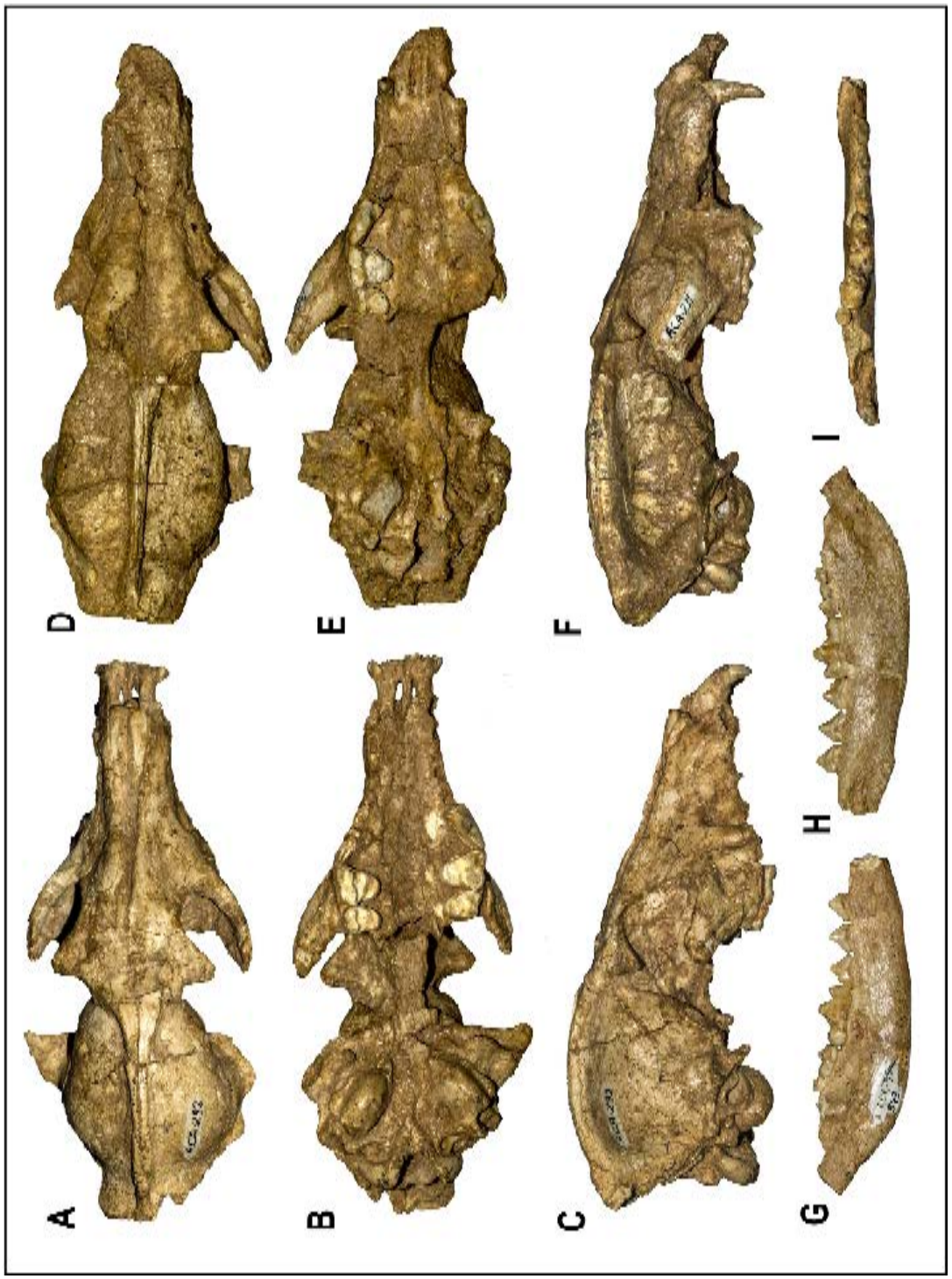
A
B
C
D
E
F
G
H
I

Nyctereutes sp. from Çalta the presence of a prominent M1 parastyle and a pointy mesiobuccal corner. *N. donnezani* and *N. lockwoodi* have a rounded mesiobuccal margin of the M1, yet with different shapes. *N. abdeslami* shows a sharp-edged mesiobuccal corner but a reduced parastyle. The occlusal morphology of the M1 of the sample from Çalta is almost squared, as the mesial side of the trigon (*i.e.*, paracone and metacone) and the lingual portion of the trigon (*i.e.*, the level of the protocone and metaconule) are similar in size, with a lobed distolingual expansion made by the high and well developed hypocone (Fig. 3.7.3.3.). This morphology contrasts with that of *N. tingi*, in which the M1 is elongated buccolingually; it possesses a mesiodistally narrow portion at its midpoint level and is only slightly curved distally. The European *N. donnezani* possesses a buccolingually shorter M1 compared to *N. tingi*, in occlusal view. The M1 metaconule of *Nyctereutes* sp. from Çalta has a large base, larger than that of *N. donnezani*, but similar to *N. abdeslami*, *N. lockwoodi*, *N. megamastoides* and *N. sinensis*. One of the most evident features of the M1 of *Nyctereutes* sp. from Çalta is the development of the mesial cingulum. The enlargement is present in other species (as pointed out in section 3.6.), with a variable degree of prominence: from *N. donnezani* and *N. vulpinus*, in which it is present but not very conspicuous, to *N. abdeslami* and *N. megamastoides*, where it juts mesially and possesses cusp-like folds of the enamel (see Fig. 3.7.3). The M1 specimens from Çalta shows this expansion of the mesial cingulum with cusp-like structures, less prominent mesially than in *N. megamastoides* or *N. abdeslami*, but unlike the simple condition of *N. donnezani*, *N. sinensis* and *N. vulpinus*. The M1 talon expands lingually (Fig. 3.7.3), in contrast to other *Nyctereutes*. Only *N. abdeslami* is close to this morphology. The M2 metaconule of *Nyctereutes* sp. from Çalta is fairly evident on the distal side of the tooth, in occlusal and distal views, but the postprotocrista is incomplete or tends to stretch towards the base of the metacone. Among *Nyctereutes*, the M2 postprotocrista generally fails to reach the metaconule, with the exception of *N. lockwoodi*, *N. sinensis* and *N. vulpinus*. The

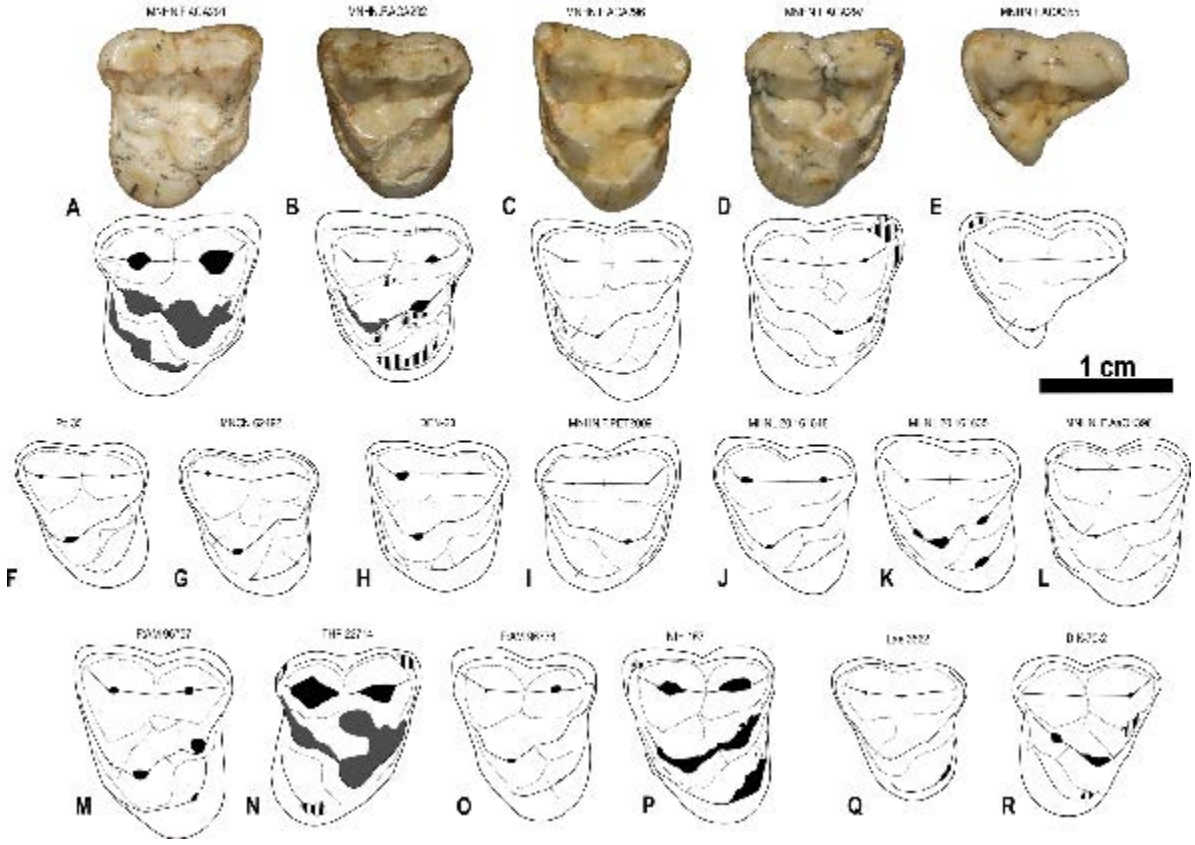

Figure 3.7.3 – Schematic comparison of the M1 in several *Nyctereutes* spp. **A-E**: *Nyctereutes* sp. nov. from Çalta (Turkey), **A**: **MNHN.F.ACA291**, right M1; **B**: **MNHN.F.ACA292**, left M1; **C**: **MNHN.F.ACA296**, left M1; **D**: **MNHN.F.ACA297**, right M1; **E**: **MNHN.F.ACA355**, fragmented left M1. **F-G**: *Nyctereutes donnezani*, **F**: **Pp 35**, left M1 from Perpignan (France); **G**: **MNCN 62492**, left M1 from Layna (Spain). **H-I:** *Nyctereutes megamastoides*, **H**: **DFN-20**, left M1 from Dafnero-1 (Greece); **I**: **MNHN.F.PET2009**, right M1 from Perrier-Les Etouaires (France). **J-K**: *Nyctereutes vulpinus* from St. Vallier (France), **J**: **MHNL 20.161635**, left M1; **K**: **MHNL 20.161648**, left M1. **L**: *Nyctereutes abdeslami* from Ahl al Oughlam (Morocco), **MNHN.F.AaO934**, right M1. **M-N**: *Nyctereutes tingi* from Yushe Basin (China), **M**: F:AM 96757, left M1; **N**: THP 22714, right M1. **O-P**: *Nyctereutes sinensis*, **O**: F:AM 96778, left M1 from Yushe Basin (China); **P**: NIH 167, left M1 from Nihewan Basin (China). **Q**: *Nyctereutes barryi* from Laetoli (Tanzania), **Lae 3562**, left M1. **R**: *Nyctereutes lockwoodi* from Didika (Ethiopia), **DIK-70-2**, right M1.

second and third lower premolars do not show any accessory distal cuspulids or a cingulid bounding the distal margin of the tooth, unlike *N. barryi*, *N. tingi* and *N. megamastoides* and resembling *N. donnezani*, *N. sinensis* and *N. vulpinus*. The m1 is stout, with a relatively enlarged distal portion compared to the trigonid one, similar

to that of *N. abdeslami*, *N. megamastoides*, *N. sinensis*, *N. terblanchei* and *N. vulpinus,* in which the talonid is as large as the trigonid or even larger buccolingually. Unlike *N. barryi*, *N. donnezani*, *N. terblanchei*, *N. tingi* or *N. sinensis*, *Nyctereutes* sp. from Çalta possesses a marked transverse cristid between the hypoconid and the entoconid of the m1. This evident connection between the talonid cuspids is unusual for *N. barryi*, *N. donnezani*, *N. terblanchei*, *N. tingi* or *N. sinensis*, whereas it is often found in the m1 of the extant *N. procyonoides* and of the fossil *N. abdeslami* and *N. megamastoides*.

3.7.5. Discussions

3.7.5.1. Phylogenetic analysis and biogeographic implications

In the literature, the "evolution" of the hypotheses regarding the centre of origin of raccoon dogs followed the description of new species. In their pivotal work, Soria & Aguirre (1976) identified Western Europe as the centre of origin of the Eurasian *Nyctereutes*. Apart from the record of Venta del Moro, recently reassessed and considered to represent a member of *Eucyon* Tedford & Qiu, 1996 (see Montoya et al., 2009; Rook, 2009), the records of *N. donnezani* from Perpignan and Layna (Neogene Mammal Zone, MN15) were the oldest then known. After the description by Tedford & Qiu (1991) of *N. tingi* from the localities of the MN14–15, East Asia was selected as the "cradle" of *Nyctereutes*. Much evidence argues in favour of this hypothesis, such as: the evolutionary history of the Canidae confined to North America (Tedford et al., 2009); the dispersal events into Asia began in late Miocene times and involved only a few taxa (Wang and Tedford, 2008); the absence of North American taxa of the tribe Vulpini showing affinity with (or similarity to) *Nyctereutes*. The recent description of a late Messinian member of *Nyctereutes* (*Nyctereutes*? sp.) in Lissasfa, Morocco by Geraads (2011), from a single maxillary fragment with damaged P4 and M1 apparently complicates the scenery. Nevertheless, its attribution remains doubtful, at both a specific and a generic

level. Some of the features possessed by the taxon from Lissasfa (*e.g.,* markedly large-based P4 paracone; the position of the infraorbital foramen very close to the rostral margin of the orbit; and the outline of the zygomaticomaxillary suture, in lateral view) cannot be found in other *Nyctereutes* spp. These morphologies resemble those of the specimens of *Lupulella mohibi* Geraads, 2011 from Sidi Abderrahmane (Morocco), which is related to the lineage of extant side-striped and black-backed jackals. Note, however, that this site is much younger than Lissasfa. These considerations cast doubts on the interpretation of this fossil as a *Nyctereutes* and of its reliability as evidence of a latest Miocene raccoon dog in Africa.

From the present cladistic analysis, all the species of *Nyctereutes* cluster in a monophyletic clade separated from Miocene Vulpini and Vulpini-like taxa *e.g., V. stenognathus* and *M. macconnelli*. This configuration has significant meaning for the biogeography of the Plio-Pleistocene *Nyctereutes*. Our analysis seems to support the idea of Tedford & Qiu (1991), as *N. tingi* stems at the base of the clade of the raccoon dogs, thus confirming its primitiveness recognized by many authors. Its first record comes from the deposits of the Yushe Basin (China), dated around 5.3–4.8 Ma (Tedford & Qiu, 1991), and it is up to now the oldest recorded species of the whole genus. The position of *N. barryi* in Fig. 3.7.1 confirms the hypothesis of Werdelin & Dehghani (2011), who deemed *N. barryi* to be an intermediate between *N. tingi* and *N. donnezani*. Indeed, the characteristics possessed by the African species are suggestive of basal position among *Nyctereutes*, probably resulting from an early dispersion of primitive, *N. tingi*-like raccoon dog from Eurasia into the African continent. *N. donnezani*, which supposedly derived from *N. tingi* (Tedford & Qiu, 1991), in our analysis apparently diverged within the *Nyctereutes* clade after the first dispersal event in Africa. The differences between this species and *N. tingi* (*e.g.,* the development of the subangular lobe and of the angular process, and the m2 entoconid) do not support a direct ancestor-descendant relationship between

them. The fairly primitive morphology possessed by *N. lockwoodi* (as described by Geraads et al., 2010) is confirmed by the position close to *N. donnezani*. Interestingly, our result supports the close relationship between *N. lockwoodi* and *N. terblanchei*, proposed by Geraads et al. (2010), but contrasts with the authors' hypothesis of a possible different generic attribution for *N. lockwoodi*. The two African species cluster together in clade within the lineage of *Nyctereutes* (Fig. 3.7.1). The position of such clade suggest that these species arose as the result of a second dispersion event from Eurasia into Africa subsequent to that of *N. barryi*. Recently, Reynolds (2012) questioned whether *N. terblanchei* belongs to *Nyctereutes*. Some of the arguments supporting such conclusion appear unsatisfactory, for instance treating some features as intraspecific variability (*e.g.,*development of the subangular lobe, inclination of the rostral side of mandibular ramus) rather than diagnostic features; or the biometric comparison between phylogenetically distant taxa of Canidae. The resulting consensus tree rules out the possibility of a reclassification of *N. terblanchei* to a different genus, confirming the view of Ficcarelli et al. (1984). A general consensus in the literature (*inter alios* Tedford & Qiu, 1991) appears to consider *N. tingi* as the ancestor of the morphologically derived *N. sinensis*. Nonetheless, the consensus tree shows a great distance between the two species and indicates a different origin for the latter. In Fig. 3.7.1, *N. vulpinus* is located between *N. donnezani* and *N. sinensis*. This imply that a fairly primitive taxon, yet unrecorded in the fossil record, might be the common ancestor of the *N. vulpinus* and *N. sinensis* lineages (see node F, Fig. 3.7.1). From a stratigraphic point of view, *N. sinensis* is more ancient than *N. vulpinus*, since the first known remains of the former are late Early Pliocene in age (ca 4.0 Ma, Yushe Basin, China), whereas the latter is recorded in Early Pleistocene (ca 2.3 Ma, Saint-Vallier, France). , *N. vulpinus* shows an array of characters typical of more ancient species (*e.g.,*a crest-like mastoid process, a relevant difference between the m1 hypoconid and entoconid and the absence of distal accessory cuspids

on the m3), which suggests a divergence from an older species of *Nyctereutes*, probably similar to *N. donnezani*. Monguillon et al. (2004) proposed two different hypotheses for the origin of *N. vulpinus* from St. Vallier, namely, from a taxon of the lineage *N. donnezani-N. megamastoides* (*sensu* Soria & Aguirre, 1976) or from the lineage of *N. tingi* (Monguillon et al., 2004: S187). The present analysis favours the former proposition. Moreover, *N. vulpinus* is regarded here as a species that diverged earlier than *N. sinensis* in the clade of Eurasian *Nyctereutes*. The relatively limited Early Pliocene fossil record of the genus may explain this pattern. One possible explanation is that *N. vulpinus* was derived from a species that retained fairly archaic traits and dispersed to Europe from the East. In any case, a close relationship between *N. sinensis* and *N. vulpinus* is evident from the analysis. *N. abdeslami*, *N. megamastoides*, *Nyctereutes* sp. from Çalta, and the extant species *N. procyonoides* are members of a clade characterised by derived features, *e.g.,*subquadrate upper molars and the presence of the *crista transversa* on the m1. Note that this clade is the most strongly supported and reliable on the tree (bootstrap value= 82; decay value= 6, Fig. 3.7.1). In literature, Argant (2004) proposed a possible affinity of the Earliest Pleistocene Moroccan species *N. abdeslami* to the other Eurasian species. This species appears to be markedly separated from the other African species (i.e. *N. barryi*, *N. lockwoodi* and *N. terblanchei*), resulting in its inclusion in the same clade with the extant raccoon dog and the widespread Eurasian *N. megamastoides*. This evidence suggests that *N. abdeslami* was probably a Eurasian taxon that dispersed in Africa during the Pliocene. *N. megamastoides* and *N. procyonoides* are confirmed as morphologically derived species, with the former with more apomorphies compared to the latter. Despite the long hiatus in the Asian record, the extant *N. procyonoides* is considered to be derived from *N. sinensis* (Soria & Aguirre, 1976; Tedford & Qiu, 1991). The present analysis suggests an alternative: *N. procyonoides* may have derived from the same Asian taxon close to *N. sinensis* that gave origin to *N. abdeslami* and the common ancestor of *Nyctereutes*

from Çalta and *N. megamastoides*. Therefore, although the relationship between the two species (*N. procyonoides* and *N. sinensis*) remains, the latter is unlikely to be the direct ancestor of the former.

The results of the analysis on the sample from Çalta confirms the morphometric and morphologic data, which contrast with the attribution in literature (Ginsburg, 1998). Besides the presence of a few primitive characters (*e.g.,*the rostrocaudal elongation of the cranium and the development of the subangular lobe on the mandible), the cladistic analysis reveals that it belongs to the group of most derived *Nyctereutes*. By far the closest relationship seems to be with *N. megamastoides* than to any other member of the genus. The combined evidence of the morphometric analyses, the morphological features and phylogenetic reconstruction support the attribution of the sample from Çalta to a new species. The affinities of *Nyctereutes* sp. from Çalta fit in the pattern outlined by the most recent discovery from western Europe. In the Spanish site of Layna (MN15), Bartolini Lucenti et al. (2018) recognised a *N. megamastoides*-like taxon that coexisted alongside the primitive *N. donnezani*. This morphologically derived sample from Layna was excluded from the present cladistic analysis due to the limited number of specimens and their as yet uncertain specific attribution. Nevertheless, the combined evidence resulting from the two sites of Layna and Çalta (which are roughly coeval, respectively, at 3.91 Ma, Domingo et al., 2013, and 4.0 Ma, Bernor & Sen, 2017) favours the hypothesis of an earlier appearance and dispersion of morphologically derived forms of *Nyctereutes* in the western part of Eurasia than previously proposed. This is consistent with the eastern Eurasian record of the first occurrence of morphologically derived species, which appeared in China in the Early Pliocene (see Tedford & Qiu, 1991), and supports the pattern of westward expansion and radiation across Eurasia.

3.7.5.2. Chronological implications

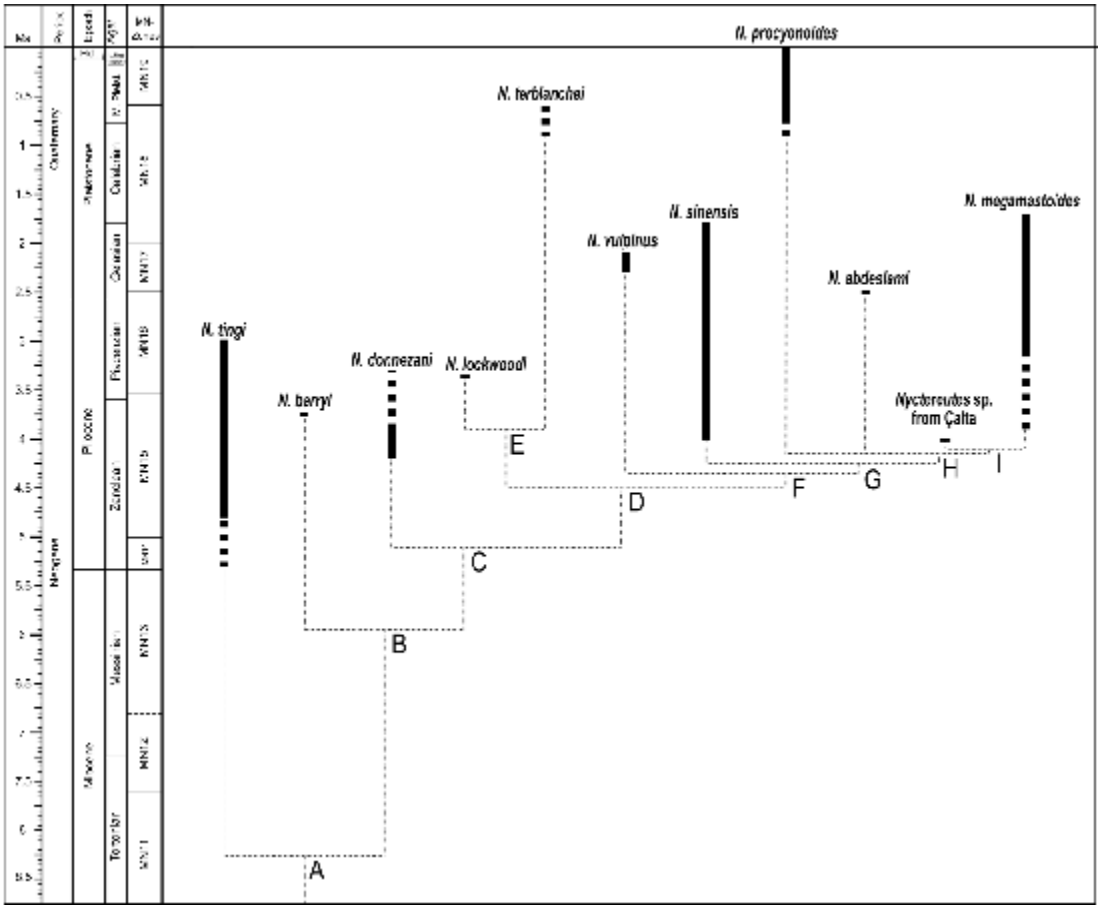

Figure 3.7.4 – Chronogram obtained from the strict consensus tree. Time scale follows Hilgen et al. (2012). Solid lines represent the reliable distribution of a taxon, whereas dashed ones the uncertainty of their exact chronostratigraphic dating. The pproposed divergency times were estimated to minimize the ghost lineages.

The cladogram was projected on a time scale to get a better understanding of the divergence times between the resulting clades (Fig. 3.7.4). The origin of the phyletic lineage of *Nyctereutes* could be parsimoniously individuated in the MN9, during the late Tortonian. The first members of this lineage should be derived from a primitive member of the Vulpini tribe, probably not very much different from the earliest members of the *Vulpes* genus. The last common ancestor of all known *Nyctereutes* probably lived in the MN11 (Late Miocene) (Fig. 3.7.4, node A). Nevertheless, no *Nyctereutes* fossils from as early as the late Tortonian are known, either in Eurasia or in North America. Notably, the presence of an early fox was reported in Africa ca. 7 Ma (de Bonis et al., 2007). These findings testify to the

passage of Beringia by the Old-World foxes before MN13. The common ancestor of *Nyctereutes* could have had some derived features, *e.g.,*low-crowned canines, clearly rugose surface of parietals, incipient development of a subangular lobe (see the description of node A in "Results" for the complete list). Considering that the oldest known *Nyctereutes* is *N. tingi* from the earliest Pliocene of the Yushe Basin, the hypothesis of an upper Miocene origin for the genus seems highly plausible. The lineage of *N. barryi* (node B, Fig. 3.7.4) originated around 6 Ma, in the upper Messinian. As noted above, other Vulpini dispersed to Africa during the MN13, so a dispersal to Africa of a primitive *Nyctereutes*-like species in the latest Miocene is likely. The Zanclean was a time of radiation for the genus as possibly the majority of its lineages arose in this period (Fig. 3.7.4). This is confirmed by several authors (e.g., Tedford & Qiu, 1991; Bartolini Lucenti, 2018). The lineage of *N. donnezani* diverged from other *Nyctereutes* much later in the early Zanclean (MN14; node C, Fig. 3.7.4). The early Zanclean (MN14) originated the subclade of *N. lockwoodi* and *N. terblanchei* (node D, Fig. 3.7.4), whereas the divergence between them might have occurred in the MN15 (node E, Fig. 3.7.4). The longest ghost lineage in the evolutionary history of the Eurasian *Nyctereutes* is that which led to *N. vulpinus*. This species probably diverged in the late Zanclean stage (MN15; node F, Fig. 3.7.4). Nonetheless, remains of *N. vulpinus* are not known until the Gelasian stage (MN17), ca. 2.3 Ma. This implies a hidden history of this species of slightly less than 2 Myr. The clades including *N. sinensis* and the more derived species diverged in the latest M14-earliest MN15 (node G, Fig. 3.7.4) and 4.2 Ma (node H, Fig. 3.7.4), respectively. Finally, the clade formed by *N. megamastoides* and *Nyctereutes* sp. from Çalta is parsimoniously dated to have diverged around 4.1 Ma, in MN15. These data agree with the pattern of dispersal that emerged from the identification of *Nyctereutes* cf. *megamastoides* from Layna (Spain), as explained above.

3.7.5.3. Ecomorphological implications

The evolutionary history of the genus *Nyctereutes* was marked by the acquisition of features adapted to a hypocarnivorous and generalist diet (see *inter alios* Soria & Aguirre, 1976; Ward & Wurster-Hill, 1990; Tedford & Qiu, 1991; Bartolini Lucenti et al., 2018), as also confirmed by the present analysis (Fig. 3.7.1). Several cranial and dentognathic characteristics are involved in this process. Some cranial features include the rostrocaudal elongation of the cranium and the development of the sagittal crest, insertion point of the *m. temporalis*. One the most prominent and renown *Nyctereutes* characteristics is the morphology of the angular and subangular regions of the mandible. The area is fundamental in the masticatory mechanics as several muscles are inserted on this area: the *mm. digastricus*, *masseter*, and *pterygoideus medialis* (Gaspard, 1964; Evans & Lahunta, 2013). The latter are attached to the angular process, laterally the *m. masseter* and medially the *m. pterygoideus medialis*, while the *m. digastricus* inserts on the subangular region of the mandibular corpus. These muscles, together with the *m. temporalis*, acts antagonistically to open (*m. digastricus*) and close (*mm. masseter*, *pterygoideus*) the mouth. Thus, changes in the anatomy of the angular and subangular regions affect the efficiency of chewing, enabling the exploitation of diverse food items. Extant *N. procyonoides* possesses a marked subangular lobe, more developed compared to other living canids, with the exception of *Otocyon megalotis* (Gaspard, 1964). Unlike *Otocyon*, *N. procyonoides* possesses a dorsoventrally enlarged and knob-like angular process, thus, with larger insertion areas for the *mm. masseter* and *pterygoideus medialis*. This implies different chewing capabilities (Ward & Wuster-Hill, 1990; Macdonald, 2001), as opposed to the insectivorous *Otocyon* (see Clark, 2005). According to several authors (*inter alios* Soria & Aguirre, 1976; Tedford & Qiu, 1990), such set of hypocarnivorous dentognathic features was acquired by *Nyctereutes* during the evolutionary history of the genus. Indeed, the oldest taxon, *N. tingi*, shows several primitive features suggestive of a modest hypocarnivorous diet, such as reduced sagittal crest, hook-shaped angular process, absence of a

subangular lobe, mesiodistally elongated molars. The earliest appearance of the subangular lobe, although reduced, is in *N. donnezani*. This species, as opposed to *N. tingi*, also shows deeper angular processes and larger molars. *N. barryi*, the oldest species of the African record, has several dentognathic features shared with *N. tingi*, although it possesses buccolingually shorter M1 and proportionally larger talonid of the m1. Clearly derived species, like *N. megamastoides* and *N. sinensis*, are characterized by the prominent subangular lobe, the enlarged angular process and the wider upper and lower molars. The enlargement of the molars is fundamental for an efficient hypocarnivorous diet: the increase of the crushing surface guarantees the access to a wider range of foods. Asahara & Takai (2016) showed that subtle differences in the diet of extant and fossil canids (and particularly raccoon dogs) could be detected with the molar ratio method. Indeed, tendencies to hypocarnivory are not only expressed by larger area of the lower molars *per se*, rather by the ratio between the areas of the m2 and of that of the m1. Differences between extant populations and between the extant and the fossil species of *Nyctereutes* has been pointed out (Asahara, 2014; Asahara & Takai, 2016; section 3.5.-3.6.). Fig. 3.7.5 shows the values of some of the species considered in the phylogenetic analysis (the lower carnassial of *N. lockwoodi* are unknown). Of all fossil *Nyctereutes*, *N. tingi* has the lowest molar ratio (=m2/m1) value but the largest occlusal surface of the m1, as expected by its large size (Fig. 3.7.5). Considering its morphological features, this position fits with the interpretation of a modest hypocarnivory compared to the other fossil *Nyctereutes*. The only exception is *N. vulpinus*. Indeed, the phylogenetically close *N. barryi* and *N. donnezani* (Fig. 3.7.1) are considerably smaller compared to *N. tingi* but both their molar indices are larger compared to the latter, implying a larger grinding surface and a more hypocarnivorous diet. In the case of *N. barryi*, this difference is not connected with the acquisition of other dentognathic features among which, primarily, the subangular lobe (see Werdelin & Dehghani, 2011). On the contrary, in *N. donnezani*, the larger m2/

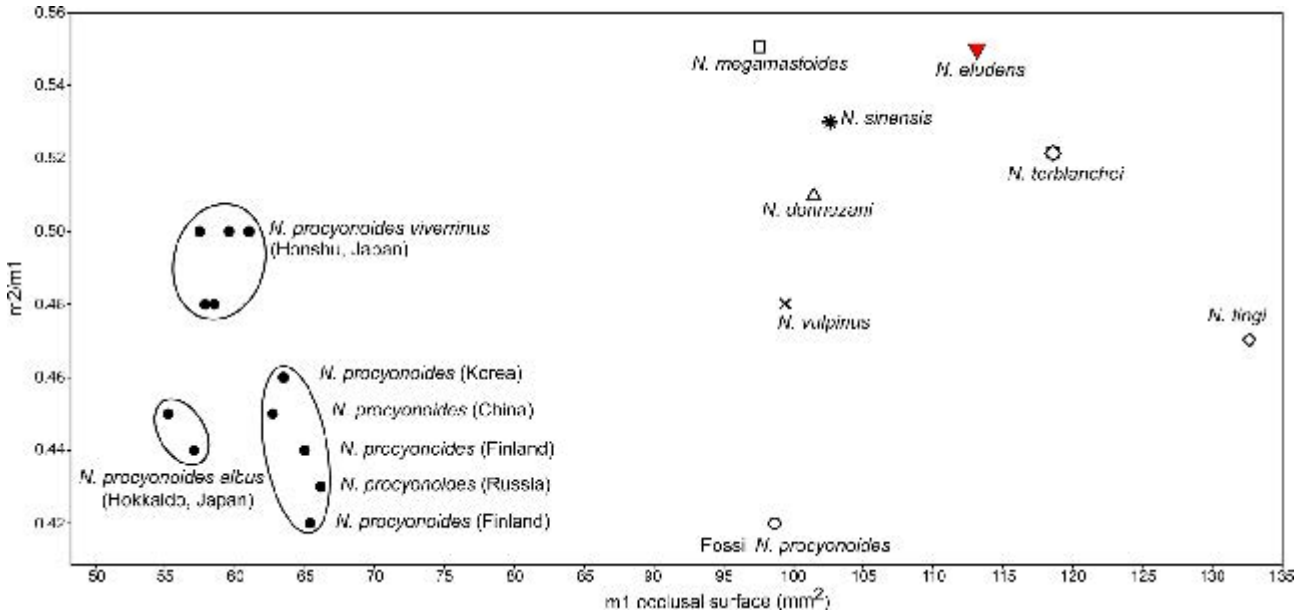

Figure 3.7.5. Biplot of the m2/m1 scores against the m1 occlusal surface (in mm²) in various species and subspecies of *Nyctereutes*. Fossil species are represented by average values. Black circles represent extant taxa; asterisk represents *N. sinensis* from the Yushe Basin (China) [n=22]; open square represents *N. megamastoides* (from Kvabebi, Georgia and Senéze, France) [n=5]; X represents *N. vulpinus* from St. Vallier (France) [n=8]; open triangle represents *N. donnezani* (from Perpignan, La Gloria 4 and Layna) [n=7]; plus represent N. barryi from Laetoli (Tanzania) [n=3] diamond represents *N. tingi* from Yushe Basin (China) [n=4]; square represents *N. abdeslami* from Ahl al Oughlam (Morocco) [n=3]; starry diamond represents *N. teblanchei* from South Africa [n=6]; red inverse triangle represent *Nyctereutes* nov. sp. from Çalta [n=3]. Updated from section 3.5 and 3.6.

m1 value is also supported by the presence of a modest subangular lobe, a deeper angular process, and the incipient enlargement of the upper and lower molars (Figs. 3.7.3 and 3.7.5). Therefore, the difference between the *N. barryi* and *N. tingi*, both primitive in their morphologies, testify to specific dietary preferences or even adaptations to distinct habitat conditions between Earliest Pliocene northern Chinese environments and the late Early Pliocene East African ones. Among the derived species of the Eurasian clade (Fig. 3.7.1), *N. abdeslami* and *N. vulpinus* have peculiar molar index value. Although retaining a developed subangular lobe, comparable to that of *N. sinensis*, *N. vulpinus* possesses the lowest m2/m1 value of the morphologically-derived fossil species (Fig. 3.7.5), suggestive of a more

carnivorous diet compared to *N. megamastoides* and *N. sinensis*. This is confirmed by the presence of several dental features (e.g., the relatively longer upper and lower premolars and lower carnassial and reduced m2, see Soria & Aguirre, 1976). Interestingly, the angular process of *N. vulpinus* appears relatively reduced and hooked compared to the knob-like shape possessed by *N. sinensis* and particularly *N. megamastoides*. *N. abdeslami* possesses the highest ratio of the genus. As Asahara & Takai (2016) noted, such high molar ratios can nowadays be found only in *Vulpes pallida* (Cretzschmar, 1827) and in *O. megalotis*, respectively mainly herbivorous (Sillero-Zubiri, 2004) and insectivorous (Clark, 2005). This implies that, like these two extant taxa, *N. abdeslami* might have been a strongly hypocarnivorous species, more adapted than the other raccoon dogs to a diet mainly composed of vegetables matter, invertebrates and, rarely, small vertebrates. The other Pliocene-early Early Pleistocene species of Eurasia (*Nyctereutes* sp. nov. from Çalta, *N. megamastoides* and *N. sinensis*) show a higher degree of hypocarnivory compared to the primitive species. Besides their different morphology of the subangular region, *Nyctereutes* sp. nov. from Çalta and *N. megamastoides* possess the highest values of the molar ratio, supporting their close phylogenetic affinity (Fig. 3.7.1). Of the African clade, *N. terblanchei* has comparable values of the molar index to *N. barryi*, although possessing a subangular lobe and a rather enlarged angular process.

The combined results of the molar ratio method and the phylogenetic analysis applied to the fossil species reveals some interesting patterns of characters. The dental features appear to change at a different rate as opposed to mandibular and cranial ones. As already pointed out by Asahara & Takai (2016), dental features, such as the molar ratio, represent principally dietary adaptations, whereas the development of craniomandibular characteristics appears to be a phylogenetic signal. This interpretation is consistent with the pattern discussed above, particularly of *N. barryi* and *N. vulpinus*.

3.7.6. Conclusions

The present paper reports the first cladistic analysis of a large dataset of fossil species of *Nyctereutes* coming from more than thirty sites across the Old World. The analysis is based on 118 cranial, dentognathic, cerebral and postcranial characters on 11 species of *Nyctereutes*, and with *L. vafer* as an outgroup. The analysis revealed that raccoon dogs form a distinctly monophyletic clade. The basal position of *N. tingi* in the clade confirms as the most basal and most primitive species of the genus. At the same time, the resulting tree excludes the hypotheses that *N. tingi* is the ancestor of either *N. sinensis* (as proposed by Tedford & Qiu, 1991) or *N. vulpinus* (as suggested by Monguillon et al., 2004). Similarly, the position of *N. barryi* confirms the observation of the Werdelin & Dehghani (2011) as intermediate between *N. tingi* and *N. donnezani*. The early differentiation of *N. barryi* represent the first event of dispersion of the genus from Eurasia into Africa, whereas that of *N. donnezani* testifies to the westward expansion across Eurasia. A second event of dispersion into Africa is recorded in the analysis by the clade that comprises *N. lockwoodi* and *N. terblanchei*. Although *N. vulpinus* and *N. sinensis* appear to be quite related to one another, although the first record of *N. sinensis* precedes that of *N. vulpinus* by nearly 2 Myr. The most supported cluster of the analysis is the crown group, which comprises *N. abdeslami*, *N. procyonoides*, *Nyctereutes* sp. from Çalta and *N. megamastoides*. The high number of synapomorphies of the cluster testifies to the derived state of these species. Although *N. procyonoides* and *N. sinensis* remain related to one another, the results refute the idea of a direct derivation for anagenesis of these species. The inclusion of *N. abdeslami* in this crown group implies that the species evolved in Eurasia and subsequently dispersed into North Africa (supporting the observations made by Argant, 2004). The record of Çalta is strikingly peculiar. Described as *N. donnezani*, the evidence of the morphometric similarities shown in setion 3.6. challenges this former attribution. Considering the complex pattern of morphological features retained by *Nyctereutes* from Çalta

(described here for the first time in detail), and the results of the phylogenetic analysis, a new species is proposed here for this sample. Considering the supposed divergence times of the various species of the genus *Nyctereutes*, the evolutionary history of this group is clearly still poorly known, especially in Mio-Pliocene times.

3.7.7. Appendix

3.7.7.1. List of cranial, dentognathic, cerebral and postcranial characters

Cranial:

1) Ratio between the neurocranium and the facial length (NCL/FL) (modified from Zrzavý et al., 2018): (0) <80%; (1) >80%.
2) Nasal length, caudal margin (modified from Tedford et al., 1995; see Fig. 3.7.6): (0) short or at level of the frontomaxillary suture; (1) long, usually extends posteriorly beyond the frontomaxillary suture.
3) Nasofrontal suture outline, in dorsal view (modified from Prevosti, 2010; see Fig. 3.7.6): (0) U-shaped; (1) V-shaped.
4) Position of the caudal margin of the infraorbital foramen, in lateral view (modified from Berta, 1988; see Fig. 3.7.7): (0) above the P3; (1) between P3-P4; (2) above the P4.
5) Inclination of the infraorbital foramen, in lateral view (modified from Zrzavý et al., 2018; see Fig. 3.7.7): (0) rostrodorsal-caudoventral; (1) vertical; (2) rostroventral-caudodorsal. Ordered.
6) Maxillofrontal suture outline, in dorsal view (modified from Prevosti, 2010; See Fig. 3.7.6): (0) U-shaped; (1) angled outline (L-shaped).
7) Infraorbital margin of the zygomatic bone (modified from Tedford et al., 1995; see Fig. 3.7.8): (0) lateral flare and eversion of the dorsal margin; (1) no lateral flare and dorsal border thickened.
8) Ratio between the zygomatic width and the condylobasal length (Zyg/CBL) (modified from Zrzavý et al., 2018): (0) 51-56%; (1) 57-59%.
9) Zygomaticomaxillary suture outline, in lateral view (modified from Tedford et al., 2009; see Fig. 3.7.7): (0) poorly marked caudal embayment; (1) straight

rostrodorsal-caudoventral line; (2) marked caudal oriented notch.

10) Ventral margin of the zygomatic arch, in lateral view (modified from Tedford et al., 1995; see Fig. 3.7.7): (0) dorsally or rostrodorsally arched; (1) low and gently curved outline.

11) Frontal process of the zygomatic bone: (0) absent; (1) present.

12) Frontal process of the zygomatic bone (see Fig. 3.7.7): (0) on the zygomatic process of the temporal; (1) on the zygomatic bone.

13) Frontal sinus (modified from Tedford et al., 1995; see Fig. 3.7.9): (0) absent; (1) present.

14) Caudal development of the frontal sinus (modified from Tedford et al., 1995; see Fig. 3.7.9): (0) poorly developed; (1) slightly developed caudally to the zygomatic process of the frontals. To score characters 17 and 18, Berta (1988) and Tedford et al. (1995) criterion to assess development of the sinus were followed, with no need to dissect the skull.

15) Depression on the dorsal surface of the zygomatic process of the frontal: (0) present; (1) absent;

16) Development of the depression on the dorsal surface of the zygomatic process of the frontal (see Fig. 3.7.10): (0) not extended on the dorsal surface of the zygomatic process; (1) strong and covering dorsal surface of the process.

17) Rugose surface of the parietals (modified from Zrzavý et al., 2018): (0) no or little rugosity; (1) distinctly rugose.

18) Interparietals (see Fig. 3.7.11): (0) extremely expanded; (1) expanded rostrally; (2) limited to the distal portion of the occipital region.

19) Shape of parasagittal ridges: (0) straight; (1) lyre-shaped;

20) Point of fusion of the parasagittal ridges, in dorsal view (see Fig. 3.7.9): (0) rostral to the frontoparietal suture; (1) at level of the frontoparietal suture; (2) caudal to the frontoparietal suture. Ordered.

21) Mesial margin of the orbit (modified from Prevosti, 2010): (0) over the mesial half of P4; (1) over the distal half of the P4; (2) over the M1.

22) Position of the external occipital protuberance, in lateral view (modified from Tedford et al., 1995; see Fig. 3.7.12): (0) rostral to the level of occipital condyles;

(1) at level of occipital condyles; (2) extends caudally compared to the occipital condyles.

23) Morphology of the occipital region, in lateral view (see Fig. 3.7.12): (0) convex caudally; (1) vertical or slightly concave caudally; (2) concave caudally.

24) Development of the nuchal crest, in caudolateral view (see Fig. S8): (0) low; (1) high.

25) Caudal expansion of the nuchal crest (see Fig. 3.7.13): (0) reduced; (1) jutting.

26) Nuchal tubercles (see Fig. 3.7.12): (0) reduced; (1) prominently developed.

27) Mastoid process, in lateral view (modified from Tedford et al., 1995): (0) crest-like; (1) enlarged, ridge-like; (2) enlarged, knob-like.

28) Morphology and development of the acoustic meatus (see Fig. 3.7.14): (0) ovoidal and wide;; (1) round and wide; (2) ovoidal and reduced.

29) Difference between the height of the acoustic meatus and that of the bulla (Modified from Berta, 1988; see Fig. 3.7.14): (0) reduced; (1) acoustic meatus reduced compared to bulla height.

30) Extension in rostrocaudal sense of paracondylar processes, in lateral view (modified from Tedford et al., 1995; see Fig. 3.7.14): (0) caudally expanded (angle >15°); (1) mostly ventral, but with a gentle posterior inclination that forms a small angle (ca. 15°) with the distal border of the tympanic bulla; (2) directed ventrally and parallel to the distal border of the bulla in lateral view.

31) Paracondylar processes (modified from Tedford et al., 1995; see Fig. 3.7.14): (0) large, expanded caudally; (1) reduced.

32) Curvature of the medial wall of the paracondylar processes, in ventral view (modified from Tedford et al., 1995; see Fig. 3.7.15): (0) arched, with medial concavity; (1) sigmoidal, with large base.

33) Level of fusion of the paracondylar processes and the bulla (modified from Prevosti, 2010; see Fig. 3.7.14): (0) free tip; (1) fused for all its length.

34) Palatine fissures, in ventral view (modified from Tedford et al., 1995; see Fig. 3.7.16): (0) mediolaterally compressed and elongated; (1) distally enlarged.

35) *Sutura palatina transversa*, rostral margin (see Fig. 3.7.17): (0) approximately at level with P4 paracone; (1) at level with P4 protocone; (2) at level with P4

metastyle.

36) *Sutura palatina transversa*, outline in ventral view (see Fig. 3.7.17): (0) marked caudal concavity; (1) reduced curvature, larger caudal concavity.

37) Accessory *foramina palatina*: (0) absent; (1) present.

38) Palate length, caudally (modified from Zrzavý et al., 2018; see Fig. 3.7.17): (0) end at level to the end of the toothrow; (1) extends beyond the end of the toothrow.

39) Nasal process of the palatine (see Fig. 3.7.17): (0) absent; (1) present.

40) Outline of the caudal margin of the palatines (see Fig. 3.7.17): (0) arched, with caudal concavity; (1) bilobed, caudal concavity; (2) rectangular.

41) Rostrum width/palatine length ratio (ECW/PL) (modified from Zrzavý et al., 2018): (0) <34%; (1) >34%.

42) Hammulus (see Fig. 3.7.18): (0) parallel to the sagittal plane; (1) convergent medially.

43) Medial walls of the bullae: (0) convergent; (1) parallel.

44) Canines morphology (modified from Zrzavý et al., 2018): (0) high crowned, thin; (1) low crowned.

45) Upper premolars, in occlusal view (modified from Tedford et al., 2009): (0) compressed buccolingually and elongated distally; (1) tend to be shortened mesiodistally.

46) Mesial and distal mental *foramina* (see Fig. 3.7.19): (0) the mesial under p1 and the distal under p3; (1) the mesial between p1-p2 and the distal under p3; (2) the mesial under p1 and the distal under the distal part of p3; (3) the mesial between p1-p2 and the distal under the distal part of p3; (4) one foramen, mesial under p1.

47) Mandibular symphysis, caudal border (see Fig. 3.7.20): (0) between p2 and p3; (1) under the p2.

48) Height of the ventral border of the mandibular condyle (modified from Tedford et al., 1995; see Fig. 3.7.19): (0) high, at level of the tip of the trigonid of the m1; (1) very high, well beyond the tip of the trigonid of the m1.

49) Condyloid process: (0) slender and short mediolaterally; (1) deep and large

mediolaterally.

50) Coronoid process (modified from Zrzavý et al., 2018): (0) long at base relative to dorsoventral height; (1) short at base relative to dorsoventral height.

51) Subangular lobe: (0) absent; (1) present.

52) Development of subangular lobe (modified from Tedford et al., 1995): (0) not prominent; (1) marked.

53) Subangular area, in lateral view (see Fig. 3.7.19): (0) short dorsoventrally subangular lobe; (1) expanded dorsodistally.

54) Curvature of the subangular area, rostroventral to the angular process (see Fig. 3.7.19): (0) poorly marked concavity; (1) very marked concavity.

55) Angular process (modified from Tedford et al., 1995; see Fig. 3.7.19): (0) thin and hook-shaped and elongated; (1) thin and hook-shaped and short; (2) enlarged dorsoventrally knoblike, deep.

56) Outline of the rami of the m. *pterygoideus medialis*, on the medial side of the angular process (modified from Tedford et al., 1995; see Fig. 3.7.21): (0) larger superior fossa compared to inferior one; (1) similar sizes of the fossae; (2) inferior fossa larger or confluent.

57) Morphology of the horizontal ramus (see Fig. 3.7.19): (0) curved, scaphoid ventral margin; (1) straight ventral margin.

58) Mesial margin of the ascending ramus: (0) distally inclined ($\alpha > 90°$); (1) straight vertical ($\alpha \approx 90°$).

59) Scars of the medial *m. masseter* (modified from Zrzavý et al., 2018): (0) expanded rostrally on the lateral surface of the mandible; (1) narrow and uniform width on the lateral surface of the angular process.

60) I2–I3 diastema (modified from Tedford et al., 1995): (0) I2–I3 in contact (diastema absent); (1) present.

61) I3 medial cusp: (0) absent, (1) present

62) Diastema between P2-P3: (0) absent; (1) present.

63) Position P4 protocone: (0) slightly advanced; (1) advanced; (2) on the medial side of the tooth.

64) Outline of the mesial margin of P4, in occlusal view (see Fig. 3.7.22): (0) marked

embayment; (1) tend to be reduced; (2) straight margin (no embayment).

65) Relative size of the P4 paracone in comparison to the P4 metastyle, in occlusal view (see Fig. 3.7.22): (0) the paracone is larger mesiodistally compared to the metastyle; (1) reduced difference between the paracone and the metastyle or paracone shorter that the metastyle.

66) Morphology of upper molars (modified from Zrzavý et al., 2018; see Fig. 3.7.23): (0) larger buccolingually than mesiodistally; (1) elongated lingually and variably curved distally; (2) subquadrate.

67) M1 metacone: (0) shorter mesiodistally compared to paracone and parastyle together; (1) reduced difference between buccal cuspids of M1.

68) Size of the M1 metaconule, in occlusal view (see Fig. 3.7.23): (0) marked basal area differences compared to the protocone; (1) enlarged, reduce basal difference compared to the protocone.

69) Distal notch of the M1 (modified from Zrzavý et al., 2018; see Fig. 3.7.23): (0) markedly curved; (1) straight.

70) Mesial cingulum M1: (0) absent; (1) present.

71) Mesial cingulum M1 (see Fig. 3.7.23): (0) reduced; (1) prominent; (2) cuspule-like.

72) Ratio between length and width of the M2 (L/W) (modified from Zrzavý et al., 2018): (0) < 85%; (1) > 85%.

73) Size of the M2 paracone: (0) larger than the metacone; (1) similar to metacone.

74) Presence of the protoconule on M2 (modified from Prevosti, 2010): (0) absent; (1) present.

75) M2 metaconule: (0) absent; (1) present.

76) Shape of metaconule on M2: (0) crest-like; (1) tubercular.

77) M2 postprotocrista: (0) present; (1) absent.

78) Development M2 postprotocrista (see Fig. 3.7.24): (0) connected to metaconule; (1) incomplete; (2) connected to metacone.

79) Relative upper grinding area (modified from Zrzavý et al., 2018): (0) 0.836-0.987; (1) 0.988-1.139.

80) Development of diastema between p1-p2: (0) well developed; (1) reduced.

81) Diastema between p2-p3: (0) absent; (1) present.

82) Diastema between p3-p4: (0) absent; (1) present.

83) Length of the sectorial part of the m1, expressed as ratio between the length of the trigonid and the total length of the m1, (trm1L/m1L) (modified from Zrzavý et al., 2018): (0) > 64%; (1) < 64%.

84) Size of the m1 talonid (modified from Wang et al., 1999; see Fig. 3.7.25): (0) narrow relative to the trigonid; (1) as wide as the trigonid; (2) wider than the trigonid.

85) Development m1 entoconid (see Fig. 3.7.26): (0) separated from the hypoconid; (1) enlarged, tend to coalesce with hypoconid.

86) Crown height of the m1 talonid (see Fig. 3.7.27): (0) much lower than trigonid cuspid; (1) relatively high compared to trigonid, reduced difference in height.

87) Transverse cristid connecting talonid cuspids (see Fig. 3.7.26): (0) absent; (1) present.

88) Development m1 hypoconid and entoconid (see Fig. 3.7.26): (0) hypoconid larger compared to entoconid (approximately 2 times larger); (1) reduced difference, with the entoconid similar to hypoconid.

89) Entoconulid on m1 (as in Prevosti, 2010): (0) absent; (1) present.

90) Distal basin of the talonid (see Fig. 3.7.26): (0) distally open; (1) closed by distal cingulum.

91) Hypoconulid of the m1 (modified from Tedford et al., 1995; see Fig. 3.7.26): (0) absent; (1) present.

92) Relative lower grinding area (modified from Zrzavý et al., 2018): (0) 0.604-0.923; (1) 0.924-1.243.

93) m1 protostylid (Tedford and Wang, 2008): (0) absent; (1) present.

94) Mesiobuccal cingulum of the m2 (modified from Tedford et al., 1995; see Fig. 3.7.28): (0) small, only on the mesial part of the protoconid; (1) large expansion buccally.

95) Paraconid of the m2 (modified from Tedford et al., 2009): (0) absent; (1) present.

96) Development of the m2 paraconid: (0) small; (1) enlarged.

97) Metaconid of the m2 (modified from Berta, 1988): (0) smaller than the protoconid; (1) similar to the protoconid in size.

98) Entoconid of the m2 (see Fig. 3.7.28): (0) absent; (1) present.

99) m2 protostylid (Tedford & Wang, 2008): (0) absent; (1) present.

100) Development of entoconid of the m2 (modified from Tedford et al., 1995; see Fig. S23): (0) cristid-like lingual margin; (1) distinct cuspulid; (2) divided in two or more cuspulids.

101) m2 mesoconid (modified from Zrzavý et al., 2018): (0) absent; (1) present.

102) m2 talonid (Tedfrod & Wang, 2008): (0) short; (1) elongated distally.

103) Accessory cuspulids on m3: (0) absent; (1) present.

104) Cingulid on m3 (modified from Zrzavý et al., 2018): (0) absent; (1) present.

105) Morphology of m3 cingulid: (0) ridge-like; (1) cuspulid-like.

106) m3 talonid (modified from Tedford & Wang, 2008): (0) absent; (1) present.

107) Prorean gyrus of cerebrum (Lyras & Van der Geer, 2003): (0) small; (1) elongated bilaterally compressed.

108) Outline of the coronal and ansate *sulci* on dorsal side of the cerebrum (Lyras & Van der Geer, 2003): (0) pentagonal; (1) heart-shaped; (2) parenthesis-like; (3) orthogonal.

Postcranial:

109) Medial outline of the distocranial border of the distal epiphysis of the humerus (see Fig. 3.7.29): (0) expanded, jutting cranially; (1) L-like shape.

110) Development of the *m. ulnaris medialis* scar on the medial epicondyle of the humerus (see Fig. 3.7.30): (0) expanded; (1) reduced.

111) Position of the scar of the *m. pronator teres* related to the scar of the carpal and digital flexor muscles on the distal portion of the humerus (modified from Hildebrand, 1954; see Fig. 3.7.31): (0) the scars of *m. flexor carpi* and of the *m. flexor digitorum* lies craniodistally to that of the *m. pronator teres*; (1) the facet of *m. flexor carpi* and *flexor digitorum* at the cranial tip of the distal epiphysis; (2) the scars lies distally to the scar of the *pronator teres*.

112) Shape of the capitulum of the distal articulation of the humerus (modified from Prevosti, 2010; see Fig. 3.7.32): (0) rounded and well differentiated from the rest of the articulation; (1) less differentiated and more depressed.

113) Lateral epicondyle of the humerus: (0) expanded; (1) reduced.

114) Development of the interosseous margin of the ulna craniolaterally: (0) well

developed and jutting laterally; (1) poorly developed and no jutting laterally.

115) Height of the greater trochanter of the femur related to the height of its head (modified from Prevosti, 2010): (0) lower; (1) slightly lower; (2) approximately of the same height.

116) Tibial shaft: (0) curvature only in the proximal part; (1) sigmoid shape in cranial view.

117) Shape of the notch in the distal articulation of the tibia in anterior view (modified from Prevosti, 2010; see Fig. 3.7.33): (0) narrow and deep; (1) enlarged and deep; (2) enlarged and shallow.

118) Distal process of the medial malleolus: (0) well developed; (1) reduced.

3.7.7.2. Data matrix

see next page

Table 3.7.2 – Matrix of the 115 cranial, dentognathic, and postcranial characters used for the cladistic analysis on fossil and extant *Nyctereutes*.

	1	2	3	4	5	6	7	8	9	10	1	2	3	4	5	6	7	8	9	20	1	2	3	4	5	6	7	8	9	30	1	2	3	4	5
L. vafer	?	0	0	0;2	0;1;2	0	0	0	0	1	0	?	0	?	0	0	0	0	0	2	0	0	0	0	0	0	0	1	0	0	0	0	0	?	0
M. macconnelli	1	0	1	0	0	0	0	?	?	?	?	?	0	?	0	1	0	1	1	2	1	2	1;2	0;1	0	0	0	?	?	?	?	?	?	?	0
V. stenognathus	0	0	?	0	0	0	0	0	2	0	1	0	0	?	0	0	0	0	0	0	1	0	0	0	0	0	0	1	0	0	0	0	1	0	0
N. procyonoides	1	1	1	2	1	1	1	1	1	1	1	1	1	0	0	1	1	1	0	2	2	1	1	1	1	1	1	2	1	2	0	0	1	1	1
N. abdeslami	?	?	?	1	0	?	?	?	2	?	?	?	?	?	?	?	?	?	?	?	2	?	?	?	?	?	?	?	?	?	?	?	?	?	?
N. barryi	?	?	?	?	?	?	?	?	?	?	?	?	?	?	?	?	?	?	?	?	?	?	?	?	?	?	?	?	?	?	?	?	?	?	?
N. donnezani	?	1	0	1	0	0	1	?	2	0	1	1	0	?	0	0	1	?	0	2	2	?	?	?	?	?	0	?	?	?	?	?	?	1	1
N. lockwoodi	0	1	1	1	0	0	1	0	2	1	1	1	0	?	0	0	1	1	0	0	1	2	1	1	0;1	0	1	0	0	0	0	0	1	0	1
N. megamastoides	1	1	1	2	1;2	1	1	1	2	1	1	1	1	0	0	0	1	2	0	2	2	1	1	1	1	0	1	2	1	1	1	1	1	1	1
N. sinensis	1	1	1	0	1	0	1	0	2	1	1	1	1	1	0	1	1	0	0	1;2	2	1	1	1	1	0	1	2	1	1	0	0	1	0	0
Nyctereutes sp. Çalta	1	1	1	2	1	1	1	?	1	1	?	?	1	0	0	1	1	2	0	2	2	2	1	1	1	1	1	2	1	2	1	0	0	1	?
N. terblanchei	?	?	?	?	?	?	1	?	?	?	?	?	?	?	?	?	1	?	?	?	?	?	?	1	?	?	1	?	?	?	?	?	?	?	?
N. tingi	?	0	1	0	1	1	1	1	2	0	1	1	1	1	1	?	1	?	0	1	1	1	1	1	1	0	0	?	?	?	?	?	?	1	1
N. vulpinus	1	1	1	0	0	1	1	0	2	1	1	1	1	1	0	0	1	1	0	2	1	2	1	1	1	0	0	1	1	2	0	0	0	0	1

	36	7	8	9	40	1	2	3	4	5	6	7	8	9	50	1	2	3	4	5	6	7	8	9	60	1	2	3	4	5	6	7	8	9	70
L. vafer	0	0	0	0	2	0	0	0	0	0	4	0	0	0	0	0	?	?	0	0	0	0	0	0	0	0	0	0	0	0	0	0	0	0	0
M. macconnelli	0	0	0	0	2	?	0	?	0	0	4	0	0	?	0	0	?	?	0	0	0	0	0	0	0	1	0	0	0	1	1	0	0	0	0
V. stenognathus	0	?	0	0	0	0	?	0	0	0	0	0	0	0	0	0	?	?	0	1	0	0	0	0	0	0	0	0	0	0	0	0	0	0	1
N. procyonoides	0	1	1	1	2	0	1	1	1	1	2	1	1	1	0	1	1	0	1	3	2	1	1	0	1	0	0	1	1	1	2	1	1	1	1
N. abdeslami	?	?	?	?	?	?	?	?	1	1	4	1	1	1	0	1	1	0	0	2	0	1	1	0	?	?	?	?	1	2	0	2	1	1	0;1	1
N. barryi	?	?	?	?	?	?	?	?	1	0	2	1	?	?	?	0	?	?	0	?	?	0	0	1	0	0	0	0	0	0	0	0	1	0	0	1
N. donnezani	1	?	0	0	1	?	1	1	1	0	3	1	0	1	0	1	0	0	0	2	1	0	0	0	0	0	1	1	0	0	1	0	0	0	1
N. lockwoodi	0	?	0	?	?	?	0	1	1	1	?	?	?	?	?	1	0	0	0	2	0	?	?	1	1	0	1	0	1	0	0	1	0	0	1
N. megamastoides	1	?	0	1	1	0	1	1	1	1	1	1	1	1	0	1	1	1	1	3	1	1	1	0	0	0	0	1	2	1	2	1	1	1	1
N. sinensis	0	?	0	0	2	1	1	1	1	1	3	0	0	1	1	1	1	0	0	2	2	1	1	0	0;1	0	1	0	1	0	1	0	0	0	1
Nyctereutes sp. Çalta	?	?	0	?	?	?	1	1	1	?	2	1	?	?	?	1	0	1	?	?	?	0	?	?	0	0	0	1	1	1	2	1	1	1	1
N. terblanchei	?	?	?	?	?	?	?	?	1	0	2	1	1	?	0	1	1	1	0	2	?	1	1	1	?	0	1	?	?	?	?	0	?	?	?
N. tingi	1	?	0	?	?	?	?	1	1	0	3	0	?	?	?	0	?	0	0	1	0	0	0	0	1	0	0	0	0	0	0	0	0	0	1
N. vulpinus	1	0	0;1	1	0;1	0	1	1	1	0	4	1	1	1	1	1	1	0	0	1	0	1	1	1	1	0	1	1	1	0	1	0	0	0	1

	71	2	3	4	5	6	7	8	9	80	1	2	3	4	5	6	7	8	9	90	1	2	3	4	5	6	7	8	9	100	1	2	3	4	5
L. vafer	?	0	0	0	0	?	0	1	0	0	1	0;1	0	0	0	0	0	0	0	0	0	0	0	0	0	?	2	0	0	?	0	0	0	0	?
M. macconnelli	?	0	0	0	1	1	1	?	0	0	0;1	1	0	0	0	0	0	0	0	0	0	0	1	1	0	?	1	1	1	0	0	1	0;1	0	?
V. stenognathus	0	0	0	0	1	0	0	0	0	0	0	0	1	0	0	0	0	0	0	0	0	0	0	1	0	?	0	0	0	?	0	0	0	0	?
N. procyonoides	2	1	1	1	1	1	0	1;2	1	1	1	1	1	1	0	1	1	1	1	1	1	1	0	1	1	1	1	1	0	0	0	0	1	1	1
N. abdeslami	2	1	1	1	1	1	1	?	1	1	0;1	1	1	2	1	1	1	1	0	0	0	1	0	2	1	1	1	1	0	1	1	0	1	1	1
N. barryi	0	?	?	0	1	0	0	0	?	0	1	1	0	1	0	1	0	0	0	0	0	0	0	1	0	?	1	0	0	?	0	0	?	?	?
N. donnezani	1	0	0	0	1	0	0;1	0;1	0	1	0	1	0	1	0	1	0	0	1	0	0	0	0	1	1	0	1	1	0	0	1	0	0	0	?
N. lockwoodi	0	0	0	1	1	1	1	0	1	?	?	?	?	?	?	?	?	?	?	0	0	?	0	1	?	?	?	0	0	?	0	0	?	?	?
N. megamastoides	2	1	1	1	1	1	0;1	1	1	1	0;1	1	1	2	1	0	1	1	1	1	0	1	0	2	1	1	1	1	0	0	1	0	1	1	1
N. sinensis	1	0	0	0	1	0	0	0;1	0	0;1	0;1	1	1	1	0;1	0	0	1	0	1	1	1	0	1	0	?	1	1	0	0	0	0	1	0	?
Nyctereutes sp. Çalta	2	1	0	0	1	1	0	1	1	1	1	1	0	1;2	1	0	1	1	1	1	0	1	0	2	1	0	0	1	0	0	1	0	0	1	0
N. terblanchei	?	?	0	1	1	?	1	?	?	1	0	0	0	1	0	0	?	0	0	0	0	0	0	1	1	0	0	0	0	?	0	0	0	1	1
N. tingi	0	0	0	0	1	0	0	1	0	0	1	1	0	0	0	1	0	0	1	0	0	0	0	1	0	?	1	0	0	?	0	0	0	0	?
N. vulpinus	1	0	0	0	1	0	0;1	1	0	1	1	1	1	1	0	1	0;1	0	1	0	0	1	0	1	0	0	0	1	0	1	0	0	0	1	0

	106	7	8	9	110	1	2	3	4	5	6	7	8
L. vafer	0	?	?	?	?	?	1	?	1	?	?	?	?
M. macconnelli	1	?	?	?	?	?	?	?	?	?	?	?	?
V. stenognathus	0	0	0	?	?	?	?	?	0	0	0	0	0
N. procyonoides	0	1	1	1	1	2	0	1	1	1	1	2	1
N. abdeslami	0	?	?	?	?	?	?	?	?	?	?	?	?
N. barryi	?	?	?	?	?	?	?	?	?	?	?	?	?
N. donnezani	0	1	1	0	0	0	0	?	1	1	1	1	0
N. lockwoodi	?	?	?	?	?	?	?	0;1	?	?	?	?	?
N. megamastoides	0	1	1	1	1	1	0	1	0	2	1	2	1
N. sinensis	0	1	1	?	?	?	?	?	?	?	?	?	?
Nyctereutes sp. Çalta	0	?	?	?	?	?	?	?	?	?	?	?	?
N. terblanchei	0	?	?	?	?	?	?	?	?	?	?	?	?
N. tingi	0	1	?	?	?	?	?	?	?	?	?	?	?
N. vulpinus	0	?	?	0	0	1	1	0	1	?	0	2	1

3.7.7.3. Figures of some of the characters used in the phylogenetic analysis.

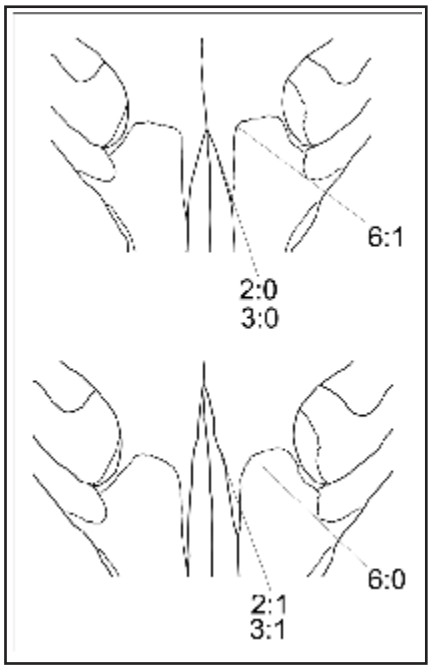

Figure 3.7.6 – Skull in dorsal view, detail of the nasofrontal and maxillofrontal region.

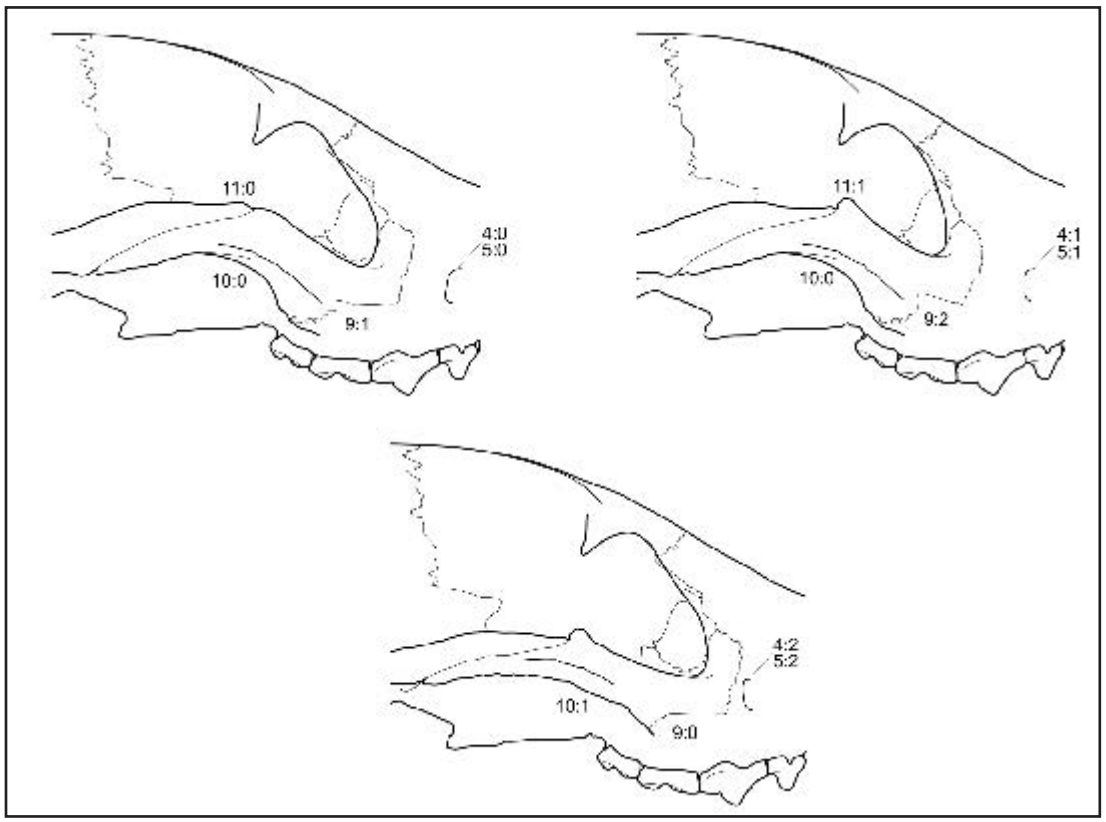

Figure 3.7.7 – Skull in lateral view, morphology of the orbit and the zygomatic region.

Figure 3.7.8 – Morphology of the infraorbital margin of the zygomatic bone, in dorsal view.

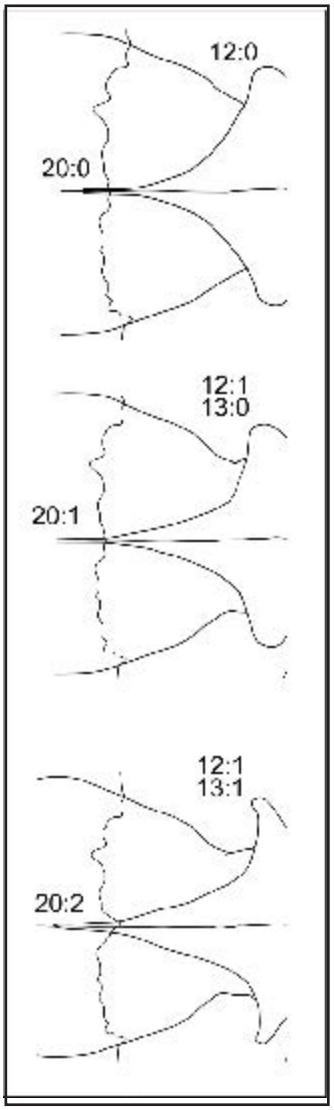

Figure 3.7.9 – Frontal sinus and position of the caudal point of sagittal crest, in dorsal view.

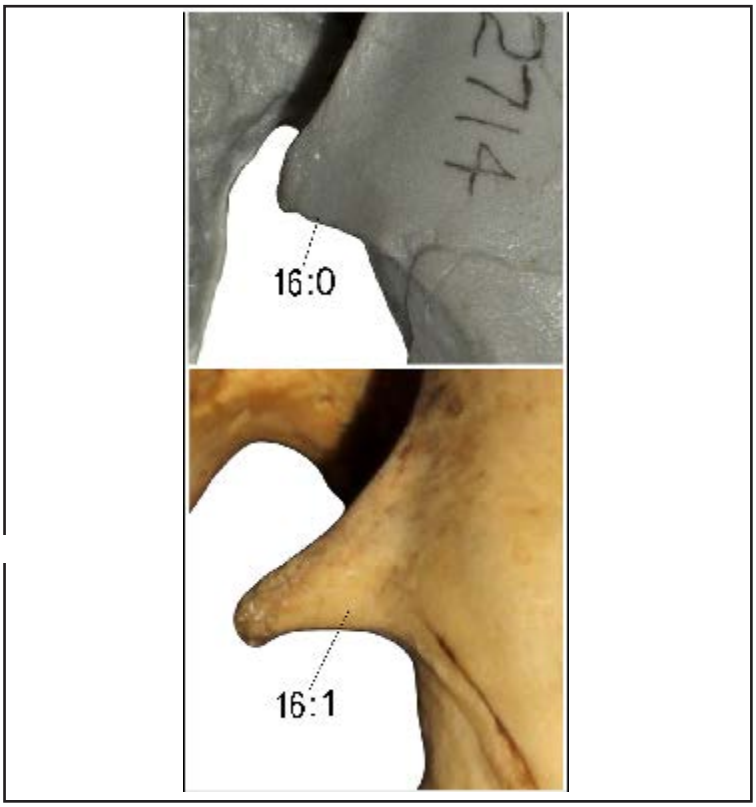

Figure 3.7.10 – Dorsal surface of the zygomatic process of the frontals, in dorsal views.

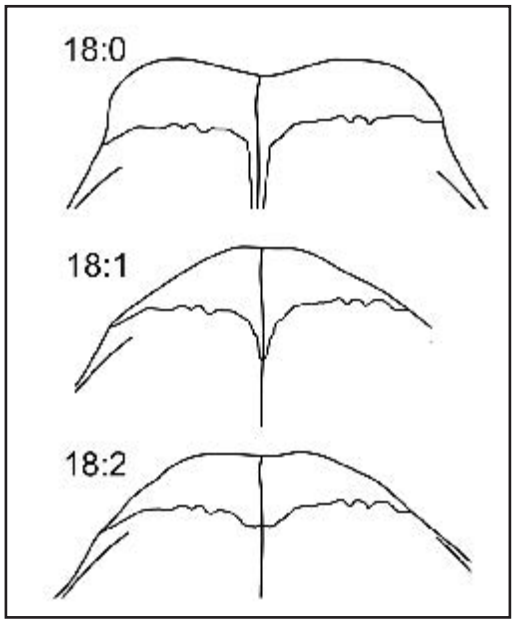

Figure 3.7.11 – Development of the rostral projection of the interparietal bone, in dorsal view.

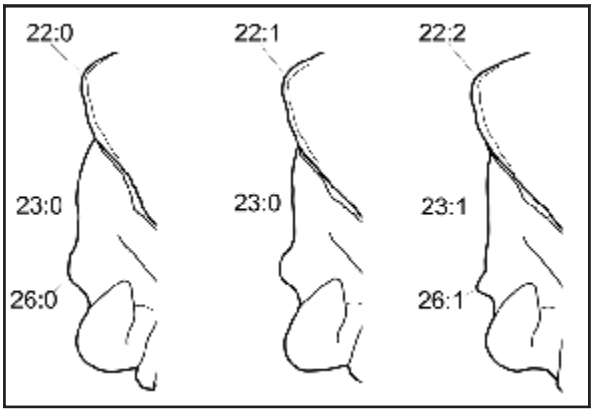

Figure 3.7.12 – Position of the external protuberance, morphology of the occipital region and development of the nuchal tubercles, in lateral view.

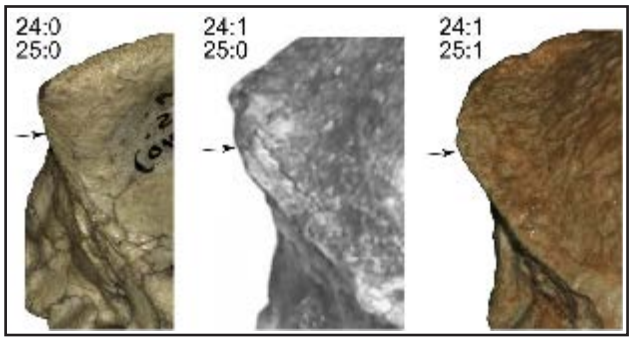

Figure 3.7.13 – Development of the nuchal crest, in lateral view.

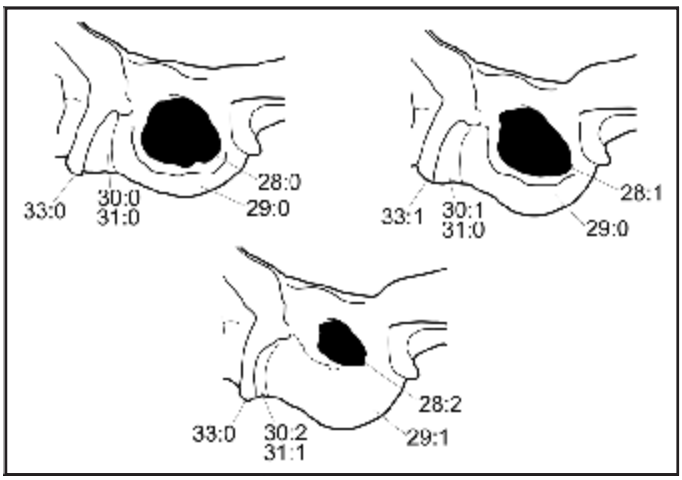

Figure 3.7.14 – Lateral shape of the bulla, the acoustic meatus and the paracondylar process, in lateral view.

Figure 3.7.15 – Shape of the medial side of the paracondylar process, in ventral view.

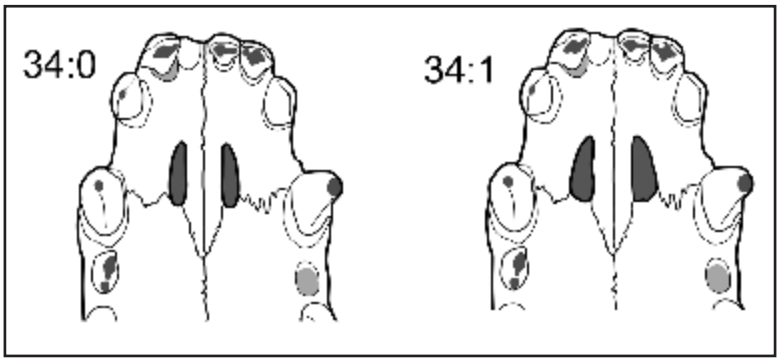

Figure 3.7.16 – Morphology of the palatine fissures, in ventral view.

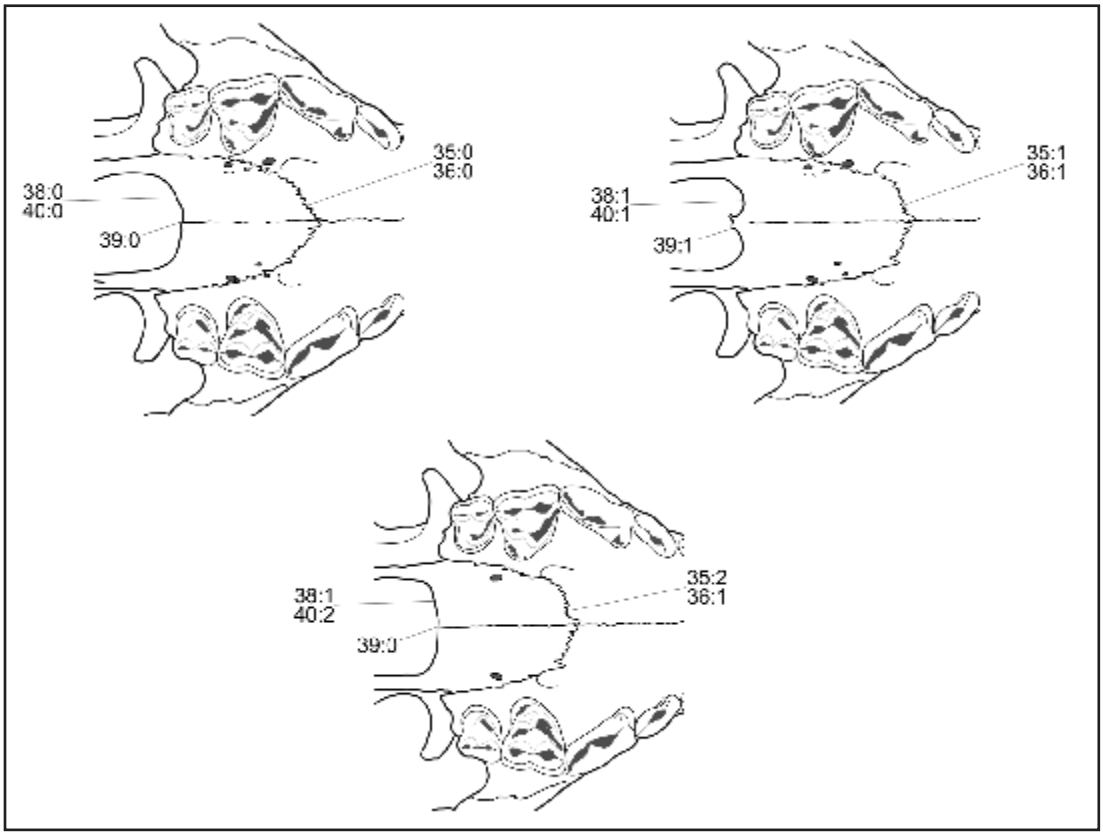

Figure 3.7.17 – Outline of the sutura palatina transversa, of the distal margin of the palatine bone and the development of the nasal process of the palatine, in ventral view.

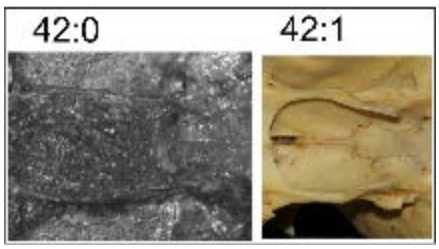

Figure 3.7.18 – Morphology of the hammulus, in ventral view.

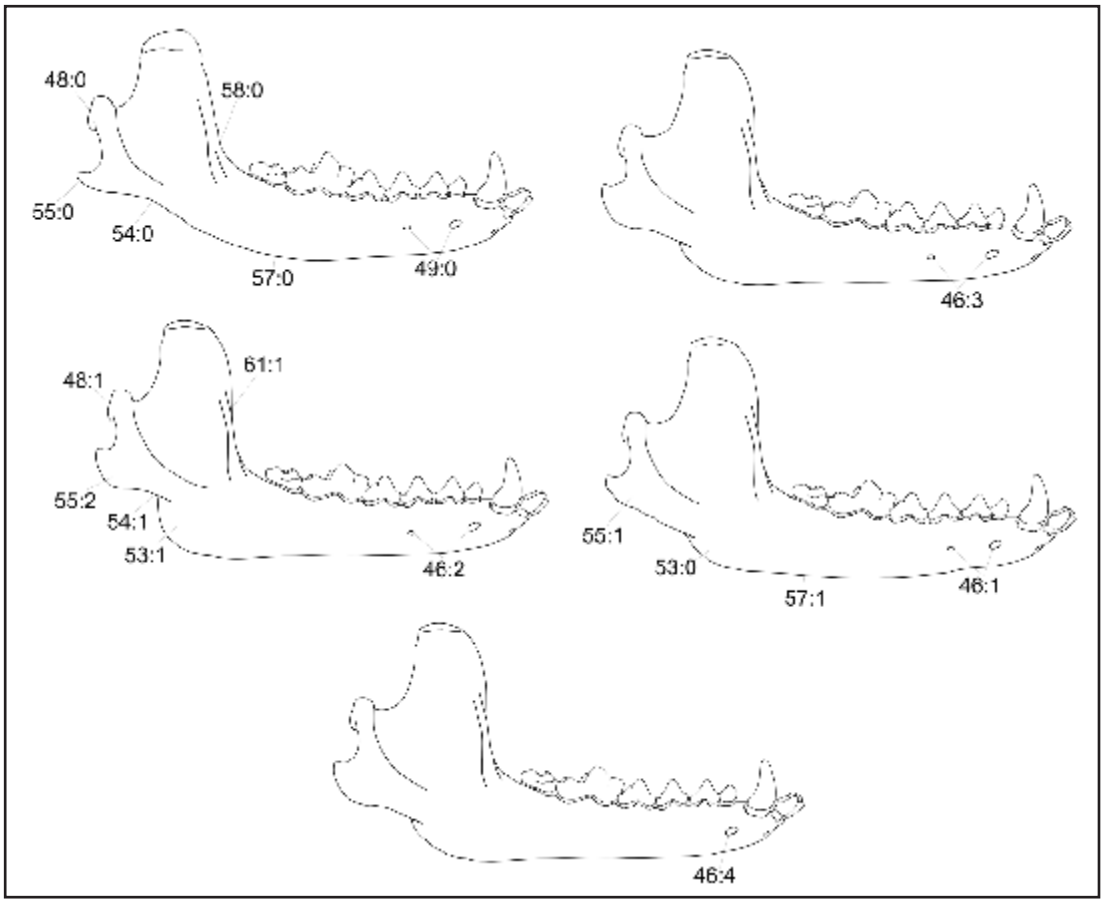

Figure 3.7.19 – Variability of position of the mental foramina, the development of the subangular lobe and of the angular process and height of the condyloid process.

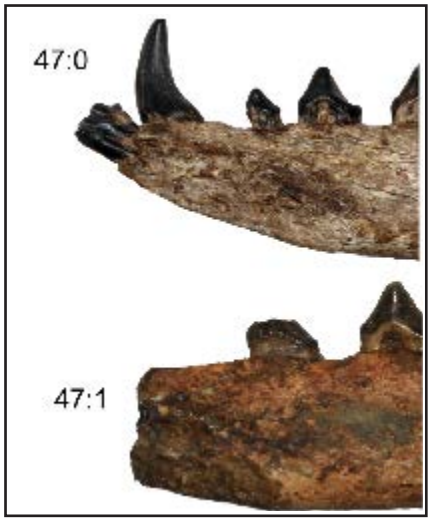

Figure 3.7.20 – Caudal extension of the mandibular symphysis, in medial view.

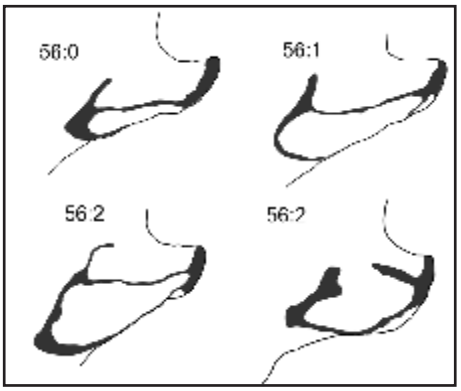

Figure 3.7.21 – Schematic outlines of the rami of the muscle *pterygoideus medialis* on the medial side of the angular process.

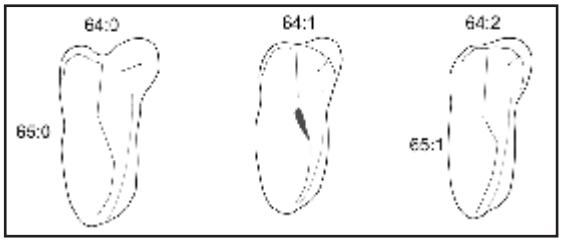

Figure 3.7.22 – P4 occlusal morphology.

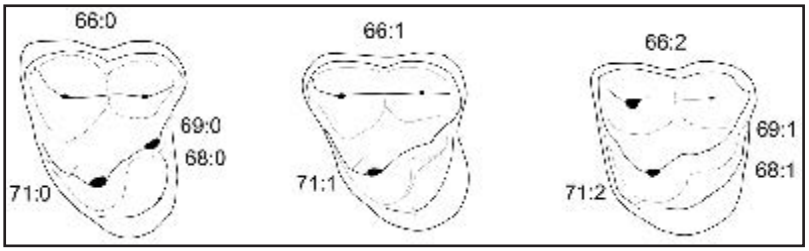

Figure 3.7.23 – Variability of the M1, occlusal view.

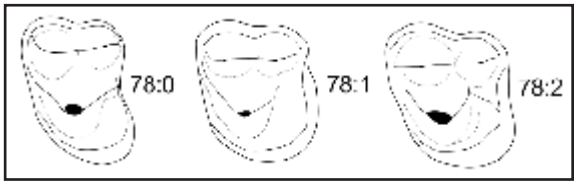

Figure 3.7.24 – Development of the M2 prostprotocrista, in occlusal outline.

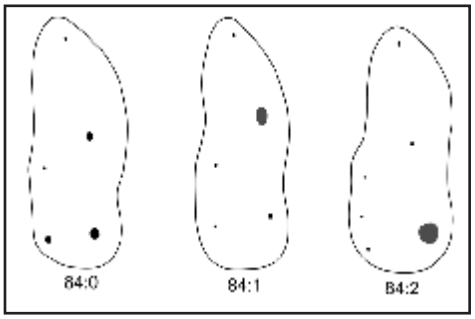

Figure 3.7.25 – m1 occlusal outline.

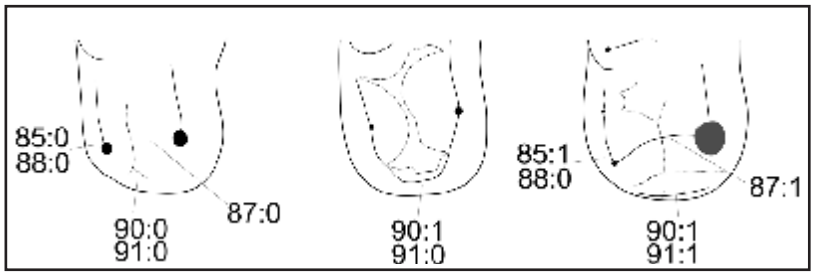

Figure 3.7.26 – Variability of the m1 talonid, in occlusal view.

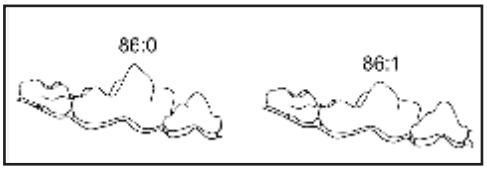

Figure 3.7.27 – Crown height of the m1, in lateral view.

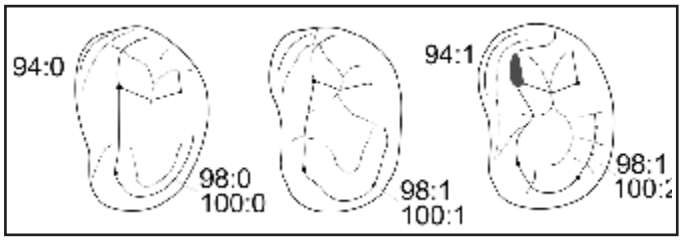

Figure 3.7.28 – Development of the m2 buccal cingulid and of the distolingual side of the m2, in occlusal view.

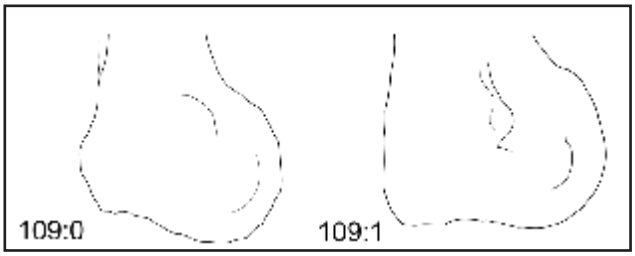

Figure 3.7.29 – Outline of the distocranial border of the distal epiphysis of the humerus, in medial view.

Figure 3.7.30 – Development of the insertion area of the *m. ulnaris medialis* on the medial epicondyle of the humerus, in medial view.

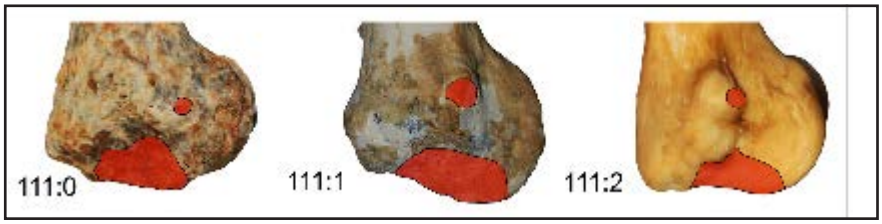

Figure 3.7.31 – Position of the scar of the *m. pronator teres* related to the scar of the *m. flexores carpalis* and digitorum on the distal portion of the humerus, in medial view.

Figure 3.7.32 – Shape of the *capitulum humeri*, in palmar view.

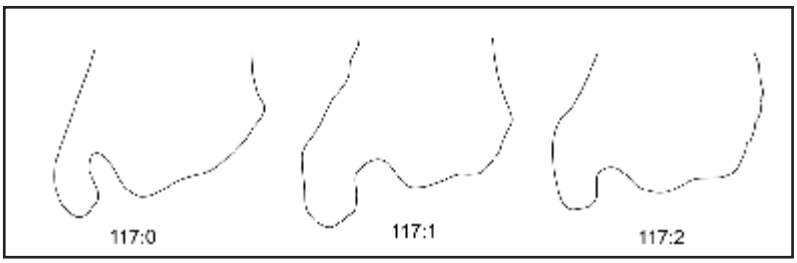

Figure 3.7.33 – Development of the distal notch on the distal articulation of the tibia, in cranial view.

3.8. The tangle of Pleistocene *Vulpes* of Europe

3.8.1. Context

The Plio-Pleistocene record of *Vulpes* in Eurasia is confused and debated. Compared to Asia, the European record is more diverse (5 taxa described) but definitely more disputed. The taxa described from western Europe are based on very scarce fossil material and, in literature, the distinction of these taxa is mainly based on size or on the chronological correlation of the site where they were recovered (*e.g.*, Bonifay, 1971; Koufos, 2018).

3.8.2. Systematic Paleontology

Order **Carnivora** Bowdich, 1821

Suborder **Caniformia** Kretzoi, 1943

Family **Canidae** Fischer, 1817

Subfamily **Caninae** Fischer, 1817

Tribe **Vulpini** Hemprich & Ehrenberg, 1832

Genus ***Vulpes*** Frisch, 1775

Vulpes alopecoides (Del Campana, 1913) *pro parte*

(Figs. 3.8.1-3.8.2; Tables 3.8.1-3.8.3)

Type specimen. IGF 12110, right maxillary fragment with M1 and M2 from Tasso (Upper Valdarno, Italy, ca. 1.8 Ma).

Referred material. V.61.1401, cranium with left P4-M2 and right P4, and a fragment of right hemimandible with m1-m2. From Villàny 3, Mészko-hegy (Hungary, Early Pleistocene, 2 Ma; Pazonyi, 2011).

Description. *Cranium.* The cranial fragment of V.61.1401 lacks the zygomatic

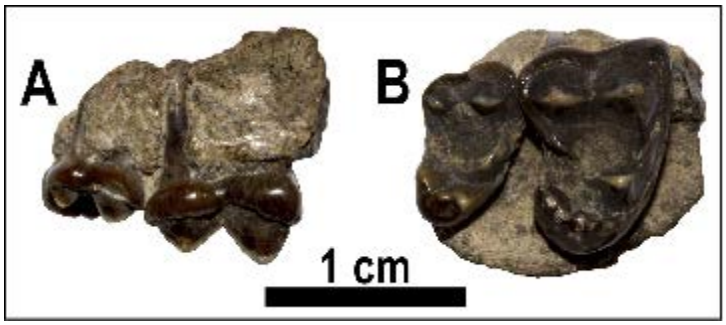

Figure 3.8.1 – *Vulpes alopecoides* type from Il Tasso. **A-B**: **IGF 12110**, maxillary fragment in buccal (**A**) and occlusal (**B**) views.

arches, the rostral tip of the incisive bone and the occipital condyles. In dorsal view, the neurocranium is larger rostrocaudally compared to the splanchnocranium, which does not seem to elongate considerably rostrally. The dorsal surface of the nasals is wide, with caudal V-shaped outline. The nasals end beyond the level of the maxillofrontal suture. In dorsolateral view this suture has an arched outline. The postorbital processes are fragmented, but on the dorsolateral surface of the frontals the vulpine crease is evident, especially on the left postorbital process. This dorsal depression is also visible in lateral view. From these processes, the parasagittal ridges extend caudally and fuse on the interparietal bone, in a dorsal, sharp and lyrate shape. The braincase is considerably inflated and pear-shaped. Although the zygomatic arches are not preserved, in lateral view, the orbit appears wide and high, and the infraorbital margin lies at level of the distal half of the P4. The external occipital protuberance is located considerably lower compared to the dorsal surface of the braincase. The caudal part of the neurocranium is characterized by a caudoventral curvature. The nuchal crest is very shallow. The tympanic bullae are considerably inflated and bulging ventrally, with a well-developed acoustic meatus. If observed ventrally, their medial walls are straight and tend to converge caudorostrally towards the sagittal plane. The palate is short, ending at level of the mesial half of the M2 (approximately at level of the M2 protocone). The difference between the width of the palate at level of the canines and that at M1 is not so marked. In the occipital region, the three-sided occipital

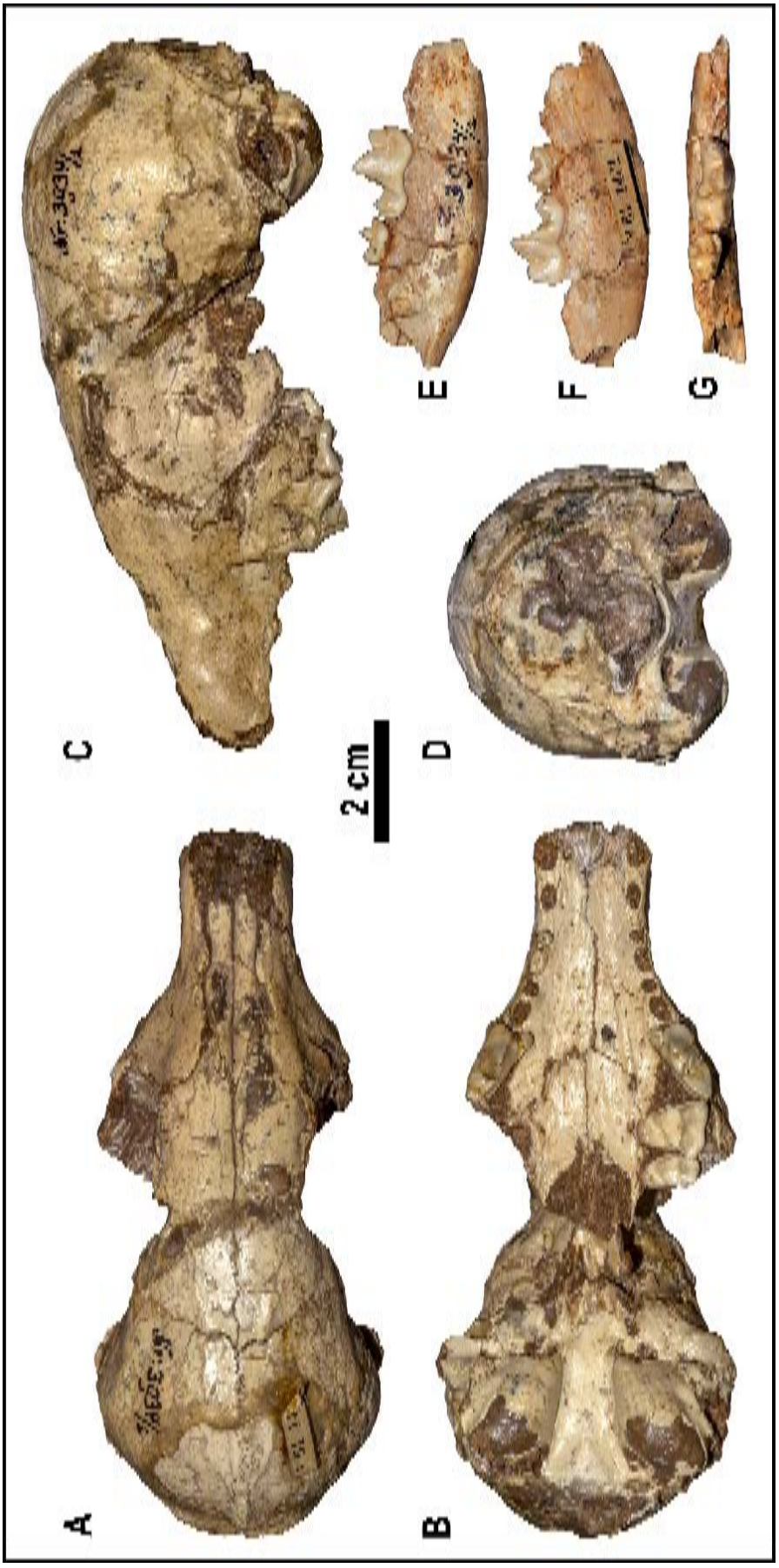

Figure 3.8.2 – *Vulpes alopecoides* from Villany 3. **A-G**: **V.61.1401**, cranium with right hemimandible fragment in dorsal (**A**), ventral (**B**), lateral (**C**), caudal (**D**), buccal (**E**), lingual (**F**), occlusal (**G**) views.

triangle is considerably reduced compared to the inflated and enlarged braincase.

Upper teeth. The P4 is fairly elongated mesiodistally. On the mesiobuccal side, no parastyle is visible. Lingually, the protocone is a well-developed and pointy cusp. In occlusal view, it is slightly advanced compared to the mesial margin of the tooth. On the distal side of the protocone, a shallow but visible cingulum extends distally from this cusp towards the more prominent, distolingual basal cingulum. The paracone is large and high. The metastyle is shorter compared to the former but still well developed. The M1 is enlarged buccolingually, compared to the mesiodistal length. The paracone is slightly larger than the metacone, but of similar height. The buccal cingulum is bulging and prominent, both in buccal and in occlusal views. Lingually, there is a large protocone, a smaller metaconule and a visible protoconule. The lingual lobe is enlarged and possesses a prominent hypocone, separated from a mesial accessory cuspule by marked furrow. The trigon and talon basins are well developed and enlarged, with the latter almost as wide as the former and surely of similar depth. The mesial cingulum is prominently developed. The M2 is considerably elongated buccolingually. Although the metacone is damaged, it seems of similar size compared to the paracone. Whereas the protocone is well-developed, the metacone is cusp-like but reduced. Lingually the hypocone is individualized from the cingulum, and an evident furrow divides the hypocone from an accessory cuspule. Both the buccal and the mesial cingula are marked.

Mandible. The mandible corpus of V.61.1401 is rather shallow. Its ventral margin is arched with a ventral convexity on lateral view. On the buccal side, the distal mental foramen emerges at level of the p3-p4 interalveolar space.

Lower teeth. The lower carnassial of V.61.1401 is well-developed and elongated mesiodistally. The paraconid is considerably shorter mesiodistally compared to the stout protoconid. The metaconid is reduced compared to the other cuspulids. It does not project lingually. On the talonid, hypoconid and entoconid are of

similar height, although the former is larger. The talonid basin is round in occlusal view, and rather deep. A small cuspulid is present between the entoconid and the metaconid, partially closing the basin on this side. The shallow but evident transverse cristid separates this basin from the distal one. A prominent cristid-like cingulid and a hypoconulid bound the distal side of the m1. This cingulid is fused to the prominent, yet short, buccodistal cingulid. The m2 has an irregularly oval shape in occlusal view, with the trigonid part considerably larger compared to the talonid one. Mesially, the paraconid is evident. It individualized by the other mesial cuspids by a rather deep groove on its distal side, but it is joined to the protoconid by a high cristid and with the base of the metaconid by a shallower one. Protoconid is slightly larger than the metaconid, in occlusal view, although the two cuspids are of comparable height. The mesiolingual cingulid is greatly expanded and girdles the lingual side of the tooth, reaching the hypoconid. The latter cuspid is enlarged whereas the entoconid is smaller and shorter. Mesial to the entoconid, there is an evident accessory cuspulid. The distal margin of the tooth is bounded by a prominent cristid-like cingulid.

3.8.3. Discussion

3.8.3.1. Comparisons to the types and paratypes of V. alopecoides*,* V. praecorsac *and* V. praeglacialis

Fig. 3.8.3 shows part of the lectotype materials chosen by Kormos (1932) in his description of *V. praeglacialis* (Figs. 3.8.3A-D and S1 A1-C2, J-K) and *V. praecorsac* (Figs. 3.8.3E-I and S1G1-G2, I1-I2), from Villany 3 and 8, Püspökfurdò/Betfia 2-4 and Nagyharsanyhegy 4. Nowadays, the Figured specimens are housed in the paleontological collections of the HNHM and MAFI. The P4 of V.61.1401 is more slender compared to *V. praecorsac* from Nagyharsanyhegy 4 and *V. praeglacialis* from Villany 8 (Fig. 3.8.3D-E), although the P4 of the maxillary fragment V.61.2164_1 resemble that of V.61.1401. The mesial embayment, so evident in

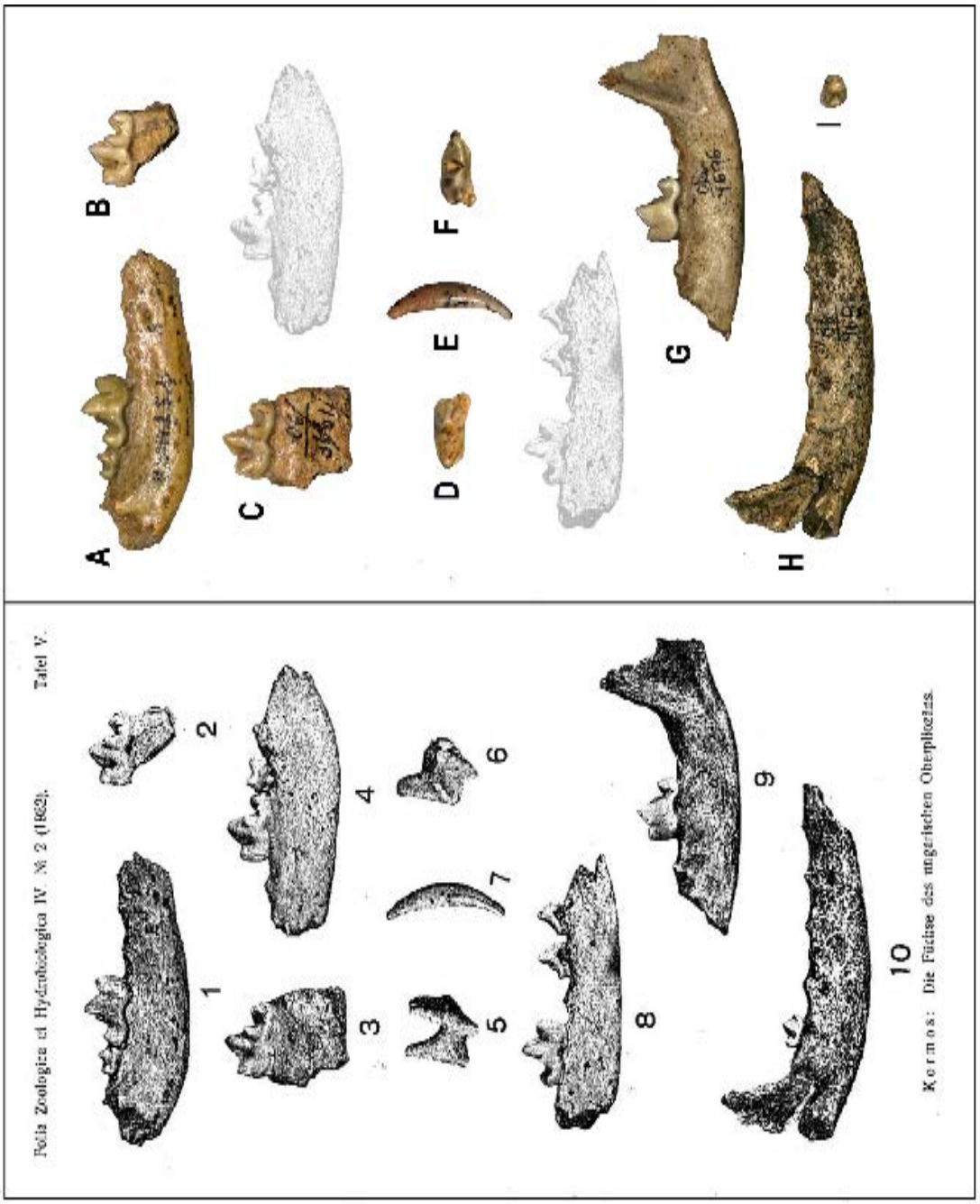
A
B
C
D
E
F
G
H
I
Fauna Zoologica et Hydrobiologica IV. № 2 (1862). Tafel V.
1
2
3
4
5
6
7
8
9
10
Kormos: Die Füchse des ungarischen Oberpliozäns.

V.61.1401, is more reduced both *V. praecorsac* and *V. praeglacialis*. In *V. praecorsac*, the protocone tend to be more reduced, less separated from the paracone, whereas in both *V. praeglacialis* and V.61.1401 it is more developed and individualized. The mesiobuccal margin of the P4 of V.61.1401 is simple, as in the paratype of *V.*

Figure 3.8.3 – The original table of Kormos (1932) depicting the material used by the author to describe *V. praeglacialis* and *V. praecorsac*, and the same specimens housed in the collections of HNHM and MAFI. **A-E**: *V. praeglacialis* from various Hungarian localities. **A**: **V.2014.2.5.1**, hemimandible from Villany 3 in buccal view. **B**: **V.2014.5.1.2**, hemimandible fragment from Villany 3 in lingual view. **C**: **V.2014.2.5.4**, hemimandible fragment from Villany 3 in lingual view. **D-E**: **V.61.2164**, left upper canine and right P4 from Villany 8, respectively, in lingual (**D**) and occlusal (**E**) views. **F-I**: *V. praecorsac* from Nagyharsanyhegy 4. **F**: **V.13.04696.0**, left P4 in occlusal view. **G**: **V.13.04696.0**, left hemimandible in lateral view. **H-I**: **V.13.04696.0**, right hemimandible with a m2 in lateral (**H**) and occlusal (**I**) views.

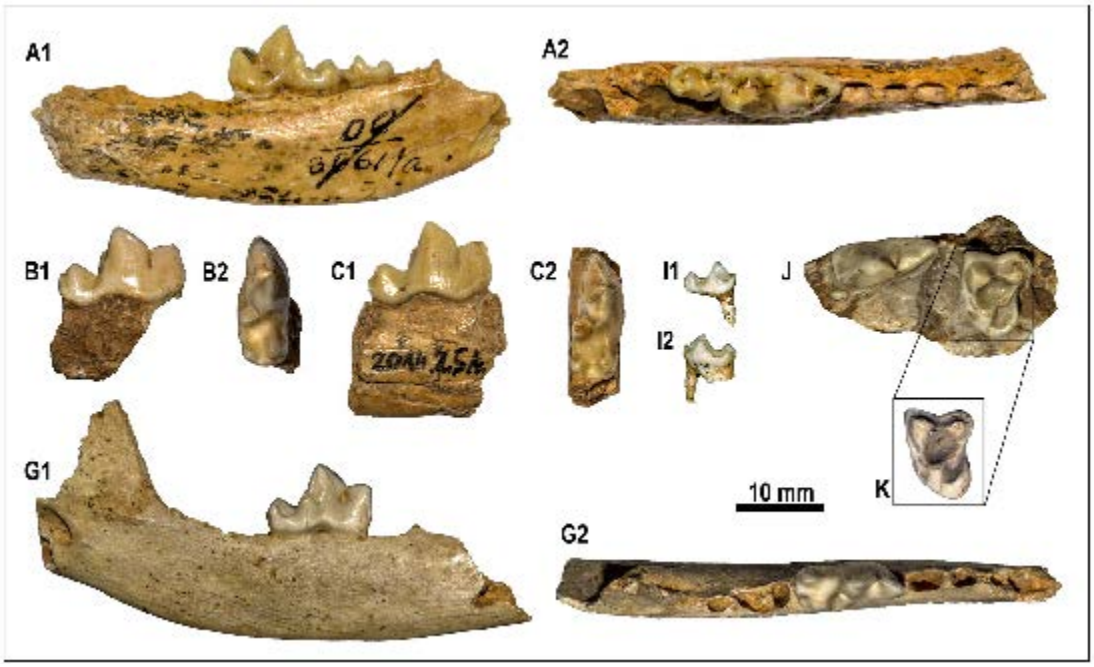

Figure 3.8.4 – Additional views of the specimens of Fig. 3.8.3. **A-C, J-K**: *V. praeglacialis* from Hungary. **A1-A2**: **V.2014.2.5.1**, hemimandible from Villany 3 in lingual (**A1**) and occlusal (**A2**) views. **B1-B2**: **V.2014.5.1.2**, hemimandible fragment from Villany 3 in buccal (**B1**) and occlusal (**B2**) views. **C1-C2**: **V.2014.2.5.4**, , hemimandible fragment from Villany 3 in buccal (**C1**) and occlusal (**C2**) views. **J-K**: **V.61.2164**, maxillary fragment from Villany 8 in occlusal view. **G1-G2**: **V.13.04696.0**, from Nagyharsanyhegy 4 in lingual (**G1**) and occlusal (**G2**) views. **I1-I2**: **V.13.04696.0**, from Nagyharsanyhegy 4 in buccal (**I1**) and lingual (**I2**) views.

praeglacialis. On the contrary, the P4 of *V. praecorsac* of Nagyharsanyhegy 4 has an evident cingulum, girdling the mesiobuccal portion of the tooth. Moreover, the metastyle in the small taxon from Nagyharsanyhegy 4 is reduced compared to that of *V. praeglacialis* and V.61.1401. The lingual expansion of the distolingual cingulum in V.61.1401 seems limited, compared to the lobe-like cingulum of *V. praecorsac* and *V. praeglacialis*. In comparison to the type specimen of *V. alopecoides* from Tasso (Upper Valdarno) the morphology of the upper molars of V.61.1401 is strikingly similar. The development of the M1 parastyle, the M1 paracone larger than the metacone but of similar height, the accessory cuspules on the distal side of the hypocone of M1 and M2, the buccolingual elongation of the M2 are all the features in common with the IGF 12110 (Fig. 2). Compared to the paratype of *V. praeglacialis* of Villany 8 (V.61.2164), the embayment between paracone and metacone on the M1 is more marked compare do that of V.61.1401. In the mesial and lingual cingula are fused together, whereas in *V. praeglacialis* the lingual cingulum ends on the prominent protocone. This morphology creates a narrower talon basin in *V. praeglacialis* compared to the wider one of V.61.1401.

The mandibular type specimens of *V. praeglacialis* come from the same locality of the considered specimen. The considered specimen shares with *V. praeglacialis* several features: the depth of the mandible at the m1; the position of the distal mental foramen (at level of the distal side of the p3, close to the interalveolar space between p3 and p4); the buccal morphology of the m1, with a stout protoconid and prominent cingulid bounding the basal portion of the buccal side of the tooth; presence of transverse cristid between m1 hypoconid and entoconid; prominence the metaconid in occlusal view; developed basin distally to the hypoconid; m2 the protoconid slightly larger than the prominent metaconid; developed m2 entoconid; and cuspulid-like cingulid bounding the lingual side mesially to the entoconid. Nevertheless, some differences can be noted: the m1 of V.61.1401 in occlusal view, shows a gentle notch between protoconid and metaconid giving the tooth a gentle

sinuous morphology; V.61.1401 possesses an accessory lingual cuspulid between m1 metaconid and entoconid like V.2014.2.5.1 and V.2014.5.1.2, although in the latter it is conspicuously developed. On the contrary, V.2014.2.5.4 that does not possess any accessory cuspulids. The m2 of V.61.1401 shows an evident paraconid, almost absent in V.2014.2.5.1. Moreover, the buccal cingulid is more developed and swollen in V.61.1401 than in the type sample of *V. praeglacialis*.

Compared to the mandibles from Nagyharsanyhegy 4 (V.13.04696.0), V.61.1401 is surely deeper and more robust (Figs 3.8.2-3.8.4). The m1 in larger but more slender compared to that of *V. praecorsac*. The paracone is shorter mesiodistally compared to the that of V.61.1401. moreover, the m1 of *V. praecorsac* lacks the transverse cristid, the accessory cuspulids on the lingual side of the talonid basin, and the m1 entoconid is reduced compared to that of V.61.1401. The development of the buccal cingulid on the m2 of *V. praecorsac* from Nagyharsanyhegy 4 is similar to that of V.61.1401 in the mesial part but in the former does not extends distally on the hypoconid as in the latter (see Figs 3.8.2-3.8.4). In occlusal morphology, the two specimens seem to be very similar. Nevertheless, there is no m2 paraconid in *V. praecorsac*'s type, and the distolingual side of the tooth does not bear accessory cuspulids.

3.8.3.2. Comparisons with selected extant species

Cranial fragments of fossil foxes are extremely rare in the fossil record of Europe. Compared to modern *V. vulpes*, the cranium appears shorter in rostrocaudal direction. The splanchnocranium rostral to the P4 is elongated in modern *V. vulpes*, whereas in V.61.1401 this portion does not consistently narrow or elongated. Although slightly larger compared to *V. vulpes*, V.61.1401, lacks the broadening of the maxilla and of the incisive bones at level of the canines typical of *V. lagopus*. The outlines of the nasofrontal and maxillofrontal sutures differ greatly between V.61.1401 and *V. corsac*, *V. lagopus* and *V. vulpes*, as in the latter, the nasals are enlarged

caudally compared to the sharp ends of those of V.61.1401. In dorsal view, the maxillofrontal suture of *V. lagopus* and *V. vulpes* has an angled outline, contrasting with the gently curved morphology of *V. corsac* and V. 61.1401. The fossil specimen possesses rostrally elongated and broad nasal processes of the frontals whereas in *V. lagopus* and *V. vulpes*, these are long but thin extensions of bone and in *V. corsac* they are thin and short. The braincase of V.61.1401 is proportionally more inflated and larger than *V. vulpes*, in which is more elongated rostrocaudally. The parasagittal ridges of *V. vulpes* and *V. lagopus* are generally straight and may fuse close to the frontoparietal suture or caudally to this point (depending on sex and ontogenetic stage). Apart from juvenile individuals, no adult these species show lyre-shaped sagittal crest. In this regard, V.61.1401 resembles *V. corsac*, although in the latter species the area between the parasagittal ridges is broader and more curved compared to the fossil specimen. Whereas nuchal crest of *V. vulpes* juts caudally, especially around the external occipital protuberance, in V.61.1401 does not, similarly to the condition of *V. corsac*, where the crest is considerably reduced. Moreover, the nuchal crest of *V. lagopus* tend to converge medially, forming a blunt pointed morphology in dorsal view. The caudal margin of the nuchal crest of *V. corsac* and *V. vulpes* has a lobed dorsal morphology. V.61.1401 is closer to the latter species, although the nuchal crest does not extend beyond the level of the external occipital protuberance, resulting in a gentle caudal curvature. The caudal portion and occipital region of the braincase of the cranium V.61.1401 are similar to those of *V. corsac*, with the marked ventrally curved cranium, very short occipital triangle compared to the skull height. On the contrary in *V. lagopus* and *V. vulpes*, the external occipital protuberance is closer to the roof of the braincase. In ventral view, the tympanic bullae of V.61.1401 possess straight medial walls that tend to converge caudorostrally towards the sagittal plane. The straight morphology resembles that of *V. corsac*. In *V. vulpes*, the medial side of the bulla is gently arched, as the mesial point tend to curve toward medially compared the distal corner

of the bulla. *V. lagopus*' morphology is similar to *V. vulpes*. Nevertheless, in the three extant species the medial walls are parallel to the sagittal plane, in ventral view. The distal margin of the palate of V.61.1401 reached the level of the M2 hypocone. This feature is somewhat intermediate between *V. vulpes* in which the palate ends at level of the distal side of the M2, and that of *V. corsac* and *V. lagopus*, in which it extends only to the mesial level of the M2. Compared to *V. lagopus*, the palate of V.61.1401 is narrower rostrally, although appears proportionally larger at level of the molars in comparison to *V. vulpes*. The P4 of V.61.1401 is slender and elongated mesiodistally. It possesses a cingulum on the mesial side of the P4 protocone similar to that of *V. lagopus* and *V. vulpes* (although, in this species, it is generally continuous on all the mesiolingual margin of the cusp). *V. corsac* does not show this cingulum. Moreover, in V.61.1401, a marked cingulum bounds all the lingual side of the P4. This feature is present in *V. vulpes*, whereas in *V. lagopus* the mesiolingual cingulum is reduced or absent, and in *V. corsac* is absent. The M1 is elongated buccolingually, with the lingual portion of the tooth not shortened if compared to the buccal side, like *V. vulpes* and in contrast to *V. corsac* and *V. lagopus*. The general development of the cusps resembles that of *V. vulpes*, whereas in *V. corsac* and *V. lagopus* the protocone tend to be enlarged and prominent and the metaconule and hypocone are comparatively reduced. In *V. corsac* the mesial cingulum is considerably reduced, unlike V.61.1401, *V. lagopus* and *V. vulpes*. The furrow that separates the M1 hypocone from the lingual cingulum is sometimes present in *V. vulpes* (see section 3.8.3.3.), whereas it is absent in *V. corsac* and *V. lagopus*. The presence of a M2 metaconule in V.61.1401 contrasts with *V. corsac* and *V. lagopus*, whereas it is similar to *V. vulpes*. In lateral view, the mesial margin of the masseteric fossa of V.61.1401 ends at level of the m3 alveolus, as in *V. lagopus* and *V. vulpes*, whereas in *V. corsac* the fossa ends caudally. The lateral outline of this region is broader compared to that of *V. vulpes* and more similar to *V. lagopus*. The lower carnassial possesses a stout metaconid, not so individualized from the

protoconid, similar to *V. corsac* and *V. vulpes*, and reduced compared to that of *V. lagopus*. Other features contrast with *V. corsac* and *V. lagopus* and resemble more *V. vulpes*: the developed entoconid; the transverse cristid connecting the talonid cuspids; the evident entoconulid; the hypoconulid and the prominent distal cingulid. Unlike *V. corsac*, the m2 of V.61.1401 possesses an entoconid, like *V. lagopus* and *V. vulpes*. Nevertheless, the former does not show mesial accessory cuspulids on the lingual side like in V.61.1401 or some *V. vulpes*.

3.8.3.3. On the variability of extant red fox: possible insights for taxonomy of fossil taxa

The morphological analysis of a homogenous sample of 45 extant *V. vulpes* coming from Italy (principally from Tuscany, held at MZUF) showed the existence of several of numerous variable features in their teeth morphology (Figs. 3.8.5-3.8.6). For instance, in the upper teeth, the mesial lobe of the P4 paracone is generally narrow (Fig. 3.8.5A) but it can also be reduced (Fig. 3.8.5E) or, on the contrary expanded (Fig. 3.8.5F). The P4 protocone is enlarged in the majority of the specimens (Fig. 3.8.5A, C), Nevertheless, in some specimens it can be reduced (Fig. 3.8.5N, Q, T), fairly prominent but partially fused to the paracone (Fig. 3.8.5I, K), or even enlarged and separated (Fig. 3.8.5G). The morphology of the mesial embayment of P4 is generally present, although it can be narrow (Fig. 3.8.5V) or wide (Fig. 3.8.5W). It is although absent in few specimens (Fig. 3.8.5Q, Y). In *V. vulpes*, generally there is no cingulum on the mesiobuccal side the P4 (in the majority of the specimens of Fig. 3.8.5), although specimens with fairly- or well-developed cingula are not so uncommon (respectively Fig. 3.8.5A, N, R, S and Fig. 3.8.5E, H, I, O, Y, Z). Rare is the presence of an individualized parastyle. This feature appears to be rarer in *V. corsac* and slightly more common in *V. lagopus* (Gimranov, 2017). Just above the mesial embayment, some P4 possess an accessory cuspule on the preparacrista (Fig. 3.8.5E, J, T). Another variable morphology of the upper carnassial of *V. vulpes*, is the morphology of the medial protocone crest and its

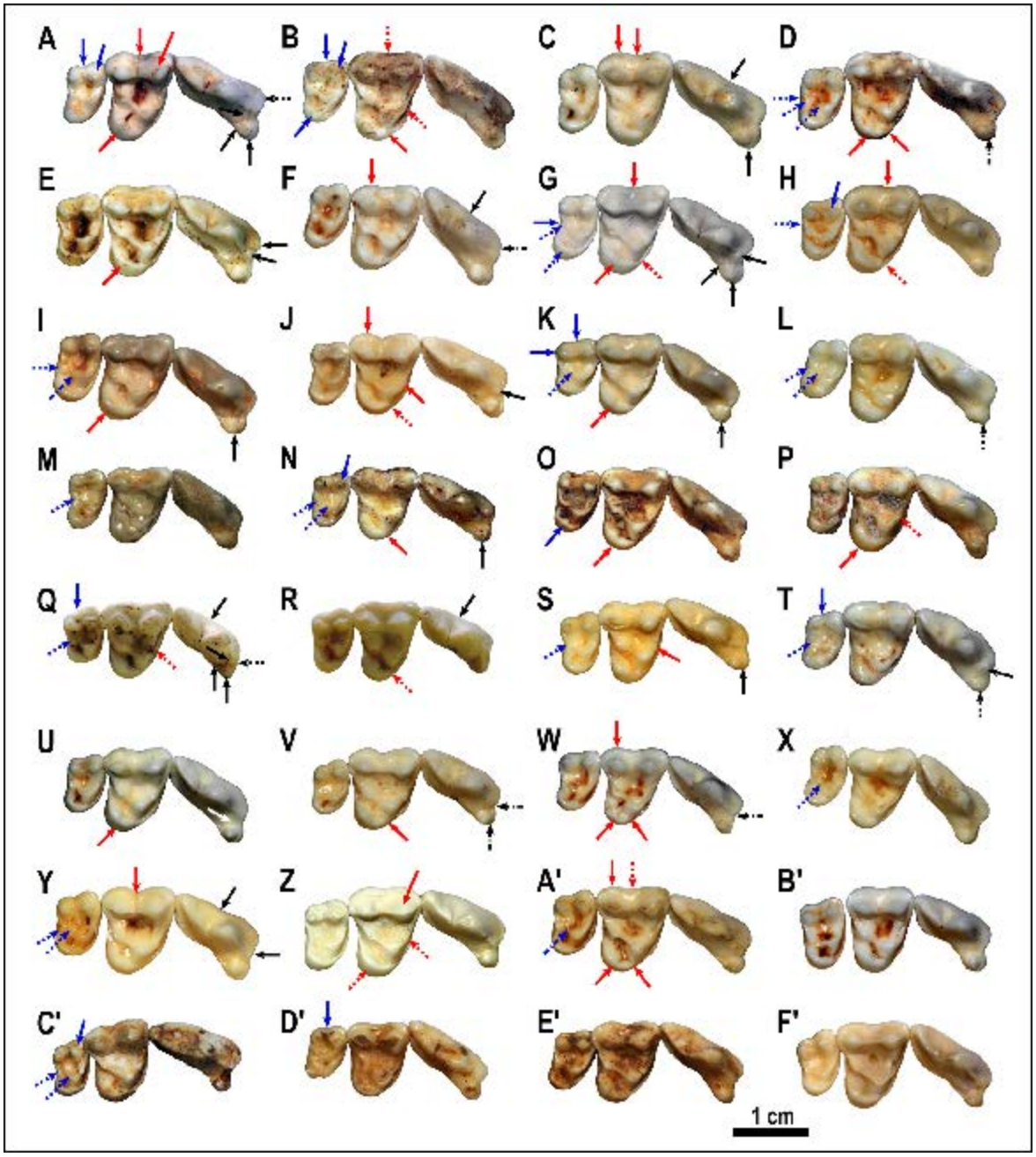

Figure 3.8.5 – Variability of the occlusal morphology of upper teeth (right P4-M2) of extant *V. vulpes* from Italy. **A**: **MZUF-1358**. **B**: **MZUF-3627**. **C**: **MZUF-3632**. **D**: **MZUF-4001**. **E**: **MZUF-4115**. **F**: **MZUF-4140**. **G**: **MZUF-4363**. **H**: **MZUF-5882**. **I**: **MZUF-6445**. **J**: **MZUF-8467**. **K**: **MZUF-9827**. **L**: **MZUF-11854**. **M**: **MZUF-11857**. **N**: **MZUF-11861**.**O**: **MZUF-12420**.**P**: **MZUF-12421**. **Q**: **MZUF-12424**. **R**: **MZUF-12426**. **S**: **MZUF-12428**. **T**: **MZUF-12429**. **U**: **MZUF-12432**. **V**: **MZUF-12433**. **W**: **MZUF-12434**. **X**: **MZUF-12708**. **Y**: **MZUF-16590**. **Z**: **MZUF-16775**. **A'**: **MZUF-18893**. **B'**: **MZUF-21735**. **C'**: **MZUF-22236**. **D'**: **MZUF-22237**. **E'**: **MZUF-22238**. **F'**: **MZUF-22289**. Legend: solid arrows, presence of feature; dotted arrows, absence of feature; dashed arrow, reduced/poorly developed feature.

relation to the preparacrista. In general, the medial crest is fused the preparacrista, but in some specimens it is incomplete or curved distally not reaching it. When it is complete, of the medial protocone crest has mainly two alternative shapes, in the occlusal view: arched, with parabola-like shape (*e.g.*, Fig. 3.8.5A, B, H, M, A') extending linguomedially and then ventrally toward the tip of the crown; or straight, that projects medially toward the lower third of the preparacrista. In the considered sample of *V. vulpes*, the latter shape is considerably the most common (see Fig. 3.8.5C, E, G, I, L, O, Q, R, V, W, X, C', F'). The protocone in *V. vulpes* is girdled by a prominent cingulum (*e.g.*, Fig. 3.8.5B, C), which nevertheless might be incomplete (Fig. 3.8.5A, I, K, S, T, V, X) and rarely absent (Fig. 3.8.5D, G, L, Q). In occlusal view, the P4 paracone is longer mesiodistally compared to the metastyle (*e.g.*, Fig. 3.8.5C, F), although there are also morphotypes with reduced difference in length between these portions of the P4 (Fig. 3.8.5Q, R, Y, B'). The development of the distolingual cingulum on P4 varies from specimens in which it is nearly absent (Fig. 3.8.5U) to other in which it is considerably evident (Fig. 3.8.5Y, B'). This cingulum generally continues mesially with a prominent cingulum (*e.g.*, Fig. 3.8.5C, E, F). In some specimens, the mesiolingual cingulum is only incipient (*i.e.*, Fig. 3.8.5A, B, D, P, R, W, X, B'), whereas others do not possess it (Fig. 3.8.5G, L, S, T, B'-C').

The occlusal morphology of the M1 is highly variable: generally buccolingually elongated, with the lingual portion smaller than buccal but not narrowed; buccolingually elongated, with narrow lingual portion (T-like morphology) (Fig. 3.8.5A, R, S, W, X, Z, F'); buccolingually elongated, with enlarged lingual portion (Fig. 3.8.5G, L, T); buccolingually shortened, subsquared (Fig. 3.8.5F, J, N, V, Y, D', E'). The M1 embayment on the buccal cingulum can be reduced (*e.g.*, Fig. 3.8.5P) or marked (*e.g.*, Fig. 3.8.5J, Y). On the M1, the development of the buccal cingulum on the metacone is present but not bulging, whereas other M1 have expanded buccal cingula (Fig. 3.8.5C, J). The hypocone lobe connects mesially to

the mesial cingulum (Fig. 3.8.5D, G, R). Another not unusual morphotypes has the M1 lingual cingulum ending on the lingual side of the protocone (Fig. 3.8.5B, J, N, V). Generally, the M1 hypocone is a cingular cusp (*e.g.*, Fig. 3.8.5E), although some specimens show a separated cusp from the cingulum by shallow furrow (Fig. 3.8.5D, G, K, O, U, W). The M2 occlusal morphology is variable: generally, it is buccolingually elongated (Fig. 3.8.5A), but it can be bean-shaped (Fig. 3.8.5G) or D-shaped, enlarged mesiodistally (Fig. 3.8.5B, K). The M2 buccal cingulum may possess a buccal notch or may not. Distally, the M2 possess a marked notch (lingually to the metacone), which can be reduced or absent in other specimens (Fig. 3.8.5D, H, I, A').

In the lower teeth, the occlusal morphology of the p4 varies in the sample, from the generalized mesiodistally elongated and oval (Fig. 3.8.6B), to the enlarged distally (Fig. 3.8.6K) or the considerably enlarged distal portion (Fig. 3.8.6M). Moreover, the distal margin can show a rounded outline (the majority of the specimens) or a more square-like one (*e.g.*, Fig. 3.8.6V). The m1 possesses a variable occlusal outline: some are slender and buccolingually compressed (*e.g.*, Fig. 3.8.6B, Q), whereas others are stout and enlarged in buccolingual sense (Fig. 3.8.6C, J, S, W). On the lingual side, the m1 protoconid possesses a gentle inflexion of the tooth (*e.g.*, Fig. 3.8.6A). In some specimens is more developed and marked (Fig. 3.8.6G, J), whereas in others is reduced, and the area is nearly convex (Fig. 3.8.6W). Generally, the m1 metaconid in *V. vulpes* is developed and individualized (*e.g.*, Fig. 3.8.6D), although some specimens might possess a developed metaconid that is less separated from the protoconid (Fig. 3.8.6J, Q, X), or a reduced and less separated one (Fig. 3.8.6L, O, P, R, S, W, A'). The presence of a transverse cristid is common in the sample (*e.g.*, Fig. 3.8.6D). This feature is particularly marked in some specimens (Fig. 3.8.6E, F, C'), whereas is completely absent or reduced in some others (Fig. 3.8.6A, C, N, R, U, F'). One of the most variable feature of the lower carnassial in the considered sample is the morphology of the lingual

cuspulids, mesial to the m1 entoconid: single reduced cuspulid, entoconulid (most of the specimens, *e.g.*, Fig. 3.8.6A); single and enlarged cuspulid, entoconulid (Fig. 3.8.6F, N, K, E'); entoconulid and mesial accessory cuspulid (Fig. 3.8.6E, D'); no cuspulid mesial to the entoconid (Fig. 3.8.6L, P). Another high variable feature is the distal margin of the m1. The margin can be characterized by: a simple cristid bounding the distal margin (Fig. 3.8.6D, E, I, J, M, C'); a distal cristid arising from an evident hypoconulid (Fig. 3.8.6C, G, H); distal accessory cuspulids, in place of a cingulid (Fig. 3.8.6A, F, N); an enlarged hypoconulid with no distal cristid or a strongly reduced one (Fig. 3.8.6B, Q, T, U, W); a reduced distal cristid or no cristid (Fig. 3.8.6Q, P, S).

On the buccal side, the m2 generally shows a marked hypoflexid (*e.g.*, Fig. 3.8.6A), which is not present in other specimens (Fig. 3.8.6J, S, W, Y, Z), giving the m2 a more ovoidal shape, instead of bean-like one. Furthermore, the m2 show a buccal cingulid that is evident on the mesiobuccal side of the protoconid (*e.g.*, Fig. 3.8.6E). In some specimens it enlarges and prominently extends distally on the buccal side of the hypoconid (Fig. 3.8.6F, I, N, U, V, D'), but in others it is reduced, limited to the mesial face of the protoconid (Fig. 3.8.6Y, W, F'). Although some m2 possess the entoconid as a single cuspid (Fig. 3.8.6F, M, T, C') or a very reduced one (Fig. 3.8.6G, U, W), the majority of the specimens show one large entoconid and a mesial accessory cuspulid (*e.g.*, Fig. 3.8.6B, E, H). Four specimens of the sample

Figure 3.8.6 – Variability of the occlusal morphology of lower teeth (left p4-m3) of extant *V. vulpes* from Italy. **A**: **MZUF-934**. **B**: **MZUF-3624**. **C**: **MZUF-3632**. **D**: **MZUF-4001**. **E**: **MZUF-4115**. **F**: **MZUF-4140**. **G**: **MZUF-4141**. **H**: **MZUF-4363**, reversed. **I**: **MZUF-5882**. **J**: **MZUF-591**. **K**: **MZUF-6445**. **L**: **MZUF-8465**. **M**: **MZUF-8467**. **N**: **MZUF-9827**. **O**: **MZUF-11857**. **P**: **MZUF-11861**, reversed. **Q**: **MZUF-11862**. **R**: **MZUF-12420**. **S**: **MZUF-12421**. **T**: **MZUF-12424**, reversed. **U**: **MZUF-12426**. **V**: **MZUF-12427**, reversed. **W**: **MZUF-12428**. **X**: **MZUF-12429 Y**: **MZUF-12430**. **Z**: **MZUF-12431**. **A'**: **MZUF-12432**. **B'**: **MZUF-12433**. **C'**: **MZUF-12434**, reversed. **D'**: **MZUF-12708**. **E'**: **MZUF-18893**, reversed. **F'**: **MZUF-22289**. Legend: solid arrows, presence of feature; dotted arrows, absence of feature; dashed arrow, reduced/poorly developed feature.

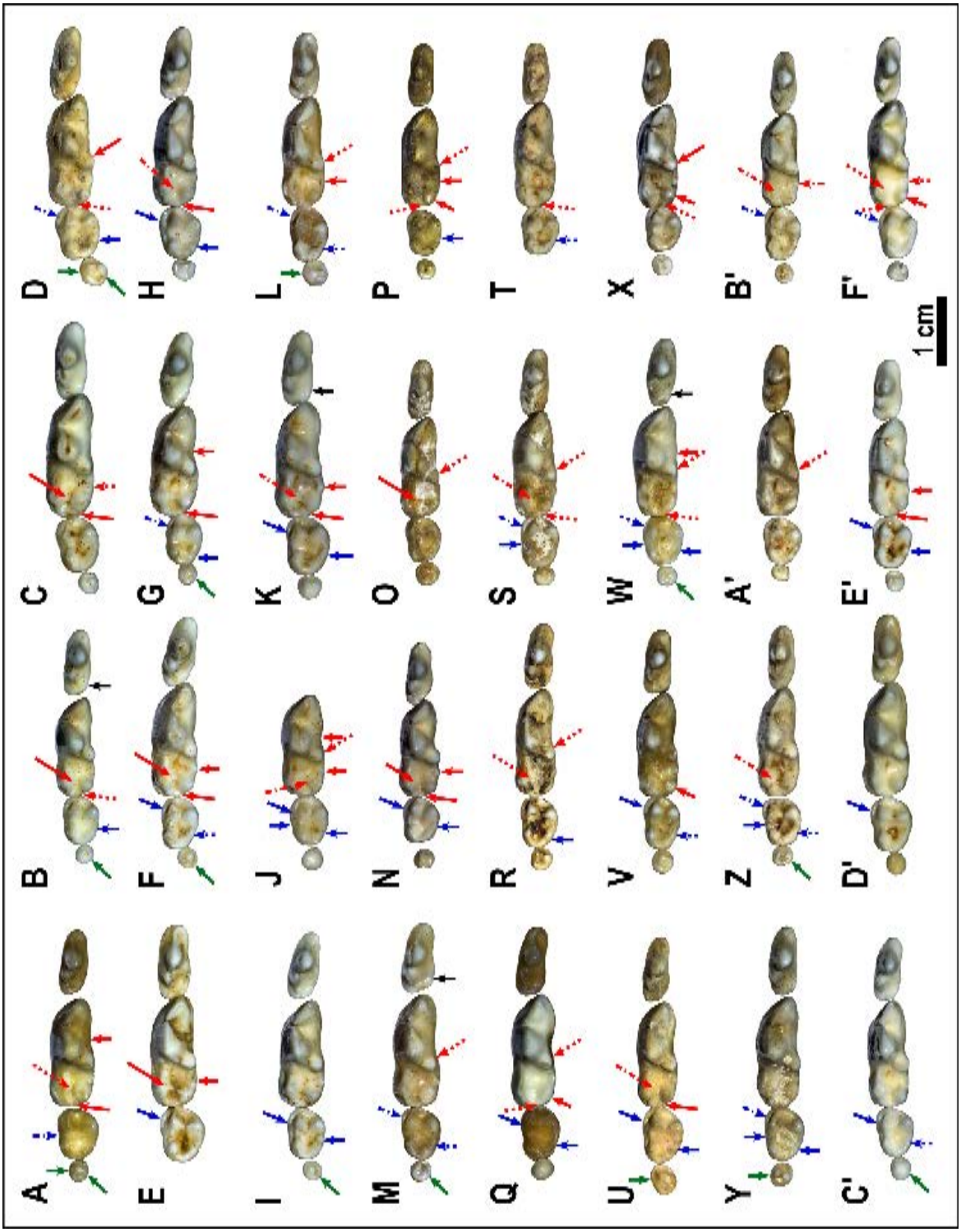
A
B
C
D
E
F
G
H
I
J
K
L
M
N
O
P
Q
R
S
T
U
V
W
X
Y
Z
A'
B'
C'
D'
E'
F'
1 cm

(MZUF-4115; MZUF-4141; MZUF-12424; MZUF-12425) do not possess m3. In the other specimens its occlusal morphology of m3 is generally small and round (*e.g.*, Fig. 3.8.6A), but it can also be large and round (Fig. 3.8.6D, L, Y) or large and oval (Fig. 3.8.6U). The cuspids present on the m3 (*i.e.*, the buccal protoconid and the lingual metaconid) are generally subequal in size (*e.g.*, Fig. 3.8.6D, H, K), although the protoconid can be larger than the metaconid (Fig. 3.8.6B, M); several specimens do not possess the metaconid but only a single buccal cuspid and a lingual cristid (Fig. 3.8.6G, I, W, Z, C') or even a single central cuspid (Fig. 3.8.6A, F, B').

This kind of variability has been documented in other populations of *V. vulpes* (Szuma, 2000; 2003; 2004; 2007; 2008a; 2008b) and even in other species of the genus (*e.g.*, *V. lagopus*, Daitch & Guralnick, 2007; Szuma 2008c; 2011; *V. corsac*, Gimranov et al., 2015; Gimranov, 2017). The size and the morphological variability results from the combination of geographic, climatic and biological factors, such as *e.g.*, latitude, habitat productivity, differential food availability, competition (on various levels, *i.e.*, intraguild, intrafamily or intraspecific), character displacement, genetic diversity and population density (Szuma, 2008b and reference therein). Different species are susceptible to different combinations of these proxies, with resulting different variability and, eventually, features. For instance, *V. lagopus* is more influenced by its evolutionary history, interspecific competition with *V. vulpes*, and diet (*i.e.*, food source variability and accessibility), whereas geographic and climatic factor are less important (Szuma, 2011). On the contrary, latitude, mean annual temperature and longitude significantly affect the distribution of morphotypes in *V. vulpes* (Szuma, 2007). Surely, the range of extant red fox is enormously larger and more diverse in terms of habitat types, conditions, etc, compared to that of *V. lagopus*, and this affects the importance of the above-mentioned factors, as also noted by Szuma (2011). Moreover, Szuma (2008b; 2011) showed that these proxies affect more severely the morphology in

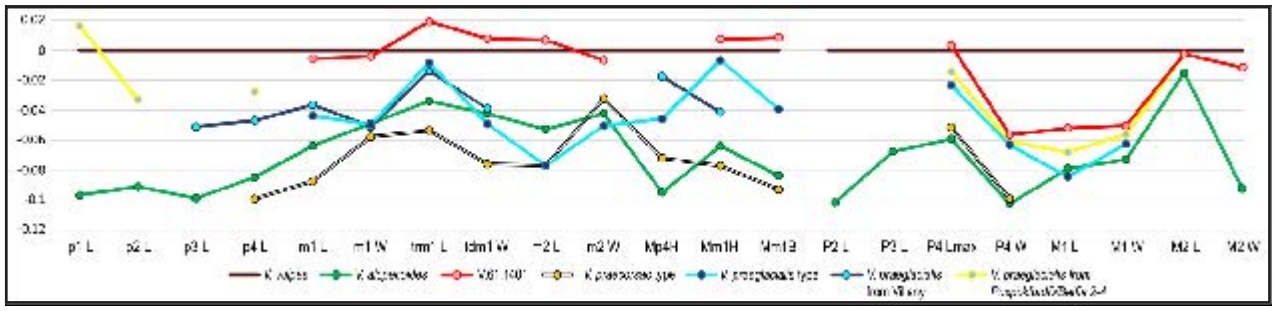

Figure 3.8.7 – Log-ratio diagram based on selected dentognathic variables in the considered specimen (V.61.1401), in *V. alopecoides* from Europe (*i.e.*, Dafnero-1, Il Tasso, La Puebla de Valverde, Kastritsi, Kvabebi, Pirro Nord, St. Vallier, Villarroya), in the samples of *V. praeglacialis* and of *V. praecorsac* from different localities of Hungary and Romania (*i.e.*, type specimens, Villany, Püspökfurdò/Betfia 2-4), housed at HNHM and MAFI as compared to extant *V. vulpes* (used as the reference baseline). The average values of *V. vulpes* result from personal measurements and literature data from Davis (1977); Gingerich et al. (1979; 1980); Szuma (2003); Altuna (2004); Hartstone-Rose et al. (2013).

case of sympatry between different species of *Vulpes* (*e.g.*, *V. vulpes-V. rueppelli* or *V. vulpes-V. lagopus*), accentuating the variability. The relation between morphotypes and climatic parameters as air moisture and mean annual temperature found by Szuma (2007) assumes great relevance for paleontological studies, although yet poorly studied.

3.8.3.4. Remarks on the intraspecific variability of the fossil European foxes

As clear from the morphological comparison between the cranium and hemimandible of *V. alopecoides* from Villany 3 (*i.e.*, V.61.1401) and the lectotype material of *V. praeglacialis* (section 3.8.3.1.) the latter species apparently represent a junior synonym of the former. This morphological datum is confirmed also by morphometric proportions. Fig. 3.8.7 show a log-ratio diagram of the dental variability of classic *Vulpes alopecoides* sites (included here Dafnero-1, Il Tasso, Kvabebi, La Puebla de Valverde, Pirro Nord, St. Vallier, Villarroya), V.61.1401, the type specimens of *Vulpes praeglacialis* and *V. praecorsac*, and the remaining specimens from Villany labelled as *V. praeglacialis* and the additional samples from Püspökfurdò/Betfia 2-4 of the both *V. praeglacialis* and *V. praecorsac*. The extant

V. vulpes was used as a standard comparison. Despite very small differences, the pattern of the type *V. praeglacialis* follows that of *V. alopecoides*, being intermediate between the large V.61.1401 and the mean *V. alopecoides* both in sized and for its proportions. The same can be said for the samples from Püspökfurdò/Betfia 2-4 and the rest of *V. "praeglacialis"* from Villany.

Less clear is position of *V. praecorsac*. From the analysis of the lectotypes used by Kormos (1932) to define it (see Figs. 3.8.3-3.8.4) some characteristics may be pointed out: the reduced but pointy P4 protocone, half fused to the paracone and not so advanced mesially; the evident mesiobuccal cingulum though no P4 parastyle; the well-developed metastyle. Moreover the mandibular corpus is shallow, with a scaphoid ventral outline in lateral view. The m1 talonid is enlarged buccolingually but a reduced in mesiodistal sense, especially in its distal portion of the talonid. The m1 metaconid is large and developed, projecting lingually. The hypoconid is prominently enlarged. No transverse cristid or lingual accessory cuspulid, mesial to the entoconid, are present. The m2 is shortened, with a prominent buccal cingulum (not extended on the hypoconid). No paraconid is present. The entoconid is well developed into a cuspid. No accessory cuspulids are present on the distolingual side of m2. Nevertheless, these features are based on single specimens, only partially and speculatively attributable to a single individual. From the same locality of V.13.04696.0, another hemimandible fragment, V.61.1372 (see later), housed in the HNHM shares with the lectotype V.13.04696.0 the shallow hemimandible corpus. In dental morphology, the two specimens share the development of the hypoconid compared to the entoconid. Despite these similarities, V.61.1372 also shows some features that resemble *V. alopecoides-V. praeglacialis*: the robustness of the mandible and of the m1, in occlusal view; the reduced but individualized m1 metaconid; the similar height of the hypoconid and entoconid, which is not as reduced as in V.13.04696.0; the presence of an incomplete crista transversa, visible on the entoconid but not on the hypoconid;

the prominent entoconulid, visible in lingual view and the distal cingulid bounding the distal side of the talonid. The similarity with these other two species is also visible in the dental proportions of *V. praecorsac*. As visible in Fig. 3.8.7, the pattern of *V. praecorsac* seems to follow that of *V. alopecoides*, especially dentally. The two species differ more in mandibular parameters: the height and the breath of the mandible at m1 of *V. praecorsac* are smaller compared to the height distally to the p4, whereas *V. alopecoides* and *V. praeglacialis* show higher and stouter mandibular corpora distal to the m1. This pattern of proportions, nonetheless, is common in the extant *V. vulpes*. If mean proportions of a natural sample are considered (*e.g.*, males, females, non-sexed individuals, Fig. 3.8.8), the variance is subtle, but if maximum and minim values or single individuals are plotted, the possible arrays of proportions become evident (despite the sex of the individuals).

The variability displayed by *V. praecorsac* fits within the intraspecific diversity displayed by extant foxes (*e.g.*, *V. vulpes*, see previous section and Figs. 3.8.5-3.8.6). On the other hand, considering the number of the specimens plausibly referred to this species and the variability of extant species (see previous section, Figs. 3.8.5-3.8.6 and Szuma, 2007; Gimranov et al., 2015; Gimranov, 2017), it might be more parsimonious to consider the whole sample of Villany, Püspökfurdò/Betfia 2-4 and Nagyharsanyhegy 4 as belonging to a single species rather than two separate ones. Nevertheless, in literature European localities of the Early and middle Pleistocene have been variously interpreted as *V. alopecoides*, *V. praecorsac* or *V. praeglacialis*. Here a number of samples of the selected sites are revised in order to understand the taxonomic nature of Early-middle Pleistocene European species. Figs. 3.8.9-3.8.11 resume the morphological and morphometric variability of these samples.

Fig. 3.8.9 show the interspecific variability of the upper carnassial and molars of *V. alopecoides*, *V. praecorsac* and *V. praeglacialis* from different European localities. As seen in Fig. 3.8.5 and testified to by Szuma (2007; 2011), in both *V. vulpes* and *V. lagopus* the occlusal outline of the P4 may vary considerably. For instance, in the

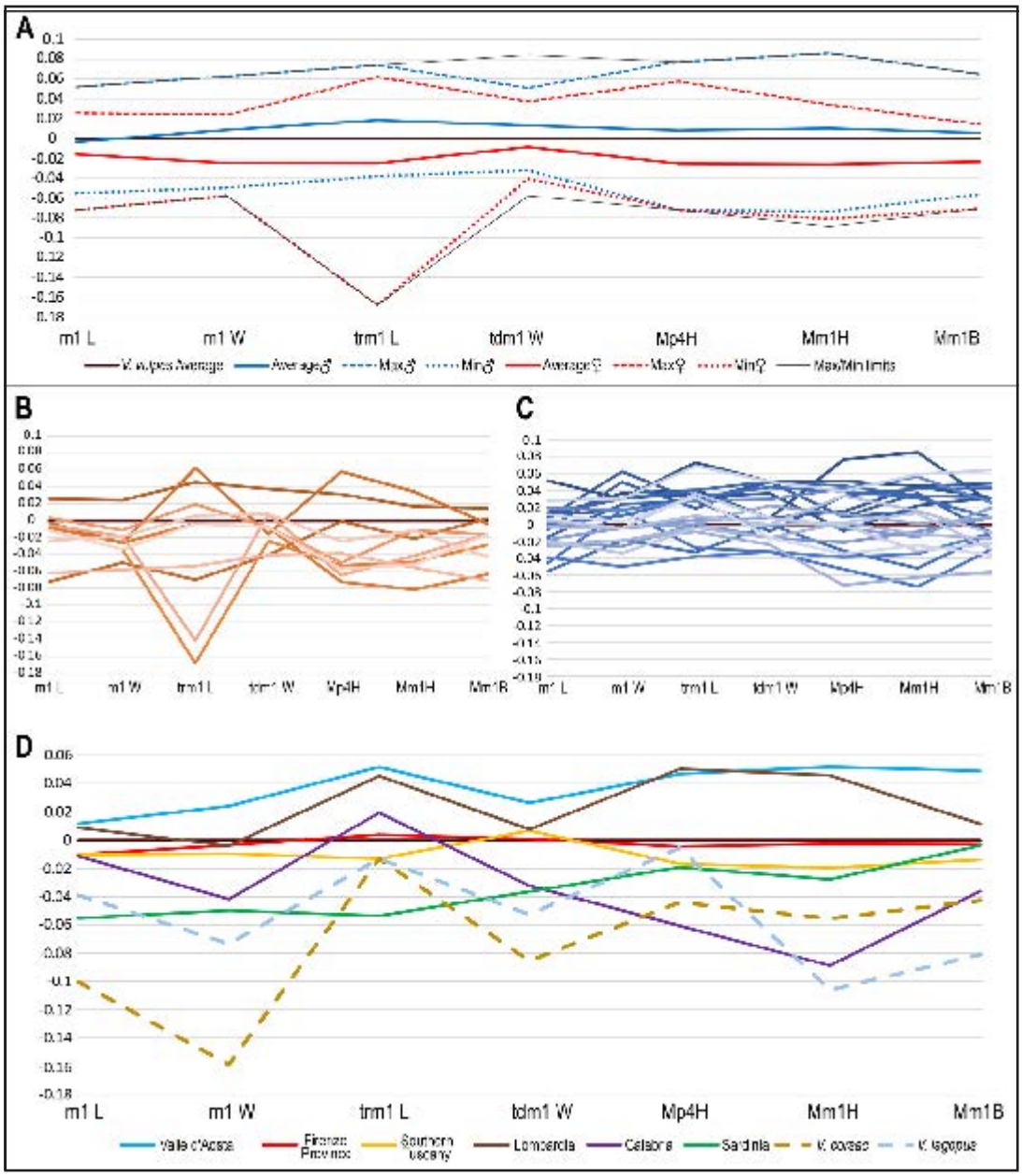

Figure 3.8.8 – Resuming log-ratio diagrams based on m1 and mandible variables in the specimens of the Italian sample of extant *V. vulpes*. **A**: Log-ratio considering the average proportions of males (blue line) and females (red lines) in the sample. Black lines are the maximum and the minimum proportions of the whole sample (*i.e.*, males, females and non-sexed specimens). **B-C**: Log-ratios based on the same proportions of A in the single female (**B**) and male (**C**) specimens. **D**: Log-ratio showing the pattern of proportion of the considered dentognathic variable of A-C in specimens from different Italian regions, in *V. lagopus* and in *V. corsac*. The reference baseline in all log-ratios is the average *V. vulpes* of Fig. 3.8.7.

development of the P4 protocone, its degree of coalescence with the paracone or expansion on the lingual side, or the mesial embayment. Fossil specimens do show a comparable degree of variability. The mesiobuccal margin of the P4 generally show a visible cingulum in all three taxa (Fig. 3.8.9B, D-G, I-J, M-N, Q, T-V), missing only in *V. alopecoides* from Villany 3, *V. praecorsac* from Somssich Hill 2 and *Vulpes* sp. from Vallparadís Estació (Fig. 3.8.9H, K, S). In occlusal view, the P4 protocone of *V. alopecoides*, *V. praecorsac* and *V. praeglacialis* from different localities generally shows a prominent cingulum (Fig. 3.8.9B-K, T-U). In V.61.2164_2 (*V. praeglacialis* from Villany 8) and in *Vulpes* from Vallparadís Estació, it is not complete, but present only on the mesial side (Fig. 3.8.9N, S), whereas it is absent in V.61.2164_1 and the unnumbered P4 from Villany 3 (Fig. 3.8.9M, Q). The medial crest of the protocone is evident in all the specimens, with the exception of few specimens of *V. alopecoides* from Apollonia-1, Pirro Nord and Villany 3 (Fig. 3.8.9E, H, I) and *V. praecorsac* from Villany 8 (Fig. 3.8.9J). In all the taxa, this crest is arched and fused with preparacrista. On the lingual side, a prominent cingulum is visible in the specimens, only in *V. praeglacialis* from Villany 8, V.61.2140_2 (Fig. 3.8.9N). On the M1, variable features are the development of the buccal notch (marked in Fig. 3.8.9A, C, H, M, R-S; reduced in Fig. 3.8.9B, D,G, P, T-V) and the buccal elongation of the lingual portion (similarly to *V. vulpes*, see Fig. 3.8.5 and Szuma, 2007). The M1 protoconule seem to be present in all the taxa, a part from *V. praecorsac* from Odessa (Fig. 3.8.9V). Unlike the condition of *V. lagopus*, the metaconule is not reduced nor shallow in *V. alopecoides*, *V. praecorsac* and *V. praeglacialis*. The hypocone of the type of *V. alopecoides* (Fig. 3.8.9A), *V. alopecoides* from Villany 3 (Fig. 3.8.9K), *Vulpes* sp. from Vallparadís Estació (Fig. 3.8.9S) and *V. praecorsac* from Somssich Hill 2 and Deutsch Altenburg 2C (Fig. 3.8.9L, T) is individualized from the lingual cingulum by an evident furrow. The mesial side of the lingual cingulum generally continues in the mesial cingulum (Fig. 3.8.9A, D, G-H, P, R, U-V). *V. praecorsac* from Somssich Hill 2 and Deutsch Altenburg 2C and

V. praeglacialis from Villany 8 (respectively, 3.8.9L, T and Fig. 3.8.9M) show the lingual cingulum ending on the lingual side of the protocone. This morphology can also be seen in some specimens of *V. vulpes* (Fig. 3.8.5). The M2 is generally elongated lingually, although in *V. alopecoides* from St. Vallier and Kastritsi (Fig. 3.8.9B, G), the buccal side is enlarged. The paracone is generally larger than the metacone in all the taxa, although in the specimen from Vallparadís Estacio is particularly enlarged, also marked by a prominent cingulum (Fig. 3.8.9S). Lingual to the paracone, from the large M2 protocone the postprotocrista continues reachingthe distal margin, where a small metaconule is visible. The presence of an evident metaconule contrasts with the general condition of *V. lagopus*, where no metaconule is present and the postprotocrista generally does not reach the distal margin (see also Szuma, 2011; Gimranov, 2017). On the contrary, this morphology of the M2 resembles *V. vulpes.* As in the M1, the M2 hypoconid of *V. alopecoides* from Il Tasso (Fig. 3.8.9A) is individualized from the lingual cingulum

Figure 3.8.9 – Detailed pictures of the P4-M2 of fossil *Vulpes* from several European localities. **A-I**: *V. alopecoides* from Europe. **A**, **IGF 12110**, right M1-M2 (type) from Il Tasso. **B**: **MHNL 20.161684**, right P4-M2 from St. Vallier. **C**: **IPS 36793**, left P4-M2 (reversed) from Villarroya. **D**: **PP 789**, left P4-M2 (reversed) from Pirro Nord. **E**: **PU104618**, right P4 from Pirro Nord. **F**: **PU104805**, left P4 (reversed) from Pirro Nord. **G**: **KSR- PO221**, P4-M2 (reversed) from Kastritsi. **H**: **V.61.1401**, P4-M2 (reversed) from Villany 3. **I**: **APL-20**, right P4 from Apollonia-1 (attributed to *V. praeglacialis* by Koufos, 2018). **J-L**: *V. praecorsac* from Hungary. **J**: **V.13.04696.3**, type left P4 from Nagyharsanyhegy 4 (reversed). **K**: **VER.2018.2676**, left P4 from Somssich Hill 2 (reversed). **L**: **VER.2018.2682**, right M1 from Somssich Hill 2. **M-Q**: *V. praeglacialis* from Hungary. **M**: **V.61.2164_1**, left P4-M1 from Villany 8 (reversed); **N**: **V.61.2164_2**, right P4 from Villany 8. **O**, unnumbered specimen, left M2 from Villany 3 (reversed). **P** unnumbered specimen, right M1 from Villany 3. **Q**, unnumbered specimen, left P4 from Villany 3. **R**: *V. praeglacialis* from Venta Micena. **IPS 45634** (cast), right M1. **S**: *Vulpes* sp. from Vallparadís Estació. **EVT 14942**, left P4-M2 (reversed). **T**: *V. praecorsac* from Deutsch Altenburg 2C. **UWPI 2275/13/10**, left P4-M2 (reversed). **U**:*V. praeglacialis* from Deutsch Altenburg 2C. **UWPI 2275/13/11**, right P4-M2. **V**: *V. praecorsac* from Odessa Catacomb. **O-7764**, right P4-M2. Legend: solid arrows, presence of feature; dotted arrows, absence of feature; dashed arrow, reduced/poorly developed feature.

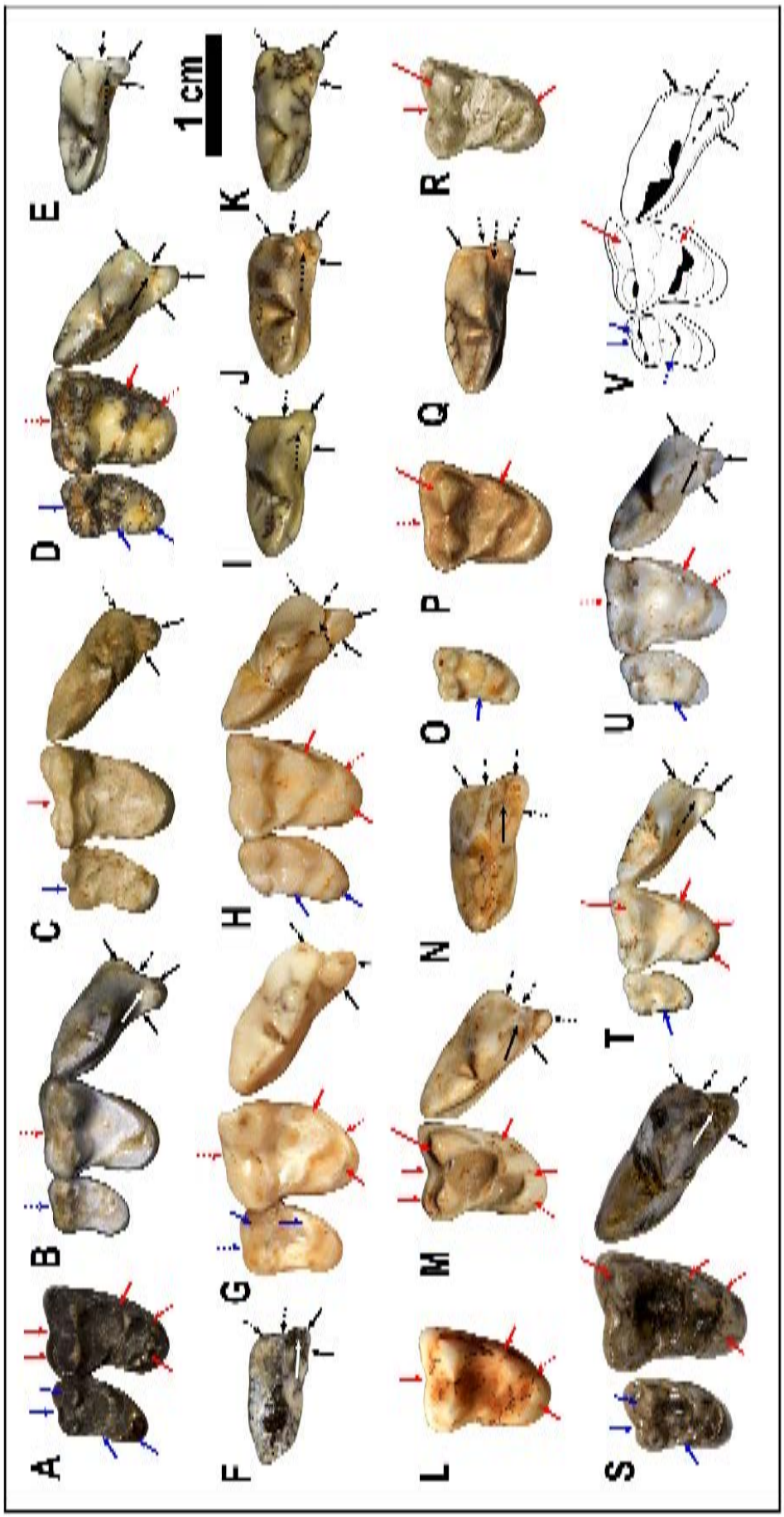
A
B
C
D
E
1 cm
F
G
H
I
J
K
L
M
N
O
P
Q
R
S
T
U
V

by a marked furrow. The same morphology is visible in the specimens from Pirro Nord (Fig. 3.8.9D) and Villany 3 (Fig. 3.8.9H).

Fig. 3.8.10 shows the variability of the morphologies of p4-m3 of the three fossil taxa from renowned European sites. Gimranov et al. (2015) noted that the presence on the p4 of a mesial accessory cuspulid is frequent in *V. corsac*. In contrast, *V. lagopus* and *V. vulpes* do not show such feature, almost completely. In *V. alopecoides*, the p4 does not generally possess any mesial accessory cuspulid, although two specimens (from Dafnero-1 and Pirro Nord, respectively Fig. 3.8.10A and I) do have it. No mesial cuspulid is visible in *V. praecorsac* and *V. praeglacialis* specimens, a part from the specimens of Odessa Catacombs (Fig. 3.8.10M'). As observed in the previous section, the occlusal morphology of the p4 varies in *V. alopecoides*, in *V. praecorsac* and in *V. praeglacialis*. One of the most important features historically used to discriminate between *V. alopecoides-V. praeglacialis* and *V. praecorsac* is the morphology of the m1 talonid and particularly the presence of the transverse cristid. As in extant *V. vulpes*, all three considered fossil species show a larger hypoconid compared to the entoconid. This difference is modest, especially in height, in *V. alopecoides* and *V. praeglacialis* (see Fig. 3.8.10A-M, W-G', K'-L'). The m1 entoconid is reduced in some *V. praecorsac*'s specimens (the type from Nagyharsanyhegy 4, Fig. 3.8.10O, but especially in that Püspökfurdò/Betfia 2-4 and Odessa Catacombs, Fig. 3.8.10Q, M'-N') whereas generally in those from Somssich Hill 2 and Deutsch Altenburg 2C it is not (*e.g.*, Fig. 3.8.10R-V, J'). This reduction is also a feature of in some specimens of *V. alopecoides* (*e.g.*, in Pirro Nord, Fig. 3.8.10J) or *V. praeglacialis* from Hungary (Fig. 3.8.10X, D'). As far as the transverse cristid is concerned, Fig. 3.8.10 shows that indeed some specimens attributed to *V. praecorsac* does not possess this cristid (Fig. 3.8.10O, Q-R, T, M'-N'). Nevertheless, several other *V. praecorsac* specimens have evident partial or complete cristids (Fig. 3.8.10P, S, U, J'). Moreover, it is not uncommon to find lower carnassials of *V. alopecoides* ad *V. praeglacialis* with no or incomplete

transverse cristids (*i.e.*, Fig. 3.8.10A, B, G, C', G'). The presence of a modest number of specimens without or with extremely reduced transverse cristids (*i.e.*, morphotypes P1 and P2 of Szuma, 2004) is documented in the modern-day *V. vulpes* (Szuma, 2004; 2007). The opposite condition, *i.e.*, the presence of the cristid in species where it is generally absent (P3-P4 morphotypes of Szuma, 2004), is also fairly common in extant *V. lagopus* (Szuma, 2004). Another variable features of the m1 is the development entoconulid. This cuspulid is present in *V. alopecoides* and generally present in *V. praeglacialis* (is absent only in Cal Guardiola specimen, Fig. 3.8.10G'). Although the type of *V. praecorsac* and some specimens from different localities does not possess it (Fig. 3.8.10O, Q, U and M'), the majority shows an evident cuspulid (Fig. 3.8.10P, R-T, N'). A cingulid generally bounds the distal margin of the m1 in *V. alopecoides*, *V. praeglacialis* and also in *V. praecorsac*. Nevertheless, some specimens do not possess it (Fig. 3.8.10A, B, O, Q, B', K', M'-N'). On the m2, the development of a buccal cingulid is variable in *V. alopecoides*. It can be reduced (Fig. 3.8.10D), developed around the protoconid (*e.g.*, Fig. 3.8.10B), considerably developed and expanded distally on the hypoconid (*e.g.*, Fig. 3.8.10A, L). Similarly, in *V. praecorsac* it varies from being prominent around the protoconid to expanded distally. The presence of m2 entoconulid or accessory cuspulids on the lingual margin of the m2 is fairly common feature in all three fossil taxa.

The degree of morphological variability possessed by the three known European fossil taxa (*i.e.*, *V. alopecoides*, *V. praecorsac* and *V. praeglacialis*) seems comparable to the intraspecific variability displayed by modern foxes' species like *V. vulpes* (from the present analysis, see section 3.8.3.2. and Figs. 3.8.5-3.8.6; for literature data see *inter alios* Szuma, 2000, 2003, 2004; 2007; 2008a; 2008b), *V. lagopus* (see *inter alios* Daitch & Guralnick, 2007; Szuma, 2008c; 2011; Gimranov et al., 2015; Gimranov, 2017), or even *V. corsac* (see Gimranov et al., 2015; Gimranov, 2017). As clear from Figs. 3.8.9-3.8.11, no peculiar or specifically distinctive patterns arise

from the analyses of upper and lower teeth morphology. The variable features (*e.g.*, central protocone crest and the mesial cingula on P4; the lingual cingulum of M1; the transverse cristid on m1; reduction of m1 entoconid; m1 entoconulid) are distributed randomly within the samples and also among individuals, without homogeneity. Considering the shown degree of interspecific variability (lower than the intraspecific one displayed by the *V. vulpes*) and the heterogeneous

Figure 3.8.10 – Detailed pictures of the p4-m3 of fossil *Vulpes* from several European localities. **A-M**, *V. alopecoides* from Europe. **A**: **DFN-22**, left p4-m3 from Dafnero-1. **B**: **DFN-172**, right p4-m2 from Dafnero-1 (reversed). **C**: **DFN-190**, left p4-m3 from Dafnero-1. **D**: **MG 29-2013/461**, right m1-m2 from Kvabebi (reversed). **E**: **IPS 27246**, left m1-m2 from La Puebla de Valverde. **F**, **IPS 27247**, left m2 from La Puebla de Valverde. **G**, **IPS 27248**, right m1 from La Puebla de Valverde. **H**, **IPS 27259**, right p4-m3 from La Puebla de Valverde. **I**: **PN 28**, left p4-m1 from Pirro Nord. **J**: **PU104721**, right m1 from Pirro Nord (reversed). **K**: **PU106227**, right m1 from Pirro Nord (reversed). **L**: **V.61.1401**, right m1-m2 from Villany 3 (reversed). **M**: **APL-11**, right p4-m2 from Apollonia-1 (reversed). **N-V**: *V. praecorsac* from Hungary. **N-O**: **V.13.04696.0** (type), right m2 (reversed) and left m1 from Nagyharsanyhegy 4. **P**: **V.61.1372**, left p4-m1 from Villany 8. **Q**: **V.13.04785.0**, right m1 talonid from Püspökfurdò/Betfia 2-4 (reversed). **R**: **VER.2018.2630**, left m1 from Somssich Hill 2. **S**: **VER.2018.2638**, right m1 from Somssich Hill 2 (reversed). **T**: **VER.2018.2641**, left m1 from Somssich Hill 2. **U**: **VER.2018.2676**, left m1 from Somssich Hill 2. **V**: **VER.2018.2678**, left p4 and m2 from Somssich Hill 2. **W-D'**: *V. praeglacialis* from Hungary. **W**: **V.2014.2.5.1** (type), right m1-m2 from Villany 3 (reversed). **X**: **V.2014.5.1.2** (type), right m1 from Villany 3 (reversed). **Y**: unnumbered specimen, right m1-m2 from Villany 3 (reversed). **Z**, **V.2014.2.5.2**, left p4-m1 from Villany 3; **A'**: **V. 2014.2.5.4**, right m1 from Villany 3 (reversed); **B'**: **V.13.3632_c**, right m1 from Villany 3 (reversed). **C'**: **V.13.3632_d**, left m1 from Villany 3. **D'**, **V.13.10754.1**, right m1 from Püspökfurdò/Betfia 2-4 (reversed). **E'-F'**: *V. praeglacialis* from Petralona. **E'**: **PET-1600**, left m1-m2. **F'**: **PET-1602**, right m1-m3 (reversed). **G'**: *Vulpes praeglacialis* from Cal Guardiola. **IPS 14748**, right m1-m2 (reversed). **H'-I'**: *Vulpes* sp. from Vallparadís Estació. **H'**: **EVT 14842**, right m1 (reversed); **I'**: **EVT 14942**, left p4-m1. **J'**: *V. praecorsac* from Deutsch Altenburg 2C. **UWPI 2275/13/17**, left p4-m2. **K'-L'**, *V. praeglacialis* from Deutsch Altenburg 2C. **K'**: **UPWI 2275/13/1**, right p4-m3 (reversed); **L'**: **UPWI 2275/13/26**, right m1-m3 (reversed). **M'-N'**: *V. praecorsac* from Odessa Catacomb. **M'**: **O-1519**, left m1-m2; **N'**: **O-1520**, right m1 (reversed). Legend: solid arrows, presence of feature; dotted arrows, absence of feature; dashed arrow, reduced/poorly developed feature.

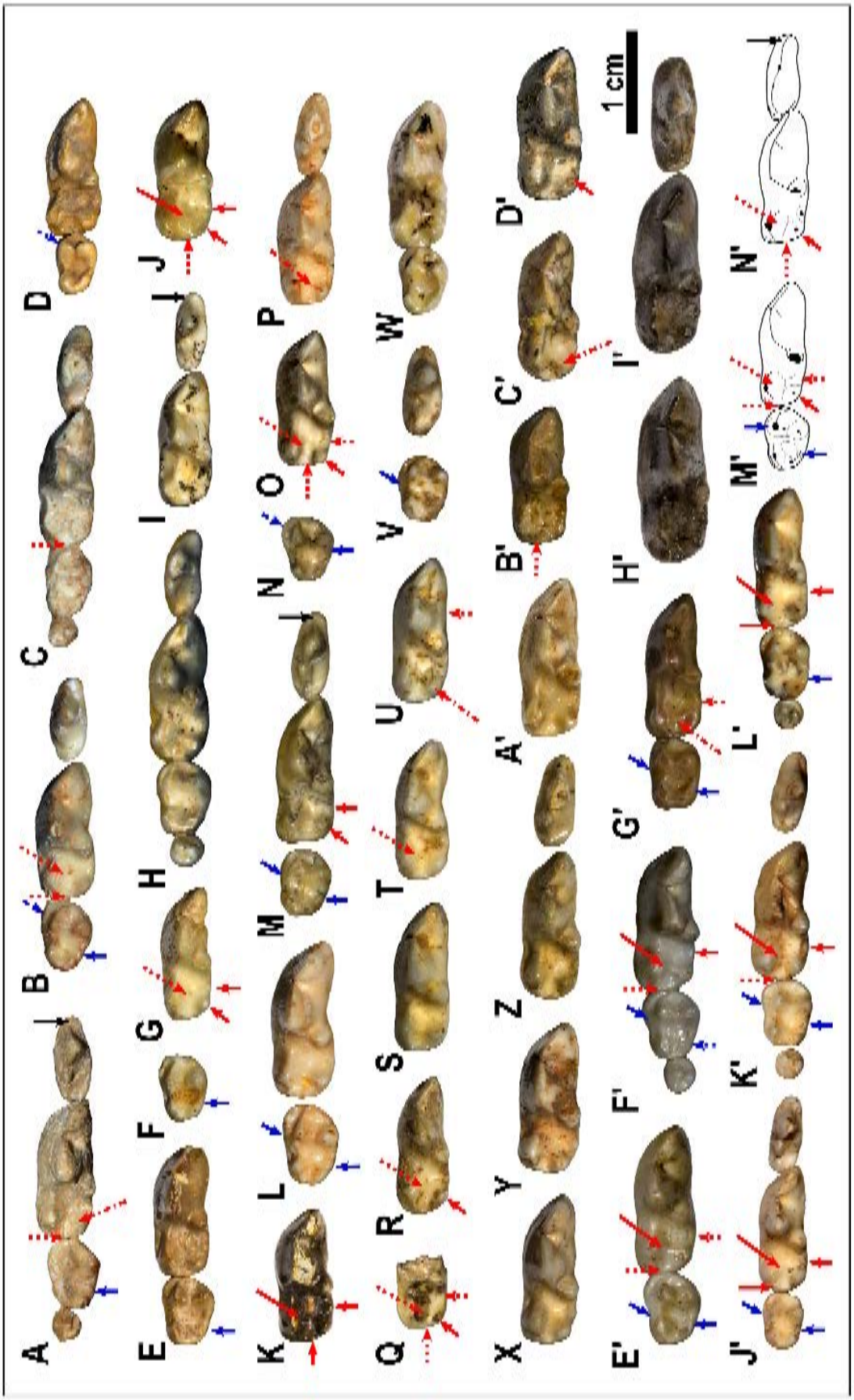
A
B
C
D
E
F
G
H
I
J
K
L
M
N
O
P
Q
R
S
T
U
V
W
X
Y
Z
A'
B'
C'
D'
E'
F'
G'
H'
I'
J'
K'
L'
M'
N'
1 cm

nature, the hypothesis of taxonomical distinction in three species does not appear parsimonious. As evident from the section 3.8.3.1., the type material of *V. praeglacialis* described from Kormos (1932) and the other material from Hungary (*i.e.*, from Villany 3, Villany 8 and Püspökfurdò/Betfia 2-4) do not show features distinctive from *V. alopecoides*. This is also true for the other occurrences attributed to *V. praeglacialis*: Apollonia-1 (Koufos, 2018); Cal Guardiola (Madurell-Malapeira et al., 2009); Deutsch Altenburg 2C (Rabeder, 1976); Petralona (Baryshnikov & Tsoukala, 2010); Venta Micena (Madurell-Malapeira et al., 2014). The features possessed by the sample of *V. praecorsac* of Somssich Hill 2 do not fit with the specific attribution. The mesial cingula on the P4 (mesiobuccal, that around the protocone, and the mesiolingual one), the development of the cusps on the M1, the presence of the cristid transversa on m1, the developed m1 entoconid (compared to the type *V. praecorsac*), the evident entoconulid and the marked buccal cingulid on the m2 are all features typically possessed by *V. alopecoides* (as visible from Figs. 3.8.9-3.8.11). Therefore, this sample can be reascribed to the latter species. The sample of *V. praecorsac* from Deutsch Altenburg 2C does not show distinctive morphological features compared to that of *V.* "*praeglacialis*" from the same site. The whole sample might be ascribed to *V. alopecoides*. The comparative analyses on the teeth morphologies suggest another important aspect. Considering that specimens confidently attributable to *V. praecorsac* (*i.e.*, coming from the site of original description) are very few, and the striking dental similarity with the sample of *V. alopecoides* from European localities, the hypothesis of a plausible synonymy between these two species seems supported. Indeed, as it is defined (*i.e.*, based on the scanty Hungarian material; without a certain diagnostic feature, but rather an inconsistent pattern of characteristics) *V. praecorsac* cannot be considered as a valid species. It is more parsimonious to ascribe its specimens to *V. alopecoides* (Del Campana, 1913).

The inclusion of *V. praecorsac* and *V praeglacialis* in *V. alopecoides*, does not exclude

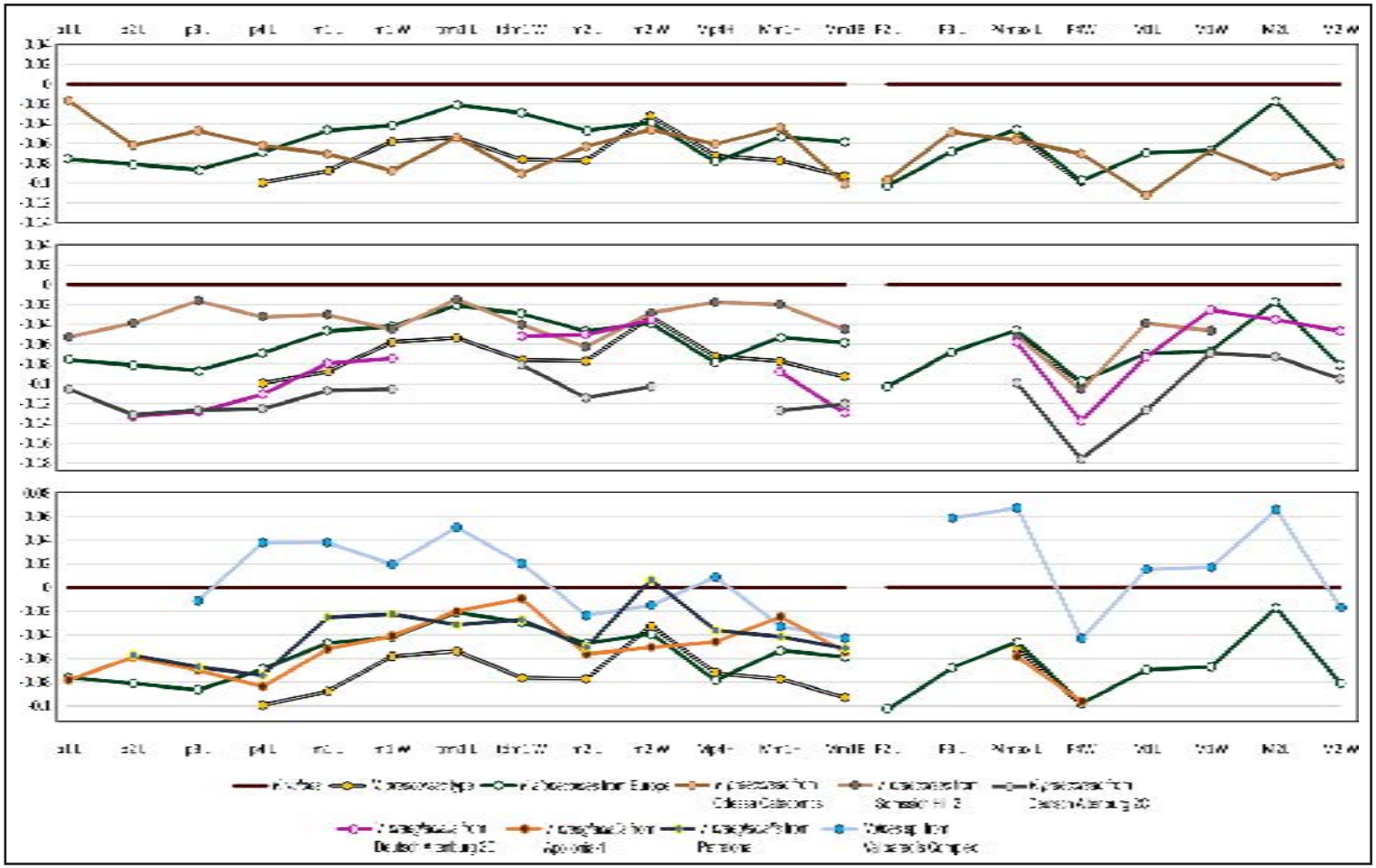

Figure 3.8.11 – Log-ratio diagram based on selected dentognathic variables in *V. alopecoides s. l.* from Europe (*i.e.*, also including the specimens previously attribute to *V. praeglacialis*), in *V. praecorsac* and in other *Vulpes* spp. samples of Europe (*i.e.*, Odessa Catacombs, Somssich Hill 2, Deutsch Altenburg 2C, Apollonia-1, Petralona) as compared to extant *V. vulpes* (used as the reference baseline). In all log-ratios, the average of *V. vulpes* are the same as in Fig. 3.8.7.

the possible existence of another species of *Vulpes* in the Plio-Pleistocene of Eurasia. Indeed, *V.* "*praecorsac*" from Odessa Catacombs possesses distinctive characteristics compared to the other European samples. This is evident considering the morphology of the upper teeth (*e.g.*, the buccolingually enlarged P4, the M1 considerably stout and elongated mesiodistally) but also some lower teeth features testify to this distinction (*e.g.*, the considerable reduction of the m1 entoconid compared to the hypoconid, and its distolingual position in the talonid, the proportional reduction of the metaconid). This taxon could represent a different form, early arrived to Europe, later replaced by *V. alopecoides*-like foxes.

The log-ratio diagrams in Fig. 3.8.11 show the dental proportion variability of fossil samples compared to modern *V. vulpes*. The dental proportions of *V. praecorsac* were left separated from those of *V. alopecoides* to better compare the fossil samples attributed to this taxon and, also, to show the similarity between the two taxa. Dental proportions displayed by log-ratios do not have direct connection with phylogenetic affinities as shown by some research, rather comparable diet preference (Bartolini Lucenti & Rook, 2016; Bartolini Lucenti et al., 2017; see also sections 3.2.-3.4. and 3.9.-3.11.). This appears particularly true for foxes, as shown in Fig. 3.8.8C, in which different samples of extant *V. vulpes*, mean proportions of *V. lagopus* and *V. corsac* were plotted against the mean average of red fox (only for selected parameters as the measurements of the carnassial and height and breadth of the mandible at level of the m1). Several of the pattern displayed by the samples do not follow the average *V. vulpes*. On the contrary, the arctic fox and the corsac fox are rather similar one another. *V. corsac* and *V. lagopus* share a more carnivours diet, being hunters and scavengers, compared to the more generalist *V. vulpes* (Larivière & Pasitschniak-Arts, 1996; Audet et al., 2002; Clark et al., 2009). This preference reflects in different proportions of their teeth. Different populations of the extant red fox exploit different food source and this difference might result in a different pattern compared to the average (in relation to the sample size). In fossil species,

some interesting elements arise. The *Vulpes* from Odessa Catacombs, although similar in size to *V. alopecoides* and *V. praecorsac* show some peculiarity, especially in the upper teeth proportions, confirming the morphological data. The sample from Somssich Hill 2 is generally larger compared to *V. alopecoides* and *V. praecorsac*. Apart from the length of the p3, proportionally larger compared to p2 and p4, the other proportions resemble the *V. alopecoides*' ones. Two species were recognized from the sample of Deutsch Altenburg 2C but their proportions, like their morphologies, are strikingly similar one another. This evidence supports the ascription of the sample to a single taxon, whose pattern does not differ greatly from *V. alopecoides*. The sample of Apollonia-1 and Petralona confirm the morphological data of strong affinity to *V. alopecoides* from Europe. Although it does not show morphological distinctive features from *V. alopecoides*, the sample from Vallparadís Site Complex is considerably larger when compared to the former species. Its dental proportions, the upper teeth do not differ from the average *V. alopecoides*, whereas lower teeth proportions partially differ. This difference could be due to the scantiness of the record of *Vulpes* it Vallparadís Site Complex (NISP=2).

3.8.4. Conclusions

The present revision of the fossil material of *Vulpes* coming from the Hungarian sites, particularly from the Early Pleistocene Villany 3, dated to the, has revealed that the provisional attribution to *Vulpes praeglacialis* (Kormos, 1932) might not be correct. Indeed, the well-preserved cranial specimen V.61.1401 shows remarkable resemblance in upper teeth morphologies to the type specimen of *Vulpes alopecoides* (Del Campana, 1913) from Il Tasso. To test this hypothesis, the three most renowned species from the Europe have been reviewed, starting from their type specimens and descriptions. Moreover, the variability of extant foxes' species has been investigated, both directly and from literature, in order to obtain valid inferences on the intra- or interspecific variation of the fossil taxa.

Part of the of the problematic surrounding fossil foxes is the scantiness of their fossil record and, consequently, of their type material. The comparison between these materials and the correctly attributed V.61.1401 points out the synonymity between *V. alopecoides* and *V. praeglacialis*, with the latter as a junior synonym of the former. The smaller *V. praecorsac* is even more elusive in the fossil record compared to the other two taxa. The features classically used to discriminate between this species and other taxa (*e.g.*, reduction of m1 entoconid or absence of transverse cristid) are not homogeneously possessed by the type samples, and considering the great variability of modern *V. corsac*, *V. lagopus* and *V. vulpes* on these characteristics cautions is advisable. Moreover, the fossil specimens of *V. alopecoides s. l.* show a considerable degree of variation. All considerate, the inclusion of *V. praecorsac* in *V. alopecoides* appears a more parsimonious hypothesis. This simplification of the fossil record of Europe, does not exclude the possible existence of other species of *Vulpes* in the Plio-Pleistocene of Europe and Eurasia. Nevertheless, as it is defined, *V. praecorsac* does not show significant and substantial diagnostic features allowing to discriminate from *V. alopecoides* of Italy, Spain, France, Greece and Hungary.

3.8.5. Appendix

3.8.5.1. Tables of measurements of the specimens V. 61.1401.

Table 3.8.1 – Cranial measurements of V.61.1401, *V. alopecoides* from Villany 3 (Hungary).

Cat. N°	Element	Eu	PoCW	SH	PwP1	LBu	M2B	AC-M2 L	M1-M2 L
V.61.1401	cranium and L hemimandible fr.	44.12	20.3	38.3	10.5	21.5	27.1	49.5	13.9

Table 3.8.2 – Upper teeth measurements of V.61.1401, *V. alopecoides* from Villany 3 (Hungary).

Cat. N°	Element	P4 L	P4 Lmax	P4 W	M1 L	M1 W	M2 L	M2 W
V.61.1401	cranium and L hemimandible fr.	13.2	14.4	6.4	8.73	10.7	5.3	8.3

Table 3.8.3 – Lower teeth measurements of V.61.1401, *V. alopecoides* from Villany 3 (Hungary).

Cat. N°	Element	m1 L	m1 W	trm1 L	tdm1 W	m2 L	m2 W	Mm1H	Mm1B
V.61.1401	cranium and L hemimandible fr.	14.8	6	9.7	5.7	7.4	5.2	14.1	7.2

3.9. REVISING *"CANIS" FEROX* AND THE ECOMORPHOLOGY OF SOME LONG-GONE DOGS

3.9.1 Context

In the complex and debated framework of early *Canis* and *Eucyon*-like species across the world, the morphological features of *Canis ferox* were reviewed in the taxonomical and ecological framework of Mio-Pliocene Oloarctic Canini. Despite these taxonomical issues, *Eucyon* has been regarded as a genus of primitive canids, intermediate between the derived clades that radiated in the American continent and in the Old World during the Pliocene (namely the group of *Canis sensu lato* and that of South American canids; see Tedford & Qiu, 1996). The common dental features of Mio-Pliocene *Eucyon*-like taxa (from both North America and Eurasia) are suggestive of adaptations to a mesocarnivorous diet. Only two exceptions are currently known: one is *Nurocyon* showing a shift towards hypocarnivory (*i.e.*, thanks to a clear enlargement of the upper molars grinding area, with marked development of the cusps); the second one is *E. marinae* for which Spassov & Rook (2006), suggested a plausible adaption to a highly carnivorous diet somewhat similar to modern coyotes. Nevertheless, no research has methodically investigated the diet of *Eucyon* species yet. Subsequently, the results of the morphological and morphometric analyses on this taxon were tested using particular cranial and dental morphometric ratios (see section 2.2.3.). The selected ratios are here used for the first time to test the dietary preference of *Eucyon*-like taxa. The ratios used here and their description are reported in Table 3.9.1. All indices were calculated as in Van Valkenburgh (1989) and Van Valkenburgh & Koepfli (1993).

3.9.2. Systematic Paleontology

Order **Carnivora** Bowdich, 1821

Suborder **Caniformia** Kretzoi, 1943

Abbreviation	meaning
RBL	Relative blade length of the lower carnassial, obtained dividing the lenght of the trigonid part of the lower carnassial by the maximum length of the m1.
RPS	Fourth lower premolar shape, measured dividing its width by its mesiodistal length.
RLGA	The relative lower grinding area measured as the square root of the summed areas of the m1 talonid and m2, divided by the length of the m1 trigonid. Area was estimated as the product of the width and length of the talonid of m1 and of the m2.
RUGA	Relative upper grinding area measured as the square root of the summed areas of the upper molars divided by the anteroposterior length of the P4. Area was estimated by the product of width and length of M1 and M2.
M1BS	Length of the m1 trigonid relative to the dentary length, estimated as the ratio between the mesiodistal length of the trigonid and the dentary length (rostrocaudal length between the mesial side of the lower canine and the caudal margin of the mandibular condyle.
M2S	Relative size of the m2 estimated as the area of the lower m2 and the dentary length. Area is measured as in RLGA and dentary length as in M1BS
IxM2	Relative resistance of the dentary to bending in parasagittal plane as estimated by the second moment of area of the at the interdental gap between the first and second molars between m1 and m2 relative to the dentary length.
MAT	Mechanical advantage of the temporalis muscle, measured as the distance from the mandibular condyle to the apex of the coronoid process (see Fig. 3.9.2) divided by dentary length (measured as in M1BS)
MAM	Mechanical advantage of the masseter muscle, measured as the distance from the mandibular condyle to the ventral border of the mandibular angle (see Fig. 3.9.2) divided by dentary length (measured as in M1BS)
I2	Relative size of the second upper incisor, measured by the square root of the basal area of I2 divided by the condylobasal length of the skull. The area of the incisor was obtained as the product of the basal mesiodistal length and mediolateral width of the I2 (measured at the alveolus)
I3	Relative size of the third upper incisor, measured by the square root of the basal area of I3 divided by the condylobasal length of the skull. The area of the incisor was obtained as the product of the basal mesiodistal length and mediolateral width of the I3 (measured at the alveolus)
C1	Relative size of the upper canine, measured by the square root of the basal area of canine divided by the condylobasal length of the skull. The area of the canine was obtained as the product of the basal mesiodistal length and mediolateral width of the canine (measured at the alveolus)
C1C1	Relative width of the rostrum measured at level of the canines and divided by the condylobasal length of the cranium
UM2/1	Ratio of the square root of theare of the M2 and the square root of the area of the M1. The areas were measured as in RUGA

Table 1 Morphometric ratios used in the analyses and their definition, following Van Valkenburg & Koepfli (1993); Friscia et al. (2007).

Family **Canidae** Fischer, 1817

Subfamily **Caninae** Fischer, 1817

Tribe **Canini** Fischer, 1817

Subtribe **Canina** Fischer, 1817

Genus ***Eucyon*** Tedford & Qiu, 1996

Eucyon ferox (Miller & Carranza-Castañeda, 1998)

(Fig. 3.9.1; Tables 3.9.4-3.9.7)

Canis davisi Gustafson, 1978: 36.

Canis ferox Miller & Carranza-Castañeda, 1998: 549.

Canis ferox Tedford et al., 2009: 105 *pro parte*

Type. IGM 1130, fragmented cranium with poorly preserved left and right P3-M2; left hemimandible with fragmented p1, p3-p4 and preserved m1-m2. Postcranial elements (partially figured by Miller and Carranza-Castaneda, 1998) include an atlas fragment, a broken axis, III cervical vertebra, three thoracic vertebrae, a left scapula, a left and right humerus, a left femur, a patella, a right tibia, a right IV and a right V metacarpals, a left calcaneus, navicular, cuboid, cuneiform, left and right proximal epiphysis of the II metatarsals, nine phalanges.

Type locality. Rancho San Martin locality, Rancho Viejo village (Guanajuato, Mexico), lower portion of Rancho Viejo Beds (Carranza et al., 1994), late Hemphillian (ca 4.95-4.80 Ma, Flynn et al., 2005).

Paratypes. F:AM 49298 (Fig. 3.9.1), skull with left P2-M2 and right I1-I3, P2-M2, and mandible almost complete (right is broken distally to the m3 and lacks the ascending ramus), with left c1-m3 and right i3-p4, broken m1, m2-m3; axis and III cervical vertebra, one thoracic and two caudal vertebrae, broken pelvis. Golgotha Watermill Pothole site (Spring Valley, Lincoln County, Nevada), late Hemphillian.

F:AM 75848, skull composed of crashed cranium with left P1-M2 and right C-M2 and a right hemimandible with c, broken p2, p3-m2; F:AM 75821, left hemimandible with p2-m, probably same individual as F:AM75848; Redington Quarry (San Pedro River Valley, Pima County, Arizona), late Hemphillian (Quiburus Formation).

Age. late Hemphillian (North America Land Mammal Age); latest Miocene/earliest Pliocene.

Referred material. Bird Bone Quarry (Big Sandy Formation, late Hemphillian, Arizona): F:AM 63035, left and right hemimandible fragments with left c-m2 and right, p2, broken p3, p4, m1 and m2; F:AM 72556, left humerus; F:AM 72566, left radius; F:AM 72569A, left ulna; F:AM 72581, left metacarpal II; F:AM 72577, II, III, metacarpals and incomplete IV metacarpal; F:AM 72572A, left tibia; F:AM 72572C, left tibia; F:AM 72572B, left tibia; F:AM 72610, left II metatarsal; F:AM 72585B, left metacarpal II; F:AM 72611, left II metatarsal; F:AM 72587D, left II metatarsal; F:AM 72589B, IV left metatarsal; F:AM 72589A, right IV metatarsal.

Clay Bank Quarry (Big Sandy Formation, late Hemphillian, Arizona): F:AM 63060, right hemimandible fragment c–m2; 61612, left hemimandible fragment with p4, broken m1, and m2.

Redington Quarry (Arizona): F:AM 75822, right hemimandible fragment with m1–m2.

Leyden locality (Chamita Formation, late Hemphillian, New Mexico): F:AM 27388, left partial ramus with p3–p4 alveoli and m1–m2.

Comparison and Remarks

Reviewing the North American fossil Caninae, Tedford et al. (2009) supported the generic attribution of "*Canis*" *ferox* by Miller & Carranza-Castañeda (1998) for the retention in this taxon of some apomorphic features, distinctive when compared to the coeval *E. davisi*. These include the extension of the sagittal crest onto the frontals; the large fossa for the superior branch of the medial pterygoid muscle; the supraoccipital shield with triangular shape in caudal view; the inion that overhangs the occipital condyles in lateral view; and the ratio of radius/tibia length 80-90%

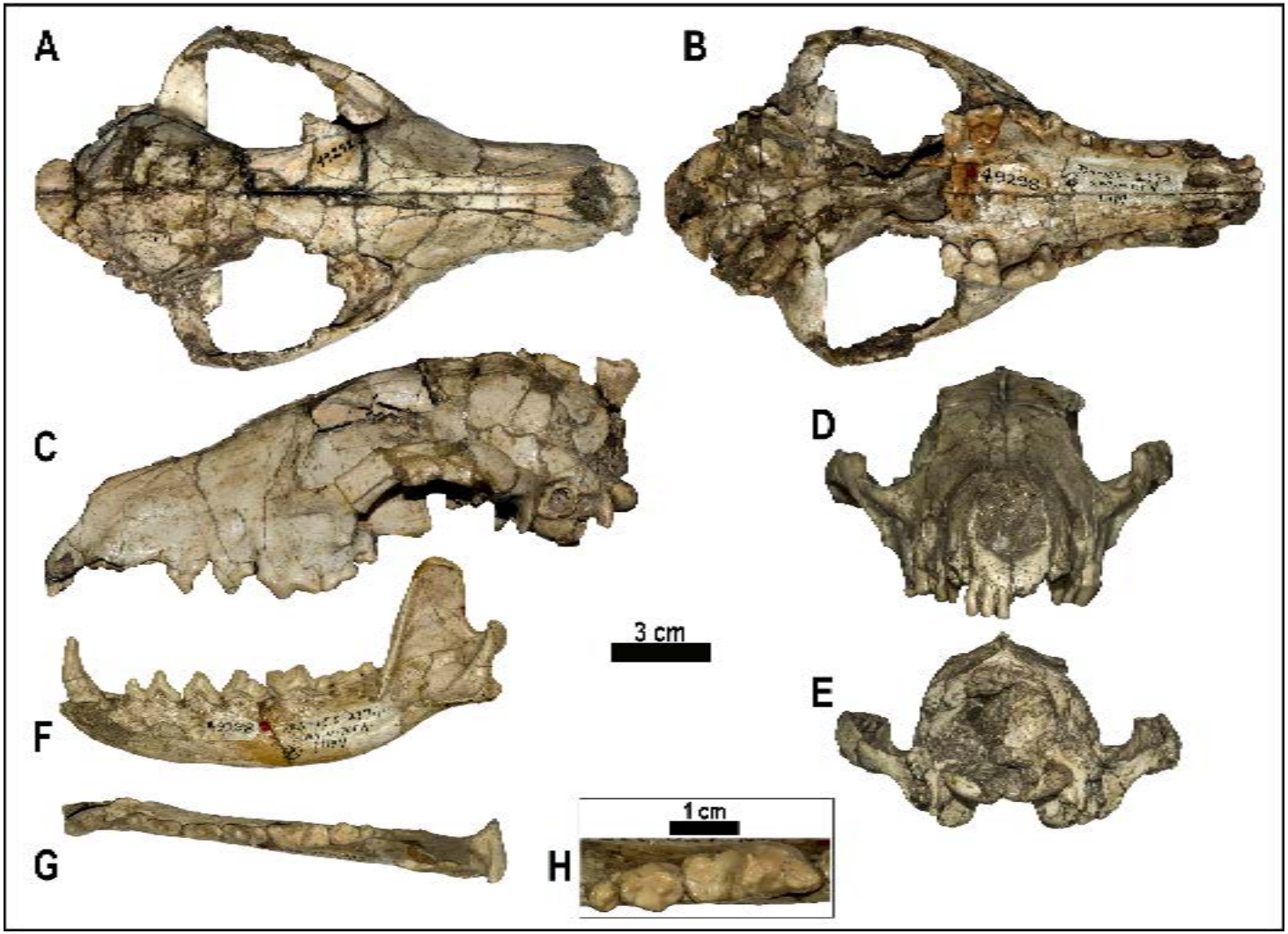

Figure 3.9.1 – Paratype material of *Eucyon ferox* (Miller & Carranza-Castañeda, 1998), F:AM 49298, skull. **A-E**: cranium in dorsal (**A**), ventral (**B**), left lateral (**C**), rostral (**D**), and caudal (**E**) views. **F-H**: left hemimandible in buccal (**F**) and occlusal (**G**) views. **H**: detailed occlusal view of the m1-m3.

(character matrix of cladistic analysis in Tedford et al., 2009: 162). This revision of the (para)type and referred material in comparison to the *Eucyon*'s variability across North America and the Old World reveals a different scenario (Fig. 3.9.2). For instance, in dorsal view, the supraoccipital shield shows an enlargement of the nuchal crest in the area of the external occipital protuberance (*e.g.*, F:AM 49298) typical of *Eucyon* species (*e.g.*, *E. adoxus*, *E. davisi*, *E. zhoui*) or in *Eucyon*-like taxa (*e.g.*, "*E.*" *kuruksaensis* or *N. chonokhariensis*). Compared to these species, this enlargement is less marked but certainly the paratype specimens of "*C.*" *ferox* do not possess the pointy and elongated shape of the external occipital protuberance on the dorsal part of the supraoccipital shield typical of early *Canis* members, like *C. lepophagus*, or even more recent ones as *C. edwardii*. Moreover, in these early *Canis* (*i.e.*, *C. lepophagus* and *C. edwardii*), the lateral expansion of the nuchal crest appears to angle forward more in lateral view, as opposed in "*C.*" *ferox*. In the latter species, this projection is prominent in lateral view, and it reflects in the inion strongly overhanging the occipital condyles (even in the type specimen, see Tedford & Qiu, 1996). On the contrary, in the crania of "*C.*" *ferox* the external occipital protuberance extends until the level of the condyles or slightly beyond them, similar the condition visible in *E. davisi*, *"E." kuruksaensis*, and *N. chonokhariensis* (Fig. 3.9.2). Curiously, some specimens of *E. zhoui* do possess caudal extension of the inion, prominently beyond the level of the occipitals. The "distinctly triangular" shape of the occipital region "with sharp, pointy apex" of the type specimen from Rancho San Martin described by Miller and Carranza-Castañeda (1998: 551), should be regarded as a morphology produced by breakage and/or some degree of diagenetic deformation, as the type specimen IGM 1130 is poorly preserved (Miller and Carranza-Castañeda, 1998). Moreover, "*C.*" *ferox* from Nevada, Arizona and New Mexico possesses several features that fit in the diagnosis of the genus *Eucyon* (Fig. 3.9.2) such as the reduced development of the I3 compared to the I2, with a poorly developed basal cingulum; the absence of the M2 metaconule but with a feeble

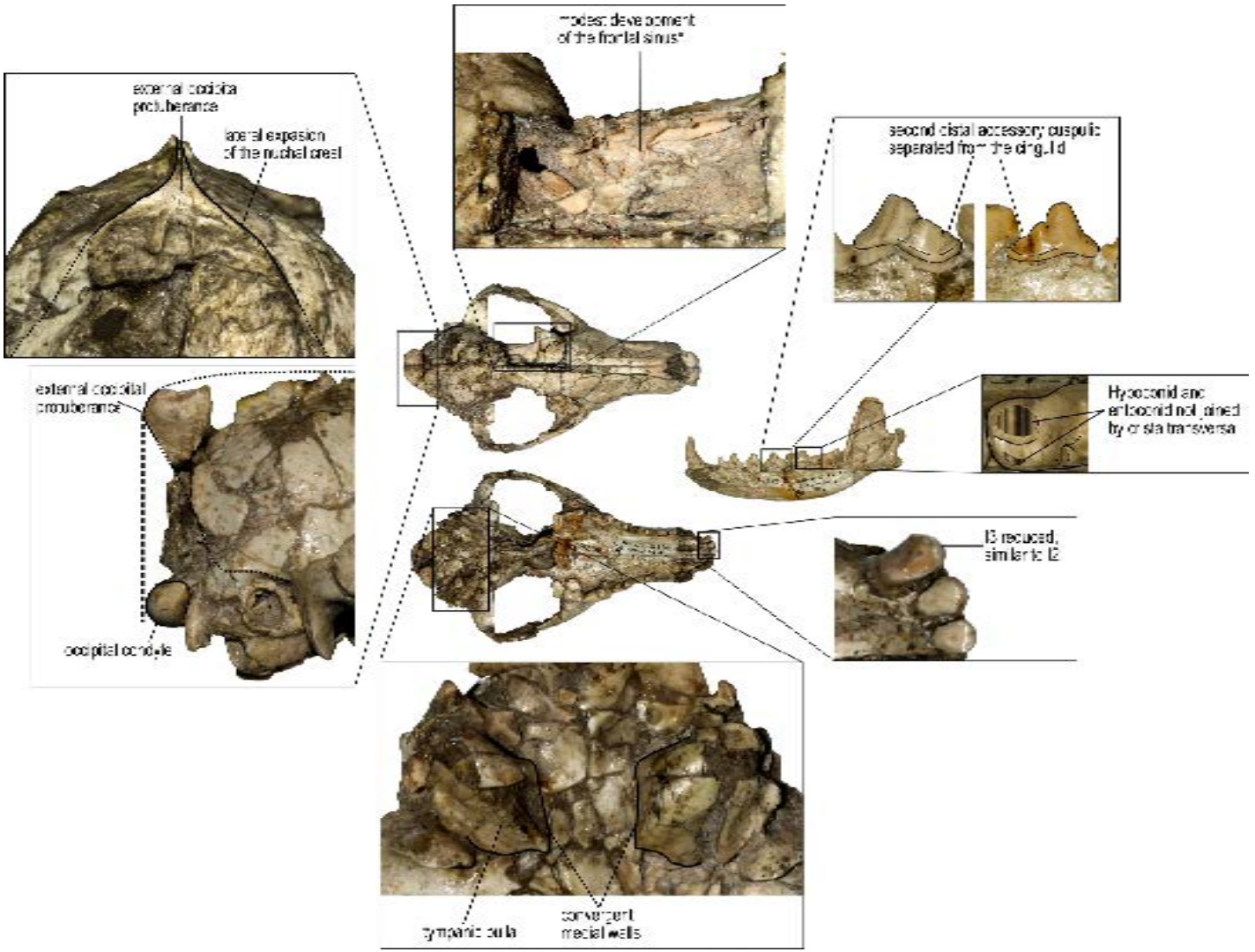

Figure 3.9.2 – Cranial and dentognathic characteristics consistent with genus *Eucyon* displayed by the paratype of "*Canis*" *ferox* specimen (F:AM 49298). Asterisk: morphology of the sinus cavity revealed by a section (removing the left side of the top of orbit and postorbital area) of the cranial specimen F:AM 49298.

postprotocrista; the lack of the transverse cristid connecting m1 entoconid and hypoconid (Figs. 3.9.1 and 3.9.2), and the radius/tibia ratio inferior to 80% (as given in Tedford et al., 2009). Even if used as phylogenetic characters by Tedford et al. (2009), the forelimb and hindlimb proportions and the ratios calculated on them show a great range of variability among the different canid taxa. In general terms, *Eucyon* taxa should possess a primitive state of radius/tibia ratio <80%, whereas a *Canis* species should show ratios of 0.80. As expected, *C. lepophagus*, *C. edwardii* and *Canis thöoides* Tedford et al., 2009 have high mean ratios (value=0.87; 0.88; 0.90 respectively; Table 7 in Tedford et al., 2009), but *E. davisi* possesses a mean radius/tibia ratio of 0.83. Moreover, one of the lowest values of radius/tibia ratio [the smallest being that of the ancestral *Leptocyon vafer* (Leidy, 1858), see Tedford et al., 2009] is shown by "*C.*" *ferox*, ratio=0.79, value considerably smaller than that of *Vulpes stenognathus* Savage, 1941 (ratio=0.86). Other putative diagnostic features of the genus are variable among the several described species, such as the size of M1 paracone and metacone, which are similar to one another in *E. davisi* from China and North America or *E. odessanus* from Odessa Catacombs but prominently different (with the paracone larger than the metacone) in *E. adoxus* or in *E. zhoui*. The development of the frontal sinus in the area posterior to the postorbital processes is similar to that of *E. davisi* but it tends to expand caudally, without reaching the frontoparietal suture (Fig. 3.9.2). The overall pattern of inflation of the sinus is similar to that of *E. zhoui* from Yushe Basin, *E. adoxus* from St. Estève, and that of *N. chonokhariensis*. Notably, Sotnikova (2006) and Sotnikova & Rook (2010) recognized a certain degree of affinity between *Nurocyon*, *E. adoxus* and "*C.*" *ferox*. In dorsal view, the caudally elongated shape of the frontals in the area of the postorbital constriction of "*C.*" *ferox* resembles the condition possessed by *N. chonokhariensis*, although this feature is particularly developed in this latter species. Indeed, this portion of the frontals is considerably inflated in *N. chonokhariensis*, so the frontal shield shows a marked and deep medial depression, more

developed compared to that of "*C.*" *ferox*. Several other cranial features allow to distinguish "*C.*" *ferox* material from *N. chonokhariensis*, *e.g.*, the broader muzzle, in dorsal view, and palate, in ventral one; the caudal extension of the distal part of the palatine, so that the palate ends well beyond the end of the toothrow. In lateral view, the frontals and the sagittal crests are more prominent in *N. chonokhariensis*, whereas the zygomatic process of the frontal in "*C.*" *ferox* is more developed, large and blunt compared to the Asian canid. The paracondylar processes in "*C.*" *ferox* are shorter compared to the dorsoventral height of the bulla, whereas in *N. chonokhariensis* they reached the ventral development of the bulla. In both taxa, these processes fuse to the bulla all along their length. The occipital regions markedly differs in the two species: the dorsal portion of the nuchal crest of *N. chonokhariensis* has a marked dorsally convex outline followed ventrally by a gentle lateral constriction, resulting in a bell-like shape of the occipital region in caudal view. In "*C.*" *ferox*, instead, the nuchal crest is slightly curved and poorly constricted laterally. Moreover, the occipital condyles in "*C.*" *ferox* are more slender and dorsoventrally compressed in comparison to those of *N. chonokhariensis*. In the latter, the mastoid process is prominent, ridge-like and evident in caudal view, whereas the former possesses a knob-like process but with a reduced lateral expansion. No mandibular specimens of *Nurocyon* are available at present; therefore it is impossible to assess the morphology of such elements. Despite a superficial similarity, we deem the two taxa to be rather distinct from one another.

Another key feature for carnivoran taxonomy is the morphology of the tympanic bulla (*inter alios* Fejfar et al., 2012; Bartolini Lucenti et al., 2017, Bartolini Lucenti, 2018; Rook et al., 2018). Many fossil *Canis* from Eurasia and North America (*e.g.*, *Canis etruscus* Forsyth Major, 1877 and *Canis arnensis* Del Campana, 1913 from Upper Valdarno, *Canis chihliensis* Zdansky, 1924 from Yushe Basin, *C. lepophagus* from Cita Canyon, TX, or St. David Quarry, AZ) possess the tympanic bulla with parallel medial walls, if observed in ventral view. Modern *Canis* species (*i.e.*, *C. an-*

thus, *C. aureus*, *C. latrans*, *C. lupus*, *C. simensis*) and the fossil *Canis mosbachensis* Soergel, 1925 and *Canis dirus* Leidy, 1858 show caudorostrally divergent medial walls. In *E. davisi* from North America and Asia, this feature resembles the condition shared by the majority of *Vulpes* spp., *i.e.* caudorostrally convergent outline of the medial walls. On the contrary, in *E. zhoui* and *E. adoxus* they are parallel. *Nurocyon* shares this latter morphology. The paratype specimen of "*C.*" *ferox* F:AM 49298 has clearly rostrally convergent medial walls, resembling the condition of *E. davisi*, rather than any other *Canis* species (Fig. 3.9.2).

The dental morphologies of "*C.*" *ferox* differ from the other Mio-Pliocene medium-sized canines (Fig. 3.9.3). In occlusal view, the P4 of "*C.*" *ferox* is stout, enlarged buccolingually and well developed. The robustness of this tooth contrasts with the shape of *Eucyon* spp. (including *E. cipio*), in which this tooth is more slender. In *C. lepophagus*, *C. edwardii*, and *C. thöoides*, the P4 is not enlarged and robust as in "*C.*" *ferox*. Unlike *E. davisi*, *E. zhoui*, and *C. lepophagus*, the protocone in "*C.*" *ferox* is reduced, not distinctively separated from the paracone. Furthermore, it lies at the level of the mesial margin of the P4 and does not project lingually. The protocone does not possess a high and sharp-pointed tip, in contrast to *Eucyon* spp. (*e.g.*, *E. davisi* or *E. zhoui*) or even numerous Pliocene *Canis* [the American *C. lepophagus*, *C. thöoides*, *C. edwardii*, or the Asian *Canis palmidens* (Teilhard de Chardin and Piveteau,1930) and *C. chihliensis* from Nihewan and Yushe basin]. The morphology of this cusp is similar to that of *E. cipio*. The paracone is stout and the metastyle is elongated distally. The M1 morphology is very peculiar, as it is reduced in buccolingual width. The paracone is considerably larger compared to the metacone, although the latter cusp is well-developed. This feature contrasts with *E. davisi* from Yushe Basin and North America, *E. odessanus* from Odessa Catacombs, *N. chonokhariensis* from Chonokhariakh, and *C. lepophagus* from North America that show the M1 cusps of comparable size, and resembles the condition of *E. adoxus* from St. Estève, *E. cipio* from Los Mansuetos, *"E." kuruksaensis* from Kuruksay,

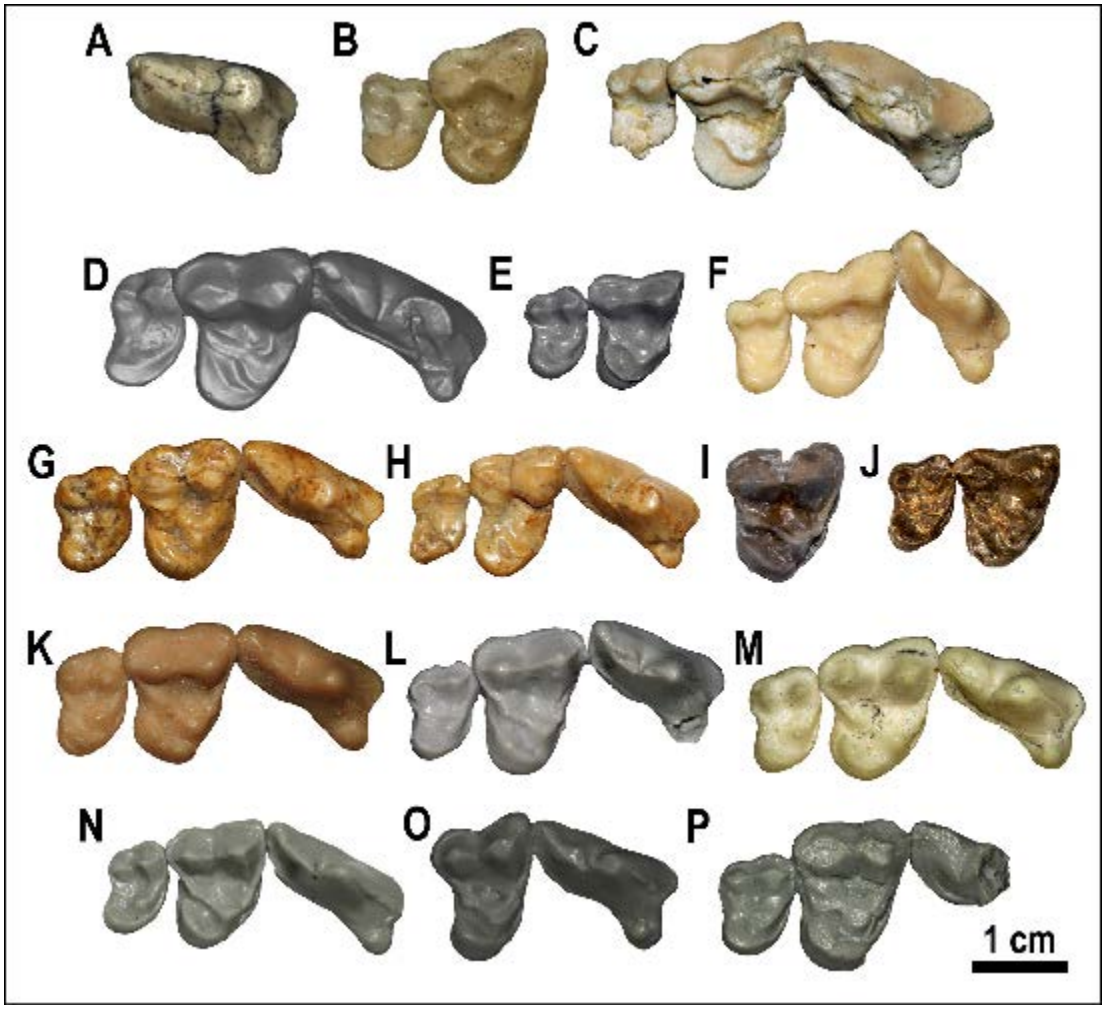

Figure 3.9.3 – Morphology of P4-M2 of various *Eucyon* and *Eucyon*-like taxa of Mio-Pliocene. **A-C**: *Eucyon ferox* from North America. **A-B**: **F:AM 49298**, detailed view of the left P4 reflected (**A**) and of the right M1-M2 (**B**) of the paratype cranium from Golgotha Watermill Pothole (U.S.A.). **C**: **F:AM 75848**, detailed view of the paratype cranium from Redington Quarry (U.S.A.). **D**: *Eucyon cipio* from Concud Cerro de la Gariata (Spain). **IPS 1988**, right maxillary fragment. **E-H**: *Eucyon davisi* from North America. **E**: **UCMP545**, type maxillary fragment from Rattlesnake creek (U.S.A.). **F**: **F:AM 63009B**, cranium from Clay Bank Quarry (Arizona). **G**: **F:AM 97057**, cranium from Xiakou (China). **H**: **F:AM 97059**, cranium from Xiakou (China). **I**: *Eucyon monticinensis* from Brisighella (Italy). **BRS 24-12**, right M1. **J**: *Eucyon debonisi* from Venta del Moro (Spain). **MNCN-VM-1**, maxillary fragment. **K-L**: *Eucyon zhoui* from Yushe Basin (China). **K**: **F:AM 97048**, cranial fragment from Zhaozhuang. **L**: **THP 10199**, type cranium from Yinjiao. **M**: *Eucyon adoxus* from St. Estève (France). **Rss 45**, type cranium. **N**: *Eucyon odessanus* from Odessa catacomb (Ukraine). **PIN 390-156/7018**, maxillary fragment. **O**: "*Eucyon*" *kuruksaensis* from Kuruksay (Kazakhstan). **PIN 3120-251**, type cranium. **P**: *Nurocyon chonokhariensis* from Chonokhariakh (Mongolia). **PIN 2737-257**, type cranium.

and *E. zhoui* from Yushe Basin. The buccal cingulum, both in occlusal and in buccal views, is prominent, continuous and almost shelf-like. The mesiobuccal side of the M1 has a sharp wedged shape, with a prominent parastyle. One of the most peculiar features of the M1 of "*C.*" *ferox* is the enlargement of the protocone, especially in comparison to the almost crest-like metaconule. Moreover, the lingual lobe of M1 tends to be reduced and with a semicircular outline in occlusal view, without expanding considerably lingually. In *Eucyon* spp., *"E." kuruksaensis* and *N. chonokhariensis* the M1 metaconule is evident as a cuspule, individualized from the postprotocrista. In the latter species, the lobe bearing the hypocone is generally more expanded lingually than in "*C.*" *ferox*. The M2 of "*C.*" *ferox* is reduced in buccolingual length relative to the M1, with an enlarged paracone and reduced metacone. By contrast, in *E. adoxus* from St. Estève, *E. davisi* from Yushe basin and North America, *E. debonisi* from Venta del Moro, *E. zhoui* from Yushe Basin, and *N. chonokhariensis* from Chonokhariakh the M2 are enlarged buccolingually and the metacone is equal in size with the paracone.

The mandible corpus in the type and paratypes of "*C.*" *ferox* is generally stouter and deeper compared to those of coeval and younger *Eucyon* species, or even to *C. thöoides* and *C. lepophagus* (Fig. 3.9.1). On the p4, the presence of a second accessory cuspulid, distal to the first one, has been described as an autopomorphy of *Eucyon* shared with *Canis* group (Tedford and Qiu, 1996). Whereas in *Canis* this cuspulid is fused to the distal cingulid, in *E. davisi* from Yushe Basin and North America and *E. odessanus* from Odessa Catacombs and Alatini the cuspulid is visibly identified from the bulging distal cingulid. In early species of *Canis*, *e.g. C. lepophagus* from North America (Tedford et al., 2009) or *C. palmidens*, a similar cuspulid is present but very reduced. In "*C.*" *ferox* the development of this feature resembles that of *E. davisi* from North America and Asia or *E. odessanus* from Odessa Catacombs. The majority of the m1 of the considered sample of "*C.*" *ferox* possess a reduced metaconid, closely attached to the protoconid. Only F:AM

63060 and F:AM 75848 show a more individualized m1 metaconid slightly projecting to the lingual side, in comparison to the other specimens but still reduced compared to other Mio-Pliocene American and Asian taxa, *e.g.*, *E. davisi* from Yushe Basin and North America, *E. adoxus* St. Estève, *E. zhoui* from Yushe Basin, *E. monticinensis* from Cava Monticino, *E. marinae* from Muhor-Erig, *E. odessanus* from Alatini and Odessa Catacombs, *Eucyon*? *skinneri* Tedford et al., 2009 from Nebraska, *C. lepophagus* from North America, and *C. thöoides* from Arizona. A condition similar to that of "*C.*" *ferox* can be noted in *E. cipio*. Furthermore, the m1 of "*C.*" *ferox* possesses an entoconid strongly reduced compared to the hypoconid, a condition shared with other allied or coeval canids although the size of the hypoconid relative to the talonid is similar to that of *E. marinae*, *E. minor*, and especially *E. cipio*. The m2 occlusal shape of *E. davisi*, *E. marinae*, *E. odessanus* and *E. zhoui* is rectangular, unlike "*C.*" *ferox* and *E. minor* that show a three-sided shape. This shape is due to the reduced talonid that, in the lingual part, does not project markedly on the lingual side. The m2 of "*C.*" *ferox* is characterized by the greater size of the protoconid compared to the metaconid, which is very reduced in size and height. This morphology differs from other *Eucyon*-like canids, which generally possess equal-sized protoconid and metaconid, with the exception of *E. minor* from Nihewan. The m3 in "*C.*" *ferox* is round in occlusal view. It is almost single-cusped, as the protoconid is considerably larger compared to the lingual cristid-like cuspulid. In *E. davisi* from both North America and China, *E. minor* from Nihewan, *E. odessanus* from Odessa Catacombs and Alatini, and *E. zhoui* possess a more oval m3, particularly for the development of a bulging cingulid that girdles the base of the occlusal surface of the tooth. Moreover, the m3 cuspulids are very similar in size in these species, unlike the condition of "*C.*" *ferox.* Although currently referred to this species, the medium-sized canid materials coming from other localities of North America (*e.g.*, UNSM locality Kx 113, Nebraska; Rexroad Local Fauna locality 3, Kansas; or the Hagerman fauna, Idaho) point

out that these samples do not fit in the diagnostic features showed by the type and paratype specimens of "*C.*" *ferox*. These specimens were ascribed to *C. lepophagus* by several researchers (Bjork, 1970; Nowak, 1979), yet they might represent a different, possibly new, species of *Canis*.

Potential convergence on hypercarnivory

Cranial and mandibular features

Several of the dental features displayed by "*C.*" *ferox* appear to be convergent to those in highly carnivorous canids, both extant and extinct. Among Caninae several species display such specialization. For instance, the fossil taxa of *Xenocyon* and the extant *Lycaon* and *Cuon* possess derived dental and skeletal features towards this dietary adaptation that prominently distinguish them from *Canis* spp. Within the genus *Canis*, the various species have various dietary habits, from mesocarnivory to hypercarnivory (see *inter alios* Nowak, 2005). These diet preferences are reflected in cranial and dentognathic morphologies; *e.g.*, the strong adaptations of *C. simensis*, as pointed out by Rook and Azzaroli, 1996. More clearly, hypercarnivorous taxa show similar specializations of certain features, probably as a result of convergent selection of more effective characteristics to a particular diet. For instance, the development of the frontal sinus is a characteristic often found in predatory carnivorans (Moore, 1981; Tanner et al. 2008). In modern Caninae, this is evident in *C. lupus*, *L. pictus*, and *C. alpinus*, in which the frontal sinus can be enlarged in rostrocaudal direction, as in the former, or shorter but considerably inflated compared to mesocarnivorous canids, in the latter two. Unlike condition of *Canis*, with a general inflation of the frontal shield area, "*C.*" *ferox* shows a less bulging frontal shield but considerably caudally elongated sinuses, close to frontoparietal suture (similar to the condition of *C. lupus*, and close-allied species). Whereas *Eucyon* species possess sharp-pointed postorbital processes generally slightly pointing caudally (*e.g.*, *E. davisi*, *E. zhoui*), *Canis* ones have three-sided and more rounded ones

(*e.g.*, *inter alios*, *C. lepophagus*, *C. arnensis*, *C. armbrusteri*, *C. lupus*). The zygomatic processes of the frontals of "*C.*" *ferox* are pointy and moderately arched distally. A convergent feature retained by numerous highly carnivorous taxa within Canidae is the deepening of the mandibular corpus at the level of the carnassial (*i.e.*, increasing dorsoventral height of the corpus), compared to close-allied species. The deep morphology of the mandible repeatedly independently appeared during Canidae evolution, *e.g.* within Borophaginae (Wang et al., 1999), in *V. lagopus* (Wang and Tedford, 2008), in *C. armbrusteri-C. dirus* (Tedford et al., 2009), in *C. lupus*, in *C. chihliensis* (see Tong et al., 2012), and in the *Xenocyon* lineage (*inter alios* Rook, 1994; Madurell-Malapeira et al., 2013). The type and paratype specimens of "*C.*" *ferox* show a rather deep mandible corpus at the level of the lower carnassial.

Upper and lower dental features

Dental morphology is by far the anatomical part of carnivorans that most correlates with diet. Common specializations involve the reduction of the P4 protocone; development of the slicing part of molar to the detriment of the crushing, M1 paracone enlarged compared to the metacone, considerably reduced M2, reduction or absence of the m1 entoconid, development of m2 buccal cuspids, and reduction or loss of the m3 (Biknevicius & Van Valkenburgh, 1996). The occlusal surface of the P4 protocone of *C. lupus*, *Lycaon* and *Cuon* (as well as in extinct species of *Xenocyon*, *e.g.*, *X. lycaonoides*) is blunt as the cusp is reduced to a crest-like fold of the enamel, unlike the condition of hypocarnivorous species (*e.g.*, *N. procyonoides*), in which the protocone is high and pointy. The specimens of "*C.*" *ferox* do not show a cusped protocone possibly similar to the former species. Although the buccal margin of the M2 of "*C.*" *ferox* possesses the bilobed morphology of *Eucyon* spp., unlike the latter, the tooth is buccolingually shortened compared to the mesiodistal length (whereas in *Eucyon* the M2 is rather elongated; see *inter alios E. davisi* from Yushe Basin and North America). Some hypercarnivorous species,

e.g., *X. lycaonoides* and *L. pictus*, possess a M2 reduced in buccolingual length while elongated in the mesiodistal sense.

Features of "Canis" ferox

As described above, the precise reassessment of the morphologies possessed by the type and paratype specimens of "*C.*" *ferox* advise to reconsider the validity of the diagnostic features that support its attribution to *Canis*. The larger size compared to *Eucyon* spp. or the inflation of the frontal sinus should not be considered reliable evidence of phylogenetic affinity. The latter feature is also influenced by dietary adaptations (Moore, 1981), like the development of the dimples of the *m. pterygoideus medialis* on the medial side of the angular process (Gaspard, 1964). The shape of the occipital triangle is difficult to assess in the type specimen IGM 1130 for its fragmented nature, whereas in the paratype F:AM 49298 the occipital region has a rounded dorsal margin (rather than triangular). Moreover, the inion does not overhang the occipital condyles, as in *Canis sensu lato*. "*C.*" *ferox* do not possess other *Canis* features such as the markedly enlarged I3 compared to the I2. The cristid connecting m1 entoconid and hypoconid cannot be seen in "*C.*" *ferox*. Altogether, the development of the features suggests a more plausible attribution to the genus *Eucyon*.

Morphometric comparisons

Log-ratio diagrams were used to investigate the affinity of *Eucyon ferox* to other early Canini of North America and of Eurasia. Fig. 3.9.4 shows the cranial variability of some of the most complete species of *Eucyon* (*i.e.*, *E. adoxus* and *E. zhoui*), of *N. chonokhariensis*, of *"E." kuruksaensis* and of *E. ferox*, all compared to *E. davisi*. In size, *E. ferox* is considerably larger than *E. davisi*. Compared to *E. adoxus* and *E. zhoui*, it is generally of greater size, apart for the postorbital constriction. The large-sized *Nurocyon* is close to *E. ferox* (note the total length, width of the braincase and

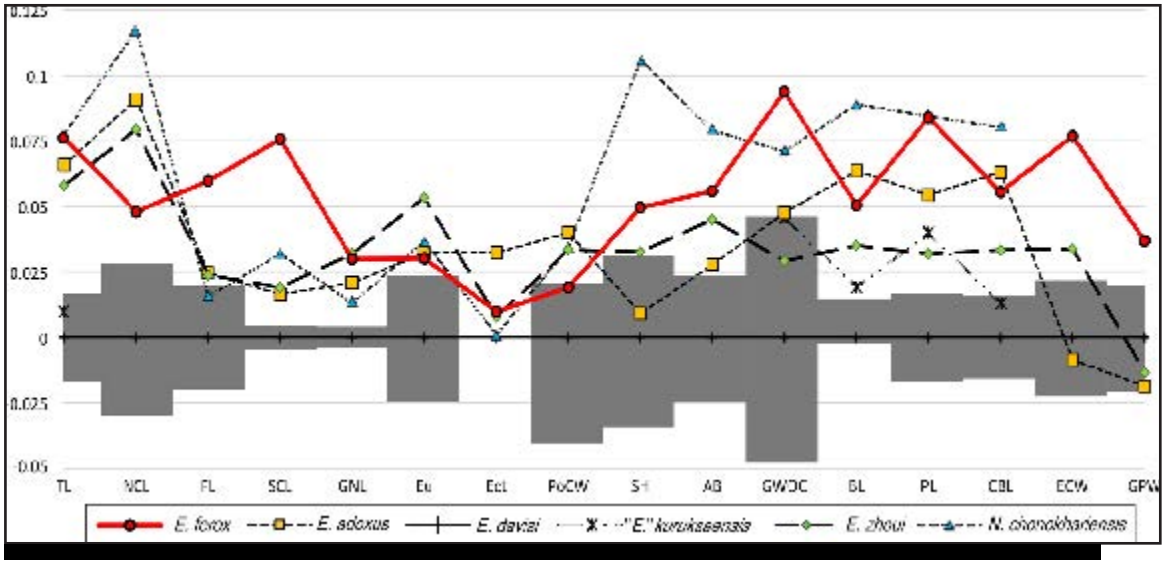

Fig. 3.9.4 – Log-ratio diagram based on selected cranial variables in the type and paratypes material of *E. ferox* as well as in other late Miocene-Early Pliocene *Eucyon* and *Eucyon*-like taxa ("*E.*" *kuruksaensis*, *E. adoxus*, *E. zhoui*, *N. chonokhariensis*) as compared to *E. davisi* (used as the reference baseline). The grey bars are ±1 σ for the individuals used to typify the standard.

palate length, almost equal), and both taxa have a great range of variation in cranial measurements, compared to the reference *E. davisi*. Considering the patterns of proportions, it is clear that *E. ferox* shows a peculiar set of proportions compared to the other *Eucyon* spp. and *N. chonokhariensis*. Only the arrangement of *"E." kuruksaensis* resembles that of *E. ferox*, although being smaller. Fig. 3.9.4 also points out the remarkable similarity between *E. zhoui* and *E. adoxus* is remarkable. They differ only for the braincase width-width across the postorbital processes, height of the cranium without the sagittal crest-greatest width of the occipital condyles and condylobasal length-width of the muzzle externally to the canines. Despite its size, *N. chonokhariensis* shares with the latter two species the majority of its proportions, diverging in the elongated muzzle (see the splanchnocranial length) and the higher cranium, both with or without sagittal crest (Fig. 3.9.4). The latter three proportions resemble those of *E. ferox*. The dental proportions (Fig. 3.9.5) confirm *E. ferox* as one of the largest taxa of the Mio-Pliocene medium-sized Canini. As shown in the same figure, the peculiar pattern of dental variables of *E. ferox* is not shared by any other taxa, apart from *E. cipio* (Fig. 3.9.5A). Although *"E." kuruksaensis* and *E.*

minor partially resemble the proportion of lower teeth (Fig. 3.9.5C), *E. cipio* better approximates the dental pattern of *E. ferox*. Combining the distinctive features with the morphometric results, it appears clear that *E. ferox* was a unique taxon of the Miocene canine guild of North America, which possessed several derived features (especially dentally) together with many primitive ones (particularly in the cranium but also in the dental morphologies). Although only known for a scarce record, the older Western Eurasian *E. cipio* retains comparable dental features and morphometric pattern to those of *E. ferox*. As questioned for the former taxon, the results presented here add new information in support of the generic attribution based on morphological data of *E. cipio* as well as *E. ferox*.

3.9.4. Results

3.9.4.1. Variability of canids with different dietary preferences

As teeth morphology and their relative size are the features most influenced by the dietary habits of an animal, we used a log ratio diagram on canids with different dietary adaptations and phylogenetically unrelated. In their pivotal work, Van Valkenburgh & Koepfli (1993) established four distinct groups, according to morphologies and the proportion of vertebrate prey in their diet (>70% in Group 1 and 2; 70-50% and <50% in Group 3 and Group 4, respectively; Van Valkenburgh & Koepfli, 1993). Group 1 and 2 differ in their habit of hunting large prey, Group 1, or small prey, Group 2. Fig. 3.9.6 shows the pattern of dental proportions of selected extant canids, one of Group 2, Group 3 and Group 4 and two of Group 1, and the fossil *E. cipio* and *E. ferox* as compared to *E. davisi*, chosen as a standard reference. Besides the phylogenetic distance and size difference, the taxa of Group 1 (*C. lupus*, *L. pictus*) and Group 2 (*V. lagopus*) show a remarkably similar pattern of proportions. By contrast, teeth proportions of *C. latrans* (Group 3, mesocarnivores) and *N. procyonoides* (Group 4, omnivores that occasionally take small prey) shows a different and distinct pattern. The proportions of *E. cipio* and *E. ferox*

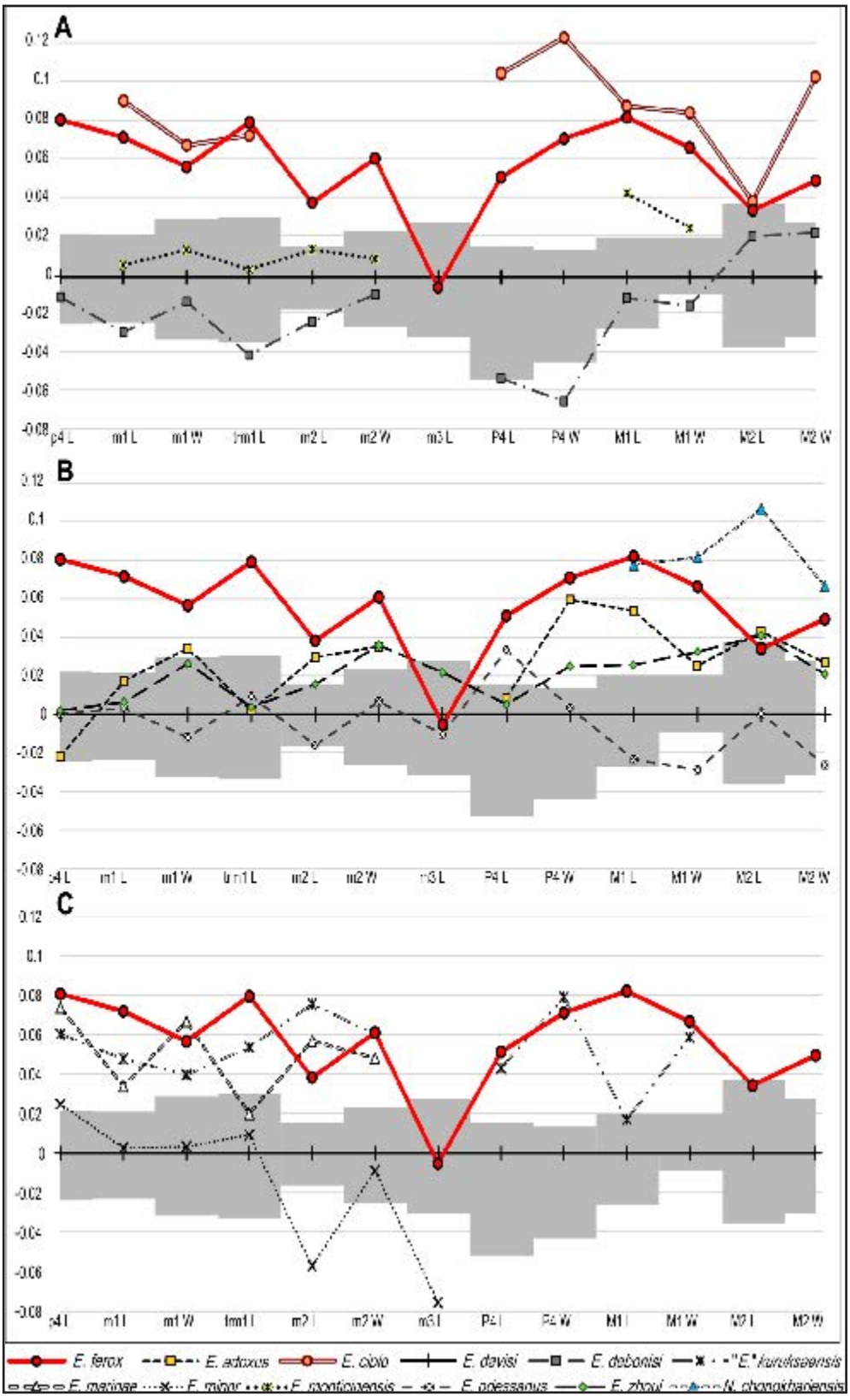

Figure 3.9.5 – Log-ratio diagram based on selected upper and lower dental variables in the type and paratypes material of *E. ferox* as well as in other late Miocene-Early Pliocene *Eucyon* and *Eucyon*-like taxa as compared to *E. davisi* (used as the reference baseline). The grey bars are ±1 σ for the individuals used to typify the standard.

clearly differs from those of *C. latrans* and *N. procyonoides*, especially considering the upper teeth (P4-M2). The trigonid blade of the lower carnassial of *E. cipio* and *E. ferox* is proportionally longer compared to *C. latrans*, whereas *N. procyonoides* is characterized by a considerably buccolingually enlarged lower carnassial. In size, *E. cipio* and *E. ferox* are close in size to *C. lupus* and *V. lagopus*. The lower forth premolar of *E. ferox* is proportionally longer compared to the lower carnassial like in *V. lagopus*. The relative width of the m1 of *E. ferox* is narrow compared to *C. lupus* and *L. pictus*, whereas resembles the condition of *V. lagopus*. The m2 of *E. ferox*, *C. lupus* and *L. pictus* is stout and enlarged buccolingually compared to the mesiodistal length, unlike *V. lagopus*. The upper teeth of *E. cipio* show a pattern that is approximated by *C. lupus* and *V. lagopus* (*e.g.*, the reduced length of the M1 compared to the P4; the width of the first molar proportionally similar to it length). In *E. ferox* the proportions of the upper teeth resemble the pattern of *L. pictus*, although smaller. The only difference is the buccolingually larger M2, more similar to *C. lupus* and *E. cipio*.

3.9.4.2. Morphometric ratios and diet investigation

Van Valkenburgh (1989) was among the first to use morphometric ratios to quantify difference in diet among carnivorans, showing that canids display a reduced degree of diet variation, compared to other families of Carnivora. Using selected parameters (as the relative length of the trigonid, RBL, the size of the p4, RPS, taking into account body size) at a smaller scale, difference within Canidae is visible (Fig 7). *C. lupus*, *L. pictus* and *C. alpinus* are distant from more generalist canids, centered in the tridimensional morphospace (*i.e.*, *V. vulpes*, *C. latrans*, *C. aureus*, *L. mesomelas*), for their high values of RBL and RPS that reflect their predilection of meat items and the high resistance of the p4 to biting stress. On the most negative corner of the plot lie *N. procyonoides*, an opportunistic and hypocarnivorous species. The arrangement of canids in Fig. 3.9.7 agrees with the dietary habits of

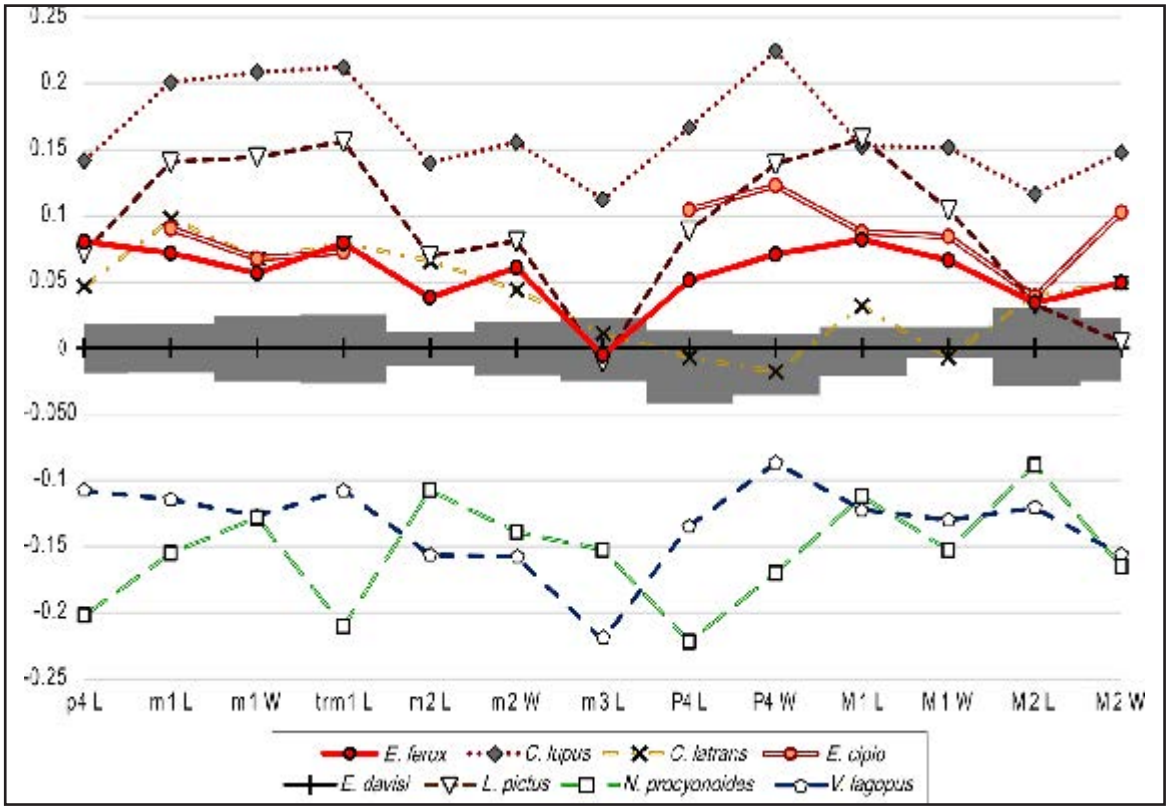

Figure 3.9.6 – Log-ratio diagram based on selected upper and lower dental variables in the type and paratypes material of *E. ferox* and *E. cipio* compared to some extant canids (*C. lupus*, *L. pictus*, *N. procyonoides*, *V. lagopus*). *E. davisi* is used as the reference baseline. The grey bars are ±1 σ for the individuals used to typify the standard.

the taxa and it is consistent with the results for all Carnivora (particularly those of Van Valkenburgh, 1989: Fig. 15.8). Plotting the extinct taxa *E. ferox*, *E. adoxus*, *E. davisi*, *"E." kuruksaensis*, and *E. zhoui* (Fig. 3.9.7), we see that *Eucyon* species (*E. adoxus*, *E. davisi*, *E. zhoui*) lie in the proximity of the central group. Separated from the central clump, arise *"E." kuruksaensis* and *E. ferox*. Of the two, *E. ferox* possesses the largest p4 and the relatively longest m1 trigonid blade of all the other fossil taxa considered. This results in a decentralized position, projected towards the position of *C. lupus* and *L. pictus*. Although the reconstructed body size of *E. ferox*, based on its condylobasal length of the cranium, is smaller than those of the latter species, it is very similar to the average one of *C. alpinus*. Uncertain is the condition of *"E." kuruksaensis*, whose value of RPS and RBL are close to those of *V. lagopus*, although considerably larger in size. To further investigate the variability of the

studied fossil species, and particularly of *E. ferox*, we used biplots and a three-dimensional plot of Van Valkenburgh & Koepfli (1993)'s morphometric ratios. The absence of morphological features related to a prominently hypocarnivorous diet in *E. ferox* led us to exclude the members of Group 4 from the following plots. The tridimensional space formed by three of these ratios (the relative length of the upper second incisor and canines and the mandible rigidity) is reported in Fig. 3.9.8. Additional plots are reported in Fig. 3.9.11. All species of Group 1 show increased value of resistance, whereas the other extant species have considerably lower values. For I2 and C1, *C. lupus* and *L. pictus* possess the largest ratios of the extant stock, whereas *C. alpinus* and *Speothos venaticus* (Lund, 1842) are close to *V. lagopus* (Group 2) and *C. latrans* (Group 3). As in Fig. 3.9.7, the fossil *E. adoxus*, *E. davisi*, and *E. zhoui* cluster together in the center of the morphospace, close to *V. vulpes*. *E. ferox* is prominently separated from the other species, for all the considered ratios. Although its indices are smaller, the isolated position of *E. ferox* in the morphospace is similar to *C. lupus* and *L. pictus*, which lie far from the central cluster of the other canids, fossil and extant.

3.9.4.3. Prey size

The estimation of typical prey size of fossil *Eucyon* followed the least squared regression of Van Valkenburgh et al. (2003). The results of the method applied to our sample of *Eucyon* and *Eucyon*-like taxa are reported in Table 3.9.2. All of the species apparently consumed prey considerably smaller than themselves. Although, as known from literature (*inter alios*, Van Valkenburgh & Koepfli, 1993), prey size is related to size of the predator, some interesting pattern are evident. Although of comparable size, the maximum depth of the mandible of *E. davisi*, *E. monticinensis*, *E. odessanus* and *E. zhoui* suggests possible different prey size. Particularly *E. monticinensis*, although probably smaller that *E. zhoui*, hunted larger prey compared to the latter. In *E. ferox* the difference between predator and prey size is

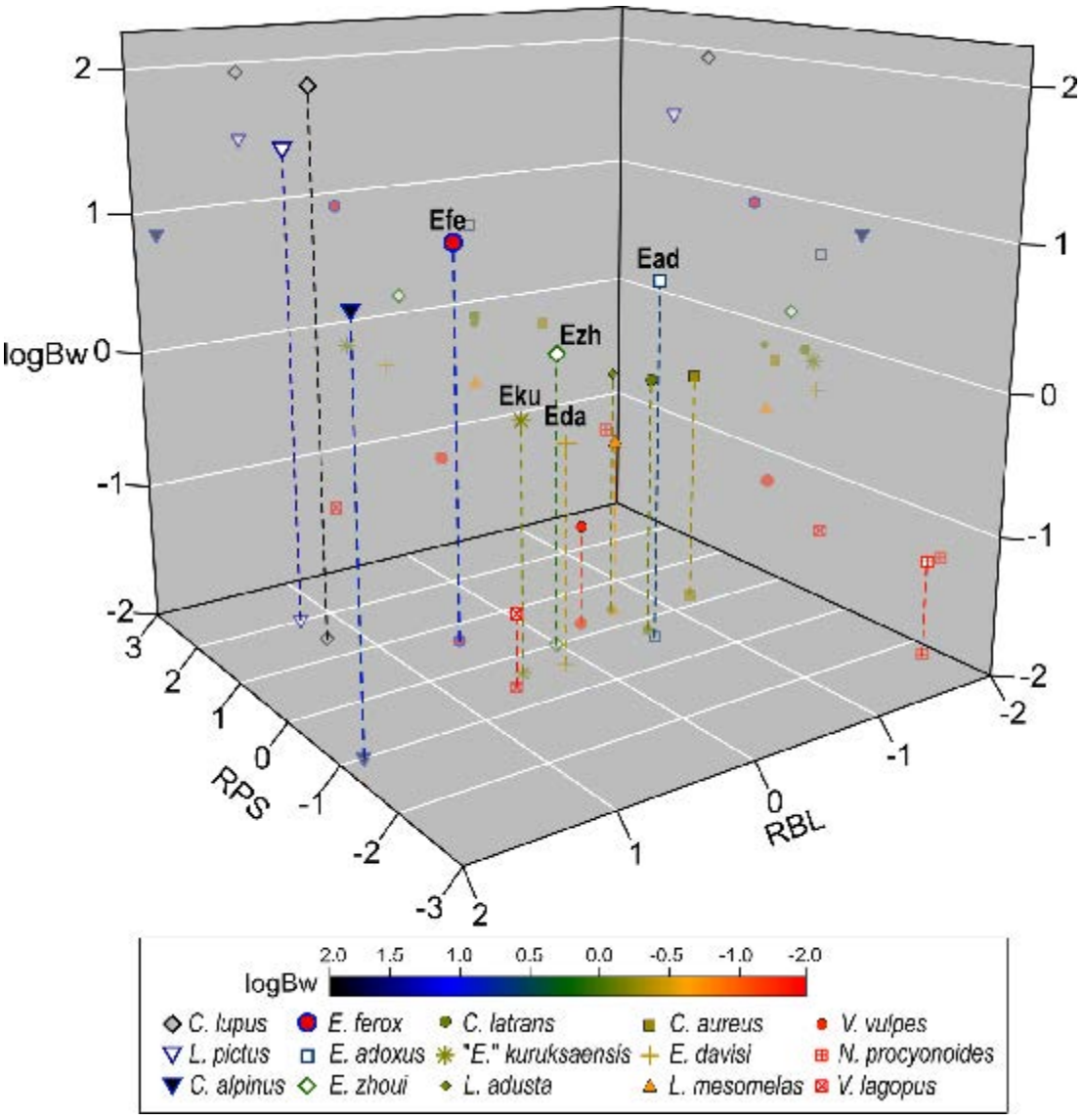

Figure 3.9.7 – Morphospace of dietary preferences of extant and extinct canids obtained by the relative premolar size (RPS), relative length of the trigonid blade (RBL) and logarithm of the body size (logBW). Color code identifies the variation of body size. Data on extant species are partially taken from Van Valkenburgh (1989). Abbreviations: **Ead**, *E. adoxus*; **Eda**, *E. davisi*; **Efe**, *E. ferox*; **Eku**, "*E.*" *kuruksaensis*; **Ezh**, *E. zhoui*.

reduced (ca 20% compared to 66-94% of the other *Eucyon* spp.). Unfortunately, no mandibular specimen of *E. cipio* has been recovered, thus preventing estimation for this species.

3.9.4.4. Analysis of variance

The results of tests of significant difference between *E. ferox* and the dietary groups

	Max. Jaw depth (mm)	Estim. Body size (kg)	Estim. Prey size (kg)
E. ferox	23.15	18±2	14
E. adoxus	19.65	14	5
E. davisi	16.65	11±1	2
E. debonisi	13	10±1	1
E. monticinensis	18.7	12±1	5
E. odessanus	16.95	11±1	2
E. zhoui	17.65	13±1	3

Table 3.9.2 – Jaw depth values (measured buccally at level of m1-m2 interalveolar space), estimated body size (methods of Van Valkenburgh, 1990) and estimated typical prey size (according to least regression equation of Van Valkenburgh et al., 2003) for Holarctic *Eucyon* and *Eucyon*-like taxa. Both estimated sizes are rounded to the nearest kilogram.

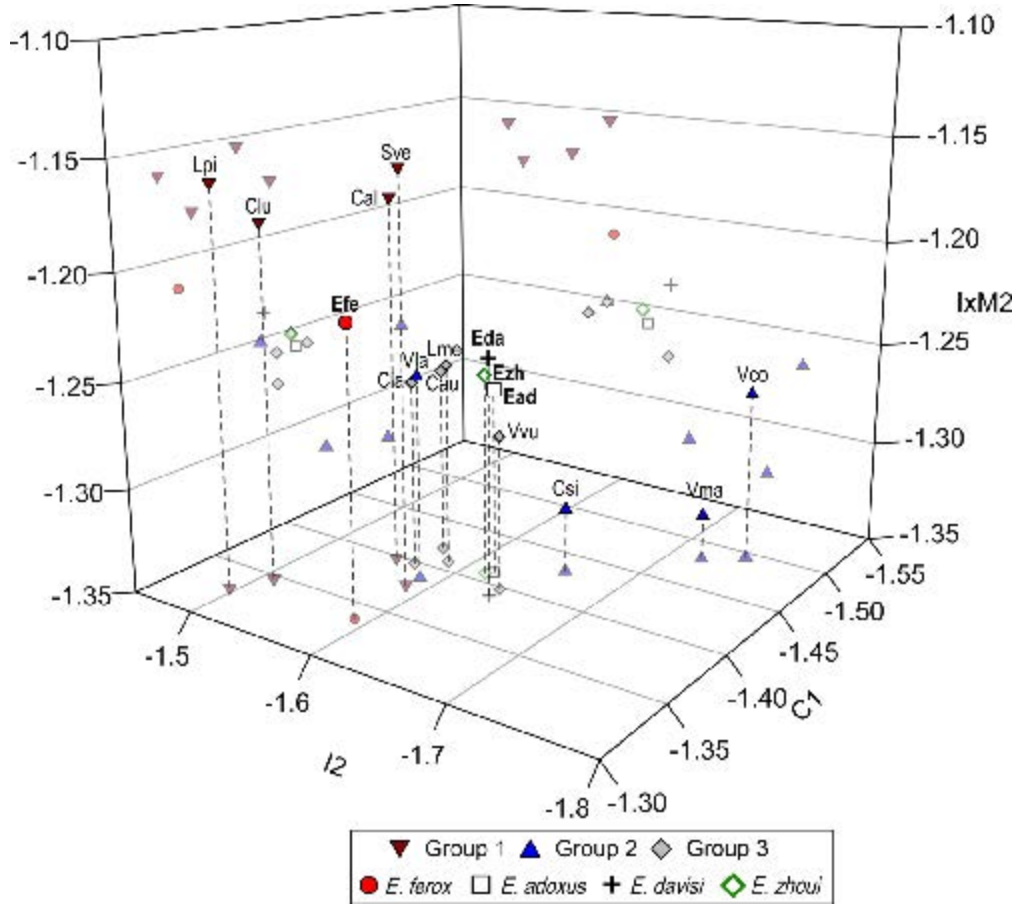

Figure 3.9.8 – 3D scatter-plot obtained plotting the relative size of the second upper incisor (I2), and of the upper canine (C1) and the relative resistance of the dentary to bending in the sagittal plane (IxM2). Groups follow Van Valkenburgh & Koepfli (1993). Abbreviations: **Cal**, *C. alpinus*; **Clu**, *C. lupus*; **Csi**, *C. simensis*; **Ead**, *E. adoxus*; **Eda**, *E. davisi*; **Efe**, *E. ferox*; **Eku**, "*E.*" *kuruksaensis*; **Ezh**, *E. zhoui*; **Lme**, *L. mesomelas*; **Lpi**, *L. pictus*; **Sve**, *S. venaticus*; **Vco**, *V. corsac*; **Vla**, *V. lagopus*; **Vma**, *V. macrotis*; **Vvu**, *V. vulpes*.

of Van Valkenburgh & Koepfli (1993) ($p<0.05$) is reported in Table 3.9.3. As opposite to Group 1 (hypercarnivores hunter of large prey), *E. ferox* differs for the larger grinding area of lower molars (RLGA), the reduced mechanical advantage of the *m. masseter* (MAM) and the reduced relative width of the cranium across the canines (C1C1). The latter two features are also different from those of Group 2 (hypercarnivores hunting small prey). Moreover, the increased mandibular rigidity (IxM2) and the relative stoutness of the canines (C1) are further differences between *E. ferox* and Group 2. Six of the 13 ratios differ significantly between *E. ferox* and Group 3 (mesocarnivores), whereas the fossil species differs significantly from Group 4 (omnivores that occasionally take small prey) in all the ratios (Table 3.9.3). Apparently, *E. ferox* cannot be included in any of the dietary groups of modern canids, despite possessing numerous similar morphometric ratios with Group 1 and 2.

3.9.4.5. Principal and discriminant analyses

The results of a principal component analysis based on 12 variables are reported in Fig. 3.9.9 (see section 3.9.7.). In this analysis, we included all four Groups described by Van Valkenburgh & Koepfli (1993). PC1, which accounts for 63.9% of total variance, has positive loadings for the majority of the original variables (see Table 3.9.8), and it is largely influenced by the cranial, upper teeth and mandibular resistance. On this axis, the canids of Group 1 (on the positive end) are well divided from those of the other groups, sparsely spread. The extinct species, apart from *E. ferox*, lie on the positive side of the graph, in the space where Group 2 and Group 3 overlap. *E. ferox* is isolated from the fossil taxa, but close to *V. lagopus* and toward species of Group 1. PC2 accounts for 14.1% of variance and it is majorly influenced by the relative grinding areas (positively) and the lower teeth ratios (*e.g.*, RBL, negatively). Most of the members of Group 4 possess positive values, whereas the rest of the extant species vary and overlap considerably along this axis. Fossil species show small values (positive in *E. adoxus* and *E. zhoui*, and

	E. ferox		Group 1	Group 2	Group 3	Group 4
RBL	0.697 (0.012)	3,4	0.657 (0.03)	0.646 (0.028)	0.638 (0.018)	0.63 (0.042)
RLGA	0.721 (0.022)	1,3,4	0.683 (0.77)	0.762 (0.067)	0.805 (0.053)	0.907 (0.108)
RUGA	0.873 (0.042)	4	0.844 (0.1)	0.919 (0.07)	0.896 (0.046)	1.066 (0.091)
M1BS	0.099 (0.001)	4	0.103 (0.009)	0.091 (0.007)	0.103 (0.007)	0.088 (0.009)
M2S	0.056 (0.002)	3,4	0.051 (0.009)	0.052 (0.004)	0.061 (0.006)	0.061 (0.005)
IxM2	0.061 (0.004)	2,3,4	0.068 (0.004)	0.051 (0.005)	0.055 (0.002)	0.05 (0.006)
MAT	0.249 (0.012)	4	0.264 (0.012)	0.232 (0.021)	0.243 (0.014)	0.227 (0.014)
MAM	0.367 (0.020)	1,2,3,4	0.427 (0.004)	0.354 (0.028)	0.389 (0.015)	0.341 (0.038)
I2	0.025 (0.001)	4	0.029 (0.003)	0.022 (0.003)	0.026 (0.003)	0.019 (0.003)
I3	0.029 (0.001)	4	0.033 (0.003)	0.029 (0.005)	0.031 (0.003)	0.023 (0.004)
C1	0.046 (0.001)	2,3,4	0.043 (0.004)	0.037 (0.004)	0.039 (0.002)	0.032 (0.006)
C1C1	0.181 (0.004)	1,2,4	0.211 (0.021)	0.166 (0.018)	0.173 (0.008)	0.161 (0.013)
UM2/1	0.644 (0.042)	4	0.522 (0.096)	0.633 (0.016)	0.626 (0.047)	0.70 (0.044)

Table 3.9.3 Mean values and ratios with standard deviations for *E. ferox* and the dietary groups of Van Valkenburgh & Koepfli (1993). Ratios are defined in Table 3.9.1.

negative in *E. davisi* and *E. ferox*). The results of the discriminant analysis on the 12 variables used for the PCA on the fossil species and the dietary groups are shown in Fig. 3.9.10. The Axis 1 accounts for the 64.6% of the total variance. Major positive loadings for this axis (Table 3.9.9) are upper teeth ratios (*e.g.*, the relative length of the upper second and third incisors, of the canines) and of the mandible (the mandibular rigidity to bending on the sagittal plane and the moment of advantage of the *m. masseter*), whereas the major negative influence are the relative development of the upper molars and the upper and lower grinding area. On this axis the extant dietary groups are well separated from the Group 4 (on the negative end) to the Group 1 (on the positive end). The fossil species, *E. adoxus*, *E. davisi*

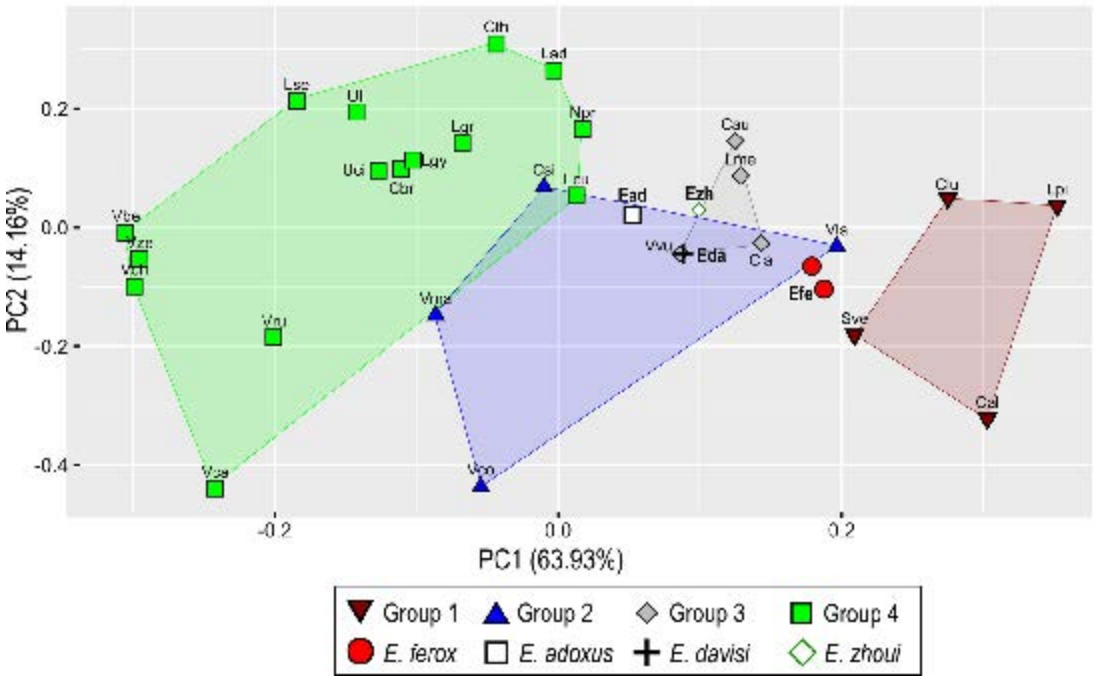

Figure 3.9.9 – Principal Component Analysis diagrams of extant and extinct canids resulting from the dietary relevant morphometric ratios of Table 3.9.1. Groups follow Van Valkenburgh & Koepfli (1993). Abbreviations: **Cal**, *C. alpinus*; **Cbr**, *C. brachiurus*; **Clu**, *C. lupus*; **Csi**, *C. simensis*; **Cth**, C. *thous*; **Ead**, *E. adoxus*; **Eda**, *E. davisi*; **Efe**, *E. ferox*; **Eku**, "*E.*" *kuruksaensis*; **Ezh**, *E. zhoui*; **Lad**, *L. adusta*; **Lcu**, *L. culpaeus*; **Lgr**, *L. griseus*; **Lgy**, *L. gymnocercus*; **Lme**, *L. mesomelas*; **Lpi**, *L. pictus*; **Lse**, *L. sechurae*; **Npr**, *N. procyonoides*; **Sve**, *S. venaticus*; **Uci**, *U. cinereoargenteus*; **Uli**, *U. littoralis*; **Vbe**, *V. bengalensis*; **Vca**, *V. cana*; **Vch**, *V. chama*; **Vco**, *V. corsac*; **Vla**, *V. lagopus*; **Vma**, *V. macrotis*; **Vru**, *V. rueppelli*; **Vvu**, *V. vulpes*; **Vze**, *V. zerda*.

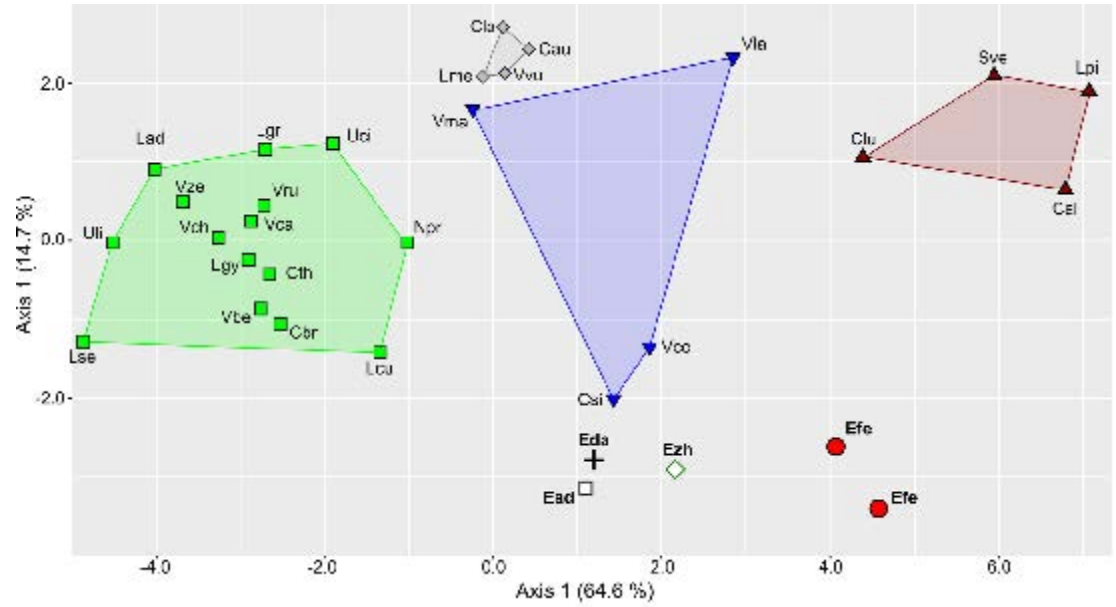

Figure 3.9.10 – Linear Discriminant Analysis diagrams of extant and extinct canids resulting from the dietary relevant morphometric ratios of Table 3.9.1. Legend and Abbreviations as in Fig. 3.9.9. Groups follow Van Valkenburgh & Koepfli (1993)..

and *E. zhoui,* lie within in the variability of Group 2 species. *E. ferox* is isolated from the fossil taxa, lying where Group 1 and Group 2 overlap. The Axis 2, which accounts for the 14.7% of the variability, is positively affected by dental ratios relative surface of upper molars, the relative length of the trigonid blade, and the relative lower grinding area. Negative loadings include cranial (relative width of the muzzle at canines), dental (relative length of the upper incisors), and mandibular ratios (resistance to bending of the dentary). The analysis reveals a relevant degree of separation between the dietary groups of modern canids, with the species of Group 1, 3 and 4 fairly clustered with taxa of the same group. Group 2 shows a more scattered pattern in the morphospace. The fossil species has positive values for both Axis 1 and 2. *E. adoxus*, *E. davisi* and *E. zhoui* lie close to the variability of Group 2. *E. ferox* is separated from all the extant groups.

3.9.5. Discussion

Heretofore, *Eucyon* species have been regarded as jackal-like canids limited to the medium-sized niche of canids, larger than foxes and probably similar in behavior to the extant coyotes (*C. latrans*) or jackals (*C. aureus*, *L. mesomelas*). The dental morphology possessed by *Eucyon* spp. is consistent with a mesocarnivorous diet, close to the latter species. On the one hand, no analyses have investigated this hypothesis. On the other, the current redescription of the *E. ferox* implies that the ecological diversity of these medium-sized canids might be underestimated, confirming the idea of Rook (2009) in including the highly carnivorous "*C.*" *cipio* in *Eucyon*. Indeed several of the peculiar features possessed by both *E. ferox* and *E. cipio* favor the hypothesis of a strongly carnivorous diet, *e.g.*, the stout P4, development of the M1 protocone and a crest-like metaconule, reduced m1 metaconid and enlarged buccal cuspids of m1-m3 compared to the reduced lingual ones (see Crusafont-Pairó & Truyols-Santonja, 1956 on terminology of "hypercarnivory" and "hypocarnivory"). Similar morphological features characterize numerous

fossil and extant canids renowned for their carnivorous diet, for instance, *C. armbrusteri*, *C. lupus* or *V. lagopus* (besides their hunting strategy). In hypercarnivorous canids as the genus *Xenocyon*, or in *L. pictus* and *C. alpinus* these features are further developed. On the contrary, taxa with a hypocarnivorous diet enlarge the grinding portion of teeth and develop lingual and accessory cusps on molars, *e.g.*, *Metalopex*, *Urocyon* Baird, 1857 and *Nyctereutes* (see Tedford & Wang, 2008; Tedford et al. 2009; section 3.5-3.6). In Fig. 3.9.6 morphometric variability of modern canids belonging to different dietary groups and of *E. ferox* and *E. cipio* is plotted against *E. davisi*, used as a standard reference. Interestingly, distantly related canids like *C. lupus*, *L. pictus* and *V. lagopus* (see among others Zrzavý et al., 2018) possess similar dental patterns, especially if compared to other extant canids (*e.g.*, *C. latrans*, which is closely related to *C. lupus*). These similar patterns reflect the their hypercarnivorous diet (Mech, 1974; Audet et al., 2002; Davies-Mostert et al., 2013), besides the different hunting strategies (prey size, pack- vs solitary hunting, etc.). *E. ferox* and *E. cipio* evidently differ from *C. latrans* (Group 3) and *N. procyonoides* (Group 4). Their proportions appear intermediate between those of *C. lupus*, of *L. pictus* and of *V. lagopus*, although not identical to any of them. In general terms, the pattern of these two fossil species, also considering their morphological features, favors the interpretation of a highly carnivorous diet. As prey size is a discriminant factor between the two dietary groups of hypercarnivorous canids we used the least squared regression of Van Valkenburgh et al. (2003) to estimate typical prey size of fossil species of *Eucyon* (Table 3.9.2). Unlike other *Eucyon* and *Eucyon*-like taxa, whose prey size appears to be smaller than one-third of the predator, *E. ferox* was probably the only species to hunt prey size close to its size. This is the same result Van Valkenburgh & Koepfli (1993) obtained in the analysis of the extant dietary groups: prey of species of Groups 2, 3 and 4 is considerably smaller than their size, whereas species of Group 1 are the only extant canids to hunting larger prey. Carbone et al. (1999; 2007) showed that carnivoran species that weigh more

than 21 kg are forced by metabolic constraints to prey on large animals. Although with such results, the authors do not imply that smaller species cannot hunt prey larger than themselves, it should be noted that in modern canids, at least two notable exceptions exist. Of the large-sized hypercarnivorous species, *L. pictus* and *C. lupus* weigh more than the size limit of 21 kg and cooperatively hunt ungulates larger than themselves. Even *C. alpinus* and *S. venaticus* are hypercarnivorous and highly social hunters (both part of Group 1 of Van Valkenburgh & Koepfli, 1993). The latter two species are considerably smaller than wolves and African wild dogs, as the weight of females of *C. alpinus* ranges between 10-13 kg, whereas males are between 15-21 kg (approximated mean body mass of ca 15 kg; Nowak, 2005; Castelló, 2018). *Speothos* Lund, 1839 is even smaller, as its weight ranges between 5-8 kg (de Mello Beisiegel & Zuercher, 2005; Nowak, 2005; Castelló, 2018). Applying the least square regression method to *Cuon*, whose body mass and mean jaw depth are similar to the reconstructed and measured ones for *E. ferox* (dhole's jaw depth=23.3 mm, Van Valkenburgh et al., 2003), we would never include the dhole among the social, hypercarnivorous canids specialized in killing prey heavier than themselves. Although not conclusive to demonstrate the predatory behavior of an animal, the set of specialized morphological and morphometric features retained by both *Cuon* and *Speothos* at least allows to clearly acknowledge their dietary preferences. The morphologies and proportions of *E. ferox* are not extremely specialized as *Cuon* or *Lycaon*, but they support the hypothesis that the Mio-Pliocene taxon had a markedly carnivorous diet.

Several studies have recognized the importance of morphometric ratios in the reconstruction of the diet of extant and fossil species (Van Valkenburgh, 1989; Van Valkenburgh & Koepfli, 1993; Van Valkenburgh et al., 2003). The latter parameter remains a key factor leading to alternative predatory strategies (*i.e.*, as pack- or solitary hunters) and driving the choice of prey (*i.e.*, in relation to predator-prey size), as pointed out by Van Valkenburgh & Koepfli (1993) and Carbone et al.

(1999; 2007). Regarding phylogeny, the ratios were tested and revealed a clear dietary signal, independent from phylogeny (Van Valkenburgh & Koepfli, 1993). We used here several of the morphometric ratios by these authors to investigate for the first time the dietary habits of *E. ferox* and other Mio-Pliocene *Eucyon* and *Eucyon*-like taxa. The majority of *Eucyon* species (*E. adoxus*, *E. davisi*, *E. zhoui*) in Fig. 3.9.7 lie close to the central group composed of canids of dietary Group 3. The species of this latter group are considered as generalist feeders (Nowak, 2005), with both vertebrate, non-vertebrate and vegetal incomes in their diets (*i.e.*, with adaptation to a mesocarnivorous diet). Size is also comparable between the two groupings, with the exception of *E. adoxus*, which is rather large-sized. It is possible to suppose a similar diet for the three fossil medium-sized *Eucyon* spp. As far as morphology is concerned, *E. adoxus* possesses an elongated snout, with evident diastemata between premolars, which perfectly match during occlusion (in a way similar to *C. latrans* and, particularly, *C. simensis*). *"E." kuruksaensis* lie close to *V. lagopus*, a hypercarnivorous species hunter of small prey. Although larger in size, the former could have had a similar diet as the arctic fox. Considering the power of explanation of the variables used in the three-dimensional plot (see Van Valkenburgh, 1989), the separated position of *E. ferox* in the volume appears to support the morphological interpretation of a hypercarnivorous diet, different from that of extant large and small hypercarnivorous canids.

The peculiarity of the lower teeth ratios in *E. ferox* is also confirmed by other ratios, known as indicators of predatory behaviors, specially for killing and consumption of large prey (Van Valkenburgh & Koepfli, 1993): the increased strength in the mandible, large upper incisors and canines. Although, peculiar dietary specializations of the groups are reflected in their teeth morphology as well as other ratios, related to processing of the different food item (*i.e.*, prevalently meat in Groups 1 and 2, with a large income of plant and arthropods in Groups 3 and 4), species of Groups 1 and 3 may be able to kill taxa of similar size (*i.e.*,

larger than themselves; see *inter alios*, Bekoff & Gese, 2003). This might result in similar values of the relative size of the upper second incisor and canine, as the rostral portion of the muzzle is one of the parts of the cranium that receives major stress during predation of such prey. On the contrary, the frequency of stress on the mandible is crucial for the development of the high resistance to bending (Van Valkenburgh & Koepfli, 1993; Biknevicius & Van Valkenburgh, 1996) and, therefore, IxM2 is a good discriminant between modern dietary groups, as visible Fig. 3.9.8.

The values of mandible rigidity for the three *Eucyon* spp. (*E. adoxus*, *E. davisi* and *E. zhoui*) seems to testify to a regime of stresses comparable to that of members of Group 3 but also of *V. lagopus*, whereas the relative size of upper teeth is very close to *V. vulpes*. These lower values of fossil *Eucyon* species, excluding *E. ferox*, might testify to the limited or less frequent habit to hunt large prey. On the contrary, the high values of I2 and C1 might be indicative of the ability of *E. ferox* to hunt large prey, unlike Group 2 species. Moreover, its larger values of the mandible resistance to bending stresses compared to Groups 2 and 3, but considerably lower than those of Group 1, support a different diet and hunting strategy compared to extant dietary groups. The difference between *E. ferox* and Groups 2-3 is also statistically significant for the mandible rigidity and the relative size of the upper canine (see Table 3.9.3), close to values of Group 1. The mechanical advantage of the *mm. temporalis* and *masseter* is larger compared to the average of Group 2, probably in relation to the bite strength needed to hunt large preys. Compared to hypercarnivores of Group 1, *E. ferox* possess slender muzzles at level of the canines and larger lower grinding area.

The principal and discriminant analyses summarize and confirms the results discussed above. Modern dietary groups are well separated one another, though Group 2 has a wide range. Overall, the results of the PCA indicate that three of extinct species are close to Group 2 and Group 3, whereas *E. ferox* project towards

hypercarnivorous species of Group 1, as *V. lagopus*. The discriminant analysis confirms the peculiarity of the set of morphometric ratios possessed by the fossil species compared to the extant dietary groups. Particularly *E. ferox* lie outside the variability of any dietary group. Van Valkenburgh (1989) put forward the idea that the empty spaces in the dietary morphospace might have once been filled by extinct Carnivora species. This might have been the case of *E. adoxus*, *E. davisi* and *E. zhoui*, with their interesting intermediate position between Group 2 and Group 3. As far as *E. ferox* is concerned, several of its morphometric values and patterns shown here do not find any evident extant parallel. Thus *E. ferox* represent an ecomorphotype that no longer exists among canids.

The dietary differences between *E. davisi* and *E. ferox* explains the sympatry of such species in the Late Miocene of North America. Although sympatry among fossil Caninae based on ecological preferences has already been described in literature (*e.g.*, Tedford et al., 2009; Rook et al., 2017), even within the same genus (Bartolini Lucenti et al., 2018), quantitative evidence of such ecological separation is reported here for the first time. Interesting future development of these research could consider the interaction between *E. ferox* and other members of Canidae of comparable chronology, shading new light in the ecology of Late Miocene fossil species.

3.9.6. Conclusions

Late Miocene to Early Pliocene times in North America (Hemphillian-Blancan) and Asia (early Yushean) were a time of radiation for numerous taxa of Caninae (Tedford and Qiu, 1991; 1996; Tedford et al., 2009, Sotnikova & Rook, 2010). In this phase, *Eucyon* and *Eucyon*-like taxa thrived across the Holarctic (Rook, 2009). The peculiar *Eucyon ferox* has been widely considered as the oldest *Canis* known (Miller & Carranza-Castaneda, 1998). Nevertheless, the type specimens from Mexico, Nevada and Arizona share numerous cranial and dentognathic features

with species of the genus *Eucyon* that are unusual for *Canis* (*e.g.*, lobed expansion of the nuchal crest in dorsal and caudal view, inion extending only to the level of the occipital condyles in lateral view, I3 similar sized to the I2 without a prominent basal cingulum, no M2 metaconule and reduced postprotocrista, absence of crista transversa on m1, radius/tibia ratio <0.8). The evidence of a highly carnivorous diet supported by the dental morphologies of *Eucyon ferox* suggests that the shared features with *Canis* (*e.g.*, the enlargement of the frontal sinus) might not be expression of phylogenetic affinity but rather the result of convergent ecological adaptations. The ascription of the type material of "*C.*" *ferox* to *Eucyon* reopens the question of the origin of *Canis*. The latter genus seems thus appearing in more recent times that previously thought, and the earliest representative of *Canis* remains *C. lepophagus* from the Early Pliocene (Blancan) of Cita Canyon in Texas (Tedford et al., 2009).

No research has ever investigated the diet of *E. ferox*, *Eucyon* spp. or even *Eucyon*-like taxa therefore morphometric ratios were used to assess their possible dietary preferences. *E. adoxus*, *E. davisi*, and *E. zhoui* generally show intermediate adaptations of the dietary ratios, partially similar to those of Group 2 and partially Group 3 (Van Valkenburgh & Koepfli, 1993). Their diet was probably a transitional mesocarnivorous diet, with consistent portion of meat in the diet and these taxa where mainly capable of hunting small prey (Table 3.9.2), only rarely preying on large animals. Different the results for *E. ferox*: the rather large body mass (ca 18 kg ± 2) confirms the morphological evidence in showing that the taxon was most probably a hypercarnivorous canid capable of hunting prey close to its size. It is difficult to assess if it preyed on prey larger than itself (Group 1 of Van Valkenburgh & Koepfli, 1993) or smaller ones (Group 2). Though the hypercarnivore features of *C. alpinus* are considerably more developed compared to those of *E. ferox*, the body mass and certain morphometric parameters (*e.g.*, the height of the mandible) are similar to the extant social canid, yielding comparable results. Considering

all the pattern of morphological characteristics and morphometric ratios, the ecomorphotype of *E. ferox* represent a unique case among the array of the trophic adaptations of fossil Canini during Mio-Pliocene times.

3.9.7. Appendix

3.9.7.1. Resuming measurements of Eucyon ferox

see next page

Table 3.9.4 Cranial measurements of the type and paratype specimens of *E. ferox*. Abbreviations: see section 2.4.

Locality	Cat. Num.	Element	TL	NCL	FL	SCL	GNL	Eu	Ect	PoCW	SH	AB	GWOC	BL	PL	CBL	ECW	GPW	M1-M2L
Rancho San Martin	**IGM 1130**	skull	177.6	76.6	102.9	-	-	-	43.4	28.1	-	-	-	-	-	-	-	51.1	-
Golgotha Water Mill	**F:AM 49298**	skull	185.4	81.6	105.2	89.6	65.9	-	46	27.7	54.5	40	35.1	160.1	93.9	176	31.3	52.5	18.6
Redington quarry	**F:AM 75848**	skull	196.3	-	-	-	-	-	-	-	-	-	-	-	-	188	-	-	22.2

Table 3.9.5 Upper teeth measurements of the type and paratypes specimens of *E. ferox*.

Locality	Cat. Num.	Element	P1 L	P1 W	P2 L	P2 W	P3 L	P3 W	P4 L	P4 W	M1 L	M1 W	M2 L	M2 W
Rancho San Martin	**IGM 1130**	skull	-	-	-	-	-	-	16.5	7.2	-	-	6.1	-
Golgotha Water Mill	**F:AM 49298**	skull	-	-	11.7	4.4	13.2	4.9	19	10.1	12	13.3	7.6	9.5
Redington quarry	**F:AM 75848**	skull	6.6	4.5	12	4.1	15.3	-	20.1	10.5	14.5	16.6	7.4	10.2

Table 3.9.6 Mandibular measurements of the type and paratypes specimens of *E. ferox*. Abbreviations: see section 2.4.

Locality	Cat. Num.	Element	Mp4H	Mm1H	Mm1B	HR	Ac1-m2 L	LLPR	LLMR
Rancho San Martin	**IGM 1130**	skull	20.8	20.8	8.9	51.5	76.4	42.6	
Golgotha Water Mill	**F:AM 49298**	skull	21.8	21.8	9.7	45.9	78.8	43.1	32.6
Bird bone quarry	**F:AM 63035**	Hemimandibles	22.3	-	9.1	-	83.4	45.4	-
Bird bone quarry	**F:AM 63060**	Hemimandible	11.9	-	3.7	-	76.7	36.1	-
Bird bone quarry	**F:AM 61612**	Hemimandible	-	-	-	-	-	-	-
Leyden Locality	**F:AM 27388**	Hemimandible	-	-	7.9	-	-	-	-
Redington quarry	**F:AM 75821**	hemiandible	21.5	24	11	-	-	-	36.3
Redington quarry	**F:AM 75822**	hemimandible	-	-	-	-	-	-	-
Redington quarry	**F:AM 75848**	skull	21.6	24.5	10.7	60.8	79.3	-	-

Table 3.9.7 Lower teeth measurements of the type and paratypes specimens of *E. ferox*.

Locality	Cat. Num.	Element	p1 L	p1 W	p2 L	p2 W	p3 L	p3 W	p4 L	p4 W	m1 L	m1 W	trm1 L	m2 L	m2 W	m3 L	m3 W
Rancho San Martin	**IGM 1130**	skull	3.7	3	-	-	10.7	3.8	-	-	18.6	7.4	13.2	5.7	-	-	15.7
Golgotha Water Mill	**F:AM 49298**	skull	6.2	4	10.6	4.4	12	5	14.1	5.6	19.7	8.1	13.2	6.6	4.4	4.3	19.3
Bird bone quarry	**F:AM 63035**	Hemimandibles	4.4	2.8	10.2	4	11.7	4.2	V	5.5	19.9	8.1	13.6	-	-	-	18.7
Bird bone quarry	**F:AM 63060**	Hemimandible	4.6	2.8	10.3	3.7	11.4	4.2	13	5.6	20.4	7.7	13.1	6.4	-	-	12.1
Bird bone quarry	**F:AM 61612**	Hemimandible	-	-	-	-	-	-	-	-	-	-	-	7.6	-	-	-
Leyden Locality	**F:AM 27388**	Hemimandible	-	-	-	-	-	-	-	-	19.3	7.7	13.6	6.5	-	-	-
Redington quarry	**F:AM 75821**	hemiandible	-		11.2	4.8	12.7	4.8	14.6	6.2	22.8	9.4	15.8	6.8	4.3	3.8	18
Redington quarry	**F:AM 75822**	hemimandible	-	-	-	-	-	-	-	-	23.7	9.4	17.1	7.2	-	-	-
Redington quarry	**F:AM 75848**	skull	-	-	-	-	12.5	-	14.8	-	21.8	8.6	14.7	6.6	-	-	-

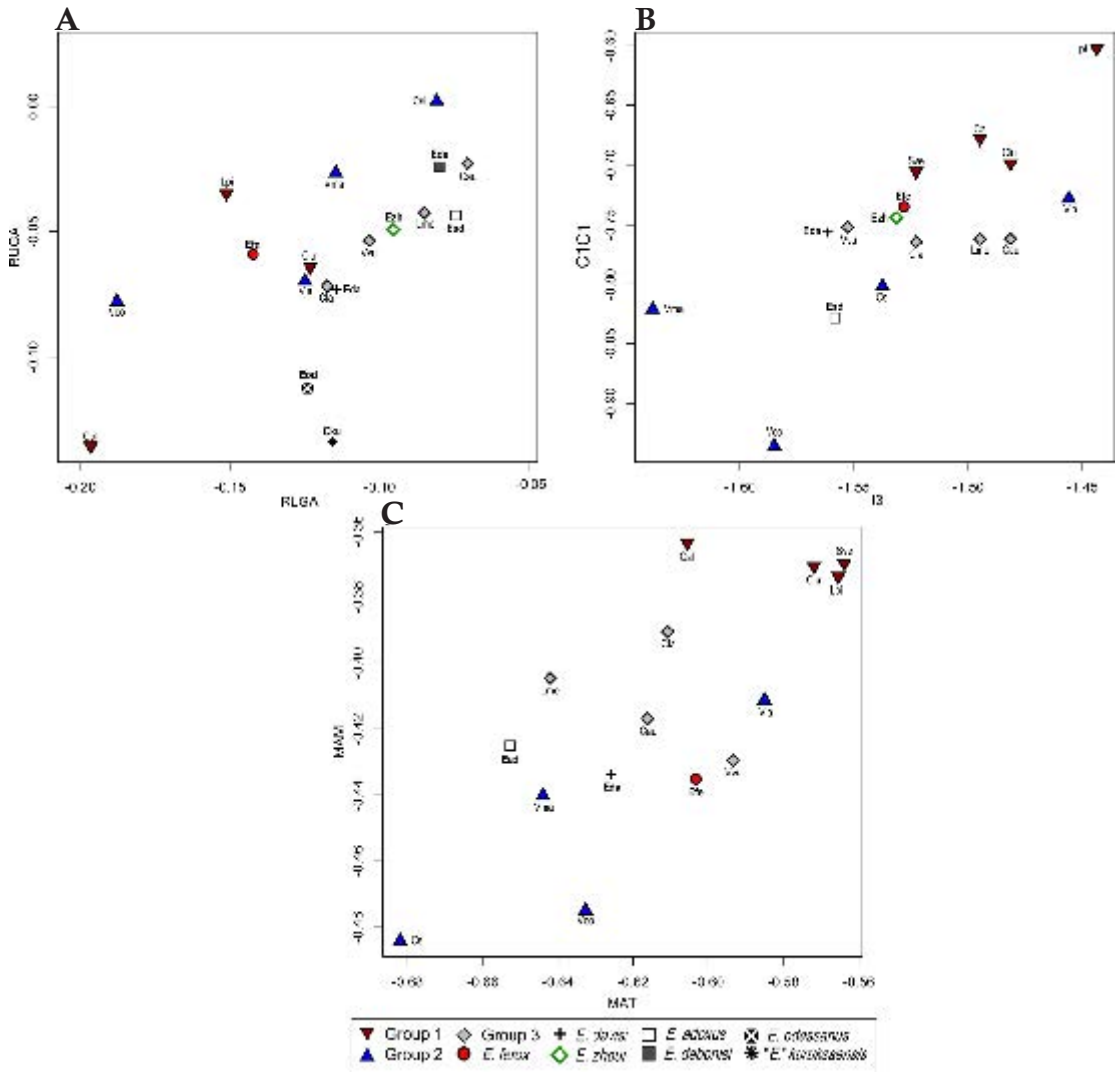

Figure 3.9.11 – 2D and 3D scatter-plot diagrams of selected morphometric ratios informative of the dietary habits in extant and extinct canids. **A**, Relative lower (RLGA) and upper (RUGA) grinding areas. **B**, Relative size of the third upper incisor (I3) and relative rostral breath of the cranium (C1C1). **C**, Mechanical advantage of the *m. temporalis* (MAT) and of the *m. masseter* (MAM).

3.9.7.2. Additional plot on morphometric ratios

Comment on the additional graphs, Fig. 3.9.11: *E. ferox* is generally distant from the other fossil species, often positioned close to highly carnivorous species of Group 1. The exception is Fig. 3.9.11C, where it seems that the fossil species possess intermediate value of MAM, whereas MAT is lowest in *E. adoxus* and highest in *E. ferox*, and *E. davisi* lies in an intermediate position. Although Van Valkenburgh & Koepfli (1993) deemed these parameters as important discriminators among

canid dietary groups, a scattered range of ratios is observed, especially for Group 2. Moreover, members of Group 3 have greater MAT and MAM values compared to members of Group 2, apart from *V. lagopus*. Indeed, only the species of Group 1 seems to be closely grouped, as its members are characterized by high values of both indices. Biknevicius & Ruff (1992) showed that, among Carnivora, increased forces applied on the sagittal plane results in stronger and more resistant mandibular corpora (also confirmed by several recent studies, *inter alios* Meloro, 2011; Figuerido et al., 2013). In Canidae, Van Valkenburgh & Koepfli (1993) found that high values of bending resistance of the dentary are associated with the largest ones for incisors and canines. Altogether these features appear essential for modern canids that prey on large ungulates (Biknevicius & Van Valkenburgh, 1996).

3.9.7.3. Loadings of Principal Component Analysis on the 12 morphometric ratios estimated for fossil Eucyon *and living Canidae.*

Table 3.9.8 – Loadings of the PCA analysis on morphometric ratios of fossil *Eucyon* and living Canidae.

	PC1	**PC2**	**PC3**	**PC4**	**PC5**	**PC6**
Eigenvalue	0.0294499	0.00652073	0.00314143	0.00246289	0.00126171	0.00113556
Variance %	63.932	14.156	6.8197	5.3467	2.739	2.4652
	PC1	PC2	PC3	PC4	PC5	PC6
RBL	0.011611	-0.20883	0.10817	0.024852	0.14755	0.097
RLGA	-0.17617	0.62007	0.11732	-0.029116	-0.10384	-0.26603
RUGA	-0.20839	0.31087	-0.35108	0.17449	-0.053425	0.32614
M1BS	0.1082	-0.30607	0.40449	0.22869	0.10565	0.21256
M2S	-0.13202	0.39583	0.6626	0.22416	0.055643	-0.11225
IXM2	0.28057	0.023625	-0.22304	0.24686	-0.047293	-0.084135
MAM	0.20667	0.035917	-0.12616	0.2074	-0.78677	-0.11804
I2	0.50394	0.22933	0.15757	-0.039798	-0.0076965	0.47702
I3	0.49956	0.14395	0.1847	-0.42032	-0.15915	0.12524
C1	0.41035	0.19492	-0.23847	-0.17245	0.45671	-0.47413
C1C1	0.24258	0.16864	-0.15801	0.69469	0.27383	0.11348
UM2/1	-0.20997	0.28865	-0.2054	-0.26647	0.14194	0.50373

3.9.7.4. Loadings of Discriminant Analysis on the 12 morphometric ratios estimated for fossil Eucyon *and living Canidae*

Table 3.9.9 Loadings of the discriminant analysis on morphometric ratios of fossil *Eucyon* and living Canidae.

	Axis 1	**Axis 2**	**Axis 3**	**Axis 4**
Eigenvalue	12.565	2.8662	2.3564	1.2676
Variance %	64.6	14.7	12.11	6.52
	Axis 1	Axis 2	Axis 3	Axis 4
RBL	0.0028231	-0.0046965	-0.000978	-0.002147
RLGA	-0.013756	-0.0026803	0.0039135	-0.002656
RUGA	-0.010397	0.00041633	0.0066966	0.015217
M1BS	0.0064604	0.0054321	0.003423	-0.011845
M2S	-0.010374	-0.0007949	0.0056619	-0.015381
IXM2	0.012557	0.0016524	0.012776	0.0002132
MAM	0.0095245	0.0062592	0.0054616	-0.008456
I2	0.020516	0.0095668	0.0085032	-0.023141
I3	0.020257	0.0095851	-0.005991	-0.024334
C1	0.016214	-0.002493	0.0062743	-0.016827
C1C1	0.010078	0.006953	0.019157	0.0020883
UM2/1	-0.011402	-0.0036048	-0.001984	0.0013742

3.10. A new medium-sized canid from Wadi Sarrat (Tunisia)

3.10.1. Geological setting, paleontological and archeological record

The Wadi Sarrat basin is located in northwestern Tunisia, close to the Algerian border (Fig. 3.10.1). It has an extension of 2188 km^2 and an average altitude of 700 m a.s.l. It is oriented east-west and surrounded by calcareous mountains of Cretaceous (Aptian) and Eocene age. This sedimentary basin was formed at the end of the early Pleistocene and was endorheic, with a central shallow lake, during the middle Pleistocene. The Wadi Sarrat Basin has a rich continental Pleistocene record. The fossil bed is situated within a more than 6m thick palustrine black series of more than 5km of exposure, and it is composed of conglomerates, gravels, sands, silts, and clays (Fig. 3.10.2). Above a discontinuity, it is superposed by a brown sedimentary series dominated also by conglomerates, gravels, sands, and clays. The partial cranium of *Canis* (OS10-02) was found in a conglomerate level, 4m below the top of the Black series, close to the river bed, at 2 meters from the systematic excavation undertaken during years 2010, 2012 and 2014 (Martínez-Navarro et al., 2014).The fossil assemblage of large mammals of Wadi Sarrat is dominated clearly by the record of abundant remains of a primitive *Bos primigenius*. The fauna from the early middle Pleistocene black level, dated 0.7 Ma, is composed by Suidae indet., *Hippopotamus* sp., *B. primigenius*, *Gazella* sp., *Ceratotherium simum* and *Equus* sp.; in addition to these larger taxa, seven small mammals species have been determined (*i.e.*,, one of the order Eulipotyphla, *Crocidura* sp., and six rodents, *Mus* aff. *spretus*, *Mus* cf. *hamidae*, *Paraethomys* cf. *rbiae*, *Praomys* sp., *Meriones* sp. and *Eliomys* sp.), as well as also other small vertebrates such as one fresh water fish (Cyprinidae indet.), two anurans, one terrapin, three squamates, and one small-sized bird. Also there is a rich malacofauna assemblage, composed of six gastropods and only one bivalve (see Martínez-Navarro et al., 2014; Mtimet et al., 2014; Karoui-Yaakoub et al., 2016).A combination of

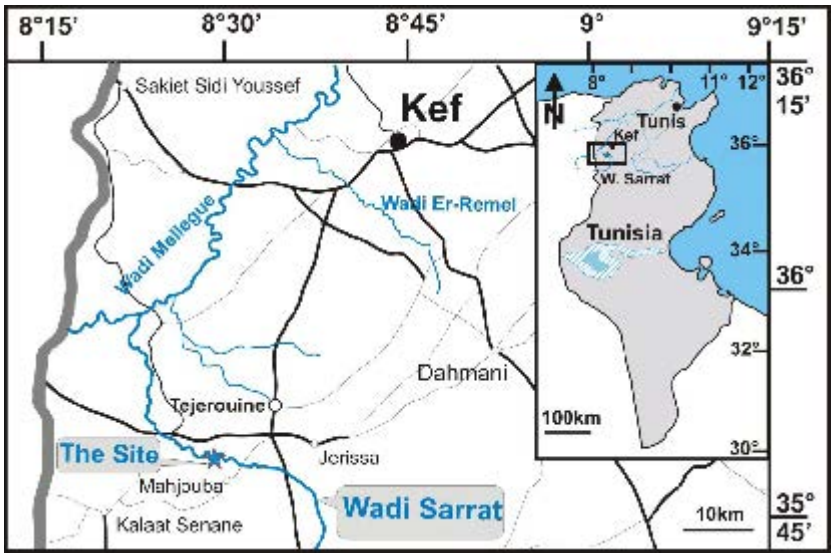

Figure 3.10.1 – Geographic localization of the Wadi Sarrat basin.

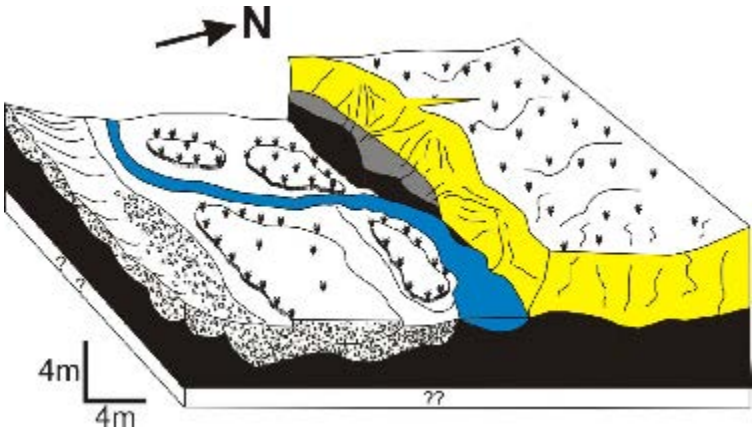

Figure 3.10.2 – Bloc diagram of the geologic layers present in the Wadi Sarrat site.

paleomagnetic data together with the record of small mammals from the black level of Wadi Sarrat at the locality, where the earliest *Bos primigenius* cranium and the *Canis* cranium were found, indicates that the site can be confidently dated to the base of the middle Pleistocene, around ~0.7 Ma (Martínez-Navarro et al., 2014). The climatic and paleoecological data are basically supported by the good record of reptiles, amphibians and mollusks. The presence of the common toad indicates that the site of Wadi Sarrat was under the influence of a warmer climate and wetter than it is today, probably tropical hot and humid. Consequently, the fossil assemblage, considered as a whole, may suggest that the site was formed during a period of more humid and temperate climate than today. Such moister climatic conditions may be related to an interglacial period of the middle Pleistocene

(Martínez-Navarro et al., 2014; Karoui-Yaakoub et al., 2016). Some lithic tools were recovered in situ (flakes, fragments of nucleus, etc.) during three seasons of systematic excavation in Wadi Sarrat. In the black level, associated with several fossil bones, including a craniums of *Bos primigenius* and *Canis*, evidence was found of a knapping strategy organized around the core's periphery. The lithic assemblage of core and the removed flakes, falls within the variability of the Mode 2 or Acheulian technological complex (Martínez-Navarro et al., 2014).

3.10.2. Systematic Paleontology

Order **Carnivora** Bowditch, 1821

Suborder **Caniformia** Kretzoi, 1938

Family **Canidae** Fischer, 1817

Subfamily **Caninae** Fischer, 1817

Tribe **Canini** Fischer, 1817

Genus ***Canis*** Linnaeus, 1758

Canis othmanii Amri et al., 2017

(Fig. 3.10.3)

Holotype. OS10-02 cranial fragment with both palates, with right maxillary fragment preserving P1-P2, distal part of the P3 and P4–M1 and left maxillary preserving I1, P1, P3, and the mesial portion of P4.

Derivatio nominis. it is dedicated to the discoverer of the fossil and the site, Abdelhak Othmani, who together with his family are long-time owners of the land where the site of Wadi Sarrat is located, and have been great supporters of this research. Type locality: the early middle Pleistocene black level of Wadi Sarrat; UTM coordinates: X 0454811, Y 3963837; Kef province, Tunisia (Fig. 3.10.1).

Description. *Cranium*. OS10-02 (Fig. 3.10.3) shows exclusively the maxillae, both palates and the long right nasal bone. It is small but robust. In lateral view, the skull profile seems to be quite steep, and the maxillofrontal suture seems very high. The palate seems to be rather wide.

Upper teeth. The only incisor preserved is a robust and wide I1. Its occlusal surface is worn. Both canines are missing, but their alveoli show a rather consistent mesiodistal enlargement (*e.g.*, the alveolus of the left canine is 12.8 mm long). The first upper premolar is single-rooted, has a conical crown and a quite elongated talon. It is low-crowned and enlarged buccolingually. The P2 is elongated mesiodistally and does not present any distal accessory cusp. The P3 is slightly longer than the P2 and it presents a small distal accessory cusp behind the protocone. The right P3 is broken and the mesial alveolus shows signs of reabsorption. In the upper carnassial, the protocone slightly projects mesially compared to the mesial border of the tooth. The metastyle is rather low and elongated mesiodistally. The P4 shows a strong lingual cingulum. The M1 is elongated buccolingually with a rather enlarged and rounded talon, which is poorly arched distally. The paracone and the metacone are almost equal in size. On the mesiobuccal margin, the parastyle is prominent. On the talon, the well-developed metaconule and the worn protocone and protoconule are evident. The hypocone is only slightly individualized from the lingual cingulum. The measurements are shown in the Table 3.10.1.

Comparisons. The P4 possess an individualized protocone, which projects slightly beyond the mesial margin of the tooth, unlike *C. aureus*, *C. anthus*, *L. mesomelas* or C. *lupus*. This feature also contrasts with the condition seen in European Early Pleistocene canids like *C. mosbachensis* from Pirro Nord, Cueva Victoria and Untermassfeld or with *C. arnensis* and *C. etruscus* from Upper Valdarno, where the protocone lies at level of the mesial margin of the P4 or is placed more lingually. The mesial projection of the P4 protocone is similar to that of *L. adusta*, but the

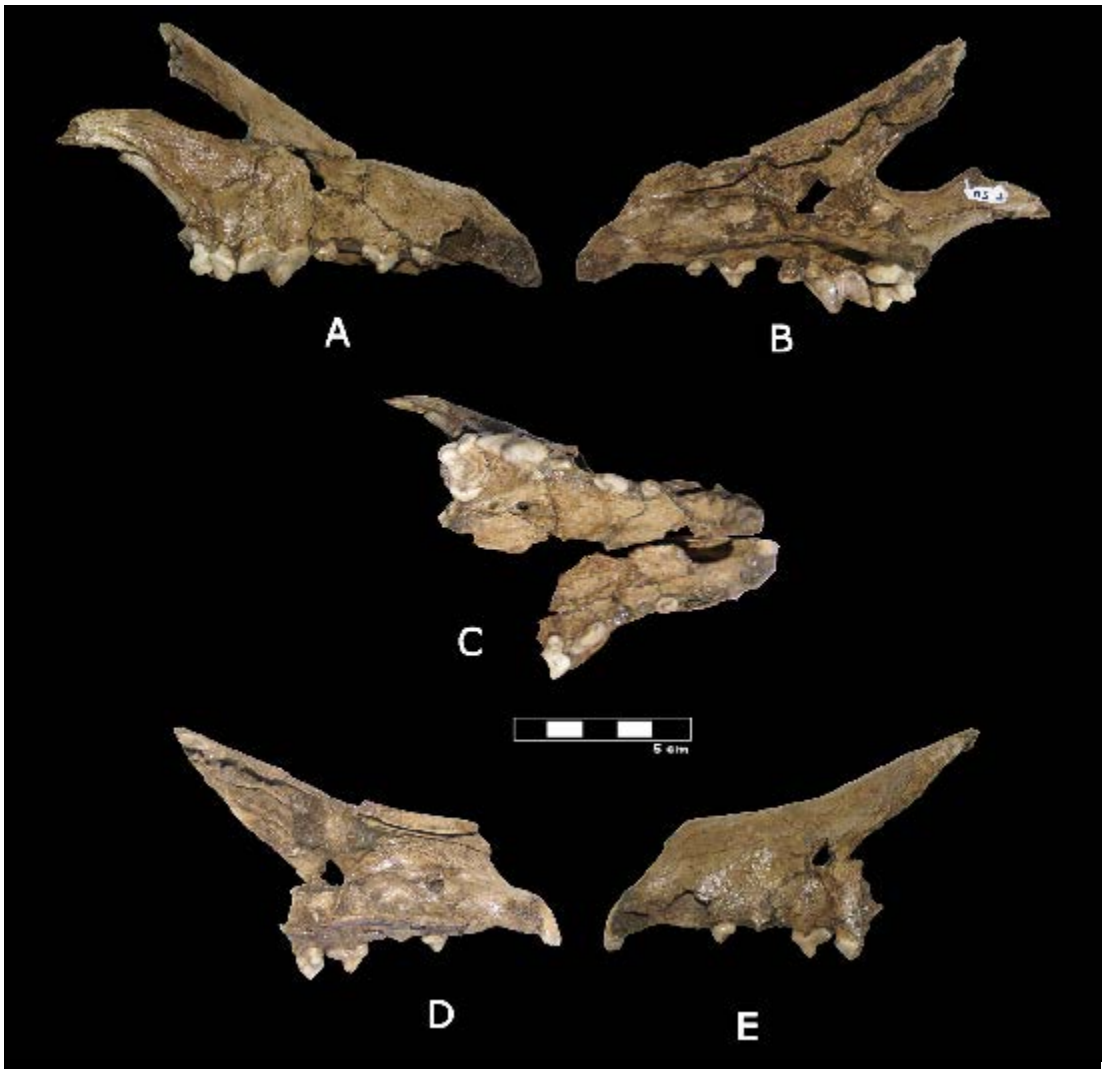

Figure 3.10.3 –*Canis othmanii* sp. nov from Wadi Sarrat. **A-E**: **OS10-02**, cranium in right lateral (**A**), right medial (**B**), and occlusal (**C**), left medial (**D**), left lateral (**E**) views. The scale bar equals 5 cm.

	Right		Left	
	L	**W**	**L**	**W**
I1	-	-	4.3	5.4
P1	7.4	4.4	6.5	4.4
P2	11.1	4.7	-	-
P3	-	-	12.3	4.9
P4	20.5	10.4	20.7	11.1
M1	14.5	18.8	-	-
P1-P4	55.3	-	-	-

Table 3.10.1 – Dimensions of two maxillary fragments of *Canis othmanii*. (OS10- 02). All measurements are in mm.

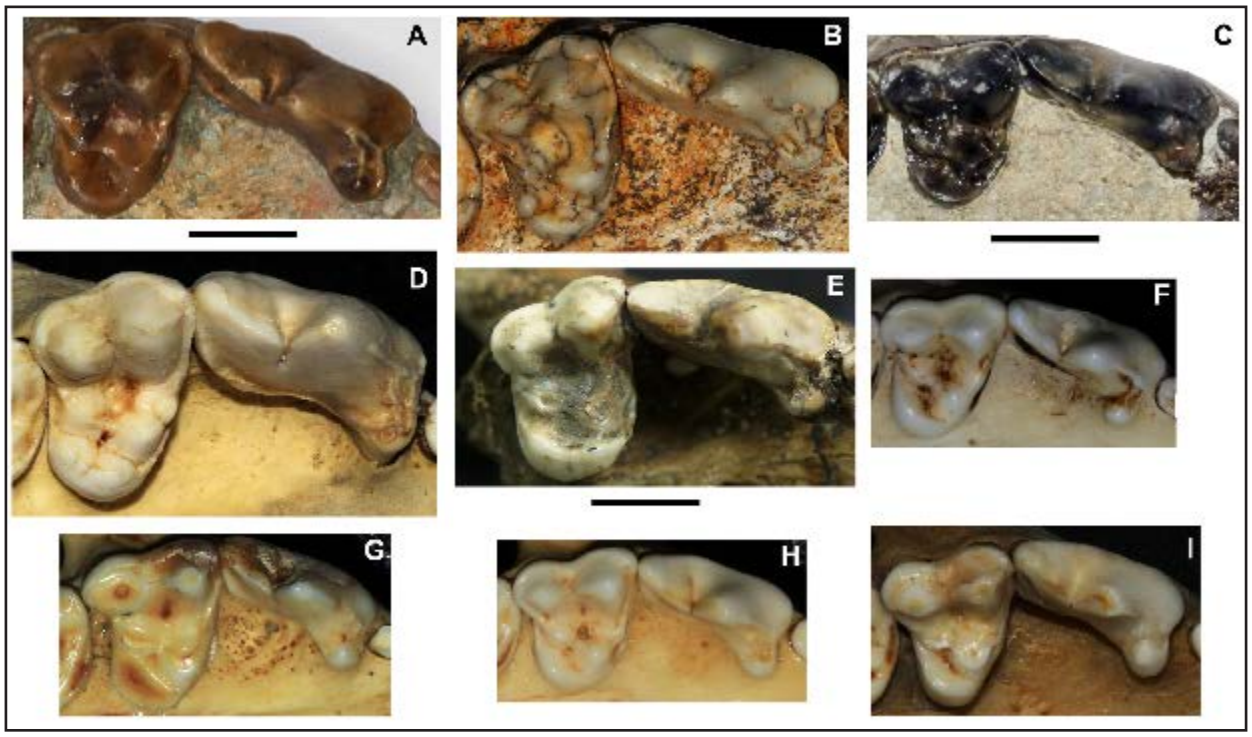

Figure 3.10.4 – The upper carnassial and M1 of some extant and fossil species. **A**: *C. etruscus* – IGF 12867V. **B**: *C. mosbachensis* – DE 2 ac. **C**: *C. arnensis* – IGF 7919V. **D**: *C. lupus* – MZUF-11874. **E**: *C. othmanii* – OS10-02. **F**: *C. anthus* – MZUF-1842. **G**: *L. adusta* – MZUF-8496. **H**: *L. mesomelas* – MZUF-1898. **I**: *C. aureus* – MZUF11880. The scale bar equals 1 cm.

latter canid has a stouter protocone compared to that of the *Canis* specimen from Wadi Sarrat. The metastyle is elongated mesiodistally, similar to *C. arnensis*, although the paracone is higher than in that species (Bartolini Lucenti & Rook, 2016). The M1 is particular in shape as its talon is large mesiodistally and not arched backwards as in other extant or fossil canids (see Fig. 3.10.4). Moreover, the mesiodistal breadth of the trigon is similar to that of the talon, whereas in modern species the talon is generally narrower (see Fig. 3.10.4). In this regard, the canid from Wadi Sarrat is closer to *C. mosbachensis* from Pirro Nord, although theM1 of the latter species shows other features (*e.g.*, the larger paracone compared to the metacone; a round and large protocone basin; a prominent cingulum in the mesial and distal side of the tooth; see Bartolini Lucenti et al., 2017) which cannot be found in OS10-02. The metaconule of the M1 is particularly well developed and larger-based compared to the modern African canids (*i.e.*, *C. anthus*, *L. mesomelas*,

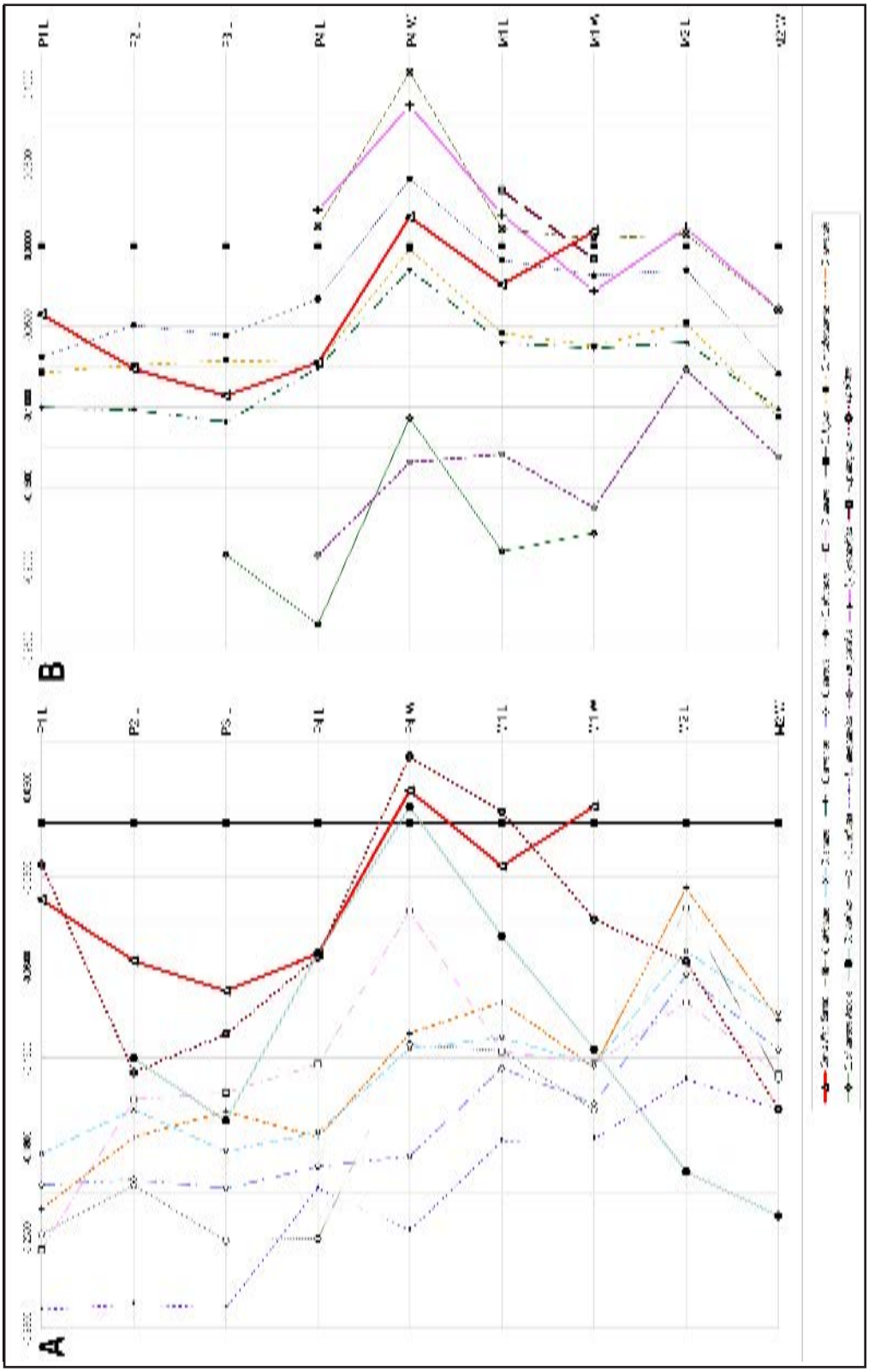

Figure 3.10.5 – Log-ratio diagram based on log-transformed mean dental measurements of extant (**A**) an extinct (**B**) species of *Canis* and *Canis othmanii*. Tooth measurements taken into consideration are shown on the right side.

L. adusta), the golden jackal (*C. aureus*) and the European fossil species *C. etruscus*, *C. mosbachensis* and *C. arnensis*. *Canis othmanii* sp. nov. lacks all the hypercarnivorous features shared by wild dog-like canids (*e.g.*, *X. lycaonoides*, *C. alpinus*, *C. africanus*) like the buccolingual enlargement of the P4; the strongly larger paracone of the M1 compared to the metacone; the short talon of the M1 with large protocone and hypocone and a reduced metaconule

Morphometric analyses. The morphometric analyses of the dentognathic material of *Canis othmanii* sp. nov. (Fig. 3.10.5A-B) shows important differences with the extant African *L. adusta*, *L. mesomelas*, *C. anthus* and Eurasian *C. aureus*. In fact, its size stands in the middle between that of modern C. *lupus* and that of the smaller jackals, as can be seen from the log-ratio diagram in Fig. 3.10.5A-B. An attribution to the coeval *X. lycaonoides* can be ruled out as the size and proportions of the latter taxon are considerably larger than the African species here considered (Fig. 3.10.5B). The same can be said about *L. pictus* and *C. alpinus*. As far as African fossil taxa are concerned, the Early Pleistocene *L. paralius* (Geraads, 2011) is smaller, with proportions more similar to modern species, particularly *L. adusta*. In fact, *L. paralius* could represent and early form of this modern jackal. The species *C. africanus* (considered here as separate taxon as in Geraads, 2011, although Martínez-Navarro & Rook, 2003 deemed it as part of *X. lycaonoides*) has proportions very close to *X. lycaonoides*, whereas *L. magnus* (see Geraads, 2011), is considerably larger than the canid from Wadi Sarrat. It also shows numerous morphological differences. *Canis* cf. *aureus* from Asbole (see Geraads et al., 2004) is much smaller in its dental proportions than the species from Wadi Sarrat. The upper dental proportions are, by all means, closer to the Eurasian stock of fossil canids like *C. arnensis*, *C. etruscus* and *C. mosbachensis*.

3.10.3. Discussions and Conclusions

3.10.3.1. Taxonomic remarks on Canis othmanii

The morphometric and anatomical features of *Canis othmanii* sp. nov., show on the one hand, significant distinction from the modern *L. adusta*, *L. mesomelas*, *C. aureus* and *C. anthus* (*e.g.*, larger size; shape of the P4 protocone; length of the M1). On the other hand, the new species does not possess peculiar hypercarnivorous dental adaptions such as *Canis* (*Xenocyon*) ex gr. *falconeri* (*sensu* Sotnikova, 2001), *X. lycaonoides* and modern *L. pictus* do have. From our analyses, it is clear that size and proportions of the teeth of *C. othmanii* sp. nov. are closer to those of the European Early-middle Pleistocene fossil canids (*i.e.*, here *C. arnensis* and *C. etruscus* from Olivola and Upper Valdarno and *C. mosbachensis* from Pirro Nord, Untermassfeld and Cueva Victoria) rather than to other African fossil and extant species, as shown in Fig. 3.10.5A-B. Nevertheless, the dental morphology of *C. othmanii* shows peculiarities, which cannot be found in other Villafranchian and Epivillafranchian species of both Africa and Eurasia.

3.10.3.2. History of Eurafrican canids

At present, the knowledge of the history and the pattern of the dispersion of Canidae in Africa is scarce, due to several issues, such as the reduced number of sites with canids, their scattered distribution in the continent, number of fossils, etc. (Geraads, 2008; Werdelin & Dehghani, 2011). The first attested record in the African continent is nowadays that of *Canis* sp. A from South Turkwel (Kenya), dated approximately between ca 3.58 and 3.2 Ma (Werdelin & Lewis, 2000; 2005). Fossil materials of *L. adusta* are reported from the 3-million-years-old South African site Makapansgat 3 (Ewer, 1956). The characteristic of the upper second molar (M2) and the relative elongation of both molars of *L. adusta* are similar to some material fragments reported from early Early Pleistocene site of Ain Boucherit (Algeria), dated to 2.3 Ma (Arambourg, 1979). A large jackal-like form is also mentioned in several sites in the Late Pleistocene in Morocco, *e.g.*,

Dar es Soltane, Doukkala II (Michel & Wengler, 1993), Zourah Cave (Aouraghe, 2000) and Cap Achakar (Ouachaou & Amani, 2002). From the Early Pleistocene site of Aïn Hanech, a maxilla of the large canid *Canis* cf. *atrox* (Arambourg, 1979) has been recovered. This specimen has then been assigned to the genus *Lycaon* by Martínez-Navarro & Rook (2003). According to Geraads (2008), the first record of a living canid in North Africa appears only in the late middle Pleistocene site of Sidi Abderrahmane (Morocco). The author assigns this material to *C. aureus*, as it "cannot be separated from" this taxon. The recovered fauna from Wadi Sarrat site is particularly similar to that living in the various extant environments of east Africa, given that some of these taxa are still existing there today. The material of *Canis* from Wadi Sarrat possesses peculiar features and proportions, which are unique among North African canids; this suggests an attribution of the specimen OS10-02 to a new species of *Canis*. The record in North Africa of a canid with morphometric affinity to Eurasian taxa is, for now, unprecedented for this age and, therefore, this has important implications for the latest Early-middle Pleistocene biogeography of canids, not only of Africa but also of the circum-Mediterranean regions, as well as of the entire Eurasia, testifying to the increasing trend of radiation and rapid dispersion of *Canis* spp. in the late Villafranchian/ Epivillafranchian (Sotnikova & Rook, 2010).

The early middle Pleistocene mammal assemblage from Wadi Sarrat is similar to that reported from other coeval sites of North Africa, where the genus *Canis* has been known since the late Pliocene. The morphological and morphometric analyses of the specimen OS10-02 show the closer similarity of this canid to Eurasian Early Pleistocene taxa rather than to North African ones, other African species of the fossil record or to the extant *C. anthus*, *C. aureus*, *L. mesomelas*, *L. adusta* and the modern *Canis lupus*. For these reasons, Wadi Sarrat material can be sensibly ascribed to *Canis othmanii* sp. nov. The record of a new taxon in a North African deposit with Eurasian affinities, during the middle Pleistocene, opens an

unprecedented scenario on the evolutionary history, biogeography and dispersion of canids in the Old world.

3.11. The Late Pleistocene *Canis lupus* (Canidae, Mammalia) from Avetrana (Apulia, Italy)

3.11.1. Context

A preliminary study of *C. lupus* from Avetrana suggested that this wolf population shows morphological and morphometric similarities to those collected from central and northern Italy, chronologically referred to MIS 3 and MIS 2, and that it is larger in body size when compared with those from the early Late Pleistocene of southern Italy (Bertè & Pandolfi, 2014).Besides this preliminary work, no other studies have been carried out on the wolf material from Avetrana with respect to the variability of Late Pleistocene wolves across Europe. The aim of this paper is to try to fill this knowledge gap with a review of the morphological and morphometric variability in the large sample of *C. lupus* of Avetrana bed 8. This review takes into consideration previously unpublished cranial, dentognathic and postcranial material recovered in this same level to provide new insights into the biochronology and paleobiogeography of modern wolves during the Late Pleistocene of Italy and Europe.

3.11.2. Geological and Biochronological framework

A rich mammal assemblage was discovered at Avetrana (Taranto, Apulia; Fig. 3.11.1) in 2003 (Bedetti et al., 2004). The site is located in an abandoned quarry, and it consists of a fossiliferous karst filled deposit within the Early Pleistocene limestone known as "Calcareniti di Gravina" (Ciaranfi et al., 1988). The faunal assemblage recovered from the filling deposits has been studied in a number of papers (Bedetti et al., 2004; Sardella et al., 2005; Petronio et al., 2008, Bertè & Pandolfi, 2014), and includes numerous bird and mammal taxa, such as:

Erinaceus europaeus Linnaeus, 1758, *Microtus* (*Terricola*) *savii* (De Selys-Longchamps, 1838), *Hystrix vinogradovi* Agryropulo, 1941, *Lepus* cfr. *europaeus* Pallas, 1778,

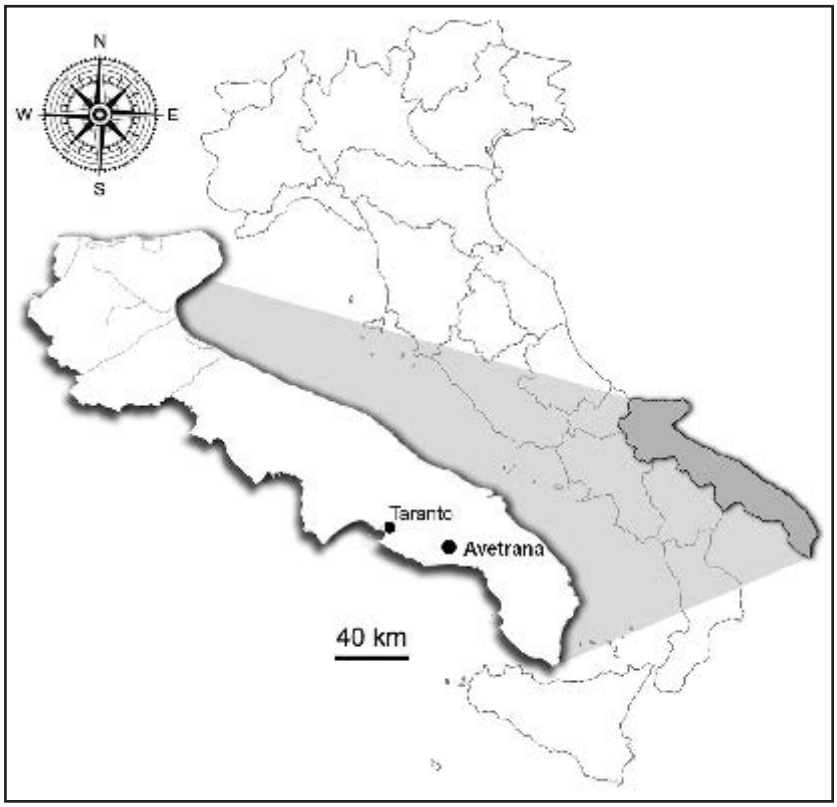

Figure 3.11.1 – Location of the Late Pleistocene site of Avetrana (Apulia, southern Italy).

Oryctolagus cuniculus (Linnaeus, 1758), *Canis lupus*, *Vulpes vulpes*, *Meles meles* (Linnaeus, 1758), *Mustela putorius* Linnaeus, 1758, *Crocuta crocuta* (Erxleben, 1777), *Lynx lynx* (Linnaeus, 1758), *Felis silvestris* Schreber, 1777, *Panthera spelaea* Goldfuss, 1810, *Stephanorhinus hemitoechus* (Falconer, 1868), *Hippopotamus amphibious* Linnaeus, 1758, *Sus scrofa* Linnaeus, 1758, *Dama dama* (Linnaeus, 1758), *Cervus elaphus* Linnaeus, 1758, *Megaloceros* sp. Blumenbach, 1799, *Capreolus capreolus* (Linnaeus, 1758) and *Bos primigenius* Bojanus, 1827.

Stratigraphically, the deposits of Avetrana have been divided into nine beds and two pockets (Sardella et al., 2005; Petronio et al., 2008; Fig. 3.11.2).

The large sample of *C. lupus* described here comes from bed 8 of the Avetrana succession (Bertè & Pandolfi, 2014). The Avetrana bed 8 is about 75 cm thick and consists of argillaceous-sandy sediments with calcareous pebbles. The bones were concentrated at the base of the layer (Sardella et al., 2005; Pandolfi et al., 2013). The mammal assemblage recovered from Avetrana bed 8 includes *M.* (*T.*) *savii, M. putorius, V. vulpes, L. lynx, P. spelaea, S. scrofa, D. dama, C. elaphus* and *B. primigenius.*

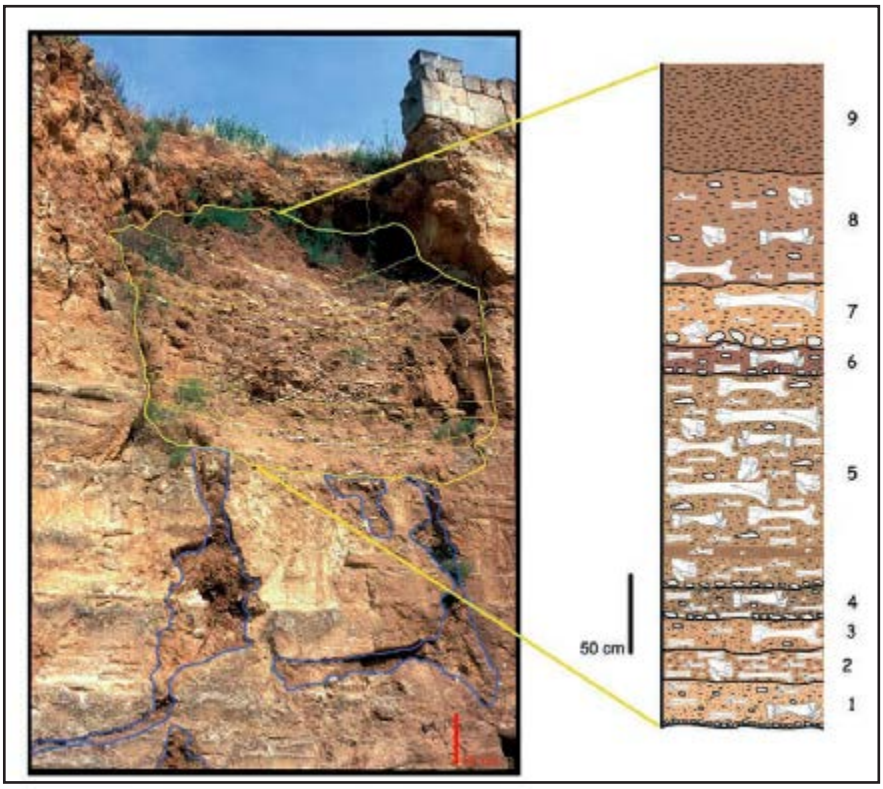

Figure 3.11.2 – Photographic and schematic representation of the stratigraphic section of the Avetrana deposit modified from Sardella et al. (2005).

Some lithic artefacts were also recovered from this layer and their study is still in progress (Pandolfi et al., 2013). The studied material is poorly preserved and most of the remains are partially embedded in reddish-brown limestone concretions. The fossil remains are often fragmented and are generally not in anatomic connection, suggesting a prolonged transport prior to the final deposition. Although recovered from the same layer as lithic artefacts, the studied material does not reveal traces or fractures attributable to human activity.

3.11.3. Systematic Paleontology

Order **Carnivora** Bowdich, 1821

Family **Canidae** Fischer, 1817

Subfamily **Caninae** Fischer, 1817

Tribe **Canini** Fischer, 1817

Genus ***Canis*** Linnaeus, 1758

Canis lupus Linnaeus, 1758

(Fig. 3.11.3)

Materials. A8-45, right maxillary fragment with P4-M2; A8-36, left maxillary fragment with M1-M2; A8C9, right maxillary fragment with P4-M1; AND-9, left I3; AND-10, left I3; Ave-07-16, left I3; AND-11 left I3; AND-35, left I3; AND-49, left I3; AND-8, right I3; AND-12, right I3; AND-13, right I3; AND-16, left C1; AND-14, right C1; AND-4, left P1; AND-15, right C1; A8-75, right P1; AND-2, right P1; AND-3, rightP1; Ave-07-01, left P4; Ave-07-04, left P4; A843b, left P4; A8-42, right P4; A8-43a, right P4; Ave8-34, right P4; Ave-07-02, right P4; Ave-07-03, right P4; AND-1, right P4; A8-13, right P4; AND-56, right P4; A8-48, left M1; AND-7, left M1; AND-15, left M1; A8-39, right M1; A8-19, right M1; A8-38, right M1; A8-68, right M1; Ave-07-05, right M1; AND-5, right M1; AND-6 right M1; AND-36, left M2; A8-25-65, left hemimandible with c1-m3; A8-28-30, left hemimandible with c1-m3; AND-18, left mandibular fragment with m1; AND-19, left mandibular fragment with p4-m2; AND-20, left mandibular fragment with m1; Ave8-16-18, left hemimandible with i3-p4; A8-20, left mandibular fragment with p4; A8-26, left mandibular fragment with c1-p3; AND-23, left mandibular fragment with p2-p3; Ave8-10, left mandibular fragment; A8-15, left mandibular fragment with p1-m2; AND-26, left mandibular fragment with m1-m2; A8-24, left mandibular fragment with m2; AND-31, left mandibular fragment with p1-p2; A8-81, right mandibular fragment with p4-m2; A8-27, right mandibular fragment with p3-m3; A8-17, right mandibular fragment with p3-m2; A8C6, right mandibular fragment with p3-m1; And-17, right mandibular fragment with m1-m2; A8-14, right mandibular fragment with p1-m2; A8-73, right mandibular fragment with p3-m1; AND-21, right p4-m1; A8C8, right mandibular fragment with p4-m1; AND-22, , right mandibular fragment with i3-p1; A8-11, right mandibular fragment with p1-p2; AND-24, right mandibular fragment with p1-p4; A8-2, right mandibular fragment; A8C2, right mandibular fragment with m1-m2; AND-25, right mandibular fragment with p1-p2; AND-27, right mandibular fragment with p1-p3; AND-28, right mandibular fragment with m2; A8-1, left hemimandible with i2-m2; A8-29, right mandibular fragment; A8C4, right mandibular fragment with p4-m2; A8-18,

right mandibular fragment with i2-i3; AND-40, left i2; AND-42, left i2; AND-44, left i2; AND-38, left i2; AND-39, left i2; AND-41, left i2; AND-43, left i3; Ave-07-08, left c1; AND-50, left c1; AND-52, left c1; AND-55, left c1; Ave-07-13, right c1; A811701, right c1; AND-51, right c1; AND-53, right c1; AND-54, right c1; AND-46, left p1; AND-45, right p1; AND-32, left p2; AND-47, left p2; A8-76, right p2; AND-30, left p3; AND-48, right p3; A8-9, left m1; A8-74, left m1; AND-57, left m1; A8-19, right m1; AND-31, left m2; AND-32, left m2; AND34, left m2; AND-29, right m2; AND-121, left m3; A8-22, distal epiphysis of right humerus; AND-58, distal epiphysis of right humerus; AND-113, proximal epiphysis of right humerus; AND-114, proximal epiphysis of left humerus; AND-122, proximal epiphysis of left humerus; AND-123, proximal epiphysis of left humerus; AND-116, proximal epiphysis of right ulna; AND-62, proximal epiphysis of left radius; AND-59, proximal epiphysis of right radius; AND-60, proximal epiphysis of right radius; AND-61, proximal epiphysis of radius; AND-63, right scapula fragments; AND-64, thoracic vertebrae; AND-65, sacrum; A8-C21, right femur; AND-71, right femur fragments; AND-66, fragmented proximal epiphysis of left tibia; AND-68, fragmented distal epiphysis of left tibia; AND-67, fragmented proximal epiphysis of right tibia; AND-69, fragmented distal epiphysis of right tibia; AND-70, right tibia fragments; AND-115, distal epiphysis of left tibia; AND-117, distal epiphysis of left tibia; AND-118, distal epiphysis of right tibia; AND-73, left calcaneus, AND-72, right calcaneus; AND-119, left calcaneus; AND-120, left calcaneus; AND-76, left astragalus; AND-77, left astragalus; AND-78, left astragalus; A8-42, right astragalus; AND-75, right astragalus; AND-80, left IV metacarpal; AND-79, right IV metacarpal; AND-83, right IV metacarpal; AND-82, left V metacarpal; AND-81, right V metacarpal; AND-86, left II metatarsal; AND-87, left II metatarsal; AND-85, right II metatarsal; AND-88, left III metatarsal; AND-89, right III metatarsal; AND-90, metapodial fragments; AND-91, metapodial fragments; AND-92, metapodial fragments; AND-93, metapodial fragments; AND-94 – AND-107, eight right and six left first phalanges; AND-108, third phalanx; AND-112, third phalanx.

Description. *Upper teeth*. The I3 is large and canine-like in general morphology. The P1 is single-cusped, oval in shape in occlusal view and pointed. The main cusps of P2 and P3 are rather low. Whereas the P2 does not possess any distal

accessory cuspid, the P3 does have one. The P4 possesses a relatively stout protocone (Fig. 3.11.3), which is generally expanded lingually, although in AVE-07-01 it is not as expanded. The tip of the protocone is rather low and not pointed. It generally lies slightly mesially, compared to the mesial margin of the P4. The P4 paracone is stout and the metastyle is long, with a groove on its buccal side. A strong cingulum is evident in the distolingual side of the tooth. The M1 possesses a considerably larger and higher paracone compared to the metacone (Fig. 3.11.3). This cusp is bounded by the buccal cingulum in way that, in the occlusal view, it shows a rounded shape. The buccal cingulum is not very prominent, except at level of the parastyle, which is rather conspicuous. The trigon basin is well developed, especially compared to the talon one, but no marked difference in depth is evident between them. A8-5 shows a small round pit in the trigon basin, most probably a caries. The M1 protocone is large-based and generally a prominent protoconule is present, although in A8-5, A8-39 and A8-65 it is rather reduced. Distally to the protocone is a short metaconule. The hypocone is rather low and poorly individualized from the lingual cingulum. The M2 is rather short, not very expanded lingually, and it possesses a paracone that is larger than the metacone (Fig. 3.11.3). The paracone is also slightly higher than the metacone, if observed in buccal view. The M2 protocone is rather large, and no metaconule is present.

Mandible. Correct assessment of the features of the mandible corpus is difficult because of the state of preservation of the specimens. Nevertheless, the corpus is rather deep dorsoventrally and elongated (Fig. 3.11.3). Two foramina are visible on the buccal surface: the larger mental foramen emerges under the interdental space between p1 and p2 and the smaller one under the mesial root of p3. The toothrow is slightly buccally convex at the p4-m1 commissure. The premolars possess short diastemata between them, especially between p2 and p3. The mandible ramus is high, with a mesiodistally large coronoid process and a conspicuous coronoid crest.

Figure 3.11.3 – *Canis lupus* from Avetrana. **A-C**: **A8-25**, right hemimandible in buccal (**A**), lingual (**B**) and occlusal (**C**) views. **D-F**: **A8-28**, left hemimandible in buccal (**D**), lingual (**E**) and occlusal (**F**) views. **G-I**: **AND-17**, right hemimandible in buccal (**G**), lingual (**H**) and occlusal (**I**) views. **J-L**: Ave8-1, right hemimandible in buccal (**J**), lingual (**K**) and occlusal (**L**) views. **M-O**: **A8-15**, right hemimandible in buccal (**M**), lingual (**N**) and occlusal (**O**) views. **P-R**: **A8-81**, left hemimandible in buccal (**P**), lingual (**Q**) and occlusal (**R**) views. **S**: **A8-36**, left maxillary fragment with M1 and M2 in occlusal view. **T**: **A8-39**, right M1in occlusal view. **U-W**: **Ave8-3**, right P4 in buccal (**U**), lingual (**V**) and occlusal (**W**) views. **X-Z**: **Ave07-2**, right P4 in buccal (**X**), lingual (**Y**) and occlusal (**Z**) views. Scale bars equal 3 cm.

Lower teeth. The p1 is single-cusped, with a short protoconid, and is single-rooted; it also possesses two small accessory cuspulids, one mesial and one distal. The p2 is rather long and oval, with no buccolingual constriction at its midpoint; it lacks any accessory cuspulids. The p3 is similar in shape to p2, but with one distal accessory cuspulid. In buccal view, the p3 emerges from a lower level when compared to the alveolar plane of p2 and p4. The p4 is a stout tooth, large and subrounded in shape (Fig. 3.11.3). It has a very large accessory cuspulid behind the protoconid and another small one on the distal cingulid. The m1 has a large paraconid with a mesial margin that is inclined distally, and in some specimens (*i.e.*, A8-C4, A8-C6, A8-28 and AND-26) is curved distally (Fig. 3.11.3). The paraconid tip is higher than the p4 protoconid tip. The protoconid is high and stout, and the metaconid is reduced and closely attached to the lingual side of the protoconid. In the shallow talonid basin, the hypoconid is prominently larger and higher than the entoconid; a sinuous crest connects them. The talonid is much lower compared to the height of the trigonid cuspids. The m2 is bean-shaped, characterised by a strong cingulid expanded mesiobuccally. The protoconid is larger and higher than the metaconid, and distally, a prominent hypoconid and a shelf-like distolingual side are evident. The m3 is a small and round tooth, with a single and prominent cuspulid in the center of the tooth.

Postcranial. Most of the postcranial elements recovered are badly preserved and fragmented. It was possible to identify which bone each specimen belonged to and to attribute them to *C. lupus*, but subtle features, such as muscular scars, etc., could not be described apart from a few exceptions. These were two fragments of humerus (A8-22 and AND-113) and a complete femur (A8-C21). Humerus. The proximal epiphysis of the humerus (AND-113) shows a knob-like and prominent *caput*. The tricipital line, in lateral view, seems to be sharp although it is broken at the level of the tuberosity of the *teres minor*. The greater tubercle is not as elevated over the *caput*. The medial view shows a round and smooth area on the greater

tubercle, for the attachment of the *m. infraspinatus*. In the cranial view, the humerus shows a rather shallow radial fossa, with an oval and wide supratrochlear foramen (Fig. 3.11.4A-B). Although broken on its caudal side, the lateral supracondylar crest in A8-22 is well developed as a moderately high ridge for the insertion of the *m. extensor carpi radialis*. In the distal epiphysis, the trochlea is slightly larger than the *capitulum humeri*. Femur. In general shape, the femur (Fig. 3.11.4C-D) has a rather straight diaphysis, in cranial view, that curves laterally only towards the distal epiphysis. In medial and lateral views, the diaphysis is curved. In cranial view, the intertrochantheric line is visible. In the medial portion it is more prominent and crest-like, corresponding to the attachment of the *m. vastus medialis*, whereas from its lateral side it is low. The long ridge for the *m. vastus medialis* departs from the lesser trochanter; this ridge extends caudally and continues in the medial lip. Near this is the lateral lip, which is less pronounced than the medial lip. Distally, two rugose and oval bulges mark the supracondylar tuberosities, with the lateral larger than the medial one. In distolateral view, a marked incision is evident for the insertion of the *m. extensor digitorum longus* and caudally, a round depression is visible, which is the attachment for the *m. popliteus*.

Morphological and Morphometric Comparisons. The scarcity of well-preserved cranial materials recovered from Avetrana bed 8 complicates any assessment of its main features. Nevertheless, tooth morphology allows us to consider the affinities and/or the differences between the Avetrana canid and the considered middle-Late Pleistocene wolves from Italian and European sites. Besides the remarkable similarity, *C. lupus* from Avetrana shows some peculiarities when compared to *C. l. italicus*; for example, it lacks the distal accessory cusp generally present in the P2 of the latter taxon. The position of the P4 protocone in the wolf from Avetrana is slightly mesially advanced when compared to the mesial margin of the P4, which is similar to *C. lupus* from Grotta Romanelli (Sardella et al., 2014) but contrasts

Figure 3.11.4 – **A-B**: **A8-22**, right distal epiphysis of humerus in cranial (**A**) and palmar (**B**) views. **C-D**: A8C-21, right femur in cranial (**C**) and plantar (**D**) views. Scale bar equals 3 cm.

with *C. lupus lunellensis* from Lunel-Viel 1 and Igue des Rameaux (Bonifay, 1971; Boudadi-Maligne, 2010) and with *C. l. italicus*, in which the protocone generally does not end beyond the mesial margin of the tooth. The M1 shows a narrowing at the level of the trigon (*e.g.*, in A8-36 and A8-68), as in other Apulian wolves like *C. lupus* of Grotta Romanelli, whereas the extant Italian wolves or *C. l. lunellensis* do not show this narrowing. Furthermore, the buccal cingulum seems more developed and prominent when compared to that of *C. l. italicus*, but is similar to the buccal cingulum of wolves from Grotta Romanelli and *C. l. lunellensis* of Lunel-Viel 1, although not as developed as in *C. mosbachensis*. The M2 of the wolf

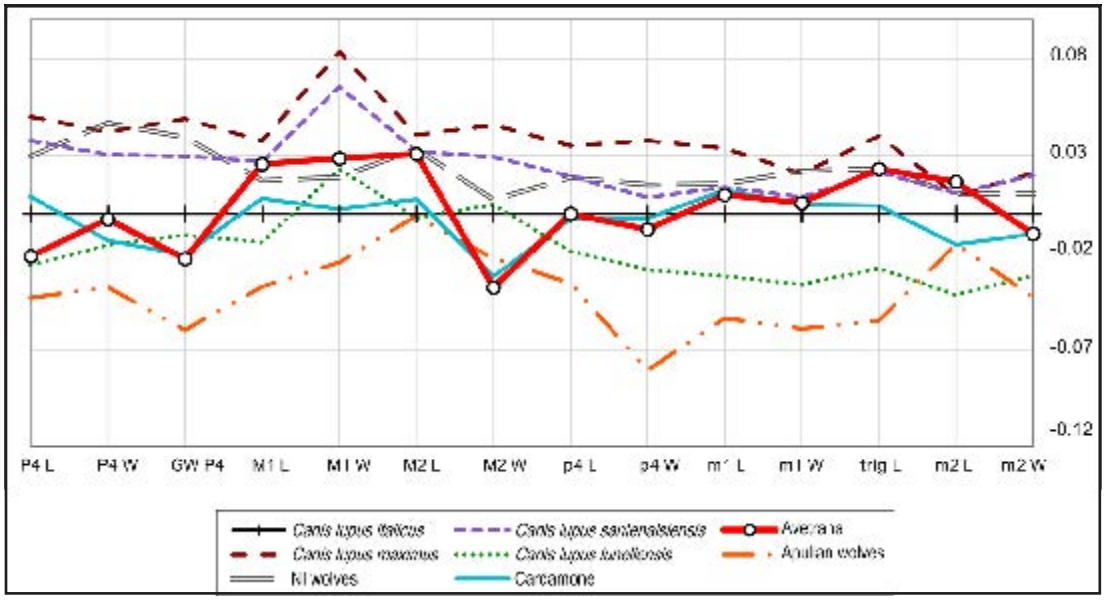

Figure 3.11.5 – Log-ratio diagram based on selected dental variables in the described (Avetrana bed 8 sample), as well as in other Late Pleistocene forms of *Canis lupus* (*C. lupus santenaisiensis, C. lupus maximus, C. lupus lunellensis,* Apulian wolves, northern Italian wolves; data taken from the literature: Bonifay, 1971; Boudadi-Maligne, 2010; 2012; Bertè, 2014) as compared to extant *Canis lupus italicus* (used as a reference baseline).

from Avetrana seems to be longer mesiodistally and shorter buccolingually when compared to that of *C. l. italicus* or *C. lupus* from Grotta Romanelli (see also Fig. 3.11.5). The lower teeth are very similar to those of modern Italian wolves and do not show significant peculiarities. In contrast to *C. lupus* from Grotta Romanelli and especially to *C. l. lunellensis*, the metaconid of the lower carnassial is rather reduced, as can be seen generally in *C. l. italicus*.

In size, the canid from Avetrana is slightly larger than the extant *C. l. italicus* (Fig. 3.11.5), especially in the upper teeth. When its tooth proportions are compared to those of the middle-Late Pleistocene French subspecies of *C. lupus* (*i.e.*, *C. l. lunellensis*, *C. l. santenaisiensis* Argant, 1989 and *C. l. maximus*), *C. lupus* from Avetrana is clearly somewhat intermediate between *C. l. lunellensis* and *C. l. santenaisiensis*, whereas *C. l. maximus* is larger, on average, than the other samples studied here. Besides this similarity in size, the pattern of dental proportions displayed by *C. lupus* of Avetrana does not follow the remarkably constant outline typical of all three

French subspecies. Indeed, the proportions of *C. l. lunellensis*, *C. l. santenaisiensis* and *C. l. maximus* (apart from the slight differences in size) seem to testify to a consistent degree of similarity among these three forms. In the scientific literature concerning the Italian fossil *C. lupus* samples, no attempt has been made to group them into different subspecies, although Sardella et al. (2014) identified that the Grotta Romanelli *C. lupus* shared an affinity with those from other southern Italian sites (*e.g.*, Ingarano, Melpignano) and named them "Apulian wolves". Here, these Apulian wolves were considered on the one side, and the "northern Italian wolves" (from localities like Broion, Buco del Frate, Pocala, etc.) on the other. The Cardamone site is considered separately because of its peculiar assemblage compared to the other southern Italian sites (see further discussion below). The French wolves, apart from differences in size (or in age between the sites), show considerable differences in comparison to these Late Pleistocene Italian wolves. When *Canis lupus* from Avetrana bed 8 is compared to the three Italian groups (*i.e.*, Apulian, northern Italian and Cardamone wolves), it shows proportions that fit the pattern of both Apulian and northern Italian groupings; therefore, it partially resembles both the variable pattern of the Apulian wolves and that of the northern Italian wolves. Interesting to note that the northern Italian proportions resemble those of the extant *C. l. italicus* especially for the lower teeth. Probably the most closely affine to Avetrana is the pattern displayed by the sample from Cardamone. Among the postcranial elements, only the fragmentary humeri (A8-22 and AND-113) and a complete femur (A8-C21) show features similar to those of extant Italian wolves and can be discussed in detail. In size, the humerus of *C. lupus* from Avetrana is similar to that of *C. l. italicus* and the Apulian wolves (Sardella et al., 2014), whereas it is slightly larger than that of *C. l. lunellensis* (Boudadi-Maligne, 2010). The proximal epiphysis of the humerus shows a knob-like and prominent caput, more "bulging" than the caput of *C. l. italicus*. The diaphysis of the humerus of *Canis lupus* from Avetrana seems to be more slender than that of *C. l. italicus*,

especially near the distal epiphysis. In cranial view, the radial fossa and the oval and wide supratrochlear foramen of the humerus (Fig. 3.11.4A-B) are similar to those of *C. l. italicus*. In the distal epiphysis, the development of the trochlea, slightly larger than the capitulum humeri, differs from that of *C. l. lunellensis* from Lunel-Viel 1, in which the trochlea has a greater extension in proximodistal sense (Boudadi-Maligne, 2010). The condition of *C. l. lunellensis* is similar to that of *C. mosbachensis* from Vértesszòlòs II. The marked narrowing that divides the capitulum from the trochlea is less pronounced in both *C. l. lunellensis* and *C. mosbachensis* in comparison to that of *C. l. italicus* and *C. lupus* from Avetrana. In the specimens of extant *C. lupus* examined for morphological comparisons, the distal articular surface of the humerus, in cranial view, has the shape of a parallelogram due to its medial and lateral sides that are strongly inclined compared to the vertical axis of the diaphysis. By contrast, this feature is less pronounced in *C. lupus* from Avetrana. Other features are similar to those of *C. l. italicus*.

In general shape, the femur (Fig. 3.11.4C-D) is very similar to that of extant wolves, although compared to that of *C. l. italicus*, it is more slender and the diaphysis appears thinner. The neck is also longer when compared to that of *C. l. italicus,* so that the femoral head is higher than the greater trochanter, in cranial view. In fact, the head projects proximomedially to a greater extent than in *C. l. italicus* and more cranially, so that, in lateral view, almost all the femoral head is visible. The greater trochanter is also shorter and has a larger gluteal tuberosity when compared to Italian wolves. In plantar view, the trochanteric fossa seems shallower but is more elongated distally, with a larger intertrochanteric crest than is seen in *C. l. italicus*.

The proportions of the complete right femur were compared, A8-C21, with that of the other middle and Late Pleistocene wolves considered in Fig. 3.11.5 (Fig. 3.11.6). As seen for the dental log-ratio diagrams, the femur of *C. lupus* from Avetrana is more similar to that of the Apulian wolves than to those of the larger *C. l. santenaisiensis* and *C. l. maximus*.

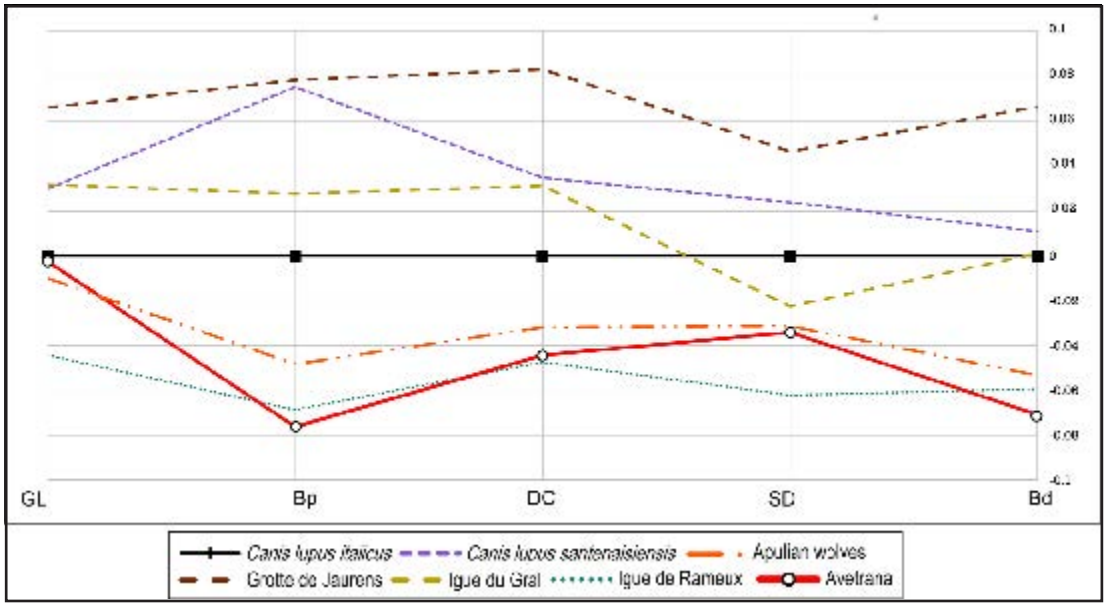

Figure 3.11.6 – Log-ratio diagram based on selected femur measurements in the described (Avetrana bed 8 sample), as well as in other Late Pleistocene varieties of *Canis lupus* (*C. lupus santenaisiensis*, *C. lupus maximus*, *C. lupus lunellensis*, Apulian wolves, northern Italian wolves; data taken from the literature: Bonifay, 1971; Boudadi-Maligne, 2010; 2012; Bertè, 2014) as compared to extant *Canis lupus italicus* (used as a reference baseline).

3.11.3. Results

A Kruskal-Wallis test performed on the datasets revealed various differences in the lengths of the upper and lower teeth in the fossil and modern wolf populations. The biometrical comparative analyses on P4 L, M1 L, and m1 L revealed a relevant difference in size between the Avetrana and the other wolf populations, as reported in Fig. 3.11.7. The length of the P4 from Avetrana was similar to that of the Apulian wolves (p value = 0.176), *C. l. lunellensis* (p value= 0.746), Cardamone (p value = 0.160), and the modern *C. l. italicus* (p value = 0.087); therefore, it differs only from the larger French forms of *C. lupus* considered here. By contrast, the lengths of both M1 L and m1 L were similar to those of the large-sized *C. l. maximus, C. l. santaineisiensis,* the northern Italian wolves from Broion, Pocala, and Buco del Frate, and the wolves from Cardamone (Fig. 3.11.7).

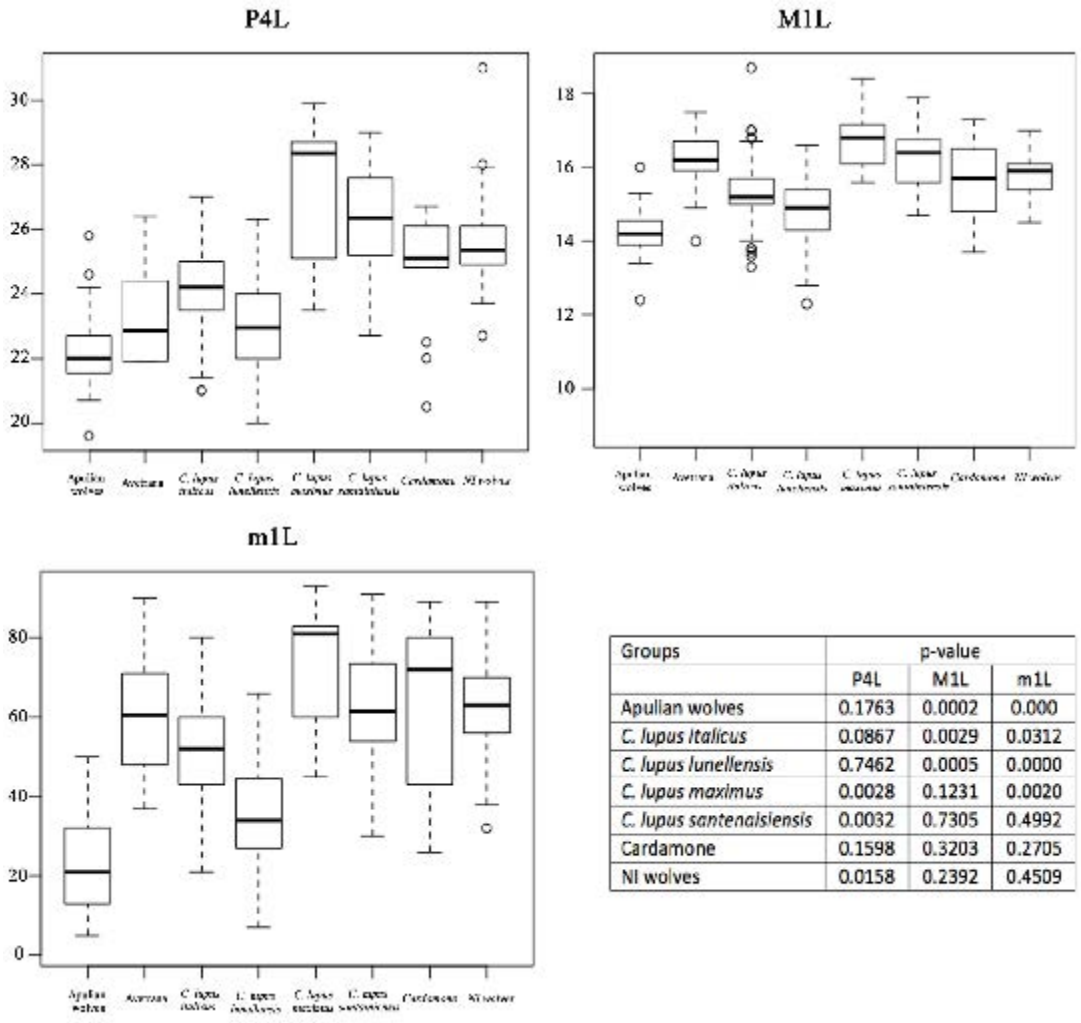

Groups	p-value		
	P4L	M1L	m1L
Apulian wolves	0.1763	0.0002	0.000
C. lupus italicus	0.0867	0.0029	0.0312
C. lupus lunellensis	0.7462	0.0005	0.0000
C. lupus maximus	0.0028	0.1231	0.0020
C. lupus santenaisiensis	0.0032	0.7305	0.4992
Cardamone	0.1598	0.3203	0.2705
NI wolves	0.0158	0.2392	0.4509

Figure 3.11.7 – Boxplot of variation length of P4 L, M1 L and m1 L from Apulian wolves, Avetrana, *C. lupus italicus*, *C. lupus lunellensis*, *C. lupus maximus*, *C. lupus santenaisiensis*, Cardamone and northern Italian wolves. (d) Table of p-values for the Kruskal-Wallis test.

3.11.4. Discussion

3.11.4.1. Variability of the Avetrana wolf population

The minimum number of individuals (MNI) of the *C. lupus* Avetrana bed 8 population, estimated from the most abundant element (the lower carnassial), is 14. The dentognathic diagnostic features of *C. lupus* are easily recognizable in the Avetrana sample, and the inter-individual variability is limited to the development of some cuspules (*e.g.*, the protoconule on the M1) and cuspulids (*e.g.*, the morphology of the mesial margin of the m1 paraconid).

The population of *C. lupus* recovered from the Avetrana bed 8 shows peculiar

morphologies and dental proportions that lie between those of the wolves recovered from other southern Italian sites (*e.g.*, Melpignano, S. Sidero, Ingarano) and those from northern Italy (Broion, Pocala, Buco del frate). According to Sardella et al. (2014) these southern Italian sites are referable to the MIS 4-3 whereas the northern Italian ones are referred to MIS 3 in Gatta et al. (2016). The dental proportions of *C. lupus* from Avetrana are similar or slightly larger than those of the extant *C. l. italicus*, apart from a few teeth, whereas its proportions are generally smaller than those of the French *C. l. maximus* (unlike reported in Bertè & Pandolfi, 2014).
Conversely, the only complete postcranial remain recovered, a right femur, is considerably smaller than the average values for *C. l. italicus*. This discrepancy agrees with the great size variability displayed by modern wolves (Klein, 1986; Dayan et al., 1991; Meiri et al., 2004). With all this considered, the average size of *C. lupus* from Avetrana is, nonetheless, larger than that of other southern Italian fossil wolves (Figs. 3.11.5 and 3.11.6).

3.11.4.2. A short review of the Late Glacial Canis lupus *of Europe*

The first anatomically modern *C. lupus* to appear in the western European fossil record is *C. l. lunellensis* from Lunel-Viel 1 (Bonifay, 1971). In size, this canid was comparable to the large-sized populations of *C. mosbachensis* from mid middle Pleistocene (Thenius, 1954; Bonifay, 1971). Large-sized individuals of *C. lupus* began to appear during the MIS 8 in the deposits of Naciekowa Cave (Poland; Van der Made et al., 2014). Since then, the tooth sizes of fossil wolf populations in Europe seem to have reached and remain within the dimensional range of variability of the modern *C. l. lupus*, *C. l. italicus,* and *Canis lupus signatus* Cabrera, 1907 (see Van der Made et al., 2014). Nevertheless, local peculiarities emerged from different timeframes during the Late Pleistocene. For example: 1) during the MIS 3 in France, two different forms of *C. lupus* occurred in different sites: the large subspecies called *C. l. maximus* in localities like Grotte de Jaurence and

Grotte de Maldidier, coeval with a "smaller" form, *C. l. santenaisiensis* from Aven de l'Arquet, (Boudadi-Maligne, 2012); 2) Flower & Schreve (2014) showed that *C. lupus* from the MIS 5a sites of the United Kingdom were larger, on average, when compared to extant *C. l. lupus* from Sweden and to those recovered in MIS 7 and MIS 3 of other British sites; 3) the complex Italian situation in which, in the last 100 kyr, *C. lupus* from southern Italy seems to have smaller proportions than those of coeval northern Italian populations (see, among others, Sardella et al., 2014).

Today, wolves are widely diffused throughout the northern hemisphere, from the high latitudes of North America to the South of India. This range is reflected in a clinal geographic variation that follows Bergmann's ecogeographical rule (Klein, 1986; Dayan et al., 1991; Meiri et al., 2004). This rule has been also applied to Neogene and Quaternary mammals and correlates with latitudinal and climatic oscillations and with glacial/interglacial cycles (Davis, 1977; Klein & Scott, 1989; Bown et al., 1994; Renaud et al., 1999; Millien et al., 2006). Indeed, during the middle and Late Pleistocene, climatic changes produced strong palaeoecological and paleoenvironmental instability that profoundly affected the vertebrate faunal assemblages.

One case study is that of Cardamone (Apulia, southern Italy), as discussed by Rustioni et al. (2003). Referable to the Last Glacial Maximum (MIS 2, 22-18 ka), the faunal assemblage of this site shows a mix of autochthonous taxa, such as *C. elaphus*, *L. europaeus*, *O. cuniculus*, *B. primigenius,* and some of the elements of the so-called *Mammuthus-Coelodonta* Faunal Complex (Kahlke, 1994), like *Mammuthus primigenius* Blumenbach, 1799, *Coelodonta antiquitati*s Blumenbach, 1799 and *E. ferus*. According to Rustioni et al. (2003), the presence of the mammoth and the woolly rhino is actually a result of the dispersal of these taxa through the lowstand of the Adriatic Sea and the connection between the Balkan region and Apulia during the MIS 2 glacial stage. The mammal assemblage known as the *Mammuthus-Coelodonta* Faunal Complex (which includes other frigophile species

related to modern *V. lagopus*, *Saiga tatarica* Linnaeus, 1766, *Ovibos moschatus* Zimmermann, 1780 and *R. tarandus*) has been considered as an indicator of cold, rapid temperature fluctuations and especially arid climatic conditions (Kahlke, 2014). This mammal assemblage was widespread in the Palaearctic during the Late Pleistocene (Kahlke, 2014) and it is also known from Italian localities, although incompletely represented in northern regions and discontinuously in some others. Some elements never reached Italy (*e.g.*, *S. tartarica* and *O. moschatus*); *Sicista* Gray, 1827 and *Ochotona* Link, 1795 are reported in Veneto and on the eastern side of central Italy (Sala et al., 1992); *M. giganteus* is recorded in central Italy (Pasini, 1970; Farina, 2011); *R. tarandus* is reported from Liguria and Friuli Venezia Giulia (Bon et al., 1991), and *Alces alces* Linnaeus, 1758 is also reported in North-eastern Italy (Breda, 2001). The *Coelodonta* Bronn, 1831 record in Italy is rather scanty, reported in a few localities from northern (Cremaschi et al., 2005; Gallini & Sala, 2001), central (Palmarelli & Palombo, 1981) and southern Italy (Petronio & Sardella, 1998; Rustioni et al., 2003). These findings testify to favorable (*i.e.*, cold and arid) environmental and climatic conditions for the dispersal of this fauna into the Italian Peninsula, which occurred many times in the Late Pleistocene. As far as *C. lupus* is concerned, from the MIS 3, the specimens from northern Italian sites (Broion, Buco del Frate and Pocala) are very similar in size to those from the MIS 3 sites of southern France, referred to by some scholars to the subspecies *C. l. maximus* (Fig. 3.11.5). Indeed, as shown in Fig. 3.11.5, the subspecies *C. l. maximus*, proposed for its greatly different size from extant and fossil wolves, is remarkably close in dental proportions to *C. l. santenaisiensis* from Aven de l'Arquet (still from MIS 3). A similarity between these wolves and *C. lupus* from Avetrana bed 8, especially when compared to southern Italian ones, had already been pointed out by Bertè & Pandolfi (2014). On the one hand, the authors explained the close morphometric affinity and the differences in morphology between the wolf of Avetrana and *C. l. maximus* with the action of similar evolutionary constraints

towards comparable specialization in diet or to an increase in size. On the other, they outlined the possibility that the morphometric likeness between Avetrana and northern Italian samples resulted as a consequence of a dispersal event of central European wolves during the MIS 4, with replacement or hybridization with the southern European ones. In southern Italy, the appearance of large-sized wolves is evident only in the final part of MIS 3, at sites like Grotta Tina di Camerota (Salerno, Campania; Martini et al., 1974), Grotta del Poggio (Salerno, Campania; Sala, 1979) and Grotta Paglicci (Foggia, Apulia; Boscato, 2004); or in the earliest MIS 2, *e.g.*, Masseria del Monte Conversano (Bari, Apulia; Anelli, 1959). The stratigraphic sequence of Grotta Paglicci has an important role in the paleontological and archaeological scenario of research on the middle–late Paleolithic of Apulia. The long and well-preserved sedimentary succession consists of 26 layers, with the most ancient ones referring to the early-middle Paleolithic and the more recent ones to the late Paleolithic. Some of these levels (level 22-23) were found to contain mammal remains and artefacts attributed to the ancient Gravettian (Boscato, 2004). The faunal assemblage includes *Equus ferus* Boddaert, 1874, *Equus hydruntinus* Regalia, 1907, *S. scrofa, B. primigenius, Capra ibex* Linnaeus, 1758*, Rupicapra* cf. *pyrenaica* Bonaparte, 1845*, C. elaphus, L. europaeus, F. sylvestris, C. spelaea, Ursus arctos* Linnaeus, 1758*, C. lupus* and *V. vulpes* (see Boscato, 2004). The radiocarbon dates indicate that the 22–23 layers accumulated from 28.1 ±0.4 ka and 26.8±0.3 ka (Palma di Cesnola, 1991). Gatta et al. (2016) suggested that Avetrana bed 8 should be referred to MIS 3 coeval to sites like Pocala Cave and Buco del Frate. In particular, the occurrences of *M.* (*Terricola*) *savii* and of the rhinoceros *S. hemitoechus* in the faunal assemblages from bed 2 to bed 7 suggest referring these layers to MIS 4–3 (78–28 ka; Vandergoes et al., 2005). In Avetrana bed 8, in addition to the occurrence of *M. savii,* the rhinoceros *S. hemitoechus* was missing. In the Apulian Peninsula, the last occurrence of the narrow-nosed rhinoceros would seem to be from Ingarano (about 41 ka BP) (Pandolfi et al., 2017). In this scenario,

the composition of the faunal assemblage from Ingarano, Pocala Cave and Buco del Frate would appear to differ from that of Avetrana bed 8. Finally, according to Bertè & Pandolfi (2014), the biochronological correlations are suggestive to consider Avetrana bed 8 as referable to the end of MIS 3. The results of the statistical analyses reveal a strong affinity between the wolf populations from Avetrana and Cardamone, previously unknown in literature. These two population differ in P4 length from northern Italian wolves and the other large *C. lupus* subspecies from MIS 3 in France (*C. l. maximus, C. l. santenaisiensis*). Recent research has examined the evolutionary trends in carnassial teeth of European Pleistocene canids (Sansalone et al., 2015). According to the authors, the lower and upper teeth in true *C. lupus* are characterised by morphometric changes through time, with significant climate influence. From the middle Pleistocene to the Holocene, the modern wolf went through an increase in dimensions of the upper and lower dentition, with the exception of the P4 length, which is characterised by stasis (Sansalone et al., 2015). Here the geographic and temporal wolf' populations were treated as separate groups from the Italian Peninsula. As shown in Fig. 3.11.7, analyzing these as separate groups indicates that the P4 length would not seem be affected by stasis during the Late Pleistocene. Indeed, the northern Italian wolves show a longer P4, similar to other large *C. lupus* subspecies from MIS 3 in France (*C. l. maximus*, *C. l. santenaisiensis*).

The record of *C. lupus* from Avetrana, characterised by larger body size than observed for the older Apulian wolf samples from the sites located in same area (*e.g.*, Melpignano, Ingarano, Grotta Romanelli), fits within the pattern of southward dispersal of the "*glacial wolves*". Although the faunal assemblage of Avetrana bed 8 (Petronio et al., 2008) includes mainly temperate taxa, a more rapid dispersal can be readily imagined for a species that today is so adaptable to a wide range of different environments and that travels a great deal (Mech, 1970), compared to the taxa that are strictly connected to glacial conditions. The peculiar

faunal assemblage of Cardamone, dated between 22 and 18 ka, records the arrival in southern Italy of the other cold taxa, referable to the *Mammuthus-Coelodonta* Faunal Complex that coexisted with the autochthonous temperate fauna.

3.11.5. Conclusions

The faunal assemblage of Avetrana bed 8 has yielded a large sample of *C. lupus*. The general morphological features of the sample do not show significant differences with the comparative samples, *i.e.*, extant wolves from Italy and fossil wolves from Italy and abroad. In terms of size, *C. lupus* from Avetrana is considerably larger than other *C. lupus* discovered in Apulian sites (*e.g.*, Grotta Romanelli, Ingarano, Melpignano; together called Apulian wolves; Sardella et al., 2014), which are rather small. On the contrary, the population of wolves from Avetrana bed 8 is very similar to the extant *C. l. italicus*, the Italian wolf, and close to wolves recovered from Late Pleistocene sites in both northern Italy and France. During the Late Pleistocene, at least until the MIS 3-2, the pattern of mensural variability of *C. lupus* across the Italian Peninsula seems to be divided in two groups: the large-sized northern Italian wolves, with dental proportions close to those of the extant *C. l. italicus*, and the small-sized Apulian wolves, with peculiar dental proportions in comparison to other wolves from Italy and Europe. This apparently simple binary pattern is the result of complex biogeographic and climatic factors. This "equilibrium" between the large-sized populations from North Italy and the small-sized ones from the southeast changes by the end of MIS 3 and the beginning of MIS 2. Contemporaneously, there is the earliest record in Apulia of the so-called *Mammuthus-Coelodonta* Faunal Complex in the locality of Cardamone. This frigophile assemblage, commonly associated with cold and arid environments or phases during the middle-Late Pleistocene of the whole Eurasia, has been recorded only sporadically in the Italian Peninsula, possibly due to the stability of micro- and/or mesoclimatic conditions favorable for other types of faunas. Nevertheless,

the record from Cardamone, like others in the same time span, testifies that Apulia was characterised by a cold and arid environment during the MIS 2. This climatic evidence supports the hypothesis that the occurrence of *C. lupus* of Avetrana bed 8, with its size and its dentognathic proportion that differ so greatly from those of the earlier Apulian wolves, is probably the result of the dispersal into southern Italy of glacial forms of wolves from other regions of Europe.

3.12. Preliminary report on the *Canis lupus* sample from Ingarano (Apulia, Italy)

3.12.1. Context

The Late Pleistocene vertebrate assemblage of Ingarano site was discovered in the first half of the 1980s, but described only in the early 1990s (Capasso Barbato et al., 1992).

The fossiliferous deposit is located near the village Apricena (Foggia, Apulia) at about 270 m a.s.l. (Fig. 3.12.1), along the Garganica railway, in a cave deposit of karst origin outcrops situated in an abandoned quarry (Capasso Barbato et al., 1992; Petronio et al., 1996; Petronio & Sardella, 1998; Bedetti et al., 2007). *Canis lupus* was reported for the first time by Capasso Barbato et al. (1992), and later new material was discovered during new excavation field campaigns in the 1990s (Petronio et al., 1996; Petronio & Sardella, 1998). Petronio & Sardella (1998) suggested that the wolf population in Ingarano site belonged to a form of rather small body size, comparable to *C. l. lunellensis* from Lunel Viel 1 and Avent de la Fage (Bonifay, 1971; Martini, 1975).

The sample of *Canis lupus* from Ingarano, with one complete cranium and three partially complete crania, never studied in detail, represent one of larger collection of *C. lupus* from Late Pleistocene Italian localities. The first description and analyses on this sample are here provided.

3.8.2. Geological and paleontological framework

The fossiliferous deposit of Ingarano is about 12 m thick karst filling succession within the Jurassic-Cretaceous limestone of the "Calcare di Sannicandro" Formation (Capasso Barbato et al., 1992; Petronio et al., 1996; Petronio & Sardella, 1998; Bedetti et al., 2007). The stratigraphy sequence included five depositional events of terrigenous sedimentation during the Late Pleistocene.

Figure 3.12.1 – Localization of the site of Ingarano, Apulia (southern Italy), from Iurino et al. (2015).

The first one is an alabastrine layer, including stalagmites and stalactites fragment and locally encrusted by phospatic materials (Petronio et al., 1996; Petronio & Sardella, 1998; Bedetti et al., 2007). The second is a phosphatic layer, locally rich in Aves and mammal remains. The layer C is a massive conglomerate layer with flattened calcareous pebbles and poorly cemented silty reddish matrix. The layer D, separated from the layer C by a discontinuity surface, is a conglomerate bed with angular clasts and calcareous matrix. The last is a conglomerate layer with angular clasts cemented by calcareous matrix (Bedetti et al., 2007). Between D and E, Mousterian lithic artefacts were discovered (Petronio et al., 1996). The rich Late Pleistocene vertebrate fauna from this site was studied by several researchers (Capasso Barbato et al., 1992; Petronio et al., 1996; Petronio & Sardella, 1998; Sardella, 2000; Petronio et al., 2006; Bedetti et al., 2007; Iurino, 2014; Iurino et al., 2015; Pandolfi & Petronio, 2017), including 41 species. Among these: *E. europaeus, Myothis blythi* (Tomes, 1857)*, O. cuniculus, L. europaeus, Microtus* sp., *Microtus* ex gr. *arvalis/agrestis, M.* (*Terricola*) *savii, Apodemus sylvaticus* Linnaeus, 1758*, Elyomis quercinus* Linnaeus, 1766*, C. lupus, V. vulpes, U. arctos, M. nivalis, Martes* sp., *Gulo*

gulo Linnaeus, 1758*, C. crocuta, F. sylvestris, Lynx* sp.*, Panthera pardus* Linnaeus, 1758 Linnaeus, 1758*, E. hydruntinus, C. elaphus, D. dama, C. capreolus, Rupicapra* sp. and *B. primigenius*. Petronio & Sardella (1998) identified a sandy-clay layer in uncertain stratigraphic relationship with the karst succession, including *P. spelaea*, *H. amphibius*, *C. antiquitatis*, *S.hemitoechus* and *Palaeoloxodon antiquus* (Falconer & Cautley, 1847) (Petronio & Sardella, 1998). The faunal assemblage was deposited in a short time-span chronologically referred to MIS 3 (Bedetti & Pavia, 2007).

3.12.3. Systematic Paleontology

Order **Carnivora** Bowdich, 1821

Family **Canidae** Fischer, 1817

Subfamily **Caninae** Fischer, 1817

Tribe **Canini** Fischer, 1817

Genus ***Canis*** Linnaeus, 1758

Canis lupus Linnaeus, 1758

(Figs. 3.12.2-3.12.6; Tables 3.12.1-3.12.4)

Materials. Cranial fragments. Unnumbered specimen (provisional number: DST-N1), cranium with left I3, P3-M2and right I3-C, P3-M2 and fragmented left mandible with m2-m3 and complete right one with c-m3. IN504, splanchnocranium with left P2-M2 and right P2, P4-M2; IN505, splanchnocranium with left P1-P2, P4-M2 and right P4-M2; IN506, cranial fragments in bone breccia; IN507, neurocranium; IN513, left maxillary fragment with P4-M1; IN514, maxillary fragment with M1-M2; IN516, left maxillary fragment with P3 and partial P4; IN517: maxillary fragment with P3; IN519, occipitals. Upper teeth. INGND52, left I2; INGND77, right I2; INGND51, right I3; INGND75, left I3; INGND76, right I3; ING528, right I3; IN521, left C1; IN523, left C1; INGND81, right P1; INGND347, left P3; IN524, right P4; IN527, right M1; IN531, right M1; IN532, left M1; IN508, left hemimandible with c1-m1; IN509, left hemimandible with m1-m2; IN510, left hemimandible with m1-m2; IN511, left hemimandible with p4-m1; IN515,

right hemimandible with p4-m1; IN522, left hemimandible fragment with c1, p2-p3; IN552, right hemimandible with m1; IN581, right hemimandible with p2-p3; IN634, left hemimandible with i1-c1, p2, p4-m2; IN635, left hemimandible with p2-m1; IN641, left hemimandible with m1; INGND338, right hemimandible with p4-m2; INGND43, right i1; INGND55, right i1; INGND69, right i1; INGND70, right i1; IN35, right i2; IN530; right i2; INGND44, right i3; INGND45, right i3; INGND46, right i3; IN529, right c1; IN 525, right m1; INGND45 left m3; ING 540, atlas; INGND946, left fragment scapula; IN037, left proximal epiphysis of humerus; INGND722, right distal epiphysis of humerus; INGND947, left distal epiphysis of humerus; INGND333, right proximal epiphysis of radius; IN533, partial left ulna; INGND87, left proximal epiphysis of ulna; INGND9, left first metacarpal; IN566, left second metacarpal; IN580, right second metacarpal; IN575, right second metacarpal; INGND140, right second metacarpal; IN567, right third metacarpal; IN569, right third metacarpal; INGND10, right third metacarpal; INGND325, left third metacarpal; IN558, left fourth metacarpal; IN638, right fourth metacarpal; IN573, right fourth metacarpal;INGND131, right fourth metacarpal; INGND308, right fourth metacarpal; IN557, right fifth metacarpal; INGND8, right fifth metacarpal INGND9, left fifth metacarpal; IN545, right femur; IN546, left distal epiphysis of femur; IN547, left distal epiphysis of femur; IN548, right proximal epiphysis of femur; IN550, right proximal epiphysis of tibia; ING549, left proximal epiphysis of tibia; ING551, right proximal epiphysis of tibia; INGND350, right proximal epiphysis of tibia; IN636, left calcaneus; INGND351, right calcaneus; ING633, right talus; IN637, right talus; INGND1, left talus; INGND22, left talus; INGND2, right second metatarsal; INGND688, left second metatarsal; IN564, left third metatarsal; IN566, right third metatarsal IN568, right third metatarsal; INGND948, left third metatarsal; IN565, left fourth metatarsal; IN665, right fourth metatarsal; INGND4, left fourth metatarsal; IN562, left fifth metatarsal; INGND306, right fifth metatarsal; IN572, IN579, IN597, IN563, IN639,IN830, INGND707,INGND708, fragments metapodial; IN576, right first phalange; IN577, left first phalange; INGND14, left first phalange; INGND15, right first phalange; INGND60, right first phalange; INGND61, right first phalange; INGND332, left first phalange; INGND949-956, fragments first phalange.

Description. *Cranium*. The muzzle relatively short and stout. In dorsal view, the cranium is relatively elongated rostrocaudally (Fig. 3.12.2). The frontal sinus is greatly developed, bulging and elongated caudally. The inflation of the sinus causes the frontals to create a marked median interfrontal fossa. The sagittal crest is developed: the parasagittal crests are fused at level of the frontoparietal suture and, on the distal side of the braincase, the crest reaches its top. In occipital view, the occipital part of the cranium has a triangular shape, marked by the sharp and prominent nuchal crests. The external occipital protuberance (inion) considerably overhangs the condyles, in lateral view (Fig. 3.12.2). In ventral view, the tympanic bullae appeared considerably inflated and hemispheric. Their medial walls are caudorsotrally divergent. Paraoccipital processes are missing. In ventral view, the palate ends at level M2. It is wide, especially at level of M1, but also enlarged in its rostral portion. The incisive foramina variably end before the distal end of C (DST-N1; IN 505) or at or slightly beyond it (IN 504) (Figs. 3.12.2-3.12.3).

Upper teeth. The I3 is enlarged, well-developed and canine-like. It possesses a prominent basal cingulum. The canine is stout. The P1 is single-cusped, oval in shape with a relatively extended distally; IN 505 possesses a mesial accessory cuspid and pointed (Fig. 3.12.3). The cusp of P2 and P3 is rather low. P2 does not possess any accessory cuspids, whereas P3 has a small one, poorly individualized from the protocone. The P4 possesses a generally reduced protocone (although it is stout in IN 505), which lies at level of the mesial margin of the tooth (in IN 504 and IN 513 the protocone is placed mesially compared to the mesial margin of the P4) (Fig. 3.12.3). All the specimens possess a great deal of dental wear on the protocone so it is difficult to assess the correct morphology of the cusp. The paracone is stout and large, and the metastyle is sharp, with a groove on the buccal side. On the distolingual side of the tooth there is a cingulum. The M1 possesses a considerably larger and higher paracone compared to the metacone. The buccal cingulum is fairly noticeable and the parastyle is rather prominent. The

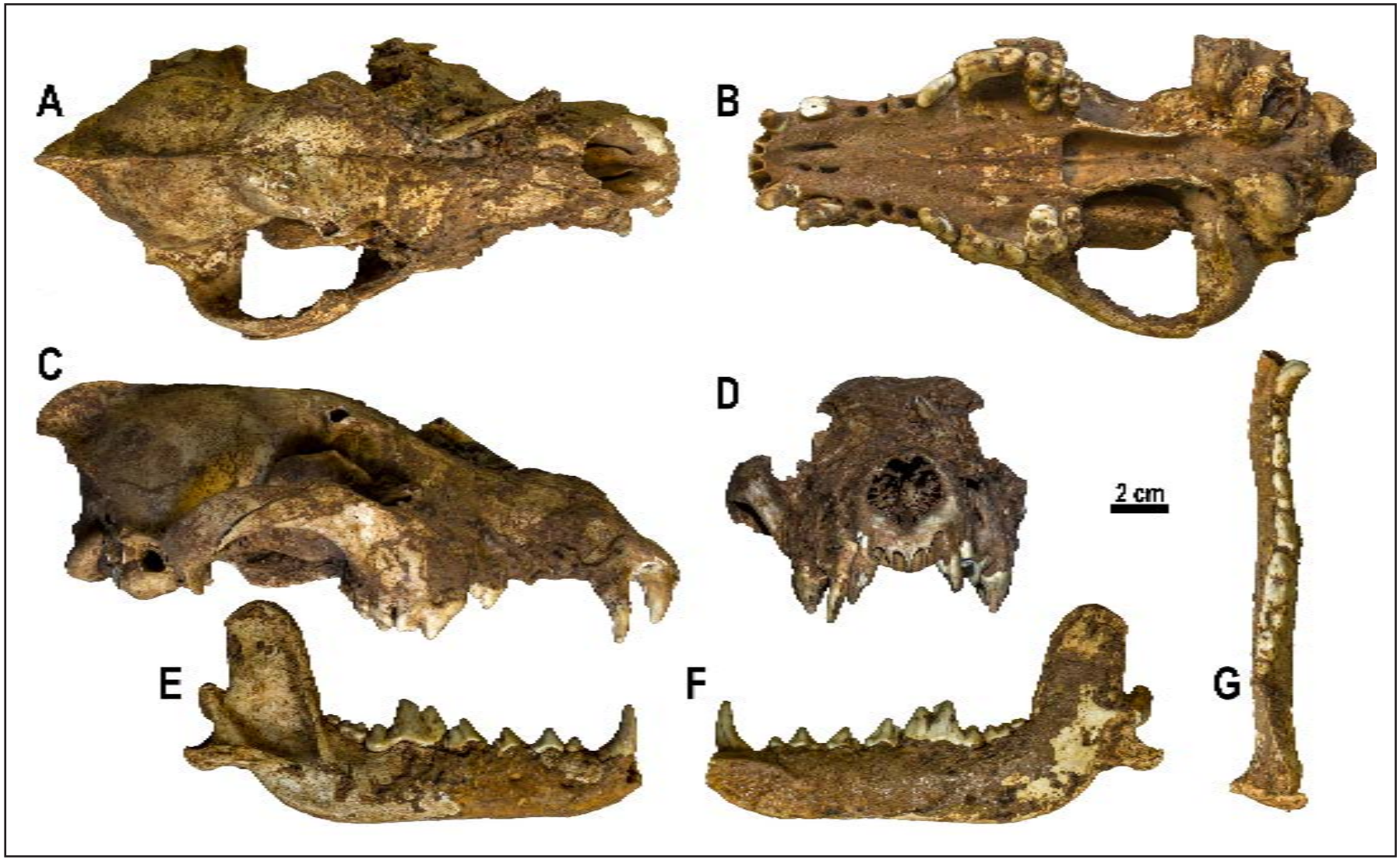

Figure 3.12.2 – *C. lupus* from Ingarano. **A-G**: **DST-N1**, skull in dorsal (**A**), ventral (**B**), lateral (**C**) and rostral views (**D**); right hemimandible in buccal (**E**), lingual (**F**) and occlusal (**G**).

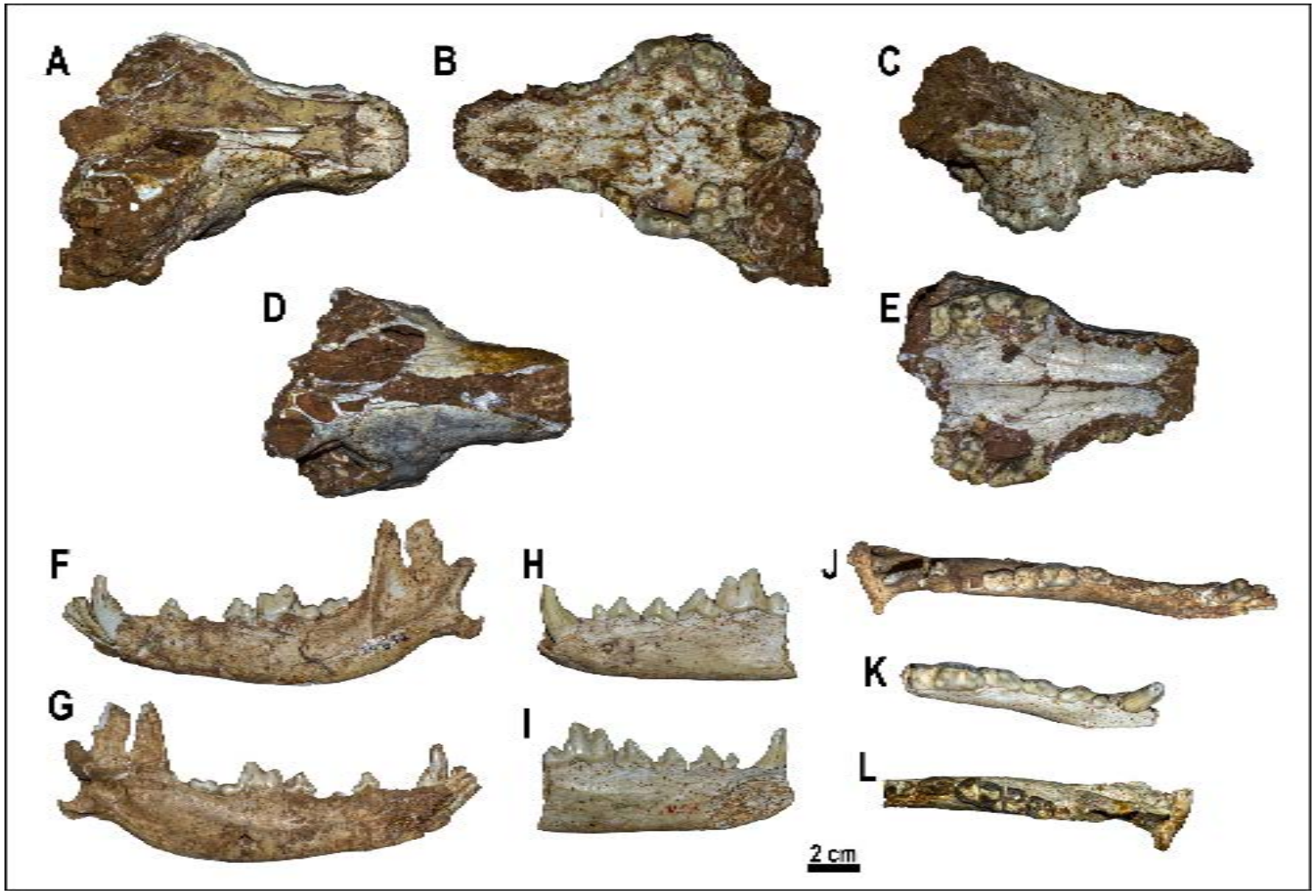

Figure 3.12.3 – *C. lupus* from Ingarano. **A-C**: **IN 504**, cranial fragment in dorsal (**A**), ventral (**B**), and lateral (**C**). **D-E**: **IN 505**, cranial fragment in dorsal (**D**) and ventral (**E**) view. **F-G, J**: **IN 634**, left hemimandible in buccal (**F**), lingual (**F**) and occlusal (**J**) views. **H-I, K**: **IN 508**, left hemimandible in buccal (**H**), lingual (**I**) and occlusal (**K**) views. **L**: **INGND338**, right hemimandible in occlusal view.

trigon basin is well developed, especially compared to the talon one (reduced to an S-shaped furrow); trigon basin is deeper than talonid one. M1 possesses a small but prominent protoconule, stout protocone and small metaconule. The hypocone is rather individualized from the lingual cingulum in the unworn specimen IN 505 (Fig. 3.12.3). The M2 is rather short (not so expanded lingually). It possesses a very large paracone and a smaller metacone (with also small difference in height). On the trigon, there is a rather large protocone and a distal cingular hypocone (Fig. 3.12.3).

Mandible. The corpus is rather deep and elongated (Fig. 3.12.3). On the buccal side, there are two foramina: the larger mental foramen under the interdental space between p1 and p2 and a smaller one under the midpoint of p3. IN635 possess an enbulgement of bone under the p2. The toothrow is arched (*i.e.* buccally convex at the p4-m1 commissure), especially IN634 (whereas the IN 508 is not so arched). Two mandibles show diastemata between premolars (especially p2-p3), DST-N1, IN634 and IN635, whereas IN 508 and INGND338 does not have it (Figs. 3.12.2-3.12.3). The mandible ramus is high, with a relatively mesiodistally large coronoid process and a conspicuous coronoid crest.

Lower teeth. The p1 is unicusped, with a short protoconid and single-rooted; it also possesses two tiny accessory cuspulids, one mesial and one distal. The p2 is buccolingually compressed, with no medial buccolingual constriction; it does not have any accessory cuspulids. The p3 is oval-shaped, with one small distal accessory cuspulid. It emerges from a lower level compared to the alveolar plane of p2 and p4 (especially visible DST-N1, IN 634 and INGND338). The p4 is a stout tooth, large and oval in shape. It shows a large and high protoconid, a very large accessory cuspulid behind protoconid and another small one on the distal cingulid. The m1 has a large and very high paraconid with a distally inclined mesial margin. Its tip is higher than that of the p4 protoconid. The protoconid is high and stout. The metaconid is reduced and closely attached to the protoconid (poorly

individualized). In the shallow talonid basin, the hypoconid is prominently larger and higher than the entoconid. The talonid is much lower compared to the height of trigonid cuspids. The m2 is bean-shaped, characterized by a strong cingulid expanded mesiobuccally; the protoconid is larger than the metaconid. Distally, there is a prominent hypoconid and a shelf-like distolingual side. The m3 is single-cusped and generally possess a cristid on the lingual side of the protoconid.

Postcranial elements. The postcranial specimens recovered from Ingarano are often fragmented and poorly preserved. The most complete specimens are a proximal portion of humerus (IN037) right radius (INGND333), a left ulna (IN 533) and a right femur (IN 545) (Figs. 3.12.4-3.12.5). Scapula. The scapula fragment INGND946 represent almost only the glenoid articular surface. The glenoid is rather shallow and with a distal oval outline. Humerus. On the proximal epiphysis, the head is stout and well developed. In proximal view, it is round in shape, and reducing the development of the lesser tubercle, on its medial side. In caudal view, the greater tubercle is developed but not so high above the *caput* (Fig. 3.12.4). The insertion area of the *m. infraspinatus* is visible on the medial side of the greater tubercle as a round and smooth area (Fig. 3.12.4). The tricipital line is prominent and sharp, in lateral view. On the distal epiphysis, the radial fossa is rather shallow, in cranial view. The supratrochlear foramen appears to be reduced and round in shape (Fig. 3.12.4D). The trochlea is slightly larger than the *capitulum humeri*. The medial epicondyle is enlarged compared to the lateral one. Radius. The radius diaphysis is flattened craniocaudally and gently arched with caudal concavity, as it is visible especially in lateral view (Fig. 3.12.4E-G). The proximal epiphysis is considerably more slender compared to the distal one. On the lateral side of the diaphysis, there is a crest-like enlargement probably related to the insertion of the *m. abductor digiti I longus*, particularly visible in caudal view. On the cranial side of the distal epiphysis, the groove of the *m. extensor digitalis communis* is modestly enlarged. Medially it is bounded by rather wide bone swelling, that bounds

medially the broad groove of the *m. extensor carpi radialis* (Fig. 3.12.4G). Almost on the lateral side of the cranial surface of the distal epiphysis, the groove of the *m. abductor digiti I longus* is considerably reduced and narrow. The ulnar notch is large, round and well-developed. Ulna. The shaft of the ulna has a trigonal section. The olecranon tuber is developed and prominent. The trochlear notch is more high than deep (Fig. 3.12.4H). The anconeal process does not overhangs the coronoid processes significantly. Femur. In general shape, the femur (Fig. 3.12.5) has a rather straight diaphysis, in cranial view. In medial and lateral views, the diaphysis is curved with a caudal concavity. The greater trochanter is reduced but pointy, and considerably shorter than the *caput* (Fig. 3.12.5A-C). On the caudal surface, two lines are visible. Of the two, the medial one is the more prominent and crest-like, marking the insertion of the *m. vastus medialis.* The lateral one is shallower (Fig. 3.12.5B). proximally, the medial line develops in a prominent crest that reaches the lesser trochanter. The median area bounded by these lines is rather wide, corresponding to the insertion of the *mm. adductores magnus et brevis*. of whereas from its lateral side it is low (Fig. 3.12.5B). Distally, the supracondylar tuberosities are evident, in caudal view. The lateral one is considerably larger than the medial one. In distolateral view, a shallow incision for the insertion of the *m. extensor digitorum longus* and caudally, a round and deep depression is visible, which is the attachment for the *m. popliteus*. There is not so much difference between the two distal condyles (Fig. 3.12.5D). Tibia. Tibias are poorly represented in the sample of Ingarano. The proximal epiphysis has triangular outline in proximal view (Fig. 3.12.5E). The tibial tuberosity is enlarged and not considerably projected cranially (Fig. 3.12.5E-F). On the contrary, the condyles made up the majority of the proximal surface. The intercondyloid eminence is fairly prominent. *Endocast*. Despite the external red-brownish calcareous incrustation that characterizes the fossil specimens, the digital endocast of DST-N1 revealed that the topology of the brain impressions in the inner walls of the braincase were

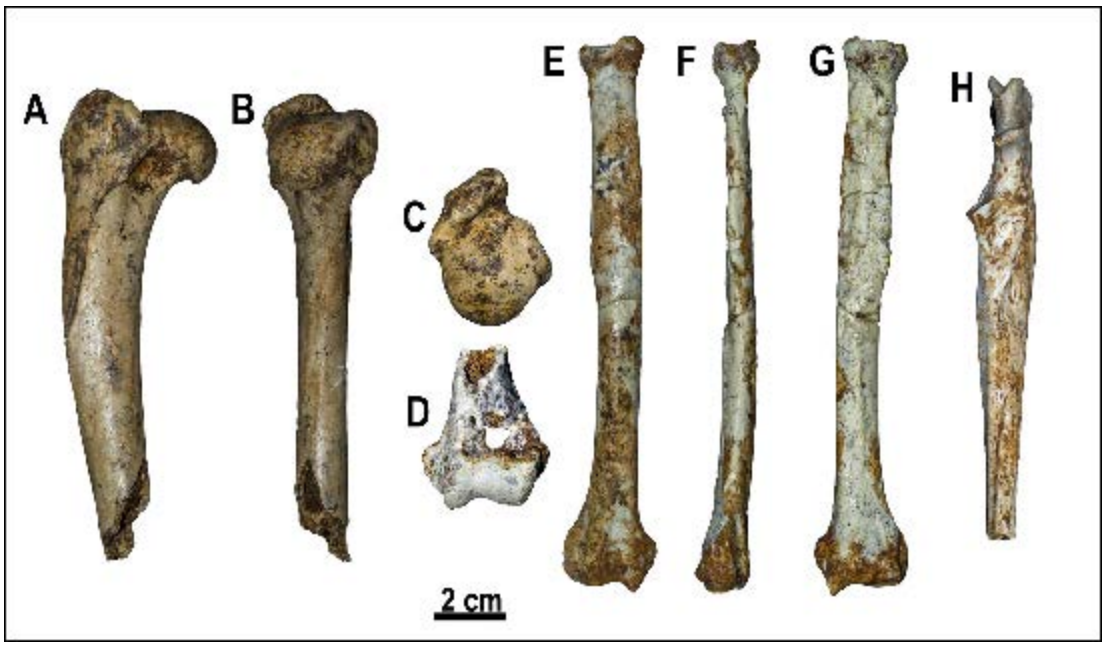

Figure 3.12.4 – *C. lupus* from Ingarano. **A-C**: **IN037**, fragment of left humerus, in lateral (**A**), palmar (**B**) and proximal (**C**) views. **D**: **INGND947**, distal fragment of a left humerus in cranial view. **E-G**: **INGND333**, right radius in cranial (**E**), lateral (**F**) and palmar (**G**) views. **H**: **IN 533,** left ulna, in cranial view.

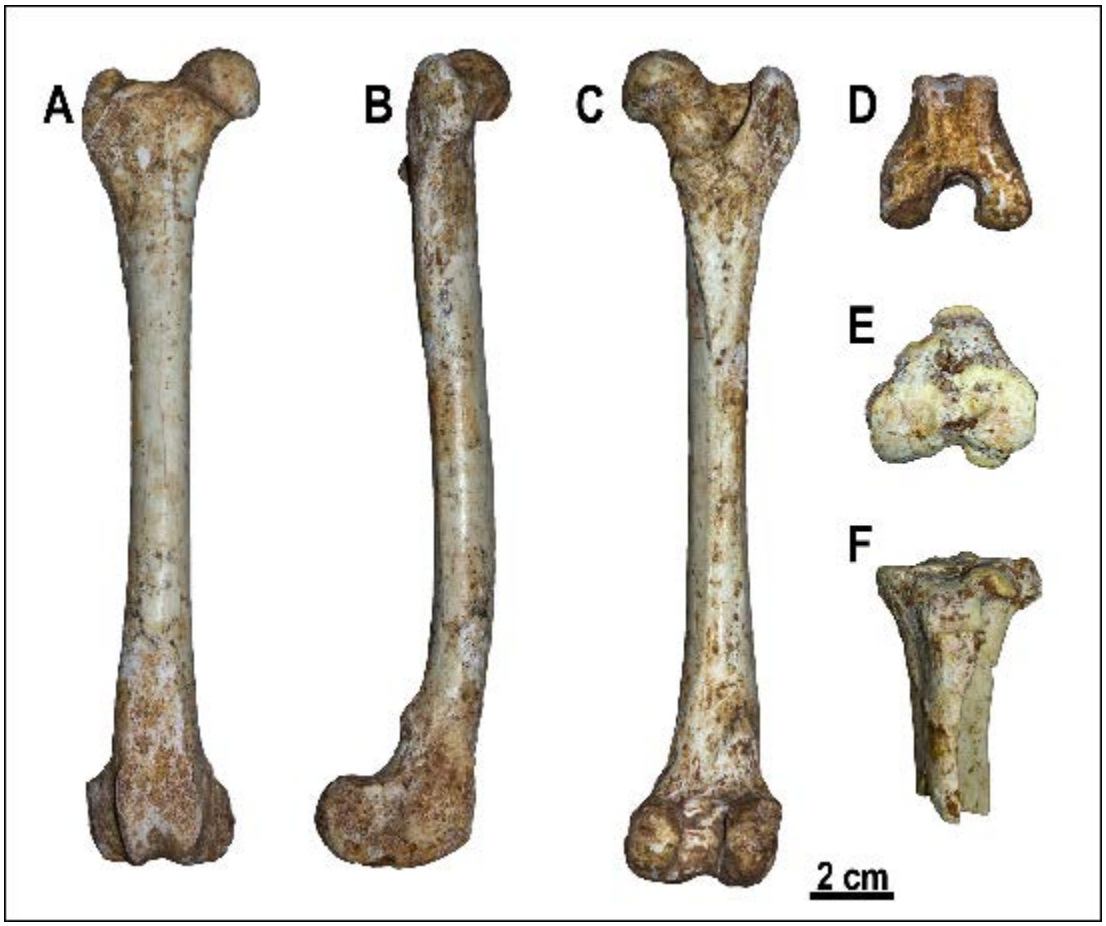

Figure 3.12.5 – *C. lupus* from Ingarano. **A-D**: **IN 545**, right femur in cranial (**A**), lateral (**B**), plantar (**C**) and distal (**D**) views. **E-F**, **ING 549**, fragment of left tibia in proximal (**E**) and cranial (**F**) views.

preserved with almost unaltered (Fig. 3.12.6). Indeed, the external surface of the endocast shows all the major *sulci* and *gyri* typical of the brain of modern wolves.

Comparisons. The cranium and cranial fragments possess all the features that characterize modern *C. lupus*, *e.g.*, the stout muzzle; rostrocaudally elongated cranium; the enlarged palate especially at level of the canines; the enlarged frontal sinus inflating the frontals and reaching the frontoparietal suture; marked sagittal crest, developed and high in the distal portion; external occipital protuberance (inion) considerably overhanging the condyles, etc. Unlike *Cuon*, relatively common element in middle-Late Pleistocene localities of Europe, both cranial and dental differences can be found in the sample of Ingarano ruling out the possible attribution of the material to this taxon. For instance, the elongation of the cranium; the development of the sagittal crest, the large and unreduced M2, the presence of the m3. Despite the specific attribution to modern wolf, some differences between fossil and extant samples can be found. Unlike the *C. lupus* from Avetrana, *C. lupus* from Ingarano possesses the distal accessory cuspule on the P2, like *C. l. italicus*. In contrast to the latter and also with *C. l. lunellensis* from Lunel-Viel 1 and Igue des Rameaux (Bonifay, 1971; Boudadi-Maligne, 2010), the P4 protocone advances slightly mesially compared to the mesial margin of the tooth. This morphology resembles both the *C. lupus* from Avetrana and that from Grotta Romanelli (see Sardella et al., 2014). The morphology of the buccal cusps is shared with that the other fossil and extant wolves, but the development of the buccal cingulum is more prominent in the sample of Ingarano than in extant *C. l. italicus* or fossil *C. l. lunellensis* and *C. l. maximus*. The marked mesiodistal narrowing possessed by *C. lupus* from Avetrana and other Apulian wolves like *C. lupus* of Grotta Romanelli, is reduced in C. lupus from Ingarano similar to the condition of the extant Italian wolves, *C. l. lunellensis* and *C. l. maximus*. Nevertheless IN 505 does possess a buccal portion of the trigon considerably larger compared to the lingual and talon ones.

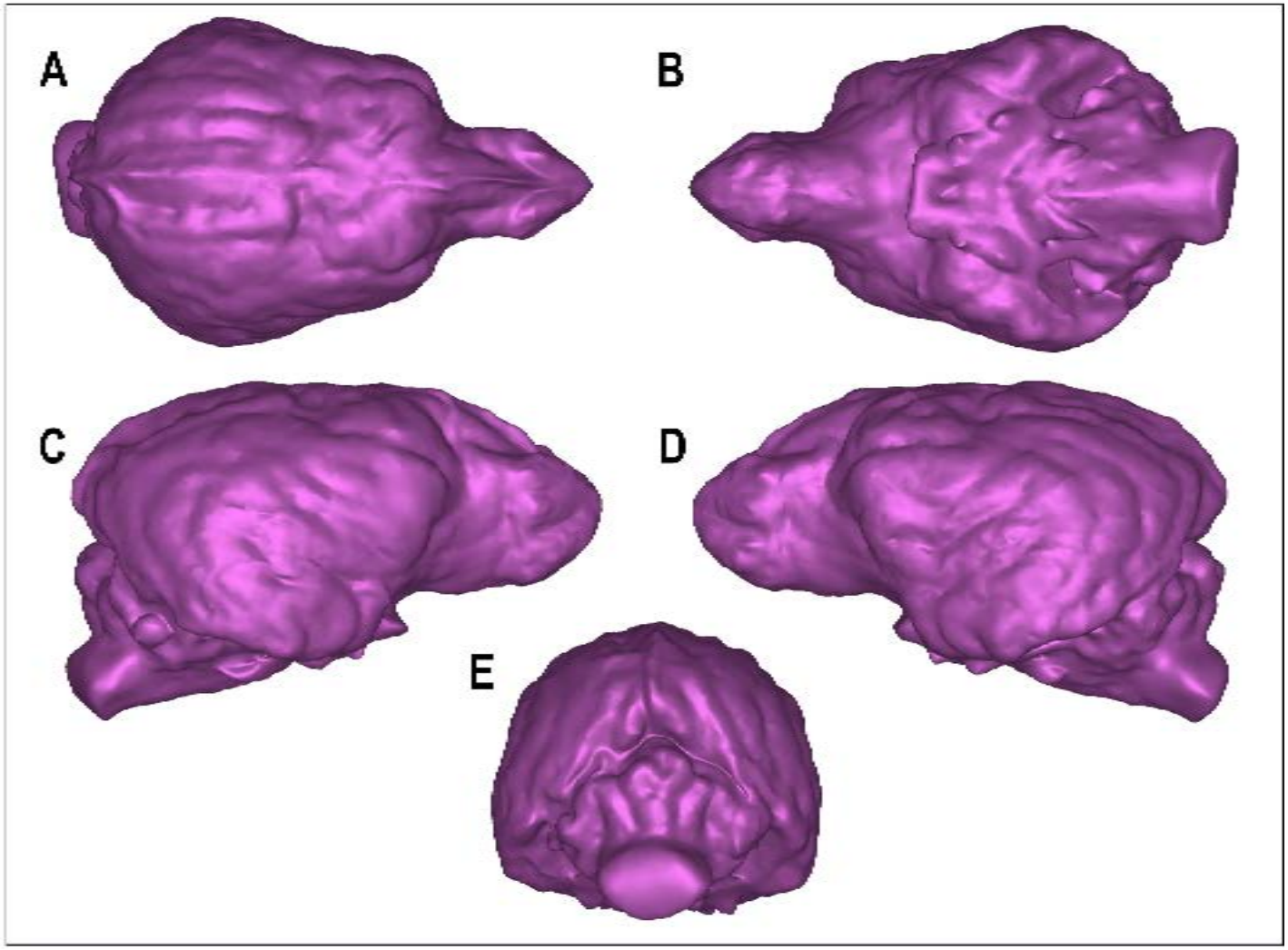

Figure 3.12.6 – *C. lupus* from Ingarano. **A-E**, digital endocast of the of the brain cavity of DST-N1 in dorsal (**A**), ventral (**B**), right lateral (**C**), left lateral (**D**) and occipital (**E**) views.

The variable occlusal morphology of the M2 resembles that of extant *C. l. italicus.* The features showed by the lower teeth do not differ with those of modern Italian wolves, without relevant peculiarities. In the lower carnassial, the metaconid is greatly reduced as *C. l. italicus* and in other fossil samples (*e.g.*, Avetrana, Lunel-Viel 1, Igue de Rameaux, Equi Cave, Canale Mussolini), whereas other do not show this reduction (*e.g.*, *C. l. maximus*). The reduction of the m1 entoconid in the sample from Ingarano contrasts with the developed one in *C. l. lunellensis* and *C. l. maximus*, in which it is generally less reduced compared to extant *C. lupus*.

Fig. 3.12.7 shows the variation of the proportion of the cranial measures in different populations of fossil wolves and the average *C. mosbachensis*, as compared to the *C. l. italicus*, used as a standard reference. *C. mosbachensis* possesses the smallest of the patterns considered. The cranial similarities between *C. lupus* from Grotta Romanelli and *C. mosbachensis* (as discussed by some authors: Bologna et al., 1994; Caloi & Palombo, 1998; Boscato, 2001; Sardella et al., 2006; 2014) do not seem to be supported by the pattern displayed in Fig. 3.12.7. This apparently confirms the attribution of Sardella et al. (2014) of the wolf of Grotta Romanelli. The similarity of the proportions of the cranial fragments from Ingarano to those of the *C. lupus* from Grotta Romanelli is evident. On the contrary, neither *C. l. lunellensis* nor the specimens from north Italian site like Broion, Grotta Ladrenizza or Pocala resemble the patter shown by *C. lupus* from Ingarano.

In size, the canid from Ingarano is smaller than the extant *C. l. italicus* (Fig. 3.12.8), in both upper and lower teeth proportions, with the exception of the M2 L. If it is compared to the middle-Late Pleistocene French subspecies of *C. lupus* (*i.e.*, *C. l. lunellensis*, *C. l. santenaisiensis* and *C. l. maximus*), *C. lupus* from Ingarano is smaller even compared to the small-sized *C. l. lunellensis*. *C. l. santenaisiensis* and *C. l. maximus* are instead considerably larger than the considered sample. The difference in size is reflected by the distinct pattern of dental proportions displayed by French taxa in comparison to *C. lupus* of Ingarano. As noted in the section

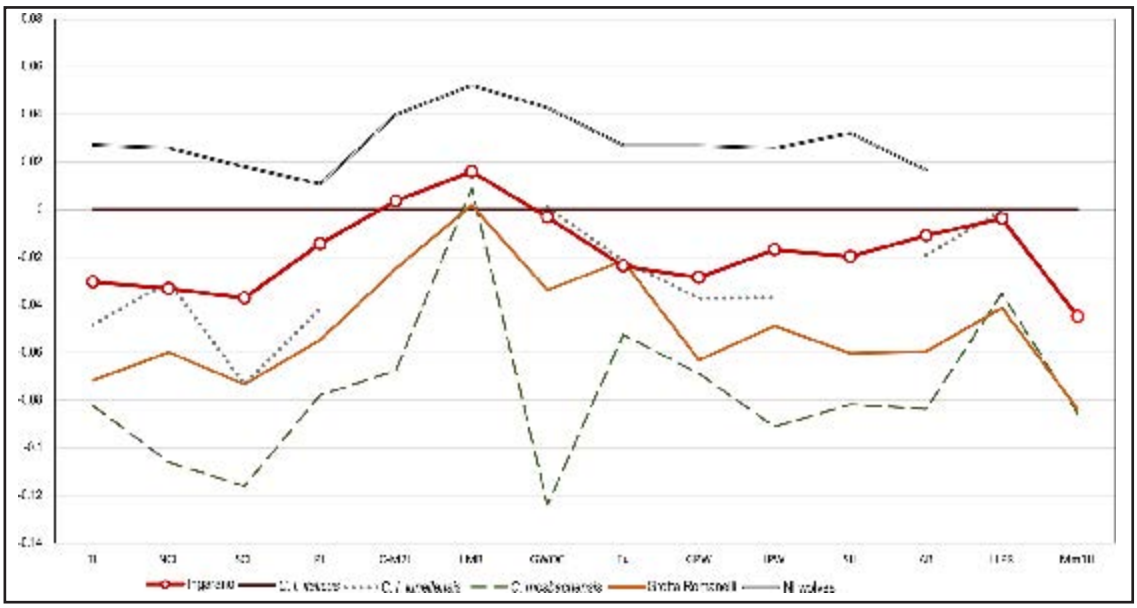

Figure 3.12.7 – Log-ratio diagram on selected cranial and dentognathic proportions. *C. l. italicus* is used as a standard reference in the comparison of *C. lupus* from Ingarano with middle-Late Pleistocene populations of wolves (*i.e.*, *C. l. lunellensis* from Lunel Viel 1, Igue de Rameaux; *C. mosbachensis* from European localities; *C. lupus* from Grotta Romanelli; and northern Italian wolves, see section 3.11. for the description of these wolves).

3.11., the proportions of *C. l. lunellensis*, *C. l. santenaisiensis* and *C. l. maximus* show a remarkable degree of similarity one another. If compared to Italian samples, several interesting aspects arise. "northern Italian wolves" group follows the discussion of section 3.11. Firstly, it is evident that none of pattern of proportions of the Italian samples resembles those of the French wolves, besides the evident difference in size. When *Canis lupus* from Ingarano is compared to the Italian taxa, it evidently shows affinity in proportions with earlier Apulian records, *i.e.*, Melpignano and especially Grotta Romanelli. On the contrary younger site like Avetrana and Cardamone are generally larger in size, particularly in lower teeth. Moreover, their patterns are more similar to that of northern Italian sites (*e.g.*, Broion, Pocala). The record of Ingarano, together with that of Melpignano and Grotta Romanelli are most variable compared to the average *C. l. italicus*. Opposite is the case of the "northern Italian wolves". Such affinity in teeth proportions between earlier Apulian record of wolves might testify to similar dietary adaptations.

The postcranial elements are considerably similar to modern *C. l. italicus*. In size,

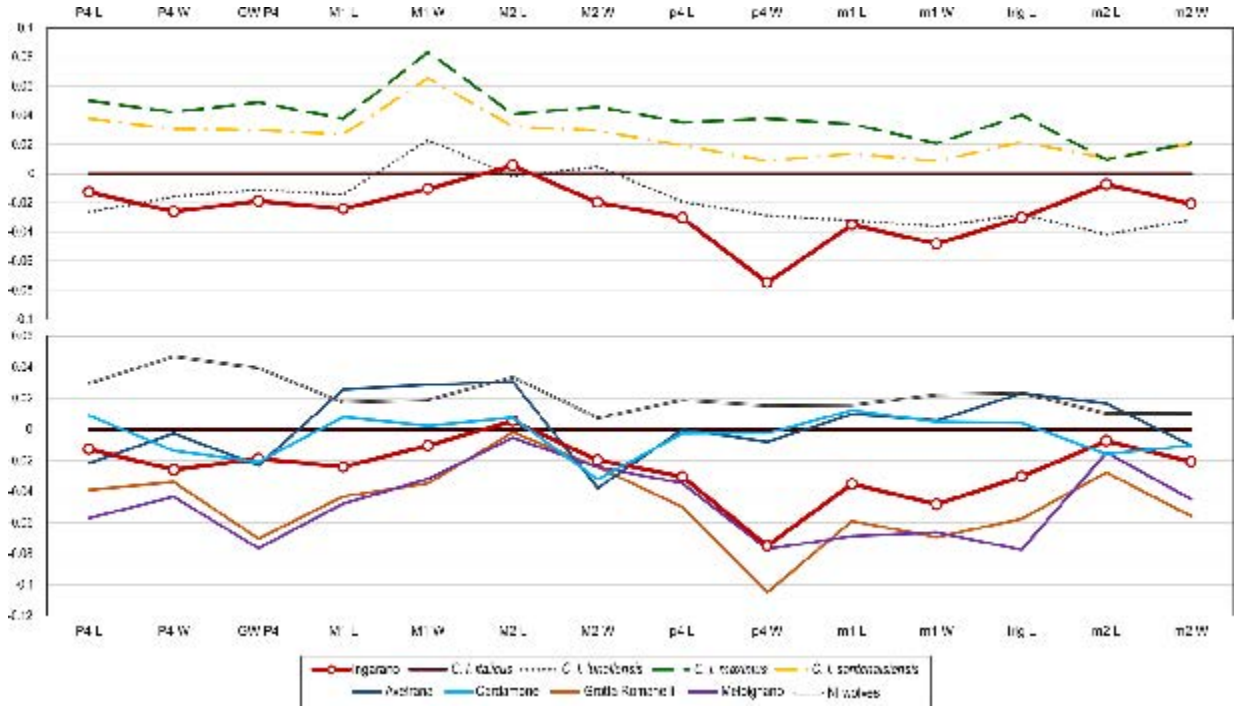

Figure 3.12.8 – Log-ratio diagram on selected upper and lower teeth proportions. *C. l. italicus* is used as a standard reference in the comparison of *C. lupus* from Ingarano with middle-Late Pleistocene populations of wolves (*i.e.*, *C. l. lunellensis* from Lunel Viel 1, Igue de Rameaux; *C. l. maximus* from from Grotte de Jaurence, Grotte de Maldidier, Igue du Gral; *C. l. santenaisiensis* from Aven de l'Arquet; *C. mosbachensis* from European localities; the sample of *C. lupus* from several Apulian localities, Grotta Romanelli, Melpignano, Avetrana, Cardamone; and northern Italian wolves).

the humerus of *C. lupus* from Ingarano is close to that of *C. l. italicus*, of *C. lupus* from Melpignano, and *C. l. lunellensis* (Boudadi-Maligne, 2010), whereas it is slightly smaller compared to the wolf from Avetrana. On the proximal epiphysis, the greater and the lesser tubercles are more developed in caudal view compared to the average *C. l. italicus*, in which these features are less prominently high, the former, or projected medially, the latter. Nevertheless, in proximal view, the lesser tubercle is more robust in *C. l. italicus* compared to the more slender one of *C. lupus* from Ingarano. No different features can be seen on the diaphysis. In contrast to *C. l. italicus* and *C. lupus* from Avetrana, radial fossa is shallower and the supratrochlear foramen is round and narrow, in the cranial view (Fig. 3.12.5). As in *C. lupus* from Avetrana, the distal epiphysis shows the trochlea that is only slightly larger

than the *capitulum humeri*. This contrasts with the morphology possessed by *C. l. italicus* and *C. l. lunellensis* from Lunel-Viel 1, in which the trochlea has a greater extension in proximodistal sense (see Boudadi-Maligne, 2010). This development of the trochlea is shared also by *C. mosbachensis* from Vértesszõlõs II. Nevertheless, the narrowing dividing the trochlea from the *capitulum* is wider and more shallow in *C. l. italicus*, *C. lupus* from Avetrana and Ingarano, compared to the marked and deep incision of *C. l. lunellensis* and *C. mosbachensis*. Similarly to the *C. lupus* from Avetrana, the cranial outline of the articular surface of the distal epiphysis of the humerus of the sample from Ingarano is almost rectangular, unlike the common parallelogram one of the extant *C. lupus*.

The radius INGND333 is complete, allowing direct comparison with extant samples. Its features fit in the variability of those of *C. l. italicus*. The ulnar notch of INGND333 is large and round, whereas generally is oval in lateral view, but shape tend to be variable in modern wolves. Compared to modern *C. l. italicus* considered as standard comparison, the coronoid processes of the ulna IN 533 seems less prominent in *C. lupus* from Ingarano. The incision of the two small processes on the cranial end of the olecranon is narrower in *C. lupus* from Ingarano compared to that of *C. l. italicus*. The other features of IN 533 do not differ from those of modern wolves. The same can be said of the femur (Fig. 3.12.6). beside the morphological affinity, the fossil specimens from Ingarano are considerably more slender and more gracile compared to the diaphysis of *C. l. italicus* but also to other fossil forms (*i.e.*, *C. l. santenaisiensis* or that of Avetrana). Unlike the wolf from Avetrana, the neck of the femur is not elongated and the greater trochanter is short, similarly to the morphology of *C. l. italicus*. In plantar view, the trochanteric fossa is deep and wide unlike the shallow and distally elongated one of *C. lupus* from Avetrana. On the diaphysis and the distal epiphysis no peculiar features are visible.

Following the comparison of section 3.11, the proportions of the femur of *C. lupus*

from Ingarano were compared to that of the other middle and Late Pleistocene wolves considered in Figs. 3.12.7- 3.12.8 (Fig. 3.12.9). In contrast with the cranial and dental log-ratios, the femur of *C. lupus* from Ingarano is more similar to that of the slender French form *C. l. lunellensis* and *C. l. italicus*, despite the considerable difference in size with the latter. Indeed, the early Apulian sample from Melpignano is closer to the sample from Avetrana rather than to *C. lupus* from Ingarano. *C. l. santenaisiensis* and *C. l. maximus* confirm as the largest taxa of all the samples.

On its inner walls, the brain cavity of DST-N1 preserves the impressions of the encephalon in very good conditions, as it is visible in Figs. 3.12.10-3.12.11. The general outline of the *sulci* and *gyri* closely resemble those of *C. l. italicus*, especially in lateral view. For instance, unlike *C. anthus*, the shape of the sigmoid *gyrus* (*i.e.*, ansate and coronal *sulci*) in dorsal views is orthogonal (*sensu* Lyras et al., 2003), like *C. l. italicus*, *C. simensis* and *C. aureus*. In *C. anthus* is heart-shaped, in dorsal view. *C. lupus* from Ingarano shares with *C. l. italicus* the elongated prorean *gyrus* are compared to the shortened one evident in the other species, especially in *C. simensis* and *C. anthus*. Nevertheless, few differences can be pointed out, especially in the general shape of the endocast. The brain of *C. l. italicus* is enlarged caudally, resulting in a pear-shaped dorsal morphology. In *C. lupus* from Ingarano, the brain is generally inflated. Indeed, this taxon does not possess an evident notch at level of the caudal side of the postcruciate *gyrus*, as visible in *C. l. italicus*.

3.12.4. Discussion and Conclusions

The minimum number of individuals (MNI) of the *C. lupus* Ingarano population, estimated from the most abundant element (the lower carnassial), is 7. The dentognathic diagnostic features of *C. lupus* are easily recognizable in the Ingarano sample, and intrasample variability is really limited (*e.g.*, prominence or slight reduction of some cuspules/cuspulids). The pattern of proportions of the population of *C. lupus* from the Ingarano is distinctively smaller than *C. l.*

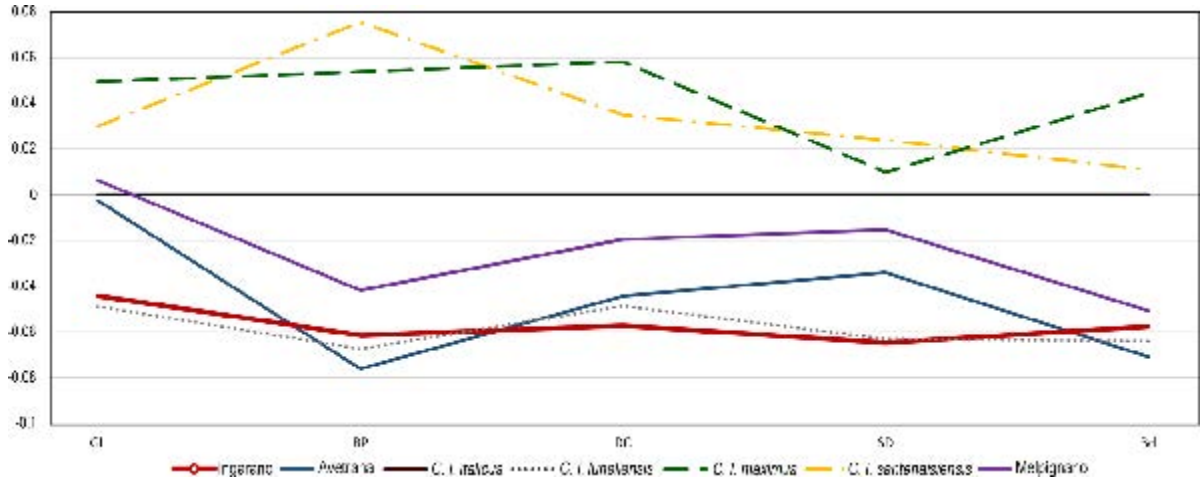

Figure 3.12.9 – Log-ratio diagram based on selected femur measurements. *C. l. italicus* is used as a standard reference in the comparison of *C. lupus* from Ingarano with middle-Late Pleistocene populations of wolves (*i.e.*, *C. l. lunellensis* from Lunel Viel 1, Igue de Rameaux; *C. l. maximus* from from Grotte de Jaurence, Grotte de Maldidier, Igue du Gral; *C. l. santenaisiensis* from Aven de l'Arquet; *C. mosbachensis* from European localities; the sample of *C. lupus* from Melpignano and Avetrana).

italicus but also if compared to the larger French forms *C. l. maximus* and even *C. l. santenaisiensis*. Compared to the Italian fossil samples, it differs from the northern Italian wolves, Avetrana and Cardamone samples for the size but also not showing their peculiar morphologies and dental. The closest in pattern of proportions are the samples recovered in Melpignano and Grotta Romanelli. Sardella et al. (2014) referred these southern sites to the late middle Pleistocene and to the MIS 4-3, and Gatta et al. (2016) related to the northern ones to the MIS 3, whereas Avetrana is probably slightly younger (*i.e.*, MIS 3-2, see section 3.11.). Cardamone is probably referable to the Last Glacial Maximum, MIS 2, 22-18 ka (Rustioni et al., 2003). The postcranial material of *C. lupus* from Ingarano is in general smaller compared to the average *C. l. italicus* and even other fossil taxa, with the exception of *C. l. lunellensis*. Even in comparison with the southern Italian samples like Melpignano, postcranial elements appear smaller (Fig. 3.12.9). Modern wolves show a great disparity in size as noted by several authors (*inter alios* Klein, 1986; Dayan et al., 1991; Meiri et al., 2004).

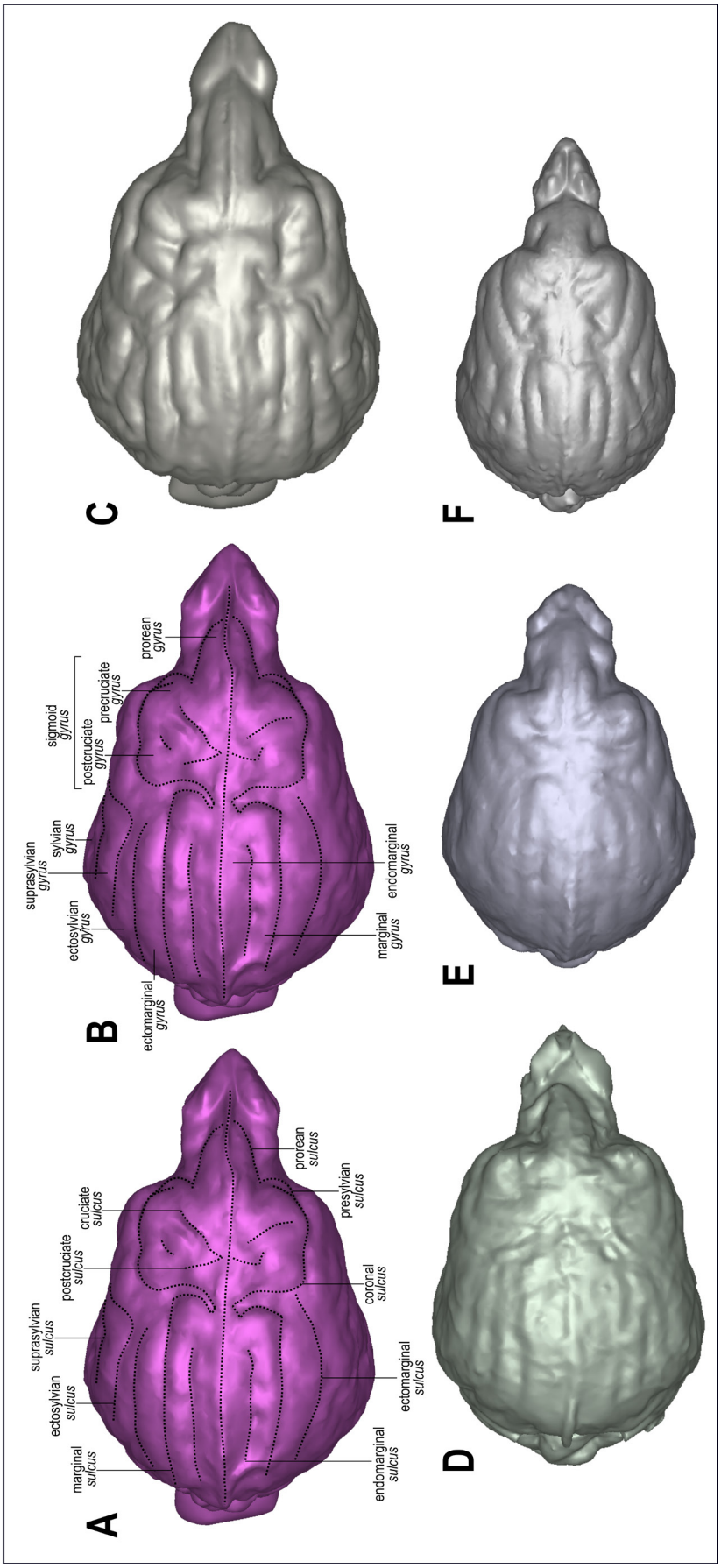

Figure 3.12.10 – Comparison between the digital endocast of *C. lupus* from Ingarano (**A-B**) and other *Canis* species: *C. l. italicus* from Tuscany (**C**); *C. simensis* from Ethiopia (**D**), *C. aureus* from Croatia (**E**), *C. anthus* from Somalia (**F**). All the endocast are shown in dorsal view. The principal terminology associated with the pattern of *sulci* and *gyri* in shown in A-B (following Lyras et al. 2003 and Evans & Lahunta, 2013).

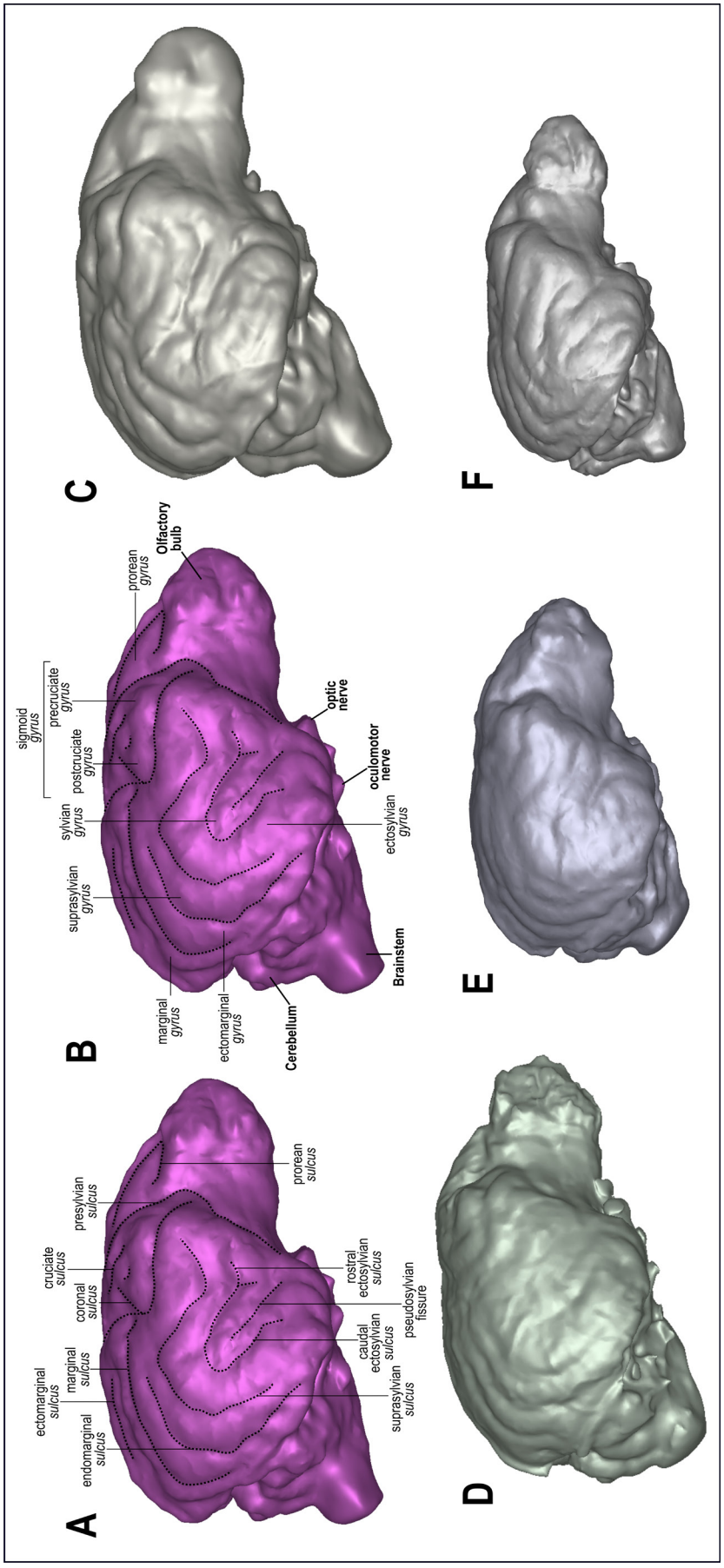

Figure 3.12.11 – Comparison between the digital endocast of *C. lupus* from Ingarano (**A-B**) and other *Canis* species: *C. l. italicus* from Tuscany (**C**); *C. simensis* from Ethiopia (**D**), *C. aureus* from Croatia (**E**), *C. anthus* from Somalia (**F**). All the endocast are shown in lateral view. The principal terminology associated with the pattern of *sulci* and *gyri* in shown in A-B (following Lyras et al. 2003 and Evans & Lahunta, 2013).

In section 3.11. was shown the coexistence of two distinct groups of wolves during the majority of the Late Pleistocene (at least until the end of the MIS 3). The size variability of *C. lupus* across the Italian Peninsula was indeed characterized by the small-sized Apulian wolves and the larger-sized northern Italian wolves. The latter group has dental proportions similar to those of the extant *C. l. italicus*. Both groups possess different patterns compared to other European fossil samples (*e.g.*, *C. l. maximus*). Despite the similarity of the postcranial material with *C. l. lunellensis*, teeth proportions and morphologies do not support the affinity, although suggested by some authors (*e.g.*, Petronio & Sardella, 1998). The morphology and the size of the sample from Ingarano appear more similar to those of the other MIS 4-3 Apulian sites like Grotta Romanelli and Melpignano. This preliminary result confirms the observations made by Sardella et al. (2014) that included the sample of Ingarano in the group of Apulian wolves. Of these records, Ingarano apparently represents one of the most recent (see Table 2 in Sardella et al., 2014). The subsequent southward dispersal of the glacial wolves first recorded in the site of Avetrana 8 (end of MIS 3) leave the *C. lupus* of Ingarano the latest occurrence of these gracile, smaller forms of wolves recorded in several sites of Apulia, but possibly spread in southern Italy.

3.12.5. Appendix

Table of measurements of the unpublished material of Ingarano (other dentognathic measurements were included in Bertè, 2013).

Table 3.12.1 – Cranial measurements (mm) of *C. lupus* from Ingarano.

Cat. N°	Element	TL	NCL	FL	SCL	GNL	Eu	Ect	PoCW	IoD	GHOr	SH	AB	GWOC	BL	PL	CBL	Zyg	ECW	GPW	MOH	M2B	LCM
DST-N1	skull	226	100.4	123.5	108.7	78.6	60.7	55.5	39.5	41.6	30.9	63.9	53.7	41.2	88.3	109.2	198.2	125.2	46.9	70.4	36.8	55.6	165

Table 3.12.2 – Measurements (mm) of associated upper teeth of *C. lupus* from Ingarano.

Cat. N°	Element	I3 L	I3 W	C L	C W	P3 L	P3 W	P4 L	P4 Lmax	P4 W	M1 L	M1 W	M2 L	M2 W	C-M2 L	M1-M2L
DST-N1	skull	8.3	7.2	11.8	8.9	15.2	6.2	23.6	25.4	11.9	14.3	18.3	7.8	10.7	93.1	22.7

Table 3.12.3 – Measurements (mm) of the mandible of *C. lupus* from Ingarano.

Cat. N°	Element	Mp1H	Mp4H	Mm1H	Mm1B	HPrac	HR	c-m2 L	c-m3 L	LLPR	LLMR
DST-N1	skull	22.7	25.3	26.4	12.3	29.1	59.8	98.6	103.3	47.1	40.6

Table 3.12.4 – Measurements (mm) of lower teeth of *C. lupus* from Ingarano.

Cat. N°	Element	c L	c W	p1 L	p1 W	p2 L	p2 W	p3 L	p3 W	p4 L	p4 W	m1 L	m1 W	trm1 L	tdm1 W	m2 L	m2 W	m3 L	m3 W
DST-N1	skull	12.9	8.7	5.6	4.2	12.4	5.5	14.3	5.6	15.2	6.7	27.6	10.5	18.5	10	9.8	7.7	5.3	4.5

3.13. Paleontology and Augmented Reality: implications and opportunities for old bones. The case of the wolf from Dmanisi

3.13.1. Context

In the complex scenario of Pliocene-Pleistocene age, recent research on canids has revealed an increasingly higher number of species than previously thought. The genus *Canis* since its early appearance in North American Late Miocene and its dispersal and radiation throughout Asia, is known to have reached the western part of Europe around 3 Ma (Lacombat et al., 2008), where the first species described is *Canis etruscus* from several sites of Europe (Cherin et al., 2014). There is wide consensus considering the modern wolf as the final stage of an evolutionary line starting with the Early Pleistocene *C. etruscus* through the Early-middle Pleistocene *Canis mosbachensis* Soergel, 1925 (see inter alios Brugal & Boudadi-Maligne, 2011). Morphologically modern wolves appear in the early Middle Pleistocene of North America (Tedford et al., 2009) and in several mid Middle Pleistocene Asian and European localities (Bonifay, 1971). In the framework of the Early and middle Pleistocene radiation of Eurasia mammals, the site of Dmanisi is celebrated for its outstanding record of early *Homo* Linnaeus, 1758 (Lordkipanidze et al., 2007; 2013; Krijgsman et al., 2019; Rightmire et al., 2019), for the state of preservations of the fossils (allowing molecular analyses on its fossils, Cappellini et al., 2019), and for the pivotal documentation of the biogeographic faunal dispersions between the three continent, Asia, Africa and Europe. Indeed, the Georgian site offers a unique glimpse on the turnovers that took place around 1.8 Ma (during the late Villafranchian Land Mammal Age) (Ferring et al., 2011; Krijgsman et al., 2019). Among the large number of mammalian taxa recovered, carnivorans are abundant: at least 13 species of five of the most common families of carnivorans are represented. Of these, *Canis* (referred to *C. etruscus* by Vekua, 1995) is by far the most represented taxon within Carnivora with ten complete crania and more than 250 cranial specimens. This rich and remarkably well-preserved sample allowed

us to assess its variability, compared to that of other Early and middle Pleistocene canids. The evidence presented here suggest an early origin of modern wolves and related species, re-describing the *Canis* from Dmanisi as a new species.

3.13.2. Methods

The 3D scan of the fossil and extant specimens was obtained with the Artec Spider laser scan at the Georgian National Museum and at in Paleo[Fab]Lab, Erath Science Dept. of the University of Florence, and through subsequent elaboration in Artec Studio 12 Professional. The 3D visualization of the cranium D64, upper and lower teeth comparison models in Augmented Reality was created following the protocols described by several authors (*e.g.*, Etienne, 2017; Carpignoli, 2019) in Visual Studio Code ver. 1.41, using AR.js and A-Frame v. 0.9.2 (www.aframe.io).

3.13.3. Systematic Paleontology

Order **Carnivora** Bowdich, 1821

Family **Canidae** Fischer, 1817

Subfamily **Caninae** Fischer, 1817

Tribe **Canini** Fischer, 1817

Genus ***Canis*** Linnaeus, 1758

***Canis* sp. nov.**

Figs. 3.13.1-3.13.4

Etymology. From the Georgian "ბორჯღალი", IPA: [bɔrʤʁali], seven-rayed symbol of the sun and eternity typical of Georgia.

Holotype. D64, almost complete skull with I1-M2 and i1-m3.

Hypodigm. Cranium and cranial fragments. 01/D01, rostral fragment with I1-I3 and

P3-M1; 02/D01, cranial fragment with I1-M2; 02/D04, maxillary fragment with M1; 02/D05, maxillary fragment with M1 and M2; 03/D25, maxillary fragment with M1-M2; D64, cranium I1-M2 and mandible I1-m3; D95&96, maxillary fragment with P4-M2; D301, cranium with I1-M2; D627, maxillary fragment with P4-M2; D760, cranial fragment; D1126, maxillary fragment with P1 and P3-M2; D1269, maxillary fragment with P3-M2; D1275, rostral fragment with I1-M2; D1275, rostral fragment with I1-M2; D1368, rostral fragment with I1-M2; D1544, cranial fragment with occipital condyles; D1702, maxillary fragment with P3-P4; D2113, maxillary fragment with P4 and M2; D2285, cranial fragment with occipitals; D2314, cranium with I1-M2; D2353, cranium with I1-M2; D2463, cranial fragment; D2588, rostral fragment with I1-M2; D2771, premaxillary fragment with I2-C1; D3222, maxillary fragment with P4-M2; D3374, cranial fragment; D3419, cranial fragment; D3420, cranium with I2 and P4-M2; D3572, cranial fragment; D3664, premaxillary fragment with I2-I3; D3712, cranial fragment; D3712, maxillary fragment with P4-M2; D3837, cranium with I2-M2; D4026, rostral fragment with I1-M2; D4116, cranium with I2-M2; D4186, cranial fragment; D4270, maxillary fragment with P4-M2; D4283, cranial fragment; D4367, premaxillary fragment with I2-I3; D4376, rostral fragment with I3-M2; D4454, premaxillary fragment with I2-I3; D4510, cranium with P2-M2; D4730, cranium with P4 and M2; D4956, rostral fragment with P2-P3; D5062, cranium with P4 and M2; D5078, cranium with P4-M2; D5188, rostral fragment with P3-M2; D5219, cranial fragment; D5246, cranial fragment; D5358, maxillary fragment with P4-M2; D5449, edentulous cranial fragment; D5553, cranium with left C1-M2 and right I2-P1; D5656, cranium with left P4-M2 and right P4-M2; Dm.6/154.1B1.7, right maxillary fragment with P4; Dm.64/62.B1x.260, cranial fragment; Dm.65/60.IV.33, maxillary fragment with M1-M2; Dm.69/62.3B1.66, cranium with left P3-P4 and right P3-M2; P089_1, occipital fragment; P101_1, fragment of frontal bones; P101_2, right maxillary fragment with C1-P2; P102, right maxillary fragment with M1-M2.

Upper dentition. D3386, left I1; D3518, left I1; D3944, right I1; Dm.66/63.B1y.45, right I1; D3334, left I2; D3335, left I2; 03/D26, left I3;D1720, left I3; D2506, left I3; D2784, left I3;D2838, right I3; D3327, right I3;D4361, left I3; D4362, left I3; 03/D02, right I3; 03/D21, left I3; Dm.61/62.B1z.40, left I3; Dm.63/61.B1x.222, left I3; D1574, right C1; D1575, right C1; D2703, right C1; D2780, right C1; D2916, left C1; D3620, right C1;

D3638, right C1; D379, right C1; D4251, right C1; D4360, right C1; D4563, right C1; D5262, right C1; D5896, left C1; P064, left C1; D2397, left P1; 03/D05, right P1; 03/D20, right P1; Dm.63/61.B1y.322, right P1; Dm.64/62.B1y.146, left P1; D5345, right P2; 03/D08, right P2; 03/D23, right P2; D1272, left P3; D2702, left P3; D2755, right P3; D3645, left P3; D4286, right P3; D4364, right P3; 03/D17, right P3; Dm.65/62.B1y.59, right P3; Dm.M6/1.II.247, right P3; D607, left P4; D1270, right P4; D1271, left P4; D3869, left P4; D4411, left P4; 03/D01, right P4; D2936, P4 and M1; D2410, right M1; D2753, left M1; 03/D14, left M1; D3519, left M1; Dm.62/62.B1z.159, right M1; Dm.69/58.B3.40, right M1; Dm.63/62.B1k.44, right M2; Dm.66/62.B1y.153, right M2.

Mandible. 05/D04, left hemimandible p2 and m1; D1, left hemimandible with i3-m2; D24, left hemimandible with c1-m2; D169, right hemimandible with p4-m3; D646, left hemimandible with c1 and p1-m3; D799, left hemimandible with m1-m3; D800, left hemimandible with p2-p3; D1079, right hemimandible dp4; D1184, right hemimandible with p1-m2; D1292, right hemimandible with p1-p4; D2023, left hemimandible with m2 and right hemimandible with p4-m2; D2460, right hemimandible with p2-m1; D2503, right hemimandible with p1- m3; D2596, right hemimandible with c1-p3; D2688, right hemimandible with c1 and p3-m2; D2882, right hemimandible with p2 and p4-m2; D2883, right hemimandible with p4-m1; D2912, right hemimandible with m2; D2913, left hemimandible with c1-p2 and p4-m2; D2914, left hemimandible; D3022, left hemimandible with m1; D3528, right hemimandible with m1-m2; D3857, left hemimandible with c1-m1; D3882, left hemimandible with p1-m1; D3906, right hemimandible with c1, p2, p4 and m1; D4279, left hemimandible; D4582, left hemimandible with p2-p3; D4871, right hemimandible with c1-m2; D4892, right hemimandible with p3-m1; D5356, right hemimandible;D5359, right hemimandible with p1-m2; D5594, right hemimandible with p1-m2; D5817, left hemimandible with p2-m1; D5554, left hemimandible with i1-p2 and m2; D5817 left hemimandible with p2-m2; Dm.27/130.1B1.1.67, right hemimandible with i2-m3; Dm.64/62.B2ak.100a, left hemimandible with m2; Dm.64/63.3B1x.256, left hemimandible with p3-m2; Dm.M6/6.II.122, right hemimandible with p3-m1.

Lower dentition. 04/D09, right i1; 04/D11, right i1; D2552, left i1; 04/D13, right i1; 04/D15, left i1; D1649, right i2; D2759, left i2; D3340, right i2; D3342, right i2; D3372, right i2; D4951, right i2; D5339, right i2; 04/D10, right i2; 04/D16, right i2; 04/D17, right i2;

04/D18, right i2; 04/D33, right i2; Dm.64/60.Va.74, right i2; P103, right i3; D648, left c1; D2612, right c1; D2837, right c1; D3271, right c1; D3491, right c1; D4412, left c1; D5261, right c1; D5361, left c1; D5561, right c1; 04/D04, left c1; 04/D05, right c1; 04/D08, right c1; Dm. 62/63.B1Z.168, right c1; Dm.63/60.2B1y._3, right c1; Dm.64/62.B2ak.9, right c1; Dm.64/64.3B1x.50, left c1; Dm.6/153.1A4.2, right c1; P104, right c1; D2763, left p1; D3339, left p1; D5342, right p1; 04/D19, right p1; 04/D20, right p1; 04/D21, left p1; 04/D23, right p1; Dm.61/62.B1z.119, left p1 and m2; D2781, right p2; 04/D32, left p2; Dm.68/61.VI.72, left p3; D3342, p3; D3372, p3; D3386, p3; D3476, p3; D3491, p3; D3493, p3; D3518, p3; D3620, p3; D3638, p3; D3329, left p3; D4347, left p3; D5736, right p3; 04/D29, left p3; 04/D31, left p3; Dm.5/153.2A4.4, right p3; Dm.63/61.1B1y.414, right p3; Dm.68/61.VI.72, left p3; Dm.M6/7.IIa.50, right p3; D3328, right p4; D4494, right p4; D595, left m1; D1418, left m1; D1961, left m1; D2504, left m1; D3476, left m1; D4497, right m1; 04/D26, left m1; 04/D27, left m1; 04/D28, right m1; D3493, left m2; Dm.M11F10/11.Bc.55, left m2; D275, left m3; D362, right m3.

Type Locality and Age: Dmanisi, Georgia; ca 1.80 Ma.

Differential Diagnosis. A medium sized canid, close or slightly smaller compared to *C. etruscus*, generally larger than other Villafranchian medium-sized canids. *Canis* sp. from Dmanisi differs from *C. arnensis* for the longer nasal bones, the well-developed frontal sinuses, the morphology of the upper molars and the hypoconid on m1 larger than entoconid in the m1. It differs from *C. etruscus* for its overall cranial architecture, including the relatively higher cranium, the profile in lateral view and shorter nasal bone and their morphology. It also differs in dental features, including the presence of accessory cuspulids on the lingual margin of m1 talonid. It is distinguished from *C. arnensis* and *C. etruscus* by the caudorostrally divergent medial walls of the tympanic bullae and few other dental features, including the deeper trigon basin compared to the talon basin on M1, the p3 that sets below the alveolar plane of p2 and p4. *Canis* sp. from Dmanisi differs from *C. mosbachensis*

for some primitive-like features, comprising the morphology of the second upper molar, the more arched lower toothrow and larger metaconid on m1. It possesses a marked apomorphy, *i.e.* the medial walls of tympanic bullae that diverge rostral direction.

Description and comparison. The cranium is moderately elongated (Figs. 3.13.1-3.13.2). Nasals are long, although not as long as in *C. etruscus* from Olivola and Pantalla. In lateral view, the profile of the cranium of *Canis* from Dmanisi is moderately arched, contrasting condition compared to the straight profile of *C. etruscus* from Olivola and Pantalla, but still less arched than in *C. mosbachensis* and *C. lupus*. The postorbital constriction is not marked for the considerable development of the frontal sinuses, which extend caudally towards the frontoparietal suture like in *C. chihliensis* from Yushe Basin, *C. etruscus* from Italy, *C. mosbachensis* from Eurasia and *C. lupus*, although reduced compared to the latter. The postorbital region is shorter compared to the elongated one of *C. lupus*, resembling other fossil species (*e.g.*, *C. mosbachensis* from Cueva Victoria, Untermassfeld, and Zhoukoudian). The supraoccipital shield has the typical *Canis* triangular shape, although less sharp compared to that of *C. mosbachensis* from Eurasia (*e.g.*, Cueva Victoria, Untermassfeld, and Zhoukoudian loc. 13) and extant *C. lupus*. In ventral view, the tympanic bullae are oval-shaped and moderately inflated. Their medial walls are not parallel, but tend to diverge in caudorostral direction, unlike *C. arnensis*, *C. etruscus*, and *C. chihliensis* from Yushe Basin (Fig. 3.13.3). There are no diastemata between the upper teeth. The protocone of the upper carnassial is poorly individualized and relatively reduced, condition similar to that found in *C. lupus*, whereas in *C. etruscus* from Italy the protocone is well separated from the rest of the tooth. The P4 also possesses a high and stout paracone, a sharp metastyle and a strong mesiolingual cingulum. On the M1, the paracone is larger and higher than the metacone as in *C. apolloniensis*, *C. etruscus*, *C. mosbachensis* and *C. lupus*.

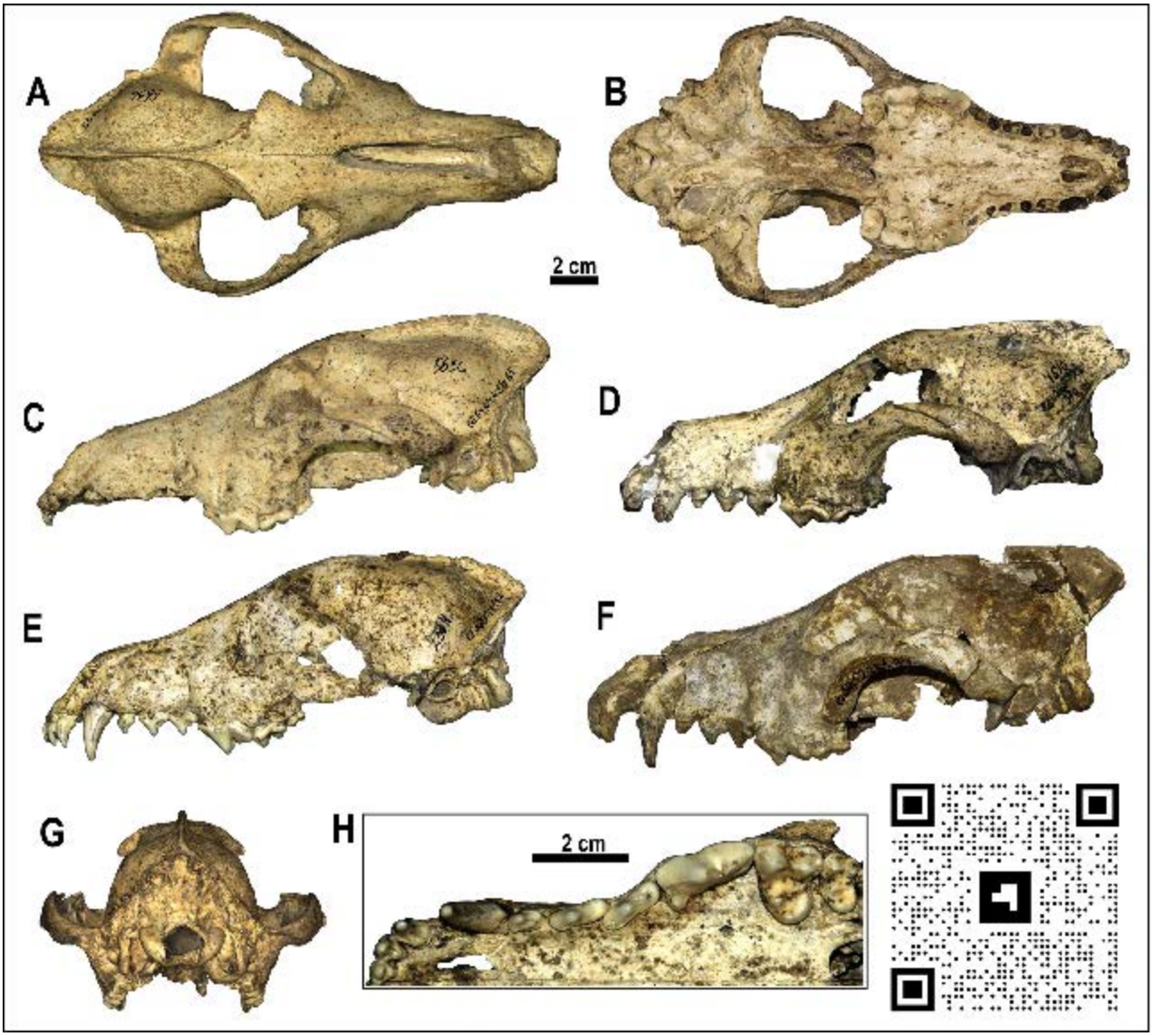

Figure 3.13.1 – *Canis* from Dmanisi. **A-C**, **G**: **D5656**, cranium in dorsal (**A**), ventral (**B**), left lateral (**C**), occipital (**G**) views. **D**: **D4510**, cranium in left lateral view (**D**). **E**: **D2314**, cranium in left lateral view (**E**). **F**: **Dm.50/52.3B1.34**, cranium in left lateral view (**F**). **H**, Detailed view of the occlusal morphology of the upper teeth of *Canis* from Dmanisi (**D2314**). Instructions: Scan the QR-code; open the link; allow the browser to access the camera of your device; point the camera towards the marker at the center of the QR-code; wait for the model to load (up to 10 sec). It is possible to turn the device around the marker (or to move the marker) to see different parts of the model (refer to section 3.13.7 for common issues).

As in these species, there is a well-developed metaconule, a high protocone and a rather individualized protoconule. The protocone basin is deeper and larger than the hypocone basin, like in *C. apolloniensis*, *C. mosbachensis* and *C. lupus*. The M1 shows a strong and well-developed buccal cingulum, expanded on both the mesial and distal sides, unlike *C. lupus* in which the cingulum is present but subdued. The morphology of the M2, in occlusal view, tends to be similar to that of *C. etruscus*, with a large buccal side. Some specimens share this more buccolingually elongated shape resembling the morphology of *C. apolloniensis* from Apollonia-1, *C. lupus* and *C. mosbachensis* from Eurasia.

The mandible of *Canis* from Dmanisi generally has a moderately deep horizontal ramus (Fig. 3.13.4), similar in size and morphology to that of *C. etruscus* from Italy, unlike *C. arnensis* from Upper Valdarno. The postcanine toothrow is slightly arched (buccally convex at the p4-m1 commissure) as generally in *C. apolloniensis*, *C. etruscus*, *C. mosbachensi*s and *C. lupus*, whereas is modestly arched in *C. arnensis* from Upper Valdarno. No diastemata between lower premolars are present. In *Canis* from Dmanisi, the p3 generally sets in the mandible below the alveolar level of the p2 and p4, as in *C. mosbachensis* and *C. lupus*. The p3 possesses a distal accessory cuspulid, generally absent in *C. apolloniensis* and *C. mosbachensis*. The p4 occlusal shape is wide and oval similar to *C. mosbachensis* from Eurasia compared the more slender shape of *C. apolloniensis* from Apollonia-1, *C. arnensis* from Upper Valdarno. The m1 paraconid is higher than the p4 protoconid, like in *C. apolloniensis* from Apollonia-1, C. *mosbachensis* from Eurasia and *C. lupus*, in contrast to *C. arnensis* and *C. etruscus*. In the lower carnassial, the metaconid is large and individualized from the protoconid larger compared to *C. apolloniensis* from Apollonia-1, *C. mosbachensis* from Eurasia and *C. lupus*, which possess a reduced metaconid, closely attached to the large protoconid. Nevertheless, it is less developed compared to C. *arnensis* and *C. etruscus*. On the talonid, the hypoconid is larger than the entoconid, although the difference between them is

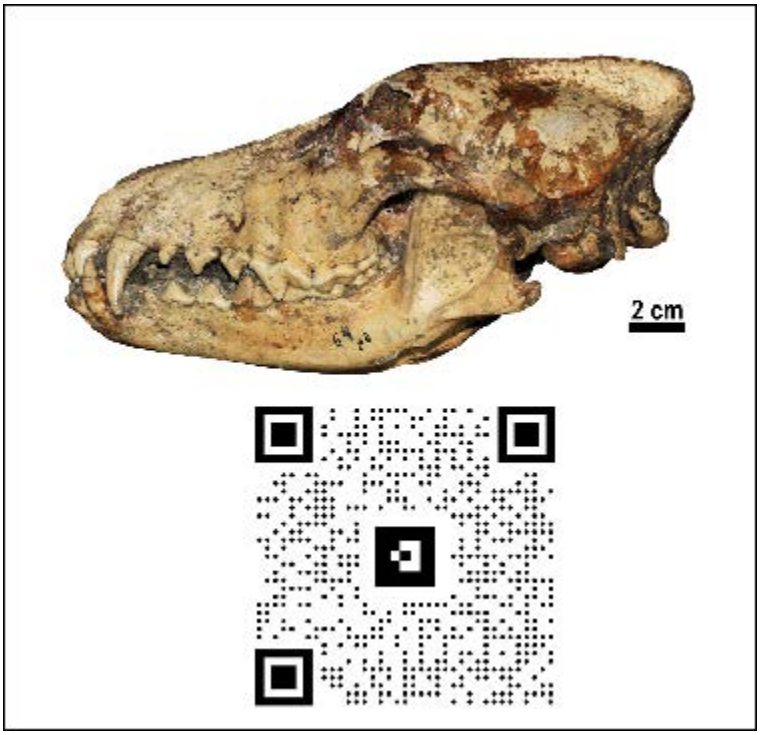

Figure 3.13.2 – D64, skull in left lateral view. Below the cranium the QR-code links to the web-app for AR visualization of D64 3D model. Instructions as in Fig. 3.13.1 (refer to section 3.13.7 for common issues). Scale bar equals 2 cm.

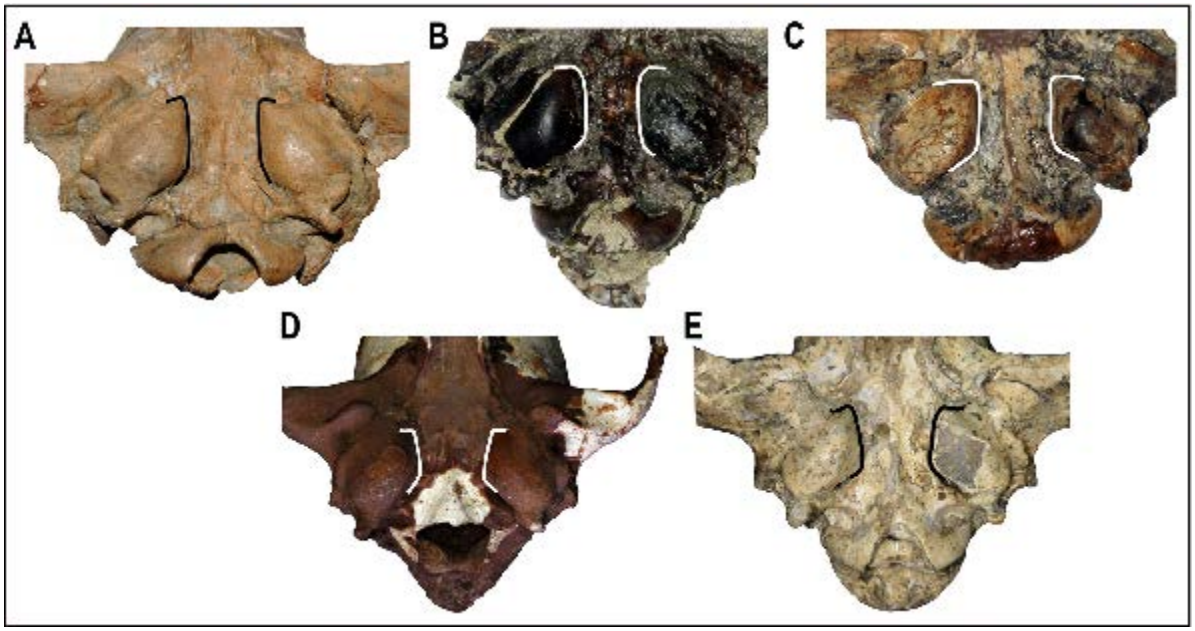

Figure 3.13.3 – Comparison of the tympanic region of *C. etruscus* from Upper Valdarno (**A**), *C. arnensis* from Poggio Rosso (**B**), *C. chihliensis* from Yushe Basin (**C**), *C. mosbachensis* from Cueva Victoria (**D**) and *Canis* from Dmanisi (**E**). Note the marked divergence of the medial walls of the tympanic bullae of *C. mosbachensis* and of *Canis* from Dmanisi. This feature is not documented in the fossil taxa but present in extant wolf-related species (like *C. lupus*, *C. anthus*, *C. aureus*, etc.).

Character	*C. etruscus*	*C. arnensis*	*C. mosbachensis*	*C. apolloniensis*	*Canis* sp. from Dmanisi	Reference
Nasal bones, in dorsal view	very long, end well beyond maxillo-frontal suture	short, end before the maxillo-frontal suture	long, end beyond maxillo-frontal suture	-	Long, end beyond maxillo-frontal suture	Sotnikova, 2001;Bartolini Lucenti et al., 2017
Nasal bones, in lateral view	straight profile in lateral view	gently dorsoventrally curved	dorsoventrally curved	-	slightly dorsoventrally curved	Bartolini Lucenti et al., 2017
GWOC/AB	> 0.9	< 0.9	< 0.9	-	< 0.9	Cherin et al., 2014
Axis of P3	inline with that of P4	inline with that of P4	generally deviates laterally from that of P4	generally deviates laterally from that of P4	may deviates laterally from that of P4	Koufos, 2018
M1 pararcone	larger than the metacone	slightly larger than the metacone	larger than the metacone	larger than the metacone	larger than the metacone	Sotnikova, 2001; Tedford et al., 2009
Trigon-talon Basins on M1	same depth	same depth	trigon basin deeper	trigon basin deeper	trigon basin deeper	Sotnikova, 2001; Bartolini Lucenti et al., 2017
Occlusal shape of the M2	triangular	short bean-like shape	buccolingually elongated bean-shaped	generally buccolingually elongated bean-shaped	generally triangular	Bartolini Lucenti et al., 2017
M2 metacone	smaller than the paracone	equal-sized with paracone	smaller tha paracone	similar to the paracone	smaller tha paracone	
Toothrow curvature	strong	slight	tend to be strong	tend to be strong	strong	Del Campana, 1913
Lower premolars protoconids	high	high	short	short	short	Bartolini Lucenti et al., 2017
p3 alveolus	at same level of p2-p4 alveoli	at same level of p2-p4 alveoli	lower in the mandible, especially distally	generally lower in the mandible	lower in the mandible, especially distally	Sotnikova, 2001
p3 distal accessory cuspulid	developed	developed	generally reduced	generally reduced	present	
p4 secondary distal cuspulid and cingulid	separated	separated	fused	fused	fused	
Mesial margin of paraconid of m1	vertical and straight	vertical and straight	inclined distally and straight/slightly curved	inclined distally and straight/slightly curved	inclined distally and straight	Bartolini Lucenti et al., 2017
Hypoconid of m1	very large	similar size with entoconid	larger than entoconid	considerably larger than entoconid	larger than entoconid	Torre, 1967; Sotnikova, 2001
Transverse cristid	straight (rarely sinuous)	straight	generally sinuous	straight (rarely sinuous)	generally sinous	Sotnikova, 2001; Bartolini Lucenti et al., 2017
m1 accessory cuspids	absent	can be present	generally present	generally present	can be present	Martinez-Navarro et al., 2009; Bartolini Lucenti et al., 2017
m2 protoconid	larger than the metaconid	equal-sized with metaconid	larger than the metaconid	larger than the metaconid	larger than the metaconid	Tedford et al., 2009
m2 distolingual cuspids	absent	entoconid evident	gnerally absent	gnerally absent	absent	Martinez-Navarro et al., 2009; Tedford et al., 2009

Table 3.13.1 – Schematic table of the main craniodental features of *C. etruscus, C. arnensis, C. mosbachensis* and *C. apolloniensis* compared to those of the canid from Dmanisi; "-" represents missing information in literature or on the specimen.

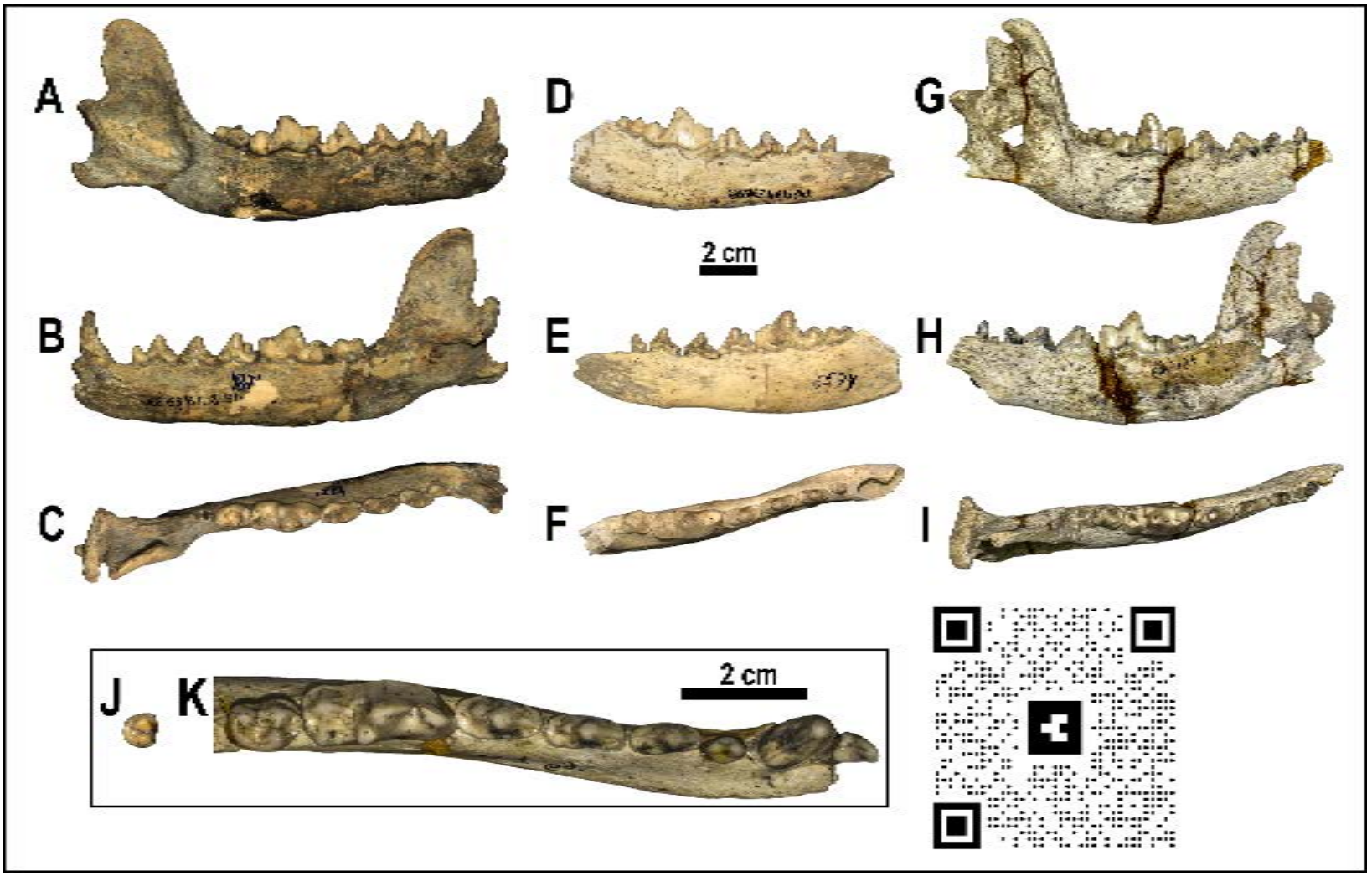

Figure 3.13.4 – *Canis* from Dmanisi. **A-C**: **D4871**, right hemimandible in buccal (**A**), lingual (**B**) and occlusal (**C**) views. **D-E**: **D5594**, right hemimandible in buccal (**D**), lingual (**E**) and occlusal (**F**) views. **G-I**: **D1184**, right hemimandible in buccal (**G**), lingual (**H**) and occlusal (I) views. Detailed occlusal morphology of the lower teeth of *Canis* from Dmanisi: D372, left m3 (**J**) and D1, left hemimandible (**K**). Instructions as in Fig. 3.13.1 (refer to section 3.13.7 for common issues). Scale bar equals 2 cm.

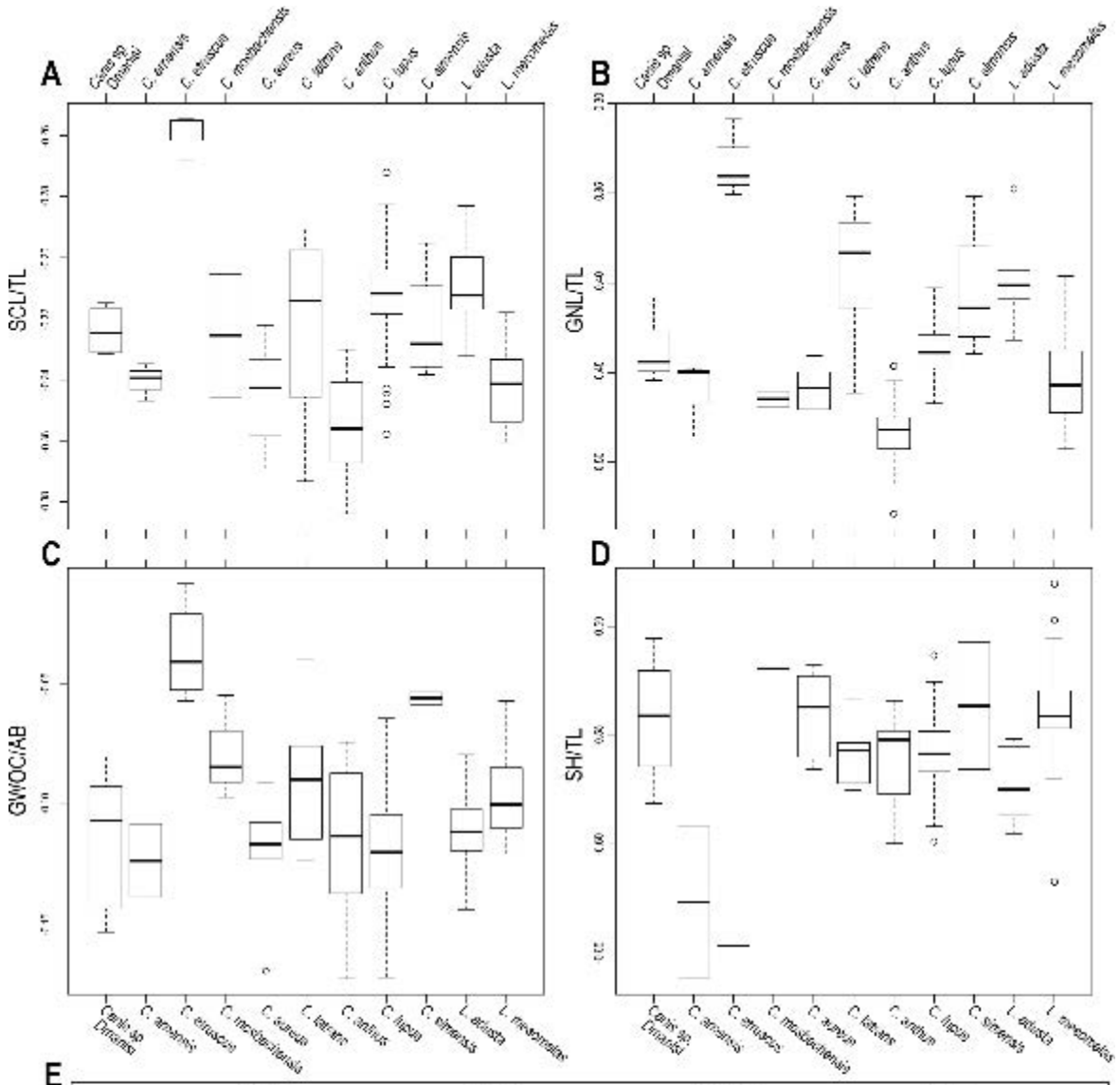

E

		SCL/TL		GNL/TL		GWOC/AB		SH/TL	
DMA	Canis sp. from Dmanisi	0.474 (0.008)	ARN, ETR, MOS, CAU, CLA, CAN, CLU, CSI, LAD, LME	0.367 (0.021)	ARN, ETR, MOS, CAU, CLA, CAN, CLU, CSI, LAD, LME	0.771 (0.050)	ARN, ETR, MOS, CAU, CLA, CAN, CLU, CSI, LAD, LME	0.286 (0.021)	ARN, CAU, CLA, CAN, CLU, CSI, LAD, LME
ETR	C. etruscus	0.551 (0.010)	DMA, ARN, MOS, CAU, CLA, CAN, CLU, CSI, LAD, LME	0.465 (0.024)	DMA, ARN, MOS, CAU, CLA, CAN, CLU, CSI, LAD, LME	0.920 (0.046)	DMA, ARN, MOS, CAU, CLA, CAN, CLU, CSI, LAD, LME	0.225	-
ARN	C. arnensis	0.457 (0.006)	DMA, ETR, MOS, CAU, CLA, CAN, CLU, CSI, LAD, LME	0.346 (0.017)	DMA, ETR, MOS, CAU, CLA, CAN, CLU, CSI, LAD, LME	0.753 (0.037)	DMA, ETR, MOS, CAU, CLA, CAN, CLU, CSI, LAD, LME	0.237 (0.027)	DMA, CAU, CLA, CAN, CLU, CSI, LAD, LME
MOS	C. mosbachensis	0.473 (0.031)	DMA, ARN, ETR, CAU, CLA, CAN, CLU, CSI, LAD, LME	0.343 (0.035)	DMA, ARN, ETR, CAU, CLA, CAN, CLU, CSI, LAD, LME	0.835 (0.042)	DMA, ARN, ETR, CAU, CLA, CAN, CLU, CSI, LAD, LME	0.303	
CAU	C. aureus	0.463 (0.015)	DMA, ARN, ETR, MOS, CLA, CAN, CLU, CSI, LAD, LME	0.346 (0.012)	DMA, ARN, ETR, MOS, CLA, CAN, CLU, CSI, LAD, LME	0.761 (0.037)	DMA, ARN, ETR, MOS, CLA, CAN, CLU, CSI, LAD, LME	0.288 (0.012)	DMA, ARN, CLA, CAN, CLU, CSI, LAD, LME
CLA	C. latrans	0.477 (0.032)	DMA, ARN, ETR, MOS, CAU, CAN, CLU, CSI, LAD, LME	0.4062 (0.033)	DMA, ARN, ETR, MOS, CAU, CAN, CLU, CSI, LAD, LME	0.817 (0.067)	DMA, ARN, ETR, MOS, CAU, CAN, CLU, CSI, LAD, LME	0.268 (0.024)	DMA, ARN, CAU, CAN, CLU, CSI, LAD, LME
CAN	C. anthus	0.442 (0.017)	DMA, ARN, ETR, MOS, CAU, CLA, CLU, CSI, LAD, LME	0.329 (0.018)	DMA, ARN, ETR, MOS, CAU, CLA, CLU, CSI, LAD, LME	0.770 (0.053)	DMA, ARN, ETR, MOS, CAU, CLA, CLU, CSI, LAD, LME	0.274 (0.013)	DMA, ARN, CAU, CLA, CLU, CSI, LAD, LME
CLU	C. lupus	0.468 (0.016)	DMA, ARN, ETR, MOS, CAU, CLA, CAN, CSI, LAD, LME	0.385 (0.011)	DMA, ARN, ETR, MOS, CAU, CLA, CAN, CSI, LAD, LME	0.754 (0.074)	DMA, ARN, ETR, MOS, CAU, CLA, CAN, CSI, LAD, LME	0.277 (0.008)	DMA, ARN, CAU, CLA, CAN, CSI, LAD, LME
CSI	C. simensis	0.476 (0.021)	DMA, ARN, ETR, MOS, CAU, CLA, CAN, CLU, LAD, LME	0.395 (0.035)	DMA, ARN, ETR, MOS, CAU, CLA, CAN, CLU, LAD, LME	0.880 (0.007)	DMA, ARN, ETR, MOS, CAU, CLA, CAN, CLU, LAD, LME	0.282 (0.028)	DMA, ARN, CAU, CLA, CAN, CLU, LAD, LME
LAD	L. adustus	0.491 (0.019)	DMA, ARN, ETR, MOS, CAU, CLA, CAN, CLU, CSI, LME	0.431 (0.026)	DMA, ARN, ETR, MOS, CAU, CLA, CAN, CLU, CSI, LME	0.775 (0.042)	DMA, ARN, ETR, MOS, CAU, CLA, CAN, CLU, CSI, LME	0.267 (0.011)	DMA, ARN, CAU, CLA, CAN, CLU, CSI, LME
LME	L. mesomeles	0.468 (0.020)	DMA, ARN, ETR, MOS, CAU, CLA, CAN, CLU, CSI, LAD	0.331 (0.033)	DMA, ARN, ETR, MOS, CAU, CLA, CAN, CLU, CSI, LAD	0.802 (0.032)	DMA, ARN, ETR, MOS, CAU, CLA, CAN, CLU, CSI, LAD	0.280 (0.020)	DMA, ARN, CAU, CLA, CAN, CLU, CSI, LAD

reduced compared to that visible in *C. lupus* and *C. etruscus*. The transverse cristid between the m1 hypoconid and entoconid is evident and generally sinuous, as in *C. mosbachensis* and *C. lupus*, unlike *C. arnensis* or *C. etruscus* from Italy. The m1 entoconid is more developed compared to *C. apolloniensis* and *C. mosbachensis*, similarly to *C. etruscus*. Accessory cuspulids may be present on the lingual side of the talonid, like in *C. apolloniensis* and *C. mosbachensis* from Eurasia. The m2 protoconid is larger compared to the metacone, unlike *C. arnensis*. Distally on the m2, there is a hypoconid and a lingual cristid, generally with no accessory cuspulids, as in *C. apolloniensis* and *C. mosbachensis* (although in the latter the m2 occlusal shape is generally more rectangular). The m3 has two cuspulids, with the buccal larger than the lingual one as in *C. etruscus* from Italy and *C. mosbachensis* from Europe, as opposed to *C. arnensis* (which has two equal-sized cuspids) and *C. lupus* (with a single and large cuspid). Table 3.13.1 resumes the major differences and similarities between Early Pleistocene European canids.

3.13.4. Results

3.13.4.1. Statistical analyses

In size, *Canis* from Dmanisi is close to *C. etruscus* and other Early Pleistocene canids of Eurasia like *C. mosbachensis* and *C. apolloniensis*, and comparable to smaller subspecies of *C. lupus* (*e.g.*, *C. l. arabs* or *C. l. pallipes*; Supplementary Information, Tables S1-S4). The results of the statistical analyses on the cranial ratios are shown in Fig. 3.13.5, whereas Tables 3.13.2-3.13.3 report those on dental measurements.

Figure 3.13.5 – Boxplots of selected cranial ratios: (**A**) relative length of the splanchnocranium, ScL/TL; (**B**) relative length of the nasals, GNL/TL; (**C**) width of the occipital condyles relative to the height of the cranium, GWOC/AB; (**D**) relative height of the cranium (comprising the sagittal crest), SH/TL. (**E**) Table showing the statistical significance of the permutation ANOVA on the considered cranial ratios. Values displayed consist of the mean and the standard deviation per each species. Abbreviations near these values indicate each species tested for statistical difference: red acronyms indicate significate difference between means ($p<0.05$). In grey, those species not differing from the mean ($p>0.05$).

		P4 L		P4 W		M1 L		M1 W	
DMA	***Canis* sp. from Dmanisi**	21.869 (1.165)	APL, ARN, ETR, MOS, CAU, CLA, CAN, CLU, CSI, LAD, LME	10.492 (0.649)	APL, ARN, ETR, MOS, CAU, CLA, CAN, CLU, CSI, LAD, LME	14.380 (0.630)	APL, ARN, ETR, MOS, CAU, CLA, CAN, CLU, CSI, LAD, LME	17.135 (0.825)	APL, ARN, ETR, MOS, CAU, CLA, CAN, CLU, CSI, LAD, LME
ETR	***C. etruscus***	22.529 (0.884)	DMA, APL, ARN, MOS, CAU, CLA, CAN, CLU, CSI, LAD, LME	10.940 (0.515)	DMA, APL, ARN, MOS, CAU, CLA, CAN, CLU, CSI, LAD, LME	14.491 (0.985)	DMA, APL, ARN, MOS, CAU, CLA, CAN, CLU, CSI, LAD, LME	16.920 (1.197)	DMA, APL, ARN, MOS, CAU, CLA, CAN, CLU, CSI, LAD, LME
ARN	***C. arnensis***	20.369 (1.009)	DMA, APL, ETR, MOS, CAU, CLA, CAN, CLU, CSI, LAD, LME	9.738 (0.844)	DMA, APL, ETR, MOS, CAU, CLA, CAN, CLU, CSI, LAD, LME	13.613 (1.147)	DMA, APL, ETR, MOS, CAU, CLA, CAN, CLU, CSI, LAD, LME	16.517 (1.064)	DMA, APL, ETR, MOS, CAU, CLA, CAN, CLU, CSI, LAD, LME
MOS	***C. mosbachensis***	21.045 (1.501)	DMA, APL, ARN, ETR, CAU, CLA, CAN, CLU, CSI, LAD, LME	10.363 (1.191)	DMA, APL, ARN, ETR, CAU, CLA, CAN, CLU, CSI, LAD, LME	13.785 (0.807)	DMA, APL, ARN, ETR, CAU, CLA, CAN, CLU, CSI, LAD, LME	16.423 (0.964)	DMA, APL, ARN, ETR, CAU, CLA, CAN, CLU, CSI, LAD, LME
APL	***C. apolloniensis***	21.620 (1.248)	DMA, ARN, ETR, MOS, CAU, CLA, CAN, CLU, CSI, LAD, LME	10.940 (0.873)	DMA, ARN, ETR, MOS, CAU, CLA, CAN, CLU, CSI, LAD, LME	14.360 (0.814)	DMA, ARN, ETR, MOS, CAU, CLA, CAN, CLU, CSI, LAD, LME	17.200 (1.304)	DMA, ARN, ETR, MOS, CAU, CLA, CAN, CLU, CSI, LAD, LME
CAU	***C. aureus***	15.623 (0.717)	DMA, APL, ARN, ETR, MOS, CLA, CAN, CLU, CSI, LAD, LME	8.066 (0.744)	DMA, APL, ARN, ETR, MOS, CLA, CAN, CLU, CSI, LAD, LME	11.206 (0.632)	DMA, APL, ARN, ETR, MOS, CLA, CAN, CLU, CSI, LAD, LME	12.856 (0.493)	DMA, APL, ARN, ETR, MOS, CLA, CAN, CLU, CSI, LAD, LME
CLA	***C. latrans***	21.550 (2.797)	DMA, APL, ARN, ETR, MOS, CAU, CAN, CLU, CSI, LAD, LME	10.813 (1.800)	DMA, APL, ARN, ETR, MOS, CAU, CAN, CLU, CSI, LAD, LME	13.913 (1.578)	DMA, APL, ARN, ETR, MOS, CAU, CAN, CLU, CSI, LAD, LME	16.294 (1.978)	DMA, APL, ARN, ETR, MOS, CAU, CAN, CLU, CSI, LAD, LME
CAN	***C. anthus***	16.251 (1.653)	DMA, APL, ARN, ETR, MOS, CAU, CLA, CLU, CSI, LAD, LME	8.345 (0.728)	DMA, APL, ARN, ETR, MOS, CAU, CLA, CLU, CSI, LAD, LME	11.620 (0.849)	DMA, APL, ARN, ETR, MOS, CAU, CLA, CLU, CSI, LAD, LME	13.440 (1.216)	DMA, APL, ARN, ETR, MOS, CAU, CLA, CLU, CSI, LAD, LME
CLU	***C. lupus***	24.222 (1.100)	DMA, APL, ARN, ETR, MOS, CAU, CLA, CAN, CSI, LAD, LME	12.777 (0.865)	DMA, APL, ARN, ETR, MOS, CAU, CLA, CAN, CSI, LAD, LME	15.320 (0.739)	DMA, APL, ARN, ETR, MOS, CAU, CLA, CAN, CSI, LAD, LME	18.403 (1.061)	DMA, APL, ARN, ETR, MOS, CAU, CLA, CAN, CSI, LAD, LME
CSI	***C. simensis***	16.214 (0.844)	DMA, APL, ARN, ETR, MOS, CAU, CLA, CAN, CLU, LAD, LME	7.647 (0.417)	DMA, APL, ARN, ETR, MOS, CAU, CLA, CAN, CLU, LAD, LME	12.302 (0.523)	DMA, APL, ARN, ETR, MOS, CAU, CLA, CAN, CLU, LAD, LME	13.485 (0.656)	DMA, APL, ARN, ETR, MOS, CAU, CLA, CAN, CLU, LAD, LME
LAD	***L. adusta***	14.247 (1.026)	DMA, APL, ARN, ETR, MOS, CAU, CLA, CAN, CLU, CSI, LME	7.510 (0.758)	DMA, APL, ARN, ETR, MOS, CAU, CLA, CAN, CLU, CSI, LME	11.454 (0.813)	DMA, APL, ARN, ETR, MOS, CAU, CLA, CAN, CLU, CSI, LME	12.763 (0.919)	DMA, APL, ARN, ETR, MOS, CAU, CLA, CAN, CLU, CSI, LME
LME	***L. mesomelas***	15.817 (1.051)	DMA, APL, ARN, ETR, MOS, CAU, CLA, CAN, CLU, CSI, LAD	7.467 (0.645)	DMA, APL, ARN, ETR, MOS, CAU, CLA, CAN, CLU, CSI, LAD	10.627 (0.707)	DMA, APL, ARN, ETR, MOS, CAU, CLA, CAN, CLU, CSI, LAD	12.789 (0.873)	DMA, APL, ARN, ETR, MOS, CAU, CLA, CAN, CLU, CSI, LAD

Table 3.13.2 – Table showing the statistical significance of the Kruskal-Wallis test on the considered upper teeth measures (in mm). Values displayed consist of the mean and the standard deviation per each species. Abbreviations near these values indicate each species tested for statistical difference: red acronyms indicate significate difference between means ($p<0.05$). In grey, those species not differing from the mean ($p>0.05$).

		m1 L		m1 W		trm1 L	
DMA	***Canis* sp. from Dmanisi**	23.415 (1.423)	APL, ARN, ETR, MOS, CAU, CLA, CAN, CLU, CSI, LAD, LME	9.516 (0.585)	APL, ARN, ETR, MOS, CAU, CLA, CAN, CLU, CSI, LAD, LME	15.747 (1.099)	APL, ARN, ETR, MOS, CAU, CLA, CAN, CLU, CSI, LAD, LME
ETR	***C. etruscus***	24.742 (1.160)	DMA, APL, ARN, MOS, CAU, CLA, CAN, CLU, CSI, LAD, LME	9.896 (0.577)	DMA, APL, ARN, MOS, CAU, CLA, CAN, CLU, CSI, LAD, LME	16.747 (0.885)	DMA, APL, ARN, MOS, CAU, CLA, CAN, CLU, CSI, LAD, LME
ARN	***C. arnensis***	21.133 (0.694)	DMA, APL, ETR, MOS, CAU, CLA, CAN, CLU, CSI, LAD, LME	8.272 (0.629)	DMA, APL, ETR, MOS, CAU, CLA, CAN, CLU, CSI, LAD, LME	14.2 (0.449)	DMA, APL, ETR, MOS, CAU, CLA, CAN, CLU, CSI, LAD, LME
MOS	***C. mosbachensis***	23.728 (1.194)	DMA, APL, ARN, ETR, CAU, CLA, CAN, CLU, CSI, LAD, LME	9.261 (0.672)	DMA, APL, ARN, ETR, CAU, CLA, CAN, CLU, CSI, LAD, LME	16.007 (0.871)	DMA, APL, ARN, ETR, CAU, CLA, CAN, CLU, CSI, LAD, LME
APL	***C. apolloniensis***	22.65 (0.597)	DMA, ARN, ETR, MOS, CAU, CLA, CAN, CLU, CSI, LAD, LME	8.930 (0.119)	DMA, ARN, ETR, MOS, CAU, CLA, CAN, CLU, CSI, LAD, LME	15.225 (0.263)	DMA, ARN, ETR, MOS, CAU, CLA, CAN, CLU, CSI, LAD, LME
CAU	***C. aureus***	18.345 (0.529)	DMA, APL, ARN, ETR, MOS, CLA, CAN, CLU, CSI, LAD, LME	7.220 (0.288)	DMA, APL, ARN, ETR, MOS, CLA, CAN, CLU, CSI, LAD, LME	12.101 (0.515)	DMA, APL, ARN, ETR, MOS, CLA, CAN, CLU, CSI, LAD, LME
CLA	***C. latrans***	20.605 (2.889)	DMA, APL, ARN, ETR, MOS, CAU, CAN, CLU, CSI, LAD, LME	7.979 (1.197)	DMA, APL, ARN, ETR, MOS, CAU, CAN, CLU, CSI, LAD, LME	14.185 (2.637)	DMA, APL, ARN, ETR, MOS, CAU, CAN, CLU, CSI, LAD, LME
CAN	***C. anthus***	17.358 (0.932)	DMA, APL, ARN, ETR, MOS, CAU, CLA, CLU, CSI, LAD, LME	6.635 (0.437)	DMA, APL, ARN, ETR, MOS, CAU, CLA, CLU, CSI, LAD, LME	11.737 (0.826)	DMA, APL, ARN, ETR, MOS, CAU, CLA, CLU, CSI, LAD, LME
CLU	***C. lupus***	27.611 (1.541)	DMA, APL, ARN, ETR, MOS, CAU, CLA, CAN, CSI, LAD, LME	11.306 (0.925)	DMA, APL, ARN, ETR, MOS, CAU, CLA, CAN, CSI, LAD, LME	19.788 (1.278)	DMA, APL, ARN, ETR, MOS, CAU, CLA, CAN, CSI, LAD, LME
CSI	***C. simensis***	19.156 (0.908)	DMA, APL, ARN, ETR, MOS, CAU, CLA, CAN, CLU, LAD, LME	6.923 (0.463)	DMA, APL, ARN, ETR, MOS, CAU, CLA, CAN, CLU, LAD, LME	13.110 (0.639)	DMA, APL, ARN, ETR, MOS, CAU, CLA, CAN, CLU, LAD, LME
LAD	***L. adusta***	16.222 (1.078)	DMA, APL, ARN, ETR, MOS, CAU, CLA, CAN, CLU, CSI, LME	6.689 (0.486)	DMA, APL, ARN, ETR, MOS, CAU, CLA, CAN, CLU, CSI, LME	10.133 (0.754)	DMA, APL, ARN, ETR, MOS, CAU, CLA, CAN, CLU, CSI, LME
LME	***L. mesomelas***	16.921 (0.648)	DMA, APL, ARN, ETR, MOS, CAU, CLA, CAN, CLU, CSI, LAD	6.663 (0.312)	DMA, APL, ARN, ETR, MOS, CAU, CLA, CAN, CLU, CSI, LAD	11.163 (0.625)	DMA, APL, ARN, ETR, MOS, CAU, CLA, CAN, CLU, CSI, LAD

Table 3.13.3 – Table showing the statistical significance of the Kruskal-Wallis test on the considered lower teeth measures (in mm). Values displayed consist of the mean and the standard deviation per each species. Se above for abbreviation an conlor code

C. etruscus is considerably different in cranial proportions as opposed to the others species. Particularly compared to *Canis* from Dmanisi, all the considered ratios (SCL/TL, GNL/TL, GWOC/AB, SH/TL) of the Etruscan wolf are different. The ratios of *Canis* from Dmanisi are more similar to *C. mosbachensis*, *C. arnensis* and C. *lupus*. Even several dental measures (Tables 3.13.2-3.13.3) confirm the statistical difference between *Canis* from Dmanisi and *C. etruscus*. Only the first upper molar does not differ statistically between the two taxa, whereas in the proportions of this tooth *Canis* from Dmanisi differs from *C. mosbachensis*. This confirms the morphological similarity between the *C. etruscus* and *Canis* from Dmanisi in upper molar gross morphology and might explain the confusion and the consequent ascription of the Georgian sample to *C. etruscus*.

3.13.4.2. Log ratios

The results of the log ratio diagrams are shown in Figs. 3.13.6-3.13.7. Cranially (Fig. 3.13.6) *Canis* from Dmanisi most clearly differs in size and general proportions from *C. arnensis* from Upper Valdarno (see also Tables 3.13.4-3.13.7). Although, the size of the Georgian material is close to *C. etruscus* from Olivola, Upper Valdarno and Pantalla, their proportion pattern is inverse in several ratios (Fig. 3.13.6), SCL, GNL, Eu, Ect, PoCW, SH. Unlike the previous species, when compared to the considered sample of *C. mosbachensis*, the pattern of *Canis* from Dmanisi is remarkably similar to the former, besides the general larger size of *Canis* from Dmanisi. A difference between these two taxa lie in the less constricted postorbital constriction of C. *mosbachensis* compared to the skull height.

Even in dental proportions (Fig. 3.13.7), the difference between *Canis* from Dmanisi and *C. arnensis*, both in size and pattern, is confirmed. *C. etruscus* confirms as the largest of western Eurasian species in almost every ratio, with the exception of the M2. Some peculiarities in its proportions, compared to the other fossil species, can be identified: *e.g.*, unlike *Canis* from Dmanisi, *C. apolloniensis* and

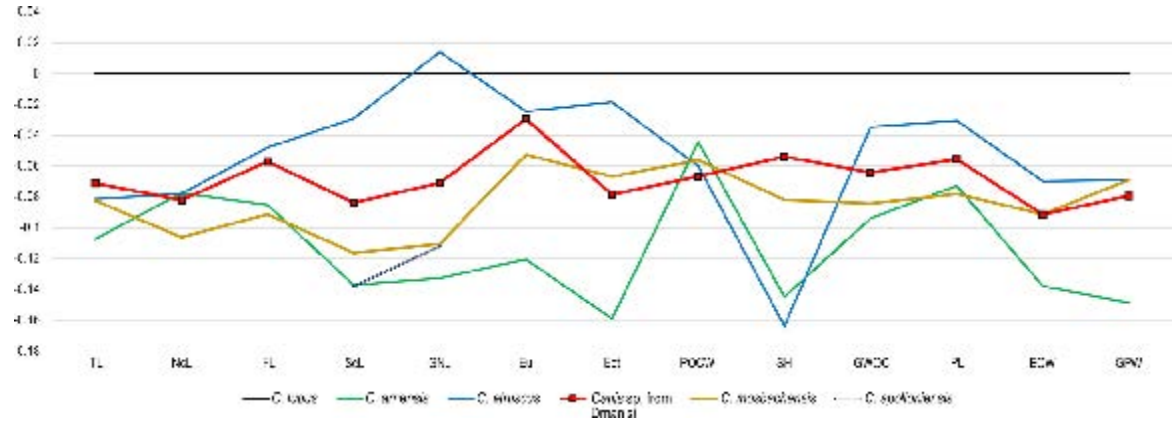

Figure 3.13.6 – Log-ratio diagram based on selected cranial variables in the described (Dmanisi material) as well as in other Early Pleistocene species of *Canis* (*C. etruscus*, *C. arnensis*, *C. mosbachensis*; data taken from the literature: Sotnikova, 2001; Martínez-Navarro et al., 2009; Petrucci et al., 2013; Bartolini Lucenti et al., 2017) as compared to extant *C. lupus* (used as the reference baseline). Abbreviations: section 2.4.

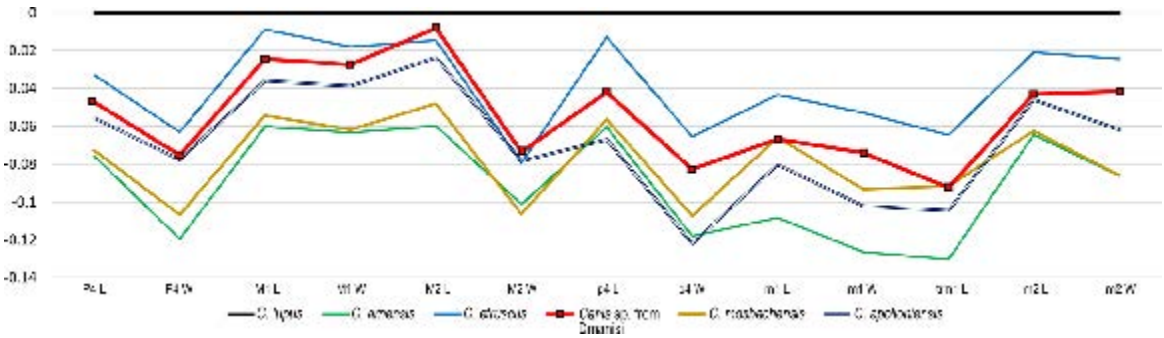

Figure 3.13.7 – Log-ratio diagram based on selected dental variables in the described (Dmanisi material) as well as in other Early Pleistocene species of *Canis* (*C. apolloniensis*, *C. arnensis*, *C. etruscus*, *C. mosbachensis*; data taken from the literature: Sotnikova, 2001; Martínez-Navarro et al., 2009; Petrucci et al., 2013; Bartolini Lucenti et al., 2017; Koufos, 2018) as compared to extant *C. lupus* (used as the reference baseline).

C. mosbachensis, the M1 is proportionally longer compared the M2. C. arnensis follows the pattern of the reference *C. lupus*, although significantly smaller. The m1 of *C. etruscus* is buccolingually larger compared to *C. apolloniensis*, *C. arnensis* and *C. mosbachensis*, whereas is more similar to the pattern of *Canis* from Dmanisi. Despite the similar width the m1 with *C. etruscus*, the upper teeth proportions of *Canis* from Dmanisi are extremely similar to *C. apolloniensis* from Apollonia-1 and *C. mosbachensis* (which are also clearly similar one another), despite the larger size of the former. In contrast to the other species, *Canis* from Dmanisi appear to have

the m2 proportionally similar to *C. lupus*.

3.13.4.3. Principal Component Analysis

The results of the PCA are reported in Fig. 3.13.8. The PC1, which accounts for most of the variance (93.7%), has positive and similar loading for all the analyzed original variables (Table 3.13.7), thus being largely influenced by size but also, to some extent, by cranial shape. PC1 segregates modern wolves (on the positive end) from other extant canids (jackals and golden wolves, on the negative end). Extinct species (*Canis* from Dmanisi, *C. mosbachensis*, *C. arnensis* and *C. etruscus*) occupy an intermediate position without overlapping with (albeit being closer to) the modern wolf variation. Of these extinct species, *Canis* from Dmanisi, *C. etruscus* and *C. mosbachensis* are more similar to modern gray wolves, whereas *C. arnensis* is more similar to the jackal-like species. The PC2 only accounts for 2.2% of total variance, being dominated positively by postorbital constriction, width of the braincase, the width across the zygomatic process of the frontals and by the greatest width of the palate, and negatively by the total length, the nasal length, cranial height without the sagittal crest, the width of the muzzle across the upper canines, and the palate length. All the investigated taxa overlap to a large extent for PC2, except for *C. etruscus* as compared to both *C. mosbachensis* and *C. arnensis*. *Canis* from Dmanisi tends to partially overlap with *C. etruscus* and *C. mosbachensis*.

3.13.5. Discussion

The results of the statistical analyses on cranial ratios clearly point out the peculiarity of *C. etruscus* compared to other known fossil and extant species (Fig. 3.13.5), confirming the observations by Cherin et al. (2014). The uniqueness of this extinct species, even in dental measures, differs from the morphometric patterns or ratio possessed by the Georgian sample (Fig. 3.13.5 and Tables 3.13.2-3.13.3), historically synonymized under the same specific name (Vekua, 1995). Our results

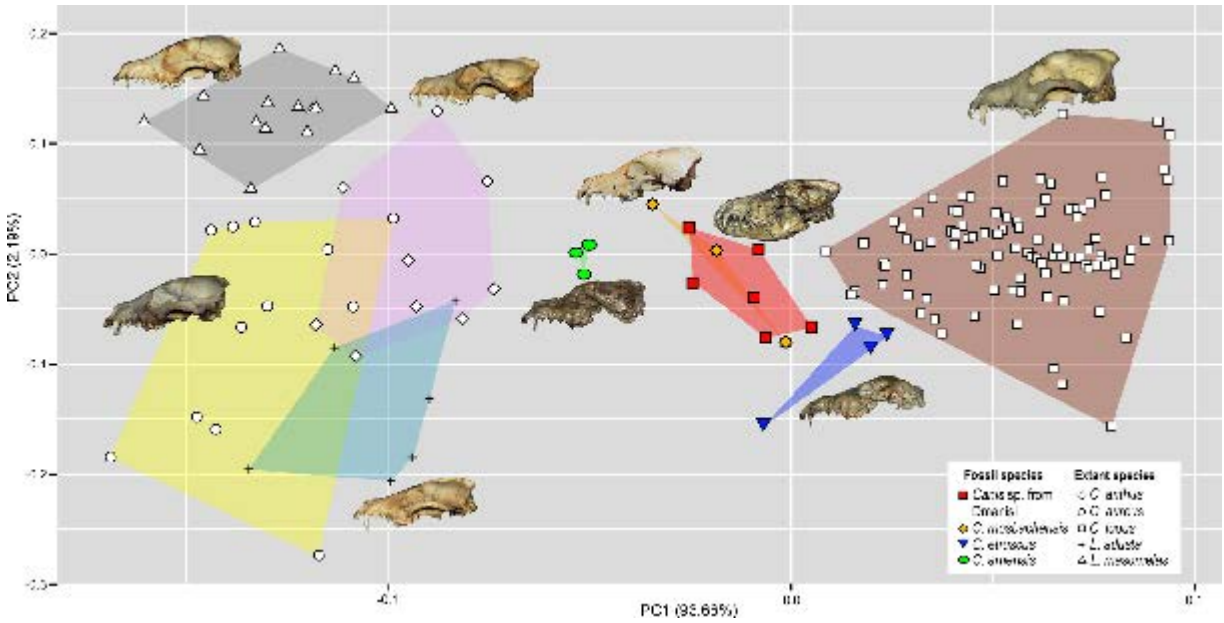

Figure 3.13.8 – Principal Components Analysis (PCA) based on selected log-transformed cranial measurements on extant and fossil species of the general *Canis* and *Lupulella*. Symbols are explained in the legend.

firmly challenge this interpretation. Further support to the distinction between the two taxa comes from the log ratio diagrams (Figs. 3.13.6-3.13.7) and the Principal Component Analysis (Fig. 3.13.8). All evidence considered, the material of *Canis* from Dmanisi cannot be ascribed to *C. etruscus*. Several of the morphometric and morphological results, for instance in the cranial log ratio diagram (Fig. 3.13.6), point out to a closer affinity of *Canis* from Dmanisi to the late Early Pleistocene *Canis* ex gr. *mosbachensis* (*C. mosbachensis e.g.*, from Untermassfeld, Sotnikova, 2001; Iberian Peninsula, Bartolini Lucenti et al., 2017; Pirro Nord, Petrucci et al.,2013; *C. mosbachensis variabilis* from Zhoukoudian localities, Jiangzuo et al., 2018; and *C. apolloniensis* from Apollonia-1, Koufos, 2018), rather than to *C. etruscus*. In addition to the affinity with these fossil taxa, *Canis* from Dmanisi shares also affinities with the group of wolf-related canids (see Lindblad-Toh et al., 2005), *e.g.*, the caudorostrally divergent tympanic bullae; p3 alveolus at a lower level than p2-p4 (Figs. 3.13.1-3.13.4). Indeed, the divergent walls of the bullae is shared by *C. lupus*, other wolf-related canids and *C. mosbachensis* (see Bartolini Lucenti et al., 2017), as opposed to any other extinct species (Figs. 3.13.1-3.13.3). Nevertheless,

some other features of the sample from Dmanisi are more primitive, *e.g.*, blunt or subrounded dorsal outline of the nuchal crest, reduced caudal elongation of the postorbital region; relatively developed crushing surface of the molars; presence of an accessory cuspulid on p3. This combined pattern of features (similar to both primitive- and derived-like canids), unlike any other early Early Pleistocene canids, supports the ascription of the sample to a new species, *Canis* sp. nov. from Dmanisi.

The new identity of *Canis* from Dmanisi casts some doubts on the current interpretation of the origin of modern wolf lineage. The wide consensus in scientific literature supports that *C. lupus* and its lineage originates during the Early Pleistocene with the primitive *Canis etruscus* (Torre, 1967; Kurtén, 1968; Musil, 1972; Sotnikova, 2001; Sotnikova & Rook, 2010), from which derived *C. mosbachensis* in the second half of the Early Pleistocene to first half of the middle Pleistocene. Despite the taxonomical debate (Mecozzi et al., 2017), *C. mosbachensis* is widely considered the ancestor of *C. lupus* (in addition to the former: Brugal and Boudadi-Maligne, 2011; Sardella et al., 2014). Sotnikova & Rook (2010) were the first to suggest a possible alternative classification for the *Canis* of Dmanisi and the plausible ancestry of *C. lupus*. Following recent molecular evidence (*e.g.*, Koepfli et al., 2015; Viranta et al., 2017) the possible early presence of *C. lupus* in the early Middle Pleistocene deposits of Alaska (Tedford et al., 2009), some authors (Bartolini Lucenti et al., 2017; Jiangzuo et al., 2018) put forward the idea that *C. mosbachensis*, as a large-ranged and time-spanned species, might be related to the crown species of the wolf lineage (*i.e.*, *C. latrans*, *C. anthus* and *C. lupus*). Koepfli et al. (2015) estimated the time of divergence between the *C. anthus* and the *C. latrans-C. lupus* clade around ca. 1.3 Ma and between *C. latrans* and *C. lupus* around 1.1 Ma. This suggests that the Early Pleistocene was a time of high diversification in modern canids, as is also confirmed by fossil record. In this framework, the privileged geographical position of the Caucasian region reveals its importance

in canids' evolutionary history, as a noted by Sotnikova & Rook (2010). Indeed, the Caucasus sets as a crossroads between three continents, and its peculiar biotic evolution testifies to its role of key region in evolution of Old-World faunas since Miocene times (Krijgsman et al., 2019). The discovery of a previously undescribed taxon in Dmanisi, with some modern features as opposed to *C. etruscus*, close but more primitive compared to *C. mosbachensis*, changes radically the idea of *C. lupus* evolution as it is conveyed today, invalidating the paradigm *C. etruscus-C. mosbachensis-C. lupus* lineage. As probable ancestor of *C.* ex gr. *mosbachensis*, *Canis* sp. nov. might also represent one of the latest common ancestors of the crown clade of modern *Canis* species (*C. latrans*, *C. anthus*, *C. lupus*).

3.13.6. Conclusions

The extensive record of *Canis* from the Dmanisi is outstanding both for its state of preservation and abundance. Several morphological and morphometrical patterns challenge the previous attribution to *C. etruscus* and favor the ascription of the taxon to a new species. The record of Dmanisi has already changed our understanding of evolutionary history of different species, like in the case of the rhino "*Stephanorhinus*" (Cappellini et al., 2019), or of the genus *Homo* (Rightmire et al., 2019 and reference therein) as the first discovery of the earliest Out-of-Africa hominids. The description of *Canis* sp. nov. from Dmanisi forces to delineates a new picture for the evolutionary history of modern wolves and wolf-like canids. Instead of considering the rather primitive species *C. etruscus* as the ancestor of *C. lupus*, the similarity between *Canis* sp. from Dmanisi and *C. mosbachensis* suggest to acknowledge in the species from Dmanisi the ancestor of modern wolf-related canids. The exquisite conservation of the fossil specimens of *Canis* sp. from Dmanisi offers the perfect subject to the application of useful 3D and digital imaging techniques, like the use of Artec Spider laser scan combined with Augmented Reality (AR). Such web-app reveals as a powerful and useful

tool to help visualization of the specimens digitalized, allow comparisons between with real specimens and the considered ones and may boost the visibility of the research.

3.13.7. Appendix

3.13.7.1. Resuming measurements of Canis *from Dmanisi.*

see next page

Table 3.13.4 – Resuming table of cranial measurements of *Canis* from Dmanisi.

	TL	NCL	FL	SCL	GNL	Eu	Ect	POCW	SH	AB	GWOC	BL	PL	CBL	Zyg	ECW	GPW
mean	205.8	89.7	117.4	97.7	75.2	59.9	51.3	37.0	59.1	45.5	35.8	182.6	99.2	189.1	116.0	34.4	62.7
sd	13.718	3.967	6.630	6.795	7.851	5.232	-	1.840	5.217	1.831	1.013	11.576	5.217	11.024	1.167	1.494	3.121
count	4	4	3	4	4	4	1	3	7	6	6	5	8	6	2	10	10

Table 3.13.5 – Resuming table of upper teeth measurements of *Canis* from Dmanisi.

	C L	C W	P1 L	P1 W	P2 L	P2 W	P3 L	P3 W	P4 L	P4 W	M1 L	M1 W	M2 L	M2 W	LCR	LPR	LMR
mean	10.2	6.3	6.7	4.2	11.6	4.6	13.1	5.1	21.7	10.7	14.5	17.3	8.2	10.7	74.4	56.4	22.8
sd	0.673	0.484	0.369	0.353	0.603	0.326	0.702	0.403	0.937	0.566	0.558	0.797	0.529	0.856	3.416	3.465	0.945
count	27	24	19	17	21	19	33	32	45	39	43	40	39	38	14	14	31

Table 3.13.6 – Resuming table of mandibular measurements of *Canis* from Dmanisi.

	Mp4H	Mm1H	HR	LLPR	p2-p4 L	LLMR	m1-m2 L
mean	22.8	23.7	57.3	44.1	38.6	38.3	34.0
sd	1.449	1.736	2.687	2.395	1.931	2.076	1.441
count	23	20	4	11	11	5	13

Table 3.13.7 – Resuming table of lower teeth measurements of *Canis* from Dmanisi

	c L	c W	p1 L	p1 W	p2 L	p2 W	p3 L	p3 W	p4 L	p4 W	m1 L	m1 W	trm1 L	tdm1 W	m2 L	m2 W	m3 L	m3 W
mean	10.2	6.6	5.2	3.6	10.8	4.9	11.8	5.0	14.0	6.5	23.4	9.4	15.7	9.1	10.4	7.7	5.1	4.8
sd	0.830	0.621	0.501	0.290	0.699	0.450	0.722	0.489	0.737	0.477	1.373	0.492	0.875	0.586	0.563	0.481	0.470	0.478
count	24	24	13	11	21	19	22	21	23	22	24	25	23	22	25	24	6	6

3.13.7.2. Loadings of the PCA

Tab. 3.13.8 – Results of the Principal Components Analysis based on log-transformed cranial measurements in extant and fossil *Canis*.

	PC1	PC2	PC3	PC4	PC5
Standard deviation	0.2572	0.0393	0.03214	0.02662	0.01888
Proportion of Variance	0.9366	0.02187	0.01462	0.01003	0.00505
Cumulative Proportion	0.9366	0.95845	0.97307	0.9831	0.98815

	PC1	PC2	PC3	PC4	PC5
TL	0.359023	-0.16602	0.075228	-0.03605	0.374715
GNL	0.39156	-0.41205	-0.31463	-0.55	-0.25716
Eu	0.177523	0.077632	0.157352	0.042951	-0.52183
Ect	0.345549	0.414068	-0.76318	0.337015	0.078222
PoCW	0.245993	0.756139	0.298756	-0.49741	0.032286
AB	0.339318	-0.04093	0.365569	0.384602	0.371671
PL	0.327721	-0.17243	-0.00491	-0.26058	0.397743
GPW	0.356866	0.018771	0.168077	0.256971	-0.41444
ECW	0.395552	-0.14719	0.192296	0.226952	-0.21423

3.13.7.3. AR guide to use it

To visualize the QR-code: choose any free application from the App Store/Play Store.

iOS devices

To visualize the Augmented Reality web-app:

1) Allow Safari to open the camera of the iPhone: Go to Setting > Safari > turn on "Camera & Microphone Access" under the "Privacy & Security" submenu.

2) Scan the QR-Code.

3) Open the link in Safari (NB. the web-app does not work in Chrome for iOS or other browsers)

4) Confirm the use of the camera by the browser.

5) Point at the marker, wait the for the model to load.

Best model-rendering performances if the scene is in landscape mode (allowing the phone to automatically rotate the view)

Android devices

To visualize the QR-code: choose any free application from the App Store.

To visualize the Augmented Reality web-app:

1) Scan the QR-Code.

2) Open the link in your browser (*e.g.*, Chrome)

3) Confirm the use of the camera by the browser.

4) Point at the marker, wait the for the model to load.

Best model-rendering performances if the scene is in landscape mode (allowing the phone to automatically rotate the view).

3.14. A new species of dog from the Early Pleistocene site of Venta Micena (Orce, Baza Basin, Spain)

3.14.1 Context

The village of Orce (Granada, Baza Basin, SE Spain) is known in the paleontological literature since 1981, when the site of Venta Micena was first published (Moyà-Solà et al., 1981). Since then, the region of Orce became one of the most important paleontological and prehistoric sites of the Quaternary of Europe. Indeed, the findings of the earliest occurrence of a fossil hominin of the continent in the site of Barranco León (BL), dated to 1.4 Ma (Toro-Moyano et al., 2013), the huge assemblages of Oldowan tools of BL and Fuente Nueva-3 (FN-3), roughly coeval to the former, and the clear evidence of anthropic action on large mammal carcasses in FN-3 (Espigares et al., 2003) are some of the elements that testifies to the uniqueness and value of Orce site complex. In this context, the site of Venta Micena, found in 1976 by a team directed by J. Gibert, is the best-known paleontological locality of Orce. Dated to ca. 1.6 Ma, it is an 80-120 cm thick horizontal stratum with ca.1 km^2 of areal extent that encloses a dense accumulation of fossil remains of vertebrates beautifully preserved in marly-limestones (*e.g.*, in the 360 m^2 surface excavated up to date, >24,000 fossils of large mammals have been unearthed). For this reason, it represents the most abundant Early Pleistocene record of all the European continent (Moyà-Solà et al., 1987; Martínez-Navarro, 1991; Martínez-Navarro & Palmqvist, 1995; Palmqvist et al., 1996; 1999; 2003; 2008; 2011; Arribas & Palmqvist, 1998; Espigares, 2010; Ros-Montoya et al., 2012; Martínez-Navarro et al., 2011; 2014).

Here the fossil material of *Canis mosbachensis* from Venta Micena is re-described. the site that records the earliest occurrence of the species. The taxonomical attribution of this sample has been a matter of debate in the literature. The first reviews of this carnivore fossil material by Pons-Moyà (1987) described the medium-sized canid specimens as *C. etruscus mosbachensis* and *Cuon priscus* according to their

size, morphology and, in case of the latter attribution, to a badly restored lower carnassial, which resembled those of extant dholes. Later, after a new restoration, this specimen and the other ascribed to *C. e. mosbachensis* were attributed to *C. etruscus* by Martínez-Navarro (1991, 1992). Rook (1993) and Rook & Torre (1996) pointed out the resemblance of this Venta Micena canid to *C*anis aff. *arnensis*, which is comparable in size to the canid from the Italian site of Pirro Nord. Finally, Martínez-Navarro (2002) ascribed this material to *C. mosbachensis*, that would be the earliest occurrence of this species in Europe (Bartolini Lucenti et al., 2017).

3.14.2 Geological background

The paleontological site of Venta Micena is located in the Baza and Guadix Basin (Fig. 3.14.1), a large NE-SW elongated basin (ca.110 km long) which extends for ca. 4,000 km^2 and is situated in the contact between the External and Internal Zones of the Betic Cordillera (Oms et al., 2011; García-Aguilar et al., 2014; 2015). After its uplift around 8 Ma (Hüsing et al., 2010, and references therein) the depression has been characterized by an old set of sediments (Late Miocene marine deposits), overlapped by a modern set of sediments with an angular unconformity (Latest Miocene to Middle Pleistocene continental deposits (Vera, 1970; García-Aguilar & Martín, 2000; Viseras et al., 2005; García-Aguilar & Palmqvist, 2011; García-Aguilar et al., 2014). The Baza and Guadix depression includes two different depocenters: the Guadix Basin, in the SW sector, and the Baza Basin, in the NE one (García-Aguilar et al., 2014). The continental infilling consists of a ca. 600 m-thick continuous succession and has been historically divided into three formations (with different facies that change laterally): (i) the Guadix Formation, which includes alluvial-fluvial sediments (Guadix Basin); (ii) the Gorafe-Huélago Formation, formed by carbonate lacustrine sediments (Guadix Basin); and (iii) the Baza Formation, consisting of lacustrine limestones, marls and gypsum (Baza Basin) (Vera, 1970).

The badlands landscape visible nowadays in the sedimentary depression is the

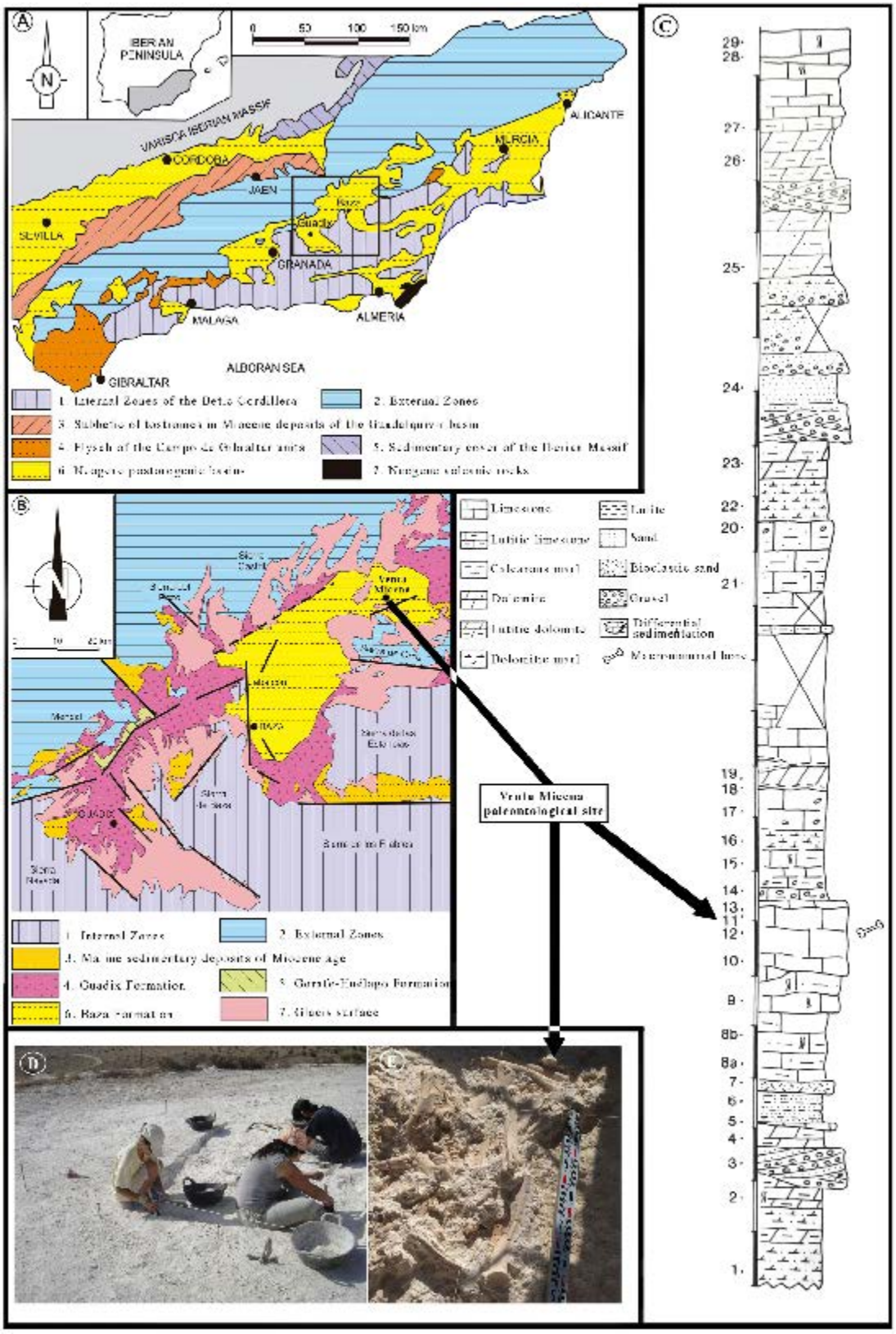

Figure 3.14.1 – **A**: Geographic and Geologic map of the Betic Chain (from García-Aguilar et al., 2014); **B**: Geologic map of the Baza and Guadix Basin (from García Aguilar et al., 2014); **C**: stratigraphic series of Venta Micena (from Anadón et al., 1987); **D**: excavation at Venta Micena during the 2005 season; and **E**: Detail of the excavation during the 2005 season.

result of an intense erosion that took place after the capture hydrographic network of the Baza Basin by a tributary of the Guadalquivir River (the Guadiana Menor River) during latest Middle Pleistocene times (García-Tortosa et al., 2008).

All the formations of the Baza and Guadix Depression preserve abundant Plio-Pleistocene paleontological assemblages (Martínez-Navarro, 1992; Arribas & Palmqvist, 1998; Palmqvist et al., 2005; 2011; Martínez-Navarro et al., 1997; 2010, 2014; Ros-Montoya, 2010; Espigares, 2010; Oms et al., 2000; 2011; Espigares et al. 2013). Vera et al. (1985) recognized three members within the Baza Formation, composed, from bottom to top, of : (i) limestones with lignite clay intercalations; (ii) a "red detrital member", with fluvio-alluvial plain mudstones; and (iii) limestones and carbonate silts precipitated in shallow lacustrine context with local fluvial contributions (Oms et al., 2000). The Early Pleistocene site of Venta Micena is located at the bottom of the uppermost member. Its local stratigraphy (Fig. 3.14.1) consists of six units in a 20-m-thick section of calcareous sediments (for further details of these units, see Anadón et al.,1987; Turq et al., 1996). This faunal assemblage is typical of the *Allophaiomys pliocaenicus* (=*A. ruffoi*) zone (MmQ2 biozone: Agustí et al. 1986), biochronologically placed in between the older Georgian site of Dmanisi, and the younger Italian site of Pirro Nord.

3.14.3. Systematic Paleontology

Order **Carnivora** Bowditch, 1821.

Family **Canidae** Fischer, 1817.

Subfamily **Caninae** Fischer, 1817.

Tribe **Canini** Fischer, 1817.

Genus ***Canis*** Linnaeus, 1758.

Canis* nov. sp. ex gr. *C. mosbachensis

Figs. 3.14.2 and 3.14.3

1986 *Canis etruscus mosbachensis*: Agustí et al.

1986 *Cuon priscus*: Agustí et al.

1987 *Canis etruscus mosbachensis*: Pons-Moyà

1987 *Cuon priscus*: Pons-Moyà

1992 *Canis etruscus:* Martínez-Navarro

1993 *Canis* aff. *arnensis*: Rook

1996 *Canis* cf. *arnensis*: Rook & Torre

2002 *Canis mosbachensis*: Martínez-Navarro, 2002.

2010 *Canis mosbachensis*: Boudadi-Maligne, 2010.

2011 *Canis mosbachensis*: Brugal & Boudadi-Maligne

2012 *Canis mosbachensis*: Ros-Montoya et al.

2014 *Canis mosbachensis*: Madurell-Malapeira et al.

Diagnosis. Medium-sized canid; M1 paracone higher and enlarged compared to the metacone; strong and lobed buccal cingulum; large M1 protocone and crest-like metaconule; M2 hypocone reduced; p3 alveolus lower than those of p2 and p4 on the alveolar plane of the mandible; short-crowned lower premolars; buccolingually compressed m1; m1 metaconid reduced; sinuous crista transversa connecting hypoconid and entoconid; m1 entoconid reduced; m2 metaconid reduced compared to the development of the protoconid and hypoconid.

Holotype. VM-2253, right hemimandible with p4-m2.

Lectotypes. VM-2258, maxillary fragment with P4-M2; and VM-4109, right M1 and M2.

Referred specimens. Cranial fragments. VM-2258, maxillary fragment with P4-M2; VM-2260, maxillary fragment with P4-M2; VM-2262, maxillary fragment with M1-M2; VM-10308, maxillary fragment with M1-M2;

Upper teeth. VM-10375, right I2; VM-10405, left I2; VM-10378, right I3; VM-10479, left I3; VM-10376, left P2; VM-10498, right P2; VM-10488, right P3; VM-10379, right P4; VM-10467, left P4; VM-10480, left P4; VM-10494, left P4; VM-10495, left P4; VM-4109_1, right M1; VM-10408c, left M1; VM-10466, left M1;

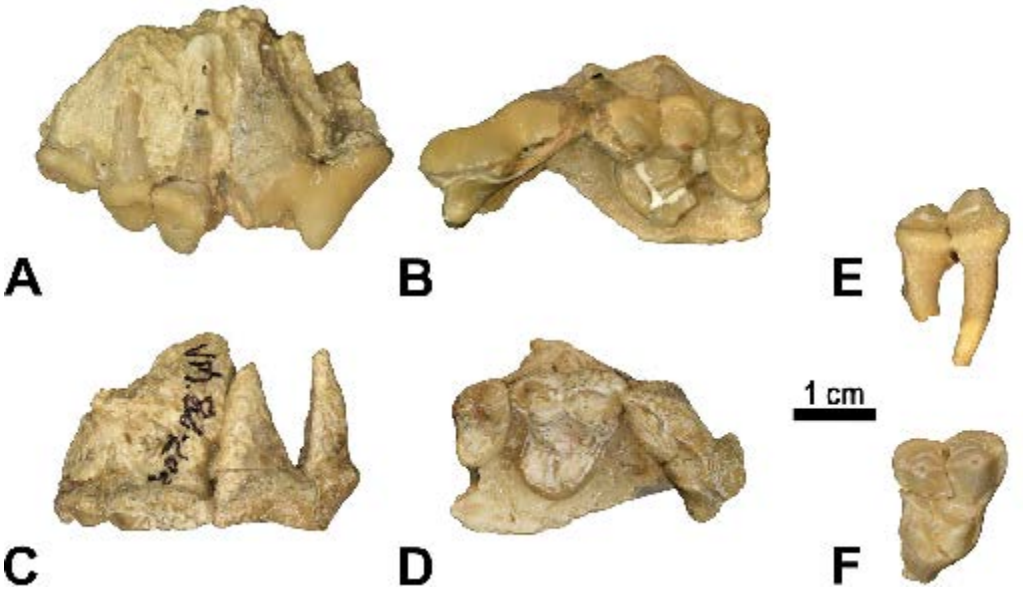

Figure 3.14.2 – *Canis* sp. nov. from Venta Micena. **A-B**: **VM-2258**, right maxillary fragment with P4-M2, in buccal (**A**) and occlusal (**B**) views. **C-D**: **VM-2260**, right maxillary fragment with P4-M2, in buccal (**C**) and occlusal (**D**) views. **E-F**, **VM-4109**, left M1, in buccal (**E**) and occlusal (**F**) views.

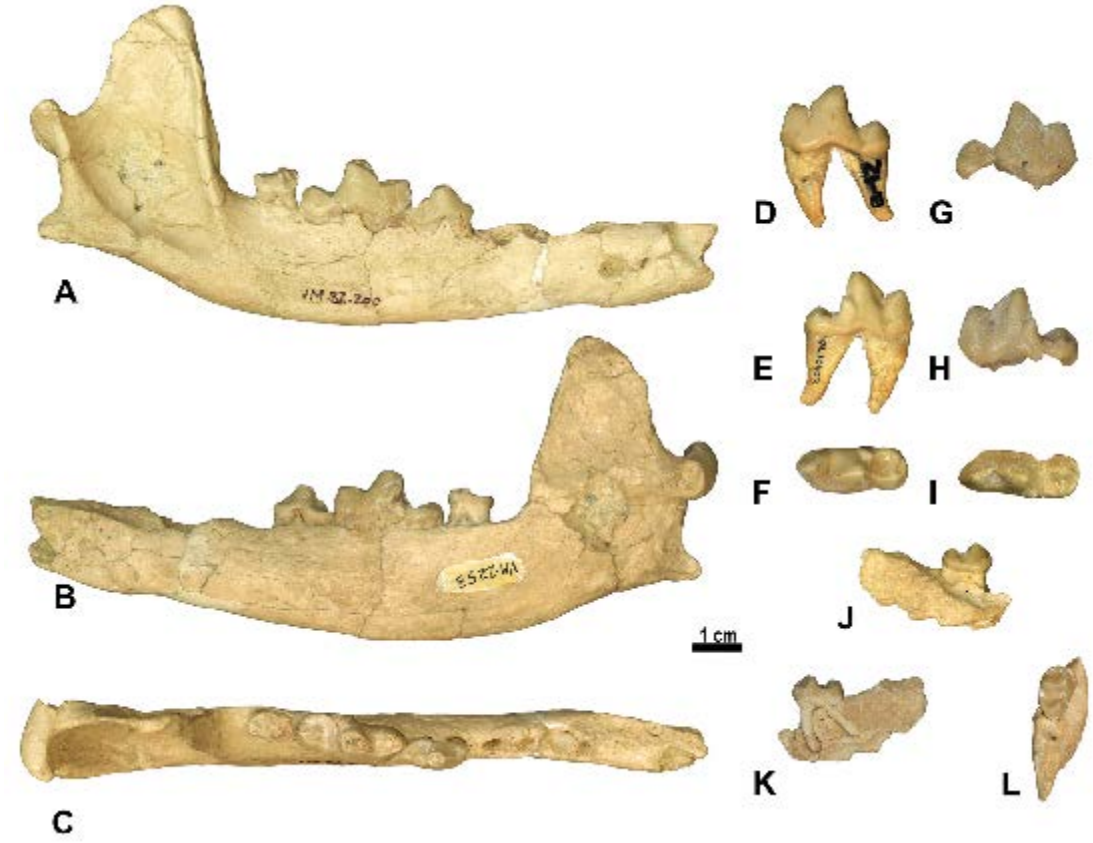

Figure 3.14.3 – *Canis* sp. nov. from Venta Micena. **A-C**: **VM-2253**, right hemimandible with p4-m2, in buccal (**A**), lingual (**B**) and occlusal (**C**) views. **D-F**: **VM-10403**, left m1, in buccal (**D**), lingual (**E**) and occlusal (**F**) views. **G-I**, **VM-10404**, left M1, in buccal (**G**), lingual (**H**) and occlusal (**I**) views. **J-L**: **VM-10408**, right hemimandible fragment, in buccal (**J**), lingual (**K**) and occlusal (**L**) views.

VM-10470, left M1; VM-4109_2, right M2; VM-4585, left M2; VM-10382, left M2; VM-10497, left M2;

Mandible. VM-2253, right hemimandible with p4-m2; VM-2254, right hemimandible with m2; VM-10408a, hemimandible with m2; VM-13295_4, right hemimandible;

Lower dentition. VM-10390, right i1; VM-10391, left i1; VM-10361, left i2; VM-10388, left i2; VM-10483, right p1; VM-10484, left p1; VM-10360, left p2; VM-10485, right p2; VM-10468, left p4; VM-13295_1, right p4; VM-9322, right m1; VM-10403, left m1; VM-10404, left m1; VM-13295_2, left m1; VM-13306, right m1; VM-4440_1, right m2; VM-4440_2, right m2; VM-10406, left m2; VM-10408d, right m2; VM-13295_3, right m2.

Description. *Upper dentition*. The I1 and I2 have two small basal cuspules, one on each side of the main cusp. The I3 is caniniform, with no accessory cuspulids and shows a well-developed distobuccal cingulum. The upper canine is flattened buccolingually, with an oval outline in occlusal view. The P1 is single-rooted, with a conical crown. The P2 has no accessory cuspules. The P3 is similar in morphology to the P2, but shows a single accessory cusp. The P4 has a reduced protocone, poorly expanded lingually and rather close to the paracone. The latter is well-developed and stout. The cingulum extends on the distolingual part of the tooth. Of the buccal cusps of M1, the paracone is larger and higher than the metacone. The protocone is well-developed, prominent and individualized. No protoconule is present. The postprotocrista is shallow and connects the protocone directly to the distal cingulum, as the metaconule is reduced to a shallow crista. The hypocone is prominent and rather individualized from the lingual cingulum. The trigon basin is wider and deeper than the talon basin. The latter is shallow and well-developed. The M2 is smaller than the M1, but similar in occlusal morphology. It is buccolingually elongated. The M2 paracone is larger than the metacone, the protocone is well-developed and the hypocone is cingular. The cingulum is well-

developed (Fig. 3.14.2).

Mandible. The corpus is low and slender, with a curved ventral border and a slightly arched toothrow with labial convexity, in dorsal view. When observed in lateral view, the ramus is high and forms a right angle with the corpus. On the lateral side of the mandible, the masseteric fossa is deep and broad. VM-2253 is the best-preserved hemimandible and may belong to an adult individual not displaying the p1 and m3 alveoli (though the former seems to be reabsorbed after the tooth was lost during life). The condyloid process is developed and medially inclined (Fig. 3.14.3).

Lower dentition. The incisors are flattened buccolingually, with a single distal accessory cuspulid. The p1 is single-rooted and single-cusped. The p2 is elongated mesiodistally, with a slightly enlarged distolingual portion and a small distal accessory cuspulid on the distal cingulid. The p3 is similar to the p2 but mesiodistally larger. It has a high protoconid and a small cuspulid on the distal cingulid. The p4 is mesiodistally larger than the p3, being elongated mesiodistally with the distolingual portion slightly inflated. It has two well-developed accessory cuspulids, individualized from the distal cingulid. A small cuspulid is evident on the mesiolingual cingulid. The m1 paraconid is well-developed and higher compared to the p4 protoconid, if observed in buccal view. The mesial margin of the paraconid is inclined distally. The m1 has a high and distally inclined protoconid as well as a smaller mesial paraconid. The metaconid is reduced but rather individualized from the protoconid. Its tip is pointed distally, especially in VM-10403. Regarding talonid cuspids, the hypoconid is the larger compared to the entoconid. There is a prominent transverse cristid between both cuspids, with a prominent sinuous outline in occlusal view. The talonid basin is deep, although it is small and closed lingually by a cristid-like entoconulid. Mesially to this cuspulid, there is a shallow cristid that develops to the distal side of the metaconid. The mesial margin of the hypoconid shows a crest. A small accessory tubercle is present on the distobuccal wall of the protoconid. The distal portion of the lower carnassial generally shows

a variably developed cristid-like cingulid, which separates a shallow space between the hypoconid and the entoconid. A distobuccal cingulid is present. VM-10403 also possess a mesiolingual cingulid. The m2 has an almost oval shape, in occlusal view. The mesiobuccal cingulid is markedly enlarged, especially compared to the distal portion of the tooth. The m2 possesses two mesial cuspids, a large and stout protoconid and a smaller metaconid. Distally, the well-developed hypoconid is the only cuspid of the talonid. The protoconid is generally higher than the other two cuspids. A high cristid bounds the distolingual margin of the tooth, enclosing the well-developed talonid basin (Fig. 3.14.3).

3.14.4. Results

3.14.4.1. Comparisons with C. arnensis *and* C. etruscus *from Italy*

The general size and tooth morphology are close to *C. arnensis* (and C. *mosbachensis*) but smaller than *C. etruscus* (see Figs. 3.14.4 and 3.14.5). In upper teeth morphology, *Canis* sp. from Venta Micena differs from the type sample of *C. arnensis* from Il Tasso and that of Poggio Rosso (Bartolini Lucenti & Rook, 2016) as well as from that of *C. etruscus* from Olivola, Upper Valdarno and Pantalla (Cherin et al., 2014) in several features, such as: the P4 protocone is reduced in lingual development and does not possess a sharp-pointed cusp, unlike *C. arnensis* and *C. etruscus*. In *Canis* sp. from Venta Micena, the M1 paracone is considerably larger than the metacone unlike *C. arnensis* where the cusps are of similar size, but also *C. etruscus* in which the difference is reduced. In the latter, the molars are elongated buccolingually in occlusal view, whereas in *Canis* sp. from Venta Micena they do not and show a marked distolingual curvature. The trigon basin in the M1 of *Canis* sp. from Venta Micena is deeper than the talon one, whereas these basins have equal depth in both *C. etruscus* and *C. arnensis* (Fig. 3.14.5), and the talon basin does not tend to reduction as in *Canis* sp. from Venta Micena. Moreover, the M2 of *C. etruscus* is mesiobuccally enlarged compared to the more slender morphology of *Canis* sp. from Venta Micena in occlusal view. Additionally, *Canis* sp. from Venta

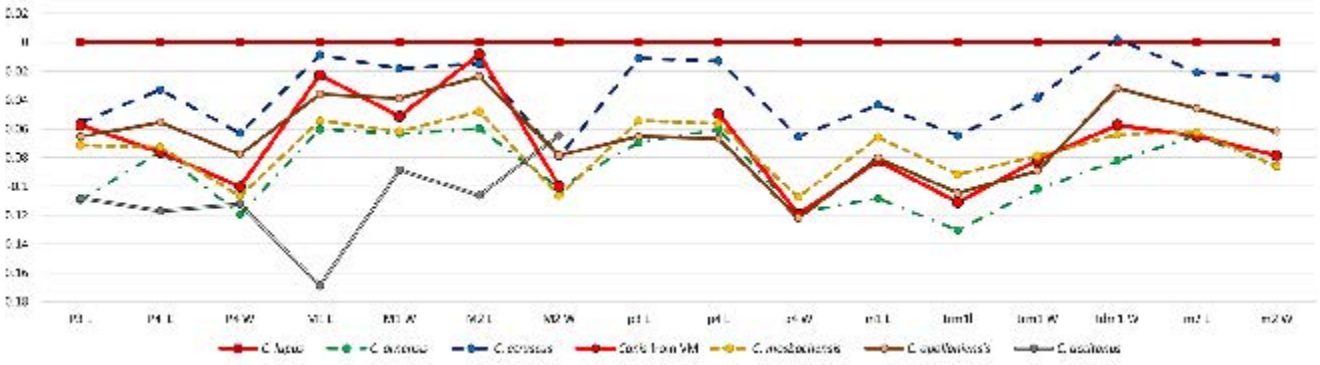

Figure 3.14.4 – Log-ratio diagram based on selected dental variables in the described material as well as in other Early Pleistocene species of *Canis* (*C. etruscus*, *C. arnensis*, *C. mosbachensis*, *C. apolloniensis*, *C. accitanus*, data taken from the literature: Sotnikova, 2001; Garrido and Arribas, 2008; Martínez-Navarro et al., 2009; Petrucci et al., 2013) as compared to extant *C. lupus* (used as the reference baseline).

Micena lacks other peculiar features of *C. arnensis* from Il Tasso and Poggio Rosso, and of *C. etruscus* from Olivola, Upper Valdarno and Pantalla, like *e.g.*, the well-developed metaconid of m1, generally lingually displaced; the strongly developed P4 protocone and the absence of cuspulids on the lingual margin of m1 of *C. etruscus*; as well as the reduced difference between the hypoconid and entoconid of m1 and the presence of accessory cuspids on the lingual side of m2 of *C. arnensis*.

3.14.4.2. Comparisons with C. etruscus *and* C. accitanus *from Fonelas P1 and* Canis *from Dmanisi*

As noted above, two small-to-medium-sized *Canis* species have been described in the Spanish site of Fonelas P1: *Canis etruscus* and the new species *C. accitanus* Garrido and Arribas, 2008. In comparison to *C. etruscus* of Fonelas P1, in addition to the above-mentioned differences, *Canis* sp. from Venta Micena shows a greater development of the M1 buccal cingulum and proportionally reduced M1 metacone, metaconule and M2 protocone. In the type specimen of *C. accitanus*, the development of the P4 protocone does not resemble that of *Canis* sp. from Venta Micena. In the former, it is large and expands lingually, whereas in the latter the protocone is less separated from the paracone, smaller and characterized by a blunt cusp. The cingula of the M1 (*i.e.*, the buccal and the mesial ones) in *C.*

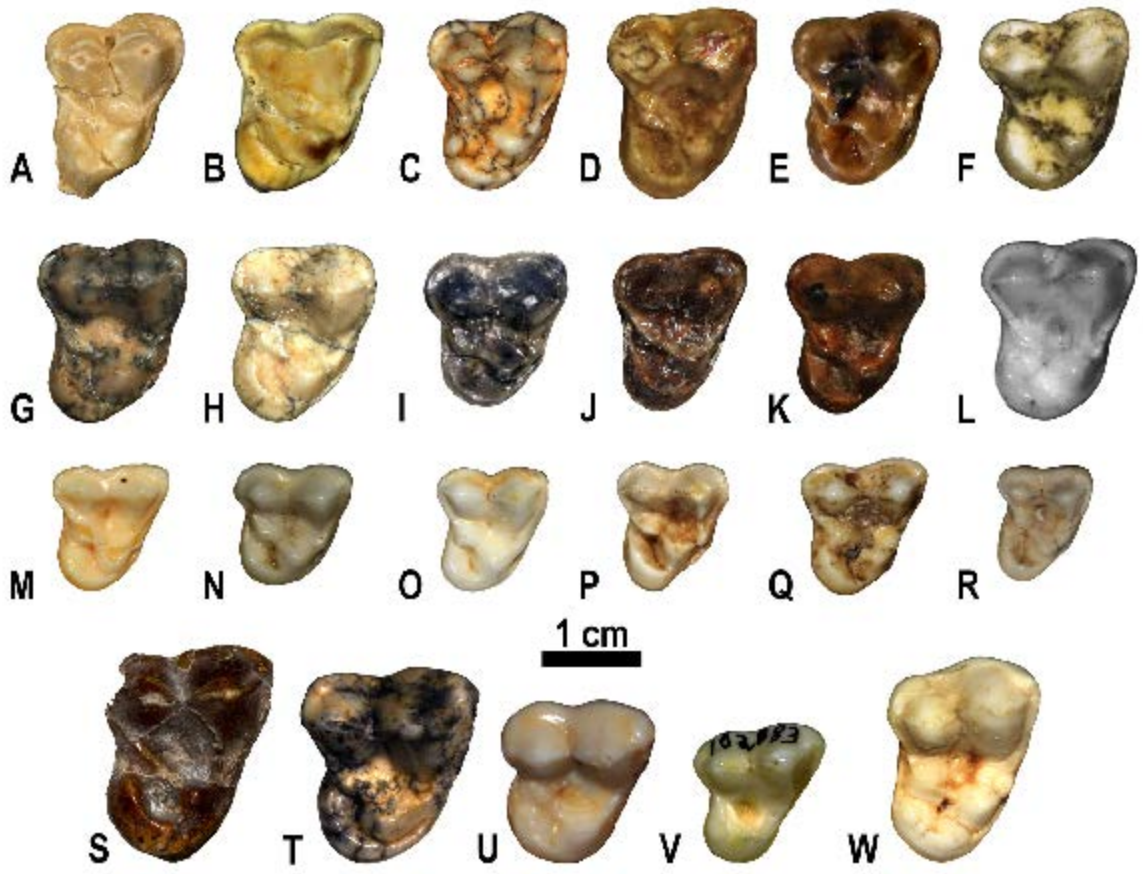

Figure 3.14.5 – **A**: **VM-2258**, *Canis* sp. nov. from Venta Micena; **B**: **EVT-6530**, *Canis mosbachensis* Soergel, 1925 from Vallparadís Section; **C**: **DE2 ac**, *Canis mosbachensis* Soergel, 1925 from Pirro Nord; **D**: **IGF 4407**, *Canis etruscus* Forsyth Major, 1877 from Olivola; **E**: **IGF 12867**, *Canis etruscus* Forsyth Major, 1877 from Matassino (Upper Valdarno); **F**: **D2314**, *Canis etruscus* Forsyth Major, 1877 from Dmanisi; **G**: **APL-16**, *Canis apolloniensis* Koufos and Kostopoulos, 1997 from Apollonia-1; **H**: **APL-254**, *Canis apolloniensis* Koufos and Kostopoulos, 1997 from Apollonia-1; **I**: **IGF 7919V**, *Canis arnesis* Del Campana, 1913 from Poggio Rosso; **J**: **IGF 867**, *Canis arnesis* Del Campana, 1913 from the Upper Valdarno; **K**: **IGF 869**, *Canis arnesis* Del Campana, 1913 from the Upper Valdarno; **L**: **FP1-2001-0434**, *Canis accitanus* Garrido & Arribas, 2008 from Fonelas P-1 (from Garrido & Arribas, 2008); **M**: **AMNH-52049**, *Lupulella adusta* (Sundevall, 1847) from Zaire; **N**: **MZUF-1898**, *Lupulella mesomelas* (Schreber, 1775) from Ethiopia; **O**, **MZUF-1851**, *Canis* "*aureus*" Linnaeus, 1758 from Somalia; **P**: **MZUF-11879**, *Canis aureus* Linnaeus, 1758 from Dalmatia; **Q**: **CE-818**, *Canis simensis* Rüppell, 1840 from Ethiopia; **R**: **MZUF-418**, *Canis latrans* Say, 1823 from Mexico; **S**: **IGF 883**, *Lycaon falconeri* (Forsyth Major 1877) from the Upper Valdarno; **T**: **PP 186**, *Lycaon lycaonoides* (Kretzoi, 1938) from Pirro Nord; **U**: **AMNH-82082**, *Lycaon pictus* (Temminck, 1820) from Kenia; **V**: **AMNH-102083**, *Cuon alpinus* (Pallas, 1811) from Java; **W**: **MZUF-11874**, *Canis lupus* Linnaeus, 1758 from Italy.

accitanus are poorly developed compared to those of *Canis* sp. from Venta Micena. The former also shows an evident protoconule and a tubercular metaconule, in contrast to the features of the sample from Venta Micena. The M2 of *C. accitanus* possesses similarly sized buccal cusps, whereas *Canis* sp. from Venta Micena shows a markedly enlarged M2 paracone in comparison to the metacone. The buccal cingulum of *Canis* sp. from Venta Micena is continuous along the buccal side of the M2. In contrast, in *C. accitanus* it girdles the buccal cusps and forms a feeble yet visible notch between them. Fonelas P1 is roughly coeval to the site of Dmanisi, which preserves one of the most remarkable records of *C.* "*etruscus*". Compared to *Canis* sp. from Venta Micena, this sample shares also the differences above-mentioned, although it also shows some similarities. In the upper teeth, the P4 protocone is reduced, the M1 buccal cingulum is more developed compared to *C. etruscus* of Fonelas P1 and Italy, the M1 metaconule is reduced although still tubercular, rather than crest-like as in *Canis* sp. from Venta Micena. Of the features of the lower teeth that resemble *Canis* sp. from Venta Micena, the most prominent are the short morphology of lower premolar in buccal view, the reduction of the m1 metaconid compared to *C. arnensis* and *C. etruscus* from Fonelas P1 and the Italian sites, and the sinuous transverse cristid connecting the hypocone and the entoconid.

3.14.4.3. Comparisons with latest Early Pleistocene C. mosbachensis *of Europe*

Numerous features suggest a close affinity to *C. mosbachensis* from Pirro Nord, Untermassfeld (see Sotnikova, 2001), Cueva Victoria and Vallparadís Section. For instance, the alveolus of the p3 sets lower level in the corpus of the mandible in comparison to those of p2 and p4. The morphology of the lower premolars resembles that of *C. mosbachensis*, with a mesiolingual stout expansion expanded and a low inclined mesial border (state 3 of character 61 described by Prevosti, 2010). *C. etruscus* from Olivola and Upper Valdarno and *C. arnensis* from Upper Valdarno differ greatly from these morphologies, *e.g.*, in showing a higher angle

of inclination of the premolar crown in lateral view (more similar to the condition of state 2 of character 61 in Prevosti, 2010). The lower carnassial testifies to this affinity to *C. mosbachensis*. For instance, the presence of a sinuous crest connecting the hypoconid and the entoconid of m1, or the metaconid separated from the protoconid but not projecting lingually. Other features are the depth of the M1 trigon basin, deeper than the talon basin or the M1 hypocone, and the protocone of similar height (see Fig. 3.14.5). These are all derived features commonly present in *C. mosbachensis*. Even the teeth proportions are suggestive of a close affinity to *C. mosbachensis* (see Fig. 3.14.4). In contrast to the latter, *Canis* sp. from Venta Micena does not possess the protoconule of the M1 and the metaconule is strongly reduced, crest-like in shape in occlusal view. This morphology bears resemblance with the condition seen in the M1 of the type specimen of the primitive hypercarnivorous canid *Lycaon falconeri* Forsyth Major, 1877.

The ratio between P4 L/M1-M2 L (CI) for *Canis* sp. from Venta Micena has an average of 86.2. This value contrasts with the mean values of other Villafranchian canids of western Europe, like *C. etruscus* (mean: 97.9), *C. arnensis* (mean: 99.1) and *C. mosbachensis* (mean: 97.1) as shown in Table 3.14.1.

3.14.4.4. Comparisons with C. apolloniensis

Compared to late Early Pleistocene species, *Canis* sp. from Venta Micena shows affinity to *C. apolloniensis* from Apollonia-1. Indeed, the morphology of the upper and lower teeth, as well as the mandible are close to the Greek canid, although some slight but significant differences might be pointed out. For instance, *C. apolloniensis* possesses more lingually elongated upper molars, in occlusal view, and the M1 trigon basin is proportionally larger compared to that of *Canis* sp. from Venta Micena. The metaconule is evidently cuspule-like in *C. apolloniensis*, as in *C. mosbachensis* from other European localities, whereas *Canis* sp. from Venta Micena has a crista-like M1 metaconule. The cingular hypocone of the M1 of *C. apolloniensis* is larger at its base and expands lingually, whereas in *Canis* sp. from

	Canis from VM	*C. mosbachensis*	*C. etruscus*	*C. arnensis*	*C. lupus*	*C. aureus*	*C. anthus*
min	85.9	94.7	94.8	93.4	91.3	81.6	76.8
max	86.5	110.6	103.7	105.4	119.0	92.5	97.2
mean	86.2	99.3	97.9	99.1	102.5	87.5	86.7
st. dev.	0.4	5.2	2.7	3.8	5.0	2.9	4.7
count	2	7	11	9	138	14	35

	C. anthus	*C. simensis*	*C. latrans*	*L. adusta*	*L. mesomelas*	*Ly. pictus*	*Cu. alpinus*
min	76.8	77.2	91.8	67.8	72.5	85.2	104.4
max	97.2	84.7	111.6	79.9	101.3	95.5	113.4
mean	86.7	81.2	98.3	75.1	93.0	90.6	108.7
st. dev.	4.7	2.1	6.5	2.9	5.8	3.0	4.5
count	35	8	13	52	29	14	3

Table 3.14.1. Resuming table of the P4 L/M1-M2 L in various species of extant and fossil Canidae.

Venta Micena it is stout and shorter, in buccolingual sense when observed in occlusal view. The m1 of *C. apolloniensis* is more compressed buccolingually and the entoconid is less reduced compared to the new Spanish species (Fig. 3.14.5).

3.14.4.5. Comparisons with Early Pleistocene canids from eastern Asia

Compared to the medium-sized *C. palmidens* from the type locality of Nihewan Basin and from the Yushe Basin, or to the large-sized *C. chihliensis* from Shanshenmiaozui (see Tong et al., 2012) and from the Yushe Basin, there are several differences that can be noticed. The P4 paracone of *Canis* sp. from Venta Micena is slender in buccal view, and the metastyle appears to be more elongated compared to the mesiodistally short one of *C. palmidens* and *C. chihliensis*. Particularly, the P4 of the latter species is considerably stouter and buccolingually large. Compared to *Canis* sp. from Venta Micena (and even more to *C. palmidens*), the P4 protocone of *C. chihliensis* is reduced and half fused to the paracone. The distolingual cingulum of the P4 is more prominent in *C. palmidens* from Nihewan and in *C. chihliensis* from Shanshenmiaozui and Yushe Basin in comparison to that of *Canis* sp. from Venta Micena. The occlusal outline of the M1 of *Canis* sp. from Venta Micena differs from that of *C. palmidens* from Nihewan and Yushe Basins and *C. chihliensis* from Shanshenmiaozui and Yushe Basin, as in the latter, it is buccolingually elongated, whereas in the former the tooth is proportionally shortened and more

distally arched. Unlike *Canis* sp. from Venta Micena, the M1 metaconule of *C. palmidens* from Nihewan and Yushe Basins is a prominent cuspule, connected to the large protocone by a sharp postprotocrista. The metaconule in *C. chihliensis* from Shanshenmiaozui is reduced but still cuspule-like, in contrast to *Canis* sp. from Venta Micena. On the contrary, *Canis* sp. from Venta Micena' morphology is similar to that of the specimen of *C. chihliensis* from Yushe Basin, where the metaconule is considerably reduced, close to the fossil *Lycaon* spp. The hypocone is more prominent in *Canis* sp. from Venta Micena than in *C. palmidens* and the trigon basin is deeper than the talon in the Spanish taxon compared to latter. In *C. chihliensis* the hypocone is greatly enlarged, compared to the two medium-sized taxa. The M2 is bean-shaped in *C. palmidens* from Nihewan and Yushe Basins, with a developed lingual lobe, whereas in *Canis* sp. from Venta Micena this portion is reduced in occlusal view. The notch on the distal side of the M2, visible in *C. palmidens*, is strongly reduced in *Canis* sp. from Venta Micena. In *C. chihliensis* from Yushe Basin, the M2 is buccolingually reduced with no distal notch. The lower carnassial of *C. palmidens* shows rather large metaconid and an entoconid slightly smaller compared to the hypoconid. *Canis* sp. from Venta Micena possesses a reduced metaconid, poorly individualized from the protoconid, although not as reduced as in *C. chihliensis* from Shanshenmiaozui. The entoconid of *Canis* sp. from Venta Micena is proportionally smaller than those of *C. chihliensis* and *C. palmidens*, and it is connected to the hypoconid with a prominently sinuous transverse cristid. Although also possessed by *C. chihliensis* from Shanshenmiaozui and *C. palmidens* from Nihewan and Yushe Basins, this cristid is generally straight. On the m2 of *Canis* sp. from Venta Micena, the entoconid is reduced, whereas it is developed in *C. palmidens* from Nihewan and Yushe Basins. *C. chihliensis* from Shanshenmiaozui has a conspicuously enlarged buccal cuspids on the m2, unlike the morphology possessed by *Canis* sp. from Venta Micena.

In comparison to the extensive record of the late Early-Middle Pleistocene *C. mosbachensis variabilis* from Zhoukoudian localities (Jiangzuo et al., 2018) some

differences can be listed. Whereas, the P4 paracone and metastyle are similar to those of *Canis* sp. from Venta Micena, the P4 protocone is generally larger and tend to be well separated from the paracone. In occlusal morphology, the sample of *C. m. variabilis* from Zhoukoudian possess a rather elongated lingually M1 resembling the condition of modern *C. lupus*, and unlike the specimens from Venta Micena. Other features of *C. m. variabilis* contrast with *Canis* sp. from Venta Micena, *e.g.*, the paracone circa two times the size of the metacone; the development of the metaconule, the large hypocone lobe. For the same reason, the sample of *C.* aff. *mosbachensis* from Ningyang differs from *Canis* sp. from Venta Micena. Other Asian samples are more similar to *Canis* sp. from Venta Micena, *e.g.*, those of *C. mosbachensis* of Gongwangling (see Jiangzuo et al., 2018). Nevertheless, as for the European *C. mosbachensis*, the M1 hypocone of *Canis* sp. from Venta Micena is more developed and the metaconule is crest-like compared to the morphology of the sample from Gongwangling. Even in lower teeth morphology, the sample of *C. m. variabilis* from Zhoukoudian and *C.* aff. *mosbachensis* fron Ningyang differ from *Canis* sp. from Venta Micena (see Jiangzuo et al., 2018). In the former Chinese taxa, the hypocone is considerably enlarged and tend to be centralized compared to the position of the cuspids of *Canis* sp. from Venta Micena. In the latter the entoconid is less reduced compared to *Canis* sp. from Venta Micena, and the crista transversa is straight instead of sinuous as in the Spanish taxon.

3.14.4.6. Paleoecology

Four out of 36 species of extant canids (the Eurasian and north American grey wolf, the African painted dog, the Indian dhole and the south American bush dog) are considered hypercarnivorous (*i.e.*, vertebrate meat constitutes >90% of their diet). The other canid species are more omnivorous and can be further subdivided in three dietary groups, although their trophic characterization is not as accurate: mesocarnivores (>50% of meat in diet, mostly from small vertebrates), hypocarnivores (small vertebrates represent <50% of diet, with variable proportions

of eggs, fruits, vegetal matter and insects making up the balance) and insectivores (>50% insects in diet).

According to Van Valkenburgh (1989; 1991) and Palmqvist et al. (1999; 2002), the trigonid blade of the lower carnassial (m1) is longer mesiodistally in hypercarnivorous canids and three of them (the dhole, hunting dog, and bush dog) share a trenchant heeled shape of the talonid , bearing a single, centrally-positioned blade-like hypoconid. *C. lupus* shows a moderately trenchant talonid, asymmetrically bicuspid, with a large, buccally positioned hypoconid and a lingually reduced entoconid. The functional significance of this condition is a lengthening of the effective cutting blade of the carnassial. Other dental modifications associated with hypercarnivory include the reduction of the metaconid of m1 and the reduction (in the m2) or complete loss of the last postcarnassial molar (the m3). In contrast, the two cusps of the talonid basin are subequal in size in the more omnivorous canids, their trigonid (lower carnassial blade) is proportionally shorter and the lower grinding area (*i.e.*, talonid basin of m1 and postcarnassial molars) is larger compared to that of hypercarnivorous species. For this reason, the ratio between the length of the trigonid divided by the length of the talonid and the second lower molar was used as a parameter allowing the investigation of the dietary adaptations of the fossil specimens analysed in this study. Moreover, given that efficient flesh-eating carnivorans use to have a deeper and shorter mandibular ramus compared to other carnivores (Figueirido et al., 2011), a second variable was estimated as the depth of the horizontal ramus, measured at the contact between m1 and m2, divided by mandibular length between the distal (posterior) border of the lower canine and the tip of the jaw condyle.

The combination of these morphometric indexes (Fig. 3.14.6) allows to discriminate between the hypercarnivorous canids, which show an enlarged trigonid blade in the lower carnassial and a more stoutly built mandible, and those species not specialized in hunting large prey. Although there is a substantial overlap between mesocarnivores and hypocarnivores, among omnivores show higher values in both

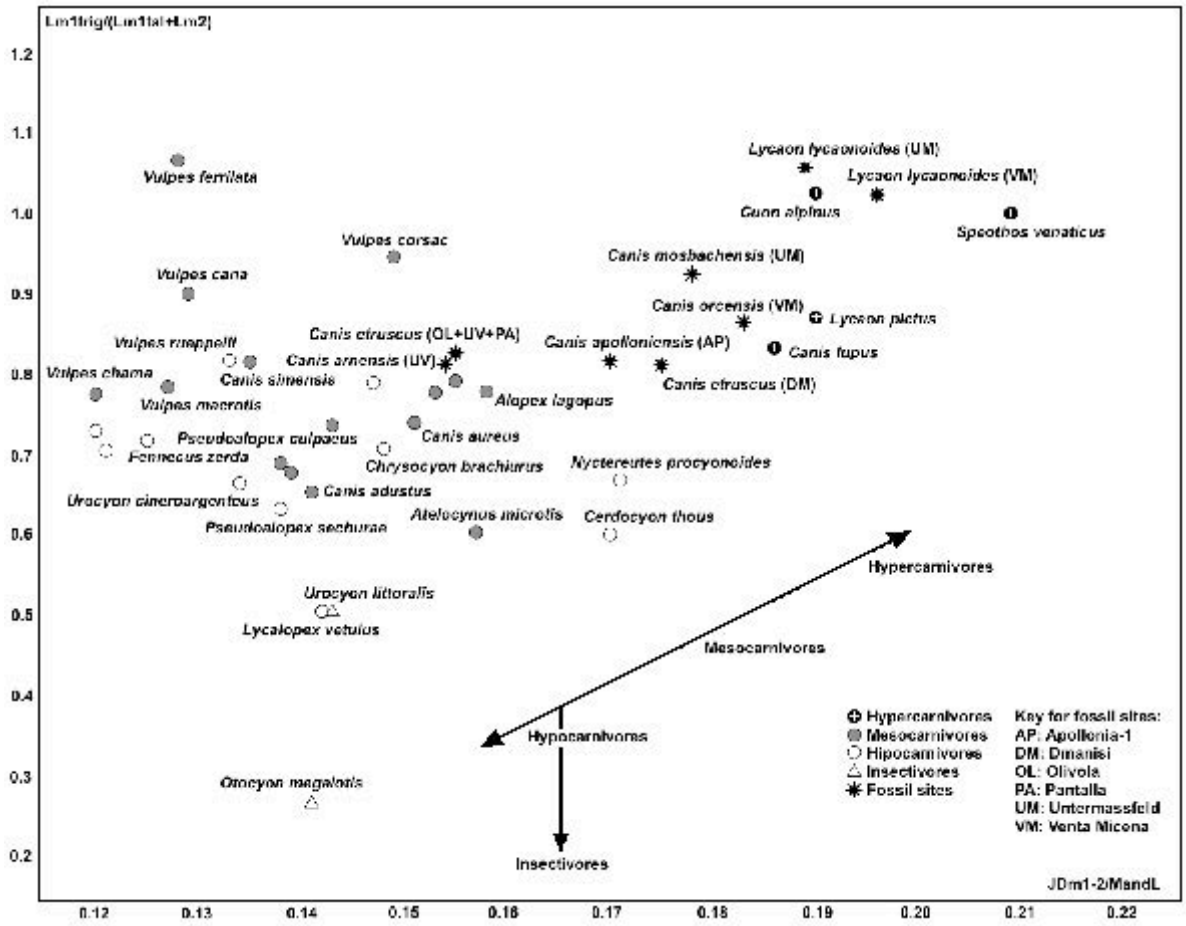

Figure 3.14.6 – Scatterplot for the extant canid species and selected Early Pleistocene specimens of *Canis* between the relative depth of the mandible (JDm1-2/MandL, X-axis), calculated as the depth of the horizontal ramus at the m1-m2 contact divided by mandibular length between the distal border of the lower canine and the tip of the jaw condyle, and the relative length of the carnassial blade (Lm1trig/(Lm1tal+Lm2), Y-axis), estimated as the ratio between the length of the m1 trigonid and the length of the m1 talonid plus the length of second lower molar.

indexes in most cases, and the two truly insectivorous species show a comparatively reduced trigonid in the carnassial. Concerning the fossil specimens, *Canis* sp. from Venta Micena from Venta Micena and *C. mosbachensis* from Untermassfeld show values closer to the hypercarnivores than those of other extinct forms, for both indexes. Moreover, *C. apolloniensis* from Apollonia and *C. etruscus* from Dmanisi show values that lie halfway between the mesocarnivores and the hypercarnivores, while *C. arnensis* from Upper Valdarno and *C. etruscus* from Olivola, Upper Valdarno and Pantalla take values close to the mesocarnivores. These results indicate that although there is substantial variability among the Early Pleistocene medium-sized canids, the canid from Venta Micena probably consumed a greater percentage of

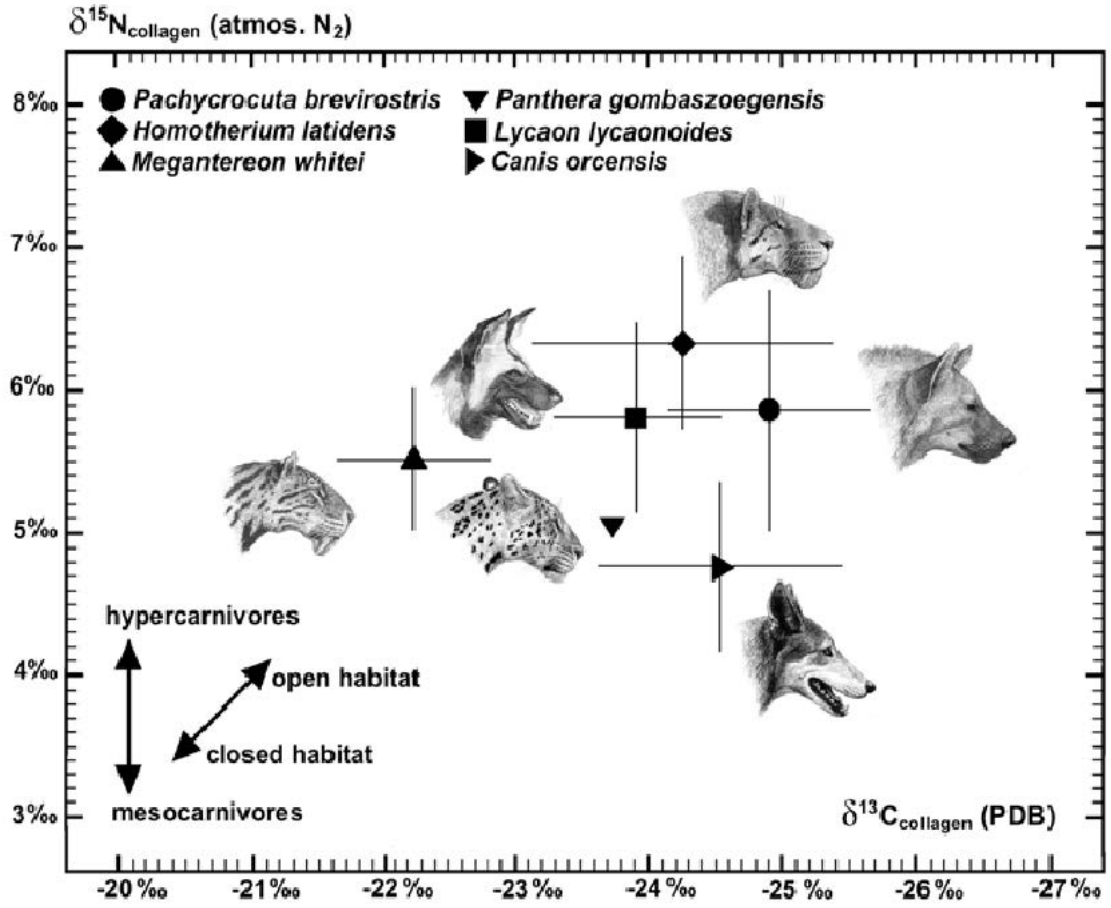

Figure 3.14.7 – Isotopic data ($\delta^{13}C$ values, X- axis; $\delta^{15}N$ values, Y-axis) measured in samples of bone collagen from the carnivorous species identified in the Early Pleistocene site of Venta Micena. The symbols indicate the species means and the lines represent one standard deviation below and above these means (data from Palmqvist et al., 2008).

vertebrate meat than the other fossil forms.

Moreover, isotopic data retrieved from bone collagen of the members of the carnivore guild from this site (Fig. 3.14.7) show that the $\delta^{15}N$ values of *Canis* sp. from Venta Micena are lower than those of the hypercarnivore *L. lycaonoides,* which suggests a lower consumption of ungulate prey, but close to the values of pantherine cat *P. gombaszoegensis* and, to a lesser extent, those of sabre-tooth *M. whitei.* This confirms that the medium-sized canid from Venta Micena had more hypercarnivorous dietary habits that other Early Pleistocene canids of similar size (except Untermassfeld) or the extant omnivorous species of this family.

3.14.5. Discussion and Conclusion

The taxonomy and systematics of the Early Pleistocene canids of Europe and Asia is a still much-debated topic. The middle/late Villafranchian faunal turnover, around 2.0 Ma, when the large canids became common in western Asia and Europe, is well-known from several Italian assemblages, especially those of Upper Valdarno, with the record of three species of large canids: *Lycaon falconeri*, *Canis etruscus* and *C. arnensis* (Forsyth-Major, 1877; Del Campana, 1913; Azzaroli, 1977, 1983).

The large-sized canid from Venta Micena, ca. 1.6 Ma, was interpreted by Martínez-Navarro and Rook (2003) as an evolved chrono-species than *Lycaon falconeri*, and it was ascribed to *L. lycaonoides*, similar therefore to later forms of this lineage, found in other numerous late Villafranchian and Epivillafranchian assemblages (Rook and Martínez-Navarro, 2010).

Similarly, the sample of *Canis* from Venta Micena possesses consistent differences with the first representatives of this genus in western Europe, *i.e.*, the Italian populations of *C. etruscus* and *C. arnensis* from the Upper Valdarno, Olivola and Il Tasso and Poggio Rosso. On the contrary, *Canis* sp. from Venta Micena shows a number of features (*e.g.*, the mesiodistally elongated lower carnassials, with a rather reduced metaconid and a sinuous crista transversa connecting the hypoconid and entoconid) resembling *C. etruscus* from Dmanisi and also some late Early Pleistocene taxa ex gr. *C. mosbachensis* (*e.g.*, *C. apolloniensis* from Apollonia-1, but particularly *C. mosbachensis* from Pirro Nord, Untermassfeld, Cueva Victoria and Vallparadís Section), as also noted by several author in literature (among others, Rook & Torre, 1996). Nevertheless, *Canis* sp. from Venta Micena possesses peculiarities that contrast with the typical *C. mosbachensis*, such as the strong reduction of the metaconule of M1 and the enlargement of the M1 paracone compared to the metacone. Most probably, *Canis* sp. From Venta Micena is a chrono-species that connects the earlier forms of small-to-medium-sized canids from the middle-late Villafranchian transition located at the Olivola and Tasso Faunal units to the posterior latest Late Villafranchian and Epivillafranchian *Canis*

mosbachensis in the European continent, and *Canis mosbachensis variabilis* from the late Early and Middle Pleistocene assemblages of eastern Asia (Jiangzuo et al., 2018)..

4. Conclusions

The numerous analyses performed in the present study attempted to improve the scientific knowledge on two important and fascinating groups of Carnivora: Canidae of the genera *Nyctereutes*, *Vulpes*, *Eucyon* and *Canis* and the enigmatic fossil representants of the tribe Lyncodontini (Mustelidae). In this last section, the records of the considered taxa are reinterpreted under the light of the results presented in the previous sections. Several questions still need to be answered and the use of digital imaging techniques and associated methodologies could help solving some of these issues in the next future.

4.1. The tribe Lyncodontini

The dispute on the taxonomy and relationship to and between Lyncodontini is still ongoing and harsh. The scantiness and incompleteness of the fossil record affects the interpretation and the fuels the confusion and disagreement. New and recent research, such as the first record of the African continent (Geraads, 2016) or the description of more complete cranial specimens of *Oriensictis* (Jiangzuo et al., 2019) testify to biogeographical dispersal events and paleoecological condition, previously undetected and probably underestimated. The revision of *Martellictis ardea* and the description of the rich sample from Monte Tuttavista (the most extensive record of Lyncodontini from insular context and, possibly of the whole Old World) attempts to shed new light on this interesting yet confused group. The nomenclature querelle, the coexistence of the peculiar and shared features, and a preliminary phylogeny on the genera of Lyncodontini support the erection of the genus *Martellictis* to include the taxon *M. ardea*, always difficult to relate with other Plio-Pleistocene taxa. Its record starts from the Slovakian site of Ivanovce (MN15, see Fejfar et al., 2012; Fig. 4.1). This small-sized mustelid was probably intermediate between a Eurasian badger and a beech-marten (Fig. 4.2) The other famous Lyncodontini *Pannonictis* appears in other European localities are those of

Etulia (Moldova) and Wölfersheim (Germany) more or less coeval to Ivanovce. Earlier records are come from the late Miocene *Hipparion* beds from China (Zdansky, 1927), but their attribution to *Pannonictis* remains doubtful (Fig. 4.1). During the Late Pliocene-Early Pleistocene, other taxa appeared in eastern Asia and Europe, such as *Eirictis* from Mongolia and China (Sotnikova et al., 2002; Qiu et al., 2004). These findings testify to the beginning of a radiation that reached its peak during the first half of the Early Pleistocene (see Fig. 4.1; García et al., 2008). Indeed, all the species of the tribe Lyncodontini known from literature appeared during the Gelasian and the early Calabrian, and became important elements of the continental faunas of the period. Among these taxa, *M. ardea* surely represented a common and widespread lyncodontine. Considering its unusual set of features, difficult to be recognized from fragmented fossils, the revision of fossil samples housed in the museum and institutions might reveal additional record of this species. Other important and renowned species are the widespread and large-sized *P. pliocaenica*, the smaller sized *P. pilgrimi* (both from Hungary) and *P. nestii* described from Italian and Spanish sites (*e.g.*, Upper Valdarno, Martelli,

Figure 4.1 – Updated chronological scheme of the known occurrences of Lyncodontini in the fossil record of the Old World. In red are reported those record resulting or modified by the results of the present study. Degree of inclination of locality names approximate the degree of uncertainty on their dating. Data from: Forsyth Major (1901); Martelli (1906); Pei (1934); Teilhard de Chardin & Leroy (1945); Schaub (1949); Villalta (1952); Viret (1954); Rabeder (1976); Jánossy (1986); Willemsen (1988); Ferrandini & Salotti (1995); Masseti (1995); Rook (1995); Burgio & Fiore (1997); Spassov (2000); Morlo & Kundrát (2001); Sotnikova et al. (2002); Abbazzi et al. (2004); Qiu et al. (2004); García & Howell (2008); García et al. (2008); Jin & Liu (2009); Ogino & Otsuka (2009); Colombero et al. (2012); Fejfar et al. (2012); Koufos (2014); Madurell-Malapeira et al. (2014); Geraads (2016); Jiangzuo et al. (2019). **Abbreviations** – **Atap. TE**, Atapuerca Trinchera Elefante (Spain); **B. Leon 5**: Barranco Leon 5 (Spain); **DA 2C**, Deutsch Altenburg 2C (Austria); **HBc**, *Hipparion* Bed (China); **JYc**, Jinyuan Cave (China); **LIV**, Livakkos (Greece); MT, Monte Tuttavista (Italy); **PLEt**, Perrier-Les Etouaires (France); **VLR**, Villarroya (Spain); **ZKD**, Zhoukoudian (China).

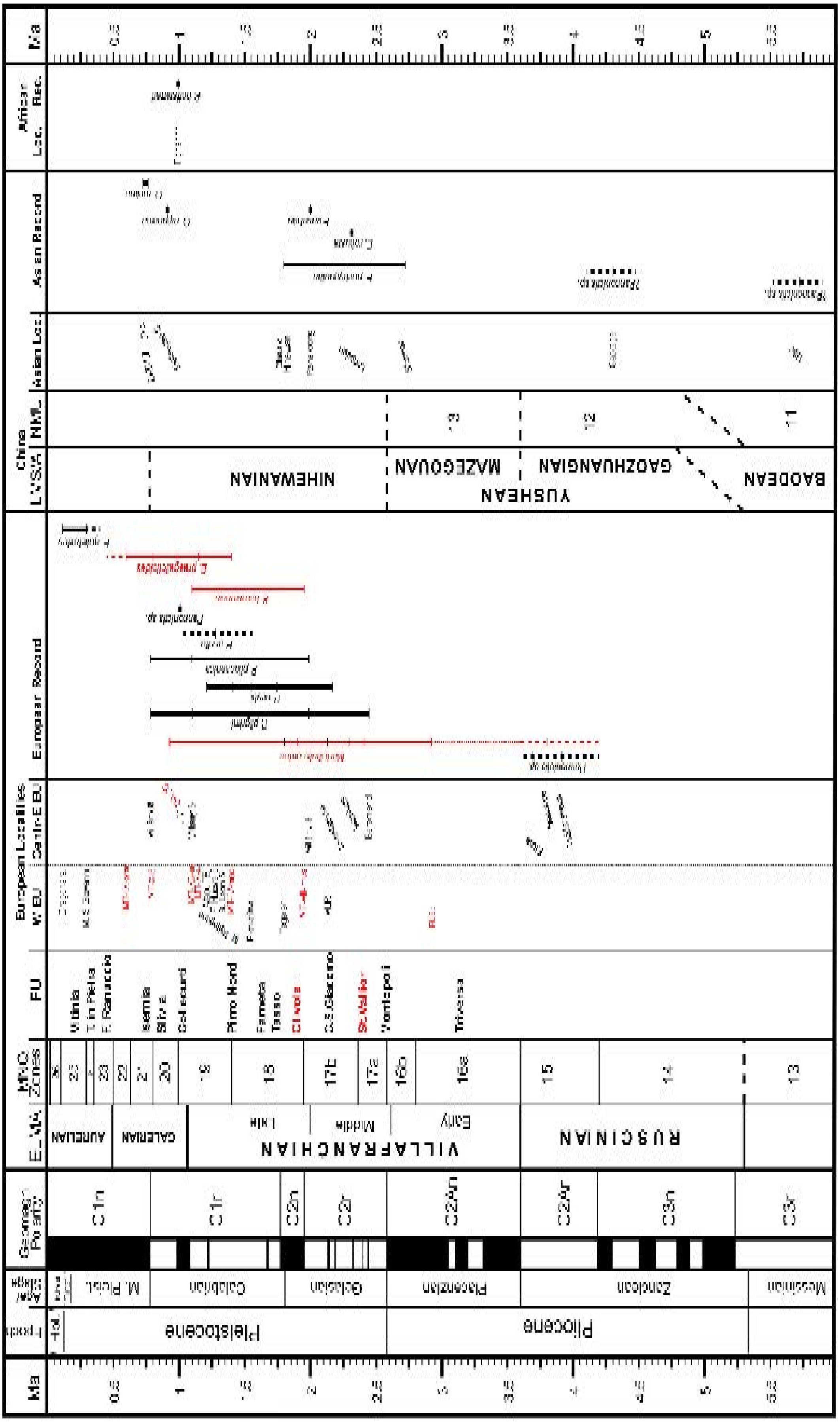
Ma
African Loc. Rec.
Asian Record
Asian Loc.
China NMU
LMS/A
NIHEWANIAN
MAZEGOUAN
GAOZHUANGIAN
YUSHEAN
BAODEAN
European Record
European Localities Centr-E EU
W EU
FU
MNQ Zones
E_MA
AURELIAN
GALERIAN
VILLAFRANCHIAN
Early
Middle
Late
RUSCINIAN
Geomag. Polarity
C1n
C1r
C2n
C2r
C2An
C2Ar
C3n
C3r
M. Pleist.
Calabrian
Gelasian
Piacenzian
Zanclean
Messinian
Pleistocene
Pliocene
Vitinia
Isernia
Pirro Nord
Triversa
Olivola
Costa S.Giacomo
Montopoli
St.Vallier

1906; and Sima del Elefante of Atapuerca, García & Howell, 2008). By the end of the Early Pleistocene, *Pannonictis* and *Martellictis* disappears from Europe as *Eirictis* in east Asia. The only African occurrence, *P. hoffstetteri* from Tighennif, "opens the hunt" to fossil members of the tribe in the African continent. The latest records of Lyncodontini in the Old World are those of the Sardinian and Corsican *E. galictoides*, surviving until late middle Pleistocene times. A number of fossil Lyncodontini in Eurasia are reported from insular context in the Early and middle Pleistocene. An interesting and still unclear record is that of the Sicilian *P. arzilla* (De Gregorio, 1886) from Monte Pellegrino (Sicily), dated to the Early Pleistocene. Several dentognathic similarities clearly suggest a relationship between this taxon and the other continental Lyncodontini. Most probably with the Italian *P. nestii* (see Rook, 1995). Nevertheless, Burgio & Fiore (1997) maintained the name *Mustelercta* as subgenus, stressing its distinction from the continental species. Further studies might clarify the taxonomical identity of this taxon in relation to the other Pleistocene circum-Mediterranean species. Recently Jiangzuo et al. (2019) included the genus *Oriensictis* under *Enhydrictis* on the basis of recently discovered cranium from Jinyuan cave (middle Pleistocene; Puwan, Danlian, China). The similarity between the Chinese skull and the Sardinian species are visible. Nonetheless, this grouping challenges the present hypotheses on the origin, radiation and dispersion of the clade of Lyncodontini without strongly supporting arguments or evidence of the intercontinental dispersion of these mustelids, or of their ancestors. Moreover, the dental differences between O. *nipponica* (the more primitive of the species of *Oriensictis*, see Ogino & Otsuka, 2008; Jiangzuo et al., 2019) and *Enhydrictis* (both *E. praegalictoides* and *E. galictoides*), could not be ruled out as interspecific variability. The cranial similarity might have resulted from convergency to similar environments and selective pressures. The lack of any record of *Enhydrictis*/*Oriensictis* out of their area of description (*i.e.*, Sardinia and eastern Asia) does not favor the inclusion of the latter genus in *Enhydrictis*.

Figure 4.2 – Reconstruction of *Martellictis ardea*. Recostructed shoulder height: ca 19 cm. Artwork made by Dr. Flavia Strani (Università di Roma).

Until new evidence from central Asia or eastern Europe are found, it seems more prudent to leave the genera separated.

Among the insular record of lyncodontines, the new taxa from the Early and middle Pleistocene deposits of Monte Tuttavista are relevant species in the panorama of Old-World Lyncodontini. The combined information obtained by the analysis of the extensive record of Monte Tuttavista and the specimens from Monte S. Giovanni suggest that *Enhydrictis* was a genus of medium-sized mustelids, approximately close in size to a modern Eurasian badger, probably larger than the modern greater grison (*G. vittata*). *E. praegalictoides* (Fig. 4.3) was slightly smaller compared to *E. galictoides*, but their appearances should have been similar one another. The scarcity of *P. baroniensis* in the fossil record of Monte Tuttavista, especially in comparison to *E. praegalictoides*, complicates the reconstruction of the possible affinities with other taxa. Particularly regarding its most probable continental ancestor. Further studies, centered on the whole sample of Lyncodontini from Monte Tuttavista, would help clarifying the patterns of colonization and dispersion of their lyncodontine ancestors in the Mediterranean islands, and across the Old World. The relationship between Old World and New World lyncodontines, the arise of the extant species and the cause of the extinction of the Eurasian and African representative of the tribe are some of the issues that remain open for further research. These questions could be answered only taking

Figure 4.3 – Reconstruction of the life appearance of *Enhydrictis praegalictoides*. Artwork made by Dr. Flavia Strani (Università di Roma).

into consideration the extensive record of this enigmatic group of mustelids at a global scale.

4.2. The genus *Nyctereutes*

The genus *Nyctereutes* appeared at the beginning of the Pliocene in eastern Asia, probably as the result of the burst of radiation of Canidae after their dispersal from the American continent by the end of the Miocene (Tedford & Qiu, 1991; Wang & Tedford, 2008). During the Late Pliocene and the Early Pleistocene (Gelasian), the genus reached its greatest diversity (Fig. 4.4). The western expansion towards Africa and Europe is rather early in the history of the genus, as in Spain *N. donnezani* is recorded in the site of La Gloria 4 (ca 4.2 Ma) and *N. barryi* in Laetoli (Tanzania; 3.7-3.6 Ma). Both these species, as the earlier *N. tingi*, are primitive taxa (*i.e.*, lacking the dentognathic features possessed by modern *N. procyonoides* and adapted to hypocarnivory). These mesocarnivorous species persisted in the Old World until 3 Ma and then disappeared (Fig. 4.4). In literature, the commonly known derived species (*i.e.*, possessing dentognathic features specialized to hypocarnivory like *N. procyonoides*) are the Chinese *N. sinensis* and the European *N. megamastoides* and *N. vulpinus*. Their certain appearance in the fossil record is around 4.0 Ma for *N. sinensis* in the Yushe Basin and S. Giusto for *N. megamastoides* (Tedford & Qiu, 1991; section 3.3.; Fig. 4.4). *N. vulpinus* appears during the Gelasian, in St. Vallier and in La Puebla de Valverde (Fig. 4.4). At present it is only known from these localities. The arrival of the derived *N. megamastoides* in Europe apparently replaced the other primitive species, unlike *N. sinensis* that co-occurred with *N. tingi* in the Yushe Basin. The analysis of the sample from Layna (Early Pliocene, Spain), historically attributed to *N. donnezani* (Soria & Aguirre, 1976), suggest a different hypothesis. Along with the most complete cranium of *N. donnezani* (MNCN-63662), some specimens do not show the diagnostic features of this species and do not even fit in its morphological and morphometric variability.

The comparisons of these fossils to other Eurasia taxa show an evident affinity to the derived species *N. megamastoides*. Considered the early age of Layna, this record predates the first occurrence of this species of ca 700 ka. It is, therefore, preferable to referred the specimens to *N.* cf. *megamastoides*. Nevertheless, this record represents the earliest appearance of a derived species in western Europe and the only case of coexistence of two distinct taxa of *Nyctereutes* (one primitive and the one derived) in the European fossil record. Clearly, the discovery of *N.* cf. *megamastoides* in Layna affects the present hypotheses concerning the origin of derived species of raccoon dogs across the Old World and has implication on our understanding of the pattern of evolution and dispersal of these species around the Old World. The early occurrence of taxa with dental morphologies and proportion close to those of derived taxa in the late Early Pliocene of western Eurasia is confirmed by the record of Çalta (Turkey; ca 4 Ma, see Fig. 4.4). The revision of this sample, ascribed to *N. donnezani*, with the support the first phylogenetic analysis that consider the fossil species of *Nyctereutes*, points out the peculiar nature of the Turkish raccoon dog. Instead of clustering with primitive species (*e.g.*, *N. tingi, N. donnezani* and *N. barryi*), the *Nyctereutes* from Çalta groups with the most derived species *N. abdeslami*, *N. megamastoides* and the extant *N. procyonoides*. The results urge a redescription of the sample and support the erection of a new species, considering the unusual and mosaic pattern of primitive-like and derived

Figure 4.4 – Updated chronological scheme of the known occurrences of *Nyctereutes* spp. in the fossil record of the Old World. In red are reported those record resulting or modified by the results of the present study. Degree of inclination of locality names approximate the degree of uncertainty on their datings. Data from literature are those of Fig. 1.9. **Abbreviations** – **AaO**, Ahl al Oughlam (Morocco); **CDP**, Collepardo (Italy); **Chikoian FC**, Chikoian Faunal Complex (Mongolia, Russia); **ELFN**, Elandfontein (South Africa); **LPVv**, La Puebla de Valverde (Spain); **Laetoli UB**, Laetoli Upper Beds (Tanzania); **MEL**, Megalo Emvolon (Greece); **PLEt**, Perrier-Les Etouaires (France); **Tabun C**, Tabun Cave (State of Palestine); **VLR**, Villarroya (Spain); **ZKD**, Zhoukoudian (China).

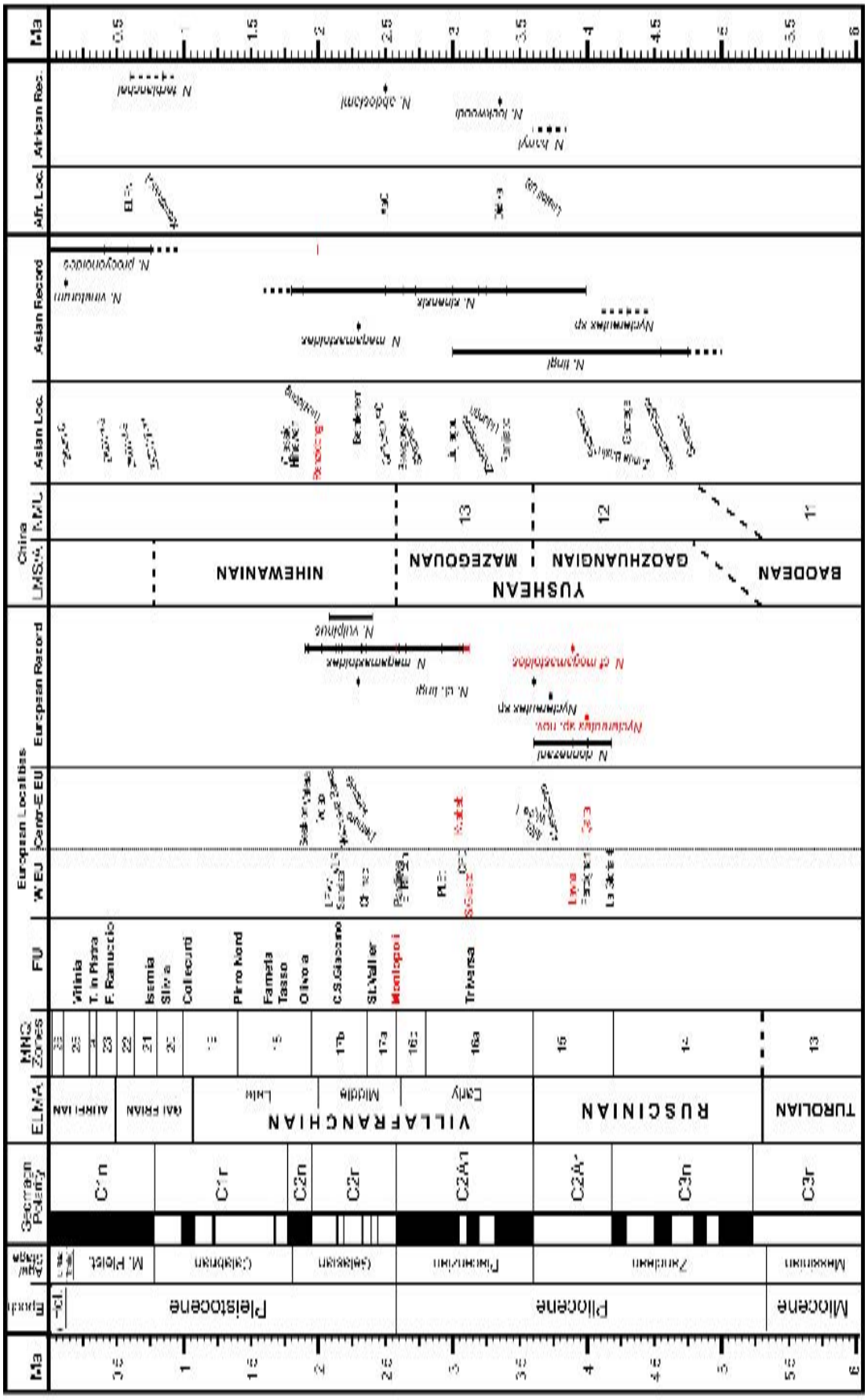

dentognathic features (*e.g.*, poor development of a subangular lobe but enlarged crushing surface of the molars). This taxon, preliminary referred to as *Nyctereutes* sp. nov. (Fig. 4.5), confirms an early wave of dispersion of morphologically derived species that took place before 4 Ma. The phylogenetic analysis also revealed other unexpected patterns of affinity. For instance, the two species (*N. lockwoodi* and *N. terblanchei*) cluster together in a separate clade from the Eurasian taxa, indicating that the African stock of raccoon dogs might have followed a separate but parallel evolutionary history from the Eurasian species. Although, more recent, the morphology of *N. vulpinus* is suggestive of closer affinity to primitive-like species rather than to *N. megamastoides* and *N. sinensis*. The earliest Early Pleistocene record of *N. abdeslami* from Morocco is a clear evidence of a new dispersion of raccoon dogs from Eurasia into the African continent. The presumed ancestor-descendant relationship between the Plio-Pleistocene *N. sinensis* and the extant *N. procyonoides* does not find support in resulting tree topology. The origin of the living raccoon dog probably lies in an undescribed form of *Nyctereutes* present in the eastern Asia in Early Pleistocene (probably already present in Renzidong, as testified by its peculiar molar ratio values).

4.3. The genus *Vulpes*

The record of *Vulpes* across the Old World is scarce and confused. Compared to the extant diversity, the fossil taxa described are fewer and, in some cases, dubious. In Eurasia, the fossil known species are five, three of which from western Eurasia. Compared to Chinese record, the species form Europe (*i.e.*, *V. alopecoides*, *V. praecorsac* and *V. praeglacialis*) have been described in the first half of the 1900 century, on fragmented material coming from different sites of various age. For

Figure 4.5 – Life restoration of *Nyctereutes* sp. nov. from Çalta, Early Pliocene of Turkey (ca. 4.0 Ma, MN15). Artwork by Dr. Flavia Strani (PaleoFactory, Dipartimento di Scienze della Terra, Sapienza Università di Roma).

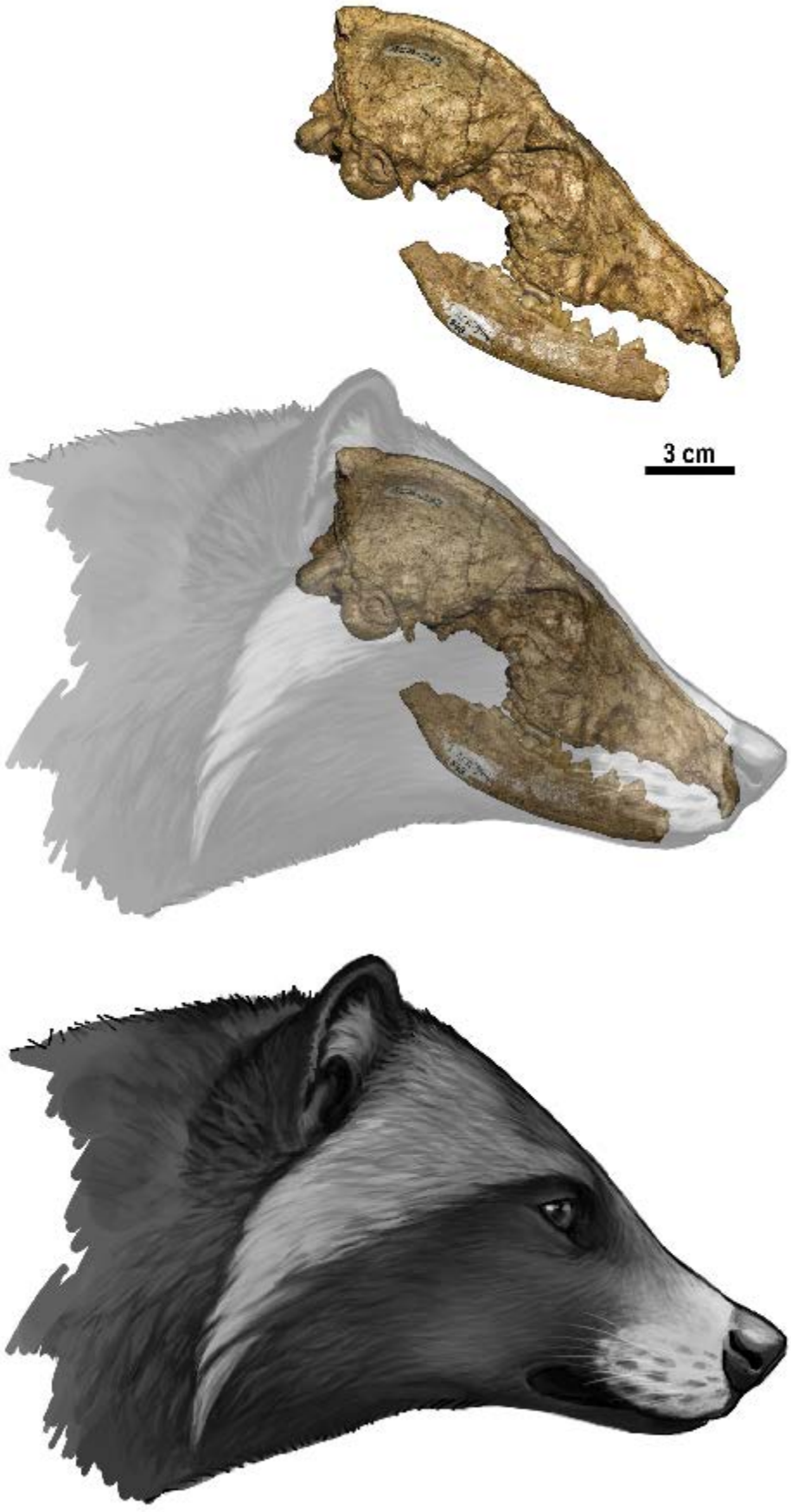
3 cm

instance, the type of *V. alopecoides* is a small maxillary fragment with M1-M2 or *V. praecorsac* comes from three different localities of the Early and middle Pleistocene of Hungary and Romania. As a result, the main element used in scientific literature to discriminate between the three species were chronology and size. This created a real taxonomic tangle in the European fossil record of *Vulpes*. After nearly a century from their original descriptions, no consistent revision of these material was made. For this purpose, the material from the Early Pleistocene of Hungary was revised. Taking into consideration the variability of selected modern species (*i.e.*, *V. vulpes*, *V. lagopus*, *V. corsac*) through direct observations and literature evidence, the variability showed by the three fossil taxa, *i.e.*, the degree of fossil interspecific variation, is inferior compared to the extant intraspecific variation of modern species. Given the size of the type samples of each species and the variability possessed, it seems plausible to ascribe the known Late Pliocene and earliest middle Pleistocene foxes to *V. alopecoides* (Fig. 4.6). Only the sample *V. praecorsac* from Odessa truly differs from the other analyzed. It might indeed represent a different species than that attribute by Odintzov (1965) and a currently on-going revision could clarify its taxonomical status (Ivanoff pers. comm.). Several issues remain to

Figure 4.6 – Updated chronological scheme of the known occurrences of fossil *Vulpes* spp. in both the Old and New World. In red are reported those record resulting or modified by the results of the present study. Degree of inclination of locality names approximate the degree of uncertainty on their datings. Data from literature are those of Fig. 1.11. **Abbreviations** – **AaO**, Ahl al Oughlam (Morocco); **APL1**, Apollonia-1 (Greece); **Atap. TD6**, Atapuerca Trinchera Dolina 6 (Spain); **Atap. TE**, Atapuerca Trinchera Elefante (Spain); **B. Leon 5**: Barranco Leon 5 (Spain); **CGR**, Cal Guardiola (Spain); **DA 2C**, Deutsch Altenburg 2C (Austria); **DrMk**, Drimolen Makondo (South Africa); **ELFN**, Elandfontein (South Africa); **EVT**, Vallparadís Estació; **F. Nueva 3**, Fuente Nueva 3; **LPVv**, La Puebla de Valverde (Spain); **LVal**, Le Vallonnet (France); **Mkps3**, Makapansgat 3 (South Africa); **NHH4**, Nagyharsanyhegy 4; **OCat**, Odessa Catacombs (Ukraine); **OH1-GR1**, Oulad Hamida1-Grotte des Rhinoceros (Morocco); **SH2**, Somssich-Hill 2; **Th1-GH**, Thomas 1 Quarry-Grotte des Hominides (Morocco); **ThCr**, Thousand Creek (U.S.A.); **VLR**, Villarroya (Spain); **ZKD**, Zhoukoudian (China).

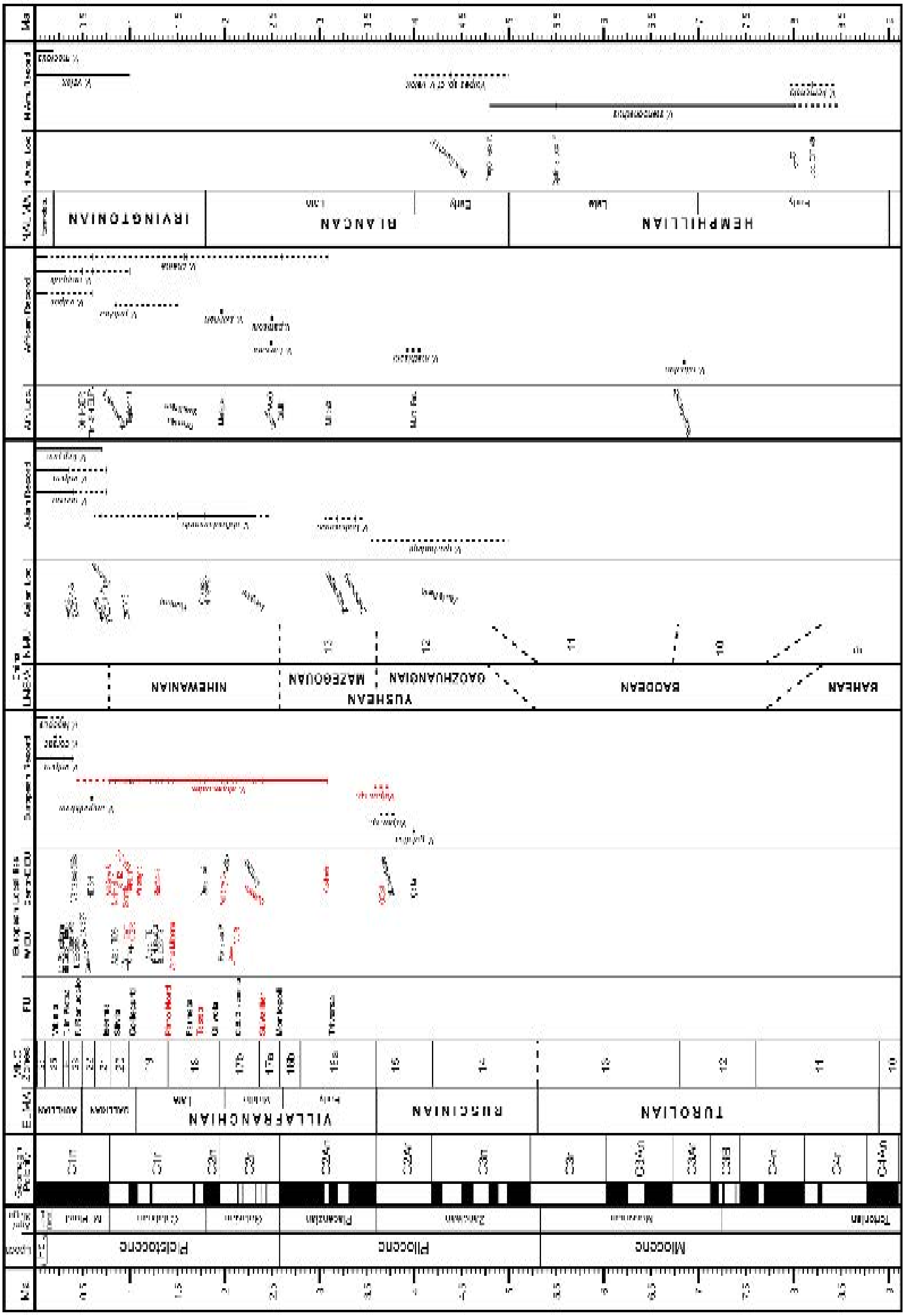
IRVINGTONIAN
BLANCAN
HEMPHILLIAN
NIHEWANIAN
MAZEGOUAN
GAOZHUANGIAN
YUSHEAN
BAODEAN
BAHEAN
VILLAFRANCHIAN
RUSCINIAN
TUROLIAN
Pleistocene
Pliocene
Miocene

be answered. For instance, the true relationship between *V. alopecoides* and modern *V. vulpes* (or other circum-Mediterranean species). The latter appears in the site of Lunel Viel 1 in the middle Pleistocene, yet its origin is still dubious, and never been studies in details. In the new framework of European foxes, a revision of the enigmatic species *V. angustidens* of Hundsheim could also help understanding the middle Pleistocene diversity (or morphological variation) of the genus *Vulpes*. The tangle surrounding the European species affected the possibility of consistent and accurate comparisons with Chinese taxa like *V. beihaiensis* and *V. chikushanensis*.

4.4. The genus *Eucyon*

The taxonomic status of the genus *Eucyon* (Fig. 4.7) is debated as some author questions the attribution of some species (Geraads, 2011; Werdelin et al., 2015). Indeed, the possible existence of undescribed extinct taxa (species or even genera) in the Pliocene fossil record of the Old World and New World is a plausible hypothesis (see Sotnikova & Rook, 2010), as proved by the strange *Nurocyon chonokhariensis* (see Sotnikova, 2006). Nevertheless, several cranial, dentognathic and postcranial characteristics seems to be shared by several species ascribed to *Eucyon* (see Tedford et al., 2009; Rook, 2009). Among them, the inion extended caudally till the level of the occipital condyles; the reduced and incisive-like I3 (rather than canine-shaped), the reduced M2 postprotocrista without a metaconule, absence of

Figure 4.7 – Updated chronological scheme of the known occurrences of *Eucyon* spp. in both the Old and New World. In red are reported those record resulting or modified by the results of the present study. Degree of inclination of locality names approximate the degree of uncertainty on their datings. Data from literature are those of Fig. 1.13. **Abbreviations** – **AEVL 1**, Amba east Vertebrate Locality 1 (Ethiopia); **ALA**, Alatini (Greece); **BRS-CM**, Brisighella-Cava Monticino (Italy); **CAS**, Casino Basin (Italy); **Chkh-1**, Chonokhariakh-1 (Mongolia); **ELFN**, Elandfontein; **KN-LsC**, Khirgis Nur Lower subcomplex (Mongolia); **KN-UsC**, Khirgis Nur Upper subcomplex (Mongolia); **OCat**, Odessa Catacombs (Ukraine); **Po-Le**, Podpusk-Lebyazh'e (Mongolia); **SdN**, Sangin Dalay Nur (Mongolia); **ThCr**, Thousand Creek (U.S.A.); **VER**, Verduno (Italy); **VMo**, Venta del Moro (Spain).

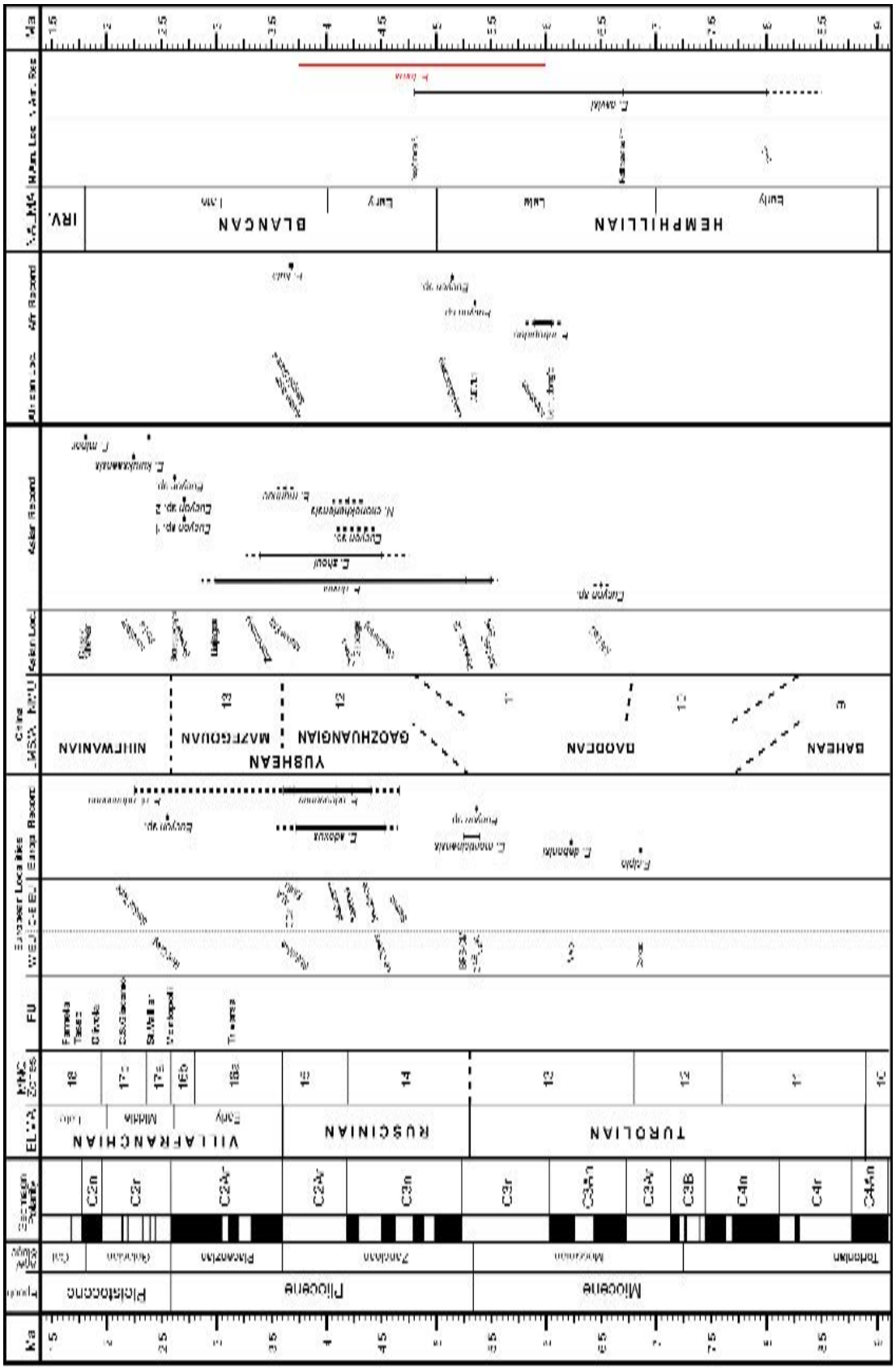

crista transversa on m1, radius/tibia ratio <80%. Such set of features should be used for the attribution to *Eucyon*. Revising several taxa ascribed to *Eucyon* and the type and paratype material of *C. ferox* (the earliest species of the genus *Canis*, see Miller & Carranza-Castañeda, 1998), it was possible to recognize the presence of these features in the latter taxon and propose a redescription as *Eucyon ferox*. The attribution of the North American species to *Eucyon*, extends the presence of the genus in the American continent at least until the early Blancan (Early Pleistocene) (Fig. 4.7). The basal position in the tribe Canini and the dental morphologies of the most renowned member of *Eucyon*, *i.e.*, *E. davisi*, lead researcher to consider these canids as adapted to a mesocarnivorous diet, between modern coyote (*C. latrans*), jackals (*C. aureus*, *L. mesomelas*) and the red fox (*V. vulpes*). In contrast to this interpretation, some evidence of certain species, for instance *E. cipio* and *E. ferox*. Particularly, in the latter several morphologies (interpreted as features of phylogenetic relevance, as the enlargement of the frontal sinus) might support a different ecological interpretation. Nevertheless, dietary preferences of *Eucyon* spp. as well as other Pliocene canids of Eurasia and North America has never been tested. The results of various analyses support the interpretation of generalized mesocarnivory for some species of *Eucyon* (*i.e.*, *E. adoxus*, *E. davisi*, and *E. zhoui*) comparable to that of *C. latrans*, *C. aureus*, and *L. mesomelas*. The results for *E. ferox* confirm the interpretation based on morphological ground: this medium-large-sized canid (Fig. 4.8) was a carnivorous species, with similarities with other hypercarnivorous species. Therefore, *E. ferox* is the first species of *Eucyon* that shows such dietary adaptation, but possibly not the only one. Similar morphologies can be found in the type specimens of *E. cipio* from Spain. Following these ecological and taxonomical results, a large and extensive Holarctic and African revision of *Eucyon* is desirable, in order to clarify the position of problematic species and rule out the issues regarding its diagnostic features of the genus. Although the record in both the Old and New World is relatively scanty, a phylogenetic analysis including

Figure 4.8 – Life restoration of *Eucyon ferox* from North America. Artwork by Dr. Flavia Strani (PaleoFactory, Dipartimento di Scienze della Terra, Sapienza Università di Roma).

the largest number of species as possible could relate the different taxa, giving hints on the possible relationships between the extant taxa and the fossil ones.

4.5. The genus *Canis*

The fossil record of the genus *Canis* and of its closely-related taxa, *i.e.*, *Xenocyon*, *Lycaon*, *Cuon*, *Lupulella*, is relatively more abundant compared to other canids (*e.g.*, *Vulpes*). In recent years, more and more researchers have added valuable contributions to our knowledge of the evolutionary history of Canini (*e.g.*, Tedford et al., 2009; Jiangzuo et al., 2018). Nevertheless, much remains to be clarified. In the present work, only few of these topics have been considered. As explained in the previous paragraph (section 4.5.) several morphologies of the type and paratypes of *C. ferox*, up to now the oldest *Canis* of the fossil record, are more consistent with a reattribution of the specie to *Eucyon*. As a consequence of this new taxonomical interpretation, the earliest record of *Canis* remains that of *C.*

Figure 4.9 – Resuming chronological scheme of the known occurrences of species of *Canis s.l.* group in both the Old and New World. In red are reported those record resulting or modified by the results of the present study. Generic names of the fossil species were reported as described by original authors (see text). Degree of inclination of locality names approximate the degree of uncertainty on their datings. Data from literature are those of Fig. 1.14. **Abbreviations** – **AaO,** Ahl al Oughlam (Morocco); **ABou**, Aïn Boucherit (Algeria); **AHan**, Aïn Hanec (Algeria); **APL1**, Apollonia-1 (Greece); Ata**p. TD6**, Atapuerca Trinchera Dolina 6 (Spain); **Atap. TE**, Atapuerca Trinchera Elefante (Spain); **B. Leon 5**: Barranco Leon 5 (Spain); **CGR**, Cal Guardiola (Spain); **Chikoian FC**, Chikoian Faunal Complex (Mongolia, Russia); **DA 2C**, Deutsch Altenburg 2C (Austria); **DrMk**, Drimolen Makondo (South Africa); **ELFN**, Elandfontein (South Africa); **EVT**, Vallparadís Estació; **F. Nueva 3**, Fuente Nueva 3; **TSn**, Fan Tsun (China); **HDSH**, Hundsheim (Germany); **K Fora KBS**, Koobi Fora KBS (Kenya); **Laetoli UB**, Laetoli Upper Beds (Tanzania); **LVal**, Le Vallonnet (France); **Mkps3**, Makapansgat 3 (South Africa); MOSB, Mosbach (Germany); **OH1-GR1**, Oulad Hamida1-Grotte des Rhinoceros (Morocco); SSMZ, Shanshenmiaozui (China); **Stkfn**: Sterkfontein (South Africa); **Th1-GH**, Thomas 1 Quarry-Grotte des Hominides (Morocco); **ThCr**, Thousand Creek (U.S.A.); **UISIW**, Upper Indian Siwalik (India); **UPSIW**, Upper Pakistan Siwalik (Pakistan); **ZKD**, Zhoukoudian (China).

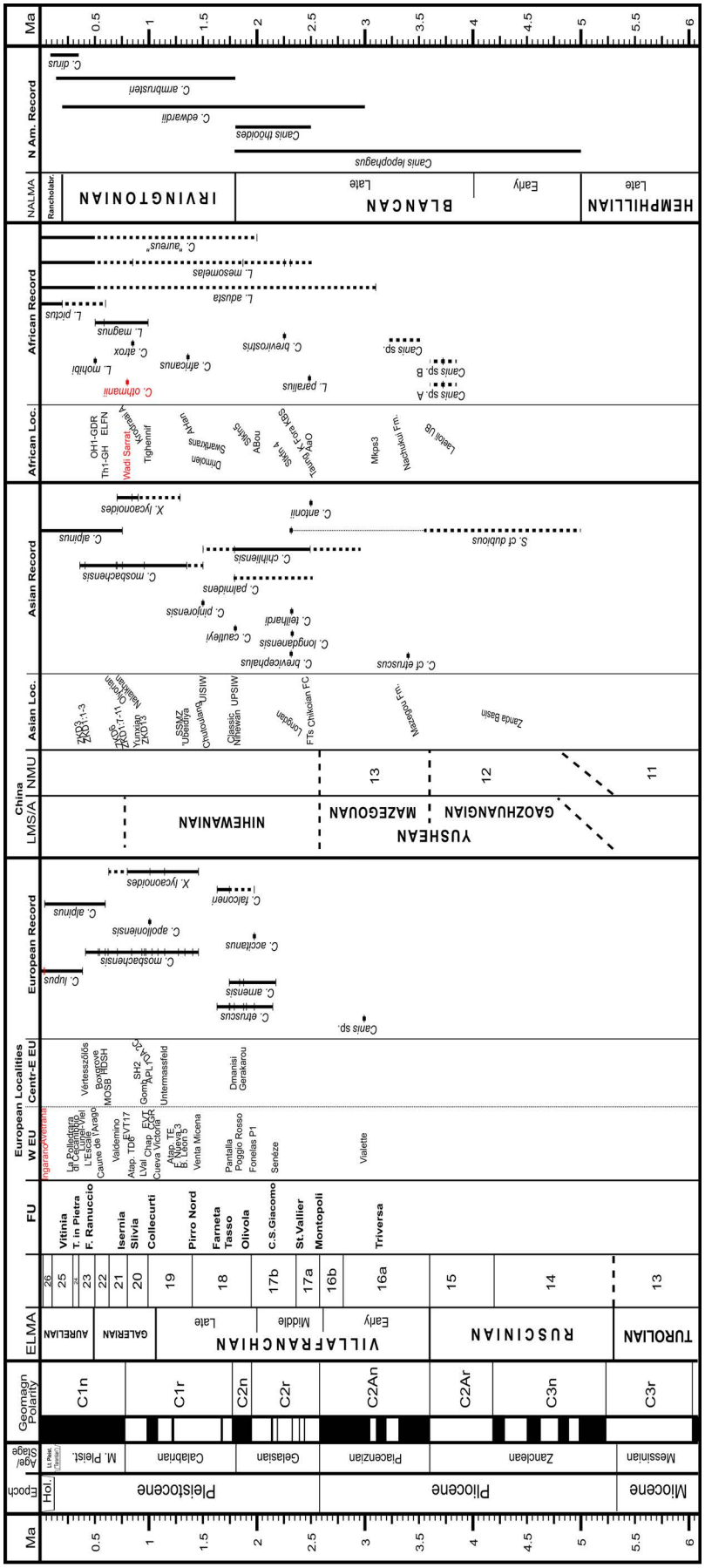
Ma
Epoch
Stage/ Stage
Geomagn Polarity
ELMA
FU
European Localities W EU
Centr-E EU
European Record
LMS/A
NMU
China
Asian Loc.
Asian Record
African Loc.
African Record
NALMA
N Am. Record
Pliocene
Pleistocene
Messinian
Zanclean
Piacenzian
Gelasian
Calabrian
M. Pleist.
Hol.
C1n
C1r
C2n
C2r
C2An
C2Ar
C3n
C3r
TUROLIAN
RUSCINIAN
VILLAFRANCHIAN
GALERIAN
AURELIAN
Vitinia
T. in Pietra
F. Ranuccio
Isernia
Slivia
Collecurti
Pirro Nord
Farneta
Tasso
Olivola
C.S.Giacomo
St.Vallier
Montopoli
Triversa
Vialette
Zanda Basin
Mataegou fm.
Classic Nihewan
Longgan
FTs Chikotan FC
Ubeidiya
Chkovalevka
Yunxian
Gongwangling
Nihewan
YUSHEAN
GAOZHUANGIAN
MAZEGOUAN
NIHEWANIAN
HEMPHILLIAN
BLANCAN
IRVINGTONIAN
Canis lepophagus
C. edwardii
C. ambrusteri
C. dirus
C. "aurus"
L. mesomelas
L. adusta
L. dictus
L. magnus
C. atrox
L. mohlbi
C. ottmanii
C. africanus
C. brevirostris
L. parafilus
Canis sp.
Canis sp. B
Canis sp. A
Ladgali UB
Nadrkhuul Fm.
Mkps3
Taung K-Tuff KBS
Shkln 4
ABou
Shkln
Dmanisi
Swartkrans
Ahhan
Dmitolen
OH1-GDR
Th1-GH
ELFN
Wadi Sarrat
Tighennif
Koobanan A
L. dictus
C. alpinus
X. lycaonoides
C. mosbachensis
C. palmidens
C. chilhiensis
C. piniforensis
C. tellhardi
C. gaudryi
C. longdanensis
C. brevicephalus
C. cf etruscus
C. antonii
S. cf dubious
C. lupus
C. mosbachensis
C. apollioniensis
C. accitanus
C. arnensis
C. etruscus
C. falconeri
X. lycaonoides
C. alpinus
Canis sp.
Vértesszőlős
Bovorgove
MOSB
HDSH
SH2
OAK-2C
Gom
APL1
Untermassfeld
Dmanisi
Gerakarou
La Polledrara
di Cecanibbio
L'Escale
Caune de l'Arago
Valdemino
Atap. TD6
EVT17
LVal
Chap
EVT
Cueva Victoria
OGR
Atap. TE
E. Nueva 3
B. León 3
Venta Micena
Pantalla
Poggio Rosso
Fonelas P1
Senèze
Rgarrab/Ahnedaline
26
25
2c
23
22
21
20
19
18
17b
17a
16b
16a
15
14
13
0.5
1
1.5
2
2.5
3
3.5
4
4.5
5
5.5
6

lepophagus from the Early Pliocene (Blancan times) of Cita Canyon in Texas (see Tedford et al., 2009; see Fig. 4.9). In the Old World, *Canis* arrived after 3.5 Ma but became an important element of the Eurasian and African faunas from the Latest Pliocene-Early Pleistocene (Fig. 4.9). As some authors have noticed (*inter alios* Sotnikova & Rook, 2010), during this period subsequent events of dispersal across Eurasia resulting in the radiation of many different species. Whereas the eastern Eurasian species are still problematic and would need a solid and consistent revision, the record of western Eurasia is better known. Two distinct moments can be identified. During the first, spanning approximately from the Latest Pliocene and the Gelasian, three forms of medium-/large-size canids are known across western Eurasia: the large, possibly hypercarnivorous *Canis falconeri*; *C. etruscus*, which was more or less the size of modern small wolf; and the jackal-sized *C. arnensis*. The second phase took place around 1.4 Ma and it is characterized by the arrival of the more derived *C. mosbachensis* and *X. lycaonoides*, which became common and widespread element of the European faunas from Spain to Georgia during the late Calabrian and the middle Pleistocene (Fig. 4.9). The African record in considerably scantier. The Late Pliocene-Early Pleistocene times appear to be characterized by jackal-like taxa. The record of *C. africanus* in Aïn Hanech, very similar to *X. lycaonoides*, represents the spreading into Africa of a Eurasian species of wild dog. Likewise, the Tunisian record of *C. othmanii*, correlated with the earliest middle Pleistocene, is relevant for its morphological and morphometric affinities. This species does not resemble any of the living species of jackals nor even other Early-middle Pleistocene canids from north and central Africa. Rather *C. othmanii* shares similarities with Eurasian species. The presence of a North African canid, distinct from fossil and extant African species, is important for several reason. Firstly, for instance, it is an unprecedented record for the Epivillafranchian of North African. Moreover, it also has important biogeographic implication, as it implies that in the late Villafranchian-Epivillafranchian remained a time of radiation and rapid

dispersal of *Canis* spp.

The study of the Late Pleistocene samples from Avetrana and Ingarano was carried out in order to understand the variability of fossil populations of wolves from Apulia in response to climatic oscillations that affected the last 120 ka. During the early Late Pleistocene, southern Italian populations ("Apulian wolves" of Sardella et al., 2014), *e.g.*, from Grotta Romanelli, Melpignano, possessed comparatively smaller size and some different morphological features compared to ones from northern Italy. The preliminary analyses on the sample from Ingarano (MIS 3), confirms that this sample belongs with the group of southern Italian wolves, being smaller and more slender compared to the robust wolves of northern Italy. The sample from Avetrana bed 8 (correlated to the late MIS 3 probably close to the transition to MIS 2), important phase in the southern Italian record of fossil wolves. Comparing this sample with that of the so-called Apulian wolves, it is clear that *C. lupus* from Avetrana bed 8 does not belong to them. Apart from minor difference, the increased size fit with the proportions of northern Italian Late Pleistocene wolves. Therefore, the population of *C. lupus* from level 8 of Avetrana marks the dispersal into southern Italy of "glacial" forms of wolves from northern Italy or even other regions of Europe. At present, there are no synthetic study of the size variability of Italian wolves during the Late Pleistocene. Such study, along with aDNA analyses on selected samples, not only could implement and confirm these local results, but would allow us to get better understanding of the framework of the dynamics that took place in the Italian peninsula during the last glacial periods (MIS 4-MIS 2).

4.6. Insights and perspectives

Along with more traditional and widely-used techniques, in recent years 3D imagine has revolutionized the way of doing research. Less than twenty-fifteen years ago, the possibility to access to these technologies was limited, either due to

the elevated costs of the devices but also for the quality of the digital data obtained. Nowadays, cheaper (or less expensive) solutions with high definition are becoming more and more available. In paleontology, pioneering studies and methodologies were used in the paleoanthropological research (see Zollikofer & de Leon, 2005) and later influencing the non-human branch of the field (see Cunningham et al., 2014; Sutton et al., 2014). In vertebrate paleontology, digital imaging has open new opportunities and approaches to evaluate aspects otherwise difficult to assess, like 3D geometric morphometrics, Finite Element Analysis (FEA), paleoneurology, etc. In recent years, such analyses are performed more and more often with open-source software and platforms (*e.g.*, the programming language environment R), therefore increasing their potential of spread and availability. The ever-changing and ever-updating digital environments also offer significant and ready-to-use opportunities for the dissemination of the scientific work carried out. The use of such techniques might help solving some of the issues regarding the evolutionary history, taxonomy and ecomorphology of some of the Canidae and Mustelidae discussed in this thesis. For instance, the ecology of the genus *Enhydrictis.* Although it was described more than a century ago, there is no agreement on the hypothesis of an aquatic life-style (as suggested by numerous authors, *e.g.*, Forsyth Major, 1901; Ficcarelli & Torre, 1967; Rook, 1995; García & Howell, 2008; and questioned by Bate, 1935; Kurtén, 1968). Nevertheless, no specific work has investigated this aspect of the ecology of *Enhydrictis* yet. 3D imaging (laser scans or CT scan) coupled with geometric morphometry methodologies, would allow to perform precise comparisons and analyses to try and test such hypothesis. The tomographic scan of the crania of *E. ferox* and other well-preserved specimens of *Eucyon* spp. would allow to assess development of features relevant for predation and feeding activity. Moreover, it would grant access to a number of useful data such as bone density or other parameters. Finally, it would enable analyses like FEA evaluating stress distribution under different predatory activity (bite, prey hold,

etc.), biomechanically characterizing the feeding ecology of such extinct canids. Among Carnivora, paleoneurological studies have been carried out on a number of taxa, with "physical" (*i.e.*, molding the brain cavity of the selected taxon) or digital approaches (*inter alios* Radinsky, 1969; 1973; Lyras & Van der Geer, 2003; Iurino et al., 2015; Vinuesa et al., 2015; Petrovič et al., 2018). On Canidae and Mustelidae opportunities of research could still be applied. Although, numerous works have investigated the macro- and microevolution of the brain of Canidae (Lyras et al., 2001; Lyras & Van der Geer, 2003; Lyras, 2009; Ivanoff et al., 2014), no studies have applied digital techniques or performed geometric morphometrics on the endocasts. On the contrary, the brain morphology of the fossil Eurasian Lyncodontini has never been analyzed.

Augmented reality (AR) is a technology that permits to interact with computer-generated objects (sensu lato from 2D pictures, videos to 3D objects) in the real world context in real-time, allowing the users to perceive the real environment surrounding the digital rendering (Azuma, 1997; Zhou et al., 2008; Lee, 2012). Thus, differing from Virtual Reality (VR), in which users are immersed in a digital/computer-generated environment, AR can be considered a mixed-reality (Bowen et al., 2014). Although AR is no more a brand-new technology (as its first applications date back to the 1990s) its potentiality to paleontology and museology seems underestimated (at the very least, in Italian institutions). AR applications cover a diverse range of fields, from medicine to manufacturing, from aeronautics to entertainment and tourism (Bowen et al., 2014). Particularly in educational sciences, AR has revealed its pedagogical potential, as much research documented (see Lee, 2012; Akçayır and Akçayır, 2017 and references therein). Nevertheless, no or little use has been made in scientific research and, particularly, in paleontology. Of the wide range of possible types of AR (see Bowen et al., 2014's review), a marker-based one was chosen here as, probably, the first application of AR to paleontology (further discussion see Kan et al., 2011). Using the easy-to-use, open-source and marker-

Figure 4.10 – Example of the Augmented Reality web-app. Comparison between the cranium of an modern *C. lupus* and the 3D model of D64 (not to scale).

based tools like AR.js and A-Frame, it was possible to create a simple web-app as the mean through which render the digital objects (in this case previously scanned fossil specimens of fossil *Canis* from the site of Dmanisi; section 3.13). A QR-code and a marker allowed to access the web-app and dispaly the 3D digital fossil. The easiness in the use of such web-app is meant to provide a simple-to-interact tool for readers who want to test the AR contents and do not have particular computer-related skills. Following the motto of the A-Frame team "show, don't tell". The use of AR of digitalized fossil specimens, as in section 3.13., allows to: increase the accessibility to superb fossils like D64 (Fig. 3.13.2); show the true tridimensional morphology of the specimens, their tiniest features (as dental cuspules/cuspulids); and even perform digital comparisons between different species (Figs. 3.13.1 and 3.13.3). Most importantly, all of this can be achieved simply by using a mobile device. The implementation of such effective tools is valuable to other researchers as it permits them to operate their observation of the 3D model better than using 2D photos or even stereophotography. Moreover, the use of a marker may consent to even compare the 3D objects to a real one (for instance to a cranium of an extant

canid, e.g., *C. lupus*, Fig. 4.10) placed near the marker, to directly see similarities and/or difference.

Bibliographic references

Abbazzi L, Angelone C, Arca M, Barisone G, Bedetti C, Delfino M, Kotsakis T, Marcolini F, Palombo MR, PaviaM, Piras P, Rook L, Torre D, Tuveri C, Valli AMF, Wilkens B (2004) Plio–Pleistocene fossil vertebrates of Monte Tuttavista (Orosei, eastern Sardinia, Italy), an overview. Riv It Paleontol Strat 110, 681–706

Abbazzi L, Arca M, Tuveri C, Rook L (2005) The endemic canid *Cynotherium* (Mammalia, Carnivora) from the Pleistocene deposits of Monte Tuttavista (Nuoro, eastern Sardinia). Riv It Paleontol Strat 111, 497–511

Agnarsson I, Kuntner M, May–Collado LJ (2010) Dogs, cats, and kin: a molecular species–level phylogeny of Carnivora. Mol Phylogenet Evol 54, 726–745

Aguirre E, Hoyos M, Mensua S, Morales J, Pérez González A, Quirantes J, Sánchez L, Soria D (1974) Cuenca del Jalón, in Aguirre E., Morales J. (eds) Libro–Guía del Coloquio Internacional sobre Biostratigrafía Continental del Neógeno superior y Cuaternario inferior, CSIC, Madrid, pp 13–45

Aguirre E, Morales J, Soria D (1981) Accumulated bones in a Pliocene cave in Cerro Pelado, Spain. Natl Geogr Soc Res Rep 13, 69–81

Agustí J, Antón M (2002) Mammoths, sabertooths and hominids. Columbia University Press

Agustí J, Moyà–Solà S, Pons–Moyà J (1986) Venta Micena (Guadix–Baza basin, South–eastern Spain): its place in the Plio–Pleistocene mammal succession in Europe. Geol Romana 25, 33–62

Agustí J, Cabrera L, Garcés M, Krijgsman W, Oms O, Parés JM (2001) A calibrated mammal scale for the Neogene of western Europe. State of the art. Earth Sci Rev 52, 247–260

Agustí J, Vekua A, Oms O, Lordkipanidze D, Bukhsianidze M, Kiladze G, Rook L (2009) The Pliocene–Pleistocene succession of Kvabebi (Georgia) and the background to the early human occupation of Southern Caucasus: Quat Sci Rev 28, 3275–3280

Akçayır M, Akçayır G (2017) Advantages and challenges associated with augmented reality for education: A systematic review of the literature. Edu Res Rev 20, 1-11

Alberdi MT, Cerdeño E, López–Martínez N, Morales J, Soria MD (1997) La fauna

villafranquiense de El Rincón–1 (Albacete, Castilla–La Mancha). Estudios Geol 53, 69–93

Alcalá Martínez L, Montoya P (1989–1990) Las faunas de macromamíferos del Turoliense inferior español. Paleontol Evol 23, 111–119

Alcalá–Martínez L (1994) Macromammiferos neogenos de la fosa de Alfambra–Teruel. PhD Thesis; Teruel, Museo Nacional de Ciencias Naturales, 1–554

Allen GM (1938) The mammals of China and Mongolia, Vol. 1. New York: The American Museum of Natural History

Altobello G (1921) Fauna dell'Abruzzo e del Molise. Mammiferi. IV. I Carnivori (Carnivora). Colitti e Figlio, Campobasso, pp 38–45

Amri L, Bartolini Lucenti S, Mtimet MS, Karoui-Yaakoub N, Ros-Montoya S, Espigares MP, Boughdiria M, Nebiha Bel Haj Ali N, Martínez-Navarro B (2017) *Canis othmanii* sp. nov. (Carnivora, Canidae) from the early Middle Pleistocene site of Wadi Sarrat (Tunisia). CR Palevol 16, 774-782.

Anadón P, Julià R, De Deckker P, Rosso J-C, Soulié-Marsché I (1987) Contribución a la Paleolimnología del Pleistoceno inferior de la cuenca de Baza (sector Orce-Venta Micena). Paleontol y Evol Mem Esp 1, 35–72

Anelli F (1959) Prime ricerche paleontologiche della grotta della Masseria del Monte Conversano –Murge di Bari. Le Grotte d'Italia, 3, 1–26

Angelone C, Tuveri C, Arca M, López Martínez N, Kotsakis T (2008) Evolution of Prolagus sardus (Ochotonidae, Lagomorpha) in the Quaternary of Sardinia Island (Italy). Quat Int 182, 109–115

Anzidei AP, Bulgarelli GM, Catalano P, Cerilli E, Gallotti R, Lemorini C, Milli S, Palombo MR, Pantano W, Santucci E (2012) Ongoing research at the late Middle Pleistocene site of La Polledrara di Cecanibbio (central Italy), with emphasis on human–elephant relationships. Quatern Int 255, 171–187

Aouraghe H (2000) Les carnivores fossiles d'El Harhoura 1, Temara, Marroc. L'Anthropologie 104, 147–171

Arambourg C (1979) Les vertébrés Villafranchiens d'Afrique du Nord (Artiodactyles, Carnivores, Primates, Reptiles, Oiseaux). Fondation Singer Polignac, Paris

Argant A (2004) Les Carnivores du gisement Pliocène final de Saint–Vallier (Drôme, France). Geobios 37, 133–182

Argyropulo AJ (1941) Rodents and insectivores of the Quaternary fauna of Binagady. Priroda 3, 88–91

Arribas A, Palmqvist P (1998) Taphonomy and paleoecology of an assemblage of large mammals: hyaenid activity in the lower Pleistocene site at Venta Micena (Orce, Guadix-Baza Basin, Granada, Spain). Geobios 31, 3–47

Asahara M (2013a) Shape variation in the skull and lower carnassial in a wild population of raccoon–dog (*Nyctereutes procyonoides*). Zool Sc 30, 205–210

Asahara M (2013b) Unique inhibitory cascade pattern of molars in canids contributing to their potential to evolutionary plasticity of diet. Ecol Evol 3, 278–285

Asahara M (2014) Evolution of relative molar sizes among local populations of the raccoon dog (*Nyctereutes procyonoides*) in Japan. Mammal Study 39, 181–184

Asahara M, Takai M (2016) Estimation of diet in extinct raccoon–dog species by the molar ratio method: Acta Zool (Stockholm) 98, 1–8

Asahara M, Saito K, Kishida T, Takahashi K, Bessho K (2016) Unique pattern of dietary adaptation in the dentition of Carnivora: Its advantage and developmental origin. Proc R Soc B 282, 20160375

Atickem A, Stenseth NC (2011) The cryptic African wolf: *Canis aureus lupaster* is not a golden jackal and is not endemic to Egypt. PLOS One 6, e16385

Audet AM, Robbins CB, Larivière S (2002) *Alopex lagopus*. Mammalian species 713, 1–10

Azzaroli A (1977) The Villafranchian stage in Italy and the Plio–Pleistocene boundary. Giorn Geol 41, 61–79

Azzaroli A (1983) Quaternary mammals and the end-Villafranchian dispersal event– a turning point in the history of Eurasia. Palaeogeogr Palaeoclimat Palaeoecol 44, 117–139

Azzaroli A, De Giuli C, Ficcarelli G, Torre D (1982) Table of the stratigraphic distribution of terrestrial mammalian faunas in Italy from the Pliocene to the early Middle Pleistocene. Geogr Fis Dinam Quat 5, 55–58

Azzaroli A., De Giuli C, Ficcarelli G, Torre D (1988) Late Pliocene to early mid–Pleistocene mammals in Eurasia: faunal succession and dispersal events. Palaegeogr Palaeoclimatol Palaeoecol 66, 77–100

Baird SF (1857) Mammals: upon the zoology of the several Pacific railroad routes. Reports, explorations and surveys for railroad route from Mississippi River to Pacific

Ocean 8, Washington DC, Tucker

Bardeleben C, Moore RL, Wayne RK (2005) A molecular phylogeny of the Canidae based on six nuclear loci. Mol Phylogenetics Evol 37, 815–831

Baron D, Negrini RM, Golob, EM, Miller, D, Sarna–Wojcicki A., Fleck RJ, Hacker B, Erendi A (2008) Geochemical correlation and $^{40}Ar/^{39}Ar$ dating of the Kern River ash bed and related tephra layers: Implications for the stratigraphy of petroleum–bearing formations in the San Joaquin Valley, California. Quat Int 178(1), 246–260

Barone R (1966) Anatomie comparée des mammifères domestiques (Vol 1). Paris

Bartolini Lucenti S (2018) Revising the species "*Mustela*" *ardea* Gervais, 1848–1852 (Mammalia, Mustelidae): *Martellictis* gen. nov. and the systematics of the fossil "Galictinae" of Eurasia. CR Palevol 17, 522-535

Bartolini Lucenti S, Rook L (2016) A review on the Late Villafranchian medium–sized canid *Canis arnensis* based on the evidence from Poggio Rosso (Tuscany, Italy). Quat Sci Rev 151, 58–71

Bartolini Lucenti S, Alba DM, Rook L, Moyà–Solà S, Madurell–Malapeira J (2017) Latest Early Pleistocene wolf–like canids from the Iberian Peninsula. Quat Sci Rev 162, 12–25

Bartow JA, Pittman GM, Gardner M (1983) The Kern River Formation, southeastern San Joaquin Valley, California. US Geol Surv Bull 1529–D, 17

Baskin JA (1998) Mustelidae, in Janis C, Scott KM, Jacobs LL (eds), Evolution of Tertiary Mammals of North America. Cambridge University Press, Cambridge, United Kingdom, pp 152–173

Baskin JA (2011) A new species of *Cernictis* (Mammalia, Carnivora, Mustelidae) from the Late Miocene Bidahochi Formation of Arizona, USA. Paleontol Electronica 14, 11

Bates DMA (1937) Palaeontology: The fossil fauna of the Wady el–Mughara caves, in Bates DMA (ed) The Stone Age of Mount Carmel. Excavations at the Wady El–Mughara, vol 1, part 2, Clarendon Press, Oxford, pp 137–233

Bedetti C, Bellucci L, Conti N, Coppola D, Di Canzio E, Pavia M, Petronio C, Petrucci M, Salari L, Sardella R (2004) Prima segnalazione di una fauna pleistocenica a vertebrati rinvenuta ad Avetrana (TA). IV Giorn Paleontol, 21–23 Maggio, Bolzano

Bedetti C, Pavia M (2007) Reinterpretation of the Late Pleistocene Ingarano cave deposit based on the fossil bird associations (Apulia, South–eastern Italy). Riv It Paleontol

Strat 113, 487–507

Bekoff M, Gese EM (2003) Coyote (*Canis latrans*). USDA National Wildlife Research Center–Staff Publications 224

Bell T (1826) Zoological meeting. Zool J Linn Soc 2, 552–554

Benvenuti M, Dominici S, Rook L (1995) Inquadramento stratigrafico–deposizionale delle faune a mammiferi villafranchiane (unità faunistiche Triversa e Monopoli) del Valdarno Inferiore nella zona a sud dell'Arno (Toscana). Il Quaternario 8, 457–464

Bernor RL, Sen S (2017) The Early Pliocene *Plesiohipparion* and *Proboscidipparion* (Equidae, Hipparionini) from Çalta, Turkey (Ruscinian Age, c. 4.0 Ma). Geodiversitas 39, 285–314

Berta A (1981) The Plio–Pleistocene hyaena *Chasmaporthetes ossifragus* from Florida. J Vert Paleontol 1, 341–356

Berta A (1988) Quaternary evolution and biogeography of the large South American Canidae (Mammalia: Carnivora). Univ Calif Public Geol Sci 132, 1–49.

Bertè DF (2014) L'evoluzione del genere *Canis* (Carnivora, Canidae, Caninae) in Italia dal wolf–event a oggi: implicazioni biocronologiche, paleoecologiche e paleoambientali. 390 pp. PhD Dissertation, Sapienza, Università di Roma, Roma

Bertè DF (2017) Remarks on the skull morphology of *Canis lupaster* Hemprich & Herenberg, 1832 from the collection of the Natural History Museum "G. Doria" of Genoa, Italy. Nat H Sci 19–29

Bertè DF, Pandolfi L (2014) *Canis lupus* (Mammalia, Canidae) from the Late Pleistocene deposit of Avetrana (Taranto, Southern Italy). Riv Ital Paleontol S 120 (3), 367–379

Biknevicius AR, Ruff CB (1992) The structure of the mandibular corpus and its relationship to feeding behaviors in extant carnivorans. J Zool 228, 479–507

Biknevicius AR, Van Valkenburgh B (1996) Design for killing: craniodental adaptations of predators. In Gittleman JL (ed) Carnivore behavior, ecology and evolution. Vol. 2. Cornell Univ. Press, Ithaca, NY, pp 393–428

Bjork PR (1970) The Carnivora of the Hagerman Local Fauna, (late Pliocene) of southwestern Idaho. Trans Am Phil Soc 60, 1–54

Blasius AWH (1884) Der japanische Nör, Foetorius Itatsi. Bericht der Naturforsch Gesellschaftsgründung 13, 9

Blumenbach JF (1799) Handbuch der Naturgeschichte. Sechste Auflage, Dieterich, Göttingen

Boddaert P (1784) Elenchus animalium. Volumen I. Sistens quadrupedia huc usque nota, erorumque varietates. CR Hake Roterdami

Boitani L (1995) Ecological and cultural diversities in the evolution of wolf–human relationships, in Carbyn LN, Fritts SH, Seip DR (eds), Ecology and conservation of wolves in a changing world. Occasional Publication 35, pp. 3–11. Canadian Circumpolar Institute, Edmonton, Alberta, Canada.

Boitani L, Lovari S, Vigna Taglianti A (2003) Fauna d'Italia. Mammalia III. Carnivora – Artiodactyla Calderini ed, Bologna

Bojanus LH (1827) De uro nostrate eiusque sceleto commentatio scripsit et bovis primigenii sceleto auxit. Nova Acta Physico–Medica Academiae Caesareae Leopoldino–Carolinae Naturae Curiosorum 13, 411–478

Boldrini R, Palombo MR, Barbieri M, Iacumin P, Melis R (2010) The Middle Pleistocene fossiliferous sequence of Grotta dei Fiori (Sardinia, Italy): multidisciplinary analysis. Boll Soc Pal It 49, 123–134

Bon M, Piccoli G, Sala B (1991) I giacimenti quaternari di vertebrati fossili nell'Italia nord–orientale. Mem Soc Geol 17, 185–231

Bonifay MF (1971) Carnivores quaternaires du Sud est de la France. Memoir Mus Natl Hist, Série C, 21, 43–377

Bornholdt R, Helgen K, Koepfli KP, Oliveira L, Lucherini M, Eizirik E (2013) Taxonomic revision of the genus *Galictis* (Carnivora: Mustelidae): Species delimitation, morphological diagnosis, and refined mapping of geographical distribution. Zool J Linn Soc 167, 449–472

Boscato P (2004) I macromammiferi dell'Aurignaziano e del Gravettiano antico di Grotta Paglicci, in Grenzi C (ed) Paglicci, l'Aurignaziano e il Gravettiano antico. Foggia, pp 49–62

Bose PN (1880) Undescribed fossil Carnivora from the Siwalik Hills. J Quat Geol Soc London 36, 119–136

Boudadi–Maligne M (2010) Les Canis pleistocenes du sud de la France: approche biosystematique, evolutive et biochronologique, 451 pp. PhD Dissertation, Université Bordeaux 1.

Boudadi–Maligne M (2012) Une nouvelle sous–espèce de loup (*Canis lupus maximus* nov. subsp.) dans le Pléistocène supérieur d'Europe occidentale. CR Palevol 11, 475–484

Boule M (1889) Le *Canis megamastoides* du Pliocene moyen de Perrier (Puy–de–Dôme). Bull Soc Géol Fr 17 321–330

Bowdich TE (1821) An Analysis of the Natural Classification of Mammalia, for Use of Students and Travelers. J. Smith, Paris, pp 115

Bower M., Howe C, McCredie N, Robinson A, Grover D (2014) Augmented Reality in education–cases, places and potentials. Edu Media Int 51(1), 1-15

Bown TM, Holroyd PA, Rose KD (1994) Mammal extinctions, body size, and paleotemperature. Proc Natl Acad Sci USA 91, 10403–10406.

Brandy LD (1978) Donées Nouvelles sur l'évolution du rongeur endémique fossils corso–sarde *Rhagamys* F. Major (1905) (Mammalia, Rodentia). Bull Soc Geol Fr 7, 831–835

Bravard A (1828) Monographie de la montagne de Perrier et de deux espèces fossiles du genre *Felis*. Dufour et Docagne, Paris, 1–128

Bravard A (1843) Considérations sur la distribution des mammifères terrestres fossiles dans le département du Puy–de–Dome, in Lecoq H (1843) Annales scientifiques, littéraires et industrielles de l'Auvergne, Vol. 16, Académie des sciences, belles–lettres et arts de Clermont–Ferrand, Thibaud–Landroit libraires–éditeurs

Bravard A (1846) Sur les animaux fossiles de l'Auvergne. Bull Soc Geol de France, series 2eme, tome III, 197–198

Brazeau MD (2011) Problematic character coding methods in morphology and their effects. Biol J Linn Soc 104, 489–498.

Breda M (2001) *Alces alces* (Linnaeus, 1758) del Pleistocene superiore e dell'Olocene antico in Italia Nord–Orientale. Boll Mus Civico Storia Nat Verona 25, 27–39.

Bronn HG (1931) Italiens Tertiär-Gebilde und deren organische Einschlüsse: vier Abhandlungen. Groos, Heidelberg,

Brookes J (1827), in Griffith E, Smith C, Pidgeon E (eds) The Animal Kingdom Arranged in Conformity with Its Organization by the Baron Cuvier, with Additional Descriptions of all the Species Hitherto Named, and of Many Not Before Noticed. G. B. Whittaker, London, pp 392

Broom R (1939) A preliminary account of the Pleistocene carnivores of the Transvaal

caves. Ann Transvaal Mus 19, 331-338.

Broom R (1948) Some South–African Pliocene and Pleistocene mammals. Ann Transvaal Mus 21, 1–28

Broom R, Schepers GWH (1946) The South African fossil ape–men: the Australopithecinae (No. 2). Pretoria: Transvaal Museum.

Brugal JP, Boudadi–Maligne M (2011) Quaternary small to large canids in Europe: taxonomic status and biochronological contribution. Quatern Int 243, 171–182

Bryant HN, Russell AP, Fitch WD (1993) Phylogenetic relationships within the extant Mustelidae (Carnivora): appraisal of the cladistic status of the Simpsonian subfamilies. Zool J Linn Soc 108, 301–334

Bryant HN (1992) The Carnivora of the Lac Pelletier lower fauna (Eocene: Duchesnean), Cypress Hills formation, Saskatchewan. J Paleontol 66, 847–855

Burgio E, Fiore M (1997) *Mustelercta arzilla* (De Gregorio, 1886) un elemento villafranchiano nella fauna di Monte pellegrino (Palermo, Sicilia). Il Quaternario 10, 65–74

Cabrera A (1907) Los lobos de Espana. Bol Real Soc Esp Hist Nat VII, 193–198

Cabrera A (1940) Notas sobre carnivoros sudamericanos. Notas Mus La Plata, Zool 5: 1–22

Caloi L, Palombo MR (1996) Latest Early Pleistocene mammal faunas of Italy, biochronological problems. Il Quaternario 8, 391–402

Caloi L, Palombo MR, Papini G (1982) Studio biometrico sui crani di lupo appenninico (Canis lupus italicus, Altobello). Convegno Nazionale Gruppo Lupo Italia, 1–2 Maggio, Civitella Alfedena.

Cappellini E, Welker F, Pandolfi L, Ramos-Madrigal J, Samodova D, Rüther PL, Fotakis AK, Lyon D, Moreno-Mayar JV, Bukhsianidze M, Rakownikow Jersie-Christensen R, Mackie M, Ginolhac A, Ferring R, Tappen M, Palkopoulou E, Dickinson MR, Stafford Jr TW, Chan YL, Götherström A, Nathan SKSS, Heintzman PD, Kapp JD, Kirillova I, Moodley Y, Agustí J, Kahlke R-D, Kiladze G, Martínez-Navarro B, Liu S, Sandoval Velasco M, Sinding M-H S, Kelstrup CD, Allentoft ME, Orlando L, Penkman K, Shapiro B, Rook L, Dalén L, Gilbert MP, Olsen JV, Lordkipanidze D, Willerslev E (2019) Early Pleistocene enamel proteome from Dmanisi resolves *Stephanorhinus* phylogeny. Nature 574(7776), 103-107

Carbone C, Georgina MM, Roberts SC, Macdonald DW (1999) Energetic constraints on

the diet of terrestrial carnivores. Nature 402, 286–288

Carbone C, Teacher A, Rowcliffe JM (2007) The cost of carnivory. PLoS Biology 5, e22

Carbonell E, Bermúdez De Castro JM, Parés JM, Pérez–González A, Cuenca–Bescós G, Ollé A, Mosquera M, Huguet R, Van Der Made J, Rosas A, Sala R, Vallverdú J, García N, Granger DE, Martinón–Torres M, Rodríguez XP, Stock GM , Vergès JM, Allué E, Burjachs F, Cáceres I, Canals A, Benito A, Díez C, Lozano M, Mateos A, Navazo M, Rodríguez J, Rosell J, Arsuaga JL (2008) The first hominin of Europe. Nature 452(7186), 465–469

Carbyn LN (1987) Gray wolf and red wolf, in Novak N, Baker JA, Obbard ME, Malloch B (eds), Wild Furbearer Management and Conservation in North America. Ontario Minintry of Natural Resources, Toronto, Ontario, pp 378–393

Carpignoli N (2019) AR.js – The Simplest Way to get Cross-Browser Augmented Reality on the Web. Medium 11 May 2019. https://medium.com/swlh/ar-js-the-simplest-way-to-get-cross-browser-augmented-reality-on-the-web-10cbc721debc

Carranza–Castañeda O, Petersen M, Miller WE (1994) Geology of the Northern San Miguel Allende area. Brigham Young Univ Geol Stud 40, 1–9

Castelló JR (2018) Canids of the World: Wolves, Wild Dogs, Foxes, Jackals, Coyotes, and Their Relatives. Princeton University Press.

Chen L, Zhang H (2012) The complete mitochondrial genome and phylogenetic analysis of *Nyctereutes procyonoides*. Acta Ecol Sin 32, 232–239

Cherin M, Bertè DF, Rook L, Sardella R (2014) Re–defining *Canis etruscus* (Canidae, Mammalia): a new look into the evolutionary history of Early Pleistocene dogs resulting from the outstanding fossil record from Pantalla (Italy). J Mam Evol 21, 95–110

Ciaranfi N, Pieri P, Ricchetti G (1988) – Note alla Carta Geologica delle Murge e del Salento (Puglia centromeridionale). Mem Soc Geol It 41, 449–460

Clark HO (2005) *Otocyon megalotis*. Mammalian Species 766, 1–5

Clark J (1936) Part I: Insectivora and Carnivora, in Scott WB, Iepsen GL (eds) The mammalian fauna of the White River Oligocene. Trans Am Phil Soc, new series 28, 1–153

Clauzon G, Le Strat P, Duvail C, Do Couto D, Suc JP, Molliex S, Bache F, Besson D, Lindsay EH, Opdyke ND, Rubino JL, Popescu SM, Haq BU, Gorini C (2015) The

Roussillon Basin (S France): A case–study to distinguish local and regional events between 6 and 3 Ma. Mar Pet Geol 66, 18–40

Clutton–Brock J, Corbet GG, Hills M (1976) A review of the family Canidae, with a classification by numerical methods. Bull Brit Mus Nat Hist 29, 119–199

Cohen C (1999) L'homme des origines. Savoirs et fictions en Préhistoire. Ed du Seuil, París

Colombero S, Pavia M, Rook L (2012) *Pannonictis nestii* (Galictinae, Mustelidae), a new element in the vertebrate association of the human site of Pirro Nord (Italy, Early Pleistocene). Geodiversitas 34, 665–681

Cope ED (1879) Observations on the faunae of the Miocene Tertiaries of Oregon. Bull US Geol Geogr Surv Territories 5, 55–69.

Cope ED (1892) A hyena and other Carnivora from Texas. Am Nat 26, 1028–1029

Cremaschi M, Ferraro F, Peresani M, Tagliacozzo A (2005) La Grotta di Fumane: nuovi contributi su stratigrafia, cronologie, faune a miromammiferi ed industrie musteriane. J Archaeol Sci 37, 758–768

Cretzschmar JC (1826) Atlas zu der Reise im nördlichen Afrika von Eduard Rüppell, Säugethiere. Frankfurt am Main, Senckenbergischen naturforschenden Gesellschaft, pp 78.

Crusafont Pairó M (1950) El primer representante del genero *Canis* en el Pontiense eurasiatico (*Canis cipio* nova sp.). Boll Real Soc Española Hist Nat Geol 48, 43–51

Crusafont–Pairó M, Truyols–Santana J (1956) A biometric study of the evolution of fissiped carnivores. Evolution 10, 314–332

Cuarón AD, Martínez–Morales MA, McFadden KW, Valenzuela D, Gompper ME (2004) The status of dwarf carnivores on Cozumel Island, Mexico. Biodiversity and Conservation 13(2), 317–331 https://doi.org/10.1023/b:bioc.0000006501.80472.cc

Cunningham JA, Rahman IA, Lautenschlager S, Rayfield EJ, Donoghue PC (2014). A virtual world of paleontology. Trends Ecol Evol 29, 347–357

Cuvier FG (1817) Le règne animal distribué d'après son organisation: pour servir de base a l'histoire naturelle des animaux et d'introduction a l'anatomie comparée. Déterville, Paris. Vol 1

Cuvier FG (1821) *Mydaus meliceps*. Histoire Naturelle des Mammiféres 3, 1–2

Cuvier FG (1825) Histoire naturelle des Mammiféres, avec des figures originales, colorées, desinées d'apres des animaux vivants. Paris, 2, 1–3, Plate 203

Cuzin F (2013) *Poecilictis libyca* Lybian Striped Weasel, in Kingdon J, Hoffmann M (eds), The Mammals of Africa. V. Carnivores, Pangolins, Equids and Rhinoceroses, Bloomsbury, London, UK, pp 90–92

Daitch DJ, Guralnick RP (2007). Geographic variation in tooth morphology of the arctic fox, *Vulpes* (*Alopex*) *lagopus*. J Mammal 88(2), 384-393

David A (1869) Extrait d'une lettre du mem, datee de la Principaute Thibetaine (independente) de Moupin, le 21 Mars 1869. Nouv Arch Mus Hist Nat 5, 12–13.

Davies-Mostert HT, Mills MG, Macdonald DW (2013) Hard boundaries influence African wild dogs' diet and prey selection. J App Ecol 50, 1358–1366

Davis S (1977) Size variation of the fox, *Vulpes vulpes* in the palaeartic region today, and in Israel during the late. Quat J Zool 182, 343–351

Dayan T, Simberloff D, Tchernov E, Yom–Tov Y (1991) Calibrating the paleothermometer: climate, communities, and the evolution of size. Paleobiology 17, 189–199

de Bonis L, 1997. Precisions sur l'age geologique et les relations phyletiques de Mustelictis olivieri nov. sp. (Carnivora, Mustelidae), carnassier de l'Oligocene inferieur (MP 22) des phosphorites du Quercy (France). Geobios 20, 55–60

de Bonis LD, Peigné S, Likius A, Mackaye HT, Vignaud P, Brunet M (2007) The oldest African fox (*Vulpes riffautae* n. sp., Canidae, Carnivora) recovered in late Miocene deposits of the Djurab Desert, Chad. Naturwissenschaften 94, 575–580

De Gregorio A (1886) Intorno ad un deposito di roditori e di carnivori sulla vetta di Monte Pellegrino. Atti Soc Toscana Sci Nat 8, 3–39

de Mello Beisiegel B, Zuercher GL (2005) *Speothos venaticus*. Mammalian species 783, 1–6

De Selys–Longchamps E (1838) Etudes de micrommalogie. Revue des musaraignes, des rats et des campagnols, suivie d'une index mèthodique des mammifères d'Europe. Roret.

Del Campana D (1913) I cani Pliocenici di Toscana. Palaeontog Ital 19, 189–254

Del Campana D (1917) Sulla presenza di (*Canis*) *Cerdocyon megamastoides* Pomel, nel Pliocene del Valdarno Inferiore. Riv It Paleont 23, 1–8

Delisle I, Strobeck C (2005) A phylogeny of the Caniformia (order Carnivora) based on

12 complete protein–coding mitochondrial genes. Mol Phylogenet Evol 37, 192–201

Dennell R. (2010) "Out of Africa I": current problems and future prospects, in Fleagle JG, Shea JJ, Grine FE, Baden AL, Leakey RE (eds) Out of Africa I: the first hominin colonization of Eurasia. Springer Science & Business Media. Springer, Dordrecht, pp 247–273

Depéret C (1890) Les Animaux Pliocènes du Roussillon. Mem Soc Geol Fr 3, 5–195

Desmarest AG (1822) Mammalogie ou description des especes de mammiferes. Seconde partie, contenant les ordres de Rongeurs des Edentes, des Pachydermes, des ruminans et des Cetaces. En encyclopedie methodique, 196 vols. Paris: Veuve Agasse 7, 277–555

Djikia N (1968) Historical Development of Akchagylian Malacofauna from eastern Georgia. Mecniereba, Tbilisi

Domingo L, Koch PL, Fernández MH, Fox DL, Domingo MS, Alberdi MT (2013) Late Neogene and early Quaternary paleoenvironmental and paleoclimatic conditions in southwestern Europe: isotopic analyses on mammalian taxa. PLoS One 8, e63739.

Domingo MS, Alberdi MT, Azanza B. (2007) A new quantitative biochronological ordination for the Upper Neogene mammalian localities of Spain. *Palaeogeogr Palaeoclimatol Palaeoecol*, 255, 361–376

Dong W, Liu J, Fang Y (2013) The large mammals from Tuozidong (eastern China) and the Early Pleistocene environmental availability for early human settlements. Quarter Int 295, 73–82

Dragoo JW, Honeycutt RL (1997) Systematics of mustelid–like carnivores. J Mammal 78, 426–443

Driesch von den A (1976) A guide to the measurement of animal bones from archaeological sites. Peabody Mus Bull 1, 1–137

Duval M, Falguères C, Bahain J-J, Grün R, Shao Q, Aubert M, Hellstrom J, Dolo J-M, Agustí J, Martínez-Navarro B, Palmqvist P, Toro-Moyano I (2011) The challenge of dating Early Pleistocene fossil teeth by the combined uranium series–electron spin resonance method: the Venta Micena palaeontological site (Orce, Spain). J Quat Sci 26, 603–615

Eizirik E, Murphy WJ, Koepfli K–P, Johnson WE, Dragoo JW, Wayne RW, O'Brien SJ (2010) Pattern and timing of diversification of the mammalian order Carnivora inferred from multiple nuclear gene sequences. Mol Phylogenet Evol 56, 49–63

Ellerman JR, Morrison–Scott TCS (1951) Checklist of palearctic and Indian mammals, 1758 to 1946. London: British Museum (Natural History)

Engesser B (1976) *Tyrrhenoglis majori*, ein neuer fossiler Gliride (Rodentia, Mammalia) aus Sardinien. Eclog Geol Helv 69,783–793

Erbajeva M, Alexeeva N (2013) Late Cenozoic mammal faunas of the Baikalian Region: composition, biochronology, dispersal, and correlation with Central Asia. Fossil mammals of Asia: Neogene biostratigraphy and chronology, 495–507.

Ercoli MD (2015) Morfología del aparato músculo–esqueletario del postcráneo de los mustélidos (Carnivora, Mammalia) fósiles y vivientes de América del Sur: implicancias funcionales en un contexto filogenético. Unpublished PhD Thesis, Universidad Nacional de La Plata, La Plat

Erxleben JCP (1777) Systema regni animalis per classes, ordines, genera, species, varietates cum synonymia et historia animalium. Classis I, Mammalia. Impensis Weygandianis, Lipsiae [Leipzig], Saxony.

Espigares MP (2010) Análisis y modelización del contexto sedimentario y los atributos tafonómicos de los yacimientos pleistocénicos del borde nororiental de la cuenca de Guadix-Baza. Ph. D. Dissertation. University of Granada, Spain

Espigares MP, Martínez-Navarro B, Palmqvist P, Ros-Montoya S, Toro I, Agustí J, Sala R (2013) *Homo* vs. *Pachycrocuta*: Earliest evidence of competition for an elephant carcass between scavengers at Fuente Nueva-3 (Orce, Spain). Quat Int 295, 113-125

Etienne J (2017) AR-Code: a Fast Path to Augmented Reality. Medium 4 Apr 2017. https://medium.com/arjs/ar-code-a-fast-path-to-augmented-reality-60e51be3cbdf

Evans HE, De Lahunta A (2013) Miller's anatomy of the dog. Elsevier Health Sciences.

Ewer RF (1956) The fossil carnivores of the Transvaal caves: Canidae. Proc Zool Soc London 126, 97–119

Ewer RF, Singer R (1956). Fossil Carnivora from Hopefield. Ann S African Mus 42, 335–347

Falconer H. & Cautley P. T. (1847). Fauna antiqua sivalensis, being the fossil zoology of the Siwalik Hills, in the North of India Illustrations, Smith, Elder and Co, London

Falconer H (1865) On the species of Mastodon and Elephant occurring in the fossil state in Great Britain. Part. II Elephant. Quarterly J Geol Soc London 21, 253–332

Farina S (2011) Late Pleistocene–Holocene mammals from "Canale delle Acque Alte (Canale Mussolini)" (Agro Pontino, Latium). B Soc Paleontol Ital 50, 11–22

Fejfar O, Sabol M, Tóth C (2012) Early Pliocene vertebrates from Ivanovce and Hajnáčka (Slovakia). VIII. Ursidae, Mustelidae, Tapiridae, Bovidae and Proboscidea from Ivanovce. Neues Jahrb Geol Paläontol 264, 95–115

Ferring R, Oms O, Agustí J, Berna F, Nioradze M, Shelia T, Lordkipanidze D (2011) Earliest human occupations at Dmanisi (Georgian Caucasus) dated to 1.85–1.78 Ma. Proc Natl Acad Sci 108(26), 10432-10436

Ferrandini J, Salotti M (1995) Decouverte d'importants remplissages fossiliferes d'age Pleistocene superieur et Holocene dans le Karst de la region d'Oletta (Haute Corse). Geobios 28, 117–124

Ficcarelli G, Torre D (1967) Il mustelide *Enhydrictis galictoides* del Pleistocene della Sardegna. Paleontogr Ital 63 (30), 139–161

Ficcarelli G, Torre D, Turner A (1984) First evidence for a species of raccoon dog, *Nyctereutes* Temminck, 1838, in South African Plio–Pleistocene deposits. Boll Soc Paleont It 23, 125–130

Figueirido B, MacLeod N, Krieger J, De Renzi M, Pérez-Claros JA, Palmqvist P (2011) Constraint and adaptation in the evolution of carnivoran skull shape. Paleobiology 37, 490–518

Filhol H (1890) Étude sur les mammifères de Sansan. Bibl Ht Études, Section Sci Nat 37, 1–319

Finarelli JA (2008) A total evidence phylogeny of the Arctoidea (Carnivora: Mammalia): Relationships among Basal Taxa. J Mammal Evo 15, 231–259

Fischer G (1817) Adversaria Zoologica. Mem Soc Imp Nat Mosc 5, 357–446

Flower WH (1869) On the value of the characters of the base of the cranium in the classification of the order Carnivora and on the systematic position of *Bassaris* and other disputed forms. Proc Zool Soc Londo, 4–37

Flower LO, Schreve DC (2014) An investigation of palaeodietary variability in European Pleistocene canids. Quaternary Sci Rev 96, 188–203

Flynn LJ, Tedford, R.H., Qiu Z (1991) Enrichment and stability in the Pliocene mammal faunas of North China. Paleobiology 17, 246-265

Flynn LJ, Nedbal MA (1998). Phylogeny of the Carnivora (Mammalia): congruence vs incompatibility among multiple data sets. Mol Phylogenet Evol 9, 414–426

Flynn LJ, Finarelli JA, Zehr S, Hsu J, Nedbal MA (2005a) Molecular phylogeny of the Carnivora (Mammalia): assessing the impact of increased sampling on resolving enigmatic relationships. Syst Biol 54, 317–37

Flynn LJ, Kowallis BJ, Nuñez C, Carranza–Castañeda O, Miller WE, Swisher III CC, Lindsay E (2005b) Geochronology of Hemphillian–Blancan Aged Strata, Guanajuato, Mexico, and Implications for Timing of the Great American Biotic Interchange. J Geol 113, 287–307

Flynn LJ, Finarelli JA, Spaulding M (2010) Phylogeny of the Carnivora and Carnivoramorpha, and the use of the fossil record to enhance understanding of evolutionary transformations, in Goswami A, Friscia A (eds) Carnivoran evolution: new views on phylogeny, form and function (Vol. 1). Cambridge University Press, pp 25-63

Forsyth Major CI (1875a) Considerazioni sulla fauna dei mammiferi pliocenici e post pliocenici della Toscana – I. La Fauna dei Mammiferi del Val d'Arno superiore. Atti Soc Tosc Sci Nat 1, 7–40

Forsyth Major CI (1875b) Considerazioni sulla fauna dei mammiferi pliocenici e post pliocenici della Toscana – II. L a Fauna dei Mammiferi del Pliocene inferiore (Orizzonte di Casino). Atti Soc Tosc Sci Nat 1, 223–245

Forsyth Major CI (1877) Considerazioni sulla fauna dei mammiferi pliocenici e post pliocenici della Toscana – III. Cani fossili del Val d'Arno superiore e della Valle d'Era. Atti Soc Tosc Sci Nat 3, 207–227

Forsyth Major CI (1901) On *Enhydrictis galictoides*, a new fossil from Sardinia. Proc Zool Soc Lond 2, 625–628

Fortelius M, Werdelin L, Andrews P, Bernor RL, Gentry A, Humphrey L, Mittmann H–W, Viranta S (1996) Provinciality, diversity, turnover, and paleoecology on land mammal faunas of the later Miocene of western Eurasia, in Bernor RL, Fahlbusch V, Mittmann H–W (eds) The Evolution of western Eurasian Neogene Mammal Faunas. New York, Columbia University Press, pp. 414–448

Frechkop S (1959) De la position systematique du genre *Nyctereutes*. Bull Mus R Hist Nat Belg 35, 1–20

Frisch JL (1775) Das Natur–System der vierfüßigen Thiere, in Günther CF (ed) Tabellen,

darinnen alle Ordnungen, Geschlechte und Arten, nicht nur mit bestimmenden Benennungen, sondern beygesetzten unterscheidenden Kennzeichen angezeigt werden zum Nutzen der erwachsenen Schuljugend:, Glogau, pp 1–30

Fulton TL, Strobeck C (2006) Molecular phylogeny of the Arctoidea (Carnivora): Effect of missing data on supertree and supermatrix analyses of multiple gene data sets. Mol Phylogenet Evol 41, 165–181

Furlong EL (1932) A new genus of otter from the Pliocene of the northern Great Basin Province. Carnegie Inst Wash Yearb 418, 93–103

Gallini V, Sala B (2001) Settepolesini di Bondeno (Ferrara – eastern Po Valley): the first example of mammoth steppe in Italy. World of Elephants – International Congress, Rome 2001, 272–275

García N (2008) "New Eucyon remains from the Pliocene Aramis Member (Sagantole Formation), Middle Awash Valley (Ethiopia)." *Comptes Rendus Palevol* 7, 583–590

García N, Arsuaga JL (1999) Carnivores from the Early Pleistocene hominid– bearing Trinchera Do lina 6 (Sierra de Atapuerca, Spain). J Hum Evol 37 (3/4), 415–430

García N, Arsuaga JL, Bermédez de Castro JM, Carbonell E, Rosas A, Huguet R (2008) The Epivillafranchian carnivore *Pannonictis* (Mammalia, Mustelidae) from Sima del Elefante (Sierra de Atapuerca, Spain) and a revision of the Eurasian occurrences from a taxonomic perspective. Quatern Int 179, 42–52

García N, Howell F (2008) New discovery of a large mustelid – *Pannonictis* cf. *nestii* – (Carnivora: Mammalia) from the early Pleistocene locality of Sima del Elefante (Sierra de Atapuerca, Spain). Paleontograph Abt A 284, 1–16

García-Aguilar JM, Guerra-Merchán A, Serrano F, Palmqvist P (2014) Ciclicidad sedimentaria en depósitos lacustres evaporíticos tipo playa-lake del Pleistoceno inferior en la cuenca de Guadix-Baza (Cordillera Bética, España). Bol Geol Min 124, 239–251

García-Aguilar JM, Guerra-Merchán A, Serrano F, Flores-Moya A, Delgado-Huertas A, Espigares MP, Ros-Montoya S, Martínez-Navarro B, Palmqvist P (2015) A reassessment of the evidence for hydrothermal activity in the Neogene-Quaternary lacustrine environments of the Baza basin (Betic Cordillera, SE Spain) and its paleoecological implications. Quat Sci Rev 112, 226–235

García-Aguilar JM, Martín JM (2000) Late Neogene to recent continental history and evolution of Guadix-Baza basin (SE Spain). Rev Soc Geol Esp 13, 65–77

García-Aguilar JM, Palmqvist P (2011) A model of lacustrine sedimentation for the Lower Pleistocene deposits of Guadix-Baza basin (southeast Spain). Quat Int 243, 3–15 García Tortosa FJ, Sanz de Galdeano C, Alfaro P, Jiménez Espinosa R, Jiménez Millán J, Lorite Herrera M (2008) Nueva evidencia sobre la edad del tránsito endorreico-exorreico de la cuenca de Guadix-Baza. Geogaceta 44, 211–214

Garrido G (2008) El registro de *Vulpes alopecoides* (Forsyth–Major, 1877), *Canis etruscus* Forsyth–Major, 1877 y *Canis* cf. *falconeri* Forsyth–Major, 1877 (Canidae, Carnivora, Mammalia) en Fonelas P–1 (Cuenca de Guadix, Granada) in Arribas A (ed) Vertebrados del Plioceno Superior terminal en el suroeste de Europa: Fonelas p–1 y el proyecto Fonelas. Cuadernos del Museo Geominero, nº 10. Instituto Geológico y Minero de España, Madrid, pp 159–186

Garrido G, Arribas A (2008) *Canis accitanus*: a new species of canid (Canidae, Carnivora, Mammalia) from the late Upper Pliocene Fonelas P-1 site (Guadix basin, Granada), in Arribas A (ed), Vertebrados del Plioceno superior terminal en el suroeste de Europa: Fonelas P-1 y el Proyecto Fonelas.Cuadernos del Museo Geominero, nº 10. Instituto Geológico y Minero de España, Madrid, 2008, 187–199

Gaspard M (1964) La région de l'angle mandibulaire chez les Canidae. Mammalia 28, 249–329

Gasparik M, Pazonyi P (2018) The macromammal remains and revised faunal list of the Somssich Hill 2 locality (late Early Pleistocene, Hungary) and the Epivillafranchian faunal change. Fragm Palaeontol Hung 35, 153–178

Gatta M, Rolfo M. F, Petronio C, Salari L, Silvestri L (2016) Late Pleistocene skeleton of *Canis lupus* L., 1758 from Grotta Mora Cavorso (Jenne, Latium, central Italy). CR Palevol 15, 941–949

Gaubert P, Bloch C, Benyacoub S, Abdelhamid A, Pagani P, Djagoun CA, Couloux A, Dufour S. Reviving the African wolf *Canis lupus lupaster* in North and West Africa: a mitochondrial lineage ranging more than 6,000 km wide. PLoS One 7, e42740

Gaur R (1987) Environment and ecology of early man in Northweston India. BR Publishing Corp, Delhi.

Gazin CL (1942) The late Cenozoic vertebrate faunas from the San Pedro Valley, Ariz. Proc US National Museum 92, 475–518

Gazin CL (1942) The late Cenozoic vertebrate faunas from the San Pedro Valley, Ariz. Proceedings of the United States National Museum 92: 475–518

Geoffroy Saint–Hilaire E, Cuvier FD (1795) Memoire sur une nouvelle division des mammifires, et sur les principes qui doivent servir de base dans cette sorte de travail. Magasin Encyclopedique, Millin, Noel et Warens, Paris 2, 164–190

Geoffroy Saint–Hilaire E, Cuvier FD (1824) Histoire Naturelle des Mammifères, Tome Deuxième (Chez A. Belin)

Geraads D (1997) Carnivores du Pliocène terminal de Ahl al Oughlam (Casablanca, Maroc). Geobios 30, 127–164

Geraads D (2008) Plio–Pleistocene Carnivora of northwestern Africa: A short review. CR Palevol 7, 591–599

Geraads D (2011) A revision of the fossil Canidae (Mammalia) of north-western Africa. Palaeontology 54 (2), 429–446

Geraads D (2016) Pleistocene Carnivora (Mammalia) from Tighennif (Ternifine), Algeria. Geobios 49, 445–458

Geraads D, Alemseged Z, Reed D, Wynn J, Roman DC (2004) The Pleistocene fauna (other than Primates) from Asbole, lower Awash Valley, Ethiopia, and its environmental and biochronological implications. Geobios 37, 697–718

Geraads D, Alemseged Z, Bobe R, Reed D (2010) *Nyctereutes lockwoodi*, n. sp., a new canid (Carnivora: Mammalia) from the middle Pliocene of Dikika, Lower Awash, Ethiopia. J Vert Paleont 30, 981–987

Geraads D, Drapeau MS, Bobe R, Fleagle JG (2015) *Vulpes mathisoni*, sp. nov., a new fox from the Pliocene Mursi Formation of southern Ethiopia and its contribution to the origin of African foxes. J Vert Paleontol 35(4), e943765

Gervais P (1844) *Lycondon*, in d'Orbigny (ed). Dict Univ Hist Nat 4, 685

Gervais P (1848–1852) Zoologie et Paléontologie françaises, premiere édition, tome II et III. Paris (Bertrand). https://doi.org/10.5962/bhl.title.39473

Gervais P (1859) Zoologie et Paléontologie françaises, deuxième édition. Paris (Bertrand). http://numerique.bibliotheque.toulouse.fr/ark:/36254/B315555103_A101

Ghezzo E, Rook L (2014). *Cuon alpinus* (Pallas, 1811) (Mammalia, Carnivora) from Equi (Late Pleistocene, Massa–Carrara, Italy): anatomical analysis and palaeoethological

contextualisation. *Rendiconti Lincei 25*, 491–504

Gibert L, Scott GR, Montoya P, Ruiz–Sanchez FJ, Morales J, Luque L, Abella J, Lería M (2013) Evidence for an African–Iberian mammal dispersal during the pre–evaporitic Messinian. Geology 41, 691–694

Gilbert C, Ropiquet A, Hassanin A (2006) Mitochondrial and nuclear phylogenies of Cervidae (Mammalia, Ruminantia): Systematics, morphology, and biogeography. Mol Phylogenet Evol 20, 101–117

Gimranov DO, Kosintsev PA, Gasilin VV (2015) Species diagnostics of corsac (*Vulpes corsac*), fox (*Vulpes vulpes*), and arctic fox (*Vulpes lagopus*) according to ontological characteristics of mandible teeth. Zool J 94(11), 1338-1338 (in russian).

Gimranov DO (2017) Species diagnostics of the corsac (*Vulpes corsac*), fox (*Vulpes vulpes*) and arctic fox (*Vulpes lagopus*, Carnivora, Canidae) using the upper teeth. Zool J 96.6, 684-697

Ginsburg L (1998) Le gisement de vertébrés pliocènes de Çalta, Ankara, Turquie. 5. Carnivores. Geodiversitas 20, 379–396

Ginsburg L, Morales J (1992) Contribution à la connaissance des Mustélidés (Carnivora, Mammalia) du Miocène d'Europe *Trochictis* et *Ischyrictis*, genres affines et genres nouveaux. CR Acad Sci II 315:111–116

Gliozzi E, Abbazzi L, Argenti A, Azzaroli A, Caloi L, Capasso Barbato L, Di Stefano G, Esu D, Ficcarelli G, Girotti O, Kotsakis T, Masini F, Mazza P, Mezzabotta C, Palombo MR, Petronio C, Rook L, Sala B, Sardella R, Zanalda E, Torre D (1997) Biochronology of selected Mammals. Molluscs and Ostracodes from the Middle Pliocene to the Late Pleistocene in Italy. The state of the art. Riv Ital Paleontol Strat 103, 369–388

Goldfuss GA (1810) Die Umgebungen von Muggensdorf. Ein Taschenbuch für Freunde der Natur und Alterumskunde. Erlangen, Palm

Golobov PA, Catalano SA (2016) TNT version 1.5, including a full implementation of phylogenetic morphometrics. Cladistics 32, 221–238

Gompper ME, Petrites AE, Lyman RL (2006) Cozumel Island fox (*Urocyon* sp.) dwarfism and possible divergence history based on subfossil bones. J Zool 270(1), 72–77 https://doi.org/10.1111/j.1469–7998.2006.00119.x

Goswami A (2010) Introduction to carnivoran evolution, in Goswami A, Friscia A (eds) Carnivoran evolution: new views on phylogeny, form and function (Vol. 1).

Cambridge University Press, pp 1–24

Goswami A, Friscia A (eds) (2010) Carnivoran evolution: new views on phylogeny, form and function (Vol. 1). Cambridge University Press.

Gradstein F, Ogg J, Smith A (eds) (2004) A Geologic Time Scale 2004. Cambridge University Press, Cambridge.

Gray J (1827) Synopsis of the species of the class Mammalia, in Cuvier G (ed) The Animal Kingdom Arranged in Conformity with its Organization, additional descriptions by Edward Griffith and others, London: George B. Whittaker,Vol. 5, pp 1-391

Gray J (1834) Illustration of Indian zoology, consisting of coloured plates of new or hitherto unfigured Indian animals from the collection of Major General Hardwicke. Fol London 2, pl 1

Gray J (1837) Description of some new or little known Mammalia, principally in the British Museum Collection. Charlesworth's Magazine of Natural History 1, 577–587

Grewal SK, Wilson PJ, Kung TK, Shami K, Theberge MT, Theberge JB, White BN (2004). A genetic assessment of the eastern wolf (*Canis lycaon*) in Algonquin Provincial Park. J Mammal 85, 625–632

Haba C, Oshida T, Sasaki M, Endo H, Ichikawa H, Masuda Y (2008) Morphological variation of the Japanese raccoon dog: Implications for geographical isolation and environmental adaptation. J Zool 274, 239–247

Haile–Selassie Y, Howell FC (2009) Carnivora in Haile-Selassie Y, WoldeGabriel G (eds) *Ardipithecus kadabba.* Late Miocene Evidence from the Middles Awash, Ethiopia. University of California Press, Berkeley, pp 237–276

Hall ER (1935) A new mustelid genus from California. J Mammal 16, 137–138

Hamilton Smith C (1839) The Canine Family in general or the genus *Canis*, in Jardine W (ed) The naturalist's library, vol. 18. Natural history of dogs, vol. 1. Edinburgh: WH Lizars, pp 267

Hamilton Smith C (1842) Introduction to the Mammalia. The Naturalist's Library 13, 1–299

Hammer Ø (2016) PAST. PAleontologial STatistics. Version 3.14. Reference manual: Natural History Museum, University of Oslo

Hammer Ø, Harper DAT, Ryan P.D. (2001) – PAST: Paleontological statistics software

package for education and data analysis. Palaeontol Electron 4: art. 4.

Harrison T (2011) Paleontology and geology of Laetoli: Human evolution in context. Springer

Hartstone–Rose A, Kuhn BF, Nalla S, Werdelin L, Berger LR (2013) A new species of fox from the *Australopithecus sediba* type locality, Malapa, South Africa. Trans R Soc South Africa 68 (1), 1–9

Hay OP (1921) Descriptions of species of Pleistecene vertebrata, types or specimens most of which are preserved in the United States National Museum. Proc US Nat Mus 59, 599–642.

Hemmer H, Kahlke R–D, Vekua A (2004) The Old World puma – *Puma pardoides* (Owen, 1846) (Carnivora: Felidae) in the Lower Villafranchian (Upper Pliocene) of Kvabebi (east Georgia, Transcaucasia) and its evolutionary and biogeographical significance. Neues Jahrb Geol Paläontol 233, 197–231

Hemprich FG, Ehrenberg CG (1828–1834) Symbolae physicae, seu icones et descriptiones corporum naturalium novorum aut minus cognitorum quae ex itineribus per Libyam, Aegyptium, Nubiam, Dongalam, Syriam, Arabiam et Habessiniam, pars zoologica II, anima. Berlin, Officina Academica

Henning W (1966) Phylogenetic Systematics. Urbana: Univ Illinois Press

Hershkovitz P (1949) Status of names credited to Oken, 1816. Am Soc Mammal 30, 289–301

Hibbard CW (1941) New Mammals from the Rexroad Fauna, Upper Pliocene of Kansas. Am Midl Nat 26, 337–368

Hilgen FJ, Lourens LJ, Van Dam JA, Beu AG, Boyes AF, Cooper RA, Krijgsman W, Piller WE, Wilson DS. The Neogene Period, in Gradstein F, Ogg JG, Schmitz MD, Ogg GM, editors. The Geologic Time Scale 2012 2–Volume Set; 2012. pp. 923–978.

Hilzheimer M (1906) Die geographische Verbreitung der afrikanischen Grauschakale. Zoologischer Beobachter 47, 363–373

Hirasawa M, Kanda E, Takatsuki S (2006) Seasonal food habits of the raccoon dog at a western suburb of Tokyo. Mammal study 31, 9–14

Hodgson BH (1838) Proceedings of learned societies. Ann Nat His 1, 1–152

Hornaday WT (1904) A new species of raccoon dog. Ann Rep New York Zool Soc 8,

71–73

Horowitz A (1979) The quaternary of Israel. Academic Press.

Hough JR (1948) The auditory region in some members of the Procyonidae, Canidae and Ursidae: Its significance in the phylogeny of the Carnivora. Bull Am Mus Nat Hist 92, 67–118

Hough JR (1953) Auditory region in North American fossil Felidae: Its significance in phylogeny. US Geol Surv Professional Papers 243, 95–115

Howard O, Clark J, Murdoch JD, Newman DP, Sillero–Zubiri C (2009) *Vulpes corsac* (Carnivora: Canidae). Mammalian Species 832, 1–8

Howell FC, García N (2007) Carnivora (Mammalia) from Lemudong'o (Late Miocene: Narok District, Kenya). Kirtlandia56, 121–139

Hoyos M, Soler V, Rodríguez E, Carracedo JC, Chicharro PM (1987) Posición magnetoestratigráfica de los yacimientos de vertebrados neógenos de Algora y Layna (Cordillera Ibérica). Reunión de Paleomagnetismo. Arenys de Mar, Spain

Hunt RM (1974) The auditory bulla in Carnivora: An anatomical basis for reappraisal of carnivore evolution. J Morph 143, 21–76

Hunter L (2011) Carnivores of the World. Illustration by Barrett, P. Princeton: Princeton University Press

Huxley TH (1880) On the Cranial and Dental Characters of the Canidæ. Proc Zool Soc London 48, 238–288

Hüsing SK, Oms O, Agustí J, Garcés M, Kouwenhoven TJ, Krijgsman W, Zachariasse WJ (2010) On the late Miocene closure of the Mediterranean-Atlantic gateway through the Guadix basin (southern Spain). Palaeogeogr Palaeoclimat Palaeoecol 291, 167–179

Illiger K (1815) Überblick der Säugethiere nach ihrer Verteilung über die Welttheile. Ab König Akad Wiss Berlin Jähren 1804–1811, 39–159

International Commission on Zoological Nomenclature (1999) International Code of Zoological Nomenclature, fourth ed. International Trust for Zoological Nomenclature, London

Iurino DA, Profico A, Cherin M, Veneziano A, Costeur L, Sardella R (2015). A lynx

natural brain endocast from Ingarano (Southern Italy; Late Pleistocene): Taphonomic, Morphometric and Phylogenetic approaches. Hystrix 26, 110-117

Ivanoff DV (1996) Systematic position of "*Vulpes*" *odessana* Odintzov, 1967 (Carnivora, Canidae) from the Ruscinian of the northern Black–Sea maritime province. Enigmatic Organisms in the Evolution and Phylogeny. Palaeontol Inst Moscow, Abstracts, 37–39

Ivanoff DV (2000) Origin of the septum in the canid auditory bulla: Evidence from morphogenesis. Acta Theriol 45, 253–270

Ivanoff DV (2001) Partitions in the carnivoran auditory bulla: their formation and significance for systematics. Mammal Reviews 31, 1–16

Ivanoff DV (2007) Unlocking the ring: Occurrence and development of the uninterrupted intrabullar septum in Canidae. Mammal Biol 72, 145–162

Ivanoff DV, Wolsan M, Marciszak A (2014) Brainy stuff of long–gone dogs: A reappraisal of the supposed Canis endocranial cast from the Pliocene of Poland. Naturwissenschaften 101, 645–651

Janis CM (1993) Tertiary mammal evolution in the context of changing climates, vegetation, and tectonic events. Ann Rev Ecol Syst 24, 467–500

Jánossy D (1986) Pleistocene Vertebrate Faunas of Hungary. Akadémiai Kiadó, Budapest

Jefferson GT (1991) A catalogue of late Quaternary vertebrates from California. Part 2. Mammals. Nat. Hist. Mus. Los Angeles County Techn Rep 7, 1–129

Jiangzuo Q, Liu J, Wagner J, Dong W, Chen J (2018) Taxonomical revision of fossil Canis in Middle Pleistocene sites of Zhoukoudian, Beijing, China and a review of fossil records of *Canis mosbachensis variabilis* in China. Quat Int 482, 93-108

Jiangzuo Q, Liu J, Jin C, Song Y, Liu S, Lü S, Liu J (2019) Discovery of *Enhydrictis* (Mustelidae, Carnivora, Mammalia) cranium in Puwan, Dalian, Northeast China demonstrates repeated intracontinental migration during the Pleistocene. Quat Int 513, 18-29

Jin CZ, Liu JY (2009) Paleolithic Site–The Renzidong Cave, Fanchang, Anhui Province. Science Press, Beijing

Johnson WE, Eizirik E, Pecon–Slattery J, Murphy WJ, Antunes A, Teeling E, O'Brien SJ (2006) The Late Miocene radiation of modern Felidae: a genetic assessment. Science 311, 73–77

Johnston CS (1938) Preliminary report on the vertebrate type locality of Cita Canyon, and the description of an ancestral coyote. Am J Sc 35: 383–390

Kahlke RD (1994) Die Entstehungs–, Entwicklungs– und Verbreitungsgeschichte des oberpleistozänen *Mammuthus–Coelodonta*–Faunenkomplexes in Eurasien (Großsäuger). Abh Senckenb Naturforsch Ges 546, 1–164

Kahlke RD (2014) The origin of Eurasian Mammoth Faunas (*Mammuthus–Coelodonta* Faunal Complex). Quat Sci Rev 96, 32–49

Kahlke RD, García N, Kostopoulos DS, Lacombat F, Lister AM, Mazza PPA, Spassov N, Titov VV (2011) western Palaearctic palaeoenvironmental conditions during the Early and early Middle Pleistocene inferred from large mammal communities, and implications for hominin dispersal in Europe. Quat Sci Rev 30(11–12), 1368–1395 https://doi.org/10.1016/j.quascirev.2010.07.020

Karoui–Yaakoub N, Mtimet MS, Bejaoui S, Amri L, Khalloufi N, Ben Aissa L, Martinez–Navarro B, (2016) Middle–to–Late Pleistocene malacofauna from the archaeo–paleontological site of Oued Sarrat (Tajerouine area, NW Tunisia). Arab J Geosci 9, 345

Kauhala K, Viranta S, Kishimoto M, Helle E, Obara I (1998) Skull and tooth morphology of Finnish and Japanese raccoon dogs. Ann Zool Fennici 35, 1–16

Kauhala K, Auniola M (2001) Diet of raccoon dogs in summer in the Finnish archipelago. Ecography 21, 151–156

Kaup JJ (1829) Skizzirte Entwickelungs–Geschichte und Natürliches System der Europaischen Thierwelt. C. W Leske, Darmstadt, Germany.

Kaup JJ (1835) Das Thierreich in seinen Hauptformen systematisch beschrieben. Darmstadt. https://doi.org/10.5962/bhl.title.130484

Kavanagh KD, Evans AR, Jernvall J (2007) Predicting evolutionary patterns of mammalian teeth from development. *Nature* 449, 427–432

Keen JA, Grobbelaar CS (1940) The comparative anatomy of the tympanic bulla and auditory ossicles, with a note suggesting their function. Trans Royal Soc S Africa 28, 307–329

Kemp TS (2005) The origin and evolution of mammals. Oxford University Press

Kim SI, Park SK, Lee H, Oshida T, Kimura J, Kim YJ, Nguyen ST, Sashika M, Min MS (2013) Phylogeography of Korean raccoon dogs: Implications of peripheral isolation

of a forest mammal in east Asian. J Zool 290, 225–235

Kim SI, Oshida T, Lee H, Min MS, Kimura J (2015) Evolutionary and biogeographical implications of variation in skull morphology of raccoon dogs (*Nyctereutes procyonoides*, Mammalia: Carnivora). Biol J Linnean Soc 116, 856–872

Kleiman DG (1967) Some aspects of social behavior in the Canidae. Am Zool 7, 365–372

Klein RG (1986) Carnivore size and Quaternary climatic change in Southern Africa. Quaternary Res 26, 153–170

Klein RG, Scott K (1989) Glacial/Interglacial size variation in fossil spotted Hyena (*Crocuta crocuta*) from Britain. Quaternary Res 32, 88–95.

Koepfli KP, Deere KA, Slater GJ, Begg C, Begg K, Grassman L, Lucherini M, Veron G, Wayne RK (2008) Multigene phylogeny of the Mustelidae: resolving relationships, tempo and biogeographic history of a mammalian adaptive radiation. BMC Biol 6, 1–22

Koepfli KP, Pollinger J, Godinho R, Robinson J, Lea A, Hendricks S, Schweizer RM, Thalmann O, Silva P, Fan Z, Yurchenko AA, Dobrynin P, Makunin A, Cahill JA, Shapiro B, Álvares F, Brito JC, Geffen E, Leonard JA, Helgen KM, Johnson WE, O'Brien SJ, Van Valkenburgh B, Wayne RK (2015) Genome–wide evidence reveals that African and Eurasian golden jackals are distinct species. Curr Biol 25, 2158–2165

Koepfli K–P, Deere KA, Slater GJ, Begg C, Begg K, Grassman L, Lucherini M, Veron G, Wayne RK (2008) Multigene phylogeny of the Mustelidae: resolving relationships, tempo and biogeographic history of a mammalian adaptive radiation. BMC Biol 6, 1–22

Kormos T (1931) *Pannonictis pliocaenica* n. g. n. sp., a new giant mustelid from the Late Pliocene of Hungary. Ann Inst Reg Hung Geol 29, 1–16

Kormos T (1932) Die Füchse des ungarischen Oberpliozän: Fol Zool Hydrobiol 4, 167–188

Kormos T (1933) Neue und wening bekannte Musteliden aus dem ungarischen Oberpliozän. Fol Zool Hydrobiol 5, 129–158

Kormos T (1931) Oberpliozäne Wühlmäuse von Senèze (Haute–Loir) und Val d'Arno (Toscana). Schweiz palaeontol Abh 51, 1–14

Kosintsev P (2007) Late Pleistocene large mammal faunas from the Urals. Quat Int 160, 112–120

Kostopoulos DS, Sen S (1999) Late Pliocene (Villafranchian) mammals from Sarikol Tepe, Ankara, Turkey. Mitt. Bayer Staat Paläontol Hist Geol 39, 165–202

Kotlia BS (1987) A new Pleistocene canid from the Upper Karewas of Kashmir basin, India. J Palaeontol Soc India 32, 108–113

Kotsakis T, Barisone G, Rook L (1997) Mammalian biochronology in an insular domain: the Italian Tertiary faunas. Mém Trav EPHE Inst Monpellier 21, 431–441

Koufos GD (1987) *Canis arnensis* Del Campana, 1913 from the Villafranchian (Villanyian) of Macedonia (Greece). Paleontol Evol 21, 3–10

Koufos GD (1992) The Pleistocene Carnivores of the Mygdonia basin (Macedonia, Greece). Ann Paleontol 78 (4), 205–257

Koufos GD (1993) Late Pliocene carnivores from western Macedonia (Greece). Paläontologische Zeitschrift 67 (3/4), 357–376

Koufos GD (1997) The canids *Eucyon* and *Nyctereutes* from the Ruscinian of Macedonia, Greece. Paleontol Evol 30–31, 39–48

Koufos GD (2014) The Villafranchian carnivoran guild of Greece: implications for the fauna, biochronology and paleoecology. Integr Zool 9, 444–460

Koufos GD (2018) New Material and Revision of the Carnivora, Mammalia from the Lower Pleistocene Locality Apollonia 1, Greece. Quaternary 1 (1), 6

Koufos GD, Kostopoulos DS (1997a). Biochronology and succession of the Plio–Pleistocene macromammalian localities of Greece. *Mémoires et travaux de l'Institut de Montpellier*, (21), 619–634.

Koufos GD, Kostopoulos DS (1997b) New Carnivore material from the Plio–Pleistocene of Macedonia (Greece) with a description of a new canid. Münchner Geowiss Abhlungen 34, 33–63

Kretzoi M (1938) Die Raubtiere von Gombaszög nebst einer Übersicht der Gesamtfauna. Ein Beitrag zur Stratigraphie des Altquartaera. Ann Mus Nat Hung 31, 88–157

Kretzoi M (1943) *Kochictis centenii* n. g. n. sp., ein alterümlicher Creodonte aus dem Oberoligozän ienbenbürgens. Földtany Közlöny 52, 190–195

Krijgsman W, Tesakov A, Yanina T, Lazarev S, Danukalova G, Van Baak CGC, Flecker R, Frolov P, Hoyle TM, Jorissen EL, Kirscher U, Koriche SA, Kroonenberg SB, Lordkipanidze D, Oms O, Rausch L, Singarayer J, Stoica M, van de Velde S, Titov

VV, Wesselingh FP (2019) Quaternary time scales for the Pontocaspian domain: Interbasinal connectivity and faunal evolution. Earth Sci Rev 188, 1–40

Kurtén B (1965) The Carnivora of the Palestine Caves. Acta Zool Fenn 107, 3–74

Kurtén B (1968) Pleistocene mammals of Europe. Aldine Publishing Company, Chicago

Kurtén B, Crusafont-Pairó M (1977) Villafranchian carnivores (Mammalia) from La Puebla de Valverde (Teruel, Spain): Comm Biol Soc Scient Fennica 85, 1–39

Kurtén B, Anderson E (1980) Pleistocene Mammals of North America. New York: Columbia University Press

Kurtèn B, Werdelin L (1988) A review of the genus *Chasmaporthetes* Hay, 1921 (Carnivora, Hyaenidae). J Vert Paleontol 8, 46–66

Leidy J (1858) Notice of remains of extinct Vertebrata, from the valley of the Niobrara River, collected during the exploring expedition of 1857, in Hayden FV (ed) Nebraska, under the command of Liet. G. K. Warren, U. S. Topographical Engineer, by, Geologist to the expedition. J Acad Nat Sci Phila 10: 20–29

Li Q, Wang X, Qiu Z (2003) Pliocene mammalian fauna of Gaotege in Nei Mongol (Inner Mongolia), China. Vertebrata PalAsiatica 41, 104– 114

Li Y, Zhang Y, Wu X, Ao H (2014) Late Cenozoic Climate Change in Asia (Vol. 16)

Lindblad-Toh K, Wade CM, Mikkelsen TS, Karlsson EK, Jaffe DB, Kamal M, Clamp M, Chang JL, Kulbokas III EJ, Zody MC, Mauceli E, Xie X, Breen M, Robert K. Wayne RB, Ostrander EA, Ponting CP, Galibert F, Smith DR, deJong PJ, Kirkness E, Alvarez P, Biagi T, Brockman W, Butler J, Chin CW, Cook A, Cuff J, Daly MJ, DeCaprio D, Gnerre S, Grabherr M, Kellis M, Kleber M, Bardeleben C, Goodstadt L, Heger A, Hitte C, Kim L, Koepfli KP, Parker HG, Pollinger JP, Stephen MJ, Searle SMJ, Sutter NB, Thomas R, Webber C, Broad Institute Genome Sequencing Platform, Lander ES (2005). Genome sequence, comparative analysis, and haplotype structure of the domestic dog. Nature, 438, 803–819

Lindsay EH, Opdyke ND, Johnson NM (1980) Pliocene dispersal of the horse *Equus* and late Cenozoic mammal dispersal events. Nature 287, 135–138

Lindsay EH, Johnson NM, Opdyke ND, Butler RF (1987) Mammalian chronology and the magnetic polarity time scale, in Woodburne MO (ed), Cenozoic Mammals of North America: Geochronology and biostratigraphy. pp. 269–284

Link HF (1795) Beytrage zur Naturgeschichte. Ueber die Lebenskrafte in naturhistorischer

Riicksicht und die Classification der Saugethiere. K. C. Stiller, Rostock und Leipzig l, 1-126

Linnaeus C (1758) Systema naturae per regna tria naturae, secundum classes, ordines, genera, species, cum characteribus, differentiis, in Synonymis, Locis, Editio Decima, Tomus I. Laurentius Salvius, Stockholm, reformata

Linnaeus C (1766) Systema naturae per regna tria naturae, secundum classes, ordines, genera, species, cum characteribus, differentiis synonymis, locis. Regum animale. Class I, Mammalia. 12th ed. Laurentii Salvii, Stockholm

Linnaeus C (1768) Systema naturae per regna tria naturae, secundum classes, ordines, genera, species, cum characteribus, differentiis synonymis, locis. Regum animale. Class I, Mammalia. 12th ed. Laurentii Salvii, Stockholm

Lister AM (2004) The impact of Quaternary Ice Ages on mammalian evolution. Philosophical Transactions of the Royal Society B: Biological Sciences, 359(1442), 221–241

López Martínez N (1974) Evolution de la lignée d'Ochotonidés *Piezodus–Prolagus* dans le Cénozoïque d'Europe Sud–Occidentale. Unpublished Ph.D. Thesis, Université des Sciences et Techniques du Languedoc, Montpellier.

López Martínez N (1989) Revisión sistemática y biostratigráfica de los Lagomorpha (Mammalia) del Terciario y Cuaternario de España. Mem Mus Paleontol Universidad de Zaragoza 3, 5–343

Lordkipanidze, D., Jashashvili, T., Vekua, A., de León, M. S. P., Zollikofer, C. P., Rightmire, G. P., et al. (2007). Postcranial evidence from early Homo from Dmanisi, Georgia. Nature 449(7160), 305

Lordkipanidze, D., de León, M. S. P., Margvelashvili, A., Rak, Y., Rightmire, G. P., Vekua, A., and Zollikofer, C. P. (2013). A complete skull from Dmanisi, Georgia, and the evolutionary biology of early Homo. Science 342(6156), 326-331

Losey RJ, Osipov B, Sivakumaran R, Nomokonova T, Kovychev E V., Diatchina NG (2015) Estimating Body Mass in Dogs and Wolves Using Cranial and Mandibular Dimensions: Application to Siberian Canids. Int J Osteoarchaeol 25, 946–959

Lund PW (1839) Coup d'oeil sur les especes eteintes de mammiferes du Brasil; extrait de quelques memoires presentes a l'Academie royale de Copenhaguen. Ann Sci Nat 11, 214–234

Lund PW (1842) Blik paa Brasiliens Dyreverden för Sidste Jordomvaeltning. Det Kongelige Danske Videnskabernes Selskabs Naturvidenskabelige og Mathematiske Afhandlinger 9, 137–208

Luterbacher HP, Ali JR, Brinkhuis H, Gradstein FM, Hooker JJ, Monechi S, Ogg JG, Powell J, Rohl U, Sanfilippo A, Schmitz B (2004) The Paleogene Period, in Gradstein FM, Ogg JG, Smith AG (eds), A Geologic Time Scale 2004. Cambridge University Press, Cambridge, UK, pp 384–408

Lyras GA (2009) The evolution of the brain in Canidae (Mammalia: Carnivora). Scripta Geol 139

Lyras GA, Van Der Geer AA (2003) External brain anatomy in relation to the phylogeny of Caninae (Carnivora: Canidae). Zool J Linnean Soc London 138, 505–522

Lyras GA, van der Geer AA, Dermitzakis M (2001) Evolution of the brain of Plio/Pleistocene wolves. Cranium 18, 30–40

Maas B (1993) Bat–eared fox behavioural ecology and the incidence of rabies in the Serengeti National Park. Onderstepoort Vet Res 60, 389–393

MacArthur RH, Wilson EO (1963) An equilibrium theory of insular zoogeography. Evolution 17, 373–387

Macdonald DW, Sillero–Zubiri C (2004) The biology and conservation of wild canids. 464 pp. Oxford University Press, Oxford

Maddison WP, Maddison DR (2018) Mesquite: a modular system for evolutionary analysis. http://www.mesquiteproject.org

Madurell–Malapeira J, Palombo MR, Sotnikova M (2015) *Cynotherium malatestai* sp. nov. (Carnivora, Canidae) from the early middle Pleistocene deposits of Grotta dei Fiori (Sardinia, western Mediterranean). J Vert Pal 35, e943400

Madurell–Malapeira J, Ros–Montoya S, Espigares MP, Alba DM, Aurell–Garrido JA (2014) Villafranchian large mammals from the Iberian Peninsula: paleobiogeography, paleoecology and dispersal events. J Iber Geol 40, 141–155

Madurell–Malapeira J, Alba DM, Moyà–Solà S (2009) Carnivora from the late early Pleistocene of Cal Guardiola (Terrassa, Vallès–Penedès Basin, Catalonia, Spain). J Palaeontol 83, 969–974

Malcom JR (1986). Socio–ecology of bat–eared foxes (*Otocyon megalotis*). J Zool 208, 457–467

Marmi J, Lopez–Giraldez F, Domingo–Roura X (2004). Phylogeny, evolutionary history and taxonomy of the Mustelidae based on sequences of the cytochrome b gene and a complex repetitive flanking region Zool Scripta, 481–499

Marshall LG, Butler RF, Drake RE, Curtis GH (1982) Geochronology of type Uquian (Late Cenozoic) land mammal age, Argentina. Science 216, 986–989

Martelli A (1906) Su due mustelidi e un felide del Pliocene Toscano. Boll Soc. Geol It 25, 596–612. https://archive.org/details/bollettinodellas2519soci

Martin R (1971) Les affinités de *Nyctereutes megamastoides* (Pomel), canidé du gisement villafranchien de Saint–Vallier (Drôme, France). Palaeovertebrata 4, 39–58

Martin R (1973) Trois nouvelles espèces de Caninae (Canidae, Carnivora) des gisements Plio–Villafranchiens d'Europe. Doc Lab Geol Fac Sci Lyon 57, 87–96

Martínez-Navarro B (1991) Revisión Sistemática y estudio cuantitativo de la fauna de macromamíferos del yacimiento de Venta Micena (Orce, Granada). PhD Universidad Autónoma de Barcelona, Ed. Microfilm, 264 pp

Martínez-Navarro B (1992) Revisión sistemática de la fauna de macromamíferos del yacimiento de Venta Micena (Orce, Granada, España). J. Gibert (coord. edic.) Presencia humana en el Pleistoceno inferior de Granada y Murcia). Ediciones del Museo de Prehistoria José Gibert, Ayuntamiento de Orce, pp 21–86

Martínez-Navarro B (2002) Presence of African large mammals (primates, carnivores and ungulates) in the Lower Pleistocene of the Middle East and Europe in Dermitzakis, E (ed), Proceedings of the 1st International Workshop of Paleoanthropology and Paleontology 'Late Plio/Pleistocene Extinction in the Palearctic.' Lesbos Island (Greece). Ann Geol Pays Hellèniques XXXIX, 337–351

Martínez-Navarro B (2010) Early Pleistocene faunas of Eurasia and hominid dispersals. In: Fleagle JG, Shea JJ, Grine FE, Baden AL, Leakey RE (eds), Out of Africa I: Who? When? and Where?, Vertebrate Paleobiology and Paleoanthropology Series: Springer Press, Chapter 13, pp. 207–224

Martínez-Navarro B, Palmqvist P (1995) Presence of the African machairodont *Megantereon*

whitei (Broom, 1937) (Felidae, Carnivora, Mammalia) in the Lower Pleistocene site of Venta Micena (Orce, Granada, Spain), with some considerations on the origin, evolution and dispersal of the genus. J Archaeol Sci 22, 569–582

Martínez–Navarro B, Rook L (2003) Gradual evolution in the African hunting dog lineage. Systematic implications. CR Palevol 2, 695–702

Martínez-Navarro B, Belmaker M, Bar-Yosef O (2009) The large carnivores from 'Ubeidiya (Early Pleistocene, Israel): biochronological and biogeographical implications. J Hum Evol 56, 514–524

Martínez-Navarro B, Espigares MP, Pastó I, Ros-Montoya S, Palmqvist P (2014) Early *Homo* fossil records of Europe, in Smith C (ed), Encyclopedia of Global Archaeology, 2561–2570

Martínez–Navarro B, Ros–Montoya S, Espigares MP, Palmqvist P (2011) Presence of Asian origin Bovini, *Hemibos* sp. aff. *H. gracilis* and *Bison* sp., at the Early Pleistocene site of Venta Micena (Orce, Spain). Quat Int 243 54–60

Martínez-Navarro B, Turq A, Agustí J, Oms O (1997) Fuente Nueva-3 (Orce, Granada, Spain) and the first human occupation of Europe. J Hum Evol 33, 611–620

Martínez-Navarro B, Palmqvist P, Madurell-Malapeira J, Ros-Montoya S, Espigares MP, Torregrosa V, Pérez-Claros JA (2010) La fauna de grandes mamíferos de Fuente Nueva-3 y Barranco León-5: Estado de la cuestión, in Toro I, Martínez-Navarro B, Agustí J (eds), Ocupaciones Humanas en el Pleistoceno inferior y medio de la cuenca de Guadix-Baza, Memoria Científica. Junta de Andalucía. Consejería de Cultura. E.P.G. Arqueología Monográfico, pp 197–236

Martínez–Navarro B, Karoui–Yaakoub N, Oms O, Amri L, López–García J–M, Zerai K, Blain HA, Mtimet MS, Espigares P, Ben Haj Ali N, Ros–Montoya S, Boughdiri M, Agustí J, Ammar H, Maalaoui K, Om El Khir O, Sala R, Othmani A, Hawas R, Gómez–Merino G, Solè A, Carbonell E, Palmqvist P (2014).The early Middle Pleistocene archeopaleontological site of Wadi Sarrat (Tunisia) and the earliest record of *Bos primigenius*. Quat Sci Rev 90, 37–46

Martini F, Sala B, Bartolomei G, Tonon M, Cattani L (1974) La Grotta Tina a Marina di Camerota (Salerno). Boll Paletnol Italiana 81, 27–79

Masini F, Torre D (1987) Review of the Villafranchian Arvicolids of Italy. Geol Rom 26,

127–133

Masseti M (1995) Quaternary biogeography of the Mustelidae family on the Mediterranean Islands. Hystrix 7, 17–34

Matschie P (1908) Mammalia. Uber chinesische saugetiere, besonders aus den Sammlungen des Herrn Wilhelm Filcher, in Filcher W (ed) Wissenschaftliche Ergebnisse der Expedition Filcher nach China und Tibet 1903–1905, Berlin: Ernst Siegfried Mittler und Sohn, pls 5–25, pp. 134–244

Matthee CA, Van Vuuren BJ, Bell D, Robinson TJ (2004) A molecular supermatrix of the rabbits and hares (Leporidae) allows for the identification of five intercontinental exchanges during the Miocene. Syst Biol 53, 433–447

Matthew WD (1902) New Canidae from the Miocene of Colorado. Bull Am Mus Nat Hist 16, 281–290

Matthew WD (1918) Contributions to the Snake Creek Fauna. Bull Am Mus Nat Hist 38, 183–229

McGrew PO (1938) Dental morphology of the Procyonidae with a description of *Cynarctoides*, gen. nov. Field Mus Nat Hist Geol 6, 323–339.

McKenna MC, Bell SK (1997) Classification of Mammals above the Species Level. New York, Columbia University Press.

Mech LD (1970) The wolf: the ecology and behavior of an endangered species. Natural History Press, Doubleday Publishing Co, New York, USA

Mech LD (1974) *Canis lupus*. Mammal Species 37, 1–6

Mecozzi B, Iurino DA, Berté DF, Sardella R (2017) *Canis mosbachensis* (Canidae, Mammalia) from the Middle Pleistocene of Contrada Monticelli (Putignano, Apulia, southern Italy). B Soc Paleontol Ital 56, 72

Mein P (1975a) Résultats du groupe de travail des vertébrés: biozonation du Néogène Méditerranéen à partir des mammiféres, in Senes J (ed) Report on Activity of RCMNS Working Groups (1971–1975): VI Congress of the Regional Committee of Mediterranean Neogene Stratigraphy, Bratislava, pp 78–81.

Mein P (1975b) Proposition de biozonation du Néogène Méditerranéen à partir des mammiféres: Trabajos sobre Neógeno/Cuaternario 4, 112–113

Meiri S, Dayan T, Simberloff D (2004) Carnivores, biases and Bergmann's rule. Biol J

Linn Soc 81, 579–588

Melis RT, Palombo MR, Ghaleb B, Meloni S (2016) The Su Fossu de Cannas cave (Sadali, Italy): a key site for inferring the timing of dispersal of giant deer in Sardinia. Quat Res 86, 335–347

Mennecart B, Zoboli D, Costeur L, Pillola GL (2017) Reassessment of the latest Oligocene ruminant from Sardara, the last non–insular mammal from Sardinia (Italy). Neues Jahrb Geol Paläontol 286, 97–104

Merriam CH (1888) Description of a new fox from southern California. Proc Biol Soc Washington 4, 135–138

Merriam CH (1890) Results of a biological survey of the San Francisco Mountain region and desert of the Little Colorado in Arizona. North American Fauna 3, 1–136

Merriam CH (1911) Tertiary mammal beds of Virgin Valley and Thousand Creek in North–western Nevada. Part II: vertebrate faunas. Univ Calif Publ Geol 11, 199–304

Meyer von H (1842), in Lommel J (ed) Neues Jahrbuch für Mineralogie, Geologie und Paläontologie: Repertorium. Stuttgart.

Michel P, Wengler L (1993) Un site paléontologique avec des vestiges archéologiques: La carrière Doukkala II (Région de Temara, Maroc atlantique) [Paléoécologie des faunes et contribution à la connaissance du comportement humain]. Paléo 5, 11–41

Miller WE, Carranza–Castañeda O (1998) Late Tertiary canids from central Mexico. Journal of Paleontology 72: 546–556

Millien V, Lyons SK, Olson L, Smith FA, Wilson AB, Yom–Tov Y (2006) Ecotypic variation in the context of global climate change: revisiting the rules. Ecol Lett 9, 853–869

Mivart SG (1890) Dogs, jackals, wolves, and foxes: a monograph of the Canidae. RH Porter, London, England.

Moigne AM, Palombo MR, Belda V, Heriech–Briki D, Kacimi S, Lacombat F, de Lumley MA, Moutoussamy J, Rivals F, Quilès J, Testu A (2006) Les faunes de grands mammifères de la Caune de l'Arago (Tautavel) dans le cadre biochronologique des faunes du Pléistocène moyen italien. L'anthropologie 110(5), 788–831

Molina GI (1782) Saggio sulla storia naturale del Chili. Stamperia di San Tommaso d'Aquino, Bologna.

Moncunill–Solé B, Tuveri C, Arca M, Angelone C (2016) Comparing the body mass variations in endemic insular species of the genus *Prolagus* (Ochotonidae, Lagomorpha) in the Pleistocene of Sardinia (Italy). Riv It Paleontol Strat 122, 25–36

Monguillon A, Spassov N, Argant A, Kauhala K Viranta S (2004) *Nyctereutes vulpinus* comb. et stat. nov. (Mammalia, Carnivora, Canidae) du Pliocène terminal de Saint–Vallier (Drôme, France): Geobios 7, 83–88

Montoya P, Morales J, Abella J (2009) *Eucyon debonisi* n. sp., a new canidae (mammalia, carnivora) from the latest miocene of venta del moro (Salencia, Spain). Geodiversitas 31, 709–722

Morales J, Pickford M, Soria D (2005) Carnivores from the late Miocene and basal Pliocene of the Tugen Hills, Kenya. Rev Soc Geol Esp 18, 39–61

Morales J (2016) Los carnívoros de Villarroya, in Alberdi Alonso MT, Azanza Asensio B, Cervantes E (eds) – Villarroya, yacimiento clave de la paleontología riojana, pp 119–142

Mori T (1922) On some new mammals from Korea and Manchuria. Ann Mag Nat Hist 10, 607–614

Morlo M (1996) Carnivoren aus dem Unter–Miozän des Mainzer Beckens. Senckenbergiana Lethaea 76, 193–249

Morlo M, Kundrat M (2001) The first carnivoran fauna from the Ruscinium (Early Pliocene, MN 15) of Germany. Paläont Z 75, 163–187

Moullé PE (1992) Les grands mammifères du Pléistocène inférieur de la grotte du Vallonnet (Roquebrune–Cap–Martin, Alpes–Maritimes). Étude paléontologique des Carnivores, Equidé, Suidé et Bovidés. PhD Dissertation, Museum National d'Histoire Naturelle, Paris

Moyà-Solà S, Agustí J, Gibert J, Pons-Moyà J (1981) El yacimiento Cuaternario de Venta Micena (España) y su importancia dentro de los asociaciones faunísticas del Pleistoceno inferior europeo. Paleont Evol 16, 39–53

Moyà-Solà S, Agustí J, Gibert J, Vera JA (1987) Geología y Paleontología del Pleistoceno inferior de Venta Micena. Paleont y Evol, Mem Esp 1, 1–295

Mtimet MS, Karoui–Yaakoub N, López–García JM, Blain HA, Agustí J, Amri L, Martínez–Navarro B, (2014) The early Middle Pleistocene microvertebrate assemblage from Wadi Sarrat (Tunisia). XVII World UISPP Congress 2014 Burgos, 1–7. September.

Volume des abstracts, pp.100–101.

Müller S (1836) Jahresbericht tiber die Fortschritte der anatomisch–physiologischen Wissenschaften im Jahre 1834. Archiv Anat Physiol, 1–243.

Munthe K (1998) Canidae. In Evolution of Tertiary Mammals of North America: Terrestrial Carnivores, Ungulates, and Ungulate-like Mammals, in Janis CM, Jacobs L, Scott KM, Cambridge University Press, Cambridge, pp 124–143

Murphy WJ, Eizirik E, O'Brien SJ, Madsen O, Scally M, Douady CJ, Springer MS (2001). Resolution of the early placental mammal radiation using bayesian phylogenetics. Science 294, 2348–2351

Naora N (1968) The fossils of otters discovered in Japan. Mem Sch Sci Eng Waseda Univ 32, 1–11

Nascimento F (2014) On the correct name for some subfamilies of Mustelidae (Mammalia, Carnivora). Pap Avulsos Zool 54, 307–313

Novacek MJ (1977) Aspects of the problem of variation, origin and evolution of the eutherian auditory bulla. Mammal Rev 7, 131–150

Nowak RM (2005) Walker's Carnivores of the World. JHU Press.

Nowak RM (2005) Walker's Carnivores of the World. John Hopkins University Press

Odintzov IA (1965) *Vulpes praecorsac* Kormos from Pliocene deposits of Odessa. Paleont Zbornik 2 (2): 57–64 (in Russian with English summary)

Odintzov IA (1967) New species of Pliocene Carnivora, *Vulpes odessana* sp. nov. from the Karst Cave of Odessa. Paleontologicheskyi Sbornik, L'vov University 4, 130–137

Ogino S, Otsuka H (2008) New middle Pleistocene Galictini (Mustelidae, Carnivora) from the Matsugae cave deposits, northern Kyushu, West Japan. Paleontol Res 12, 159–166

Oken L (1816) Lehrbuch der Naturgeschichte (Zoologie). August Schmidt und Comp, Jena

Olfers von I (1818) Bemerkungen zu Illiger's Ueberblick der Säugthiere nach ihrer Vertheilung über die Welttheile, rücksichtich der Südamericanischen Arten (Species), in Eschwege von WL (ed) Journal von Brasilien, odor vermischte Nachrichten aus Brasilien auf wissenschaftlichen Reisen gesammelt. Heft 2 in F. Bertuch. Neue Bibliothek der wichtigsten Reisebeschreibungen zur Erweiterung der Erd– und

Völkerkunde, Band 15: 233. Weimar

Oms O, Parés JM, Martínez-Navarro B, Agustí J, Toro I, Martínez-Fernández G (2000) Early human occupation of Western Europe: Paleomagnetic dates for two paleolithic sites in Spain. PNAS 97, 10666–10670

Oms O, Anadón P, Agustí J, Julià R (2011) Geology and chronology of the continental Pleistocene archeological and paleontological sites of the Orce area (Baza basin, Spain). Quat Int 243, 33–43

Ouachaou B, Amani F (2002) Les Carnivores des gisements néolithiques et protohistoriques du Nord du Maroc. Quaternaire 13, 79–87

Pacheco FG, Santiago A, Gutiérrez JM, López–García JM, Blain HA, Cuenca–Bescós G, García N (2011). The early Pleistocene paleontological site in the Sierra del Chaparral (Villaluenga del Rosario, Cádiz, southwestern Spain). QuatInt 243, 92–104

Pálfy J, Dulai A, Gasparik M, Ozsvárt P, Pazonyi P, Szives O (2008) Catalogue of invertebrate and vertebrate paleontological type specimens of the Hungarian Natural History Museum. Hung Nat H Mus 2008. 1–209

Pallas PS (1775) Spicilegia zoological, quibus novae imprimis et obscurae animalium species iconibus, descriptionibus atque commentariis illustrantur. Gottlieb August Lange, Berolini 1, 1–44

Pallas PS (1811) Zoographia Rosso–Asiatica. Tomus Primus. Petropoli

Palma di Cesnola A (1991) La campagna di scavo 1991 a Grotta Paglicci. Atti del 13 Covegno Nazionale di Preistoria, Protostoria e Storia della Daunia, San Severo, 22–24 Novembre 1991, Foggia.

Palmarelli A, Palombo MR (1981) Un cranio di *Coelodonta antiquitatis* (Bluemenbach) (Rhinocerotidae) del Pleistocene superiore del Monte Circeo (Lazio meridionale). Boll Serv Geo Ital 102, 281–312

Palmqvist P, Arribas A, Martínez-Navarro B (1999) Ecomorphological study of large canids from the lower Pleistocene of southeastern Spain. Lethaia 32, 75–88

Palmqvist P, Mendoza M, Arribas A, Gröcke D (2002) Estimating the body mass of Pleistocene canids: discussion of some methodological problems and a new 'taxon free' approach. Lethaia 35, 358–360

Palmqvist P, Gröcke DR, Arribas A, Fariña R (2003) Paleoecological reconstruction of a lower Pleistocene large mammals community using biogeochemical ($\delta^{13}C$, $\delta^{15}N$, $\delta^{18}O$, Sr: Zn) and ecomorphological approaches. Paleobiology 29, 205–229

Palmqvist P, Martínez-Navarro B, Arribas A (1996) Prey selection by terrestrial carnivores in a lower Pleistocene paleocommunity. Paleobiology. 22, 514-534

Palmqvist P, Martínez-Navarro B, Pérez-Claros JA, Torregrosa V, Figueirido B, Jiménez-Arenas JM, Espigares MP, Ros-Montoya S, De Renzi M (2011) The giant hyena *Pachycrocuta brevirostris:* modelling the bone-cracking behavior of an extinct carnivore. Quat. Int. 243, 61–79.

Palmqvist P, Pérez-Claros JA, Janis CM, Figueirido B, Torregrosa V, Gröcke DR (2008) Biogeochemical and ecomorphological inferences on prey selection and resource partitioning among mammalian carnivores in an early Pleistocene community. Palaios 23, 724–737

Palombo MR (2006) Biochronology of the Plio–Pleistocene terrestrial mammals of Sardinia: the state of the art. Hell J Geosc 41: 47–66

Palombo MR (2009) Biochronology, paleobiogeography and faunal turnover in western Mediterranean Cenozoic mammals. Integr. Zool. 4 (4), 367–386.

Palombo MR, Ferretti MP (2005) Elephant fossil record from Italy: knowledge, problems, and perspectives. Quat Int 126/128, 107–136

Palombo MR, Rozzi R (2014) How correct is any chronological ordering of the Quaternary Sardinian mammalian assemblages? Quat Int 328, 136–155

Palombo MR, Azanza B, Alberdi MT (2002) Italian mammal biochronology from the latest Miocene to the middle Pleistocene: a multivariate approach. Geol Rom 36, 335–368

Palombo MR, Zedda M, Melis RT (2017) A new elephant fossil from the late Pleistocene of Alghero: The puzzling question of Sardinian dwarf elephants. CR Palevol 16, 841–849

Palombo MR, Sardella R, Novelli M (2008) Carnivora dispersal in Western Mediterranean during the last 2.6 Ma. Quat Int 179, 176–189

Palombo MR, Valli AM, Arca M, Tuveri C (2006) A new Bovid, *Asoletragus gentryi* gen. n. et n. sp., from Monte Tuttavista (Orosei, eastern Sardinia, Italy). Riv Ital Paleontol

S 112

Pandolfi L, Boscato P, Crezzini J, Gatta M, Moroni A, Rolfo M, Tagliacozzo A (2017) Late Pleistocene last occurrence of the narrow–nosed rhinoceros *Stephanorhinus hemitoechus* (Mammalia, Perissodactyla) in Italy. Riv Ital Paleontol S 123, 177–191

Pandolfi L, Petronio C, Salari L (2013) Catastrophic death assemblages from the Late Pleistocene of Italy: the case of Avetrana karst filling (Taranto, Southern Italy). Riv Ital Paleontol S 119, 109–124

Pasini G. (1970) Fauna a Mammiferi de Pleistocene Superiore in un paleonghittitoio carsico presso Monte Croara (Bologna). Le grotte d'Italia 4, 1–46

Patnaik R, Nanda AC (2010) Early Pleistocene mammalian faunas of India and evidence of connections with other parts of the world, in Fleagle JG, Shea JJ, Grine FE, Baden AL, Leakey RE (eds) Out of Africa I: the first hominin colonization of Eurasia. Springer Science & Business Media. Springer, Dordrecht, pp 129–143

Pazonyi P (2011) Palaeoecology of Late Pliocene and Quaternary mammalian communities in the Carpathian Basin. Acta Zool Cracov-Series A: Vertebrata, 54 (1-2), 1-32.

Pei WC (1934) On the Carnivora from locality 1 of Choukoutien. Paleontol Sinica, ser C 8, 1–239

Peigné S (2012) Les Carnivora de Sansan, in Peigné S, Sen S (eds) Mammifères de Sansan. Mem Mus Natl Hist Nat 203, Publications du Muséum, Paris, pp 559–660

Pérez B, Soria D (1989–90) Análisis de las comunidades de mamíferos del Plioceno de Layna (Soria) y La Calera (Teruel). Paleontol Evol 23, 231–238

Peters N, de Vos J (2012) A Villafranchian mustelid, *Pannonictis ardea* (Gervais, 1859) (Carnivora, Mustelidae) from Langenboom (Noord–Brabant, The Netherlands). Cainozoic Res 9, 9–14

Petronio C, Sardella R (1998) Remarks on the stratigraphy and biochronology of the Late Pleistocene deposit of Ingarano (Apulia, Southern Italy). Riv Ital Paleontol S 104, 287–294

Petronio C, Bellardini F, Arzarello M, Bedetti C, Bellucci L, Cipullo A, Di Stefano G, Pandolfi L, Pavia M, Petrucci M, Sardella R, Salari L (2008) The deposit of the Late Pleistocene from Avetrana (Taranto, Southern Italy): biochronology and palaeoecology. Il Quaternario 21, 409–422

Petrovič V, Sabol M, Šurka J, Pyszko M, Stehlík L (2018) External brain morphology of juvenile cave hyena (Crocuta crocuta spelaea) from the Jasovská jaskyňa Cave (Slovakia) revealed by X–ray computed tomography. Acta Geol Slov 10, 133–142

Petrucci M, Romiti S, Sardella R (2012) The Middle–Late Pleistocene *Cuon* Hodgson, 1838 (Carnivora, Canidae) from Italy. Boll Soc Paleont Ital 51, 138

Petrucci M, Cipullo A, Martínez–Navarro B, Rook L, Sardella R (2013) The late Villafranchian (Early Pleistocene) carnivores (Carnivora, Mammalia) from Pirro Nord (Italy). Palaeontographica Abteilung A Paläozoologie, Stratigraphie, 298: 113–145

Pilgrim GE (1932) The genera *Trochictis*, *Enhydrictis* and *Trocharion*, with remarks on the taxonomy of the Mustelidae. Proc R Soc Lond 4, 845–867

Pillans B, Gibbard P (2012) The Quaternary period, in Gradstein F, Ogg J, Schmitz M, Ogg G (eds) The Geologic Time Scale 2012. Elsevier

Piras P, Sansalone G, Teresi L, Kotsakis T, Colangelo P, Loy A (2012) Testing convergent and parallel adaptations in talpids humeral mechanical performance by means of geometric morphometrics and finite element analysis. J Morph 273, 696–711

Pitra C, Schwarz S, Fickel J (2010) Going west–invasion genetics of the alien raccoon dog *Nyctereutes procyonoides* in Europe. Eur J Wildl Res 56, 117–129

Pocock RI (1921) On the external characters and classification of the Mustelidae. Proc R Soc Lond 91, 803–837

Pocock RI (1929) The structure of the auditory bulla in the Procyonidae and the Ursidae, with a note on the bulla of Hyaena. Proc Zool Soc London 1928, 963–974

Pocock RI (1935) The races of *Canis lupus*. Proc Zool Soc London, 647–68

Poe S, Wiens JJ (2000) Character selection and the methodology of morphological phylogenetics, in Wiens JJ (ed) Washington DC, Smithsonian Institution Press, pp 20–36

Pohle H (1928) Die Raubtiere von Oldoway. Wissenschaftliche Ergebnisse der Oldoway–Expedition Herausgegeben von Prof. Dr. Reck 3, 45–54

Pomel M (1842) Nouvelle espèce de chien fossile découverte dans les alluvions volcaniques de l'Auvergne. Bull Soc Geol Fr 14, 38–41

Pomel M (1853) Catalogue méthodique et descriptif des vertebrés fossiles du bassin

de la Loire et de l'Allier. Paris

Pons-Moyà J (1981) El *Canis etruscus* Major (Carnivora, Mammalia) del Villafranquiense terminal de la Cueva Victoria. Endins 8, 43–46

Pons-Moyà J (1987) Los carnívoros (Mammalia) de Venta Micena (Granada, España). Paleont Evol, Mem Esp 1, 109–127

Pons Moya J, Crusafont–Pairó M (1978). Sobre la identidad del "*Canis*" *adoxus* Martin (1973) y su implicacion en el conocimiento del genero *Vulpes*. Acta Geol Hisp 13, 129–132

Popov VV (2001) Late Pliocene voles (Mammalia: Arvicolidae) from Varshets (North Bulgaria). Acta zoologica cracoviensia 44(2), 143–172

Popov SV, Shcherba IG, Ilyina LB, Nevesskaya LA, Paramonova NP, Khondkarian SO, Magyar I (2006) late Miocene to Pliocene palaeogeography of the Paratethys and its relationship to the Mediterranean Palaeogeogr, Palaeoclimat, Palaeoecol 238, 91–106

Popowics TE (2003) Postcanine dental form in the Mustelidae and Viverridae (Carnivora: Mammalia). J Morphol 256, 322–341

Portis A (1920) Elenco delle specie di Cervicorni fossili in Roma e attorno a Roma. Boll Soc Geol It 39, 132-139

Pradella C, Rook L (2007) *Mesopithecus* (Primates, Cercopithecoidea) from Villafranca d'Asti (early Villafranchian; NW Italy) and palaeoecological context of its extinction. Swiss J Geosci 100, 145–152

Presley SJ (2000) *Eira barbara*. Mamm Species 3, 195–202

Prevosti FJ (2010) Phylogeny of the large extinct South American Canids (Mammalia, Carnivora, Canidae) using a "total evidence" approach. Cladistic The Willi Hennig Society, https://doi.org/10.1111/j.1096-0031.2009.00298.x

Profico A, Melchionna M, Veneziano A, Raia P (2018a) Arothron: Geometric Morphometrics Analyses. R package version 1.0.0, Available at https://cran.r–project.org/web/packages/Arothron

Profico A, Schlager S, Valoriani V, Buzi C, Melchionna M, Veneziano A, Raia P, Moggi–Cecchi J, Manzi G (2018b) Reproducing the internal and external anatomy of fossil bones: Two new automatic digital tools. Am J Phys Anthropol 166, 979–986

Prothero DR, Emry RJ (2004) The Chadronian, Orellan, and Whitneyan North American

land mammal ages, in Woodburne MO (ed) Late Cretaceous and Cenozoic Mammals of North America: Biostratigraphy and Geochronology. Columbia University Press, pp 156–168

Puzachenko AY, Abramov AV, Rozhnov VV (2017) Cranial variation and taxonomic content of the marbled polecat *Vormela peregusna* (Mustelidae, Carnivora). Mamm Biol 83, 10–20

Qiu ZX, Tedford RH (1990) A Pliocene species of *Vulpes* from Yushe, Shanxi. Vertebrata PalAsiatica 28, 245–258

Qiu ZX, Deng T, Wang X (2004) Early Pleistocene Mammalian Fauna from Longdan, Dongxiang, Gansu, China. Paleont Sinica, NS C 27, 1–198

Qiu ZX, Flynn LJ (2013) Chapter 1. Yushe basin, Shanxi Province, in Tedford RH, Qiu ZX, Flynn LJ (eds) Late Cenozoic Yushe Basin, Shanxi Province, China: Geology and Fossil Mammals, History, Geology, and Magnetostratigraphy, vol. I Springer, New York, pp 1–5

Qiu ZX, Tedford RH (2013) Chapter 2. History of scientific exploration of Yushe basin, in Tedford RH, Qiu ZX, Flynn LJ (eds) Late Cenozoic Yushe Basin, Shanxi Province, China: Geology and Fossil Mammals, History, Geology, and Magnetostratigraphy, vol. I. Springer, New York, pp 7–34

Qiu ZX, Qiu Z, Deng T, Li CK, Zhang Z, Wang B, Wang X (2013). Neogene land mammal stages/ages of China. Fossil Mammals of Asia: Neogene Biostratigraphy and Chronology. Columbia University Press, New York, 29–90

Rabeder G (1976) Die Carnivoren (Mammalia) aus dem Altpleistozän von Deutsch–Altenburg 2. Mit Beiträgen zur Systematik einiger Musteliden und Caniden. Beitr Paläontol Österr 1, 5–119

Radinsky LB (1969) Outlines of canid and felid brain evolution. Ann NY Acad Sci 167, 277–288

Radinsky LB (1973) Evolution of the Canid Brain. Brain Behav Evol 7, 169–185

Radulescu C, Samson PM, Petculescu A, Stiuca E (2003) Pliocene large mammals of Romania. Coloquios de Paleontología 1, 549–558

Ramstein G, Fluteau F, Besse J, Joussaume S (1997) Effect of orogeny, plate motion and land–sea distribution on Eurasian climate change over the past 30 million years. Nature 386, 788–795

Randi E (2011) Genetics and conservation of wolves *Canis lupus* in Europe. Mammal Rev 41, 99–111

Raynal JP, Lefevre D, Geraads D, El Graoui M (1999) Contribution du site paléontologique de Lissasfa (Casablanca, Maroc) à une nouvelle interprétation du Mio–Pliocène de la Méseta. CR Acad Sci–Earth and Planetary Science 329, 617–622

Reig OA (1956) Note préliminaire sur un nouveau genre de mustélidés fossiles du Pléistocène de la République Argéntine. Mammalia 20, 223–230

Renaud S, Benammi M, Jaeger JJ (1999) Morphological evolution of the murine rodent *Paraethomys* in response to climatic variation (Mio–Pleistocene of North Africa). Paleobiology 25, 369–382

Repenning C (1967) Palearctic–Nearctic mammalian dispersal in the Late Cenozoic, in Hopkins DM (ed) The Bering Land Bridge, Stanford University Press, Stanford, pp 288–311

Reynolds SC (2012) *Nyctereutes terblanchei*: The raccoon dog that never was. S Afr J Sci 108, 1–10

Rightmire GP, Margvelashvili A, Lordkipanidze D (2019) Variation among the Dmanisi hominins: Multiple taxa or one species? Am J Phys Anthr 168(3), 481-495

Rio D, Sprovieri R, Di Stefano E (1994) The Gelasian stage: a proposal of a new chronostratigraphic unit of the Pliocene series. Riv Ital Paleontol S 100, 103–124

Rodrigues S, Avilla L, De Azevedo SAK (2015) Diversity and paleoenviromental significance of Brazilian fossil *Galictis* (Carnivora: Mustelidae). Hist Biol 28, 1–6

Rook L (1992) *"Canis" monticinensis* sp. nov., a new Canidae (Carnivora, Mammalia) from the late Messinian of Italy. Boll Soc Paleontol It 31, 151–156

Rook L (1993) I cani dell'Eurasia dal Miocene Superiore al Pleistocene Medio. PhD Dissertation, Modena, Bologna, Firenze and Roma "La Sapienza" Universities, Italy

Rook L (1995) *Pannonictis nestii* (Carnivora, Mammalia) from the late Villafranchian of Pietrafitta (Umbria, Italy). Preliminary note. Eclogae Geol Helv 88, 853–864

Rook L (2009) The wide ranging genus *Eucyon* Tedford & Qiu, 1996 (Mammalia, Carnivora, Canidae, Canini) in the Mio–Pliocene of the Old World. Geodiversitas 31, 723–741

Rook L, Azzaroli ML (1996) Remarks on the skull morphology of the endangered

Ethiopian jackal, *Canis simensis* Rüppel 1838. Rend Lincei 7, 277–302

Rook L, Torre D (1996a) The latest Villafranchian early Galerian small dogs of the Mediterranean area. Acta Zool Cracov 39, 427–434

Rook L, Torre D (1996b) The wolf-event in Western Europe and the beginning of the Late Villafranchian. N Jb Geol Paläontol Monat 8, 495–501

Rook L, Ferretti MP, Arca M, Tuveri C (2004) *Chasmaporthetes melei* n. sp., an endemic hyaenid (Carnivora, Mammalia) from the Monte Tuttavista fissure fillings (Late Pliocene to Early Pleistocene; Sardinia, Italy). Riv It Paleontol Strat 110, 707–714

Rook L, Martínez–Navarro B (2010) Villafranchian: the long story of a Plio–Pleistocene European large mammal biochronologic unit. Quat Int 219, 134–144

Rook L, Bartolini Lucenti S, Tuveri C, Arca M (2018) Mustelids (Carnivora, Mammalia) from Monte Tuttavista fissure fillings (Early and Middle Pleistocene; Orosei, Sardinia), Taxonomy and evolution of the insular Sardinian Lyncodontini. Quat Sci Rev 197, 209-223

Ros–Montoya S, Madurell–Malapeira J, Martínez–Navarro B, Espigares P, Palmqvist P (2012) Late Villafranchian *Mammuthus meridionalis* (Nesti, 1825) from the Iberian Peninsula: Dentognathic remains from Incarcal–I (Crespià, Girona) and Venta Micena (Orce, Granada). Quat. Int. doi: 10.1016/j.quaint.2012.03.007

Rovinsky DS, Herries AI, Menter CG, Adams JW (2015) First description of in situ primate and faunal remains from the Plio–Pleistocene Drimolen Makondo palaeocave infill, Gauteng, South Africa. Palaeontol Electronica 18, 1–21

Rueness EK, Asmyhr MG, Sillero–Zubiri C, Macdonald DW, Bekele A, Atickem A, Stenseth NC (2011) The cryptic African wolf: *Canis aureus lupaster* is not a golden jackal and is not endemic to Egypt. PLoS One 6: e16385

Rüppel E (1838) Neue Wirbelthiere zu der Fauna Abyssinien gehörig, Säugethiere. Siegmund Schmerber, Frankfurt ant Main

Rustioni M, Ferretti MP, Mazza P, Pavia M, Varola A (2003) The vertebrate fauna from Cardamone (Apulia, southern Italy): an example of Mediterranean mammoth fauna. Deinsea 9, 395–404

Saeki M (2009) *Nyctereutes procyonoides* (Gray, 1834), in Ohdachi SD, Ishibashi Y, Iwasa MA, Saitoh T, (eds) The Wild Mammals of Japan, Kyoto, Shoukadoh Book Sellers, pp 216–217

Sala B (1979) Le faune pré–würmienne des grands mammifères de la Grotte du Poggio (Marina di Camerota, Salerno). Atti Soc Toscana Sci Nat 86, 77–99

Sala B, Masini F (2007) The late Pliocene and Pleistocene small mammal chronology in the Italian peninsula. Quat Int 160, 4–16

Sala B, Masini F, Ficcarelli G, Rook L, Torre D (1992) Mammal dispersal events in the Middle and Late Pleistocene of Italy and western Europe. Cour For Sekenbg 153, 59–68

Salari L, Achino KF, Gatta M, Petronio C, Rolfo MF, Silvestri L, Pandolfi L (2017) The wolf from Grotta Mora Cavorso (Simbruini mountains, Latium) within the evolution of *Canis lupus* L., 1758 in the Quaternary of Italy. Palaeogeogr Palaeocl, Palaeoecol 476, 90–105

Sansalone G, Bertè DF, Maiorino L, Pandolfi L (2015) Evolutionary trends and stasis in carnassial teeth of European Pleistocene wolf *Canis lupus* (Mammalia, Canidae). Quat Sci Rev 110, 36–48

Sardella R, Bedetti C, Bellucci L, Conti N, Coppola D, Di Canzio E, Pavia M, Petronio C, Petrucci M, Salari L (2005) The late pleistocene vertebrate fauna from Avetrana (Taranto, Apulia, Southern Italy): preliminary report. Geol Alp 2, 25–29

Sardella R, Bertè D, Iurino DA, Cherin M, Tagliacozzo A (2014) The wolf from Grotta Romanelli (Apulia, Italy) and its implications in the evolutionary history of *Canis lupus* in the Late Pleistocene of Southern Italy. Quat Int 328, 179–195

Sato JJ (2016) The Systematics and Taxonomy of the World's Badger Species – A Review, in Proulx G, Do Linh San E (eds.), Badgers: systematics, biology, conservation and research techniques. Alpha Wildlife Publications, Sherwood Park, Alberta, Canada, pp 1–30

Sato JJ, Wolsan M, Minami S, Hosoda T, Sinaga MH, Hiyama K, Yamaguchi Y, Suzuki H (2009) Deciphering and dating the red panda's ancestry and early adaptive radiation of Musteloidea. Mol Phylogenet Evol 53, 907–922

Sato JJ, Wolsan M, Prevosti FJ, D'Elía G, Begg C, Begg K, Hosoda T, Campbell KL, Suzuki H (2012) Evolutionary and biogeographic history of weasel–like carnivorans (Musteloidea). Mol Phylogenet Evol 63, 745–757

Sato JJ, Wolsan M, Suzuki H, Hosoda T, Yamaguchi Y, Hiyama K, Kobayashi M, Minami S (2006) Evidence from nuclear DNA sequences sheds light on the phylogenetic relationships of Pinnipedia: single origin with affinity to Musteloidea. Zool Sci 23,

125–146

Savage DE (1941) Two new middle Pliocene carnivores from Oklahoma with notes on the Optima Fauna. American Midland Naturalist 25: 692–710

Savage DE, Downs T, Poe OJ (1954) Cenozoic landlife of southern California, in Jahns RH (ed) Geology of Southern California, California Division of Mines and Geology Bulletin 170, pp 43–58

Say T (1823) In James E (ed) Account of an Expedition from Pittsburgh to the Rocky Mountains, Performed in the Years 1819 and '20, by Order of the Hon. JC Calhoun, Sec'y of War: under the Command of Major Stephen H. Long. From the Notes of Major Long, Mr. T. Say, and Other Gentlemen of the Exploring Party, vol. IHC Carey, I Lea, Philadelphia, 503

Schaub S (1949) Révision de quelques carnassiers villafranchiens du niveau des Étouaires, montagne de Perrier, Puy–de Dôme. Eclogae Geol Helv 42, 491–506

Schinz HR (1825) G. Cuvier's Thierreich Das Thierreich eingetheilth nachdem bau der thiere als grundage iher naturgeschichte und der vergleichenden anatomie. Volume 4

Schlager S (2017) Morpho and Rvcg–Shape Analysis in R. Statistical Shape and Deformation Analysis: Methods, Implementation and Applications, 217–256

Schlosser M (1903) Die fossilen Säugethiere Chinas nebst einer Odontographie de recenten Antilopen. Abh Math–Phys Kl, K Bayer Akad Wiss 22, 1–220

Schreber JCD (1776) Die Säugethiere in Abbildungen nach der Natur mit Beschreibungen. Erlangen: Wolfgang Walther

Schreuder A (1935) A note on the Carnivora of the Tegelen Clay, with some remarks on the Grisoninae. Arch Neerl Zool 2, 73–94

Schultz JR (1938) A late Quaternary mammal fauna from the tar seeps of McKittrick, California. Carnegie Institution of Washington Contributions in Paleontol 487, 112–215.

Scott WB (1890) The dogs of the American Miocene. Princeton College Bull 2, 37–39

Secord A (1994) Corresponding interests: artisans and gentlemen in nineteenth–century natural history. The Brit J Hist of Sci 27, 383– 408

Segall W (1943) The auditory region of the arctoid carnivores. Zool Series Field Mus Nat His 29, 33–59

Sereno PC (2007) Logical basis for morphological characters in phylogenetics. Cladistics 23, 565–587

Sesé C (2006) Los roedores y lagomorfos del Neógeno de España. Estudios Geol 62, 429–480

Shaw G (1800) General zoology or systematic natural history. Volume 1. Part 2. Mammalia. G. Kearsley, London, England

Shen G, Gao X, Gao B, Granger DE (2009) Age of Zhoukoudian *Homo erectus* determined with $^{26}Al/^{10}Be$ burial dating. Nature 458(7235), 198–200

Sher AV (1986) Olyorian land mammal age of northeastern Siberia. Palaeontogr Ital 74, 97–112

Sillero–Zubiri G (2010) Family Canidae (dogs), in Wilson DE, Mittermeier RA (ed) Handbook of the Mammals of the World, Vol. 1, Carnivores. Barcelona: Lynx Edicions, pp 352–447

Sillero–Zubiri G, Macdonald DW (2004) Introduction, in Sillero–Zubiri G, Hoffmann M, Macdonald DW (eds) Canids: Foxes, Wolves, Jackals and Dogs. Status Survey and Conservation Action Plan. IUCN/SSC Canid Specialist Group. Gland, Switzerland and Cambridge, UK, pp 2–7

Simões TR, Caldwell MW, Palci A, Nydam RL (2017) Giant taxon-character matrices: quality of character constructions remains critical regardless of size. Cladistics 33, 198–219

Simpson GG (1941) Large Pleistocene felines of North America. Am Mus Novitates 1136, 1–27

Simpson GG (1945) The principles of classification and a classification of mammals. Bull Am Mus Nat Hist 85, 1–350

Simpson GG, Roe A, Lewontin RC (1960) Quantitative Zoology. Harcourt Brace, New York

Smith A (1833) An epitome of African Zoology; or, a concise description of the objects of the animal kingdom inhabiting Africa, its islands and seas. S Afr Quarterly J 2, 89

Soergel W (1925) Die Säugetierfauna des altdiluvialen Tonlages von Jockgrim in des Pfalz. Z Dtsch Geol Ges 77, 405–438

Sondaar PY (2000) Early Human Exploration and Exploitation on Islands. Tropics 10,

203–230

Sondaar PY, van der Geer AAE (2002) Plio–Pleistocene terrestrial vertebrate faunal evolution on Mediterranean islands, compared to that of the Palearctic mainland. Ann Géol Pays Hellén 39, 165–180

Sondaar PY, van der Geer AAE (2005) Evolution and extinction of Plio–Pleistocene island Ungulates, in Crégut–Bonnoure E (ed) Les ongulés holarctiques du Pliocène et du Pléistocene. Quaternaire, Int J French Quat Ass 2, 241–256

Soria D, Aguirre E (1976) El cánido de Layna: revisión de los *Nyctereutes* fósiles. Trabajos Neógeno y Cuaternario 5, 83–115

Sotnikova M (1980) Late Pliocene Mustelidae from Shamar (Mongolia). Bűll Kom Izuč Četvert Perioda 50, 138–145 [in Russian]

Sotnikova M (1989) The carnivore mammals from the Pliocene to the Early Pleistocene. Stratigraphic significance. Trans Geol Inst RAS 440, 1–122. Nauka, Moscow (in Russian)

Sotnikova M (2001) Remains of Canidae from the lower Pleistocene site of Untermassfeld, in Kahlke RD (ed) Das Pleistozän von Untermassfeld bei Meiningen (Thüringen) Teil. 2. Habelt Verlag, Bonn, pp 607–632

Sotnikova M (2004) The Middle Pliocene assemblage of Carnivore from Shamar locality (Northern Mongolia), in The International Conference on the Paleontology of the Central Asia. Paleontological Institute, Moscow, pp 54–56

Sotnikova M (2006) A new canid *Nurocyon chonokhariensis* gen. et sp. nov. (Canini, Canidae, Mammalia) from the Pliocene of Mongolia. Cour Forsch Inst Senckenberg 256, 11–21

Sotnikova M, Rook L (2010) Dispersal of the Canini (Mammalia, Canidae: Caninae) across Eurasia during the Late Miocene to Early Pleistocene. Quat Int 212, 86–97

Sotnikova M, Baigusheva VS, Titov VV (2002) Carnivores of the Khapry faunal assemblage and their stratigraphic implications. Stratigr Geol Correl 10, 375–390

Spassov N (1997) Villafranchian succession of mammalian Megafaunas from Bulgaria and the Biozonation of south–east Europe. Mém Trav Inst Montpellier 21, 669–676

Spassov N (1999) The Mammalian Megafauna from the Late Villafranchian Localities Varshets and Slivnitsa, Bulgaria and the Biochronology of the Villafranchian in S.–E. Europe. PhD Thesis (unpublished). National Museum of Natural History, Bulgarian

Academy of Sciences, Sofia

Spassov N (2000) Biochronology and zoogeographical affinities of the Villafranchian faunas of Bulgaria and South Europe. Historia Naturalis Bulgarica 12, 89–128

Spassov N (2003) The Plio–Pleistocene vertebrate fauna in South–eastern Europe and the megafaunal migratory waves from the east to Europe. Rev Paléobiol 22, 197–229

Spassov N, Rook L (2006) *Eucyon marinae* sp. nov. (Mammalia, Carnivora) a new canid species from the Pliocene of Mongolia with a review of forms referable to the genus. Riv Ital Paleontol S 112, 123–133

Spaulding M (2007) The impact of postcranial characters on reconstructing the phylogeny of Carnivoramorpha. J Vert Paleontol 27, 151A

Spencer MR, Wilberg EW (2013) Efficacy or convenience? Model–based approaches to phylogeny estimation using morphological data. Cladistics 29, 663–671

Stach J (1959) On some Mustelinae from the Pliocene bone breccia of Weze. Acta Paleontol Pol 4, 102–118

Stach J (1954) *Nyctereutes* (Canidae) w pliocenie Polski, Studia nad trzeciorzędową fauną brekcji kostnej w miejscowości Węże koło Działoszyna. Acta Geol Pol 4, 191–206

Stehlin HG (1933) Paleotologie des couches paleolithiques, in Duboid A, Stehlin HG (eds) La grotte de Cotencher, station mousterienne. Mem Soc Paleont Suisse 52/53: 33–178

Stewart JR (2008) The progressive effect of the individualistic response of species to Quaternary climatic change: an analysis of British mammalian faunas. Quat Sci Rev 27, 2499–2508

Stewart JR, Lister AM, Barnes I, Dalèn L (2010) Refugia revisited: individualistic responses of species in space and time. P Roy Soc B–Biol Sci 277, 661–671

Storr GCC (1780) Prodromus methodi mammalium. Tübingen, Reissian

Stuart AJ (1982) Pleistocene vertebrates in the British Isles. Longman, London and New York

Studiati C (1857) Description des fossiles de la breche osseuse de Monreale de Bonaria pres de Cagliari, in La Marmora A (ed) Voyage en Sardeigne 3. Arthus Bertrand, Turinn, pp 651–704

Sundevall CJ (1847) Nya Mammalia från Sydafrika. Ofv K Svenska Vet–Akad Forhandl

Stockholm 3 118–121

Sutor A, Kauhala K, Ansorge H (2010) Diet of the raccoon dog *Nyctereutes procyonoides*—a canid with an opportunistic foraging strategy. Acta Theriologica 55, 165–176

Sutton M, Rahman I, Garwood R (2014) Techniques for virtual palaeontology. John Wiley & Sons

Szuma E (2000) Variation and correlation patterns in the dentition of the red fox from Poland. Ann Zool Fenn 37, 113–127

Szuma E (2003) Microevolutionary trends in the dentition of the red fox (*Vulpes vulpes*). J Zool Syst Evol Res 41, 47–56

Szuma E (2004) Evolutionary implications of morphological variation in the lower carnassial of red fox *Vulpes vulpes*. Acta Theriol 49, 433–447.

Szuma E (2007) Geography of dental polymorphism in the red fox *Vulpes vulpes* and its evolutionary implications. Biol J Linnean Soc 90, 61–84

Szuma E (2008a) Geography of sexual dimorphism in the tooth size of the red fox *Vulpes vulpes* (Mammalia, Carnivora). J Zool Syst Evol Res 46, 73–81

Szuma E (2008b) Evolutionary and climatic factors affecting tooth size in the red fox *Vulpes vulpes* in the Holarctic. Mammal Res 53, 289–332

Szuma E (2008c) Geographic variation of tooth and skull sizes in the arctic fox *Vulpes* (*Alopex*) *lagopus*. Ann Zool Fenn 45, 185–199

Szuma E (2011) Ecological and evolutionary determinants of dental polymorphism in the arctic fox *Vulpes* (*Alopex*) *lagopus*. Ann Zoologici Fenn 48, 191–214

Taberlet P, Fumagalli L, Wust–Saucy A, Cosson J (1998) Comparative phylogeography and postglacial colonization routes in Europe. Mol Ecol 8, 1923–1934

Team RC (2000) R language definition. Vienna, Austria: R foundation for statistical computing

Tedford RH (1976) Relationship of Pinnipeds to Other Carnivores (Mammalia). Syst Zool 25, 363–374

Tedford RH, Qiu Z (1991) Pliocene *Nyctereutes* (Carnivora: Canidae) from Yushe, Shanxi, with comments on Chinese fossil raccoon dogs. Vert PalAsiatica 29, 176–189

Tedford RH, Wang X (2008) *Metalopex*, a new genus of fox (Vulpini, Canidae, Carnivora)

from the late Miocene of western North America. Nat Hist Mus Los Angel City Sci 41, 273–278

Tedford RH, Taylor B, Wang X (1995) Phylogeny of the Caninae (Carnivora: Canidae): the Living Taxa. Am Mus Novit 3146, 1–37

Tedford RH, Galusha T, Skinner MF, Taylor BE, Fields RW, Macdonald JR, Rensberger JM, Webb SD, Whisler DP (2004) Faunal succession and biochronology of the Arikareean through Hemphillian interval (late Oligocene through earliest Pliocene epochs) in North America, in Woodburne MO (ed) Cenozoic Mammals of North America: Geochronology and Biostratigraphy. pp 153–210.

Tedford RH, Wang X, Taylor BE (2009) Phylogenetic systematics of the North American fossil Caninae (Carnivora: Canidae). Bulletin of the American Museum of Natural History 325, 1–218

Tedford RH, Qiu Z, Flynn LJ (eds) (2013) Late Cenozoic Yushe Basin, Shanxi Province, China: Geology and Fossil Mammals. Springer, New York

Tedford RH, Flynn LJ, Qiu Z, Opdyke ND, Downs WR (1991) Yushe Basin, China; paleomagnetically calibrated mammalian biostratigraphic standard from the late Neogene of eastern Asia. J Vert Paleontol 11, 519–526

Tedford RH, Qiu Z (1996) A new canid genus from the Pliocene of Yushe, Shanxi Province. Vertebrata Palasiatica 34, 27–40

Teilhard De Chardin PT, Piveteau J (1930) Les mammifères fossiles de Nihowan (Chine). Annls Paléont 19, 87–119

Teilhard de Chardin P, Pei W (1941) The fossil mammals from Locality 13 of Choukoutien. Palaeont Sinica C, 11 106

Teilhard De Chardin PT, Leroy P (1945) Les mustélidés de Chine. Pub Inst Géobiologie 11, 1–56

Temminck CJ (1820) Sur le genre *Hyène*, et description d'une espèce nouvelle, découverte en Afrique. Ann Gen Sc Phys 3, 46–57

Temminck CJ (1835-1841). Monographies de Mammalogie, ou Description de Quelques Genres de Mammifères, dont les Espèces ont été Observées dans les Différents Musées de l'Europe. C. C. van der Hoek, Leiden

Temminck CJ (1838) Over de kennis en de Verbreiding der Zoogdieren van Japan. Tijdschr Natuurl Gesch Physiol 5, 273– 293

Terzea E (1996) Biochronology of the Pleistocene deposits at Betfia (Bihor, Romania). Acta Zool Cracov 39, 531–540

Thenius E (1954) Die Caniden (Mammalia) aus dem Altquartär von Hundsheim (Niederösterreich) nebst Bemerkungen zur Stammesgeschichte der Gattung *Cuon*: Neues Jahrb Geol Paläontol Abh 99, 230–286

Thomas O (1883) On *Mustela albinucha*, Gray. Ann Mag Nat Hist 1, 370–371

Thomas O (1900) New South–American mammals. Ann Mag Nat Hist 7, 148–153

Thomas O (1908) On certain African on South American otters. Ann Mag Nat Hist 8, 1–391

Thomas O, Hinton MAC (1920) On the group of African zorils represented by *Ictonyx libyca*. Ann Mag Nat Hist 5, 367–369

Thomas O (1923) On mammals from the Li–Kiang range, Yunnan, being a further collection obtained by Mr. George Forrest. Ann Mag Nat Hist 11, 655–663

Tomes RF (1857) A monograph of the genus *Lasiurius*. Proc Zool Soc London 24, 34-36

Toro-Moyano I, Martínez-Navarro B, Agustí J, Souday C, Bermúdez deCastro JM, Martinón-Torres M, Fajardo B, Duval M, Falgueres C, Oms O, Parés JM, Anadón P, Julià R, García-Aguilar JM, Moigne AM, Espigares MP, Ros-Montoya S, Palmqvist P (2013) The oldest human remain in Europe, from Orce (Spain). J Hum Evol 65, 1–9

Torre D (1967) I cani villafranchiani della Toscana. Paleontogr Ital 63, 113–138

Torre D (1974) Affinità dentali del cane della grotta di l'Escale. Riv Ital Paleontol 80, 147–156

Torre D (1979) The Ruscinian and Villafranchian dogs of Europe. Boll Soc Paleontol It 18, 162–165

Turner HN (1848) Observations relating to some of the Foramina in the Base of the Skull in Mammalia, and on the classification of the Order Carnivora. Proc Zool Soc London 63

Turner A (1996) The Big Cats and their fossil relatives. Columbia University Press, New York

Turq A, Martínez-Navarro B, Palmquist P, Arribas A, Agustí J, Rodríguez-Vidal J (1996)

Le Plio-Pléistocène de la région d'Orce, province de Grenade, Espagne: bilan et perspectives de recherche. Paléo 8, 161–204

Ungar PS (2010) Mammal Teeth: Origin, Evolution, and Diversity. Johns Hopkins University Press, Baltimore

Valenciano A, Baskin JA, Abella J, Pérez Ramos, A, Álvarez SierraMA, Morales J, Hartstone Rose A (2016a) *Megalictis*, the bone crushing giant mustelid (Carnivora, Mustelidae, Oligobuninae) from the lower Miocene of North America. PLoS One 11, e0152430

Valenciano A, Abella J, Alba DM, Robles JM, Álvarez–Sierra MA, Morales J (2018) New early Miocene material of *Iberictis*, the oldest member of the wolverine lineage (Carnivora, Mustelidae, Guloninae). J Mammal Evol, 1–21

Van der Klaauw CJ (1931) On the auditory bulla in some fossil mammals, with a general introduction to this region of the skull. Bull Am Mus Nat His 62, 1–352

Van der Made J. (1999) Biogeography and stratigraphy of the Mio–Pleistocene mammals of Sardinia and the description of some fossils. Deinsea 7, 337–360

Van der Made J, Palombo MR (2006) *Megaloceros sardus* n. sp., a large deer from the Pleistocene of Sardinia. Hell J Geosciences 41, 163–176

Van der Made J, Morales J, Montoya P (2006) Late Miocene turnover in the Spanish mammal record in relation to palaeoclimate and the Messinian Salinity Crisis. Palaeogeogr Palaeoclimatol Palaeoecol 238, 228–246

Van der Made J, Krzysztof S, Marciszak A (2014) The Polish fossil record of the wolf *Canis* and the deer *Alces*, *Capreolus*, *Megaloceros*, *Dama* and *Cervus* in an evolutionary perspective. Quat Int 326, 406–430

Van Kampen PN (1905) Die Tympanalgegend des Säugetierschädels. Gegenb Morphol Jahrb 34, 321–722

Van Valkenburgh B (1988) Trophic Diversity in Past and Present Guilds of Large Predatory Mammals. Paleobiology 14, 155–173

Van Valkenburgh B (1989) Carnivore dental adaptations and diet: a study of trophic diversity within guilds, in Gittleman JL (ed) Carnivore behavior, ecology, and evolution. Springer, Boston, MA, pp 410–436

Van Valkenburgh B (1990) Skeletal and dental predictors of body mass in carnivores, in

Damuth J, MacFadden B (eds) Body size in mammalian paleobiology: estimation and biological implications. Cambridge University Press, Cambridge, pp 181–205

Van Valkenburgh B, Koepfli KP (1993) Cranial and dental adaptations to predation in canids. Symp Zool Soc Lond 65, 15–37

Van Valkenburgh B, Sacco T, Wang X (2003) Chapter 7: Pack hunting in Miocene borophagine dogs: evidence from craniodental morphology and body size. Bull Am Mus Nat Hist 147–162

Vandenberghe N, Hilgen FJ, Speijer RP (2012) The Paleogene period, in Gradstein F, Ogg J, Schmitz M, Ogg G (eds), The Geologic Time Scale 2012. Elsevier

Vandergoes MJ, Newnham RM, Preusser F, Hendy CH (2005) Regional insolation forcing of late Quaternary climate change in the Southern Hemisphere. Nature 436, 242

Vekua A (1972) Kvabebi Fauna of Akchagylian Vertebrates (in Russian). Nauka, Moscow

Vekua A (1995) Die Wirbeltierfauna des Villafranshium von Dmanisi und Ihre biostratigraphishe bedeutung. Jb Röm-Germ Zentralmus Mainz 42, 77–180

Vera JA (1970) Estudio estratigráfico de la depresión de GuadixeBaza. Bol Geol Min 81, 429-462

Vera JA,Fernández J, López-Garrido AC, Rodríguez-Fernández J (1985) Geología y estratigrafía de los materiales plioceno-pleistocenos del sector Orce-Venta Micena (prov. Granada). Paleontol Evol 18, 3–11

Villalta JF (1952) Contribución al conocimiento de la fauna de mamíferos fósiles del Plioceno de Villarroya (Logroño). Bol Inst Geol Min España 64, 3–204

Vinuesa V, Madurell–Malapeira J, Fortuny J, Alba DM 2015. The endocranial morphology of the Plio–Pleistocene bone–cracking hyena *Pliocrocuta perrieri*: behavioral implications. J Mammal Evol 22, 421–434

Viranta S, Atickem A, Werdelin L, Stenseth NC (2017). Rediscovering a forgotten canid species. BMC Zool 2, 6

Viret J (1950) Sur l'identité générique des Mustélidés fossiles désignés sous les noms de *Pannonictis pilgrimi* et d'*Enhydrictis galictoides*. CR Somm Soc Géol Fr 9, 165–166

Viret J (1954) Le lœss à bancs durcis de Saint–Vallier (Drôme) et sa faune de mammifères villafranchiens. Nouv. Archives Mus Hist Nat Lyon 4, 1–200

Viseras C, Soria JM, Fernández J, García García F (2005) The Neogene-Quaternary basins of the Betic Cordillera: an overview. Geophys Res Abstr 7, 11123–11127

Wada MY, Imai HT (1991) On the Robertsonian polymorphism found in the Japanese raccoon dog (Nyctereutes procyonoides viverrinus). Jpn J Genet 66, 1–11

Wada MY, Lim Y, Wurster–Hill DH (1991) Banded karyotype of wild–caught male Korean raccoon dog, *Nyctereutes procyonoides koreensis*. Genomics 34, 302–306

Wallace SC, Wang X. (2004). Two new carnivores from an unusual late Tertiary forest biota in eastern North America. Nature 431(7008), 556

Wang X (1994) Phylogenetic systematics of the Hesperocyoninae (Carnivora, Canidae). Bull Am Mus Nat His 221.

Wang X, Tedford RH (1994) Basicranial anatomy and phylogeny of primitive canids and closely related miacids (Carnivora: Mammalia). Am Mus Novit 3092, 1–34

Wang X, Tedford RH (2007) Evolutionary history of Canids: 3–20, in Jensen P (ed) The Behavioural Biology of Dogs. CABI, Wallingford.

Wang X, Tedford RH (2008) Dogs, their fossil relatives and evolutionary history. Columbia University Press

Wang X, Tedford RH, Taylor BE (1999) Phylogenetic systematics of the Borophaginae (Carnivora, Canidae). Bull Am Mus Nat His 243.

Wang X, Mckenna MC, Dashzeveg D (2005) *Amphicticeps* and *Amphicynodon* (Arctoidea, Carnivora) from Hsanda Gol Formation, Central Mongolia and phylogeny of basal Arctoids with comments on zoogeography. Am Mus Novit 3483: 1–57

Wang XM, Li Q, Qiu ZD, Xie GP, Wang BY, Qiu ZX, Tseng ZJ, Takeuchi GT, Deng T (2013a) Neogene mammalian biostratigraphy and geochronology of the Tibetan Plateau, in Wang X, Flynn LJ, Fortelius M (eds) Fossil mammals of Asia: Neogene biostratigraphy and chronology, pp 274–292

Wang X, Flynn LJ, Fortelius M (eds) (2013b) Fossil mammals of Asia: Neogene biostratigraphy and chronology. Columbia University Press

Wang X, Tseng ZJ, Li Q, Takeuchi GT, Xie G (2014) From 'third pole' to north pole: a Himalayan origin for the arctic fox. Proc R Soc B: Biol Sc 281(1787), 20140893

Wang X, Li Q, Xie G (2015) Earliest record of *Sinicuon* in Zanda Basin, southern Tibet and implications for hypercarnivores in cold environments. Quat Int 355, 3–10

Ward OG, Wurster–Hill DH (1990) *Nyctereutes procyonoides*. Mamm Species 358, 1–5

Ward OG, Wurster–Hill DH, Ratty FJ, Song Y (1987) Comparative cytogenetics of Chinese and Japanese raccoon dogs, *Nyctereutes procyonoides*. Cytogenet Genome Res 45, 177–186

Ward CV, Leakey MG, Brown B, Brown F, Harris J, Walker A (1999) South Turkwel: a new Pliocene hominid site in Kenya. J Hum Evol 36, 69–95

Wayne RK, Ostrander EA (2007) Lessons learned from the dog genome. Trends Gen 23, 557–567

Wayne RK, Geffen E, Girman DJ, Koepfli KP, Lau LM, Marshall CR (1997) Molecular systematics of the Canidae. Syst Biol 46, 622–53

Werdelin L, Dehghani R (2011) Carnivora, in Harrison T. (ed.) Geology and Paleontology of Laetoli: Human evolution in context. Springer, New York, pp 189–232

Werdelin L, Lewis ME (2000) Carnivora From the South Turkwel Hominid Site, Northern Kenya. J Paleont 74, 1173–1180

Werdelin L, Lewis ME (2005) Plio–Pleistocene Carnivora of eastern Africa: species richness and turnover patterns. Zool J Linn Soc 144, 121–144

Werdelin L, Lewis ME (2013) Koobi fora research project volume 7: The carnivora

Werdelin L, Peigné S (2010) Carnivora. In Werdelin L, Sanders WJ (eds), Cenozoic Mammals of Africa. Berkeley: University of California Press. pp. 609–663

Werdelin L, Sanders WJ (2010) Cenozoic Mammals of Africa. Berkeley: University of California Press

Werdelin L, Lewis ME, Haile-Selassie Y (2015) A critical review of African species of *Eucyon* (Mammalia; Carnivora; Canidae), with a new species from the Pliocene of the Woranso-Mille Area, Afar Region, Ethiopia. Papers in Palaeontology 1, 33–40

Wesley–Hunt GD (2005) The morphological diversification of carnivores in North America Paleobiology 31, 35–55

Wesley–Hunt GD, Flynn LJ (2005) Phylogeny of the Carnivora: basal relationships among the carnivoramorphans, and assessment of the position of 'Miacoidea' relative to crown–clade carnivora. J Syst Palaeontol 3, 1–28

Westbury M, Dalerum F, Norén K, Hofreiter M (2017) Complete mitochondrial genome of a bat–eared fox (*Otocyon megalotis*), along with phylogenetic considerations.

Mitochondrial DNA B 2, 298–299

Wiley EO, Siegel–Causey D, Brooks DR, Funk VA (1991) The Compleat Cladistics. Lawrence: The University of Kansas–Museum of Natural History. Special publication 19

Willemsen GF (1988) *Mustela* and *Enhydrictis* (Carnivora, Mustelidae) from Tegelen (The Netherlands). Proc Kon Ned Akad Wetensch B Phys 91, 311–320

Wilson DE, Reeder DAM (2005) Mammal Species of the World. A Taxonomic and Geographic Reference. 3rd ed. Johns Hopkins University Press, Baltimore

Wolsan M (1993) Phylogeny and classification of early European Mustelida (Mammalia: Carnivora). Acta Theriol 38, 345–384

Wolsan M (2005) Fossil–based minimin divergence dates for the major clades of musteloid carnivorans, in Abstract of Plenary, Symposium, Poster and Oral Papers Presented at Ninth International Mammalogical Congress (IMC 9): Roles of Mammalogy on coexistence of Wild Mammals and Human, July 31–August 5, 2005, Sapporo, Hokkaido, Japan. Science Council of Japan and Mammalogical Society of Japan, Tokyo. pp. 372–373.

Wolsan M, Sato JJ (2010) Effects of data incompleteness on the relative performance of parsimony and Bayesian approaches in a supermatrix phylogenetic reconstruction of Mustelidae and Procyonidae (Carnivora). Cladistics 26, 168–194

Wozencraft WC (2008) Order Carnivora, in Smith AT, Xie Y (eds) A Guide to the Mammals of China. Princeton and Oxford: Princeton University Press, pp 388–448

Wyss AR, Flynn LJ (1993) A phylogenetic analysis and definition of the Carnivora, in Szalay FS, Novacek MJ, McKenna MC (eds) Mammal Phylogeny, New York, Springer Verlag, pp 32–52

Yensen E, Tarifa T (2003) *Galictis vittata*. Mamm Species 727, 1–8

Yonezawa T, Nikaido M, Kohno N, FukumotoY, Okada N, Hasegawa M (2007) Molecular phylogenetic study on the origin and evolution of Mustelidae. Gene 396, 1–12

Young CC (1930) On the mammalian remains from Chi Ku Shan, near Chou Kou Tien. Palaeont Sin, Ser C 7 (1), 1–19

Zammiit Maempel G, de Bruijn H (1982) The Plio/Pleistocene Gliridae from the Mediterranean Islands reconsidered. Proc Koninklijke Nederlandse Akademie van Wetenschappen B 85, 113–128

Zdansky O (1924) Jungtertiare Carnivoren Chinas. Palaeontologia Sinica C. Geological Survey of China

Zdansky O (1927) Weitere Bemerkungen über fossile Carnivoren aus China. Paleont Sinica Serie C 4, 1–30

Zhao C, Zhang H, Liu G, Yang X, Zhang J (2016) The complete mitochondrial genome of the Tibetan fox (*Vulpes ferrilata*) and implications for the phylogeny of Canidae. CR Biol 339, 68–77

Zimmermann EAW (1780) Geographische Geschichte des Menschen, und der vierfüssigen Thiere. Weygandschen Buchhandlung, Leipzig, Germany 2, 1–432

Zollikofer CP, de León MSP (2005) Virtual reconstruction: a primer in computer–assisted paleontology and biomedicine. Wiley–Interscience

Zrzavý J, Řičánková V (2004) Phylogeny of recent Canidae (Mammalia, Carnivora): relative reliability and utility of morphological and molecular datasets. Zool Scripta 33, 311–333

Zrzavý J, Duda P, Robovský J, Okřinová I, Pavelková V, Řičánková V (2018) Phylogeny of the Caninae (Carnivora): Combining morphology, behaviour, genes and fossils. Zool Scripta 47, 373–389

Acknowledgements

Three years of research allow you to visit several institutions and museums, meet and work along with several experts and scholar, open opportunities, start profitable cooperation, deepen human relationships. Therefore, the list of people/institutions to be thanked is long.

Firstly, I thank the "Pegaso" Regional Ph.D. in Earth Science of the joined Universities of Firenze, Pisa and Siena, that each year allows several young researchers to develop their Ph.D. projects and, as in my case, follow their passions.

The research has been partly supported by the SYNTHESYS Project http://www.synthesys.info/, with two projects (Project Numbers: ES-TAF-6553, HU-TAF-6520), which is financed by European Community Research Infrastructure Action under the FP7 "Capacities" Program.

Other important support came from the Erasmus+ traineeship Programme allowing a staying at the Institut Català de Paleontologia. During this traineeship, I was able to development and growth of important skills related to paleontological research, excavation and fossil restoration.

Doing paleontological research mean accessing museum or institutional collection to acquire the raw data for the forthcoming work. I am, therefore, deeply thankful to several kind and welcoming curator who welcomed me in their respective institution. I would like to thank Dr. Elisabetta Cioppi of the Geology and Paleontology section of the Natural History Museum of the University of Florence.

I thank Prof. Raffaele Sardella for granting access to the Late Pleistocene wolf collections housed in the Earth Science Department of Sapienza, University of Rome.

The availability and the kindness of Dr. Caterinella Tuveri and Dr. Marisa Arca was very important in the staying in Nuoro, Ufficio Operativo of the Soprintendenza Archeologia, Belle Arti e Paesaggio per le province di Sassari e Nuoro, despite extraordinary weather conditions.

I thank Dr. Marco Pavia of the Earth Science Department of the University of Turin for help visiting the collections of this institution.

The kindness and availability of Prof. David Lordkipanidze, Dr. Maia Bukhsianidze, Tina Gotsiridze and Dr. Nika Tsikaridze of the Georgian National Museum, for making me feel at home in my stayings in Tbilisi.

I thank Dr. Emanuel Robert of the "Laboratoire de Géologie", Université Claude-Bernard–Lyon-1 for his kindness and availability. Also Dr. Didier Berthet of the Musée des Confluences was very helpful granting access to the great collection of his institutions.I thank Prof. George Koufos, Prof. Evangelina Tsoukala and Dr. Dimitris Kostopoulos of the Earth Science Department of the Aristotle University of Thessaloniki for granting access to the vast collections of their institutions. I thank the availability and kindness of Josefina Cabarga, Dr. Susana Fraile-Gracia, Prof. Jorge Morales and Prof. Manuel Salesa in my visit to Madrid. The access to the collection of fossil mammals of the American Museum of Natural History was granted by Dr. Jim Meng and Judy Galkin, allowing to acquire a considerable amount data, precious in many ways to my research. I thank Dr. M. Gasparik, for granting access the Palaeovertebrate collection of the Hungarian Natural History Museum. I thank Dr. Christine Argot and Prof. Sevket Sen from the Paleovertebrate collection of the Musée National d'Histoire Naturelle. Prof. Denis Geraads of the MNHN was very helpful to my research, allowing to study comparison materials, data and providing casts of relevant specimens, especially of African taxa.

I am indebted to Paolo Agnelli, curators of and of the osteological collection of La Specola, Zoology section of the Natural History Museum of the University of Florence, for your availability, help and enthusiast support to my project.

I thank Dr. Giancarlo Landini, President of Fondazione Santa Maria Nuova O.N.L.U.S., Dr. Giovanniluca Dedola and Dr. Elisabetta Peruzzi, of the Azienda Sanitaria USL Toscana Centro - Ospedale S. Giovanni di Dio (Scandicci, FI) for the access and use of the medical machinery at their facility. A special thanks to Dr. Dedola for the support and kindness showed me during every scanning sessions, teaching me technical and medical principles of computed tomography and radiology. Another special thanks to Elisabetta. Your joyfulness and determination are the reason I got the fantastic and fruitful opportunity to cooperate with the machinery of S. Giovanni di Dio facility. More importantly, you and your sons, Lorenzo and Cosimo, became close friends outside of work and pleasant companions of several dinners and trips together.

Dr. David M. Alba and Dr. Joan Madurell-Malapeira were very helpful to me both professionally and personally. Their support to the research, their helpful advice in scientific issues and bureaucratic craziness were fundamental during my Erasmus traineeship. Joan, particularly, you followed me closely in these years, already before the Ph.D., taking care of me and backing me up on my projects and ideas despite your institutional and research duties. You taught me so much, from the field to the manuscript. Thank you.

I am deeply indebted to Prof. Bienvenido Martinez-Navarro for the support and help given me in the years of my Ph.D., both as a researcher and as young man. The critical discussions and the lessons you taught me have contributed to make me a better researcher. Your encouragement goes beyond work, allowing me to feel part of a group of people with mutual respect and consideration. I hope to be able to continue in this path of growth under your supervision.

A special thank goes to Prof. Pasquale Raia and to the fantastic team of researchers working in/co-working with Naples (Alessandro Mondanaro, Marina Melchionna, Silvia Castiglione, Carmela Serio, Francesco Carotenuto, Mirko Di Febbraro), who showed me the incredible "world of potentiality" of the "other" side of paleontology. I really hope to be part of this world with you.

Dr. Marco Chiari for the unexpected but valuable encouragement in a moment of introspection. The turtle just needs to keep walking.

I thank my colleagues. The ones with whom I shared the office: Omar, Luca and Antonio. I am not the perfect officemate but I really enjoyed the chat, the coffees, the discussions, the cigars, the silliness, the coffees we had in these years. To Dr. Andrea Villa, a thank for the irreplaceable support with side projects, like the Palaeontologist in Progress and VPday/IVPday. Wouldn't havr made it with your help. I thank Steven Zhang and Qigao Jiangzuo for the helpful insights on the Chinese faunas and the valuable discussions on canids and mustelids we shared in the years. Thanks to Silvia Jovells Vaqué for the friendship. Thanks to Fido (Jacopo Fidenti) for the laughs and joyful time talking of lightsabers, strange(r) things and enjoying japanise delights. A thank to Flavia Dr. Strani that has illustrated several of the animal studied in this thesis. To Leonardo Sorbelli for the fantastic covers of the thesis. I thank Beniamino Mecozzi for sharing opinions and views on the evolution and taxonomy of wolves.

This work and my professional growth would be nothing without the guidance and the constant support of my tutor, Prof. Rook. I still remember the first time I knocked on your door 8 years ago, intimidated but resolved to find someone how could help make my aspirations come true. Thank you for the opportunities you opened, for the people presented me. Thank you for the exchange of ideas and the discussions, teaching me the critical way of scientific reasoning. Thank you for the guidance in every situations of academic life, from the institutional part to the personal one. Thank you for the trust for my ten-thousand-at-a-time projects, one more dreaming than the other. Without your silent but always present and helpful advice, none could have been possible. Like a shadow that does not obscure but follows wherever you go.

Thanks to Matt for your enthusiasm and dedication. You're always at my side like a "king's hand", without me being any close to a king. Your advice, critics (sometimes partially overcritical) and support, this work would have been different, and so would I.

Last but for sure not least, thanks to Betty and Mario, who follow my personal and professional achievements with the attention and the interest typical of true and loving people before being good, understanding and present parents. I would not be half the person I am without you.